Year : 2020

Investigating calcium mediated accumulation of soil organic carbon at the Nant Valley alpage, Vaud Alps, Switzerland

Rowley Michael

Rowley Michael, 2020, Investigating calcium mediated accumulation of soil organic carbon at the Nant Valley alpage, Vaud Alps, Switzerland

Originally published at : Thesis, University of Lausanne

Posted at the University of Lausanne Open Archive http://serval.unil.ch
Document URN : urn:nbn:ch:serval-BIB_300E514243831

UNIL | Université de Lausanne

Institut des dynamiques de la surface terrestre

Faculté des Géosciences et de l'Environnement

Investigating calcium mediated accumulation of soil organic carbon at the Nant Valley alpage, Vaud Alps, Switzerland

Thèse de doctorat

Présentée à la Faculté des Géosciences et de l'Environnement de l'Université de Lausanne

Par

Mike C. Rowley

Titulaire d'un Master en Applied Sciences by Research de University of Bournemouth, UK

Jury :

Directeur de thèse, Professeur Éric P. Verrecchia

Co-directrice de thèse, Docteure Stéphanie Grand

Experte interne, Professeure Jasquelin Peña

Expert externe, Professeur Markus Kleber

Expert externe, Docteur Frank Hagedorn

Sous la présidence du Professeur Christian Kull

Lausanne, UNIL, 2020

UNIL | Université de Lausanne
Faculté des géosciences et de l'environnement
bâtiment Géopolis bureau 4631

IMPRIMATUR

Vu le rapport présenté par le jury d'examen, composé de

Président de la séance publique :	M. le Professeur Christian Kull
Président du colloque :	M. le Professeur Christian Kull
Directeur de thèse :	M. le Professeur Eric Verrecchia
Co-directrice de thèse :	Mme la Docteure Stéphanie Grand
Experte interne :	Mme la Professeure Jasquelin Peña
Expert externe :	M. le Professeur Markus Kleber
Expert externe :	M. le Docteur Frank Hagedorn

Le Doyen de la Faculté des géosciences et de l'environnement autorise l'impression de la thèse de

Monsieur Michael ROWLEY

Titulaire d'un
Master en sciences de l'environnement
de l'Université de Bournemouth

intitulée

Investigating calcium mediated accumulation of soil organic carbon at the Nant Valley alpage, Vaud Alps, Switzerland

Lausanne, le 30 mars 2020

Pour le Doyen de la Faculté des géosciences et de l'environnement

Professeur Christian Kull

“The higher organic matter contents of calcareous soils compared with adjacent non-calcareous soils was in part supposedly due to Ca-humates, but the subject has been neglected until recently”

Oades (1988).

- only to have the subject again neglected, until recently -

Acknowledgements

Firstly, I must thank Stephanie and Eric for their help throughout this process. Thank you so much for your kind aid in developing me as a scientist and for your suggestions along this journey. It was a privilege to work with you both over these last 4 (and a bit) years and I look forward to potentially working with you again in the future. I may have produced a thesis without you, but I'm damn sure that it wouldn't have been half as good (or potentially, legible)…

Thank also to Jackie, Pascal, Torsten and David for profitable discussions throughout this process and for helping me to refine several key concepts. Your patience was much appreciated.

Thanks to Jorge, Thierry, Pierre, Laetitia and Micaela for aid throughout my time in the lab. Special thoughts also go out to the late Jean-Claude for being a constant source of happiness in the lab.

Thanks to all my MSc and BSc students that have helped along the way, in the field, in the lab, and for questioning what I thought I knew. It's amazing how fragile knowledge is, when pursued by excellent questions. In chronological order: Maïté, Mélanie, Franziska, Céline, Olivia, Nicolas, and Camille.

For the team: Magali, Nathalie, Fabienne, Fina, John, Dimitri, Thuto, and Laurent, your kind words and smiles filled this time with great happiness. Much love to you all. I want to give Magali a special mention and say thanks for the collaboration, great times, and for discussing many a crazy idea.

To the office: Zwazo, Anael, Gab, and Joel, sometimes there are things that are way more important than science and I thank for you reminding me of this every day.

Special thanks to the Canton de Vaud and IDYST for financially supporting this work and the ''Conseil de coordination scientifique du Vallon de Nant'' for research permissions. Dr. Michele Gaiffe must also be thanked for lettings us adapt her figure.

Then to the Donkeys: God damn what a fun four years that was. Thanks first to Benji for the awesome cover photo, then also to: Magali, Nath, Fina, Dimitri, Gab, VJ, Nico, Camille, Seb, Femi, Ki-Ki, Anael, Zwaso, Mama G, Sté, Bax, Mo-Mo, Alexis, Anna, Sofia, Leanne, Debra, Charlotte, Julia, Pascal E, Pascal P, Inigo, Nadja, Joanne, Monica, Gilope, Lionel, Maarten, Renske, Andrea, Sassi, Moctar, Mathieu, Manu, Bruna, Mertino, Silj, Camille, Elisa, Elfie, Ignes, Noemi, Hannah, Louise, Kwaku, Nico, Josh, Alex, and to all of those I forgot to mention, you're all awesome.

Thanks to the *poubelle bois* for reminding me once a year that smashing stuff is great, drinking white wine gives me bad acid reflux and that, moderate exercise and *compacteuses* are a source of constant danger when hanging: Ki-Ki, Julien, Chef, Pantoufles, Felix, Steve, Hector, Olivier, Yannick, Samwise, Gilope, Gael.

Thanks to my family, Madjwye (especially you, for actually taking the time to read this!), Chris, Jamie, Lisa, Ney, Olde man, Marilyn, Helen, Amy and Steph x.

Erica – without you, this wouldn't have happened. Thanks for the love and journey.

Abstract - English

Soils play an essential role in the global cycling of carbon. Understanding the mechanisms behind the preservation and accumulation of soil organic carbon (SOC) is of globally recognised significance. Until recently, research into the processes that cause SOC to accumulate has predominantly focused on acidic soil environments, where SOC interacts with aluminium (Al) or iron (Fe). The interactions between SOC and calcium (Ca) have typically received less attention, particularly in humid and temperate soil environments. Consequently, the aim of this thesis was to investigate the specific role of Ca in the accumulation of SOC in humid and temperate soils.

A critical assessment of existing literature indicated that Ca could help stabilise SOC by promoting its occlusion in aggregates or its sorption to mineral surfaces. In order to investigate the effects of Ca on these SOC stabilisation mechanisms, we conducted a field study that was split into two parts. Firstly, we evaluated the effects of calcium carbonate ($CaCO_3$), a main reservoir of Ca, on the pedogenic trajectories and general biogeochemistry of humid and temperate soils in a subalpine valley of Switzerland, the Nant Valley. To isolate the influence of $CaCO_3$ from other variables, six profiles were selected that had developed under almost identical conditions for soil formation, except for the presence ($CaCO_3$-bearing) or absence ($CaCO_3$-free) of $CaCO_3$. $CaCO_3$ was present in some parts of the valley due to the variability in $CaCO_3$ content of surficial deposits issued from the Morcles Nappe. The presence of $CaCO_3$ was associated with cascading changes in soil biogeochemistry, including a higher pH, an order of magnitude higher extractable Ca, higher proportion of poorly crystalline Fe forms, and twice as much SOC.

In the second part of the study, we investigated the mechanisms behind this accumulation of SOC at the $CaCO_3$-bearing site. To separate the role of occlusion from that of sorption, we fractionated SOC into four fractions by density and sequential sonication (a free-light fraction, two occluded fractions separated at 10 and 200 J mL^{-1} sonication and a mineral-associated-fraction). There was always more occluded material at the $CaCO_3$-bearing site. Likely causes included the flocculation of soil separates by exchangeable Ca (Ca_{Exch}) and the increased cementation or stability of aggregates in the presence of high SOC content. Yet, the free-light or occluded pools played a minimal role in bulk SOC content at either site. It was instead the mineral-associated fraction that had the highest mass of SOC, closely resembling bulk SOC values. Mineral-associated SOC was nearly twice as high at the $CaCO_3$-bearing site, relative to the $CaCO_3$-free site. Mineral-associated SOC also displayed different stable carbon isotope compositions, which was potentially caused by a preferential stabilisation of SOC by either Ca or Fe oxides. Finally, this thesis highlights that pH could be used as a predictor of the dominance of different SOC stabilisation mechanisms and their effects on accumulation in soils.

Résumé - Français

Les sols jouent un rôle essentiel dans le cycle global du carbone. C'est pourquoi il est primordial de mieux comprendre les mécanismes qui préservent et accumulent le carbone organique du sol (COS). Jusqu'à présent, les recherches sur la stabilisation du COS se sont concentrées principalement sur les environnements de sols acides, où le COS interagit plus avec l'aluminium (Al) ou le fer (Fe). Les interactions entre le COS et le calcium (Ca) ont été généralement négligées, en particulier dans les sols de milieux frais et tempérés. L'objectif de cette thèse fut donc d'étudier le rôle du Ca dans l'accumulation du COS des sols frais et tempérés d'une vallée subalpine de Suisse, le Vallon de Nant.

Une évaluation de la littérature existante a montré que le Ca pouvait stabiliser le COS par occlusion dans les agrégats ou par sorption sur les surfaces minérales. Les recherches ont ensuite entrepris d'isoler les effets du calcium sur les mécanismes de stabilisation du COS grâce à une approche fondée sur deux parties complémentaires. Dans une première partie, les effets du carbonate de calcium ($CaCO_3$), réservoir principal de Ca, ont été évalués en tant que facteur agissant sur la trajectoire pédogénétique et la biogéochimie des sols du Vallon de Nant. Afin d'isoler l'influence du $CaCO_3$, six profils ont été sélectionnés. Ces profils se sont développés sous des conditions pédogénétiques similaires, à l'exception de la présence (*$CaCO_3$-bearing site*) ou de l'absence (*$CaCO_3$-free site*) de $CaCO_3$. La présence de $CaCO_3$ a conduit à un enchainement de changements dans la biogéochimie du sol, à savoir un pH plus élevé, une teneur en Ca extractible supérieure d'un ordre de grandeur, une proportion plus élevée de formes du Fe crypto-cristallines, et deux fois plus de COS, le tout par rapport à une absence de $CaCO_3$.

Dans la seconde partie de l'étude ont été étudiés les mécanismes contrôlant l'accumulation du COS dans les profils contenant du $CaCO_3$. Afin de séparer le rôle de l'occlusion de celui de la sorption, le COS a été fractionné en quatre fractions par densité et sonification séquentielle (une fraction libre légère, deux fractions occluses et une fraction intimement associée aux minéraux). Le site contenant du $CaCO_3$ était toujours plus riche en matériaux occlus, probablement à cause de la floculation des particules du sol par le Ca échangeable (Ca_{Exch}) et l'augmentation de la cimentation ou de la stabilité des agrégats du sol en raison du contenu élevé en COS. Pourtant, les fractions libre ou occluses ne représentaient qu'une partie minime du COS. La majorité du COS était présente dans la fraction associée aux minéraux, donc caractérisée par des teneurs en COS proches de celles du sol total. La teneur en COS associée aux minéraux était près de deux fois supérieure dans les profils contenant du $CaCO_3$, comparativement aux profils sans $CaCO_3$. Ce COS avait également des compositions en isotopes stables (^{13}C) différentes entre les deux sites, ce qui présuppose une stabilisation préférentielle du COS lors des associations organo-minérales. Enfin, cette thèse souligne l'importance du pH en tant que prédicteur de la dominance des mécanismes de stabilisation et d'accumulation du COS.

List of contents

List of figures

- Chapter 1 -

- Chapter 3 -

- Chapter 4 -

- Chapter 5 -

- Chapter 6 -

- Chapter 8 -

List of tables

List of equations

- Chapter 1 -

- Chapter 2 -

- Chapter 5 -

- Chapter 6 -

List of acronyms

Below is a list of all the acronyms used in this thesis. Chemical symbols will not be listed in this table. Most units from the International System of Units are not included in this table either, but a full list can be found at: https://www.nist.gov/pml/weights-and-measures/metric-si/si-units (last accessed 18/10/2019)

Acronym	Meaning	Acronym	Meaning
ATP	Adenosine triphosphate	**kyr**	A thousand years
2 θ	2 theta (angle of diffraction)	**LFs**	Light fractions including the free-light fraction and the occluded fractions
Å	Angstrom (m x 10^{-10})	**M**	Moles per litre
AGB	Aboveground biomass	**NanoSIMS**	Nano-scale secondary ionisation mass spectrometry
Al_d	Aluminium extracted by dithionite	**NEXAFS**	Near-edge X-ray absorption fine structure spectroscopy
Al_{Exch}	Salt-extractable or exchangeable Al	**NPP**	Net primary productivity
Al_o	Aluminium extracted by oxalate	**OCP**	Oxalate-carbonate pathway
B1, B2, B3	$CaCO_3$-bearing profiles	**o-LF_{10}**	Occluded density fraction separated at 10 J mL^{-1} sonication energy
BGB	Belowground biomass	**o-LF_{200}**	Occluded density fraction separated at 200 J mL^{-1} sonication energy
Ca_{Exch}	Exchangeable calcium	**o-LFs**	Occluded density fractions
CCE	Calcium carbonate equivalent	**OM**	Organic matter
CEC	Cation exchange capacity	**OMA**	Organo-mineral association
CEC_{sum}	Sum of extractable cations on the exchange complex, excluding H^+	**PCA**	Principal component analysis
$cmol_c$ kg	Centimoles of charge per kilogram	**pH**	The negative of the base 10 logarithm of the activity of hydrogen ion
CO_2^{Atm}	Atmospheric CO_2 concentrations	**PhD**	Doctor of philosophy
Cohex	Cobalt hexamine	**ppm**	parts per million
Da	A dalton or unified atomic mass unit	**PZC**	Point of zero charge
DF	Density fractionation	**RMSE**	Root mean square error
DOC	Dissolved organic carbon	**rpm**	Revolutions per minute
EDTA	Ethylenediaminetetraacetic acid	**SAS**	Statistical software
EPS	Extracellular polysaccharides / polymeric substances.	**SIC**	Soil inorganic carbon
Eq.	Equation	**SIMS**	Secondary ionisation mass spectrometry
F1, F2, F3	$CaCO_3$-free profiles	**SOC**	Soil organic carbon
Fe_d	Iron extracted by dithionite	**SOM**	Soil organic matter
Fe_o	Iron extracted by oxalate	**SPT**	Sodium polytungstate solution (density = 1.6 g cm^{-3})
Fe_o/Fe_d	Ratio of oxalate extracted iron to dithionite extracted iron	**STXM**	Scanning transmission X-ray microscopy
Fig.	Figure	**v/v**	Volume to volume
f-LF	Free-light density fraction	**XAS**	X-ray absorption spectroscopy
HF	Heavy density fraction	**XPS**	X-ray photoelectron spectroscopy
IUSS	International Union of Soil Sciences	**XRD**	X-ray diffraction
K_{Exch}	Exchangeable potassium	**XRF**	X-ray fluorescence

- This page is intentionally left blank -

- Chapter 1: General introduction -

- This page is intentionally left blank -

- General introduction foreword -

In this section the current state of the art on soil organic carbon and its biogeochemical cycling is presented. The following introduction defines the general concepts and key terms that are used regularly throughout this thesis. This introduction will also aim to place our research and the following chapters within the context of existing literature, highlighting recent paradigm shifts in our understanding of the transformation and persistence of soil organic carbon. It will then focus on some more complex concepts within the field of organo-mineral association that will be key for our general discussion (Chapter 6). It will also importantly, highlight the existing knowledge gaps that will be addressed in the research outline (Chapter 2) and following research chapters (Chapters 3-5).

1.1 - Biogeochemistry

Biogeochemistry is a scientific discipline that seeks to describe the relocation, exchanges, or cycling of elements through the Earth's surface. Elements take part in different processes as they migrate through the Earth's four spheres, the atmosphere, hydrosphere, lithosphere, biosphere, and the intersection between them, the pedosphere. The field is interdisciplinary, spanning biology, geology, physics, and chemistry, to name but a few fields, and is a fundamental building block in our understanding of natural systems (Schlesinger, 2003). Biogeochemistry is built upon two fundamental principles, the laws of thermodynamics and chemical stoichiometry (Schlesinger and Bernhardt, 2013). The 1st law of thermodynamics states that energy can never be created or destroyed, but is instead converted from one form to another. Yet, as chemical reactions are not completely efficient, some energy is lost from natural systems (typically as heat) and thus, reactions always proceed to yield a lower state of free energy (*G;* 2nd law) or higher disorder (entropy). Biological systems are highly ordered and thus, must constantly process energy or metabolise to maintain their state of low entropy. The laws of thermodynamics therefore provide a framework for understanding the movement of energy in different biogeochemical reactions and why life must metabolise.

The second fundamental principle of biogeochemistry is stoichiometry, which dictates that elemental cycles are linked through the proportional balance of elements within the structure of molecules. This principle highlights the delicate equilibrium between different elemental cycles in nature. It states that one elemental cycle may be limited by the presence or absence of another element needed to create specific molecules; for instance, the productivity of vegetation is typically limited by an environmental deficiency in N or P (Koerselman and Arthur, 1996), needed to create chlorophyll, amino acids and adenosine triphosphate (ATP). Biogeochemical constraints placed on a specific environment by stoichiometry thus enable us to model elemental cycles and their interactions with other elements on ecosystem- or larger-scales (Bashkin, 2002). With these two fundamental principles, we can begin to investigate the complex coupling of different elemental cycles such as Ca and C as they migrate through the Earth's surface, our global biogeochemical system (Lovelock, 1989).

1.2 - The Ca cycle

Calcium is an alkaline earth metal, meaning that it has a high third stage ionisation energy and is divalent. Ca is the 5th most abundant element in the Earth's crust (Wedepohl, 1995) and is considered mobile, as it is weathered relatively easily from most primary and secondary minerals, moving freely in different marine and terrestrial reservoirs. Ca is an essential nutrient in the biosphere, typically used throughout nature for structural purposes, including the stabilisation of membranes (Demarty et al., 1984), enzymes (Likens et al., 1998), or the production of essential biominerals, such as hydroxyapatite (teeth or bones; Abou Neel et al., 2016) or different forms of carbonate (protective shells; Ries et al., 2009). During the biomineralisation of carbonate ($CaCO_3$) by marine organisms, C can be sequestered

within the geologic pool when the animal dies and sink to the ocean floor (Heinze et al., 2015). This is just one of the examples in which the Ca and C cycles can be intimately coupled due to their importance within biological systems.

1.3 - The C cycle

The C cycle is of central importance to biogeochemistry because C is the fundamental building block of life. C is a non-metallic tetravalent element that has four electrons available to form covalent bonds. C is an effective catenater, binding to itself and creating long chain-like and ring structures. C shifts between different inorganic and organic phases as it moves through the geosphere, atmosphere, hydrosphere, biosphere, and pedosphere. However, it is the faster cycling biotic C cycle that has the larger fluxes as the amount of carbon taken up by the biosphere and re-released to the atmosphere is 1000 times greater than that of the geological C cycle (Archer and Barber, 2004). The biotic cycling of C starts when photosynthetic organisms (phototrophs) utilise photons at certain electromagnetic wavelengths from inbound solar radiation to create adenosine triphosphate and nicotinamide adenine dinucleotide phosphate within chloroplasts. This energy source is then used by phototrophs to reduce inorganic C (CO_2) in the Calvin cycle, releasing O_2 and C, the latter of which can be stored as fuel after being converted to a higher state of *G*, (Eq. 1.1; Benson and Calvin, 1950). Organic C is then subsequently oxidised back into a state of lower *G*, inorganic CO_2 during heterotrophic respiration (Eq. 1.2; Krebs and Johnson, 1937), which is the fundamental pathway of metabolism for nearly all remaining life forms (not accounting for chemoautotrophs).

$$CO_2 + 2H_2O \underset{\text{Light}}{\Longrightarrow} \langle CH_2O \rangle + O_2 + H_2O$$

Eq. 1.1. Reduction of inorganic carbon into a nominal carbohydrate during photosynthesis by photosynthetic organisms, utilising inbound electromagnetic wave radiation (Archer and Barber, 2004).

$$C_6H_{12}O_6 + 6O_2 \rightarrow 6CO_2 + 6H_2O + \text{ATP energy}$$

Eq. 1.2. The aerobic oxidation of glucose during glycolysis and the Krebs cycle (Krebs and Johnson, 1937) and production of energy.

1.3.1 - Global budgets and reservoirs of C

During the migration of C through both inorganic and organic forms, it is stored within different environmental reservoirs. Each reservoir has different inputs and outputs (fluxes) and processes that govern how long C may stay within a specific reservoir (residence times). Global estimates for how much C is stored within each environmental reservoir (g x 10^{15} = 1 Pg) at a specific time vary widely (Fig. 1.1) due to the intricate nature of the global system and large spatial and temporal fluctuations in elemental cycles (Schlesinger and Bernhardt, 2013).

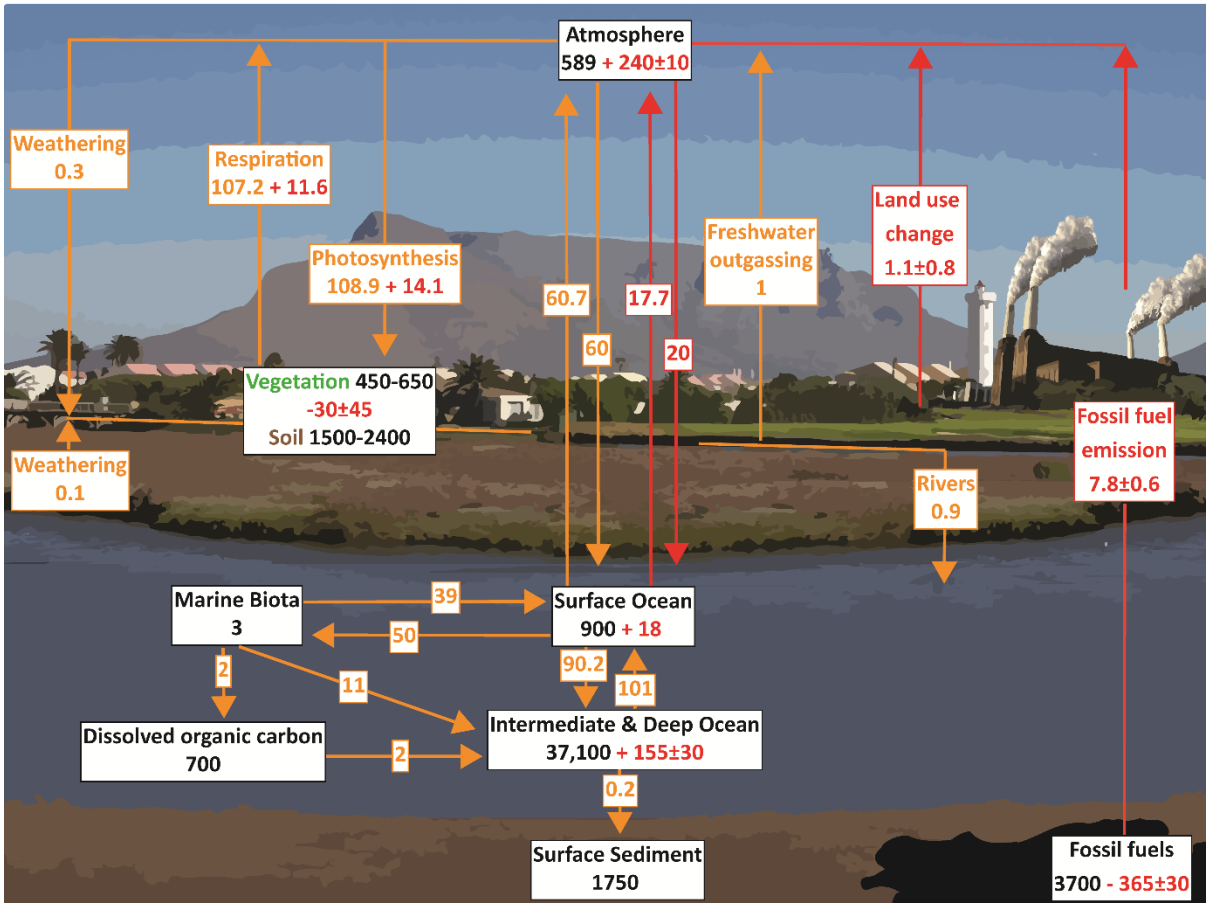

Fig. 1.1. A simplified model of the carbon (C) cycle describing the stocks of C within different environmental reservoirs (Pg C) and the fluxes of C between the different reservoirs. Fluxes (Pg C yr^{-1}) are in orange (environmental) or red (anthropogenic) boxes with accompanying arrows. Reservoirs are in black boxes with red numbers signifying anthropogenic driven changes in the stocks of the reservoirs since the industrial revolution (1750). All figures are taken from Kandasamy and Bejugam (2016). Estimates for soils vary widely, but 2400 Pg C will be used from here out.

1.3.2 - Anthropogenic effects on the C cycle

Since the start of the industrial era, humans have been extracting fossil C from an inert reservoir, combusting it, and releasing various gases into the atmosphere (CO_2, CO, CH_4, SO_2, NO_2, N_2O; Fig. 1.1), the predominant of which is CO_2. Atmospheric CO_2 concentrations (CO_2^{Atm}) have thus risen from 280±10 ppm during the several thousand years prior to the industrial revolution (1750; Prentice et al., 2001) to 407.4±0.1 ppm in 2018 (NOAA, 2019). This increase in CO_2^{Atm} protrudes from historical records (Ciais et al., 2013), as measurements of ice cores show that CO_2^{Atm} typically varied between 172–300 ppm during the last 800 kyr, between glacial and interglacial periods, respectively (Lüthi et al., 2008). It has long been known that CO_2, along with other greenhouse gases (H_2O vapour, CH_4) trap inbound infrared radiation (Tyndall, 1859), driving global temperatures (Foote et al., 1856) by increasing surface radiative forcing. This process is vital for life as it warms average global temperatures to 15°C from

-18°C, the Earth's radiative equilibrium temperature (Ahrens and Samson, 2010). However, global temperatures are rising rapidly and there is now scientific consensus (Cook et al., 2016) that anthropogenic emissions from the burning of fossil fuels is likely its main cause (IPCC, 2014). This increasing CO_2^{Atm} is in turn linked to a range of environmental issues (IPCC, 2014) and there is near global consensus that CO_2^{Atm} must be reduced (UNFCC, 2016). CO_2^{Atm} can be reduced by sequestering it through different processes and storing it in existing natural reservoirs, such as in the geosphere, hydrosphere, biosphere, or pedosphere (soils). This is supported by the European Academies Science Advisory Council who recently concluded that soils could play a major role in reducing CO_2^{Atm} (EASAC, 2018).

1.4 - Soils

Soils are complex 3-dimensional matrices formed of both mineral and organic solid matter (both living and dead), the pores of which, water (or ice) and gases pass through, all interacting in different biogeochemical processes. Soils initially form when life begins to colonise rock weathering products or sediment (regolith) at the surface of the lithosphere. The complexity of a soil then typically increases as a function of time as pedogenic processes (addition, losses, translocation and transformation) alter components differentially within the solum, causing the horizonation and forming the profile (Fig. 1.2; Schaetzl and Thompson, 2015). The evolution and development of soils through time (pedogenesis) is principally governed by four external factors: climate, topography, biota, and parent material, which function through time (Dokuchaev, 1883; Jenny, 1941). Thus, soils that have developed for a similar amount of time under near-identical external factors of pedogenesis should be relatively similar (Dokuchaev, 1883). Yet, it is often more complicated than this in the field and the effects of these factors can also be inhibited by inherent pedogenic processes or intrinsic pedogenic factors (Muhs, 1984). These intrinsic pedogenic factors can enforce a state of pedogenic inertia, preventing pedogenesis and its associated changes in biogeochemistry (Chadwick and Chorover, 2001), contributing to the spatial heterogeneity of soils. Thus, soils can vary drastically over short distances due to small differences in both external and internal factors of pedogenesis, which has a divergent influence on biogeochemical cycles, such as the C cycle.

Fig. 1.2. Two soil profiles of different pedogenic complexity. Profile A is a Regosol profile that has recently developed in a regolith (museum example of a Regosol, photo credit to Rockwurm, Creative Commons License). Contrastingly, profile B is a Podzol at Fontainebleau, France (photo courtesy of Dr. Stephanie Grand). Profile A still retains the structure of the original regolith, while profile B is formed due to the downwards translocation of carbon, iron, and aluminium through a sandy textured soil via chelation, leaving a bleached eluviation horizon over an enriched illuviation horizon.

1.4.1 - Carbon in soils

Soils play an essential role in the cycling of both inorganic (SIC) and organic carbon (SOC). Soils contain approximately 2400 Pg C, of which, 900 Pg C is SIC and 1500 Pg C SOC (Batjes, 1996; Lal, 2004). SIC is generally overlooked in soil studies, but is still important as it links the slower geologic C cycle with the faster biotic cycle of SOC (Zamanian et al., 2016). SOC consists of both living and non-living soil organic matter (SOM) that is cycling through the pedosphere (Torn et al., 2009). SOM plays a central role in many soil properties and ecosystem services, including soil fertility and the slow release of nutrients, water filtration, ecosystem functioning, structural stability, erosion prevention, and the regulation of global CO_2^{Atm} (Lal, 2009). The mass of SOM in a given space or landscape (stocks) can be summarised as the balance between inputs (fresh, transported and recycled SOM) and outputs

(dissolved organic C and respired CO_2). SOM stocks are being degraded globally, particularly by land management practices in agricultural soils (Stockmann et al., 2015), and land use change, such as deforestation (Cerri et al., 1991). This disrupts soils, their C cycle, and their associated ecosystem services, further exacerbating global CO_2^{Atm}.

The recent United Nations Sustainable Development goals (UN General Assembly, 2015) aim at reducing this degradation by moving towards sustainable agricultural practices (§ 2.4) and achieving land degradation neutrality (§ 15.3) by 2030. This is further supported by a recent movement called the "4 Per Mille Initiative". This initiative publicises the need to preserve and accumulate SOC in agricultural soils due to its important ecosystem services (Minasny et al., 2017). The project aims to reduce harmful land management practices that decrease SOC and increase the adoption of sustainable agricultural practices that contribute towards the accumulation of SOC. Through the adoption of such practices, the initiative aims to increase SOC stocks on agricultural land by 0.4 % yr^{-1} (4 ‰), which, by their calculations, would represent a C sequestration that equals current anthropogenic CO_2 emissions. Yet, to successfully implement both the United Nations Sustainable Development goals and the 4 Per Mille Initiative, key knowledge gaps regarding the degradation, retention, and preservation of SOC, and its interactions with other elements within a soil profile, must first be addressed.

1.4.2 - Decomposition

Non-living SOC (from here on out SOC) is predominantly formed of plant, but also animal / microbial matter that is at various stages of physical and oxidative transformation (decomposition). SOC is incorporated into the soil when plants or animals die and can have residence times that span several orders of magnitude (minutes to tens of thousands of years) before it is respired back to the atmosphere as CO_2 (Torn et al., 2009). During decomposition, SOC can become increasingly laden in functional groups as it undergoes oxidative transformation. Decomposition is more efficient in the presence of O_2 (aerobic); but it can also occur anaerobically, as unlike other heterotrophs, microorganisms can use a variety of chemicals as electron acceptors for the oxidative transformation of SOC (Burgin et al., 2011). There are currently three conceptual models of SOC decomposition processes (Fig. 1.3), discussed further below to give context to the evolution in our understanding of SOC's degradation and transformation within a profile.

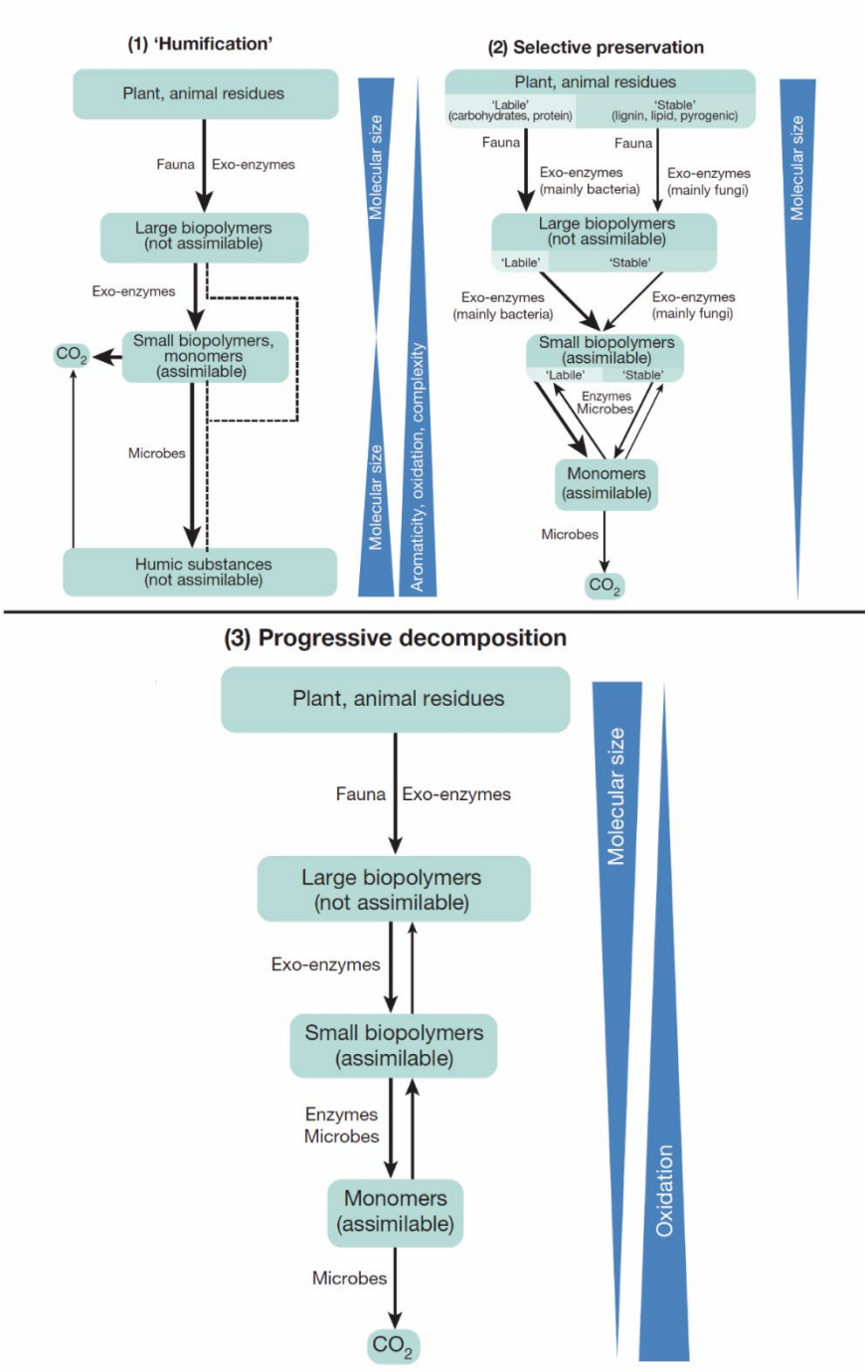

Fig. 1.3. The three competing models of decomposition within soil science, discussed further below. Image adapted from Lehmann and Kleber (2015).

1.4.2.1 - Humification

Humification is the oldest of the three models of decomposition in soils and differs from the other models by theorising that decomposition products condensate within a soil profile. These novel condensates were defined operationally as the products of alkali-based extraction methods and were thought to consist of large macromolecules of a dark nature, called humic substances. Humus was then assumed to be more resistant to decomposition, leading to its persistence and accumulation within soils (Orlov, 1995; Stevenson, 1994). Yet, the concept of humification has been recently challenged (Kelleher

and Simpson, 2006; Kleber and Lehmann, 2019; Lehmann and Kleber, 2015). Novel techniques have demonstrated that humic substances cannot be defined as a single substance and are instead, a heterogeneous mixture of simpler biochemical constituents (Kelleher and Simpson, 2006). It therefore seems as though recent evidence does not support the historic concept of humification and that these substances and their associated condensation processes do not exist within soils (Kleber and Lehmann, 2019; Lehmann and Kleber, 2015; Schmidt et al., 2011). Humification will thus not be discussed further within the context of this thesis, unless referring to ancient literature.

1.4.2.2 - Selective preservation

Another important model of understanding SOC decomposition processes is selective preservation, which is based upon the selective decomposition of certain substrates by microorganisms. Litter decomposition experiments have repeatedly shown that certain complex and more stable compounds (lignin, cutin, and suberin) have a slower turnover in organic horizons (Aber et al., 1990; Preston et al., 2009). It was thus previously assumed that this also occurred in mineral horizons and that microorganisms preferentially used less complex substrates, due to the smaller energy barriers that obstructed their utilisation. Logically, this would lead to the selective preservation and persistence of these complex substrates within a profile and their accumulation through time.

However, as hypothesised by Oades (1988), there has been little evidence for the preservation of complex materials within soil profiles. On the contrary, authors have found that simple substrates tend to persist within the soil profile, while complex substrates, like lignin, are decomposed relatively quickly (Gleixner et al., 1999; Gleixner et al., 2002). It has also been demonstrated that microorganisms can use the energy gained from simpler substrates to overcome energy barriers associated with the metabolism of more complex substrates (priming effect; Kuzyakov et al., 2000; Löhnis, 1926). Thus, the importance of selective preservation is still recognised within organic horizons or at the beginning of the decomposition continuum, but its role seems to be diminished within mineral horizons (Matteodo et al., 2018).

1.4.2.3 - Continuum

Decomposition is now commonly thought to occur in a continuum (Lehmann and Kleber, 2015). This continuum begins when organic matter is incorporated into the soil by physical or biological processes and then broken down into smaller particulate SOM by macro-endopedonic species (mites, beetles, worms, small mammals, etc...; Gobat et al., 2004). This source of particulate SOM can then be further degraded by the extra-cellular enzymes of microorganisms (fungi / bacteria), hydrolysing it from large energy rich compounds to smaller energy poor compounds (Burns, 2010). Once SOC has been broken down beyond approximately < 600 Da, it can pass directly across the cell wall of microorganisms (Decad and Nikaido, 1976) and either be incorporated into cell structures, used for storage (Mason-Jones et al., 2019), or respired and transformed into CO_2 (Section 1.4.3; Eq. 1.2).

Thus, unlike selective preservation, where SOC is preserved due to its inherent biochemical complexity, the continuum model suggests that SOC is actually more likely to persist as it becomes increasingly smaller and less complex (Lehmann and Kleber, 2015). This is because degradation processes that reprocess SOC into smaller energy poor compounds also increase the proportion of polar and ionisable functional groups in SOC (Kleber et al., 2007). In turn, the processes that inhibit the decomposition of SOC within most mineral soils, occlusion and sorption (discussed further in Section 1.5), can more readily stabilise these smaller substrates with more polar and ionisable functional groups. This hypothesis agrees with recent evidence that, rather than more complex substrates, it is instead the simpler constituents of SOC that persist within mineral soil (Gleixner et al., 1999; Gleixner et al., 2002). It therefore seems that, contrary to previous hypotheses, SOC is formed of a heterogeneous mixture of substrates at various points along a decomposition continuum (physical degradation and oxidative transformation) within mineral soil, prior to being eventually respired (Lehmann and Kleber, 2015). Furthermore, the direction of this continuum does not reverse to form more complex substrates (humification) and remains relatively disconnected from the inherent composition of particulate SOM (selective preservation) once incorporated into the mineral soil.

1.4.3 - Respiration and its global drivers

At the end of the decomposition continuum under both aerobic and anaerobic conditions, a certain fraction of C is lost and re-emitted as CO_2 or CH_4 in a process called heterotrophic respiration. Respiration rates, like any other property of a soil, are governed by the five factors of soil formation. Thus, heterotrophic respiration varies temporally and spatially, and global estimates vary widely from 43.6 to 75 Pg C yr^{-1} (Konings et al., 2019; Schlesinger and Andrews, 2000). Yet, while estimates of global respiration vary widely, it seems as though heterotrophic soil respiration is increasing globally (Bond-Lamberty et al., 2018). Recent changes in two soil forming factors (organisms and climate) could be driving these globally increasing decomposition / respiration rates and will now be explored further below.

1.4.3.1 - Increased net primary production

Photosynthetic organisms play a vital role in heterotrophic respiration as their net primary production (NPP) drives the input of new SOC into the soil reservoir. Gross primary production is defined as the amount of chemical energy stored (usually defined as carbon biomass) by photosynthetic organisms through a given time. In contrast, NPP is the chemical energy that remains stored within photosynthetic organisms after they have used photosynthate from gross primary production for cellular respiration and maintenance of existing tissues. Thus as NPP increases, there is more C input into the reservoir as SOM to be decomposed and respired back to the atmosphere, if not inhibited by other processes (Torn et al., 2009; Trumbore et al., 1995). As CO_2^{Atm} increase globally, photosynthesis (the ribulose-1, 5-bisphosphate carboxylase / oxygenase enzyme) becomes more efficient, increasing gross primary productivity world-wide in what is known as the CO_2 fertilisation effect (Braghiere et al., 2019; Ciais et

al., 2019; Frederick et al., 1973; Zhu et al., 2016). Thus, a proportion of increasing heterotrophic respiration is likely driven by increased gross primary productivity from CO_2 fertilisation.

1.4.3.2 - Climate (precipitation / temperature)

Moisture is a necessary component of decomposition, and changes in moisture regime can either increase or decrease global respiration rates. Episodic periods of drying can thus affect decomposers by reducing the availability of a necessary component of decomposition (H_2O) from substrates, enzymatic efficiency, decreasing bacterial mobility (Iovieno and Bååth, 2008) when not transported through air pockets by fungal highways (Bravo et al., 2013), and consequently, heterotrophic respiration. Contrastingly, rain events can drive sharp increases in heterotrophic respiration rates as moisture from precipitation reconnects decomposers with the necessary components of decomposition and fresh C substrates (Carbone et al., 2011; Lee et al., 2004). With a changing global climate, precipitation frequency and intensity will also be affected (Trenberth, 2011), which can directly or indirectly influence soil moisture content and heterotrophic respiration rates.

Another aspect of the changing climate that impacts global respiration rates is the increasing temperature. Biogeochemical reactions in soils, such as decomposition, are strongly temperature dependent and thus C stocks tend to be smaller in hotter environments than colder environments (Torn et al., 2009). Temperature can affect decomposition by directly influencing enzymatic kinetics, microbial dynamics, and substrate availability (Davidson and Janssens, 2006; Schipper et al., 2014). Increasing temperatures globally will likely have a positive influence on soil respiration, particularly in surficial horizons with increased SOC contents, which in turn will positively feedback into CO_2^{Atm} and global climate change (Davidson and Janssens, 2006; Jenkinson et al., 1991).

1.4.3.3 - Limiting factors

It is worth noting that neither gross primary productivity nor soil respiration increase linearly or consistently with increases in CO_2^{Atm}, moisture or temperature. Responses can display a '*plateau*' due to limiting factors. These limiting factors are numerous, but specific examples include: N or P limitation modulating photosynthesis or respiration, an increased water content reducing the availability of O_2 for decomposition as soils approach saturation point, or the stabilisation of SOC within a soil profile. These processes that stabilise SOC will now be discussed further below.

1.5 - SOC stabilisation - An ecosystem property

Soil organic carbon may be stabilised against oxidative transformation within a profile, contributing towards its persistence and accumulation while reducing heterotrophic respiration. SOC stabilisation is therefore defined as a set of processes that directly or indirectly inhibit the decomposition of organic C within a soil profile (Sollins et al., 1996). It is now thought that the stabilisation and accumulation of

SOC in mineral soils over medium- to long-time periods is predominantly driven by specific ecosystem properties (Fig. 1.4; Schmidt et al., 2011). These ecosystem properties include:

i) **The physical separation of substrates from decomposers over pluri-metric to micro-metric scales.**
ii) **Interactions between SOC and minerals or cations.**
iii) **The occurrence of temperature or moisture conditions that are incompatible with enzymatic reactions.**
iv) **Toxicity effects of metal ions like Al^{3+}.**

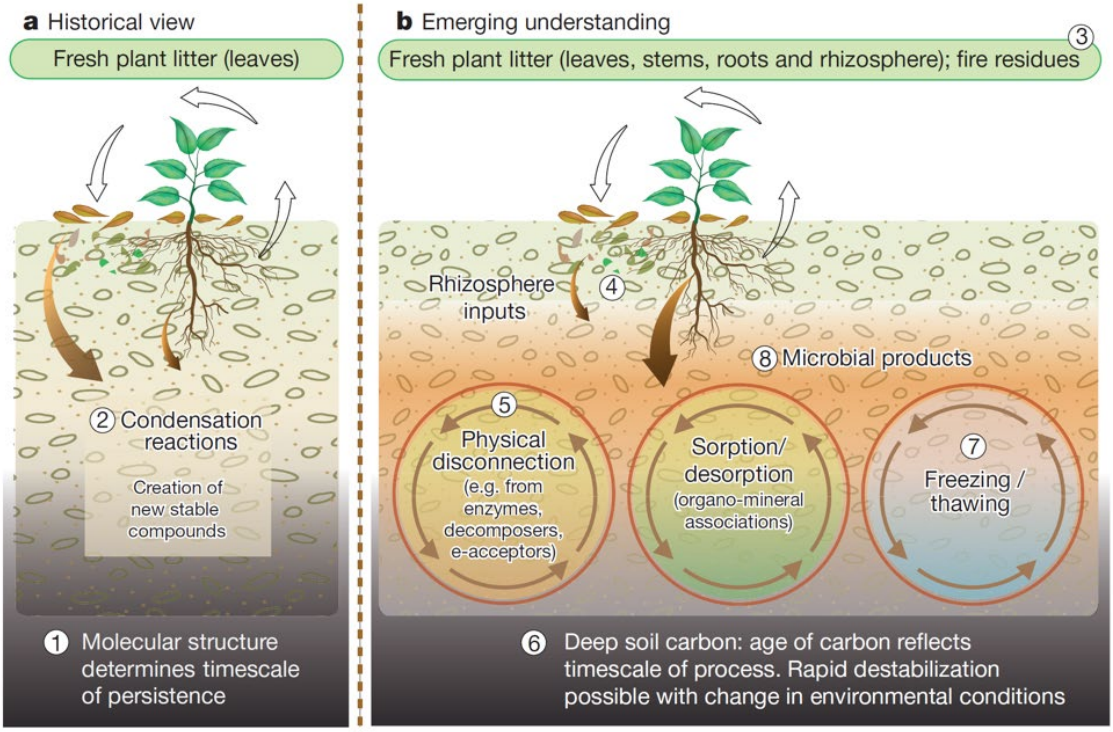

Fig. 1.4. A conceptual illustration of the emerging understanding that soil organic carbon stabilisation arises as a result of specific ecosystem properties. These properties change as one moves throughout the soil profile, meaning that different stabilisation mechanisms dominate in different horizons. This image is taken from Schmidt et al. (2011).

Calcium will more likely play a role in the first and second processes. Thus, the influence of physical separation and sorption processes on the SOC decomposition continuum (Fig. 1.5) will now be further explored in the following section, with the aim of creating a mechanistic framework for understanding the potential role of Ca in SOC stabilisation.

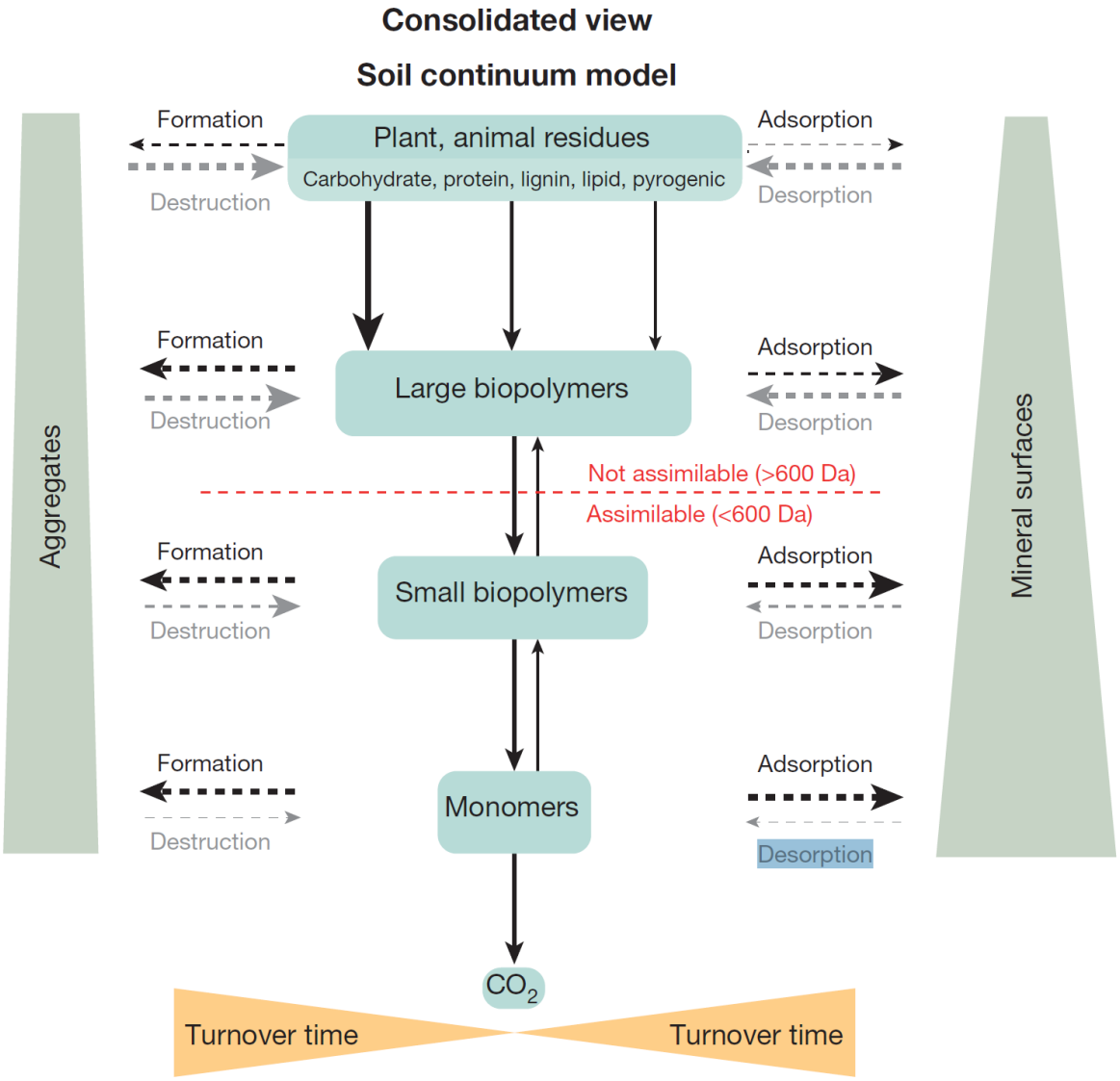

Fig. 1.5. A conceptual model of the effects of the two predominant stabilisation mechanisms at different points of the decomposition continuum. The model suggests that there is an increasing probability of stabilisation either by occlusion within aggregates or sorption onto mineral surfaces with decreasing substrate size. This image is taken from Lehmann and Kleber (2015).

1.5.1 - Physical separation

Soil organic carbon can be stabilised from decomposition if a substrate is physically separated from the necessary components of decomposition, namely decomposers, their extra-cellular enzymes, oxygen, and moisture.

Physical separation is an ecosystem property that operates on a wide range of spatial scales (pluri- to micro-metric scales) and arises due to specific physicochemical conditions in soil ecosystems. At an ecosystem scale, physical separation can stabilise large quantities of SOC in biologically-limiting environments. Specific examples include Histosols or Cryosols, where water-logged (Laine et al., 1996; Pohl et al., 2015) or frozen conditions (Grosse et al., 2011; Mueller et al., 2015) severely inhibit the

oxidative transformation of organic substrates, causing SOC to accumulate. The physical separation of substrates from decomposers and the necessary components of decomposition can also occur on much smaller spatial scales. Examples comprise SOC inclusion within a mineral or co-genetic mineral assemblage (Bindschedler et al., 2016), hydrophobic interactions creating a micellar-like structure (Chassin, 1979), SOC intercalation within phyllosilicates (Theng et al., 1986), and the separation of SOC within pedogenic aggregates (Adu and Oades, 1978).

Formation of aggregates in soil is the most widespread micro scale process that leads to the physical separation of SOC, in a mechanism typically labelled as occlusion. Soil aggregates are conglomerates of primary soil particles (Schaetzl and Thompson, 2015) and their relation to the stability or accumulation of SOC has been repeatedly demonstrated (Denef et al., 2004; Moni et al., 2010; Monreal et al., 1997; Plante et al., 2002; Skjemstad et al., 1993; Virto et al., 2008; Virto et al., 2010). Formation of aggregates has conventionally been thought to involve the electrostatic flocculation of soil separates (Ghezzehei, 2011), which are then cemented by organic or inorganic agents (Jastrow, 1996; Six et al., 2004). Aggregates can also be formed biologically during the physical meshing of soil particles by roots and fungi or the excretion of extra-cellular polysaccharides / polymeric substances by microorganisms and roots (Balesdent et al., 2000; Chenu and Cosentino, 2011; Six et al., 2004; Six et al., 2002). Microorganisms can excrete these extra-cellular polysaccharides / polymeric substances (EPS) around fresh SOC during decomposition. This EPS then adheres to soil particles, binding them together and creating a shell around the decomposing SOC nucleus, which eventually occludes the SOC residue within (Chenu and Cosentino, 2011).

When driven by biology, soil structure is typically arranged into a spatial hierarchy, with distinct physical classes of aggregates that are often classified as macroaggregates (> 250 μm) or microaggregates (< 250 μm; Asano and Wagai, 2014; Elliott, 1986; Oades, 1984; Six et al., 2004; Six et al., 2000; Tisdall, 1996; Tisdall and Oades, 1982). It is largely accepted that in this hierarchy, microaggregates are formed within macroaggregates, which then break apart because of their weaker binding agents and larger planes of weakness, distributing microaggregates into the soil matrix (Oades, 1984; Six et al., 2004; Tisdall, 1996). These microaggregates are typically considered more stable because of their stronger binding agents and reduced macroporosity, increasing the stability of SOC occluded within (Denef et al., 2004; Tisdall and Oades, 1982). Yet, despite the recent emphasis on biological controls on soil aggregation, it should be noted that soil aggregation, its hierarchy, and the occlusion of SOC are also influenced by inorganic components of the soil matrix.

Abiotic agents, such as the composition of the mineral soil matrix, can also play a dominant role in aggregate formation, occlusion, and the stabilisation of SOC. Polyvalent cations can increase aggregation in soils by flocculating negatively charged soil separates (Bronick and Lal, 2005; Érika et al., 2016; Grant et al., 1992). Inorganic components can also act as cementing agents, reinforcing

aggregates and reducing porosity, with examples including poorly crystalline minerals (Rasmussen et al., 2005), well crystallised Fe oxides (Oades and Waters, 1991; Zhao et al., 2017), or carbonates (Falsone et al., 2010; Fernández-Ugalde et al., 2014; Fernández-Ugalde et al., 2011; Virto et al., 2011). Inorganic components have been documented to reinforce both macroaggregates (Fernández-Ugalde et al., 2011; Virto et al., 2013) and microaggregates (Falsone et al., 2010). Some authors have pointed out that when predominantly controlled by inorganic agents, like Fe oxides in Ferralsols (Oxisols; Oades and Waters, 1991), soil structure may not display the hierarchical organisation commonly associated with biology. However, when compared to biotic processes, inorganic controls on SOC occlusion have received relatively little attention.

Thus, further investigation is still required into the indirect effects of inorganic components, such as Ca and $CaCO_3$, on SOC stabilisation through occlusion within aggregates, and its effects on overall SOC accumulation.

1.5.2 - Sorption

Soil organic carbon can also be stabilised within soil when it is adsorbed to reactive mineral surfaces or through other sorptive interactions with metal cations. Adsorption is defined as the adhesion and removal of atoms, ions, or molecules from a gas or liquid onto a solid surface (Sposito, 2016). Organic substrates can be adsorbed to a range of minerals. Sorptive capacity in soils is most commonly attributed to phyllosilicates (mineral clay particles), poorly crystalline minerals, Al-, Fe-, and Mn-oxides, or also to polyvalent cations, which can form bridges to mineral or other organic soil constituents. A positive relationship between the resistance of SOC to chemical oxidation and the presence of specific reactive mineral species was first described by Hosking (1932). Since then, the presence of reactive minerals or metals has been repeatedly shown to correlate with increased SOC stocks (Baldock and Skjemstad, 2000; Grand and Lavkulich, 2011; Sokoloff, 1938; Torn et al., 1997) as well as with the resistance of SOC to microbial degradation in incubation experiments (Minick et al., 2017; Rasmussen et al., 2006; Whittinghill and Hobbie, 2012). Soil organic C complexed by minerals generally exhibits older ^{14}C-derived ages than other SOC pools (Kleber et al., 2011; Rasmussen et al., 2005; Schrumpf et al., 2013; Spielvogel et al., 2008; Trumbore, 1993); thus, adsorption plays a clear role in the stabilisation of SOC over long time periods.

Sorption primarily stabilises SOC by reducing its availability for diffusive encounters with extra-cellular enzymes through the transfer of a substrate from the soil solution to a solid phase (Moni et al., 2010; Sollins et al., 1996).

Beyond the direct effect of sorption on the partitioning of SOC between the liquid and solid phases, substrates can also be stabilised by secondary mechanisms, including:

i) **steric hindrance** – a general mechanism involving the lack-of-fit between a substrate and a catalyst (an enzyme) caused by changes in tertiary structure, which is a common consequence of sorptive interactions in soil (Quiquampoix and Burns, 2007; Zimmerman and Ahn, 2010).
ii) **the inactivation of enzymes during sorption** – extra-cellular enzymes, responsible for much of SOM decomposition, can also be rendered inactive by adsorption onto mineral surfaces, due to structural modifications in their conformation at the adsorption interface (Quiquampoix and Burns, 2007).
iii) **the toxicity effects of certain metals** – it has been proposed that environmental cytotoxicity could result in the stabilisation of organics complexed by some metals such as Al (Tate and Theng, 1980). Al^{3+} is toxic and is thought to limit decomposer activity in acidic soil environments (Tonneijck et al., 2010), although evidence for this can be contradictory (Marschner and Kalbitz, 2003).

However, there is still some level of confusion regarding the chemistry involved in interactions between organic and inorganic constituents of soils. Therefore, it is necessary to briefly discuss the main bonding mechanisms between organic and inorganic soil components.

1.5.2.1 - Bonding mechanisms and the organo-mineral interface

Organic molecules can be adsorbed onto mineral or metal surfaces through a range of mechanisms in both inner and outer sphere complexes (Table 1.1). The prevalence of each bonding mechanism will vary with soil texture (proportion of fine to coarse particles), mineralogy, and cation content. Inner sphere complexes occur when a substance can closely approach a mineral's surface or metal ion, usually resulting in direct chemi-sorption (see Eq. 1.3 for an example). In outer sphere interactions, water molecules prevent the direct approach or sorption of a substance to a mineral's surface or metal ion; instead, the charges are countered through a diffuse charged zone (Oldham, 2008). In soil, inner- and outer-sphere interactions act in combination to stabilise SOC over medium- to long-time periods, so that it becomes difficult, if not impossible, to ascribe SOC stabilisation in a given horizon to specific modes of interaction. However, a basic understanding of the fundamental chemical mechanisms at play is useful to inform our interpretation of the role of Ca in SOC stabilisation and operationally-defined SOC pools.

Table 1.1. Mechanisms of interaction between soil organic carbon substrates and minerals or metal ions

Mechanism	Nature	Interaction	Description
Ligand exchange (Mikutta et al., 2014) Ligand exchange is the formation of new coordination complexes with metals	Covalent to ionic bond	Inner sphere	Strong bonding to a metal via the direct substitution of one outgoing ligand (for instance, a hydroxyl group) by an incoming one (for instance, an organic molecule with a hydroxyl, phenol, or carboxyl functional group)—see Eq. 1.3. There is no change in oxidation state at the metal centre and charge is conserved during the reaction
Chelation (Ahmed and Holmström, 2014) Chelation is the formation of polydentate coordination complexes with metals. Compared to monodentate complexes, they have a greater stability	Covalent to ionic bond	Inner sphere	A special case of ligand exchange, where the incoming ligand (usually an organic molecule) is polydentate and thus able to replace two or more of the simple outgoing ligands bound to the central metal.
Cation bridging (Iskrenova-Tchoukova et al., 2010) Cation bridging allows for the interaction of two negatively charged surfaces such as a phyllosilicate and an organic anion	Direct cation bridging; mostly ionic bond	Inner sphere	A bond formed when the hydration shell of a polyvalent cation is displaced. The organic anion becomes directly coordinated to the cation, as in ligand exchange
	Exchangeable (water) bridging Van der Waals forces (see below)	Outer sphere	Here water is not displaced and the cation interacts with the organic anion essentially through hydrogen bonding (see below). Both polyvalent and monovalent cations can participate in this type of interaction. It has sometimes been labelled 'water bridging', although this term remains ambiguous, as it has also been used to describe ligand exchange reactions. The term 'exchangeable bridging', which has been coined to describe the cation exchange phenomenon, may be more descriptive
Hydrophobic interactions (Spaccini et al., 2002) These occur whenever non-polar substances exist in a polar solvent, such as water	Entropy driven structure	Outer sphere	Aggregation of non-polar substances caused by the repulsion of hydrophobic molecule by water. Hydrophobic interactions also take place during the clustering of amphiphillic molecules into bilayers and micelles (hydrophilic exterior protecting a hydrophobic core)
Other 'weak' interactions (van der Waals) (Israelachvili, 2011) While weak, these forces are additive meaning that in complex substrates such as those commonly found in SOC, many van der Waals interactions can combine to create apparent strong sorption	Dipole–dipole force	Outer sphere	The electrostatic attraction between molecules with permanent polarity, arising from differences in the electronegativity of their atomic constituents
	Hydrogen bonding	Outer sphere	Hydrogen bonding refers to a specific type of dipole–dipole interaction, which occurs when a hydrogen atom bonded to a strongly electronegative atom (typically F, O, or N) interacts with another electronegative atom. These interactions are stronger than ordinary dipole–dipole forces

London dispersion (induced dipole) force	Outer sphere	Temporary and weak attractive force arising from the unequal movement of electrons within a molecule, turning it momentarily into a dipole. Unlike dipole–dipole interactions, the London dispersion force does not arise from a difference in the electronegativity of component atoms, but merely the correlated movements of electrons in interacting molecules

$$\| - \mathrm{M} - \mathrm{OH} + \mathrm{HO} - \mathrm{R} \rightarrow \| - \mathrm{M} - \mathrm{O} - \mathrm{R} + \mathrm{H_2O}$$

Eq. 1.3. Ligand exchange between a mineral (M) and a hydroxyl functional group on an organic substrate (R) that results in the direct and strong adsorption of soil organic carbon. Equation adapted from Huang and Schnitzer (1986).

It was previously believed that sorption of SOC through the aforementioned mechanisms occurred in a monolayer coverage on mineral surfaces. However, mineral surface loadings can be two to five times higher than would be expected during monolayer loading (Hedges and Keil, 1995). Observations of organo-mineral associations (OMA) have suggested that SOC is instead adsorbed onto distinct hotspots on reactive mineral surfaces (Mayer and Xing, 2001; Vogel et al., 2014). These SOC hotspots can be flocculated together as a result of polyvalent cation bridging or hydrophobic interactions (Table 1.1; Kaiser and Guggenberger, 2003; Kleber et al., 2007), creating a layered organo-mineral interface. Kleber et al. (2007) explored this layering in their conceptual model of the organo-mineral interface (Fig. 1.6), suggesting that the interface is organised into distinct zones of interaction, where SOC is bound with different mechanisms. These zones include a contact layer, associated with strong and direct interactions with the mineral surface, a zone of hydrophobic interactions, and a kinetic outer zone of weak interactions (Kleber et al., 2007). Polyvalent cations, like Ca^{2+}, could play an important role in the stabilisation of SOC within these different zones through cation bridging mechanisms highlighted above (Table 1.1; Fig. 1.6), but there has been very little investigation into the role of Ca^{2+} in OMA.

In theory, polyvalent cations, like Ca^{2+}, could stabilise mineral-associated SOC through cation bridging mechanisms at different zones of the organo-mineral interface, but the interactions between Ca^{2+} and SOC still requires further investigation.

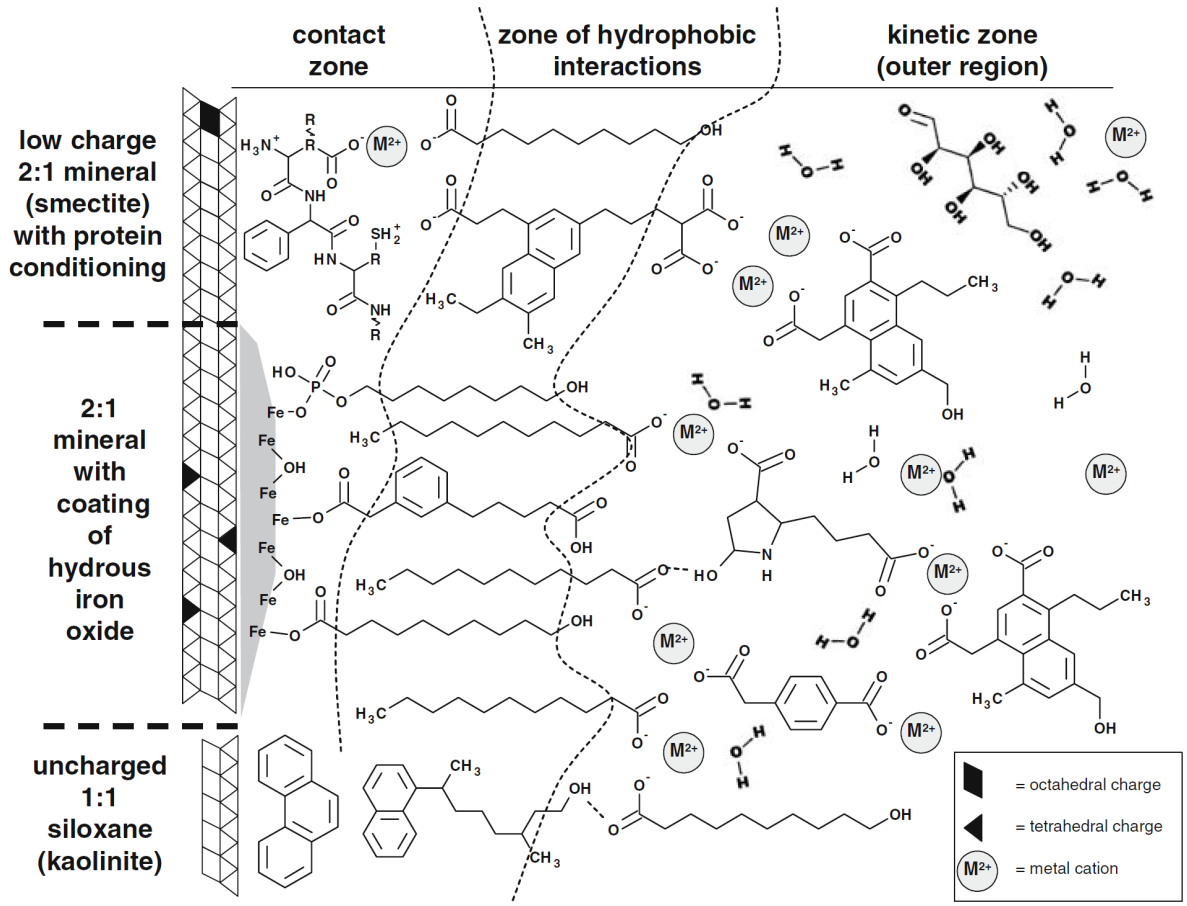

Fig. 1.6. A conceptual model of multi-layer organo-mineral association in soils, taken from Kleber et al. (2007). The model is split into three conceptual zones: the contact zone in direct association with a mineral or coating's surface, the zone of hydrophobic interactions protecting the contact zone through amphiphillic interactions, and the outer kinetic zone dominated by outer sphere cation bridging and other weak forms of organo-mineral association.

1.5.2.2 - Co-occurrence of stabilisation mechanisms

Novel techniques are enabling us to further investigate these hotspots of OMA and the mechanisms that stabilise SOC at their interfaces. Vogel et al. (2014) utilised a NanoSIMS to observe the adsorption of isotopically labelled SOC on a clay fraction during incubation. The authors found that this labelled SOC was preferentially associated with specific areas of nano-mineral clusters, such as micropores, etch pits, and cracks. As hypothesised by Kögel-Knabner et al. (2008), adsorption of SOC within these areas would provide a two-fold stabilisation of SOC. This is because, within these cracks, the physical accessibility of SOC to decomposers is reduced, while SOC is concomitantly stabilised by sorption (Chenu and Plante, 2006; Kögel-Knabner et al., 2008). Therefore, at the nanoaggregate scale, SOC could be simultaneously protected by both occlusion and adsorption (Fig. 1.7), in a stabilisation that becomes indistinguishable (Chenu and Plante, 2006; Kögel-Knabner et al., 2008; Vogel et al., 2014), questioning the conceptual segregation of the mechanisms enumerated by Sollins et al. (1996).

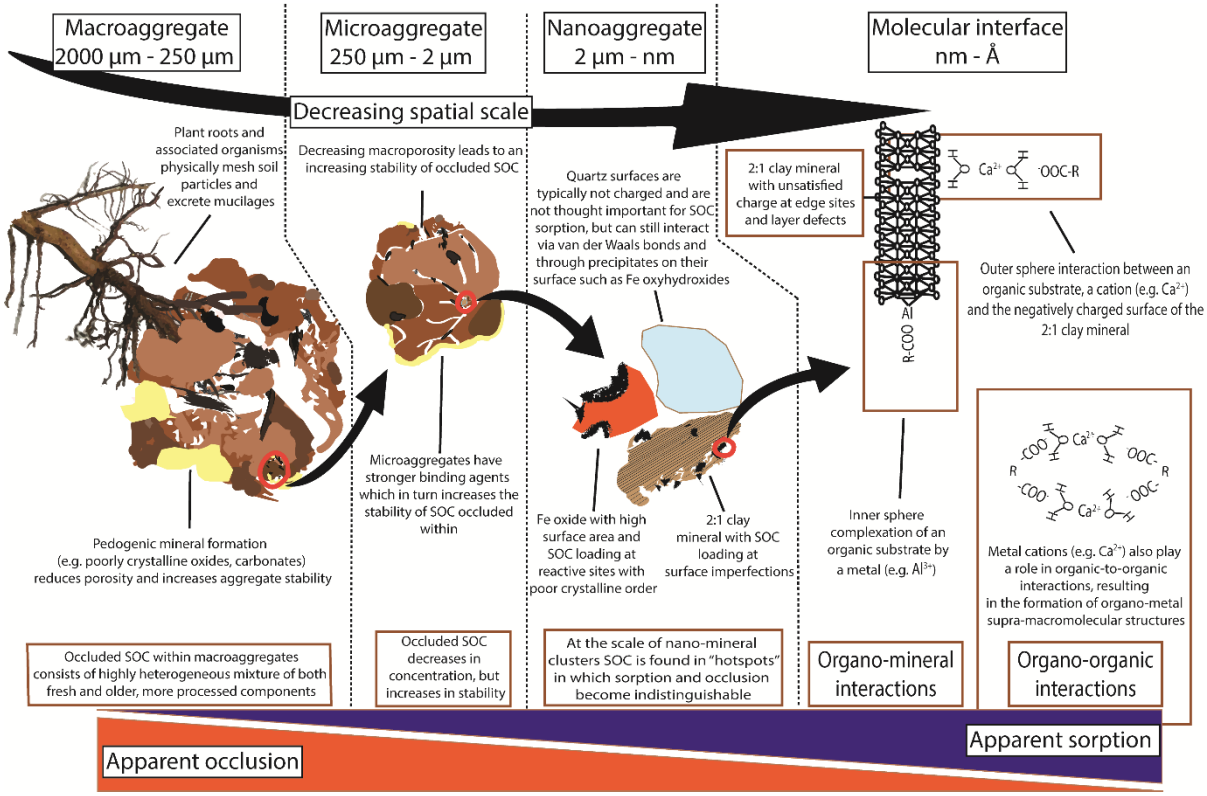

Fig. 1.7. Occlusion and sorption co-stabilise soil organic carbon at all spatial scales, but this co-occurrence becomes more apparent at the nano scale where they become operationally-indistinguishable, taken from Rowley et al. (2018).

However, at different spatial scales, the endmembers of these stabilisation mechanisms are more apparent, as large particulate organic matter stabilised through occlusion can be more easily distinguished from SOC adsorbed to clay minerals (Fig. 1.7). These endmembers, where the relative importance of a specific stabilisation mechanism is more apparent, can be fractionated into operationally-defined SOC pools (Viret and Grand, 2019). Techniques such as density fractionation and sonication can be used to separate SOC that is either free within the soil matrix, from SOC that is stabilised through occlusion within aggregates or mineral-association (Golchin et al., 1994; Kaiser and Berhe, 2014; Kaiser et al., 2012; Schmidt et al., 1999; Viret and Grand, 2019). These operationally-defined SOC pools have provided valuable insight into the mechanisms through which SOC is stabilised by Fe or Al (Golchin et al., 1994; Sollins et al., 2009; Sollins et al., 2006). Yet, there has been relatively few investigations that have fractionated Ca-rich soils, and we still do not know how Ca^{2+} influences these specific endmembers.

While a stabilisation by either occlusion or sorption can become indistinguishable at certain scales, SOC can be divided into operationally-defined SOC pools to investigate their endmembers. Yet, it remains to be seen if and how Ca could influence these operationally-defined pools of SOC.

1.5.2.3 - Preferential sorption

While selective preservation and the inherent biochemical composition of SOC seem to be relatively less important in mineral horizons, contradictorily, there is a growing consensus that sorption of organics by minerals can be preferential. This means that in the presence of certain minerals or cations, SOC of a certain composition may be more or less likely to be stabilised by sorptive interactions (Kaiser et al., 1997). Certain mineral forms in acidic soils seem to preferentially stabilise microbial matter (Spielvogel et al., 2008). Fe and Al forms are well documented to preferentially adsorb organics rich in aromatic moieties and carboxyl groups (Gu et al., 1994; Kaiser and Guggenberger, 2003; Kaiser et al., 1997). Yet, while this has been observed in acidic soils, there has been less investigation of preferential sorption in alkaline soils, rich in polyvalent cations, such as Ca; so, we still do not know whether or not Ca may preferentially influence the sorption or occlusion of specific organics in different parts of the organo-mineral interface.

Therefore, further research is still required to establish whether Ca-mediated OMA are preferential and what influence this may have on SOC in Ca-rich environments.

1.6 - The role of polyvalent cations in SOC stabilisation

As can be seen in the Table 1.1 and diagrams above (Figs 1.6 & 1.7), soil organic carbon can be stabilised through its interactions with polyvalent cations. Polyvalent cations can contribute to SOC stabilisation directly through sorption mechanisms (Table 1.1) and indirectly by flocculating soil particles and driving the formation of aggregates, and subsequent occlusion. Much of the research on flocculation thresholds has focused on acid soils dominated by Al chemistry (Boudot, 1992; Matus et al., 2006; Rasmussen et al., 2006). In these soils, it has been shown that extensive flocculation and precipitation can be expected at a C:Al ratio in the order of 10-30 or lower (Jansen et al., 2003; Scheel et al., 2007; Skjemstad et al., 1992).

Yet, the flocculation of dissolved organics by other cations, such as Ca, in natural soils has not been as extensively studied.

1.7 - The role of Ca

Of these polyvalent cations, Ca^{2+} has long been hypothesised to stabilise and positively influence the accumulation of SOC (Dokuchaev, 1883; Sokoloff, 1938). Calcareous soils have long been connected to higher SOC contents then their adjacent, non-calcareous counterparts (Oades, 1988). Yet, the stabilisation of SOC by polyvalent base cations such as Ca^{2+} have received arguably less attention since the earlier body of works by Oades (Grant et al., 1992; Muneer and Oades, 1989a; Muneer and Oades, 1989b; Muneer and Oades, 1989c; Oades and Waters, 1991; Oades, 1984; Oades, 1988; Oades, 1993; Tisdall and Oades, 1982), consequently presenting several clear knowledge gaps:

i) **Why do Ca-rich environments typically contain more SOC than their Ca-poor counterparts?**
ii) **Is this due to a stabilisation mediated by Ca?**
iii) **What are the mechanisms for this stabilisation?**
iv) **Can these mechanisms be utilised in the context of sustainable agricultural practices to promote SOC accumulation?**

1.8 - Problem statement

Soil organic carbon and its ecosystem services are of global importance (Minasny et al., 2017; UN General Assembly, 2015). There is growing consensus that geochemistry is an important predictor of SOC accumulation and its persistence in soils (Rasmussen et al., 2018). While it is well established that Fe and Al play a dominant role in the stabilisation of SOC in acidic soil environments through multiple mechanisms, our mechanistic understanding of the influence of Ca on SOC stabilisation is still weak. Ca-rich environments are often associated with significant quantities of SOC, yet we do not truly understand the mechanisms through which these environments accumulate SOC. Authors often speculate that polyvalent cation bridging and occlusion play an important role in Ca-rich environments, but more empirical data is needed to further investigate these mechanisms. Furthermore, a large proportion of research into Ca-rich soils has focused on semi-arid to arid soil environments or amended soils, thereby overlooking the role of Ca in humid and temperate soils.

> **To address the aforementioned knowledge gaps and problem statement, we must now further investigate the role of Ca in the stabilisation of SOC in humid and temperate soils.**

1.9 - Site setting - The Nant Valley

The *Vallon de Nant* (Nant Valley), Vaud, Switzerland is a humid and temperate, alpine catchment located at the frontier between the Vaud and Valais Alps (Fig. 1.8). The valley is orientated north-south and located on the Morcles Nappe, a near-recumbent anticline of Jurassic and Cretaceous shallow-water limestones, intercalated with marl and shale deposits (Austin et al., 2008). The valley was a research priority for the universities in Lausanne (*Université de Lausanne* / *École Polytechnique Fédérale de Lausanne*) and has had several teams working on the local vegetation (Dr. P. Vittoz), geomorphology (Prof. S. Lane), permafrost (Dr. Christophe Lambiel), hydrology (Prof. B. Schaefli) and river biogeochemistry (Prof. T. Battin). Previous soil science research in the valley has quantified soil respiration in the rangeland (*alpage*) and its relation to soil and vegetation type (Grand et al., 2016). There have also been several masters studies on the catchment, investigating: soil respiration (Rubin, 2013) and its environmental causes (Blattner, 2017), the classification and origin of surficial formations (Rion, 2016), their influence on soil development (Gigon, 2012), and the different reservoirs of Ca (Delasoie, 2018).

Ultimately, this site presents soils with a natural variation in Ca content, and is therefore the perfect setting for further investigating the influence of Ca on SOC stabilisation in a humid and temperate environment.

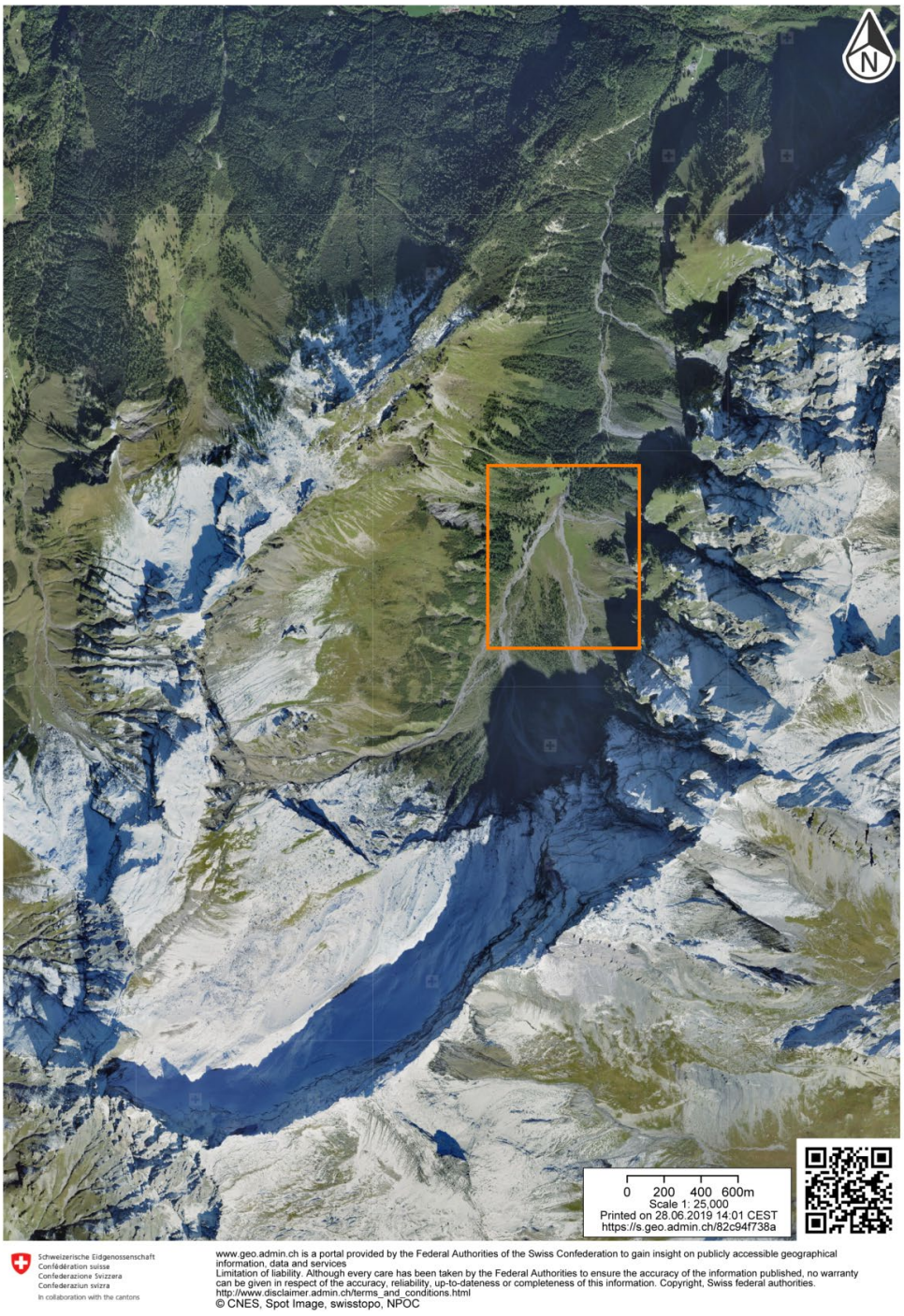

Fig. 1.8. Aerial photo of the Nant Valley (Switzerland) with the rangeland (*alpage*) marked with an orange square. This map was constructed using SwissTopo (2019). See section 8.2 for a range of different maps of the region.

- This page is intentionally left blank -

- Chapter 2: Research Outline -

2.1 - Aim

Investigate the role of Ca in the accumulation of SOC in humid and temperate soils.

2.2 - Objectives

To address this aim, this thesis will focus on four key objectives:

1. **Establish the mechanisms through which Ca can theoretically stabilise SOC.**

   Prior to investigating the role of Ca in the accumulation of SOC at the Nant Valley, we must first review existing literature to establish if and how Ca could mediate a stabilisation of SOC.

2. **Investigate the direct and indirect effects of $CaCO_3$ on soil development and biogeochemistry at the Nant Valley.**

   The objective will be to find an appropriate study site within the Nant Valley that can be used to investigate the role of Ca on soil processes. After identifying soils that have developed under similar soil forming conditions, with a natural variation in $CaCO_3$ (the main reservoir of Ca in the given geological settings). It will then evaluate how this presence or absence of $CaCO_3$ influences the pedogenesis and biogeochemistry of these soils, in an order to attempt to isolate the effects of variations in Ca on important soil processes at the Nant Valley.

3. **Evaluate the differences in SOC between the Nant Valley sites.**

   Once an appropriate study site with a natural variation in Ca is selected, we will then investigate how SOC differs between soils within this variation. We will fractionate bulk soil in an attempt to separate SOC pools related to different mechanisms of SOC stabilisation. For each fraction, we will measure the SOC content and mass in a given fraction, and characterise its degree of oxidative transformation. This will enable us to ascertain how these mechanisms differ between the sites with a natural variation in Ca at the Nant Valley.

4. **Discuss what can be inferred about the role of Ca in the accumulation of SOC**

   These previous research objectives will then be synthesised to infer how Ca may lead to SOC accumulation in cool-temperate environments. This objective will also compare our results to those within existing literature, focusing on the broader perspective of our findings and highlighting avenues for future investigation.

2.3 - Research questions

The following research questions will address the four objectives above. Each of these questions will be addressed in an individual chapter (Chapters 3 to 6). Each question is labelled with its specific Chapter Number (3 to 6) and will be redisplayed at the beginning of each chapter.

3. **Can Ca mediate a stabilisation of SOC?**
    a. What evidence exists for the stabilisation of SOC mediated by Ca?
    b. What are the mechanisms through which Ca can stabilise SOC?
    c. How could these mechanisms be measured at various spatial scales?
4. **What is the influence of small quantities of $CaCO_3$ on the pedogenesis and biogeochemistry of soils that have developed under similar soil forming conditions, in a humid and temperate environment (Nant Valley, Switzerland)?**
    a. How is the pedogenesis of soils, which have developed under otherwise similar soil forming conditions, influenced by the presence or absence of $CaCO_3$?
        i. What is the influence of $CaCO_3$ on pedogenic trajectories?
        ii. Does $CaCO_3$ create a state of pedogenic inertia?
    b. What are the fundamental differences in the biogeochemical properties caused by the presence or absence of $CaCO_3$?
        i. How does the presence or absence of $CaCO_3$ influence the amount of Ca and soil pH?
        ii. How does the presence or absence of $CaCO_3$ influence the amount of SOC?
5. **How does SOC differ at the sites with or without $CaCO_3$ at the Nant Valley?**
    a. How does bulk SOC content and stable C isotopic composition differ at sites that have formed under similar soil forming conditions with or without $CaCO_3$?
    b. Does occlusion play a larger relative role in accumulation of SOC in soils with $CaCO_3$, relative to those without?
    c. Is there more mineral-associated SOC in the soils with $CaCO_3$, relative to those without?
6. **Does Ca mediate an accumulation of SOC at the Nant Valley?**
    a. Could we isolate the role of Ca in the accumulation of SOC?
    b. What were the mechanisms through which Ca contributed to the accumulation of SOC?
    c. What are the broader applications of these findings and how do they compare to those of previous studies?

2.4 - Methodology and approach

2.4.1 - Establishing potential mechanisms for Ca-mediated SOC stabilisation

It was of the utmost importance to first establish the mechanisms through which Ca could mediate a stabilisation of SOC. This was achieved by thoroughly reviewing existing literature and evidence on the subject. Evidence of Ca-mediated SOC stabilisation is distributed amongst various domains, including soil science, biogeochemistry, microbiology, chemical modelling, and aqueous chemistry, to name but a few. Thus, this information needed to first be amalgamated within one single critical literature review that summarised the existing evidence to the best of our ability. This review aimed to identify the key knowledge gaps that remain within the field and the most appropriate methods, by which, to address them. This document highlighted the important steps that are required to further our understanding of Ca-mediated SOC stabilisation, namely:

i) **Isolate the role of Ca in the accumulation of SOC from other pedogenic variables.**
ii) **Investigate how SOC differs in otherwise highly similar, natural (unamended) sites with and without Ca.**
iii) **Isolate the role of Ca in different SOC stabilisation mechanisms, namely occlusion or organo-mineral association, and their effect on the accumulation of SOC.**

2.4.2 - Selecting an appropriate field site for the investigation of Ca-mediated accumulation of SOC

We used a field-based approach to investigate the role of Ca in the accumulation of SOC as there are very few studies that have attempted to quantify it in natural systems. To give context to future experimental studies, we must first investigate these interactions at the field scale. We attempted to isolate the role of Ca from other natural influences on SOC accumulation at the Nant Valley. SOC, like any variable in soils, is predominantly impacted by five main soil forming factors (Jenny, 1941) and as such, these factors needed to be accounted for when choosing potential study sites.

To isolate the role of Ca in SOC accumulation, the ideal study sites needed to present a natural variation in Ca, while also possessing a similar climate, topography, vegetation structure, time of development (since deglaciation), texture and silicate mineralogy. After a field campaign (2015), the Nant Valley alpage was identified as a potential study site as $CaCO_3$ was present (ascertained with HCl dropper bottle) on one side of the otherwise similar grassland and absent on the other. Furthermore, the site was practical because it is in close proximity to the University of Lausanne and was also a study priority for the Institute of Earth Surface Dynamics. This meant that there was many different research groups working in the catchment, providing potential interdisciplinary research collaborations and a larger perspective on our research. The Nant Valley alpage thus seemed to provide the perfect location to further investigate the role of Ca in accumulation of SOC, but we still needed to confirm the homogeneity of the sites, except for this source of $CaCO_3$ (Chapter 4).

2.4.3 - Investigating SOC in soils with a natural variation in Ca

The potential influence of Ca on different SOC stabilisation mechanisms was then investigated at the Nant Valley by physically fractionating soil samples into operationally-defined SOC pools. Fractionation of soils has been an important analytical tool to highlight the role of other important elements (Fe / Al) in different SOC stabilisation mechanisms and its accumulation (Golchin et al., 1994; Kaiser et al., 2002; Sollins et al., 2009; Sollins et al., 2006), but there has been less of this research in Ca-rich soils. Soils are typically fractionated by size and / or density (Viret and Grand, 2019). A recent study used size fractionation to great effect in Ca-rich Mediterranean soils, discussed further later on (Martí-Roura et al., 2019). Our approach differed because, rather than size fractionation, we fractionated our soils using density fractionation (DF) with a Na-polytungstate solution (SPT; 1.6 g cm^{-3}) and sequential sonication (Schmidt et al., 1999). The main benefit of this fractionation was that it enabled us to separate out different pools of the free particulate or occluded SOC from SOC adsorbed onto denser mineral surfaces. This thereby isolated the role of different stabilisation mechanisms in soils that had formed under similar conditions, but with a large variation in available Ca. Yet, the main difficulty to DF in Ca-rich soils is the potential precipitation of Ca-metatungstate (Rovira et al., 1998), which was ruled out during the investigation with X-ray photoelectron spectroscopy (XPS; discussed further below). While time consuming and resource heavy, the DF was carried out in triplicates to prevent random errors.

Recent studies have demonstrated that natural variations in stable C isotope compositions ($\delta^{13}C$ values) of organic carbon provide important insight into SOC accumulation of Ca-rich environments (Martí-Roura et al., 2019; Minick et al., 2017). $\delta^{13}C$ values of SOC increase when it is oxidatively transformed within a soil profile, due to the fractionation in ^{13}C during microbial activity (Boström et al., 2007), and are thus regularly used for the analysis of SOC cycling. Natural variations in $\delta^{13}C$ values of both bulk soil and density fractions were therefore analysed as an analogue for oxidative transformation within the profile. $CaCO_3$ was removed from samples using HCl fumigation, due to its higher $\delta^{13}C$ values. Furthermore, potential variations in the $\delta^{13}C$ values from below- and above-ground biomass were quantified to check that there was no variation in the $\delta^{13}C$ values of vegetation inputs between the sites. Shifts in the $\delta^{13}C$ values of SOC between our sites were then used to investigate the potential effects of an increased Ca availability on the oxidative transformation of SOC in different pools at the Nant Valley.

X-ray photoelectron spectroscopy (XPS) was also used to investigate a subset of the density fractions. XPS is an advanced surface characterisation tool that investigates the surface (< 10 nm) of samples by irradiating them with X-rays of a known energy and measuring the quantity and kinetic energy of photoelectrons that are ejected. The kinetic energy of these ejected photoelectrons is then used to calculate their binding energy (Eq. 2.1), which is indicative of the specific orbital they were ejected from (orbitals are denoted with a number and a letter after an element). The binding energy of photoelectrons, ejected from a specific orbital, can be shifted due to changes in the bonding environment of that element.

This means that we can use the XPS to qualitatively measure the surficial chemical composition of the samples, while also investigating the bonding environment of detected elements, such as Ca, W or C. The XPS accessorily enabled us to check that there had been no significant precipitation of Ca-metatungstate during the DF by evaluating surficial W contamination and by looking for Ca association in the detailed W_{4f} scans. The detailed C_{1s} spectra from the XPS analyses were also deconvoluted into sub peaks, indicative of different functional groups, to give an estimate of the oxidation state of surficial SOC in our density fractions. XPS analysis is thus complementary to the $\delta^{13}C$ values because it can be used to measure the surficial chemical composition of different samples, while concomitantly inferring differences in the speciation of SOC (Jones and Singh, 2014). Overall, all of these methods helped us to gain novel insights into the influence of Ca on SOC.

$$\text{Electron binding energy} = \text{incident photon energy} - \text{photoelectron kinetic energy}$$

Eq. 2.1. Calculating the binding energy of electrons emitted as photoelectrons from the surface of a sample irradiated by X-rays of a known energy.

2.4.4 - Choice of study design and statistical methods

As previously mentioned, initial testing revealed that there was $CaCO_3$ present on the eastern flank of the alpage (Fig. 1.8) and absent on the western flank. With the constraints of finding soils that had developed under near-identical conditions for soil formation with a natural variation in $CaCO_3$, we identified two specific sites from each side of the Nant River for further analysis. We then sampled three profiles (the descriptions of which can be found in section 8.3 in the appendices / Chapter 8) from each of these sites at the alpage. These profiles included three Phaeozems from a site with $CaCO_3$ ($CaCO_3$-bearing) and three Cambisols from a site without $CaCO_3$ ($CaCO_3$-free). The profiles were sampled at 6 / 7 different depth intervals to evaluate the evolution of SOC with depth. Samples from these profiles were transported to the University of Lausanne for further analysis. Various analyses were then completed on both the bulk soil and triplicates of density fractions.

We used linear mixed models to analyse the effects of this presence or absence of $CaCO_3$ at the alpage on different dependent variables, explored further in Chapters 4 and 5. Linear mixed models can account for the lack of independence in our measurements, caused by our sampling strategy (correlation between depth and profiles-within-sites) and triplicate measurements in the DF work. Details of the covariance structures, fixed and random effects will be explored individually in each chapter.

A brief summary of the methods used within Chapters 4 and 5 will be presented in each chapter. However, there will be an exhaustive description of the methods used within this thesis, presented in the appendices (section 8.4 in Chapter 8).

- Chapter 3: Ca-mediated stabilisation of soil organic carbon, a critical review -

The following paper is a reviewed pre-print of an open-access Biogeochemistry© publication. The introduction to the paper has been removed as some of the material was adapted and included in the general introduction. See Appendix 8.6.1 for the original copy.

- Research question Chapter 3 -

The following question and sub-questions will be addressed in this chapter:

Can Ca mediate a stabilisation of SOC?

a. What evidence exists for the stabilisation of SOC mediated by Ca?
b. What are the mechanisms through which Ca can stabilise SOC?
c. How could these mechanisms be measured at various spatial scales?

- Chapter 3 abstract -

Soils play an essential role in the global cycling of C and understanding the stabilisation mechanisms behind the preservation of SOC pools is of globally recognised significance. Until recently, research into SOC stabilisation has predominantly focused on acidic soil environments and the interactions between SOC and Al or Fe. The interactions between SOC and Ca have typically received less attention, with fewer studies conducted in alkaline soils. Although it has widely been established that exchangeable Ca (Ca_{Exch}) positively correlates with SOC content and its resistance to oxidation, the exact mechanisms behind this relationship remain largely unidentified. This synthesis paper critically assesses available evidence on the potential role of Ca in the stabilisation of SOC and identifies research topics that warrant further investigation. Contrary to the common view of the chemistry of base cations in soils, chemical modelling indicates that Ca^{2+} can readily exchange its hydration shell and create inner sphere complexes with organic functional groups. This review therefore argues that both inner- and outer-sphere bridging by Ca^{2+} can play an active role in the stabilisation of SOC. Calcium carbonate ($CaCO_3$) can influence occluded SOC stability through its role in the stabilisation of aggregates; however, it could also play an unaccounted role in the direct sorption and inclusion of SOC. Finally, this review highlights the importance of pH as a potential predictor of SOC stabilisation mechanisms mediated by Al- or Fe- to Ca, and their respective effects on SOC.

3.1 - Ca-mediated SOC stabilisation

3.1.1 - Ca-SOC interactions

Research into SOC stabilisation has typically focused on acidic soil environments and the effects of Al^{3+} or Fe^{3+} or their poorly crystalline forms on SOC (Grünewald et al., 2006; Kögel-Knabner et al., 2008). Basic soil environments, and potential interactions between the Ca and C cycles have received comparatively less attention (Grünewald et al., 2006). Yet, Ca is the most abundant alkaline earth metal in the Earth's crust, making up 2.94 % of the upper continental crust (Wedepohl, 1995). Furthermore, calcareous or Ca-rich soils cover more than 30 % of the Earth's surface (Bertrand et al., 2007; Chen and Barak, 1982) and basic soils account for at least 12 % of the world's soil resources (Grünewald et al., 2006). Ca^{2+} within a soil matrix typically originates from the weathering of lithosphere or surficial formations (Dijkstra et al., 2003; Likens et al., 1998), decomposition of Ca^{2+}-rich organic materials (Ranjbar and Jalali, 2012), the lateral movement of Ca^{2+}-rich water (Clarholm and Skyllberg, 2013), atmospheric dust deposition (Dijkstra et al., 2003; Pulido-Villena et al., 2006) or anthropogenic inputs. Ca^{2+} is weathered with relative ease from both primary and secondary minerals (Likens et al., 1998) and has therefore typically been thought to persist or accumulate chiefly in semi-arid to arid environments. However, Ca-rich environments also exist within temperate regions on soils developed from calcareous parent material, out-of-equilibrium with climate (Slessarev et al., 2016). High Ca contents are also commonly found in the topsoil of acid soils derived from crystalline lithologies due to biological cycling (Cailleau et al., 2004; Federer and Hornbeck, 1985; Grand and Lavkulich, 2013; Likens et al., 1998; Ross et al., 1991). Therefore, Ca^{2+} is an environmentally ubiquitous cation that could potentially play an unaccounted role in the stabilisation of SOC.

The first investigation into the interactions between Ca and SOC was published almost 80 years ago by Sokoloff (1938), who provided experimental evidence that organic matter solubility decreased upon addition of Ca when compared to Na addition. Since then, research in Ca-rich field environments has highlighted a positive correlation between exchangeable Ca^{2+} (Ca_{Exch}) and SOC (Fig. 3.1; Bertrand et al., 2007; Bruckert et al., 1986; Clough and Skjemstad, 2000; Duchaufour, 1982; Gaiffe et al., 1984; Oades, 1988; Paul et al., 2003; Shang and Tiessen, 2003). As an example, Yang et al. (2016) recently established that alpine grassland soils in the Neotropics contained nearly twice as much SOC (405.3 ± 41.7 t ha^{-1}) when developed on Ca-rich calcareous lithology than their acidic counterparts (226.0 ± 5.6 t ha^{-1}). Similarly, O'Brien et al. (2015) and Li et al. (2017) demonstrated that Ca_{Exch} was the strongest explanatory variable for SOC contents of grasslands. However, identification of the exact mechanisms responsible for this widespread correlation remain elusive.

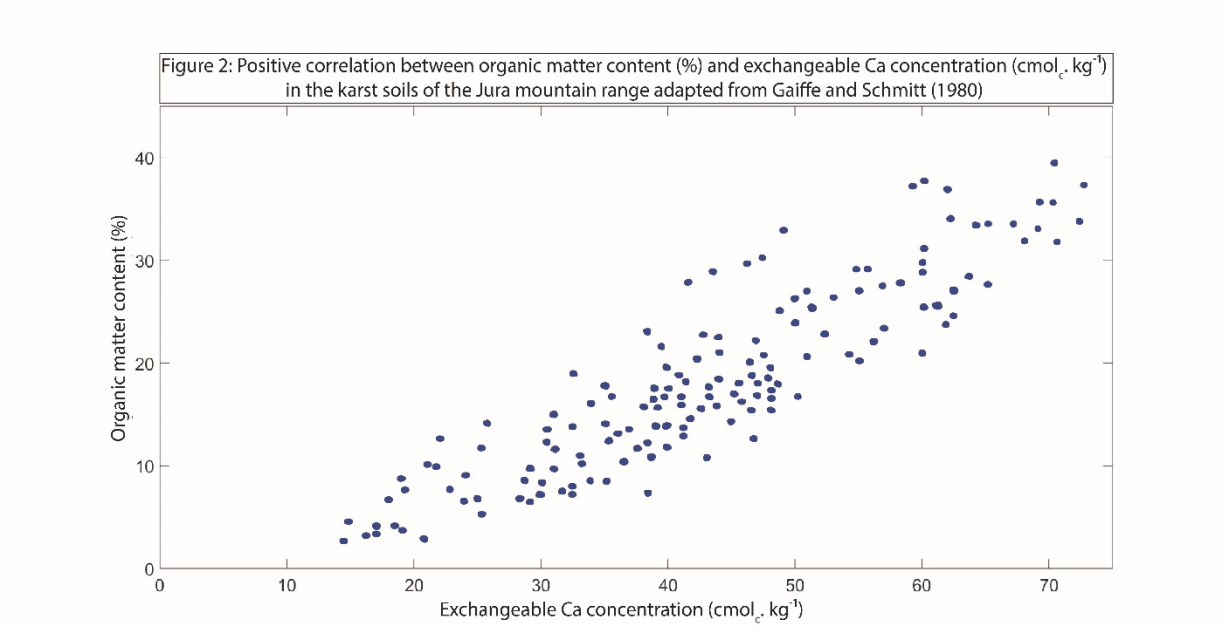

Fig. 3.1. Positive relationship between exchangeable calcium (centimoles of charge per kilogram) and soil organic carbon content (percent) in the Jura Mountains, adapted from Gaiffe and Schmitt (1980).

3.1.2 - A simple case of co-occurrence?

The positive correlation between Ca_{Exch} and SOC could be explained by their simple co-occurrence, as an increase in SOC generally increases the cation exchange capacity (CEC) of a soil (Yuan et al., 1967). Calcium is also a plant macronutrient and there is evidence that Ca also has a localised positive effect on net primary productivity (NPP) and SOM inputs through above-ground and below-ground biomass (Briedis et al., 2012b; Carmeis Filho et al., 2017; Paradelo et al., 2015). This localised effect on NPP has been shown to positively influence the accumulation of SOC in limed Ferralsols (Oxisols; Briedis et al., 2012b; Carmeis Filho et al., 2017) and could explain a portion of the differences in SOC content observed between acidic and calcareous soils. However, these explanations fail to account for the decrease in respiration rate (per unit C) associated with Ca prevalence, observed in multiple field studies (Groffman et al., 2006; Hobbie et al., 2002) or incubation experiments (Minick et al., 2017; Whittinghill and Hobbie, 2012). These results are, at first glance, counter-intuitive since the addition of Ca^{2+} to an edaphic ecosystem is also linked to a change in decomposer communities composition from fungi- to bacterial dominance (Blagodatskaya and Anderson, 1999; Rousk et al., 2010; Rousk et al., 2009) and an improvement in conditions for bacterial decomposition (Illmer and Schinner, 1991; Ivarson, 1977; Zelles et al., 1987), at least partially due to the buffering of soil pH to circumneutral levels (Narendrula-Kotha and Nkongolo, 2017). It would thus be expected that the rate of enzymatic decomposition of SOC would increase when Ca^{2+} saturates the exchange complex (Andersson et al., 1999; Chan and Heenan, 1999; Thirukkumaran and Morrison, 1996). This could be the case in the organic (litter) layer (Minick et al., 2017), but is generally not observed in the mineral soil. Contrary to hypotheses formulated in both studies, Hobbie et al. (2002) and Groffman et al. (2006) found that microbial respiration was actually

lower in Ca-rich environments, even though physicochemical conditions for microbial activity were improved. Furthermore, lab experiments have shown that Ca_{Exch} is correlated with a reduction in SOC leaching losses (Minick et al., 2017), photo-oxidation (7%; Clough and Skjemstad, 2000) and respiration (as CO_2) during incubation (Minick et al., 2017; Whittinghill and Hobbie, 2012). Therefore, Ca_{Exch} seems to be linked to a reduction in the propensity of C substrates for decomposition that is not solely linked to its effects on NPP or microbial ecology.

Consequently, this review will investigate the potential mechanisms behind the stabilisation and accumulation of SOC mediated by Ca and its mineral forms, namely their influence on:

i) **Aggregation and the occlusion of SOC.**
ii) **Inclusion of SOC within pedogenic- or biogenic-$CaCO_3$.**
iii) **Organo-mineral and organo-cation interactions.**

3.2 - Mechanisms for Ca-mediated SOC stabilisation

3.2.1 - Occlusion - Ca and aggregation

3.2.1.1 - The Ca ion and aggregates

It is widely accepted that Ca^{2+} has a significant positive effect on aggregation and soil structural stability and therefore, indirectly influences the accumulation and occlusion of SOC. Early authors demonstrated an influence of Ca^{2+} on soil aggregation (Martin et al., 1955; Peterson, 1947). This dependence was further investigated by Gaiffe et al. (1984) who demonstrated that the removal of Ca_{Exch} and its replacement by K_{Exch} led to a disruption of aggregates. As theorised by Edwards and Bremner (1967), one of the main mechanisms thought to be behind this stabilisation is the flocculation of negatively charged separates by outer sphere interactions involving Ca^{2+}, which is explored further in the following section on sorption processes. This process operates in the bulk soil and it has also been hypothesised that Ca^{2+} could play a role in flocculating particles in the gut of certain earthworm species, leading to the formation of 'Ca-humates' (Satchell, 1967). This was supported by the results of Shipitalo and Protz (1989) who utilised micromorphology and chemical pre-treatments to infer that Ca probably played a role in flocculating particles within earthworm casts of certain species, stabilising the microaggregates within them.

Another mechanism for the stabilisation of aggregates in Ca-rich environments involves the formation of complexes between Ca and high-molecular weight organic compounds such as root mucilages or microbial polysaccharides / polymeric substances. It has been shown that these substances readily complex Ca^{2+} and create gel-like structures that bind aggregates (Czarnes et al., 2000; de Kerchove and Elimelech, 2007; Erktan et al., 2017; Gessa and Deiana, 1992). In particular, galacturonic acid, a common root mucilage, displays a high affinity towards Ca, which links polymer chains to form an

adhesive matrix (de Kerchove and Elimelech, 2007). Czarnes et al. (2000) also showed that these polygalacturonic acid gels increase the hydrophobicity of aggregates, thereby increasing their stability during wetting and drying cycles. Further investigation is still needed to analyse the role that adhesive Ca-mucilage matrices play in aggregate stabilisation and the occlusion of SOC.

3.2.1.2 - The effects of carbonate on aggregates

Interactions between Ca-bearing primary and secondary minerals and soil structure have been extensively covered in the literature because of the use of liming ($CaCO_3$ addition) in agriculture. There have been many experiments that have documented the positive effects of the addition of calcite / aragonite ($CaCO_3$) or gypsum ($CaSO_4$) on the structure of non-calcareous soils (Armstrong and Tanton, 1992; Baldock et al., 1994; Briedis et al., 2012a; Grant et al., 1992; Grünewald et al., 2006; Inagaki et al., 2017; Kaiser et al., 2014; Melvin et al., 2013; Muneer and Oades, 1989a; Paradelo et al., 2016). Some authors have also assessed the effects of $CaCO_3$ removal from calcareous soils on aggregate stability, finding that the treatment reduced soil structural stability and increased porosity (Falsone et al., 2010; Muneer and Oades, 1989c; Toutain, 1974; Virto et al., 2011). Furthermore and reminiscent of the work of Oades and Waters (1991) on Fe oxides in Ferralsols (Oxisols), Fernández-Ugalde et al. (2011) demonstrated that the hierarchical model of aggregation was partially disrupted by carbonate. In the semi-arid Mediterranean soils of their study, the authors showed that the abundance of $CaCO_3$ controlled macroaggregate turnover and increased their stability, to the extent that the usual disruption of macroaggregates, leading to the release of constituent microaggregates, was prevented (Fernández-Ugalde et al., 2011; Oades, 1984).

There are several mechanisms through which $CaCO_3$ could positively affect aggregate stability and the occlusion of SOC. $CaCO_3$ is easily weathered and acts as an abundant source of Ca^{2+}, thus encouraging the flocculation of soil separates and aggregation through the mechanisms listed above (Baldock and Skjemstad, 2000; Clough and Skjemstad, 2000; Wuddivira and Camps-Roach, 2007). Carbonate ions are also capable of reprecipitation with Ca^{2+} under the right environmental conditions, forming secondary $CaCO_3$ crystals (from micrite to sparite) that cement aggregates (Fernández-Ugalde et al., 2014; Fernández-Ugalde et al., 2011; Shang and Tiessen, 2003; Virto et al., 2013). This mechanism was analysed in detail by Falsone et al. (2010), who utilised N_2 adsorption and Hg porosimetry to demonstrate that this formation of secondary $CaCO_3$ crystals decreased aggregate porosity in the 2–50 nm range and thus, decreased the accessibility of intra-microaggregate SOC to decomposers. Certain earthworm species have also been shown to cement particles that pass through their gut with a mixture of poorly crystalline biogenic carbonates (calcite, vaterite, and aragonite) excreted from their calciferous glands (Brinza et al., 2014; Edwards and Bohlen, 1995). The cementing effect of $CaCO_3$ on aggregates is well-documented in arid soils in which large quantities of pedogenic carbonates are found (Fernández-Ugalde et al., 2014; Fernández-Ugalde et al., 2011; Virto et al., 2013). However, it may also play a role

in sub-humid environments where carbonate-rich parent materials are continually getting dissolved and occasionally reprecipitated locally, but this still needs to be investigated further.

Although it is widely accepted that the occurrence of $CaCO_3$ positively affects soil structure and offers favourable conditions for the stabilisation of SOC by occlusion, its actual consequence on occluded SOC stocks is less clear. In their recent review, Paradelo et al. (2015) concluded that, while $CaCO_3$ addition had a clear positive effect on soil structure, its effect on occluded SOC stocks was uncertain. Positive (Egan et al., 2018b; Muneer and Oades, 1989a; Muneer and Oades, 1989b), non-existent (Paradelo et al., 2016), or negative effects (Chan and Heenan, 1999) of $CaCO_3$-amendment on occluded SOC have indeed been reported. In some instances, it may be difficult to disentangle the integrative effects of agricultural management from the simple effects of $CaCO_3$ additions. In natural, unamended soils, Fernández-Ugalde et al. (2014) showed that $CaCO_3$ had a positive effect on occluded SOC stocks. This finding needs to be replicated in a range of natural soils, as differences in initial conditions (e.g. texture, mineralogy, organic inputs and their distribution) could reasonably result in different outcomes.

3.2.2 - Inclusion

Inclusion is defined as the envelopment of SOC within a mineral or co-genetic mineral assemblage that leads to its physical protection (Babel, 1975). Stabilisation of SOC by inclusion works through a similar mechanism to intercalation or occlusion, by physically separating a substrate from decomposers. SOC may be trapped within any form of pedogenic carbonates, but its inclusion may not be quantitatively important when carbonate formation chiefly occurs through abiotic processes. Diaz et al. (2016) recently dated small amounts of SOC (0.1-0.5 %) included within pedogenic carbonate nodules in Cameroon with ^{14}C measurement, recording ages ranging between 8-13 kyr. This highlights the potential of this mechanism to stabilise SOC over long time periods, but probably only in small quantities.

Calcium carbonate is one of the most abundant biominerals on Earth and can be synthesised by a wide range of terrestrial organisms (Skinner and Jahren, 2007). Biomineralisation of $CaCO_3$ can either be induced within cells, mediated by biological activity that stimulates physicochemical precipitation, or initiated by the presence of an existing biological matrix that initiates crystal nucleation and growth in the extra-cellular environment (Bindschedler et al., 2016). During each of these forms of biomineralisation, SOC can become included and encapsulated within the crystal structure (Verrecchia et al., 1995). A few specific examples of biogenic carbonate forms include calcified root cells, fungal filaments and rhizoliths (calcified roots; e.g. Becze-Deàk et al., 1997; Jaillard et al., 1991; Monger et al., 1991), calcified earthworm biospheriods (Barta, 2011), and the mineralisation of bacterial or fungal organic templates (Bindschedler et al., 2014; Cailleau et al., 2009; Dincher et al., 2019). Another mechanism for the inclusion of SOC could be biomineralisation pathways such as the oxalate-carbonate pathway (Verrecchia, 1990). The oxalate-carbonate pathway involves biomineralisation of $CaCO_3$ during the bacterial catabolism of calcium oxalate-rich SOC produced by plants or fungi. It thus

intimately links SOC to the nucleation site of $CaCO_3$ biomineralisation and could allow its inclusion within the crystal matrix in both acidic (Cailleau et al., 2005; Cailleau et al., 2004; Verrecchia et al., 2006) and calcareous soils (Rowley et al., 2017). However, there has been very little direct quantification of the amounts or ^{14}C ages of SOC included within biogenic carbonate forms, which could potentially contain much higher SOC contents than abiotically-formed, pedogenic $CaCO_3$. Therefore, further investigation is now needed to quantify the inclusion of SOC within biogenic carbonate and its role in SOC cycling.

3.2.3 - Sorption - Ca, minerals and organics

3.2.3.1 - Organo-mineral associations with $CaCO_3$

Lithogenic and pedogenic $CaCO_3$ could also play a key role in the stabilisation of SOC via adsorption. Most of the research into direct organo-calcite interactions has focused on the interactions between dissolved organic carbon (DOC) and calcite in sorption experiments. Earlier work by Suess (1970) and W. Carter (1978) showed that DOC could be directly adsorbed onto $CaCO_3$, while Suzuki (2002) more recently showed that $CaCO_3$ was an effective adsorbant of DOC from black tea solutions, possibly due to its high point of zero charge (9.5; Grünewald et al., 2006). Thomas et al. (1993b) more specifically studied the affinity of different synthetic carbonates for common organic functional groups and demonstrated that calcite, dolomite, and magnesite all sorbed a wide range of organic compounds, which included carboxylic acids, alcohols, sulphates, sulfonates, amines, amino acids and carboxylated polymers. Interestingly, interaction with DOC has been shown to modify carbonate precipitation equilibria, by inhibiting either further crystal precipitation (Inskeep and Bloom, 1986; Reddy et al., 1990; Reynolds, 1978) or the dissolution of sorbent minerals (Thomas et al., 1993a). Jin and Zimmerman (2010) established that $CaCO_3$ obtained from aquifers preferentially adsorbed dissolved organic matter with a high molecular weight, which the authors attributed to a form of outer sphere interaction. It has been theorised that the kinetics of DOC adsorption by carbonates may be biphasic, occurring through an initial rapid phase of outer sphere interactions, which is then followed by a slower phase of inner sphere and hydrophobic interactions that in turn protect the carbonate surface from dissolution (Jin and Zimmerman, 2010; Lee et al., 2005; Thomas et al., 1993b). While these DOC adsorption experiments have provided interesting insight into potential $CaCO_3$-SOC interactions, there has been relatively little direct research on the adsorption of SOC by different forms of calcite / aragonite in soils. Measurements of soil carbonate content commonly differentiate between a reactive and a total pool (Pansu and Gautheyrou, 2006), but there is little evidence for the role of these operationally-defined pools in adsorption of SOC. Further research should focus on the effects of the supposedly reactive, poorly crystalline or amorphous $CaCO_3$ pool on the adsorption of SOC in natural environments.

3.2.3.2 - Outer sphere processes

Irrespective of their carbonate content, many soils have significant quantities of free Ca^{2+}, which may also contribute to the stabilisation of SOC. The widely observed correlation between Ca_{Exch} and SOC has led to the implicit assumption that Ca^{2+} predominantly affects SOC through weak outer sphere interactions (von Lützow et al., 2006), such as those contributing to the retention of exchangeable cations (Table 3.1). This form of cation bridging by Ca^{2+} has been highlighted as an important component of SOC stabilisation by many authors and is well-documented (Clough and Skjemstad, 2000; Edwards and Bremner, 1967; Oades, 1988). As illustrated in the lyotropic series, cations' outer sphere (exchangeable) behaviour is related to the size of their hydration shell and valence. This is confirmed by chemical modelling, which indicates that exchangeable bridges by Ca^{2+} typically have a larger residence time than those of monovalent cations, like Na^{+}, because the charge-to-hydration radius ratio of Na^{+} prevents it from efficiently countering the repulsion between negatively-charged surfaces (Iskrenova-Tchoukova et al., 2010; Sutton et al., 2005). Thus, Ca^{2+} is a fundamental flocculating agent of natural systems because of its ability to form efficient outer sphere bridge units.

However, it is interesting to note that Al^{3+} and H^{+} rate higher than Ca^{2+} on the lyotropic series and should thus cause similar or higher levels of apparent flocculation in soils in which they are abundant, such as most acid soils. Yet, it is widely observed that colloidal mobility is enhanced in acidic environments where Al^{3+} and H^{+} dominate and there is little or no Ca^{2+} present, such as those associated with the formation of Luvisols (Lavkulich and Arocena, 2011). It is also worth considering that the innate reversibility of outer sphere interactions should mean that exchangeable Ca bridges would not be inherently persistent in natural soils. These considerations lead us to explore the possibility that interactions between Ca and SOC are not solely attributable to outer sphere (exchangeable) processes and that, despite its correlative association with SOC, Ca_{Exch} may not be solely responsible for the bulk of SOC stabilisation in Ca-rich soils.

3.2.3.3 - Inner sphere processes

It is generally observed that each cation has a different range of interactions in soils. For instance, trivalent Fe is seldom found in large amounts as a free ion in soil, as it very readily hydrolyses to form insoluble precipitates under most environmentally-relevant conditions. Al^{3+} also hydrolyses into insoluble hydroxides at slightly acidic to basic pH, while in acidic soils, it is found to participate both in outer sphere, cation exchange and inner sphere, ligand exchange reactions. Ca^{2+} is thought to retain its hydration shell and behave strictly like an exchangeable cation, as are other 'base' cations such as Mg^{2+}, K^{+} and Na^{+} (Essington, 2015). However, in soil science, the fundamental controls on the propensity of each cation to form inner sphere complexes with SOM are not as well understood as the affinity of cations for non-specific exchange sites.

One of the reasons for this is that there are many factors that can influence inner sphere complexation of SOM by ions in the soil matrix, including characteristics of cations (ionic potential, electronegativity, polarisability of their electron cloud, hydrated radii, propensity to retain their hydration shell), of ligands (amount and type of organic functional groups), and of the environment (pH, ionic strength, solution composition, metal-to-ligand ratio, pressure and temperature conditions; Essington, 2015). Cations can be broadly split into three classes (Class A, B, and intermediate / C) based upon the polarisability of their electron cloud, which in turn, indicates how likely they are to form inner sphere complexes with specific ligands (Ahrland et al., 1958; Pearson, 1963; Schwarzenbach, 1961). Class A cations are weakly polarisable and tend to form complexes with O-containing ligands, such as carboxylate functional groups through ionic bonding. On the other hand, Class B cations have a labile electron cloud and tend to form complexes with N- or S-bearing ligands through more covalent bonding (Langmuir, 1997; Sposito, 2016). Al^{3+} and the base cations, including Ca^{2+}, are considered group A cations, indicating that they may theoretically form inner sphere complexes with widely-occurring O-bearing ligands such as carboxylate groups (Sposito, 2016). However, each cation's actual behaviour in soil cannot be predicted from one or a couple of first-principles only, as it results from the interaction of several factors. For instance, Na is not generally seen to engage in inner sphere complexation in soils, while K only does so in the interlayer of specific phyllosilicates. Advanced chemical modelling can offer insight into these issues.

Authors have modelled the interactions between DOC and Ca^{2+} in an attempt to investigate their molecular scale interactions (Aristilde and Sposito, 2008; Benedetti et al., 1995). These models suggest that Ca^{2+} can bind to SOC through both inner sphere and outer sphere processes (Bogatko et al., 2013; Iskrenova-Tchoukova et al., 2010; Kalinichev and Kirkpatrick, 2007; Sutton et al., 2005). Sutton et al. (2005) modelled the complexation of deprotonated carboxyl groups by Ca^{2+} and found that their interactions were predominantly inner sphere (75 %). The model of Kalinichev and Kirkpatrick (2007) also confirmed that Ca^{2+} could form direct cation bridges with carboxylate and to a lesser extent, phenolic and other –OH functional groups, unlike Mg^{2+}, whose hydration water is more tightly held (Dontsova and Norton, 2002; Kalinichev and Kirkpatrick, 2007; Tipping, 2005). Chemical modelling thus indicates that Ca^{2+} can interact with SOC through inner- and outer-sphere processes, thereby potentially increasing SOC stability against decomposition or leaching (Minick et al., 2017).

3.2.3.4 - Building empirical evidence for Ca-SOC interactions

While models predict that Ca^{2+} can form both inner- and outer-sphere bridges with SOC, empirical evidence of these associations in natural environments remains scarce. Density fractionation, which separates free particulate, occluded and mineral-associated SOC (Golchin et al., 1994) has the potential to offer insight. When performed sequentially (Sollins et al., 2009), density fractionation can separate SOC fractions associated with different minerals; furthermore, because the method uses extremely concentrated salt solutions (usually SPT), outer sphere associations are not expected to survive the

treatment, meaning that only strong (inner sphere) association with minerals are considered. Wen et al. (2017) recently showed that there was more SOC associated with calcite-rich than with dolomite-rich heavy fractions, possibly corroborating modelling predictions of stronger SOC association with Ca than Mg (Kalinichev and Kirkpatrick, 2007). The occluded fraction was however not separated from the mineral-associated fraction, so that the results remain somewhat equivocal. Further density fractionation studies analysing the relative role of occlusion and sorption for SOC accumulation in Ca-rich soils would undoubtedly prove informative. Density fractionation is however a costly and time-consuming technique (Poeplau et al., 2018) and may be difficult to use in calcareous soils, since polytungstate left in contact with free Ca for extended periods can precipitate as insoluble Ca-metatungstate. Methods applicable to the bulk soil would constitute useful complements to fractionation approaches.

Selective extractions on bulk soil have typically been used to analyse the effects of cation pools on SOC stocks. As indicated in Fig. 3.1, the operationally-defined Ca_{Exch} pool, extracted by salt solutions, represents a reactive and abundant pool of Ca^{2+} that is regularly correlated with SOC (Bruckert et al., 1986; Gaiffe and Schmitt, 1980; Li et al., 2017; O'Brien et al., 2015), thus highlighting its potential as an indicator variable for the measurement of Ca^{2+} interacting with SOC. However, by definition, Ca_{Exch} only represents Ca^{2+} engaged in outer sphere interactions. The selective chemical extraction of the inner sphere Ca pool, corresponding to pyrophosphate extractions for Al and Fe in acidic soil environments (Bascomb, 1968; Parfitt and Childs, 1988a; Rasmussen et al., 2006), is challenging due to the insolubility of most chelating agents once complexed by Ca (e.g., Ca-pyrophosphate or Ca-oxalate). In a recent study, van der Heijden et al. (2017) isolated a "non-crystalline pool of Ca" in acidic, base-poor soils, which may have included a significant contribution of Ca complexed by SOM, but the extract (dilute oxalic + nitric acid) was not specific to organic complexes. Extraction with other chelating agents that remain soluble in their Ca form (e.g. ethylenediaminetetraacetic acid, EDTA; Bélanger et al., 2008) or with salts of strong cation complexants (e.g. copper chloride; Barra et al., 2001; Juo and Kamprath, 1979) may also be informative.

Alternatively, X-ray absorption spectroscopy (XAS) could eventually be used to investigate the coordination environment of Ca^{2+}-SOC complexes under different environmental conditions. As an example, Martin-Diaconescu et al. (2015) have successfully probed the coordination environment of synthetic Ca complexes. While powerful, these direct spectroscopic techniques require the use of synchrotron light source and can only be applied to small amounts of samples with limited compositional complexity. We are still lacking a method that allows for the routine assessment of inner sphere Ca-SOM complexes and their relative importance in different soils, which constitutes a significant research gap given the potential for inner sphere interactions to stabilise SOM with increased efficiency (Mikutta et al., 2007), and perhaps through ecosystem disturbance events (Basile-Doelsch et al., 2009; Grand and Lavkulich, 2012).

3.3 - Implications for conceptual models of SOC cycling

Despite the growing body of evidence supporting a major role for specific soil minerals and cations in SOC stabilisation (Doetterl et al., 2015), soil mineralogy and geochemistry are largely absent from leading models of SOC cycling. The following section will discuss a few processes that have the potential to improve representations of SOC stabilisation, with particular emphasis on Ca-rich soils.

3.3.1 - Digressing from the expected profile scale depth distributions

In addition to their influence on the total amount of SOC retained in soil, polyvalent cations are suspected to influence its vertical distribution in soil profiles. Current pedometric approaches to mapping soil C acknowledge the importance of accounting for soil type when estimating the vertical distribution of SOC (Kempen et al., 2011; Wiese et al., 2016). Polyvalent cations can indeed cause departures from the generally assumed exponential decline of SOC content with depth (Hilinski, 2001). A conventional example involves Podzols characterised by the effective translocation of Al-SOC complexes to deep soil horizons (Ferro-Vázquez et al., 2014; Grand and Lavkulich, 2011). Contrastingly, Calcisols have an accumulation of Ca-saturated SOC in surface horizons (Yang et al., 2016). This accumulation of Ca-saturated SOC is likely caused by the complexation, flocculation, and precipitation of organic acids and clays in the presence of Ca, precluding their translocation to subsoil horizons. Two of the most common low molecular weight organic acids (oxalic and citric acids) in soil notably form sparingly soluble salts in the presence of Ca (Ca oxalate $K_{sp} \approx 10^{-8.5}$; Certini et al. 2000), preventing their translocation, whereas their Al and Fe counterparts are highly soluble (Gadd, 1999). The fundamental differences in how polyvalent cations modulate SOC inputs, stability and depth distributions highlight the critical importance of accounting for geochemical factors when modelling SOC.

3.3.2 - Preferential sorption in Ca^{2+} based systems

Integrating a geochemical dimension into conceptual models of SOM cycling is also important because the formation of organo-mineral complexes appears to be a preferential process, with selectivity exhibited by both the organic and mineral component (Spielvogel et al., 2008). Very little is actually known about the preferential nature of OMA in soils. To date, there is some evidence within the literature that specific organic compounds such as N-rich microbial metabolites, microbial cell-wall fragments, and possibly pyrogenic C may be selectively adsorbed by soil minerals (Brodowski et al., 2007; Jin and Zimmerman, 2010; Miltner et al., 2012; Scheel et al., 2008; Schurig et al., 2013; Spielvogel et al., 2008). Furthermore, it has been suggested that some reactive mineral surfaces, such as those of Al and Fe phases, may be disproportionally involved in the sorption of specific classes of organics, such as proteins, lignin, and phenolic compounds (Heckman et al., 2013; Kögel-Knabner et al., 2008; Xiao et al., 2015). However, there have been very few studies looking at the potential preferential sorption of organic compounds in Ca-rich edaphic environments.

If molecular scale stabilisation of SOC by Ca^{2+} predominantly occurs through inner- or outer-sphere cation bridging, then it should preferentially target functional groups such as carboxyls and phenols. Römkens and Dolfing (1998) and Kaiser (1998) accordingly demonstrated that Ca^{2+} preferentially flocculated and precipitated high molecular weight DOC compounds, which contained higher proportions of carboxylic and phenolic functional groups. There is also evidence for the preferential adsorption of negatively charged products of lignin degradation (syringyl units; Grünewald et al., 2006) and DOC (Jin and Zimmerman, 2010; Jin et al., 2014) by calcite. The implications of this hypothesis for our understanding of SOC cycling could be profound. It could potentially provide a mechanism to bridge the two competing hypotheses of SOC persistence, i.e. biochemical recalcitrance versus mineral-association, since organic compounds with different compositions could have different probabilities for sorptive preservation. This perspective is highly relevant to SOC modelling. As an example, the CENTURY model assumes universal preservation of lignin in stable SOC pools (Parton, 1996; Parton et al., 2015), which has been questioned by experimental evidence (Gleixner et al., 1999; Gleixner et al., 2002). Accruing evidence on selective sorption of specific compounds to minerals or cations, including lignin derivatives, could speak in favour of considering SOC biochemical composition as a predictor of residence time, but the parametrisation would have to be adjusted for different geochemical environments.

Conversely, Minick et al. (2017) demonstrated that high additions of Ca at the Hubbard Brook experimental forest specifically reduced the mineralisation of ^{13}C-depleted SOC, which should represent a relatively fresh pool, little affected by oxidative transformation (Rumpel and Kögel-Knabner, 2011), thus contradicting the hypothesis that Ca^{2+} preferentially stabilises oxidised SOC. Yet, stabilisation of ^{13}C-depleted SOC could simply imply that occlusion was the predominant mechanism of SOC stabilisation at the Hubbard Brook Forest. SOC occlusion could limit the mineralisation of ^{13}C-depleted sources because aggregates occlude a heterogeneous mixture of both ^{13}C-enriched, decomposed and relatively fresh, ^{13}C-depleted particulate SOM (Poeplau et al., 2018). However, this still requires further evidence. Future investigation should specifically focus on the relative importance of occlusion and adsorption for SOC stabilisation, as influenced by the geochemical environment and the composition of organic components.

3.3.3 - pH - the master variable for SOC stabilisation mechanisms?

As pH shifts from acidic to basic conditions, so does the importance of SOC stabilisation by different polyvalent cations and their mineral forms, moving from Al^{3+} or Fe^{3+} to Ca^{2+}, respectively (Tipping, 2005). The prevalence of each cation is indeed largely linked to soil pH due to the buffering capacity of primary and secondary minerals, notably calcite and Al oxides (Oste et al., 2002; Slessarev et al., 2016). As each cation is associated with different SOC stabilisation mechanisms (Fig. 3.2), this shift in pH could arguably be used to predict the content and types of SOC being stabilised in each environment. Therefore, we propose the following conceptual model: in acidic environments, complexation of organic

ligands by free Al^{3+} and Fe^{3+} as well as their mineral forms (Kalbitz and Kaiser, 2008; Scheel et al., 2008) and the cementation of aggregates by Fe oxides (Oades and Waters, 1991; Zhao et al., 2017) are likely to control SOC stabilisation. There could also be a localised effect of Ca in the topsoil of these acidic environments caused by biological cycling and resulting accumulation of Ca (Clarholm and Skyllberg, 2013). As soil pH increases above 6, Ca^{2+} becomes more prevalent and, consequently, there should be increased evidence of SOC stabilisation by inner- and outer-sphere Ca^{2+} bridging or Ca-mediated aggregation (Kayler et al., 2011). As soil pH increases further to pH > 8.4, excess Ca^{2+} will begin to precipitate physio-chemically as $CaCO_3$, reducing the stabilisation by free Ca^{2+} at the expense of $CaCO_3$-mediated mechanisms (Lindsay, 1979). When soil pH starts to increase beyond pH 9.5, soils will become increasingly sodic and dominated by Na^+, which tends to disperse soil separates, reducing occlusion (Wong et al., 2010) and sorption of SOC (Iskrenova-Tchoukova et al., 2010; Sutton et al., 2005), and consequently weaken SOC stabilisation.

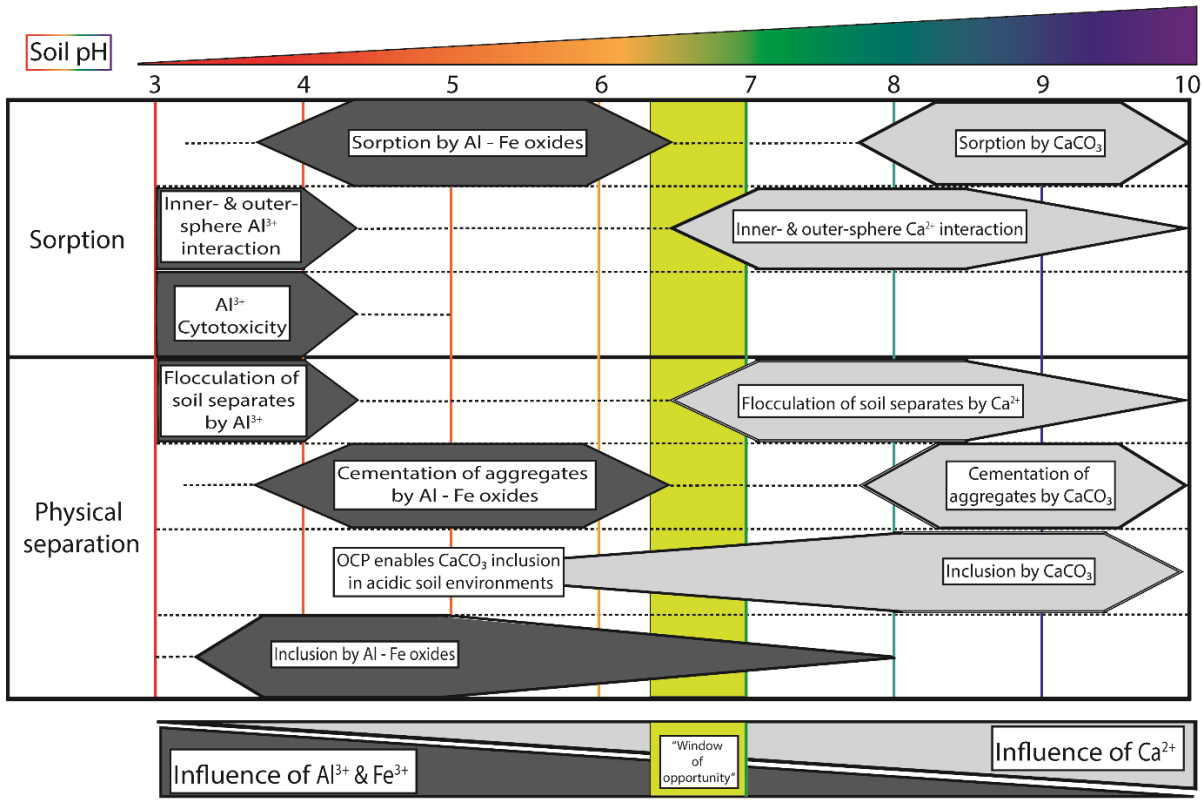

Fig. 3.2. The shifting role of polyvalent cations in the stabilisation of soil organic carbon with increasing pH. A 'window of opportunity' for microbial decomposition is highlighted in green according to the proposition of (Clarholm and Skyllberg, 2013). Thresholds are based on values available in the literature and it is expected that adjustments will occur as more results become available. Al - Fe oxides refer to true aluminium and iron oxides as well as oxyhydroxides and their poorly crystalline forms. OCP: oxalate-carbonate pathway.

As indicated by Fig. 3.2, stabilisation of SOC by polyvalent cations is expected to be weakest at near-neutral levels of pH, which also coincides with optimum conditions for bacterial mineralisation

(Groffman et al., 2006; Illmer and Schinner, 1991; Ivarson, 1977; Whittinghill and Hobbie, 2012; Zelles et al., 1987). This was suggested previously by Clarholm and Skyllberg (2013) as a "window of opportunity" (highlighted in green; Fig. 3.2) for C mineralisation. Taking this reasoning a step further, we hypothesise that low and high pH environments will afford different capacities for SOC stabilisation. Given the documented efficiency of sorption by Al and Fe forms and of aggregation by Ca, we postulate that adsorption by Al - Fe oxides generally dominates SOC stabilisation at low pH, stabilising SOC for long time periods; but as the pH increases beyond the "window of opportunity", it could be expected that the dominant stabilisation mechanism would be occlusion within aggregates, potentially involving larger amounts of SOC but for shorter durations. However, due to the relatively limited body of work on Ca-mediated SOC stabilisation mechanisms, these hypotheses currently remain speculative; the dominant SOC stabilisation mechanisms associated with each cation, the amount of SOC they can affect and the relative strength of the conferred protection still require confirmation. Nonetheless, pH has the potential to act as a fundamental indicator of the mechanisms controlling SOC stabilisation. Therefore, this review suggests that SOC models should consider incorporating pH as a master variable to represent the effects of different stabilisation mechanisms by polyvalent cations and their mineral forms on the accumulation and persistence of SOC.

3.4 - Conclusions

Although an addition of Ca^{2+} generally improves microbial conditions for decomposition by increasing pH and reducing stress from H^{+}, it can counter-intuitively reduce respiration rates through the stabilisation of SOC. The main mechanisms behind Ca-mediated SOC stabilisation are likely linked to the ability of Ca^{2+} to bridge negatively charged surfaces. Chemical modelling indicates that Ca^{2+} can bridge SOC and minerals through both inner- and outer-sphere interactions, but this still requires empirical confirmation. When scaled up, Ca bridging also positively affects soil structure; yet surprisingly little is known about the implication for the amount and stability of occluded SOC. The relative prevalence of occlusion and adsorption for SOC stabilisation in Ca-influenced soils needs to be determined, as it could have important consequences for the stabilisation of SOC in terms of its maximum amount, mean residence time but also composition. Indeed, there is some evidence that adsorption could preferentially involve some classes of organic compounds whereas occlusion may be relatively indiscriminate, at least at the macroscopic level. Soil pH could also play a fundamental role in predicting the occurrence of these stabilisation mechanisms and should be considered for inclusion in current SOC models. In order to better represent interactions between the C and Ca cycle in conceptual and numerical models of SOC cycling, we suggest that further mechanistic investigation should focus on the quantification of the relative prevalence and strength of each stabilisation mechanism and their variation across pH thresholds.

- End of publication -

Chapter 3 - Opening perspectives and recent literature

Since publication of this critical review, there have been several important articles that have helped to further illuminate the field, which will now be discussed further below. The first of these papers, was Rasmussen et al. (2018), which synthesised data from 5,500 soil profiles spanning continental scale environmental gradients. In this analysis, they showed that Ca_{Exch} strongly predicted SOC content in arid environments and called for us to move beyond clay as a sole predictor of SOC content. Another recent study (Solly et al., in review) analysed predictors of SOC content in 1000 forest soils spread throughout Switzerland. They demonstrated that CEC explained more of the variation in their dataset (35 %) than clay content (7 %) and that soil pH influenced this relationship, as effective CEC explained more variation with increasing pH (Solly et al., in review), coinciding with an increased Ca availability. While these studies do not separate out the co-localisation of Ca_{Exch} and SOC during cation exchange processes from a potential mechanism of SOC stabilisation, they do raise the potential of Ca_{Exch}, CEC and pH to modelling SOC content on national to continental scales.

Recent studies have also further investigated the potential mechanisms of Ca-mediated stabilisation of SOC in $CaCO_3$-rich soils. Chi et al. (2019) recently used *in situ* atomic force microscopy to observe how calcite gradually included SOC demonstrating the potential importance of the inclusion and sorption of $CaCO_3$ in soils with significant $CaCO_3$ contents. Another recent study, Martí-Roura et al. (2019) used size-fractionation, $\delta^{13}C$ values and incubation experiments to investigate SOC cycling and stability in arid top-soils (0-10 cm) with or without $CaCO_3$ (> 50 %). This study demonstrated that the coarse and fine fractions had similar $\delta^{13}C$ values in the $CaCO_3$-rich soils, while soils without $CaCO_3$ had higher $\delta^{13}C$ values in the fine fraction than the coarse fraction. The following research chapters will now further investigate the mechanisms of SOC stabilisation in $CaCO_3$-bearing soils and why they may have similar $\delta^{13}C$ values in different fractions, relative to soils without $CaCO_3$.

Important discoveries were also made regarding the interactions between Fe and Ca in SOC stabilisation and their coupled interaction. Sowers et al. (2018b) demonstrated that ferrihydrite adsorbed more SOC in the presence of Ca than in its absence, across a wide range of pH conditions. Sowers et al. (2018a) then used scanning transmission X-ray microscopy (STXM) paired with C-near-edge X-ray absorption fine structure (C-NEXAFS) to demonstrate that Ca was highly associated with C. The C-NEXAFS revealed that this was due to the formation of a Fe-Ca-C ternary complex, which was then further supported by another later work by the same group (Adhikari et al., 2019). This body of work opened up a whole new chapter in our understanding of Ca-SOC interactions, expanding the role of Fe beyond what was hypothesised in Fig. 3.2. The complexities of deconvoluting this relationship in a natural environment will be further explored in the following chapters.

- This page is intentionally left blank -

- Chapter 4: A cascading influence of calcium carbonate on the biogeochemistry and pedogenic trajectories of subalpine soils, Switzerland -

The following manuscript has been accepted for publication in Geoderma©. Most of the supplementary figures from this paper have been included in this chapter, but several methods-based supplementary figures and all the supplementary tables have been included in the appendices section (8.1.1).

- Research question Chapter 4 -

The following question and sub-questions will be addressed in this chapter:

What is the influence of small quantities of $CaCO_3$ on the pedogenesis and biogeochemistry of soils that have developed under similar soil forming conditions, in a humid and temperate environment (Nant Valley, Switzerland)?

a. How is the pedogenesis of soils, which have developed under otherwise similar soil forming conditions, influenced by the presence or absence of $CaCO_3$?
   iii. What is the influence of $CaCO_3$ on pedogenic trajectories?
   iv. Does $CaCO_3$ create a state of pedogenic inertia?
b. What are the fundamental differences in the biogeochemical properties caused by the presence or absence of $CaCO_3$?
   i. How does the presence or absence of $CaCO_3$ influence the amount of Ca and soil pH?
   ii. How does the presence or absence of $CaCO_3$ influence the amount of SOC?

- Chapter 4 abstract -

Soil research in temperate to humid and temperate regions has typically focused on acidic soils; there has been relatively little investigation of the effects of $CaCO_3$ on unamended soil properties or function in these environments. The object of this study was to characterise the effects of small amounts of $CaCO_3$ on pedogenic trajectories and soil biogeochemistry in a humid subalpine valley of Switzerland. To isolate the influence of $CaCO_3$, six profiles were selected that had developed under almost identical conditions for soil formation, *i.e.* climate, topography, vegetation structure, time since deglaciation, silicate mineralogy, and texture. The main difference between the profiles was that three contained a small quantity of $CaCO_3$ (< 6.2 %; thereafter, '$CaCO_3$-bearing') while the remaining three contained no detectable $CaCO_3$ (thereafter, '$CaCO_3$-free'). The presence of $CaCO_3$ was associated with cascading changes in soil biogeochemical properties. These changes included higher pH, an order of magnitude higher extractable Ca, and twice as much SOC. $CaCO_3$-bearing profiles also displayed a higher proportion of poorly crystalline Fe forms. The higher pH at the $CaCO_3$-bearing site was attributable to the weak buffering provided by $CaCO_3$ dissolution, which in turn maintained the relatively higher extractable Ca. Ca_{Exch} and other reactive Ca forms could help stabilise SOC, contributing to its accumulation through processes such as flocculation and subsequent occlusion within aggregates and / or sorption to mineral surfaces. The increased SOC, Ca_{Exch} and pH at the $CaCO_3$-bearing site could in turn be inhibiting the crystallisation of disordered Fe forms, but further research is required to confirm this effect and isolate the exact mechanisms. Overall, this study shows that the presence of small amounts of $CaCO_3$ in humid environments has a far-reaching influence on soil biogeochemical properties, and further supports the idea that indicators of Ca prevalence have the potential to improve regional SOC estimates.

4.1 - Introduction

Calcium carbonate accounts for an important fraction of C present in soils, linking the long-term geological C cycle with the faster biogeochemical cycling of SOC (Gao et al., 2017; Hasinger et al., 2015; Sanderman, 2012; Zamanian et al., 2016). Globally, the presence of $CaCO_3$ in soils is inversely correlated to effective precipitation because of its susceptibility to chemical weathering (Arkley, 1963; Jenny, 1941; Slessarev et al., 2016). However, there remains clear outliers in this global correlation, as $CaCO_3$-bearing soils can be found in humid environments and are typically related to lithological $CaCO_3$ reservoirs that are yet to be exhausted by leaching (Slessarev et al., 2016). Furthermore, while the precipitation of $CaCO_3$ by physicochemical processes is not typically favoured in humid or acidic environments (Barta et al., 2018; Cerling, 1984), it can still occur through the direct and indirect results of biological processes (Bindschedler et al., 2016; Cailleau et al., 2005; Hasinger et al., 2015). Thus, $CaCO_3$ in soils can persist in a state of disequilibrium with climate, when driven by reserves of calcareous parent material or biological processes.

The aforementioned disequilibrium is an example of pedogenic inertia, defined as the persistence of certain soil conditions or processes in spite of the presence of extrinsic pedogenic factors that favour their discontinuation (Bryan and Teakle, 1949). The extrinsic pedogenic factors refer to four of the five conventional factors of pedogenesis (parent material, biota, topography and climate; Jenny, 1941), excluding time which acts as a vector (Muhs, 1984). In the previously used example, the state of pedogenic inertia exists because an intrinsic pedogenic factor, the continued and slow dissolution of $CaCO_3$, preventing the expression of an acidic soil favoured since deglaciation by the extrinsic factor of climate (Chadwick and Chorover, 2001). This inertia in turn diverges the trajectory of pedogenesis, as evidenced by the wide array of soils that develop on parent material containing a range of varied $CaCO_3$ content in humid or mountainous environments (Kowalska et al., 2019). Unless there is a change in extrinsic factors, pedogenic inertia is by nature a transient condition that will eventually cease in a threshold response. Pedogenic thresholds are defined as limits in intrinsic pedogenic factors or soil properties, that once breached, cause rapid and irreversible transformations in pedogenesis and biogeochemistry (Chadwick and Chorover, 2001; Muhs, 1984). In the case of $CaCO_3$, a threshold may occur when its concentration becomes too low to provide pH buffering to the soil system, triggering changes in soil biogeochemistry.

The presence of $CaCO_3$ plays a commanding role in governing soil biogeochemistry. The primary mechanism for this is the buffering of soil pH caused by the consumption of H^+ during acid hydrolysis of $CaCO_3$ (Bache, 1984; Zamanian et al., 2016). pH is known as a master variable in soil ecosystems and impacts many biological and chemical processes, such as the composition of microbial communities (Bahram et al., 2018; Rousk et al., 2010), mineral weathering rates (Chadwick and Chorover, 2001), redox chemistry (Bartlett and James, 1993) and the speciation and lability of many elements (Sposito, 2016). The dissolution of $CaCO_3$ also provides a continued supply of Ca_{Exch}, which has long been

thought to promote the accumulation of SOC in $CaCO_3$-bearing soils through occlusion (Grant et al., 1992; Muneer and Oades, 1989c) and sorption processes (Edwards and Bremner, 1967; Kalinichev and Kirkpatrick, 2007; see review in Rowley et al., 2018). Recent evidence has highlighted a potential stabilisation of SOC by Fe-Ca-ternary complexation (Sowers et al., 2018a; Sowers et al., 2018b), which could be more prevalent in $CaCO_3$-bearing soils than acidic profiles with limited Ca_{Exch}. However, further research is still needed to evidence links between Ca, SOC, and reactive forms of Fe in different soil environments. In particular, the effects of small amounts of $CaCO_3$, commonly found in humid and temperate soil environments, on biogeochemistry still requires further investigation.

Therefore, the objective of this paper is to quantify the impact of small amounts of $CaCO_3$ on the pedogenesis and biogeochemistry of soils in a humid environment (Nant Valley, Vaud Alps, Switzerland). To isolate the effects of $CaCO_3$ on pedogenesis at the Nant Valley, six soil profiles were selected that had developed under near-identical conditions for soil formation (Jenny, 1941) or extrinsic pedogenic factors (Chadwick and Chorover, 2001; Muhs, 1984), except that three profiles contained a small quantity of $CaCO_3$ (< 6.2 % $CaCO_3$) while the other three were devoid of $CaCO_3$. Our hypothesis was that the presence or absence of $CaCO_3$ would trigger a threshold response, resulting in large divergences in pedogenesis and soil biogeochemistry, particularly regarding the accumulation of SOC.

4.2 - Materials and methods

4.2.1 - Site description and sampling

This study was completed in the Nant Valley (573'000, 119'000 CH1903 LV03), a partially glaciated watershed in the Vaud Alps, Switzerland. The valley is orientated north-south and situated on the Morcles Nappe, a near-recumbent anticline consisting of Jurassic and Cretaceous shallow-water limestones intercalated with marl and shale deposits (Austin et al., 2008). Sampling took place in a pastoral area of the valley floor (*ca.* 1500 m elevation above sea level), which is lightly-grazed by heifers during summer months. This area receives approximately 1800 mm yr^{-1} precipitation, has a mean annual temperature of 6°C (Vittoz and Gmür, 2008) and is typically covered in snow from December to April .

Two sampling sites were selected that represented a range of $CaCO_3$ contents, while having developed under near-identical soil forming conditions. Potential variations in the $CaCO_3$ content were identified in the field using an auger, 10 % v / v HCl and a field pH meter (Hellige pH Indicator). Retained sites were located on subalpine prairies and thus had the same vegetation structure, which had previously been characterised in detail (Grand et al., 2016; Vittoz and Gmür, 2008). Soils at each site developed in mixed alluvial, morainic and colluvial materials issued from the Morcles Nappe (Grand et al., 2016; Perret and Martin, 2014) and deposited around the time of the retreat of the Martinets Glacier (*ca.* 15 kyr; Seguinot et al., 2018). Sites all had a minimal slope, the same altitude, similar climate due to their proximity to each other (*ca.* 400 m apart) and equivalent irradiance.

Three profiles were dug at each sampling site in July - August 2016 (Fig. 4.1). Profiles were classified as Eutric Cambisols (siltic) with no HCl effervescence on the north-western bank and Cambic Phaeozems (siltic) that effervesced on the south-eastern bank of the Nant River (IUSS Working Group WRB, 2015). For brevity, the Eutric Cambisols will henceforth be labelled as $CaCO_3$-free (profiles F1, F2, F3, in fuchsia) and the Cambic Phaeozems will be labelled as $CaCO_3$-bearing (profiles B1, B2, B3, in black). Profiles were sampled at 6-7 depth intervals (see Table 4.1 included in results section) to a maximum depth of 50 cm, sampling the deepest layers first to prevent intra-profile contamination. Samples were labelled from 1 to 6 / 7 with increasing depth (*e.g.*, F1.1-to-F1.6) and then transported to the University of Lausanne in sealed bags. Aboveground biomass (AGB) was also randomly sampled from the sites to quantify potential differences in vegetation inputs at the sites.

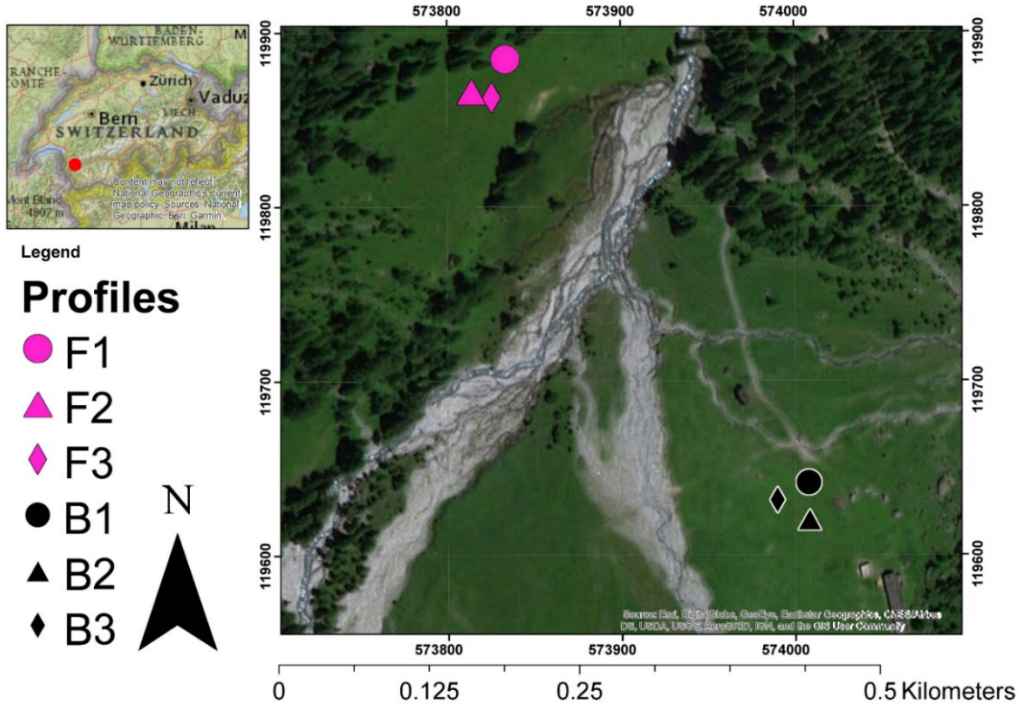

Fig. 4.1. Profile locations in the Nant Valley, Vaud Alps, Switzerland. Coordinates are in CH1903 LV03 (ESRI, 2019). Profiles labelled with an F (F1, F2, F3) are at the $CaCO_3$-free site and profiles labelled with a B (B1, B2, B3) are at the $CaCO_3$-bearing site.

4.2.2 - Laboratory analyses

Samples were air-dried and sieved to 2 mm. All analyses were completed on this fine earth fraction unless stated otherwise and results were corrected for residual humidity (van Reeuwijk, 2002). Sub-samples were ground to a fine powder (*ca.* 20 µm) for 3 min in an agate crucible with a vibrating-disc mill (Siebtechnik Schibenschwingmuhle-TS). AGB samples were oven dried (40°C), ground by hand and homogenised for further analysis. Quality control procedures included the analysis of an internal standard when appropriate, as well as the inclusion of blanks and quality checks. A minimum of 10 %

blind replicates were included in all analyses. All plastic and glassware were acid washed (3 M HCl) to remove trace contamination.

4.2.2.1 - pH and texture

Soil pH was measured potentiometrically using a glass-body combination electrode (Thermo Scientific Orion ROSS Probe) on field moist samples in a 0.1 M $CaCl_2$ solution (1:2 soil:solution mass ratio). Texture was determined using laser diffraction (0.01–2000 μm; Pansu and Gautheyrou, 2006). Pre-treatment included digestion of soil organic matter with increasing concentrations of H_2O_2 (10-35 %). During the procedure, pH was kept around neutrality with NaOH to prevent destruction of mineral components due to acidification. Samples were then shaken with sodium hexametaphosphate for 16 h to chemically disperse particles prior to measurement with a Beckman Coulter LS13320 Particle Sizing Analyser. The analyser pump speed was set at 80 % (*ca.* 9500 mL min^{-1}) and samples were weakly sonicated in both the autosampler and analyser (4 / 8 setting; *ca.* 2 J mL^{-1}) prior to measurement. The analyser was run using the default optical model (Fraunhofer.rf780d) in auto-dilution mode. Measurements were taken when an obscuration of 12 % was obtained.

4.2.2.2 - Elemental analysis

The total elemental composition was quantified on ground samples using X-ray fluorescence (XRF; PANalytical PW2400 WDXRF Spectrometer) following lithium tetraborate fusion (PANalytical Perl X3 Fuser). Results were corrected for loss-on-ignition at 1050°C (Solo 111-13/10/30). Organic C and total nitrogen were quantified on AGB and soil ground samples by dry combustion (Carlo Erba 1108 and Thermo Scientific Flash 2000 CHN Elemental Analysers). Soil samples were fumigated for 24 h with 12 M HCl in order to remove inorganic C prior to CHN elemental analysis (Harris et al., 2001; Ramnarine et al., 2011). Samples were weighed to the nearest milligram before and after fumigation to correct for mass changes. All samples gained mass due to the formation of small quantities of chloride green rust, likely formed from the reaction of Fe oxides with Cl^- (Ramnarine et al., 2011).

4.2.2.3 - Mineralogy

Bulk mineralogy was determined on ground samples prepared according to Adatte et al. (1996) using X-ray diffraction (XRD; Thermo ARL X'TRA Powder Diffractometer). Approximately 800 mg of ground sample was pressed (20 bars) in a powder holder covered with blotting paper. Pressed samples were then analysed using Cu Kα radiation at 45 kV / 40 mA with a 13 s counting time per 0.02° for 2 θ in the 1-65° range. Samples were rotated at a range of 1° min^{-1} with an acquisition step size of 0.03 – 0.05° 2 θ using a 0 / 0 type goniometer with a 250 mm radius. A spectral counter (Thermo ARL Water-cooled Silicon Detector) was used to eliminate Cu Kβ and Fe parasitic emissions. The bulk mineralogy of samples was then quantified using external standards (Adatte et al., 1996).

Samples from a randomly selected profile at each site were also prepared for clay mineralogical analysis according to Adatte et al. (1996). Briefly, samples from profiles F1 and B2 were mixed with deionised

water, agitated, and combined with 10 % HCl to remove carbonate. Insoluble residues were washed by centrifugation until neutral pH was acquired. Different size fractions (< 2 µm and < 16 µm) were separated by sedimentation according to Stokes' law. Selected fractions were then pipetted onto glass plates and air-dried. Resulting oriented slides were analysed by XRD before and after ethylene glycol solvation (heating at 450 °C).

Total carbonate content expressed as $CaCO_3$ equivalent (CCE %) was determined using a weak acid dissolution followed by measurement of the pH of the extractant (Loeppert et al., 1984). The method was selected for its reproducibility in quantifying low amounts of $CaCO_3$, for which the XRD detection limit is around 1 % (Loeppert and Suarez, 1996). The method was also adapted to measure reactive carbonates, by measuring extracts shortly after the addition of the weak acid. Briefly, 2 g of soils were placed in 50 mL centrifuge tubes and shaken on a rotary shaker (250 rpm) with 25 mL 0.4 M acetic acid. Holes approximately 1 mm in diameter were made in the lids to allow for degassing during the reaction. The pH of standards (reagent grade $CaCO_3$) and samples solutions was measured (Thermo-Fisher Scientific Orion Star A111 Probe) at 1 h (reactive carbonates) and 16 h (total carbonate) after the addition of acetic acid. Quality control was assured by running blind, analytical and spiked replicates (Loeppert and Suarez, 1996).

4.2.2.4 - Extractable cations

Fe and Al present in pedogenic oxides were extracted using a citrate-bicarbonate dithionite solution (Fe_d or Al_d; Mehra and Jackson, 1958), while poorly crystalline and monomeric Fe and Al forms were extracted with an oxalate solution (Fe_o or Al_o; McKeague and Day, 1966). The ratio of oxalate-to-dithionite extractable Fe (Fe_o/Fe_d) was used as a measure of the crystallinity of Fe oxides (Skjemstad et al., 1992). One surficial sample (B3.1) contained more Fe_o than Fe_d (*ca.* 20 %; Table 4.1). The citrate-bicarbonate dithionite extraction is typically less selective and extracts more Fe than the oxalate extraction (Dahlgren, 1994), but it can be less efficient at extracting chelated Fe (Rennert, 2019), potentially explaining the Fe_o/Fe_d ratio > 1.

Exchangeable cations were extracted from field moist samples using a 0.0166 M cobalt hexamine (Cohex; $[Co(NH_3)_6]Cl_3$) extraction (Aran et al., 2008). Pre-testing demonstrated that this extraction was the least aggressive towards carbonates (Appendix Fig. 8.19). Cation exchange capacity (CEC_{SUM}) was calculated as the sum of extracted exchangeable cations ($cmol_c\ kg^{-1}$), excluding H^+. Ca was also quantified in several other soil extracts including, in order of expected increasing extraction strength: deionised water (1:4 ratio; Tirmizi et al., 2006), 2 M KCl (1:5 ratio; Keeney and Nelson, 1982), 0.05 M disodium EDTA (1:20 ratio; Lo and Yang, 1999) and 0.5 M $CuCl_2$ extraction (1:10 ratio; Barra et al., 2001). All extracts were vacuum-filtered (0.45 µm) and diluted with 2 % HNO_3 prior to analysis on an ICP-OES (Perkin Elmer Optima 8300 Inductively Coupled Plasma–optical Emission Spectrometer).

4.2.3 - Statistical analyses of soil variables

The effects of $CaCO_3$ on soil variables were investigated using linear mixed models in SAS 9.4™. The estimation method was set to restricted (residual) maximum likelihood. Conditional residuals were plotted against predicted values to evaluate deviations from homoscedasticity and goodness of fit. Residuals were also checked for normality with QQ-plots (Galecki and Burzykowski, 2015). The significance of fixed effects was evaluated using type III F-tests. The denominators' degrees of freedom were computed using the Satterthwaite adjustment (Satterthwaite, 1946). For significant fixed effects, comparison of means was carried out using t-tests without multiple inference adjustment (Webster, 2007). The alpha level of significance was set at $\alpha=0.05$ for all tests. All reported means are conditional least-square means ± the standard error of the mean (SEM). Means for profiles are the unweighted average of sampling intervals.

Models included site ($CaCO_3$-bearing or free), depth classes and their interaction as fixed effects. Observations were blocked by profile and a different variance was computed for each site since observations from the $CaCO_3$-bearing site typically had a higher dispersion than those from the $CaCO_3$-free site. For extractable Fe, dispersion was also higher for surface samples and the variance was additionally allowed to vary with depth. To account for the autocorrelation of observations within profiles, depth was set as a repeated measure effect with a first-order autoregressive covariance structure. Choice of covariance structure was made based on the Bayesian Information Criteria.

A Pearson's correlation coefficient heat map was created to explore linear associations between variables using the Corrplot Package (Wei and Simko, 2017) in R (2019). Variables in the heat map were ordered hierarchically into two separate groups using the complete-linkage method (Sørensen, 1948). A principal component analysis (PCA) was conducted on the correlation matrix to synthesise relationships between variables. A factor analysis was completed on the first 5 principal components (accounting for > 82 % of variance) using a quartimax orthogonal rotation (Neuhaus and Wrigley, 1954). The purpose of the quartimax rotation is to minimise the number of original variables associated with each factor to simplify interpretation. Observations were then plotted according to their factor 1 and 2 scores in Matlab®.

Finally, differences in the shape of the depth curve of SOC between the sites were explored by examining scatterplots of SOC versus depth. Linear regressions were fitted to the data for each site. A higher root mean square error (RMSE) was considered as an indication of lack-of-fit (departure from the linear trend). Residuals from the linear regression were also tested for normality using the Shapiro-Wilk Test, with departures from normality used as another indicator of deviation from the linear trend.

4.3 - Results

4.3.1 - Soil texture, composition and silicate mineralogy

Soil texture was similar between the two sites (Fig. 4.2 on the following page). All samples had a silty-loam texture and were comprised of six predominant textural populations (Fig. 4.3 on the following page). There was slightly less silt at the $CaCO_3$-free site than at the $CaCO_3$-bearing site (67.3±0.7 % versus 74.1±0.4 %), and consequently more sand- (15±0.8 % versus 10.6±0.5 %) and clay-sized particles (17.8±0.3 % versus 15.3±0.3 %). The surficial samples of F1 and F2 (F1.1, F2.1, F2.2 and F2.3) as well as one deep sample (F2.6) had a more pronounced peak in the fine sand population (Fig. 4.3), which occurred at the expense of fine silt populations.

Major elemental compositions were mostly similar at both sites (Appendix Table 8.1). Ti and other transition / post-transition metals were largely invariant. The main differences pertained to Ca, which was approximately an order of magnitude higher at the $CaCO_3$-bearing site (14.7±3.3 g kg^{-1}) than at the $CaCO_3$-free site (1.9±0.2 g kg^{-1}). There was a corresponding decrease in Si at the $CaCO_3$-bearing site (299.8±1.5 g kg^{-1}), relative to the $CaCO_3$-free site (318.3±3.4 g kg^{-1}). There were also small differences in the amounts of other elements including Mg and P, which were slightly higher at the $CaCO_3$-bearing site (14.9±0.1 g kg^{-1} Mg; 4.9±0.8 g kg^{-1} P) than at the $CaCO_3$-free site (12.7±0.3 g kg^{-1} Mg; 1.4±0.1 g kg^{-1} P). K was also marginally higher at the $CaCO_3$-bearing site (26.9±0.3 g kg^{-1} versus 23.4±0.9 g kg^{-1}), while Na was slightly higher at the $CaCO_3$-free site (7.8±0.0 g kg^{-1} versus 6.4±0.1 g kg^{-1}). Overall, the main difference in major elements composition between the sites consisted of an increase in Ca at the expense of Si in the $CaCO_3$-bearing profiles.

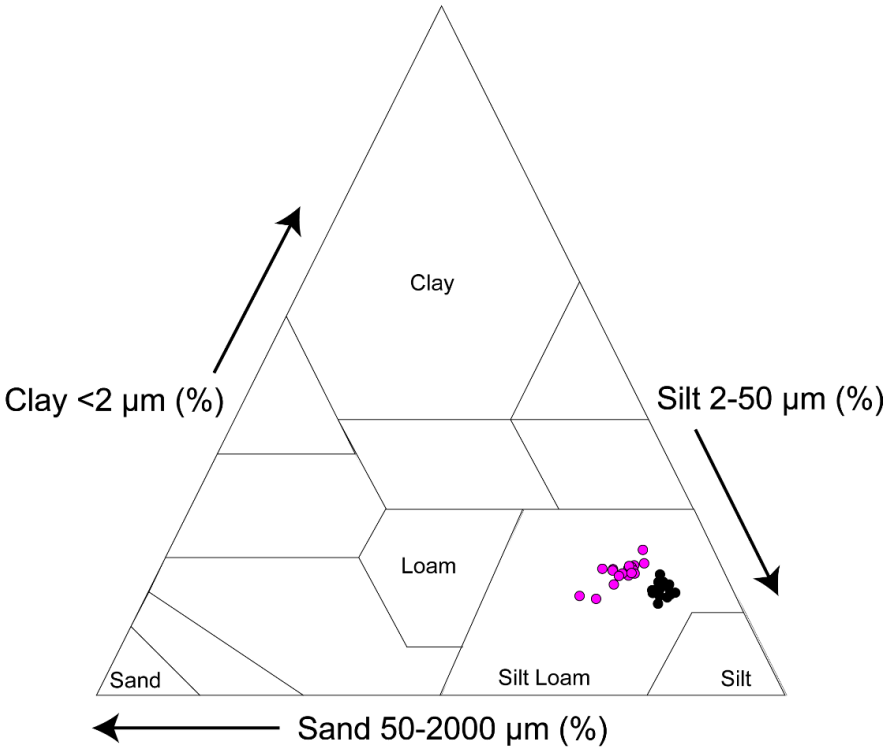

Fig. 4.2. Texture of samples from the $CaCO_3$-free (fuchsia dots) and $CaCO_3$-bearing (black dots) profiles.

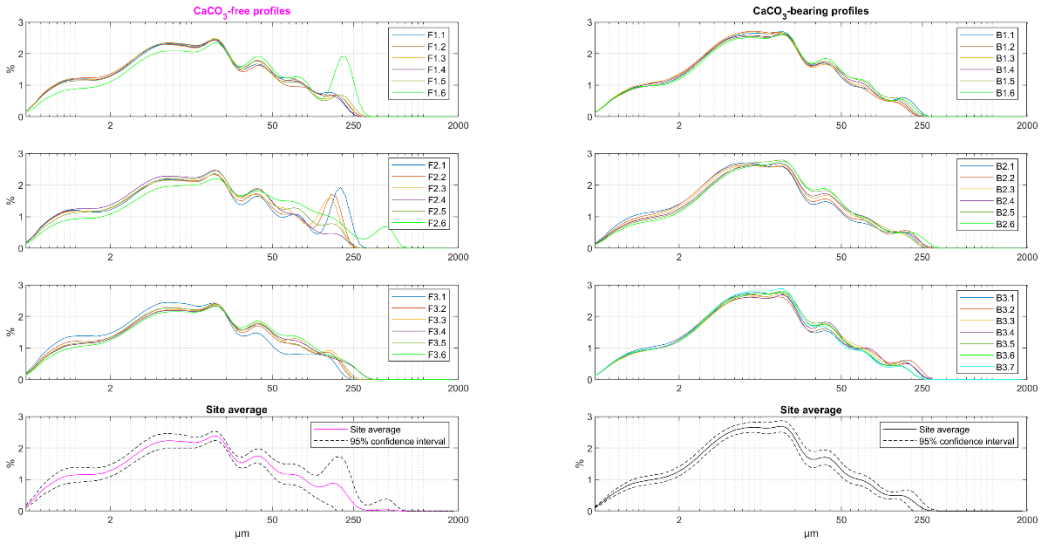

Fig. 4.3. Particle size distributions of the $CaCO_3$-free (F1, F2, F3) and $CaCO_3$-bearing (B1, B2, B3) profiles. Graphs at the bottom of the subplot are averages for sites with 95 % confidence intervals.

Table 4.1. Selected properties of the study profiles at the Nant valley. Profiles F1, F2 and F3 are Eutric Cambisols ($CaCO_3$-free) and profiles B1, B2 and B3 are Cambic Phaeozems ($CaCO_3$-bearing).

Sample name	Depth intervals (cm)	Genetic Horizons	pH	Al_{Exch} cmol.c kg^{-1}	Ca_{Exch} cmol.c kg^{-1}	CEC_{sum} cmol.c kg^{-1}	Ca_{Exch} saturation %	Al_{Exch} saturation %	TON %	SOC %	C:N ratio	Al_o g kg^{-1}	Fe_o g kg^{-1}	Al_d g kg^{-1}	Fe_d g kg^{-1}	Fe_o/Fe_d ratio
F1.1	0-5	Ah	4.1	0.4	6.2	7.3	84.9	5.7	0.6	4.7	8.0	2.6	13.2	3.2	24.0	0.6
F1.2	5-10	A1	4.3	0.3	4.5	5.3	84.9	6.4	0.4	3.0	7.5	2.8	12.5	3.3	23.0	0.5
F1.3	10-15	A2	4.3	0.2	4.1	4.7	87.0	5.2	0.3	2.3	7.3	3.1	11.8	3.3	22.3	0.5
F1.4	15-25	B1	4.5	0.2	3.8	4.6	82.8	5.1	0.2	1.6	6.8	2.6	12.1	3.8	24.6	0.5
F1.5	25-35	B2	4.5	0.2	4.1	4.6	89.1	4.5	0.2	1.3	6.1	2.9	11.2	3.9	25.4	0.4
F1.6	35-52	B3	4.6	0.1	4.3	4.6	93.3	1.5	0.2	0.9	5.3	2.5	9.1	3.0	22.8	0.4
F2.1	0-5	Ah	4.0	1.3	4.4	6.1	72.6	20.6	0.7	5.8	8.6	2.9	11.1	3.7	23.7	0.5
F2.2	5-10	A	4.2	1.5	1.6	3.2	48.4	45.7	0.3	2.4	7.7	3.1	11.5	3.6	22.1	0.5
F2.3	10-15	AB	4.2	1.4	1.5	3.0	50.0	44.5	0.3	2.3	7.5	2.8	10.6	3.9	23.1	0.5
F2.4	15-20	B1	4.3	1.0	1.7	2.8	61.1	36.7	0.3	2.0	7.3	2.9	10.8	3.7	21.8	0.5
F2.5	20-25	B2	4.4	0.9	1.6	2.6	62.9	34.5	0.2	1.5	6.7	2.8	9.9	3.9	23.3	0.4
F2.6	25-40	BC	4.4	0.8	1.6	2.5	63.5	33.1	0.2	1.0	5.6	2.1	7.4	3.0	19.7	0.4
F3.1	0-5	Ah	4.3	0.5	7.6	9.0	84.1	5.7	0.7	6.1	8.5	2.8	12.2	3.3	21.7	0.6
F3.2	5-10	A	4.4	0.9	3.2	4.5	71.2	19.8	0.4	3.4	7.8	3.0	11.6	3.6	21.8	0.5
F3.3	10-15	B1	4.5	0.9	2.6	3.8	66.9	23.5	0.3	2.3	7.4	2.7	9.9	3.6	21.5	0.5
F3.4	15-20	B2	4.4	1.1	1.7	3.0	56.4	34.8	0.3	2.0	7.3	3.0	10.6	4.3	24.6	0.4
F3.5	20-25	B3	4.5	1.1	1.9	3.2	58.1	33.8	0.2	1.7	7.4	3.2	10.5	4.1	22.9	0.5
F3.6	25-40	BC	4.5	1.1	1.7	3.1	54.3	35.9	0.2	1.5	7.5	3.2	10.1	3.8	20.5	0.5
B1.1	0-5	Ah1	6.3	0	23.2	23.7	97.6	0.0	0.8	7.7	9.2	0.9	13.1	0.9	24.7	0.5
B1.2	5-10	Ah2	6.4	0	23.0	23.4	98.4	0.0	0.8	6.8	8.9	1.0	14.0	1.0	25.4	0.6
B1.3	10-15	ABh	6.3	0	20.3	20.6	98.5	0.0	0.6	5.3	8.7	1.2	15.3	1.0	24.5	0.6
B1.4	15-20	Bh	6.4	0	16.9	17.2	98.4	0.0	0.5	4.3	8.5	1.4	17.9	1.2	26.8	0.7
B1.5	20-25	B1	6.4	0	15.2	15.5	98.3	0.0	0.4	3.4	8.3	1.2	15.3	1.2	26.3	0.6
B1.6	25-40	B2	6.3	0	11.8	12.0	98.2	0.0	0.3	2.3	7.8	1.3	13.8	1.4	29.9	0.5
B2.1	0-5	Ah1	5.7	0	23.5	23.8	98.7	0.0	0.9	8.3	9.2	1.6	17.6	1.3	20.2	0.9
B2.2	5-10	Ah2	5.7	0	18.4	18.6	98.8	0.0	0.8	7.3	9.3	1.6	20.8	1.5	25.1	0.8
B2.3	10-15	ABh	5.8	0	18.8	19.1	98.9	0.0	0.7	6.1	9.2	1.7	21.5	1.5	26.0	0.8
B2.4	15-20	Bh1	5.8	0	16.9	17.3	97.6	0.0	0.5	5.1	9.4	1.7	22.4	1.5	25.3	0.9
B2.5	20-25	Bh2	5.9	0	14.6	14.7	98.9	0.0	0.4	4.1	9.5	1.6	20.9	1.6	30.1	0.7
B2.6	25-40	BC	6.5	0	12.8	13.1	98.0	0.0	0.3	2.7	9.0	0.9	15.5	1.0	22.1	0.7
B3.1	0-5	Ah1	5.0	0	13.5	14.5	93.0	0.0	1.1	9.4	8.8	2.0	21.4	1.7	17.4	1.2
B3.2	5-10	Ah2	5.3	0	11.3	12.0	94.4	0.0	0.6	5.3	8.9	2.0	20.8	1.8	25.6	0.8
B3.3	10-15	ABh	5.1	0	12.3	12.9	95.3	0.0	0.5	5.1	9.4	1.9	21.1	1.8	26.3	0.8
B3.4	15-20	Bh	5.2	0	13.4	14.4	93.2	0.0	0.5	4.5	9.4	1.9	26.7	1.6	27.5	1.0
B3.5	20-25	B1	5.3	0	12.5	12.9	97.0	0.0	0.4	3.8	8.8	1.6	17.9	1.6	26.6	0.7
B3.6	25-30	B2	5.2	0	12.1	12.5	96.8	0.0	0.4	3.4	9.0	1.3	14.2	1.5	26.7	0.5
B3.7	30-37	BC	6.4	0	12.0	12.3	97.7	0.0	0.3	2.4	8.6	0.9	12.1	1.2	25.4	0.5

Ca_{Exch}, Al_{Exch}: exchangeable Ca and Al
CEC_{sum}: cation exchange capacity calculated as the sum of exchangeable cations, not including H^+
TON, SOC and C:N ratio: total nitrogen, soil organic carbon and the ratio of the two
Fe_o, Al_o: oxalate-extractable Fe and Al
Fe_d, Al_d: dithionite-extractable Fe and Al

Silicate mineralogy was also similar between the $CaCO_3$-bearing and $CaCO_3$-free sites (Appendix Table 8.2 & Appendix Fig. 8.1). Both sites had a bulk mineralogy that was predominated by quartz (38-41 %) and phyllosilicates (42-44 %), with small amounts of Na-plagioclase (5 %), K-feldspar (2 %) and goethite (1 %), while 8 % of the diffraction signal remained unquantified. Average Na-plagioclase content was slightly higher at the $CaCO_3$-free site (6.1±0.2 %) relative to the $CaCO_3$-bearing (4.8±0.3 %), while average content of K-feldspar was marginally higher at the $CaCO_3$-bearing site (2.2±0.1 %) relative to the $CaCO_3$-free site (1.5±0.2 %). The phyllosilicate mineralogy was also remarkably similar between the two sites and consistent throughout the analysed profiles (Appendix Fig. 8.2). The phyllosilicate population in both the randomly selected profiles (F1 and B2) was predominantly formed of chlorite and mica, with a small quantity of illite-vermiculite mixed layer minerals.

4.3.2 - Soil pH, $CaCO_3$ and Ca forms

Soil pH was higher at the $CaCO_3$-bearing site (range=5-6.5) than the $CaCO_3$-free (range=4-4.6). pH also increased significantly with depth at both sites (Table 4.1). The amount of $CaCO_3$ equivalent material (CCE) was below detectable limits in profiles from the $CaCO_3$-free site. Profiles from the $CaCO_3$-bearing site typically contained about 0.5 % reactive CCE and 0.8 % total CCE (Fig. 4.4), except for four samples also identified by XRD as containing several percent of $CaCO_3$. These four samples consisted of two surficial samples (B1.1, B1.2) and two of the deepest samples (B2.6, B3.7). The overall proportion of reactive carbonates, operationally-defined as having reacted with 0.4 M acetic acid in under 1 h, was high (74.4±3.7 % average; Appendix Table 8.2).

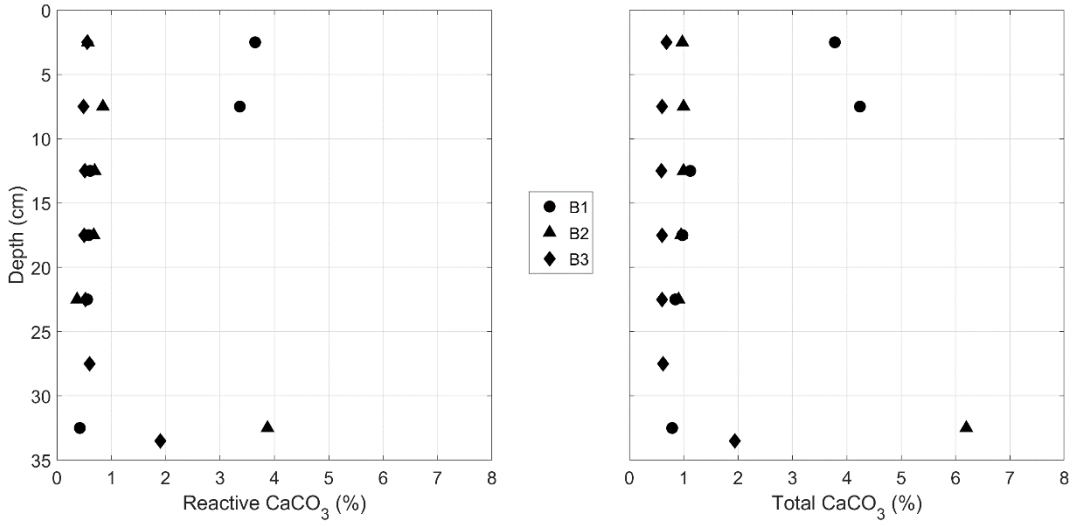

Fig. 4.4. Reactive and total contents of calcium carbonate equivalent for $CaCO_3$-bearing profiles (B1, B2, B3). Calcium carbonate equivalent contents were below the limits of detection at the $CaCO_3$-free site.

As with total Ca, extractable Ca was approximately an order of magnitude higher at the $CaCO_3$-bearing than at the $CaCO_3$-free site (Fig. 4.5). CEC_{SUM} was also higher at the $CaCO_3$-bearing (16.6±1.9 $cmol_c$ kg^{-1}) than at the $CaCO_3$-free site (4.3±0.6 $cmol_c$ kg^{-1}). This difference reflected the higher Ca_{Exch} content (Fig. 4.6) at the $CaCO_3$-bearing site (16.1±2.1 $cmol_c$ kg^{-1}) relative to the $CaCO_3$-free site (3.2±0.8 $cmol_c$ kg^{-1}), as Ca was the predominant exchangeable cation at both sites. The Ca saturation of the exchange complex was high at both sites, but was greatest and had a smaller range at the $CaCO_3$-bearing site (93-99 %) than at the $CaCO_3$-free site (48-93 %). This difference was reflected in corresponding increases in Al saturation, as exchangeable Al (Al_{Exch}) was consistently detected at the $CaCO_3$-free site only.

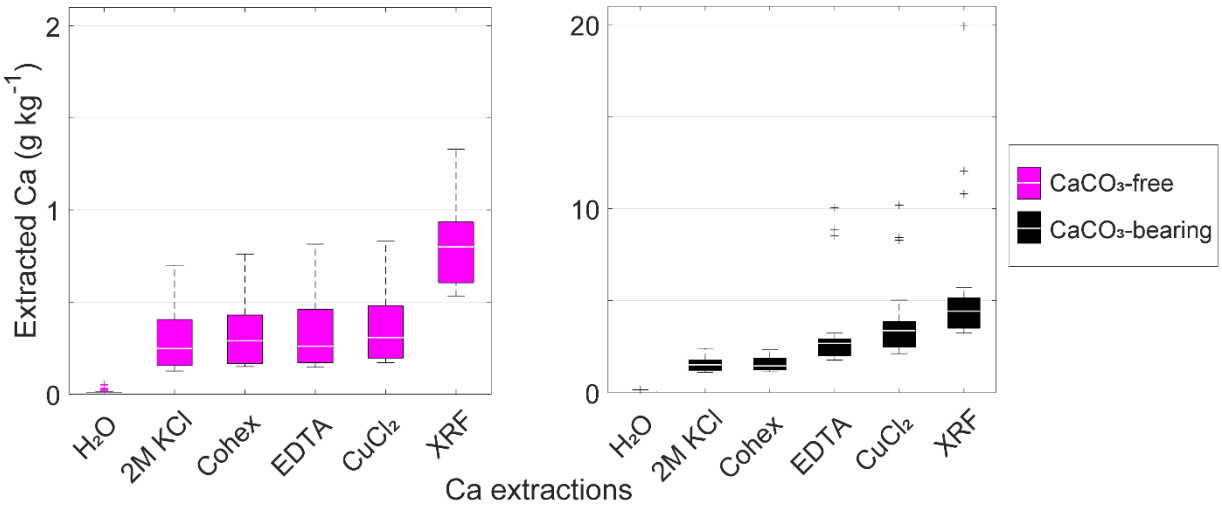

Fig. 4.5. Calcium contents of the $CaCO_3$-free and $CaCO_3$-bearing profiles. From left to right are deionised water, 2 M potassium chloride, 0.0166 M cobalt hexamine (Cohex), 0.05 M disodium EDTA and 0.5 M copper chloride extracts measured on an ICP-OES and total contents measured with X-ray fluorescence (XRF). Y scales differ by an order of magnitude. Bottom and top edges of the boxes in the box plot represent the 25th and 75th percentiles, the middle bars represent the median. Whiskers represent the range of most extreme data points not considered as outliers, while '+' represent outliers defined as values outside of the ±2.7 standard deviation range.

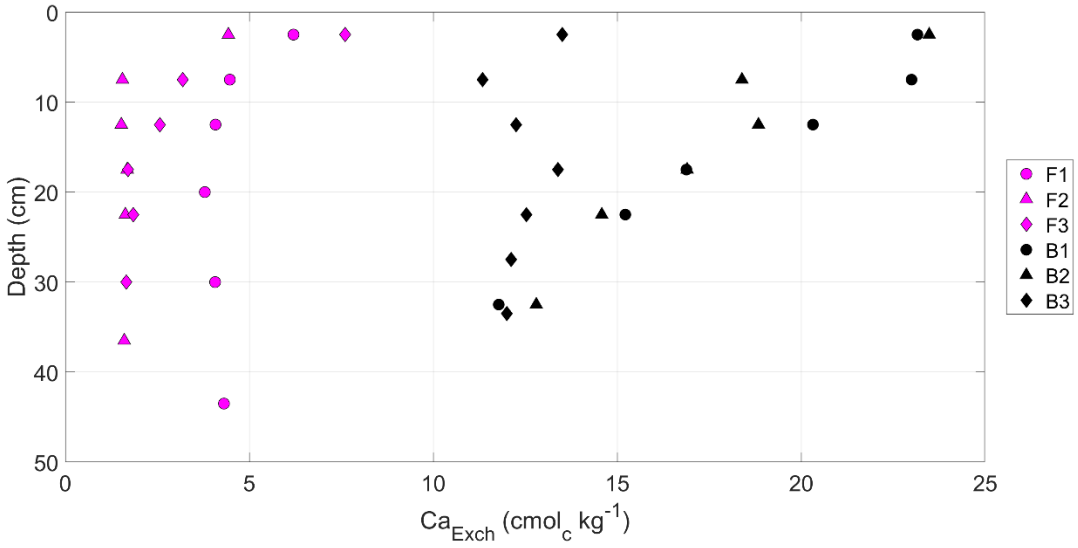

Fig. 4.6. Exchangeable calcium (Ca_{Exch}) content as a function of depth for the $CaCO_3$-free (F1, F2, F3) and $CaCO_3$-bearing (B1, B2, B3) profiles.

Extraction efficiency of Ca increased in the order of H_2O < KCl ≈ Cohex < EDTA < $CuCl_2$. 2 M KCl extracted similar amounts of Ca as 0.0166 M Cohex at both sites, indicating that these two extracts effectively targeted the classical, exchangeable pool. The EDTA and $CuCl_2$ also extracted the exchangeable Ca pool at the $CaCO_3$-free site (Fig. 4.5), but extracted more Ca at the $CaCO_3$-bearing site, particularly in the samples with higher $CaCO_3$ contents.

4.3.3 - Multivariate exploration of texture and mineralogy

Correlation analysis (Fig. 4.7) showed that there was a strong positive correlation between $CaCO_3$ and total Ca. There was also a strong positive correlation between CEC_{SUM} and Ca_{Exch}. On the other hand, there was a strong anti-correlation between Ca_{Exch} / Ca saturation and Al_{Exch} / Al saturation. Strong anti-correlations were also detected between fine silt and fine sand / clay content, reflecting the fact that soil texture was dominated by silt populations, which exerted a 'dilution' effect (Bern, 2009) on other size classes (simplex behaviour). Total Mg and total Ca were also significantly anti-correlated with changes in total Si, which dominated major element composition, highlighting another 'dilution' effect.

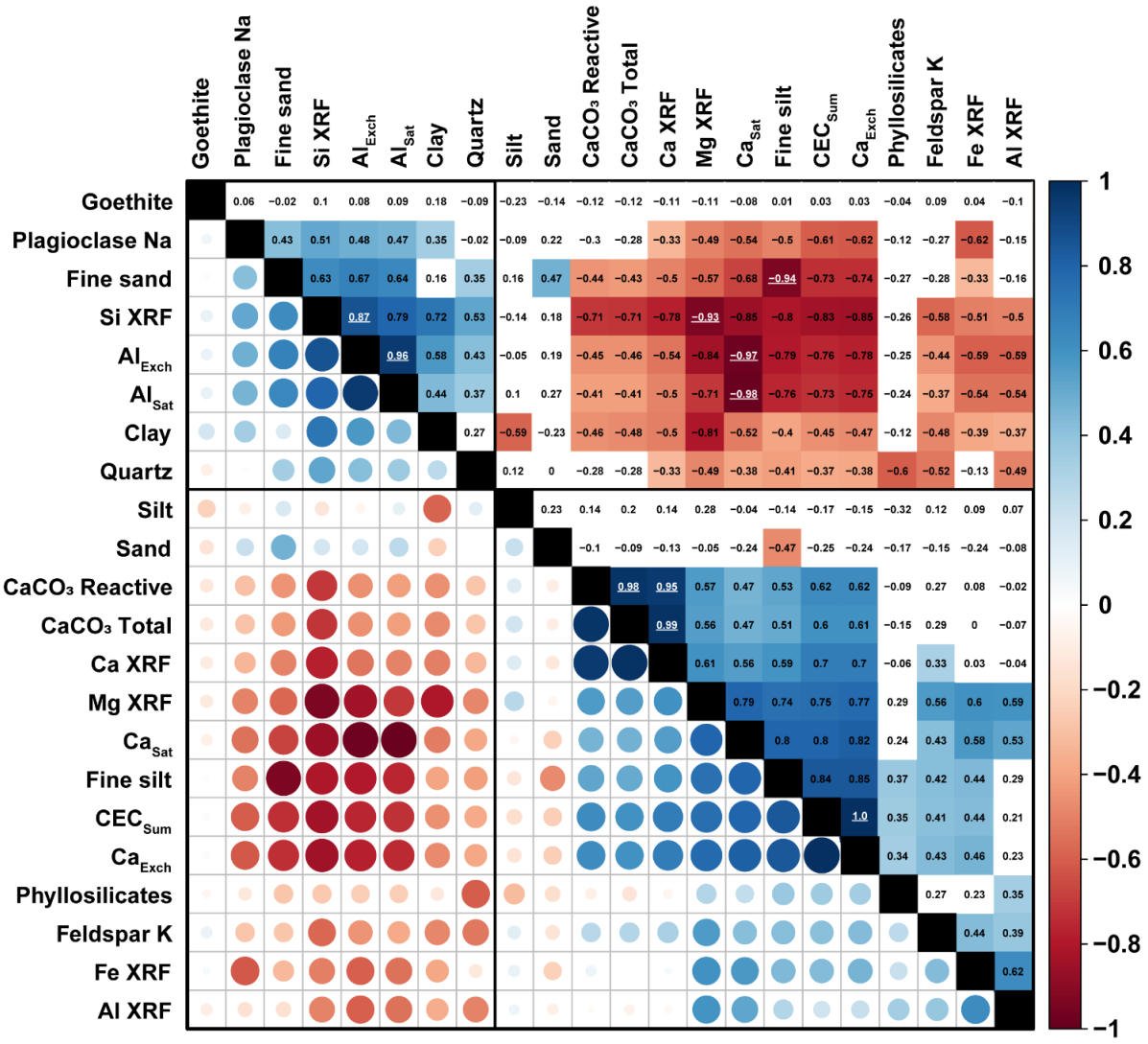

Fig. 4.7. Pearson's correlation coefficient matrix divided into two parts. The lower-left part represents the value of positive (blue) and negative (red) correlation coefficients as variations in circle size. The upper-right part displays the actual Pearson's correlation coefficients. Boxes in the upper-right part are only coloured in if the relationship is significant (α=0.05). Strong correlation coefficients are highlighted in white and underlined ($r > 0.85$). The different variables are hierarchically clustered using the complete-linkage method into two separate groups, highlighted with black rectangles in bold.

A PCA (Fig. 4.8 A) followed by a factor analysis (Fig. 4.8 B) demonstrated that sites were clearly split along multivariate factor 1 (Fig. 4.8 C). This factor represented the abundance of Ca (as shown by the correlation with total Ca, $CaCO_3$ and Ca_{Sat}) and the anti-correlation between total Ca / Mg and total Si / quartz. The second factor was a proxy for texture. There was no difference between sites along this factor, except for the fact that observations from the Ca-free site showed a higher dispersion (had both lower and higher scores than observations from the Ca-bearing site). Thus, overall differences in texture and silicate mineralogy were relatively small, but there were clear differences related to the presence or absence of $CaCO_3$, which differentiated the sites (Fig. 4.8 C).

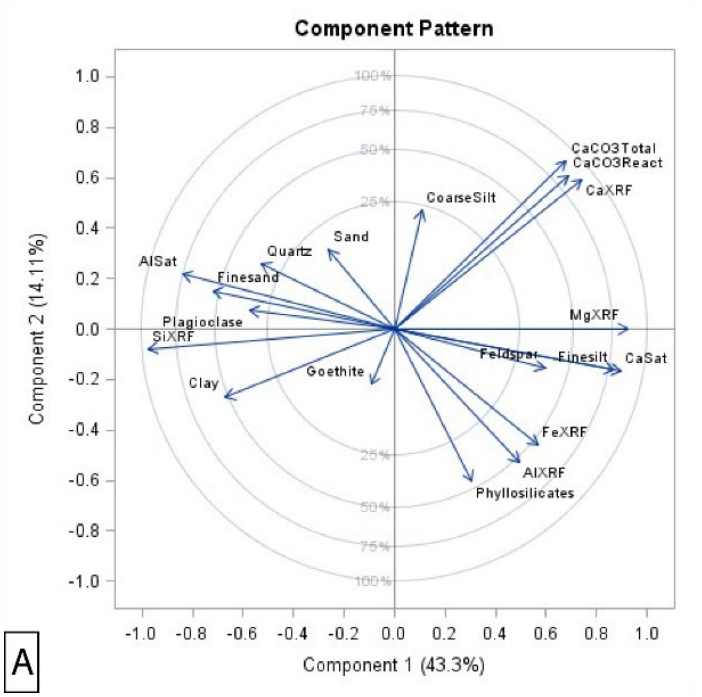
Component Pattern
CaCO3Total
CaCO3React
CaXRF
CoarseSilt
Sand
Quartz
AlSat
Finesand
MgXRF
Plagioclase
SiXRF
Feldspar
Finesilt
CaSat
Goethite
Clay
FeXRF
AlXRF
Phyllosilicates
Component 2 (14.11%)
Component 1 (43.3%)

A

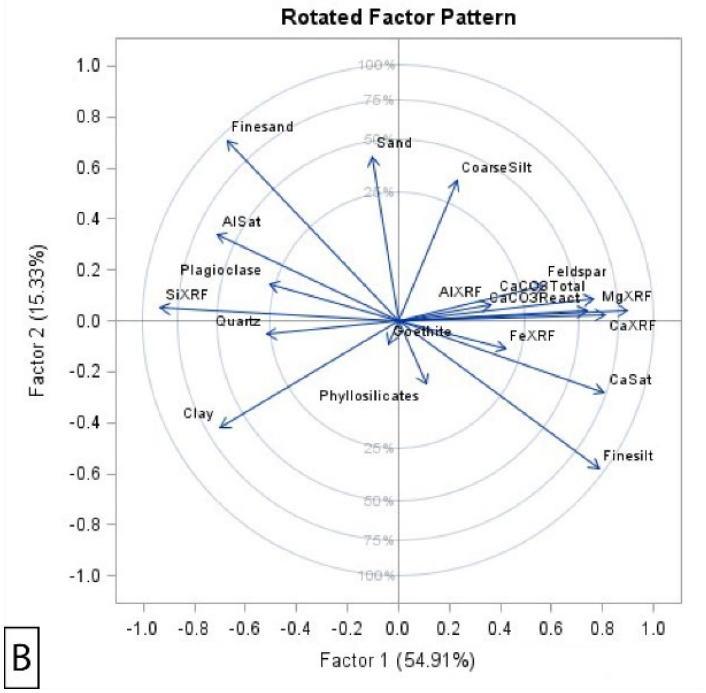
Rotated Factor Pattern
Finesand
Sand
CoarseSilt
AlSat
Plagioclase
Feldspar
AlXRF
CaCO3Total
CaCO3React
MgXRF
SiXRF
Quartz
CaXRF
Goethite
FeXRF
CaSat
Phyllosilicates
Clay
Finesilt
Factor 2 (15.33%)
Factor 1 (54.91%)

B

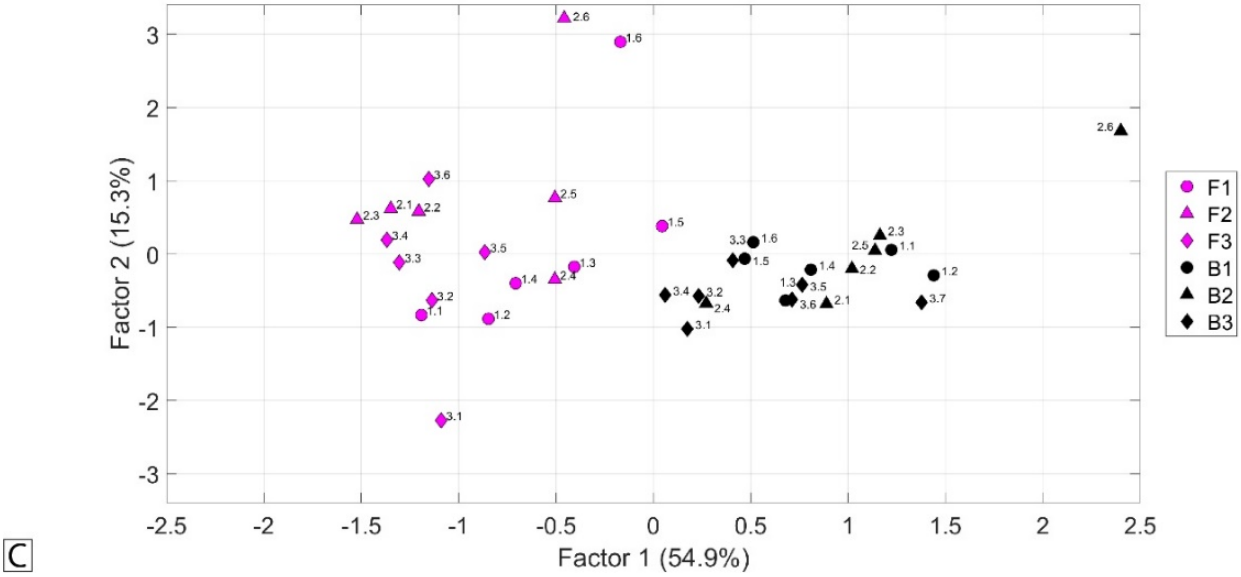

C

Fig. 4.8. Results of the principal component and factor analyses. Original variables included in the analyses were texture classes (content of clay < 2 µm, fine silt 2-20 µm, coarse silt 20-50 µm, fine sand 50-250 µm, and coarse sand 250 – 2000 µm), major elements (*e.g.*, AlXRF *etc*.), mineralogy, calcium and aluminum saturation of the exchange complex (Ca_{Sat} / Al_{Sat}). **A.)** Vector plot showing the relationships of original variables with the first and second principal components. The length of the arrow depicts the extent to which the variation in the original variable is represented in the principal components space while the direction of the arrow represents the strength of the positive or negative relation to the first or second components. Percentages indicate the amount of variance in the original dataset accounted for by each component. **B.)** Vector plot of the quartimax rotated factor pattern. Percentages indicate the amount of variance in the five-components space accounted for by each factor **C.)** Score plot of the first two factors. Observations are uniquely identified by colour (separating sites), profile number and depth interval.

4.3.4 - Organic matter and free Al / Fe

Al_o was lower at the $CaCO_3$-bearing site (1.5±0.2 g kg^{-1}) than at the $CaCO_3$-free (2.8±0.2 g kg^{-1}), and did not vary with depth. Al_o displayed a strong negative correlation with pH (Fig. 4.9; R^2=0.88). Al_d was generally equal to Al_o at the $CaCO_3$-bearing site, suggesting that dithionite and oxalate quantitatively extracted the same low-crystallinity Al pool. Al_d was however higher than Al_o at the $CaCO_3$-free site, suggesting that some Al substitution (Al incorporation into the crystalline lattice of Fe oxides dissolved by the dithionite treatment) had taken place.

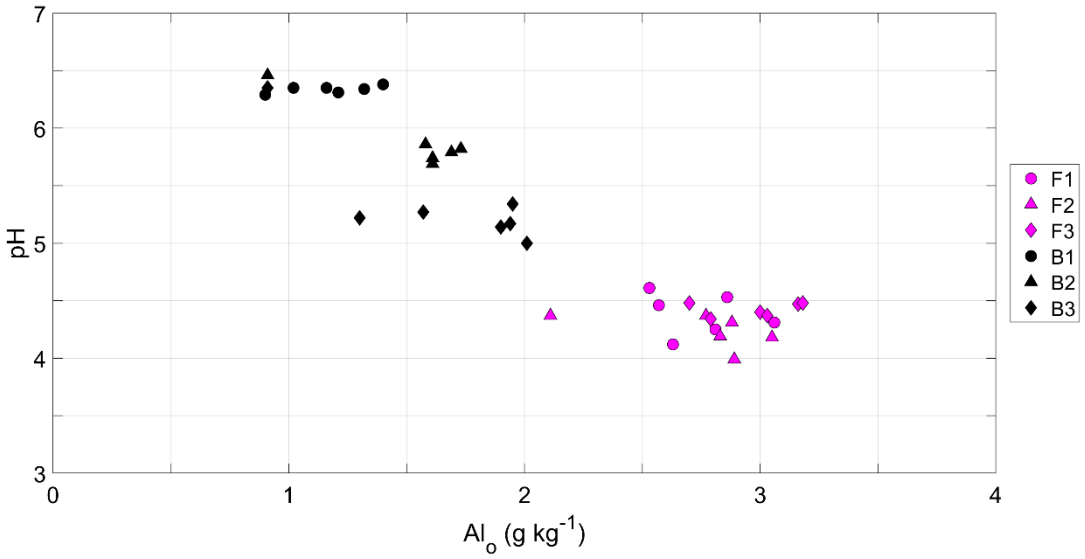

Fig. 4.9. Negative relationship between soil pH and oxalate extractable aluminium for $CaCO_3$-free (F1, F2, F3) and $CaCO_3$-bearing profiles (B1, B2, B3).

Extractable Fe was an order of magnitude higher than extractable Al at both sites. There was an effect of depth on the amount of Fe_o, which became larger mid-profile (15-20 cm). There was also a significant influence of depth on the proportion of oxalate-to-dithionite extractable Fe, which typically decreased with depth, except for samples at 15-20 cm (Fig. 4.10). Both dithionite and oxalate extractable Fe were higher at the $CaCO_3$-bearing site (Fe_d=25.3±0.3 g kg^{-1}; Fe_o=18.2±1.6 g kg^{-1}) than at the $CaCO_3$-free (Fe_d=22.7±0.4 g kg^{-1}; Fe_o=10.9±0.5 g kg^{-1}). The proportion of oxalate-to-dithionite extractable Fe was also higher at the $CaCO_3$-bearing site (0.73±0.06) than the $CaCO_3$-free (0.48±0.01). Thus, extractable Fe was more abundant and predominantly found in poorly crystalline or monomeric forms at the $CaCO_3$-bearing site.

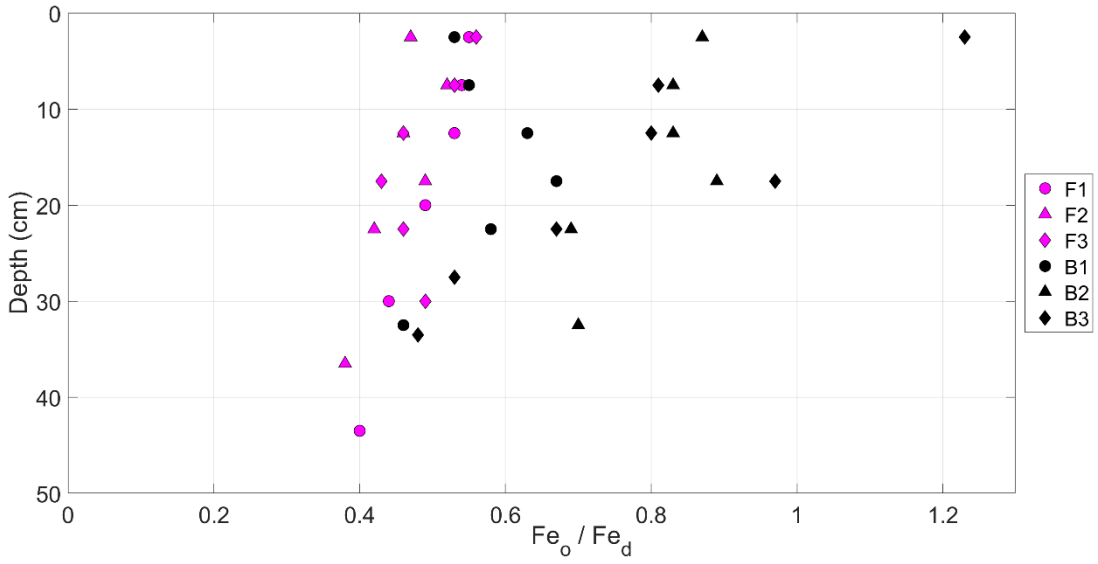

Fig. 4.10. Ratio between oxalate and dithionite extractable iron contents for $CaCO_3$-free (F1, F2, F3) and $CaCO_3$-bearing (B1, B2, B3) profiles.

Organic carbon contents of AGB were similar between the sites (Appendix Fig. 8.3). AGB estimates, reported in Blattner (2017), were 281 g m^{-2} at the $CaCO_3$-bearing sites and 350 g m^{-2} at the $CaCO_3$-free site. We thus calculated that above-ground C amounted to 110 g C m^{-2} at the $CaCO_3$-bearing site and 140 g C m^{-2} at the $CaCO_3$-free site.

In contrast, SOC was approximately twice as high at the $CaCO_3$-bearing site (5.2±0.2 %) compared to the $CaCO_3$-free soils (2.5±0.1 %), decreasing systematically with depth at both sites (Fig. 4.11). SOC decreased with depth more linearly at the $CaCO_3$-bearing site (RMSE of linear relationship=3.36) than at the $CaCO_3$-free (RMSE=6.76; Fig. 4.12 A:C). The distribution of residuals from the linear relationship between SOC and depth at the $CaCO_3$-bearing site were normally distributed (p=0.69), while the residuals at the $CaCO_3$-free site were not (p=0.02). Total nitrogen followed an almost identical pattern and was thus higher at the $CaCO_3$-bearing site (0.6±0.0 %) than at the $CaCO_3$-free (0.3±0.0 %). Total N also decreased systematically with depth. The C:N ratio was low at both sites (Fig. 4.13). It was slightly higher at the $CaCO_3$-bearing site (8.9±0.3) than at the $CaCO_3$-free site (7.2±0.3), but the differences were very small.

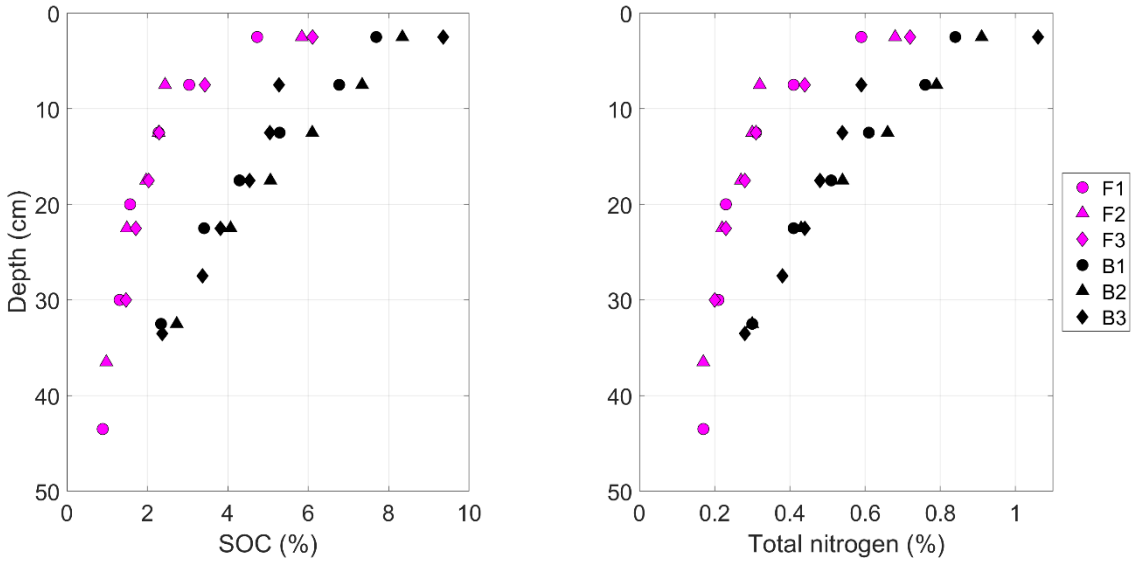

Fig. 4.11. Soil organic carbon and total nitrogen contents for $CaCO_3$-free (F1, F2, F3) and $CaCO_3$-bearing (B1, B2, B3) profiles.

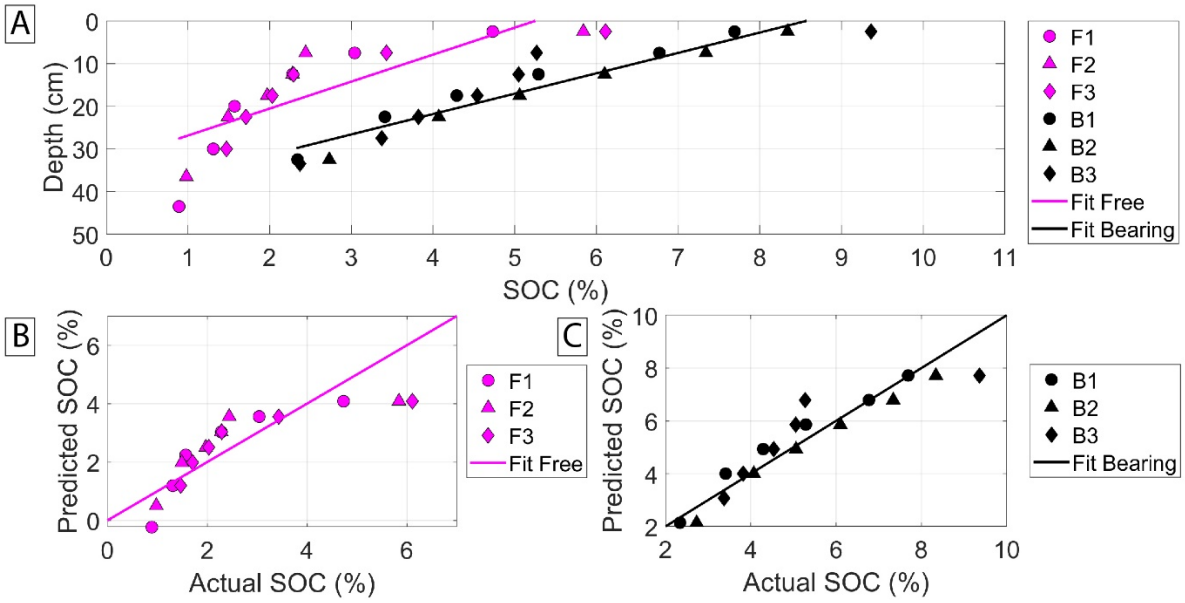

Fig. 4.12. Depth distribution of soil organic carbon (SOC) for the $CaCO_3$-free (F1, F2, F3) and $CaCO_3$-bearing (B1, B2, B3) profiles. **A)** Linear fits of SOC content as a function of depth. **B & C)** Actual versus predicted SOC contents for the $CaCO_3$-free **(B)** and $CaCO_3$-bearing **(C)** profiles, showing a clear lack-of-fit for $CaCO_3$-free profiles.

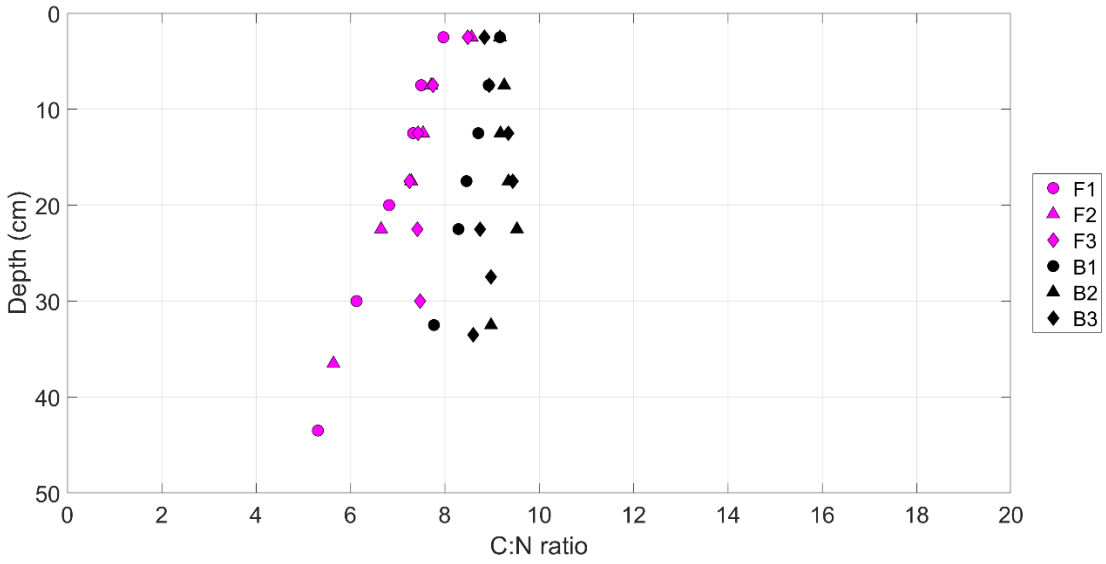

Fig. 4.13. Carbon to nitrogen ratio as a function of depth for the $CaCO_3$-free (F1, F2, F3) and $CaCO_3$-bearing (B1, B2, B3) profiles.

4.4 - Discussion

In this study, we aimed to determine the influence of small amounts of $CaCO_3$ on pedogenesis and biogeochemistry. We used a naturally occurring gradient in $CaCO_3$ content affecting otherwise highly similar soils. With the constraints of finding near-identical soil forming conditions, we retained only 6 profiles, which were all located in close proximity (< 500 m). With such a low sample size, two things must be kept in mind:

i) The generalisation of findings to other soils is not supported by this experimental layout (but remains possible if a detailed mechanistic understanding is attained).
ii) Only large effects could be statistically detected.

It was of prime importance that the soils be similar except for the presence / absence of $CaCO_3$, in order to isolate the role of $CaCO_3$ from other pedogenic variables. Homogeneity of parent material was of particular importance and is discussed further below.

4.4.1 - Parent material

Textural analysis confirmed field observations that the parent material was homogeneous, with all samples plotting within the silt loam class. Both sites had 6 predominant textural populations, the modes of which are commonly encountered in previously glaciated landscapes (Boulton, 1978). The total composition of major elements were also similar between the sites. Relatively immobile elements such as Ti and other transition / post-transition metals showed near-uniform distribution between samples from different profiles, collected at different depths, pointing to a common source for parent materials. There was however a clear increase in Ca at the $CaCO_3$-bearing sites due to the presence of $CaCO_3$. This increase in Ca also caused a proportional decrease in Si (silicates) due to a ‘dilution’ effect. The slightly

higher Mg content at the $CaCO_3$-bearing site could be due to partial substitution of Mg for Ca in calcite (0.3 % in measured coarse fragments) or the presence of poorly crystalline dolomite and accessory ferromagnesian minerals. P was also slightly elevated at the $CaCO_3$-bearing site, which could be a reflection of its lower mobility in Ca-bearing geochemical environments (von Wandruszka, 2006). K was marginally higher at the $CaCO_3$-bearing site and Na was higher at the $CaCO_3$-free site, which corresponded to small differences in K-feldspar and Na-plagioclase abundances, respectively. Neoformation of pedogenic clay was incipient at both sites, with only small quantities of an illite-vermiculite mixed-layer mineral detected (Egli et al., 2003; Zollinger et al., 2013). Most of the phyllosilicates originated from the physical disintegration of shale components of the Morcles Nappe.

While the siliceous component of the parent material at the two sites was near-homogeneous, there was a natural variation in $CaCO_3$ present at the alpage. This was likely due to the variability in $CaCO_3$ content of surficial deposits issued from the Morcles Nappe. The Grand Muveran cliffs protruding on the southeast side of the study area contain calcareous material, while the slopes of La Chaux on the northwest side essentially consist of shales. Thus, during the partial alluvio-colluvial reworking of the moraine and slope deposits that occurred following deglaciation, some carbonates were added to the $CaCO_3$-bearing site while little to no carbonates were added to the $CaCO_3$-free site.

$CaCO_3$ was identified as being predominantly reactive at the Nant Valley (Fig. 4.4) by the adapted Loeppert et al. (1984) method. This method is not typically used for the measurement of reactive carbonates, but its results were in reasonable agreement with the EDTA extraction (Appendix Fig. 8.4), which has been used previously used for the estimation of reactive carbonates (Glover, 1961). Thus, $CaCO_3$ was most likely predominantly reactive at the $CaCO_3$-bearing site, increasing the likelihood that it would play an active role in soil biogeochemistry.

Another difference between the sites was that free Fe forms were significantly less crystalline at the $CaCO_3$-bearing profiles, relative to the $CaCO_3$-free profiles. The sorption of organic colloids (Filimonova et al., 2016; Kleber and Jahn, 2007) and cations such as Ca_{Exch} (Thompson et al., 2011), which were more abundant at the $CaCO_3$-bearing site, could also have inhibited the formation of well-crystallised Fe forms. Furthermore, pH may have also indirectly influenced the crystallinity of Fe forms via its influence on their variable surface charge and their interaction with Ca_{Exch} (Schwertmann and Fechter, 1982), but this would still require further investigation. While the presence of $CaCO_3$ seemed to indirectly favour the prevalence of disordered Fe forms, the Fe_o/Fe_d ratio did not vary systematically SOC, Ca_{Exch} or pH making it hazardous to attribute the differences in crystallinity to a single factor. It seems more likely that a mixture of indirect influences of $CaCO_3$ (SOC, Ca_{Exch} and pH) were involved in explaining the decreased crystallinity of Fe forms at the $CaCO_3$-bearing site (Fig. 4.14 A).

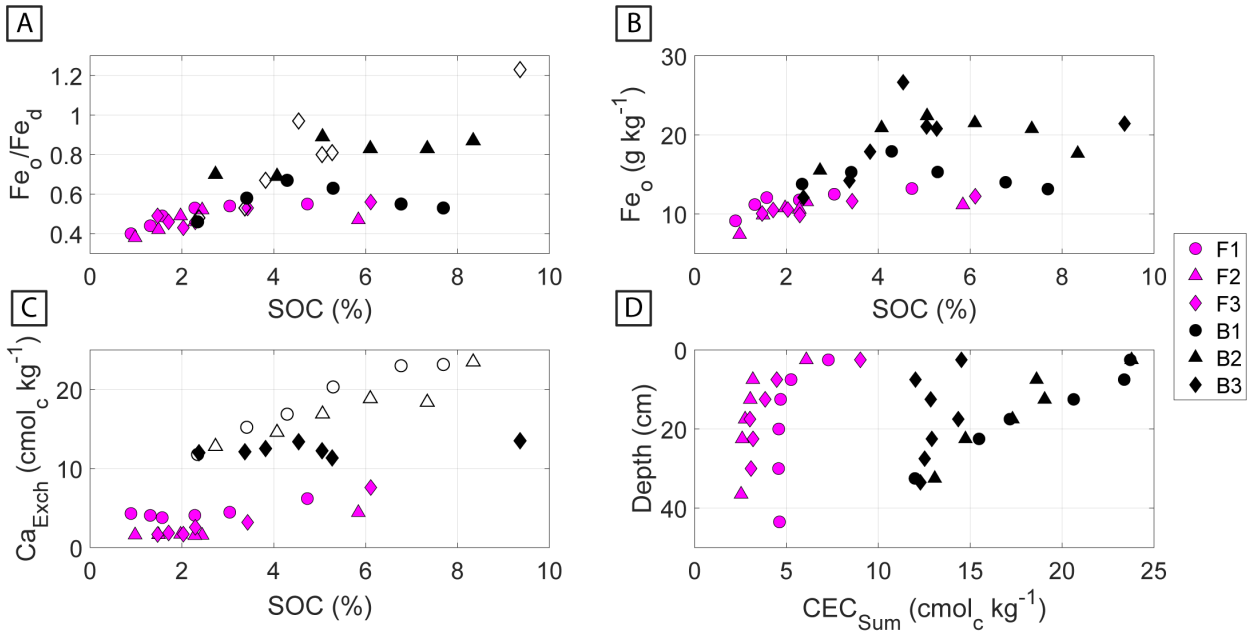

Fig. 4.14. Relationships between several edaphic variables at the $CaCO_3$-free (F1, F2, F3) and $CaCO_3$-bearing (B1, B2, B3) profiles. **A)** Relationship between the ratio of oxalate to dithionite extractable iron contents (Fe_o/Fe_d) and soil organic carbon (SOC). **B)** Relationship between oxalate extractable iron (Fe_o) and SOC. **C)** Relationship between exchangeable Ca (Ca_{Exch}) and SOC. **D)** Depth profile of cation exchange capacity (CEC_{Sum}). In panels **A & C**, profiles showing the strongest positive correlation between the dependent variable and SOC are represented by hollowed symbols.

4.4.2 - Accumulation of SOC

Soil organic carbon was approximately twice as high at the $CaCO_3$-bearing site compared to the $CaCO_3$-free site. A potential explanation for this accumulation could involve the higher primary productivity of grasses at the $CaCO_3$-bearing site. Yet, AGB was slightly higher at the $CaCO_3$-free site relative to the $CaCO_3$-bearing site. Increased root turnover or exudation at the $CaCO_3$-bearing site could explain part of the differences in SOC, but this effect should be relatively small due to the similarities between vegetation structure at the sites (Vittoz and Gmür, 2008). Instead, it was probably the difference in the efficiency of SOC stabilisation that drove the relative accumulation of SOC observed at the $CaCO_3$-bearing site.

In a previous study, Grand et al. (2016) demonstrated that soil respiration was higher at the $CaCO_3$-bearing site than the $CaCO_3$-free site for three out of four of the measured months (July-Oct.); yet estimated heterotrophic respiration (Hanson et al., 2000) was actually lower throughout the entire measurement period, when expressed per unit SOC (Appendix Table 8.3). This suggests that SOC at the $CaCO_3$-bearing site has a certain biogeochemical stability, which may be contributing towards its accumulation (Whittinghill and Hobbie, 2012). Due to similarities between the sites, this stability cannot be explained by differences in texture or clay mineralogy. Potential geochemical controls that could

influence the accumulation of SOC at the Nant Valley include the prevalence of reactive Ca and Fe forms, which are discussed further below.

4.4.2.1 - Reactive Ca forms

We found a weak positive correlation between Ca_{Exch} and SOC at our sites (Fig. 4.14 C), which was particularly evident in the $CaCO_3$-bearing profiles with higher pH and Ca_{Exch}. CEC_{sum} was also higher at the $CaCO_3$-bearing sites (Fig. 4.14 D); this was partly attributable to the higher SOC content acting as loci for cation exchange, as clay mineralogy and texture were homogeneous at the sites. Thus, the commonly observed correlation between SOC and Ca_{Exch} could partially be explained by the increase in cation exchange sites provided by SOC (Briedis et al., 2012a). However, there is evidence that Ca can also influence SOC cycling (Groffman et al., 2006; Hobbie et al., 2002; Martí-Roura et al., 2019; Minick et al., 2017; Whittinghill and Hobbie, 2012) through several mechanisms (see Rowley et al., 2018 for more details). In our study, the two-fold increase in SOC at the $CaCO_3$-bearing site supports the hypothesis that reactive Ca is causally linked to the accumulation and stabilisation of SOC. Future investigation should focus on the mechanisms through which Ca influences SOC.

4.4.2.2 - Analysing Ca forms

Exchangeable Ca may not be the only reactive Ca pool that influences SOC. It has been hypothesised that Ca could also stabilise SOC through inner sphere complexes (Rowley et al., 2018). This is supported by chemical modelling (Iskrenova-Tchoukova et al., 2010; Kalinichev and Kirkpatrick, 2007; Sutton et al., 2005), but as of yet, there is no direct evidence of this in soils. We attempted to extract more tightly bound, 'chelated Ca' pool using selective extractions, as has been done with the selective dissolution of free Fe and Al. Our more aggressive extracts, EDTA and $CuCl_2$, yielded the same quantity of Ca as the exchangeable cations extracts (KCl / Cohex) at the $CaCO_3$-free site, but more Ca than the exchangeable cations extracts at the $CaCO_3$-bearing site. This was particularly apparent in samples with higher amounts of $CaCO_3$ and it thus seems as though both EDTA and $CuCl_2$ were aggressive towards reactive $CaCO_3$, but failed to target Ca pools other than the exchangeable pool at $CaCO_3$-free sites. Thus, the existence in soils of a tightly-bound Ca pool which is distinct from reactive $CaCO_3$, and its selective extraction, remains an open question.

4.4.2.3 - Fe forms

It is widely established that poorly crystalline Fe forms can stabilise SOC (Kögel-Knabner et al., 2008; von Lützow et al., 2006). In our study, SOC displayed a weak positive correlation with Fe_o, which was particularly evident in the profiles with the highest amounts of extractable Fe (Fig. 4.14 B). The same trend was observed for the degree of crystallinity of Fe oxides (Fe_o/Fe_d; Fig. 4.14 A), as the amount of crystalline oxides was comparatively similar between profiles and it was mainly the amount of Fe_o that changed. The $CaCO_3$-bearing profiles displayed an increase in Fe_o/Fe_d ratio mid-profile (15-20 cm; Fig. 4.10), potentially due to the mobility of poorly crystalline Fe species during brief suboxic events linked

to snowmelt. It is possible that this pattern had some influence over the more linear SOC decline with depth at these sites (Fig. 4.12 A:C). Overall, our results support a positive relation between SOC accumulation and the amount of poorly crystalline Fe.

4.4.2.4 - Ca and Fe interactions

It is interesting to note that our data hint at some kind of interaction or competition between Ca and Fe forms (Fig. 4.14 A:D). Profiles B1 and B2 showed no association between SOC and Fe_o but were instead characterised by a strong correlation between SOC and Ca_{Exch}. On the contrary, in profile B3, where pH and $CaCO_3$ were slightly lower than in the other $CaCO_3$-bearing profiles, SOC was significantly related to Fe_o and much less so to Ca_{Exch}. Speculatively, we propose that some organic functional groups may interact either with exchangeable cations or with reactive oxides depending on the prevailing biogeochemical conditions (pH and the prevalence of free elements), which may lead to a change in the relative importance of SOC stabilisation mechanisms (Rasmussen et al., 2018; Rowley et al., 2018).

Furthermore, a synergistic stabilisation of dissolved organic C by poorly crystalline Fe and Ca_{Exch}, involving the formation of Fe-Ca-organic C ternary complexes, has recently been described (Sowers et al., 2018a; Sowers et al., 2018b). Hypothetically, this could also have exerted a positive feedback on the stabilisation of SOC at the $CaCO_3$-bearing sites (Fig. 4.15 A:D), as disordered Fe forms that are favoured by the higher SOC, Ca_{Exch} and pH would in turn further contribute to an accumulation of SOC, rendered particularly effective by the presence of significant amounts of extractable Ca. This potential relationship between Ca and Fe and its impacts on SOC stabilisation and accumulation should now be investigated further in Ca-rich soils.

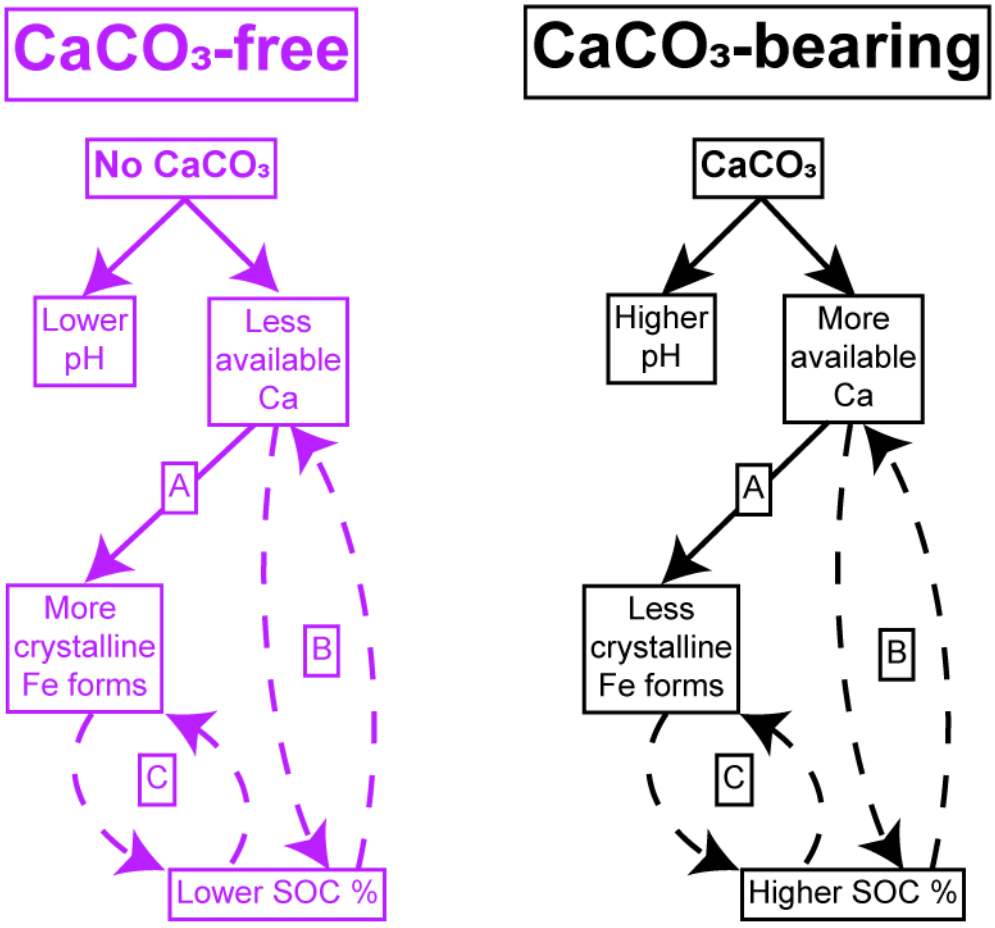

Fig. 4.15. A conceptual diagram of differences in biogeochemical properties at the $CaCO_3$-free and $CaCO_3$-bearing sites, attributable to the cascading influence of calcium carbonate. Direct one or two-ways interactions between geochemical variables are signified by straight arrows, while potential positive / negative feedback systems are signified by curved dashed arrows. The numbered interactions refer to: **A)** calcium (Ca)-Fe interactions, where sorption of Ca by Fe oxides can prevent their further crystallisation (Thompson et al., 2011). **B)** Soil organic carbon (SOC)-Ca feedback loop, where SOC can be directly stabilised by Ca (Rowley et al., 2018), while SOC also provides exchange sites for the continued retention of available Ca forms. **C)** Fe-SOC feedback loop, where poorly crystalline Fe forms retain and stabilise SOC, while SOC can also inhibit the crystallisation of Fe forms (Kleber and Jahn, 2007).

4.4.3 - Implications for modelling efforts

There is growing evidence that geochemical indicators are important parameters for modelling the persistence of SOC (Rasmussen et al., 2018; Vaughan et al., 2019). Indeed, models that infer the cycling of SOC from clay content and climate would be unable to represent the difference in SOC content attributed here to the presence or absence of $CaCO_3$. Rasmussen et al. (2018) recently questioned the use of clay and climate as sole variables for modelling SOC and our results are in close agreement with their

broader analysis of 5,500 soil profiles. Models based on climate and clay content may be particularly inappropriate in situations where soil geochemistry is in disequilibrium with climate (occurrence of pedogenic inertia) and / or variations in types and crystallinity of Fe phases exist. Furthermore, modelling the depth distribution of SOC using an exponential decay function would have also misrepresented the different SOC-depth trends present at the sites, further underestimating SOC stocks at the $CaCO_3$-bearing site. These errors could however be reduced by accounting for differences in soil geochemistry and their subsequent effects on the accumulation of SOC and its depth distribution.

4.4.4 - Synthesis - Cascading biogeochemistry

The divergence in biogeochemistry at the Nant Valley sites is caused by a state of pedogenic inertia, driven by the cascading influence of $CaCO_3$ dissolution (Fig. 4.17). The $CaCO_3$-bearing site exists in a state of disequilibrium with climate as the pedogenic threshold of $CaCO_3$ removal has not yet been breached. This threshold is unlikely to be breached in the near-future, due the presence of the adjacent calcareous cliffs and their alluvio-colluvial inputs, so that the site will likely continue to retain its Mollic nature, high pH, and base saturation (Phaeozem).

Upon weathering, reactive $CaCO_3$ buffered pH levels (Likens et al., 1998), releasing Ca_{Exch} into the soil solution. This Ca_{Exch} can stabilise SOC (Oades, 1988; Rowley et al., 2018), which likely contributed to its accumulation in the $CaCO_3$-bearing profiles (x2). The presence of $CaCO_3$ also seemed to indirectly participate in the stabilisation of poorly crystalline Fe forms, which in turn, may have exerted a positive feedback on the retention of SOC, possibly involving ternary Fe-Ca-SOC complexes (Sowers et al., 2018a; Sowers et al., 2018b).

In contrast, the $CaCO_3$-free profiles had a lower pH. These acidic conditions in turn seemed to favour the prevalence of more crystalline Fe oxides such as goethite and higher amounts of reactive Al forms such as Al_{Exch} and Al_o (Adams et al., 2000). This confirms the long-held notion that decreasing soil pH identifies a shift along a weathering sequence from Ca-to-Al dominated biogeochemistry (Adams et al., 2000; Slessarev et al., 2016). In turn, this shift can be linked to different SOC stabilisation mechanisms (Rasmussen et al., 2018; Rowley et al., 2018), which could be used to help model the persistence of SOC. Thus, this study further supports the notion that soil pH could be used as an efficient and parsimonious variable for improving regional models of pedogenesis, biogeochemical functioning, and even SOC stabilisation (Clarholm and Skyllberg, 2013; Rowley et al., 2018). Future studies should investigate the potential of soil pH as a widely available indicator to account for the effects of geochemistry on SOC and improving the accuracy of regional SOC estimates.

- End of publication -

Chapter 4 - Opening perspectives

This chapter has demonstrated that small amounts of $CaCO_3$ could have a far-reaching impact on the pedogenesis and biogeochemistry of humid environments like the Nant Valley. Now we must focus on evaluating why the $CaCO_3$-bearing site contained a two-fold increase in SOC and what mechanisms could be responsible for this increase. One way to further evaluate the differences in SOC between the sites is to fractionate soil samples into different SOC pools, representative of different forms of stabilisation. This will enable us to evaluate how much SOC is stabilised by these different SOC stabilisation mechanisms at the sites and how its properties change within these pools.

Following Chapter 3, we could expect that a proportion of the SOC accumulation that we witnessed in Chapter 4 is caused by Ca-mediated aggregation and subsequent occlusion of SOC. We can thus hypothesise that occluded SOC, separated by a density fractionation with sequential sonication, will be more abundant at the $CaCO_3$-bearing site. Furthermore, this occlusion could cause a shift in bulk SOC $\delta^{13}C$ values by physically preventing it from being oxidatively transformed. The next chapter will seek to investigate this hypothesis and the mechanisms that led to a two-fold increase in SOC at the $CaCO_3$ bearing site.

This page is left intentionally blank

- Chapter 5: The influence of Ca on soil organic carbon at the Nant Valley, Switzerland -

The following chapter is an un-submitted draft manuscript. It will eventually be submitted to Biogeochemistry© or SOIL©. Most of the supplementary figures from it have been included in this chapter, but several method-based supplementary figures and all the supplementary tables have been included in the appendices section (8.1.2).

- Research question Chapter 5 -

The following question and sub-questions will be addressed in this chapter:

How does SOC differ at the sites with or without $CaCO_3$ at the Nant Valley?

a. How does bulk SOC content and stable C isotopic composition differ at sites that have formed under similar soil forming conditions with or without $CaCO_3$?
b. Does occlusion play a larger relative role in accumulation of SOC in soils with $CaCO_3$, relative to those without?
c. Is there more mineral-associated SOC in the soils with $CaCO_3$, relative to those without?

- Chapter 5 abstract -

Geochemical indicators are emerging as important predictors of SOC and its cycling, but evidence of the influence of Ca on SOC is still scarce. This study investigated the role of $CaCO_3$ in SOC accumulation at otherwise similar sites with ($CaCO_3$-bearing) and without $CaCO_3$ ($CaCO_3$-free) in a humid subalpine valley. To isolate the role of occlusion from sorption, we fractionated samples from three profiles at each site into 4 individual fractions by density and sequential sonication (a free-light fraction, two occluded fractions separated at 10 and 200 J mL^{-1} sonication, and a heavy fraction). The SOC content, mass, stable C isotope composition ($\delta^{13}C$) and surficial chemical properties (X-ray photoelectron spectroscopy) of these separate fractions were then quantified. Our hypothesis was that Ca-mediated occlusion would play a more dominant role at the $CaCO_3$-bearing site, physical protecting SOC and preventing it from acquiring the higher $\delta^{13}C$ signature, generally associated with microbial activity.

Bulk SOC was twice as high and had lower $\delta^{13}C$ values at the $CaCO_3$-bearing site, relative to the $CaCO_3$-free site. There was also always more occluded material at the $CaCO_3$-bearing site, likely caused by the positive influence of the flocculation of soil separates by Ca_{Exch} and the increased presence of SOC on aggregation. However, contrary to our hypothesis, occluded SOC at the $CaCO_3$-bearing site was more oxidatively transformed than at the $CaCO_3$-free site and both the free-light and occluded pools played a minimal role in bulk SOC content at either site. It was instead the heavy fractions (HF) that were of clearer importance to bulk SOC content due to their larger relative masses.

The mass of mineral-associated SOC was twice as high at the $CaCO_3$-bearing site, relative to the $CaCO_3$-free site. The $CaCO_3$-free site displayed an increase in $\delta^{13}C$ values from the light fractions (LFs; free-light and occluded) to the HF, typically associated with the preferential sorption of microbial biomass by Fe oxides. Contrastingly, the $CaCO_3$-bearing site had similar $\delta^{13}C$ values in the LFs and the HF, which likely arose from two complementary mechanisms. Firstly, the $\delta^{13}C$ values and X-ray photoelectron spectroscopy (XPS) C_{1s} peak deconvolution imply that the LFs were more oxidatively transformed at the $CaCO_3$-bearing site. This was probably caused both by the better biogeochemical conditions for the oxidation of the LFs at the $CaCO_3$-bearing site and the lesser degree of mineral coating of the LFs at this site. Secondly, mineral-associated SOC also tended to have lower $\delta^{13}C$ values at the $CaCO_3$-bearing site. This was likely related to the flocculation, precipitation, and accumulation of dissolved organic carbon (DOC) with a fresher signal by Ca_{Exch} in organo-mineral association (OMA), which would have also contributed to the increased mass of SOC in the HF.

Future research should now attempt to decipher Ca-mediated OMA in similar Ca-bearing environments with advanced spectroscopy, investigating the exact mechanisms that drive a near two-fold increase in OMA.

5.1 - Introduction

Soil geochemical properties are emerging as an important predictor of SOC content and cycling, yet empirical data on how this role changes in different environments is still scarce. It is well established that Fe and Al forms can stabilise SOC (Kögel-Knabner et al., 2008; Torn et al., 1997). Moreover, Ca forms can also play a role in SOC accumulation and cycling (Martí-Roura et al., 2019; Oades, 1988; Rasmussen et al., 2018), mediating a stabilisation of SOC through several mechanisms (Rowley et al., 2018). Ca is thought to indirectly contribute to the accumulation of occluded SOC through the flocculation of soil separates and its subsequent promotion of aggregation (Muneer and Oades, 1989c; Oades, 1984; Oades, 1988). While, outer sphere polyvalent cation bridging (Clough and Skjemstad, 2000; Edwards and Bremner, 1967) and other sorption processes (Kalinichev and Kirkpatrick, 2007; Sutton et al., 2005) mediated by Ca are also thought to play a significant role in the accumulation of SOC. It has been recently demonstrated that Ca can have a synergistic effect on the sequestration of SOC by ferrihydrite (Sowers et al., 2018a; Sowers et al., 2018b), which may be particularly prevalent in Ca-rich environments (Chapter 4). However, few studies have attempted to quantify the role of these different mechanisms in SOC accumulation in soils with a variation in Ca content.

Stable C isotope compositions ($\delta^{13}C$ values) could aid in further investigating the role of these mechanisms in natural systems. Previous investigation at the Hubbard Brook experimental site has demonstrated that bulk SOC $\delta^{13}C$ values are lower after Ca-addition, relative to similar, adjacent soils with less Ca_{Exch} (Minick et al., 2017). The $\delta^{13}C$ values of SOC typically increase by approximately 1-3 ‰ with depth, which is linked to a fractionation by the activity of microorganisms (Boström et al., 2007; Hobbie et al., 1999). Increased protection of SOC within aggregates, as demonstrated in Ca-bearing environments (Muneer and Oades, 1989c), should prevent this ^{13}C fractionation by physically separating microorganisms from SOC. Thus, the relative decreases in bulk ^{13}C values measured by Minick et al. (2017) could have been indicative of the physical protection of SOC within aggregates flocculated by Ca (Chapter 3). However, this hypothesis still requires testing, fractionating and analysing the occluded SOC pool in otherwise similar soils with a natural variation in Ca_{Exch}.

Soil organic carbon stabilisation has typically been investigated in Fe and Al rich soils by fractionating bulk soil samples into individual components or pools, predominantly by size or density fractionation. Yet, few studies have attempted to fractionate soils of a Ca-bearing nature, due in part, to the complicated nature of investigating SOC cycling in $CaCO_3$-containing soils (Rovira et al., 1998). Martí-Roura et al. (2019) recently used size fractionation to successfully investigate SOC in top soils with or without $CaCO_3$ under several land uses. Their study demonstrated that SOC was higher in the carbonated forest soils, which also, unlike the sites without, displayed similar $\delta^{13}C$ values in the coarse and fine fractions. Several studies have used density fractionation on neutral soils, including dolomitic soils (Kreyling et al., 2013) or reclaimed industrial soils (Grünewald et al., 2006). Schrumpf et al. (2013)

measured several calcareous soils in their detailed study, but did not isolate the differences between $CaCO_3$-free and $CaCO_3$-bearing samples. More recently, Wen et al. (2017) utilised density fractionation to analyse differences between SOC of dolomitic and calcaric soils, but bulked the occluded and free-light fractions, thus preventing the analysis of the occluded pool. Ca-bearing soils have long been thought to impact SOC through occlusion, thus further investigation with density fractionation is still required to isolate the role of occlusion in soils with a natural variation in Ca.

Chapter 4 demonstrated that $CaCO_3$, derived from alluvio-colluvial inputs from the adjacent mountain range, had a cascading influence on the biogeochemistry of soils, formed under near-identical conditions for pedogenesis (similar climate, parent material, vegetation structure, relief, and time since deglaciation) at the Nant Valley, Switzerland. This cascading influence included a direct increase in soil pH and an order of magnitude higher Ca_{Exch} in profiles with $CaCO_3$ ($CaCO_3$-bearing; 16.1±2.1 $cmol_c\ kg^{-1}$) relative to those without $CaCO_3$ ($CaCO_3$-free; 3.2±0.8 $cmol_c\ kg^{-1}$). The $CaCO_3$-bearing site also presented a higher proportion of poorly crystalline Fe forms ($CaCO_3$-bearing 73±6 % versus $CaCO_3$-free 48±1 %), which were linked to the higher SOC and Ca_{Exch} content, known to inhibit the crystallisation of ferrihydrite to goethite (Kleber and Jahn, 2007; Thompson et al., 2011). The $CaCO_3$-bearing site contained twice as much SOC (5.21±0.16 %) as the $CaCO_3$-free site (2.54±0.11 %), which was not linked to vegetation, climatic or textural differences between the sites. Due to the otherwise similar nature of these soils and their natural variation in Ca, increased occlusion, mediated by Ca may be contributing to the higher bulk SOC content of the $CaCO_3$-bearing site.

In order to isolate the potential role of occlusion in soils with a natural variation in Ca, three profiles from the $CaCO_3$-bearing and $CaCO_3$-free site were fractionated by density and sequential sonication into four individual fractions (a free-light fraction, two occluded-light fractions separated at 10 and 200 J mL^{-1} sonication and a heavy fraction), in triplicate. The SOC content, mass, $\delta^{13}C$ composition of all these fractions, and the surficial chemical composition and bonding environment of C in a subset of these fractions were then quantified to investigate differences in SOC at the sites. Our hypothesis was that the flocculation of soil separates by Ca_{Exch} would cause relative increases in occluded SOC at the $CaCO_3$-bearing site, inhibiting the oxidative transformation of occluded material. Furthermore, we hypothesised that this inhibition caused the accumulation of SOC at this site and would result in lower bulk $\delta^{13}C$ values.

5.2 - Materials and methods

5.2.1 - Site description and sampling

This study was completed in the Nant Valley (573'000, 119'000 CH1903 LV03), a partially-glaciated alpine watershed in the Vaud Alps, Switzerland. The valley is situated on the Morcles nappe, which consists of Jurassic and Cretaceous shallow-water limestones intercalated with marl and shale deposits (Austin et al., 2008). These variations in the composition of the Morcles Nappe, ensure that there are

natural variations in the amount of $CaCO_3$ in the soils of the valley. Sampling took place in the rangeland (the alpage; Fig. 4.1) described in detail by several studies (Grand et al., 2016; Vittoz and Gmür, 2008). The alpage is approximately 1500 m above sea level, receives 1800 mm yr^{-1} precipitation, and has a mean annual temperature of 6°C (Vittoz and Gmür, 2008).

Two sampling sites were selected at the alpage after field-testing with 10 % HCl demonstrated the presence or absence of $CaCO_3$ (0-6.2 %). The texture, silicate mineralogy, and elemental composition of the sites have been previously analysed and described in detail (Chapter 4) and were highly similar. Three profiles were dug at each sampling site in July - August (Fig. 4.1; IUSS Working Group WRB, 2015) and were characterised as Eutric Cambisols (siltic) with no $CaCO_3$ ($CaCO_3$-free; F1, F2, F3) and Cambic Phaeozems (siltic) with small (< 6.2 %) quantities of $CaCO_3$ ($CaCO_3$-bearing; B1, B2, B3). Profiles were sampled at 6-7 depth intervals and labelled from 1 to 6 / 7 with increasing depth (*e.g.*, F1.1-to-F1.6) before being transported to the University of Lausanne in sealed bags. Bulk density measurements were made at three equally spaced depths at a randomly selected profile from each site (P3 & R3) according to Wiesmeier et al. (2012). Both above- and below-ground biomass (AGB and BGB, respectively) were randomly sampled from the sites to quantify potential differences in the $\delta^{13}C$ values of the vegetation.

5.2.2 - Sample preparation

Samples were air-dried and sieved to 2 mm. Subsamples of bulk samples were crushed to a fine powder for 3 min using a vibrating-disc mill and agate crucible (van Reeuwijk, 2002). $CaCO_3$ was removed from crushed bulk samples by HCl fumigation and corrected for changes in mass (Harris et al., 2001). Samples typically gained a little weight, which was caused by Cl^- sorption (Ramnarine et al., 2011). AGB and BGB samples were oven dried (40°C), ground by hand and homogenised for further analysis.

5.2.3 - Lab analysis

Quality control procedures included the analysis of an internal standard when appropriate, as well as the inclusion of blanks and quality checks. All plastic and glassware were acid washed (3 M HCl) to remove trace contamination.

5.2.3.1 - Density fractionation

Individual SOC pools were fractioned by density and sequential sonication using SPT (Na-polytungstate; Sometu-Europe). These pools included a free-light fraction (f-LF), two occluded-light fractions separated at 10 J mL^{-1} and 200 J mL^{-1} sonication energies (o-LF_{10} and o-LF_{200}, respectively), and finally, a heavy fraction (HF; Golchin et al., 1994; Poeplau et al., 2018; Viret and Grand, 2019). 7 g of soil were combined with 35 mL 1.6 g cm^{-3} SPT in 50 mL centrifuge tubes and inversed thoroughly to liberate the f-LF fraction. Samples were then left to repose for 30 min before centrifuging for 30 min at 1080 g. The suspended f-LF were carefully decanted onto 0.45 μm nitrocellulose membranes and

vacuum filtered. The f-LF remaining on the filter was then rinsed with deionised water (Schrumpf et al., 2013) and washed carefully into aluminium drying boats.

SPT was then placed back into the tubes and the remaining sample was then sonicated at 10 J mL^{-1} using a QSonica Q500 Sonicator with a model cl-334 Sonication Node, the output energy of which was calibrated calorimetrically according to Schmidt et al. (1999). Sonication energies were selected after pretesting revealed that higher sonication energies (< 590 J mL^{-1}; Schmidt et al., 1999; Kaiser and Berhe, 2014) did not alter the recovery of o-LFs at either site (data not shown; Golchin et al., 1994; Schrumpf et al., 2013). Tubes were sonicated in an ice slurry to dissipate heat transferred from the sonicator, which was ran at max 20 % amplitude. After sonication, the o-LF_{10} was then separated in the same manner as the f-LF, before sonicating the sample a second time at 190 J mL^{-1}. This second more sonication resistant occluded pool (o-LF_{200}) was then fractionated at a higher centrifuge speed (1830 g) and rinsed in the same manner as the other light fractions (LFs). The remaining HF was then rinsed with deionised water, shaking on a rotary shaker (250 rpm) for 10 mins and centrifuging at 7,500 g between rinses. A 1 mm glass bead and vortex were used to break up aggregated centrifuge pellets and ensure SPT was thoroughly rinsed from the HF (Schrumpf et al., 2013). Once rinsed, all fractions were oven dried at 65°C, crushed in a pestle and mortar, fumigated with HCl to remove $CaCO_3$ (Harris et al., 2001), and stored in glass vials. SPT was recycled several times before disposal according to Six et al. (1999). To ensure accurate and replicable fractionation, density fractionation was run in triplicate for each soil sample, the recoveries of which ranged from 98–100 % (Appendix Table 8.4). There was no o-LF_{10} recovered from sample F1.6.

5.2.3.2 - SOC and $\delta^{13}C$ values

The content of SOC and stable C isotope composition ($\delta^{13}C$ values) in both bulk samples, triplicates of density fractions, AGB, and BGB were quantified using a Carlo Erba 1108 Elemental Analyser connected to a Thermo Fisher Delta V Isotope-ratio Mass Spectrometer. Bulk SOC stocks were calculated for individual soil profiles using Eq. 5.1. The mass of SOC in different fractions was calculated by multiplying the SOC content by the mass of a given fraction. The elemental analyser was operated in continuous He flow mode via a split interface (Conflo II). Combustion of samples within pre-weighted tin capsules occurred in an O_2 atmosphere at 1020°C. Standards and blind replicates were measured throughout the run. The $\delta^{13}C$ values of samples is reported relative to known standards (Eq. 5.2). All analyses were run with a minimum of 10 % blind replicates, unless run in triplicate (DF).

$$\mathrm{SOC}_{h_z} = \sum_{z}^{h_z} \mathrm{SOC}_i \; x \; \mathrm{BD}_i \; x \; h_i \; x \; (1 - \frac{\mathrm{RF}_i}{100})$$

Eq. 5.1. Calculating the soil organic carbon stocks (kg C m^{-2}) of a specific profile from the soil organic carbon content (%) of each sample (SOC_i), the nearest corresponding bulk density measurement of each sample (BD; g cm^{-3}), a samples' height (h_i; cm), and the proportion of large (>2mm) rock fragments (RF_i; %; Wiesmeier et al., 2012) .

$$\delta^{13}\mathrm{C}_{\mathrm{unknown}} = \frac{\mathrm{R}(^{13}\mathrm{C}/^{12}\mathrm{C})_{\mathrm{unknown}} - \mathrm{R}(^{13}\mathrm{C}/^{12}\mathrm{C})_{\mathrm{standard}}}{\mathrm{R}(^{13}\mathrm{C}/^{12}\mathrm{C})_{\mathrm{standard}}}$$

Eq. 5.2. The stable carbon isotope composition is reported in per mille relative to the Vienna Pee Dee Belemnite standard (Coplen, 2011).

The ^{13}C isotopic enrichment factor (ε) was calculated individually for our sites using the Rayleigh equation (Eq. 5.3; Rayleigh, 1896), fitting our observed bulk SOC content and corresponding $\delta^{13}C$ values (Accoe et al., 2003; Accoe et al., 2002; Garten et al., 2007; Powers and Schlesinger, 2002). The initial SOC content and $\delta^{13}C$ values were taken from the surface sample (0-5 cm) of each profile. There was no significant improvement in the relationship (R^2) for the sites when the deepest samples were removed (Accoe et al., 2003; Accoe et al., 2002), so all observations are included in our ε calculations.

$$\delta = \delta_0 + \varepsilon \; \log[\mathrm{C}/\mathrm{C}_0]$$

Eq. 5.3. The Rayleigh equation describes the gradual ^{13}C enrichment of SOC resulting from isotopic fractionation associated with the oxidative transformation of C. The enrichment factor (ε) is calculated from the C content and initial C content (C_0) and the intercept (δ_0).

5.2.3.3 - X-ray photoelectron spectroscopy

All the fractions of a surface and subsoil sample from the same randomly-selected profile at each site were investigated (all fractions from samples B2.1, B2.4, F2.1, F2.4) using a PHI VersaProbe II Scanning X-ray Photoelectron Spectroscopy Microprobe (XPS; Physical Instruments AG, Germany). XPS measurements were performed at the Surface Characterization Laboratory, *Ecole Polytechnique Fédérale de Lausanne*. The topography of samples can influence XPS measurement due to photoelectron and differences in nano-, micro-, and macro-scopic electron emission geometry (Zemek et al., 2008). Thus, powdered fractions were loaded onto stubs in a homogeneous manner, attempting to reduce surface topographical differences between samples, prior to measurement with the XPS. The surface of samples (< 10 nm depth; Yuan et al., 1998) were then analysed with a monochromatic Al Kα X-ray source (1486.6 eV) of 45.7 W power and a beam size of 200 µm. The spherical capacitor was set at 45° take-off angle respective to the surface of samples. Samples were scanned twice, once coarsely (regional scans), with a pass energy of 187.85 eV, yielding the principle elements of interest. The samples were than scanned again in more detail (survey scans) using a pass energy of 46.95 eV.

Exposure time was < 30 min to prevent X-ray induced alteration of the density fractions and subsequent false structural C assignments (Dengis et al., 1995). Vacuum inside the main chamber was in low 10 torr during measurements (-7 Pa). Sample charging during analysis caused peak shifts of < 3 eV, which were corrected based on the maximum principal C_{1s} peak, centered at 285 eV (Mikutta et al., 2009).

Atomic quantification of the surface of samples was completed using a process of background linear subtraction, fitting a set of Gaussian curves to lines and converting intensities into atomic abundancies with sensitivity factors (Moulder and Chastain, 1992). Curve fitting of survey scans was performed using PHI Multipak 9.5^{TM} Software. Identification of binding energies was completed according to Moulder and Chastain (1992). Differences in C bonding environments at the surface of the fractions were evaluated by deconvoluting the C_{1s} peak into sub-peaks (Appendix Fig. 8.5; Jones and Singh, 2014). Sub-peaks were fitted with Gaussian-Lorentzian functions, the full-width-at-half-maximum was allowed to vary between 1 and 2. Spectral shifts in core level C_{1s} binding energies were assigned according to Table 5.1. The ratio of aromatic / aliphatic C to oxidised C moieties (alcoholic / phenolic, carbonyl, carboxylate) was also used as an index of the level of SOC oxidation within the fractions (Yeasmin et al., 2017).

Table 5.1. Binding energies of specific carbon C_{1s} sub-peaks and their associated C bonding environment; these figures have been adapted from Jones and Singh (2014) and Moulder and Chastain (1992).

Associated carbon bond environment	Bond type	Fixed binding energy (eV)
Aromatic / Aliphatic	C-C / C-H	285
Alcoholic / Phenolic	C-O	286.5
Carbonyl based	C=O	288
Carboxylate	O=C-O	289.5

5.2.4 - Statistical analysis

The effects of the natural variation in quantities of $CaCO_3$ on SOC and $\delta^{13}C$ values were investigated using linear mixed models. Models were fitted using SAS 9.4^{TM} with the estimation method set to restricted (residual) likelihood ratio. Residuals were checked for goodness of fit and normality with QQ-plots (Galecki and Burzykowski, 2015). Deviations from homoscedasticity were evaluated by plotting conditional residuals against predicted values. The significance of fixed effects were evaluated using type III F-tests, while the means of significant fixed effects were compared using t-tests without multiple inference adjustment (Webster, 2007). The Satterthwaite adjustment was used to compute the degrees of freedom of the denominators (Satterthwaite, 1946). All reported means are significant (α=0.05 for all tests), conditional least-square means ± the standard error of the mean.

Separate models were constructed using measurements from the bulk soil and density fractionation. Choice of covariance structure was based upon the Bayesian Information Criteria. Simpler model structures were used for the bulk observations (see Chapters 4 & 8) as they were based on singular measurements rather than triplicate measurements. Models used to analyse triplicate observations from the density fractionation included site, depth classes, the specific fractions, and their interactions as fixed effects. Depth was set as a random effect with a first-order autoregressive covariance structure to account for the spatial autocorrelation of observations within profiles. Observations were blocked by sample and each triplicate (repetition) to account for the temporal autocorrelation between replicates of the same fraction within samples. LFs and HF were given different variances to account for the greater variance in observations from the LFs.

5.3 - Results

5.3.1 - Bulk soil

Bulk SOC (%) was twice as high at the $CaCO_3$-bearing site (5.3±0.1 %) relative to the $CaCO_3$-free site (2.5±0.1 %). Total mean SOC stocks (appendix table 8.4) were thus higher at the $CaCO_3$-bearing site (22.8 kg C m^{-2}) than the $CaCO_3$-free site (12 kg C m^{-2}). Bulk SOC $\delta^{13}C$ values increased systematically with depth at both sites. As hypothesised, bulk $\delta^{13}C$ values of SOC (Fig. 5.1) were lower at the $CaCO_3$-bearing site (-26.2±0.1 ‰) relative to the $CaCO_3$-free site (-25.5±0.0 ‰). AGB $\delta^{13}C$ values were higher at the $CaCO_3$-bearing site, but BGB $\delta^{13}C$ values were indistinguishable between the sites. The $\delta^{13}C$ values of SOC were always higher than AGB and BGB measurements but this shift was smaller at the $CaCO_3$-bearing site. The ε (Fig. 5.2) was higher at the $CaCO_3$-bearing site (ε=-1.46, R^2=0.9) than at the $CaCO_3$-free (ε=-1, R^2=0.88).

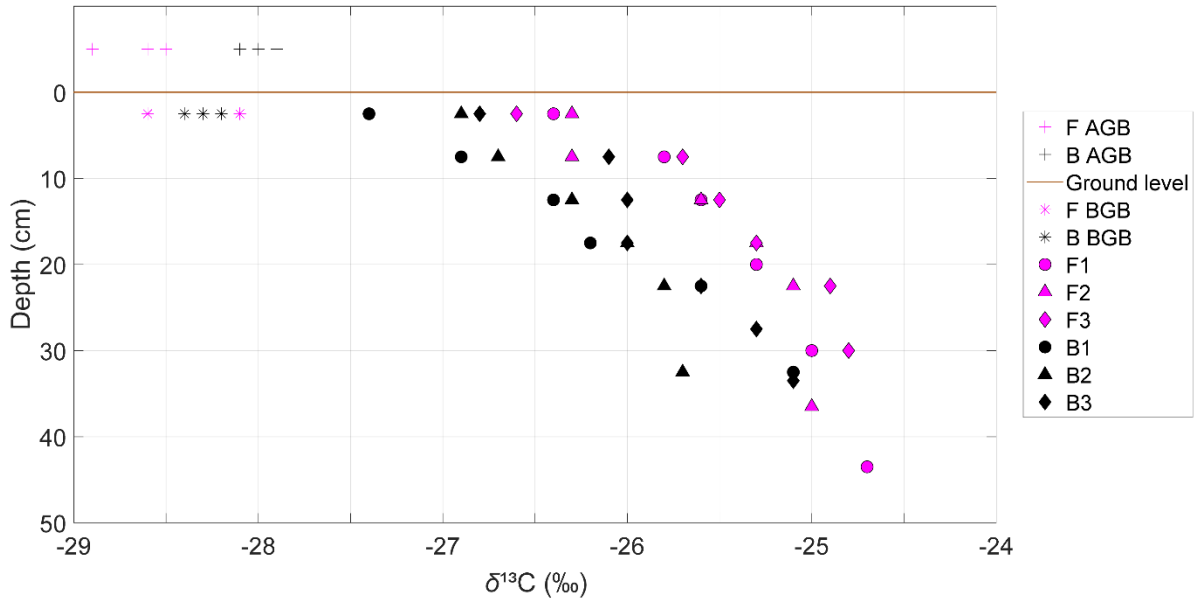

Fig. 5.1. Stable carbon isotope composition of bulk soil organic carbon, above ground- (AGB) and below-ground biomass (BGB) from the $CaCO_3$-free (F) site and the $CaCO_3$-bearing (B) site.

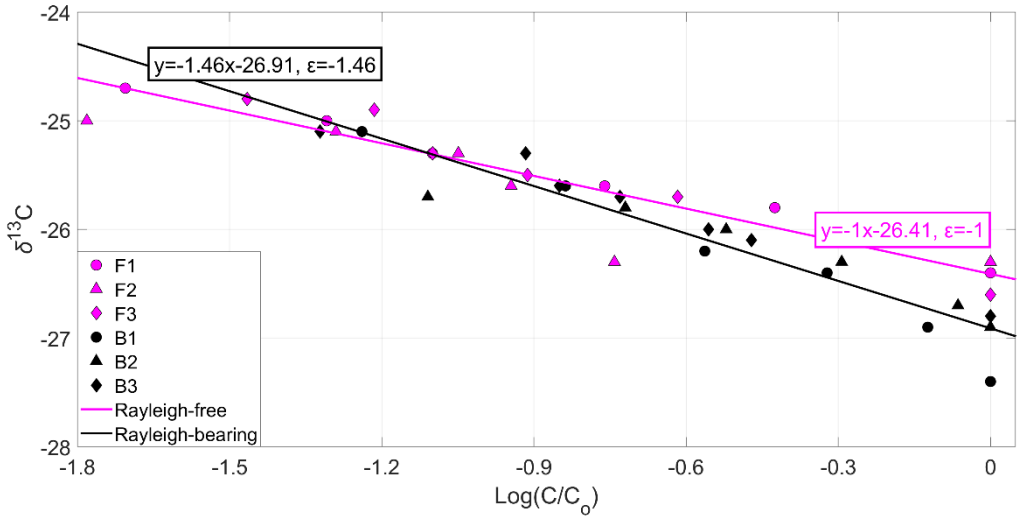

Fig. 5.2. Stable carbon isotopic enrichment factors (ε) for the $CaCO_3$-free (F) site and the $CaCO_3$-bearing (B) site, calculated using the Rayleigh equation (Eq. 5.3). ε is calculated as the slope of the relationship between bulk $\delta^{13}C$ values and the log relationship between SOC content of each sample divided by the initial SOC content (Log C/C_o).

5.3.2 - Density fractions

5.3.2.1 - Distribution of material between fractions

Out of the four density fractions and at both sites, there was always the least recovered material in the o-LF_{10}, while the HF always contained the most material (Appendix Table 8.4). The f-LF was larger than the o-LF_{200} in several samples at the $CaCO_3$-free site (Fig. 5.3 A); while, in contrast, the o-LF_{200}

was particularly large at the $CaCO_3$-bearing site (Fig. 5.3 B), always containing more material than the f-LF. The HF was at least an order of magnitude larger than the LFs (Fig. 5.3 C:D).

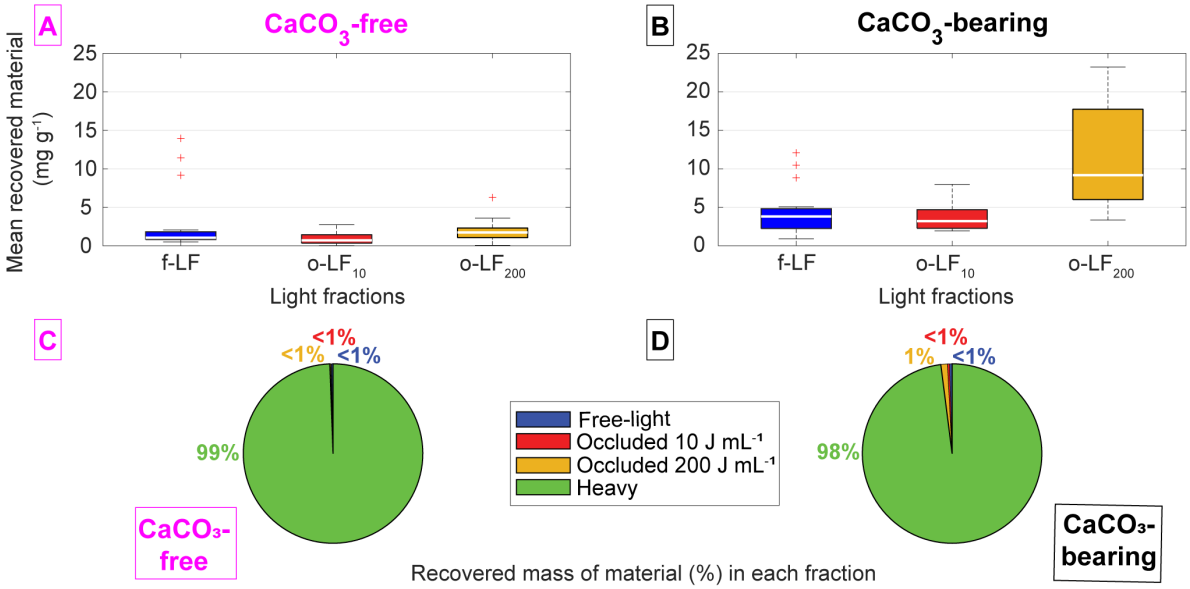

Fig. 5.3. Mass of material recovered in the fractions. **A & B)** Amount of material recovered in the light fractions (free-light and occluded fractions separated at 10 J mL^{-1} and 200 J mL^{-1}; f-LF, o-LF_{10}, o-LF_{200}, respectively) per gram of fractionated soil (mg g^{-1}) for the **(A)** $CaCO_3$-free and **(B)** $CaCO_3$-bearing samples. Bottom and top edges of the boxes in the box plot represent the 25th and 75th percentiles, the middle bars represent the median. Whiskers represent the range of most extreme data points not considered as outliers, while '+' represent values outside of the maximum potential whisker value, corresponding to ±2.7 standard deviation (outliers). **C & D)** The average amount of material in each fraction as a percentage of the total recovered material in the **(C)** $CaCO_3$-free and **(D)** $CaCO_3$-bearing samples.

5.3.2.2 - Distribution of SOC between fractions

The SOC content of each fraction was higher at the $CaCO_3$-bearing site relative to the $CaCO_3$-free site (Fig. 5.4). SOC contents of the LFs showed higher variability relative to the HF, particularly at the $CaCO_3$-free site where there was less material in the LFs. Overall the LFs had a higher SOC content at the $CaCO_3$-bearing site (22.6±1.4 %) than at the $CaCO_3$-free site (14.9±1.0 %). The SOC contents of the HF at both sites were similar to the bulk SOC contents, differing most in surficial horizons (Fig. 5.5), which had a larger proportion of recovered material in the LFs. Therefore, the SOC content was almost twice as high in the HF at the $CaCO_3$-bearing site (4.7±0.2 %) relative to the $CaCO_3$-free site (2.4±0.1 %; Fig. 5.6 A).

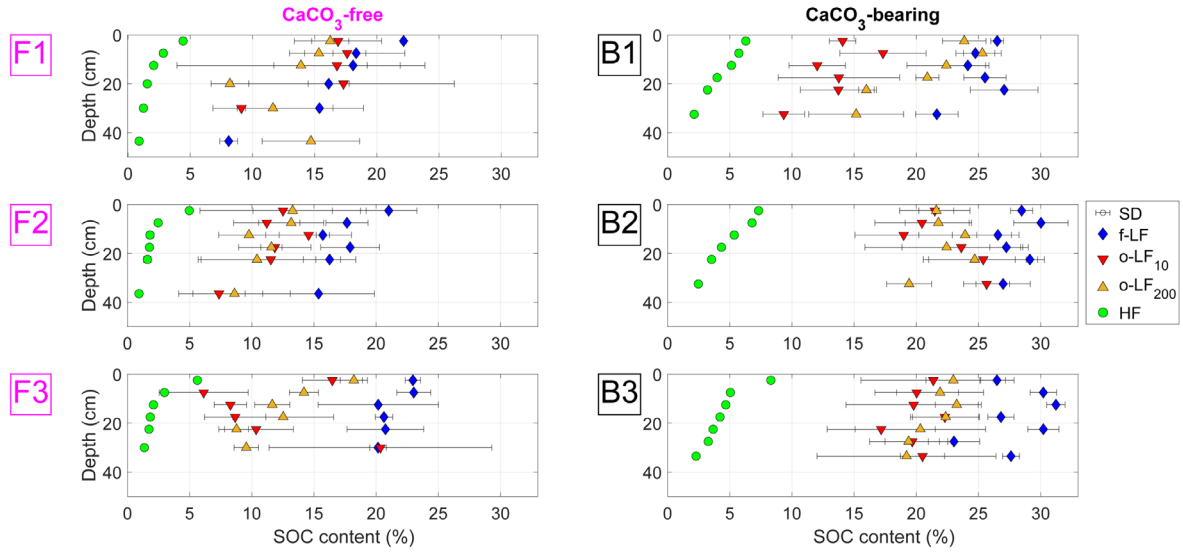

Fig. 5.4. Mean soil organic carbon content of the free-light fraction (f-LF), occluded fractions separated at 10 J mL^{-1} ($o\text{-}LF_{10}$) and 200 J mL^{-1} ($o\text{-}LF_{200}$) and heavy fraction (HF). The $CaCO_3$-free (F1, F2, F3) profiles are on the left and the $CaCO_3$-bearing profiles (B1, B2, B3) are on the right. Error bars represent the standard deviation between triplicate measurements. The amount of material recovered in $o\text{-}LF_{10}$ of F1.6 was insufficient for analysis.

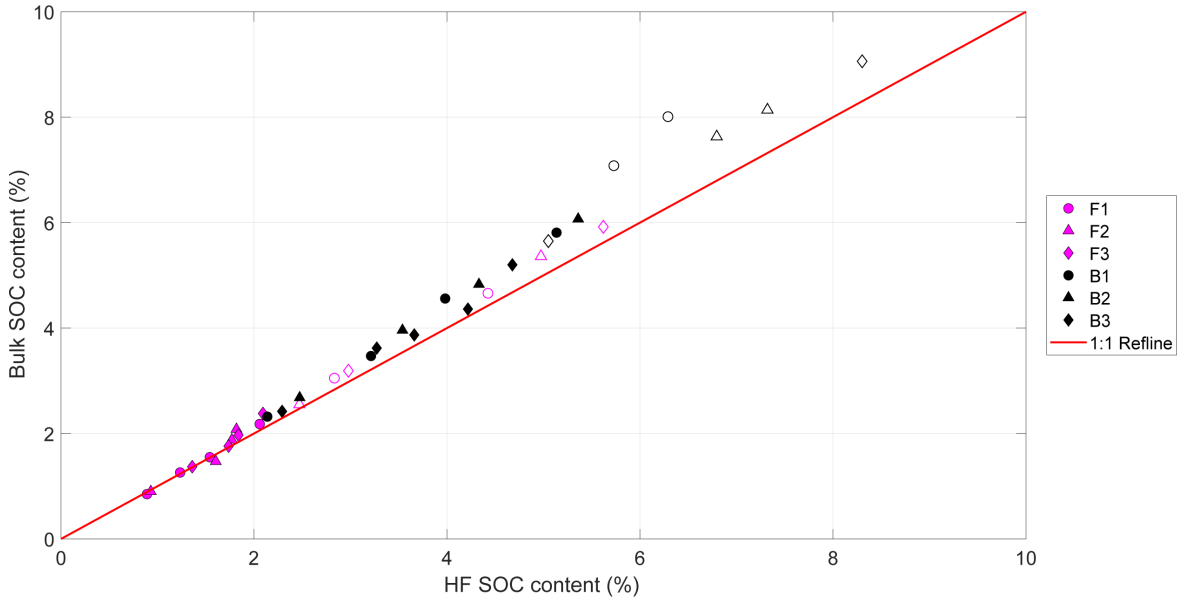

Fig. 5.5. Linear relationship between the content of soil organic carbon in the heavy fractions (mean of three triplicates) and bulk soil at the $CaCO_3$-free (F1, F2, F3) and $CaCO_3$-bearing (B1, B2, B3) profiles. A reference line representing the 1:1 relationship is plotted in red. Surficial samples tended to deviate most from the 1:1 relationship and to highlight this, the first two samples from each profile are plotted with hollow markers.

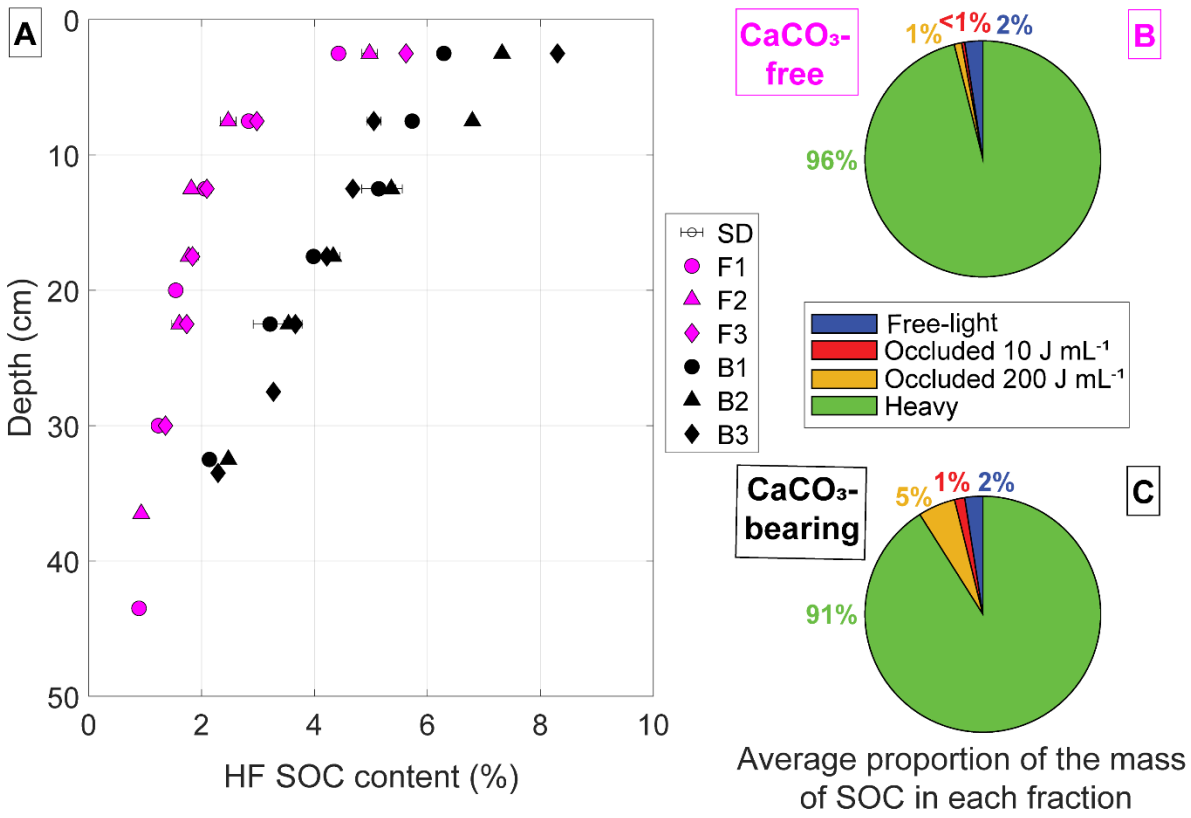

Fig. 5.6. The relatively larger role of the mineral-associated fractions in bulk SOC at our sites. **A.)** The SOC content of the heavy fractions from the $CaCO_3$-free (F1, F2, F3) and $CaCO_3$-bearing (B1, B2, B3) profiles. Error bars represent the standard deviation between triplicate measurements. **B:C)** The average proportion of SOC mass in each fraction at the **B)** $CaCO_3$-free site and **C)** $CaCO_3$-bearing site.

The mass of SOC decreased systematically with depth at both sites. The mass of SOC in the f-LF (8.6±0.8 versus 4.1±0.5 mg C) was approximately twice as high at the $CaCO_3$-bearing site. The mass of SOC in the occluded fractions was also higher at the $CaCO_3$-bearing site, but the differences between the sites were larger in the o-LF_{200} (17.7±0.8 versuss 1.7±0.5 mg C) than in the o-LF_{10} (4.8±0.8 versus 0.7±0.5 mg C). Yet, the mass of SOC in the LFs were always at least an order of magnitude lower than the HF (Fig. 5.6 B:C). Like in the bulk soil or the f-LF, the mass of SOC in the HF was nearly twice as high in the $CaCO_3$-bearing site (310.9±3.7 mg C), relative to the $CaCO_3$-free site (159.7±3.7 mg C). This meant that the mineral-associated SOC pool was the largest at the Nant Valley (Fig. 5.6 B:C) and there was nearly twice as much SOC in OMA at the $CaCO_3$-bearing site, relative to the $CaCO_3$-free site (Fig. 5.6 A).

5.3.2.3 - $\delta^{13}C$ values of fractions

As with SOC content, the $\delta^{13}C$ values of the LFs were more variable between triplicates than the HF (Appendix Table 8.5). The $\delta^{13}C$ values of the LFs at the $CaCO_3$-free site were always lower than those at the $CaCO_3$-bearing site (f-LF =-27.2±0.1 ‰ versus -25.9±0.2 ‰; o-LF_{10}= -27.9±0.1 ‰ versus -

26.5±0.2 ‰; o-LF_{200}= -27.6±0.1 ‰ versus -25.8±0.2 ‰; respectively; Fig. 5.7). Contrastingly, the $\delta^{13}C$ values of the HF at the $CaCO_3$-free profiles were typically higher than those at the $CaCO_3$-bearing site, which was particularly evident in B1 or B2, but less apparent in B3 (Fig. 5.8). Thus, the $CaCO_3$-free site displayed an increase in $\delta^{13}C$ values from the LFs to the HF, but the $\delta^{13}C$ values in the LFs were similar to the HF at the $CaCO_3$-bearing site.

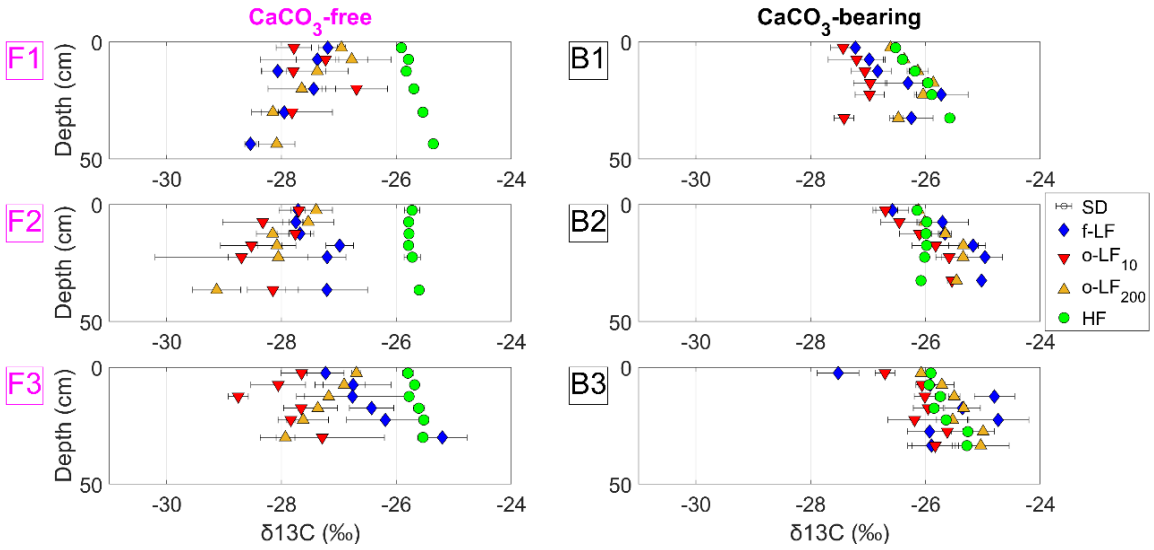

Fig. 5.7. Mean stable carbon isotope composition of the free-light fraction (f-LF), occluded fractions separated at 10 J mL^{-1}(o-LF_{10}) and 200 J mL^{-1}(o-LF_{200}) and heavy fraction (HF). The $CaCO_3$-free (F1, F2, F3) profiles are on the left and the $CaCO_3$-bearing profiles (B1, B2, B3) are on the right. Error bars represent the standard deviation between triplicate measurements. The amount of material recovered in the o-LF_{10} of F1.6 was insufficient for analysis.

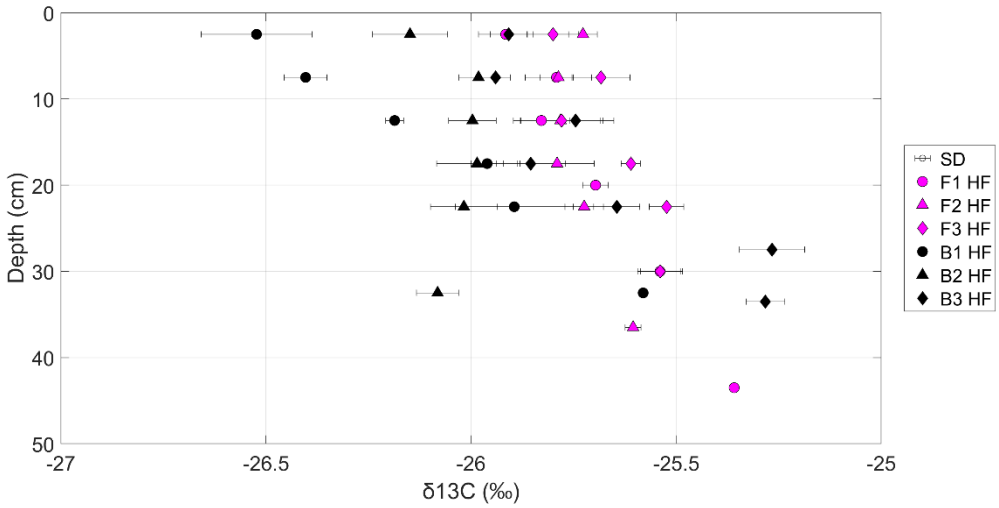

Fig. 5.8. Mean stable carbon isotope composition of heavy fractions (HF) at the $CaCO_3$-free (F1, F2, F3) and $CaCO_3$-bearing (B1, B2, B3) profiles. Error bars represent the standard deviation between triplicate measurements.

5.3.2.4 - XPS characterisation of fractions

Surficial chemical compositions

The two main elements detected by XPS were C (44-57%) and O (30-40%; Appendix Table 8.6). The high C contents were likely caused by adventitious C adsorption on the surface of the samples. As a result, the surficial composition of the fractions could not be quantitatively determined. Elements associated with the mineral phase (*e.g.* Ca, Fe, Si, Ti or Al) were all detected at low quantities. W and Cl were also detected at low quantities and probably represent residues from the fractionation and fumigation procedures, respectively.

Patterns in XPS detailed scans

While estimation of surface coverage was unreliable, qualitative information on potential differences in bonding environments between the sites could still be gained from the shape of XPS scans for different elements. Different survey scans from the different XPS analysed elements are all presented in Appendix Fig. 8.6-8.10, but several specific scans are presented below (Fig. 5.9 to 5.10). There was a slight shift in the N_{1s} peak towards more protonated N forms at the more acidic $CaCO_3$-free site (Fig. 5.9). Ca-tungstate precipitation was not evident on the details W_{4f} scans (Fig. 5.10). There also was a clear difference in the Ca_{2p} signal between the sites (Fig. 5.11). Both sites presented a peak in the $Ca_{2P1/2}$ region, but this peak was better defined in the $CaCO_3$-bearing fractions. However, the $CaCO_3$-bearing site also displayed a satellite peak in the $Ca_{2P3/2}$ region, which was not present at the $CaCO_3$-free site.

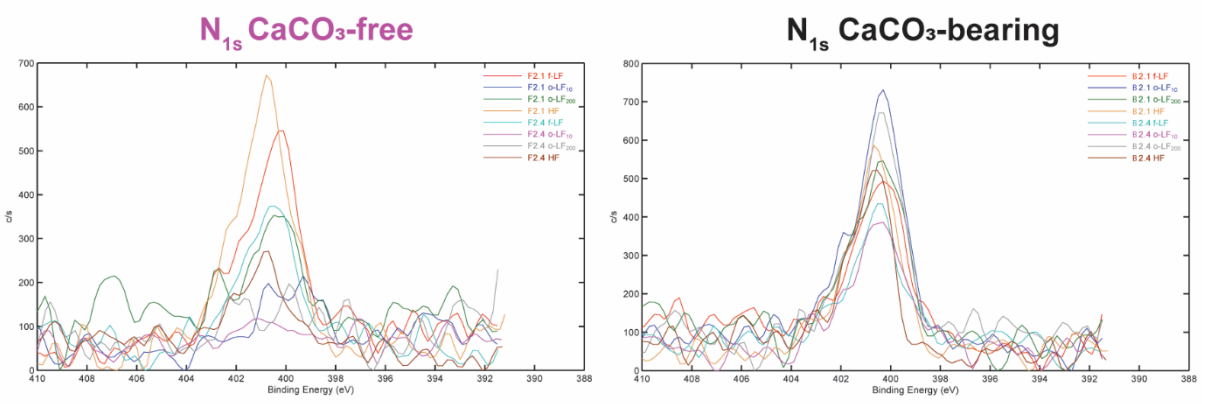

Fig. 5.9. Detailed X-ray photoelectron spectroscopy spectra in the electron binding energy range of photoelectrons ejected from the nitrogen 1s orbital. These spectra are from all of the density fractions from the $CaCO_3$-bearing (B2.1 and B2.4) and $CaCO_3$-free (F2.1 and F2.4) sample subsets.

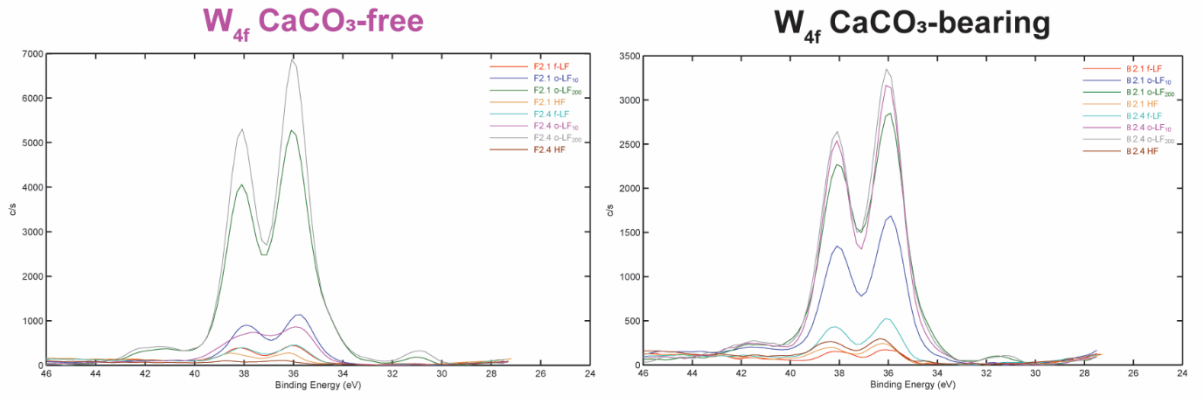

Fig. 5.10. Detailed X-ray photoelectron spectroscopy spectra in the electron binding energy range of photoelectrons ejected from the tungsten 4f orbital. These spectra are from all of the density fractions from the $CaCO_3$-bearing (B2.1 and B2.4) and $CaCO_3$-free (F2.1 and F2.4) sample subsets.

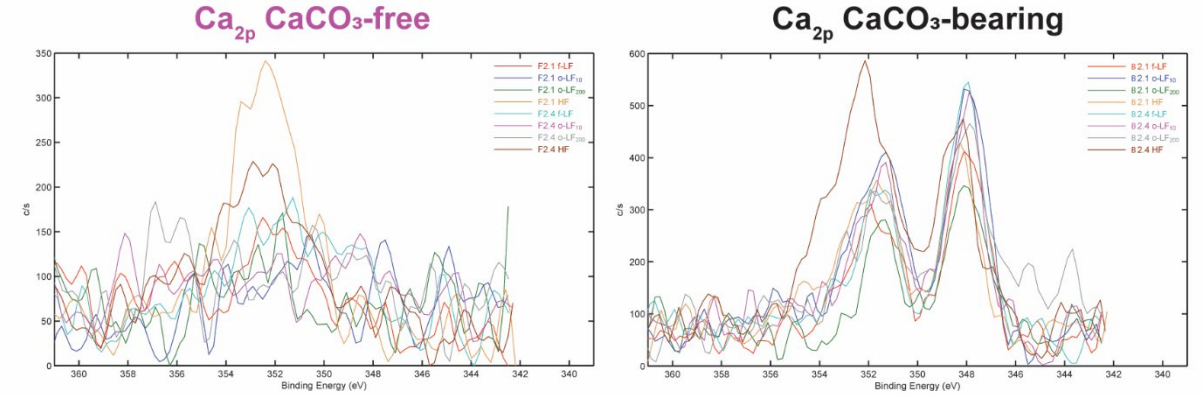

Fig. 5.11. Detailed X-ray photoelectron spectroscopy in the electron binding energy range of photoelectrons ejected from the calcium 2p orbital. These spectra are from all of the density fractions from the $CaCO_3$-bearing (B2.1 and B2.4) and $CaCO_3$-free (F2.1 and F2.4) sample subsets.

C_{1s} peak deconvolution

The deconvolution of the C_{1s} peak (Fig. 5.12; Table 5.2) indicated that the largest proportions of surficial C were always associated with aromatic / aliphatic C moieties at both sites. There was a higher proportion of carbonyl C moieties at the $CaCO_3$-free site (9.8±1.3 %) than the $CaCO_3$-bearing (14±1.1 %). The ratio of aromatic / aliphatic C to oxidised C moieties in the LFs were typically higher and more similar at the $CaCO_3$-bearing site than at the $CaCO_3$-free site. This pattern was similar to the $\delta^{13}C$ values, which were more similar between the LFs and HF at the $CaCO_3$-bearing site, relative to the $CaCO_3$-free, which displayed a larger range of $\delta^{13}C$ values between the f-LF, the occluded fractions and the HF. Yet, the ratio of aromatic / aliphatic C to oxidised C moieties contrasted the $\delta^{13}C$ values in the HF. The ratio was higher at the $CaCO_3$-bearing site HF relative to the $CaCO_3$-free and decreased with depth, while HF $\delta^{13}C$ values were higher in the $CaCO_3$-free site, and decreased with depth. Thus the C_{1s} deconvolution hinted that there was more carbonyl C at the $CaCO_3$-bearing site and that the LFs were more oxidatively transformed.

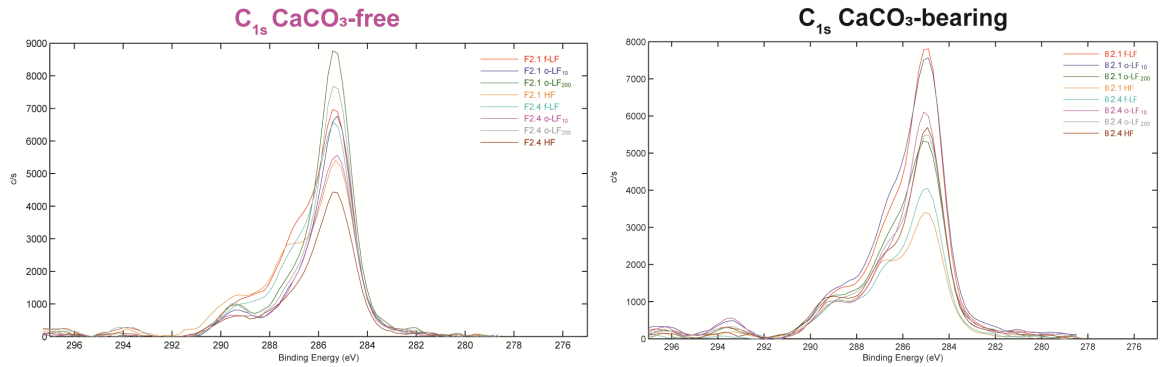

Fig. 5.12. Detailed X-ray photoelectron spectroscopy spectra in the electron binding energy range of photoelectrons ejected from the carbon 1s orbital. These spectra are from all density fractions from the $CaCO_3$-bearing (B2.1 and B2.4) and $CaCO_3$-free (F2.1 and F2.4) sample subset.

Table 5.2. Results from the deconvolution of the detailed X-ray photoelectron spectroscopy attained carbon 1s (C_{1s}) peak for the four density fractions (free-light fraction, occluded fraction separated at 10 and 200 J mL^{-1}, and heavy fraction) of samples from the $CaCO_3$-free (F2.1, F2.4) and $CaCO_3$-bearing (B2.1, B2.4) sample subsets. The first four data columns represent the percentage area of each sub-peak within the total C_{1s} peak and are indicative of different C bond environments (listed in Table 5.1). See the method section for more details on the deconvolution technique. The final column represents the ratio between the percentages of the sub-peak centred at 285 eV relative to the percentage representation of other sub-peaks.

Sample	Fractions	C-C / C-H 285 eV	C-O 286.5 eV	C=O 288 eV	O-C=O 289.5 eV	Ratio of C-C / C-H to oxidised C (C-O / C=O / O-C=O)
F2.1	f-LF	57.6	24.1	13.4	4.9	0.74
	o-LF_{10}	73.8	11.6	8.3	6.2	0.35
	o-LF_{200}	70.4	16.7	7.6	5.3	0.42
	HF	48.3	29.1	13.2	9.4	1.07
F2.4	f-LF	59.2	23.7	11.2	5.8	0.69
	o-LF_{10}	71.7	14.1	7.6	6.5	0.39
	o-LF_{200}	70.1	16.5	5.4	8.0	0.43
	HF	64.8	19.6	8.3	7.2	0.54
B2.1	f-LF	61.6	21.0	13.3	4.1	0.62
	o-LF_{10}	59.4	22.0	12.8	5.8	0.68
	o-LF_{200}	59.1	19.3	15.0	6.7	0.69
	HF	47.5	27.0	17.4	8.1	1.11
B2.4	f-LF	57.6	19.0	16.7	6.7	0.74
	o-LF_{10}	63.3	20.3	10.0	6.4	0.58
	o-LF_{200}	58.2	22.4	14.8	4.7	0.72
	HF	55.1	25.1	10.8	9.0	0.81

5.4 - Discussion

5.4.1 - Limitations of the XPS

Surficial C contents determined by XPS were higher than expected (44-57%) and did not show a consistent pattern with depth or between the C-rich LFs and C-poorer HF (Fig. 5.4). This was most probably caused by the adsorption of adventitious C by the analysed fractions when exposed to the atmosphere during the various manipulations (Greczynski and Hultman, 2017). Adventitious C is a thin film (1-2 nm) of C contamination, typically formed primarily of aliphatic / aromatic C, which is deposited onto the surface of samples upon atmospheric exposure or during the creation of a vacuum. The analysed fractions were treated identically throughout the density fractionation and fumigation processes, so it is reasonable to assume that adventitious C contamination has been homogeneous between the subsets of fractions measured with the XPS. This assumption is supported by the fact that, while there was an increased surface content of C in our samples, there was still notable differences in the C_{1s} peak deconvolution. The C_{1s} peak deconvolution can be used as an indication of the degree of oxidative transformation of surface C and agreed with patterns in the LFs $\delta^{13}C$ values, fractionated towards higher values during microbial transformation. Thus, while, in our study, the XPS surficial chemical compositions were likely biased by adventitious C, this contamination seemed to be homogeneous. Thus, the C_{1s} peak deconvolution and other specific survey scans can still help to reinforce our interpretations of the more reliable $\delta^{13}C$ data, discussed further below.

5.4.2 - Bulk values

Bulk soil organic carbon was twice as high in the $CaCO_3$-bearing site as the $CaCO_3$-free. Bulk SOC results from this study were in agreement with previous measurements with a separate CHN analyser (Appendix Fig. 8.11).Bulk SOC stocks were either higher ($CaCO_3$-bearing) or similar ($CaCO_3$-free) to a range of SOC stock measurements from grassland environments in Bavaria (Wiesmeier et al., 2012). Vegetation structure, inputs and total organic carbon contents were similar between the sites. Thus, this difference in SOC arises from a cascading influence of $CaCO_3$ on the biogeochemistry of the $CaCO_3$-bearing site (Chapter 4).

Bulk $\delta^{13}C$ values systematically increased with depth at both sites. It is widely reported in the literature that $\delta^{13}C$ values of bulk SOC increase by approximately 1-3 ‰ with depth. This fractionation is thought to arise through a combination of several mechanisms (see Boström et al., 2007 for detailed description). The most accepted of these is the fact that SOC is fractionated by the oxidative transformation of microorganisms and that there is an increasing proportion of microbial necromass with depth (Boström et al., 2007; Hobbie et al., 1999; Rumpel and Kögel-Knabner, 2011), This in turn, typically has higher $\delta^{13}C$ values and slower turnover times than plant residues, leading to its accumulation with depth and the fractionation of bulk SOC $\delta^{13}C$ values.

The bulk $\delta^{13}C$ values of the $CaCO_3$-bearing profiles were significantly lower than those of the $CaCO_3$-free profiles. The $\delta^{13}C$ differences in both AGB and BGB from vegetation at the sites were contrary to the SOC signature or negligible at the sites, respectively. This further hinted to a disconnection between the inputs from vegetation and SOC at the sites (Matteodo et al., 2018; Schmidt et al., 2011). Instead, bulk $\delta^{13}C$ values suggested that SOC had been exposed to less ^{13}C fractionation by microbial activity and was thus, less oxidatively transformed at the $CaCO_3$-bearing site, supporting previous observations from similar environments (Matteodo et al., 2018).

The ε was higher at the $CaCO_3$-bearing site (Fig. 5.2). Our ε figures rest within experimental values (Balesdent and Mariotti, 1996; Natelhoffer and Fry, 1988), but are lower than would be expected from similar forested (Accoe et al., 2003; Powers and Schlesinger, 2002) or agricultural systems (Accoe et al., 2003; Accoe et al., 2002). Due to the similarity in texture and climate between our sites, one interpretation of this result is that SOC processing of fresh soil C inputs may have been faster at the $CaCO_3$-bearing site; furthermore, this SOC may have had a greater stability at the $CaCO_3$-bearing site (Garten, 2006; Garten et al., 2000; Garten and Hanson, 2006). Yet, this relationship needs to be interpreted with caution as the Rayleigh equation is only really applicable in the case of a mono-directional isotopic enrichment system (Rayleigh, 1896). In a soil system, microbial biomass is incorporated and recycled within the residual SOC pool and as such, the ε should be interpreted with caution (Accoe et al., 2003).

5.4.3 - Light fractions

Yet, in contrast to the bulk $\delta^{13}C$ values, the LFs at the $CaCO_3$-bearing site had both higher $\delta^{13}C$ values and a higher ratio of aromatic / aliphatic C to oxidised C moieties. This seems to indicate that they had a higher degree of oxidative transformation relative to the respective $CaCO_3$-free fractions. Environments with a near-neutral pH are typically considered to present near-optimum conditions for the oxidative transformation by bacteria (Clarholm and Skyllberg, 2013; Groffman et al., 2006; Whittinghill and Hobbie, 2012). It is thus possible to suggest that biogeochemical conditions for the oxidative transformation of easily accessible SOC were better at the $CaCO_3$-bearing site. These conditions in turn could explain why more easily accessible SOC (LFs) showed increased signs of oxidative transformation at the $CaCO_3$-bearing site.

SOC contents were also lower in the LFs at the $CaCO_3$-free site. This likely indicates that there was relatively more mineral coating on the LFs at the $CaCO_3$-free site (Cerli et al., 2012), relative to the $CaCO_3$-bearing site. While XPS detected surficial abundances of Al, Fe, and SI, were largely invariant in-between the LFs at the sites, the XPS also did not detect differences between the LFs and the HF, which should have displayed a larger range of differences. Clay content (2 %) and well-crystalline Fe / Al oxides were slightly more abundant at the $CaCO_3$-free site (Chapter 4). Both of these can adsorb onto particulate organic matter, subsequently protecting it against further decomposition through multiple

mechanisms (Scheel et al., 2008). This stabilisation could potentially also explain a proportion of the differences in the oxidative transformation of the LFs between the sites. Thus, to conclude, SOC in the LFs seems to be more efficiently oxidised at the $CaCO_3$-bearing site, which is probably due to the better biogeochemical conditions for its oxidative transformation and it having a lower degree of mineral coating, relative to the $CaCO_3$-free site.

5.4.4 - Occluded pool

As hypothesised, the $CaCO_3$-bearing site had a larger occluded SOC pool relative to the $CaCO_3$-free site, particularly in the o-LF_{200} fraction. It has been repeatedly shown by numerous methods that Ca-amended soils typically have a high degree of aggregation and increased occluded SOC pools (Kaiser et al., 2014; Muneer and Oades, 1989b; Paradelo et al., 2016). In humid conditions, this is usually attributed to the abiotic flocculation of soil separates by Ca_{Exch} (Muneer and Oades, 1989c), rather than the evaporative precipitation of $CaCO_3$ and its subsequent cementation of aggregates (Fernández-Ugalde et al., 2014). An increased mass of SOC, such as that present at the $CaCO_3$-bearing site, can also positively influence biological aggregate formation (Chenu, 1989; Chenu and Cosentino, 2011), which would have also likely played a role in increasing the occlusion of SOC. In the biological theory of aggregate formation, microaggregates can be created around decomposing SOC as microorganisms emit cohesive EPS that can bind soil separates, eventually occluding the substrate within (Chenu, 1989; Chenu and Cosentino, 2011). Occluded SOC was more oxidatively transformed at the $CaCO_3$-bearing site, relative to the $CaCO_3$-free site, thereby supporting the idea that this SOC may have been occluded during biological aggregate formation processes. Thus, it is was most likely a mixture of both abiotic (Ca_{Exch}) and biotic (increased SOC) influences on aggregation that generated a larger occluded SOC pool at the $CaCO_3$-bearing site.

5.4.5 - Differences between LFs and HF

At the $CaCO_3$-free site, the LFs had significantly lower $\delta^{13}C$ values than the HF. This shift has been widely reported in numerous studies investigating the $\delta^{13}C$ values of different density fractions (Poeplau et al., 2018; Schrumpf et al., 2013). It is thought to arise from the selective preservation of ^{13}C enriched microbial matter by Fe oxides (Spielvogel et al., 2008), relative to the less decomposed and recycled SOC in the LFs. However, this contrasted our results from the $CaCO_3$-bearing site where the $\delta^{13}C$ values of the HF were similar to the LFs. A similar finding has been observed recently by Martí-Roura et al. (2019) in Mediterranean soils with $CaCO_3$ relative to those without. They fractionated their soils by size and reported a smaller shift in $\delta^{13}C$ values from coarser fractions to finer fractions. Yet, prior to further exploring this finding, the potential effects of density fractionation on these results must first be excluded.

The similarities between LF and HF at the $CaCO_3$-bearing site could have been caused by the dissolution of $CaCO_3$ and subsequent precipitation of the dense Ca-metatungstate on the LFs. If this precipitation

occurred on SOC from the LFs with a fresh signature, it could cause it to sink into the HF, creating a false equivalence between the LFs and HF, which was previously reported during a ^{14}C addition and recuperation experiment using density fractionation (Rovira et al., 1998). Firstly, it is worth noting that the Rovira et al. (1998) study was completed on soils with higher quantities of $CaCO_3$ (> 40 %) than our study (< 6.2 %), increasing the likelihood of Ca-metatungstate precipitation. Secondly, if there had been significant precipitation of Ca-metatungstate, recovery during density fractionation would have been higher at the $CaCO_3$-bearing site fractionation, which it was not (Appendix Table 8.4). Thirdly, XPS scans of the fractions revealed that W contamination was lowest in the HF, with no difference between sites. There was also no peak detected for Ca tungstate (shift towards 35 eV) in the detailed scans of the W_{4f} region (Fig. 5.10). Thus, these differences did not seem to arise due to the precipitation of Ca-metatungstate on fresh particulate organic matter. Yet, future studies should be aware of the risks of running density fractionation on $CaCO_3$-bearing soils (> 10 %).

Instead, the similarities between the LF and the HF of the $CaCO_3$-bearing site were likely caused by two complementary mechanisms.

i) **More efficient microbial community** - Firstly, as discussed above, the LFs were oxidatively transformed by microorganisms more efficiently at the $CaCO_3$-bearing site. This increased the $\delta^{13}C$ values of the LFs so that they are more similar to the HF, relative to the $CaCO_3$-free site.
ii) **Preferential stabilisation -** Secondly, organo-mineral association (OMA) in the HF may preferentially stabilise SOC with $\delta^{13}C$ values that are more similar to those of the LFs. This second point will now be expanded on and discussed further below.

5.4.6 – Heavy fractions

5.4.6.1 - Discrepancy between the HFs and the bulk soil

A discrepancy existed between the bulk and HF $\delta^{13}C$ values. The HF accounted for the largest proportion of the total SOC mass (Fig. 5.6 B & C) and should thus have had $\delta^{13}C$ values that were closely related to those of the bulk soil, particularly in deeper samples where there was less recovered material in the LFs. This difference between the bulk and HF $\delta^{13}C$ values could demonstrate that there was a larger error in our $\delta^{13}C$ measurements than evidenced by our blind replicates for bulk $\delta^{13}C$ values or error bars for the DF triplicates in Fig. 5.7. It could also be caused by an artefact of the DF, whereby we lost a proportion of the bulk depth profile of $\delta^{13}C$ values, which seems to have occurred during similar extraction procedures in similar soils (Schrumpf et al., 2013). A subset of these samples now need to be remeasured to evaluate whether this difference between bulk and HF $\delta^{13}C$ values was caused by an analytical error or an artefact of the DF. Ultimately, this discrepancy reduces the magnitude of our observations in the HF relative to our bulk observations and is thus, more likely to reduce the strength of the conclusions that we can draw from this dataset.

5.4.6.2 - Indirect role of $CaCO_3$

The mass of mineral-associated SOC was almost twice as high at the $CaCO_3$-bearing site, relative to the $CaCO_3$-free site. This accumulation is unlikely to arise as a direct result of $CaCO_3$. While there is evidence that $CaCO_3$ can directly contribute to the accumulation of SOC through sorption processes (detailed in Chapter 3) due to its high point of zero charge (PZC; Jin and Zimmerman, 2010), this evidence is limited in soils. The presence of $CaCO_3$ at the Nant Valley is instead more likely playing an indirect role in the accumulation of mineral-associated SOC in the HF at the $CaCO_3$-bearing site by acting as a reservoir of Ca or influencing the crystallinity of Fe forms.

5.4.6.3 - The direct roles of Ca and Fe

During its dissolution, $CaCO_3$ buffers soil pH and releases Ca into the soil solution, which in turn, can influence the crystallinity of Fe oxides (Thompson et al., 2011). Both this released reactive Ca (Rowley et al., 2018) and a higher proportion of poorly crystalline Fe forms (Kramer and Chadwick, 2018) have well-established links to the accumulation of mineral-associated SOC. Furthermore, Ca_{Exch} has recently been shown to positively influence the sorption of SOC by poorly crystalline Fe forms (Sowers et al., 2018b). While, the higher SOC in the HF at the $CaCO_3$-bearing site is probably stabilised by a complex mixture of organo-cation / mineral interactions involving Ca_{Exch}, poorly crystalline Fe and their interaction, the $\delta^{13}C$ values of this mineral-associated SOC may have hinted at their individual roles, developed in the following section.

5.4.6.4 - Evidence from $\delta^{13}C$ values

In Chapter 4 we suggested that Ca and Fe may co-stabilise SOC at the $CaCO_3$-bearing site, but that Ca_{Exch} was likely more dominate in B1 and B2 and poorly crystalline Fe forms in profile B3. This was because SOC displayed a positive correlation with either Ca_{Exch} (B1 & B2) or the ratio between oxalate and dithionite extractable Fe (B3) in these respective profiles (Fig. 4.14 A & C), and that poorly crystalline Fe seemed to be competing for exchange sites at B3, distorting the CEC-depth profile (Fig. 4.14 D). Interestingly, both bulk and HF $\delta^{13}C$ values (Fig. 5.6 A & B) were lower at B1 and B2, relative to B3, which had signatures that were more similar to the $CaCO_3$-free profiles. As Fe oxides are typically thought to stabilise ^{13}C-enriched SOC (Spielvogel et al., 2008), the $\delta^{13}C$ values seem to further support the idea that Fe oxides may be more dominant in B3, relative to B1 and B2. Yet, the next question is what mechanism could explain an accumulation of ^{13}C-depleted SOC in the mineral-associated fractions (HF) of profiles with higher Ca availability?

5.4.6.5 - DOC

Dissolved organic carbon (DOC) has variable $\delta^{13}C$ values and is readily eluviated and adsorbed onto soil separates differentially in different soil environments (Hagedorn et al., 2004; Kaiser et al., 2001). Minick et al. (2017) demonstrated that Ca addition suppressed the mineralisation of ^{13}C-depleted sources and the leaching of DOC. If Ca_{Exch} predominantly affects the sorption of SOC through polyvalent cation

bridging, it would be expected to flocculate, precipitate and stabilise DOC on mineral and organic surfaces as it moves throughout the soil profile. This in turn, could explain the increased mass of mineral-associated SOC and the relatively fresher $\delta^{13}C$ values of SOC stabilised in the HF of profiles with a higher Ca availability.

The flocculation and bridging of Ca_{Exch} has typically been thought to preferentially stabilise phenol and carboxyl functional groups (Kaiser, 1998; Römkens and Dolfing, 1998). However, unexpectedly, the main difference in the results from the C_{1s} peak deconvolution of the subsampled fractions was an increased presence of carbonyl C moieties at the $CaCO_3$-bearing site. This increased presence could be explained by the co-localisation of the carbonyl C sub peak with the peak of Ca-formate ($Ca[COOH]_2$; 288.6 eV), measured in standards during a previous XPS study (Demri and Muster, 1995). It would be expected that Ca-formate-like C bonds would be more abundant at the $CaCO_3$-bearing site, with its increased Ca availability, but the Ca_{2p} peak could not provide further evidence for this.

There were two peaks present in the Ca_{2p} region of the $CaCO_3$-bearing site fractions, but only one weaker peak present in the HF at the $CaCO_3$-free site (Fig. 5.11). Unfortunately, this peak could not be identified readily as there is only a small range of chemical shifts in the Ca_{2p} region (< 1 eV; Moulder and Chastain, 1992) and pre-existing data on Ca XPS is limited (Demri and Muster, 1995). While this peak cannot belong to $CaCO_3$ due to the prior fumigation process, it is still difficult to distinguish from other Ca interactions or compounds ($CaCl_2$, Fe-Ca, $Ca(COO)_2$). The small shift in the O_{1s} peak (Appendix Fig. 8.9) did not help in further distinguishing the relationship either (Demri and Muster, 1995). Further investigation with more advanced spectroscopic techniques would be needed to identify the origin of this satellite Ca peak in the HF of the $CaCO_3$-bearing samples and to further investigate Ca-mediated OMA.

Ultimately, we hypothesise that the higher mass of mineral-associated SOC at the $CaCO_3$-bearing site (commonly attributed to Ca-humate relationships; Oades, 1988) are actually caused by the sorption of DOC (Kleber et al., 2007; Minick et al., 2017), complexed predominantly by inner sphere interactions with reactive Ca forms (Rowley et al., 2018), and potentially a co-association with poorly crystalline Fe forms (Sowers et al., 2018a; Sowers et al., 2018b). However, further spectroscopic investigation is still required to confirm if Ca can form inner sphere complexes with DOC in different soils and whether this can explain a significant proportion of the SOC accumulated in the HF at the $CaCO_3$-bearing site.

5.5 - Conclusions

We investigated SOC in soils with or without $CaCO_3$ that had formed under similar conditions for soil formation, in an attempt to isolate the complex role of Ca in SOC stabilisation. Bulk SOC was twice as high and $\delta^{13}C$ were lower in the $CaCO_3$-bearing profiles, relative to the $CaCO_3$-free profiles, implying that the $CaCO_3$-bearing site contained an abundant source of relatively fresh SOC. In contrast to the

bulk signature, the LFs were more oxidatively transformed at the $CaCO_3$-bearing site. This is probably due to better biogeochemical conditions for the decomposition of easily accessible SOC in a near-neutral environment and due to the LFs having a lower degree of mineral coating at the $CaCO_3$-bearing site. Occluded pools were larger at the $CaCO_3$-bearing site, likely due to the flocculation of soil separates by Ca_{Exch} and the increased presence of SOC, both of which are known to positively influence aggregate formation. Yet contrary to our hypothesis, the LFs were of little overall significance to bulk SOC at either site due to their lower mass of SOC, relative to the HF.

It was instead the heavy fractions (HF) that dominated bulk SOC. There was twice as much mineral-associated SOC at the $CaCO_3$-bearing site, relative to the $CaCO_3$-free site. This mineral-associated SOC differed in quality from the $CaCO_3$-free site, which had higher $\delta^{13}C$ values, likely linked to the preferential stabilisation of microbially-enriched SOC by Fe oxides. Instead, the mineral-associated SOC at the $CaCO_3$-bearing site tended to have lower $\delta^{13}C$ values (particularly B1 & B2). Both the abundance and lower $\delta^{13}C$ values of mineral-associated SOC at the $CaCO_3$-bearing site are likely caused by the flocculation, precipitation and accumulation of DOC, with a fresher signal, in OMA (Minick et al., 2017). However, this would require further investigation with adsorption and leaching experiments to see if Ca does preferentially stabilise DOC with a fresher signal, measuring the $\delta^{13}C$ values of DOC. Future research should aim to decipher OMA in Ca-bearing environments, investigating the mechanisms that drive a near two-fold increase in OMA, in subalpine soils that have developed under similar conditions.

- End of draft publication -

This page is left intentionally blank

- Chapter 6: General discussion -

- Research question Chapter 6 -

The following question and sub-questions will be addressed in this chapter:

Does Ca mediate an accumulation of SOC at the Nant Valley?

a. Could we isolate the role of Ca in the accumulation of SOC?
b. What were the mechanisms through which Ca contributed to the accumulation of SOC?
c. What are the broader applications of these findings and how do they compare to those of previous studies?

- Chapter 6 foreword -

This chapter will now synthesise the previous research chapters to highlight the specific mechanisms through which Ca could have stabilised SOC, contributing to its accumulation at the $CaCO_3$-bearing site. This chapter will also place this information within the context of existing literature, examining whether or not our findings conform to previous hypotheses regarding the accumulation of SOC. It will finally examine the remaining uncertainties that still require further investigation (which will be explored further in section 7.2) and broader prospective of the findings.

6.1 - The overlooked effects of $CaCO_3$ in humid and temperate soil environments

Calcium carbonate can play an important role in the pedogenesis and biogeochemistry of a humid and temperate soil environments.

Calcite (a crystalline phase made of $CaCO_3$) is a soluble mineral and is weathered easily from humid soil environments (Schaetzl and Thompson, 2015), although it can still be precipitated from the soil solution by biomediated processes (Dincher et al., 2019; Hasinger et al., 2015; Millière et al., 2019). Contrarily, in semiarid or arid environments, $CaCO_3$ can precipitate as calcite from the soil solution during evaporation processes (Arkley, 1963; Zamanian et al., 2016). Thus, $CaCO_3$ minerals such as calcite are more commonly associated with these arid environments where they are known to accumulate (Zamanian et al., 2016). Simple evidence for this accumulation can be found in the global negative relationship between alkaline soils, buffered by $CaCO_3$ and the aridity index (precipitation / potential evapotranspiration; Slessarev et al., 2016) or the distribution of calcretes (Goudie, 1973). We will refer to the aridity index in several locations throughout this discussion; to save confusion, it is worth noting that the aridity index is inversed, meaning that illogically, a humid environment has a high aridity index (UNEP, 1992). Due to this climatic association, the biogeochemical effects of $CaCO_3$ on soils have been predominantly investigated in semiarid to arid environments, with a low aridity index.

Yet, $CaCO_3$ also exists in humid environments (Slessarev et al., 2016) and as shown in Chapter 4 and 5, it can still play a commanding role in the pedogenesis and biogeochemistry of these regions. The weathering of limestone fragments, supplied by the Morcles Nappe, acted as an intrinsic pedogenic factor, sustaining a state of pedogenic inertia in the $CaCO_3$-bearing soils at the Nant Valley (Bryan and Teakle, 1949; Muhs, 1984). This inertia bifurcated the pedogenic trajectory of the $CaCO_3$-bearing site from that of the $CaCO_3$-free site. The $CaCO_3$-free site had no $CaCO_3$ and without this reservoir, Ca_{Exch} was less abundant and more variable. It also had a lower pH due to the absence of $CaCO_3$ buffering, which may have enabled the hydrolysing effect of available Al^{3+} and its associated buffering of soil pH (Eq. 6.1; Fig. 6.1 A; Chadwick and Chorover, 2001; Thomas and Hargrove, 1984). In contrast, at the $CaCO_3$-bearing site, $CaCO_3$ dissolution directly increased soil pH and quantities of Ca_{Exch} (Eq. 6.2; Fig. 6.1 B). This dissolution also indirectly affected the crystallinity of Fe oxides and SOC accumulation at the $CaCO_3$-bearing site. The effects of this presence or absence of $CaCO_3$ on SOC will now be explored in more detail below, focusing on the specific role of Ca in the accumulation of SOC. The hypothesised mechanisms, which could explain these observations will be first synthesised in a conceptual diagram in Figure 6.1 (A:N).

A) $Al(OH)_3(s) + 3H^+(aq) \leftrightarrow Al^{3+}(aq) + 3H_2O\ (l)$

B) $Al^{3+}(aq) + H_2O(l) \leftrightarrow AlOH^{2+}(aq) + H^+(aq)$

C) $AlOH^{2+}(aq) + H_2O(l) \leftrightarrow AlOH_2^+(aq) + H^+(aq)$

Eq. 6.1. The buffering of soil pH by available aluminium (Al^{3+}). **A)** The dissolution of gibbsite ($AlOH_3$) releases Al^{3+} and consumes protons, while the progressive hydrolysis of Al^{3+}, and potential precipitation of gibbsite, releases protons. **B & C)** The progressive hydrolysis of dissolved Al^{3+}. All three equations are adapted from Chadwick and Chorover (2001). The letters in brackets refer to chemical states: solid, aqueous and liquid (s, aq, & l, respectively).

A) $CaCO_3(s) + 2H^+(aq) \Rightarrow Ca^{2+}(aq) + CO_2(g) + H_2O(l)$

B) $CaCO_3(s) + H^+(aq) \Rightarrow Ca^{2+}(aq) + HCO_3^-(aq)$

Eq. 6.2. The acid hydrolysis of calcium carbonate ($CaCO_3$), which consumes protons and liberates available calcium (Ca), **(A)** while degassing carbon dioxide (CO_2), when strong acids are acting or **(B)** bicarbonate ions when weak acids are involved. Although the yield in this chemical formula is included as a one-way direction, $CaCO_3$ may reprecipitate due to evaporation or biomediated processes; it is worth noting that reprecipitation processes through evaporation were likely limited at the Nant Valley, because of its high aridity index, but biomineralisation remains possible. The letters in brackets refer to chemical states: solid, aqueous and liquid (s, aq, & l, respectively).

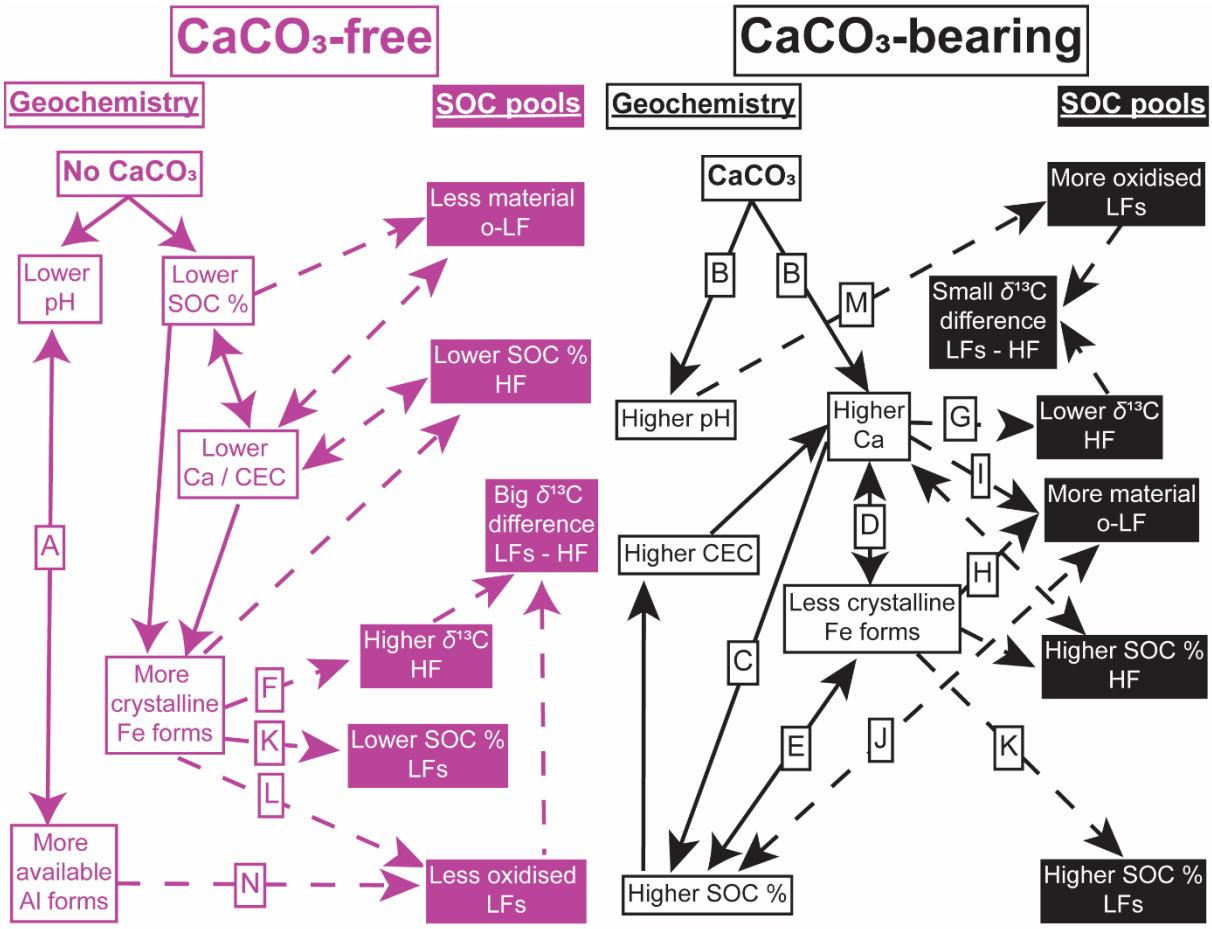
CaCO₃-free
Geochemistry
SOC pools
No CaCO₃
Lower pH
Lower SOC %
Lower Ca / CEC
More crystalline Fe forms
More available Al forms
Less material o-LF
Lower SOC % HF
Big δ¹³C difference LFs - HF
Higher δ¹³C HF
Lower SOC % LFs
Less oxidised LFs
A
F
K
L
N
CaCO₃-bearing
Geochemistry
SOC pools
CaCO₃
Higher pH
Higher Ca
Higher CEC
Less crystalline Fe forms
Higher SOC %
More oxidised LFs
Small δ¹³C difference LFs - HF
Lower δ¹³C HF
More material o-LF
Higher SOC % HF
Higher SOC % LFs
B
B
M
G
I
D
H
C
E
J
K

Fig. 6.1. Synthesis of the cascading influence of calcium carbonate ($CaCO_3$) on geochemistry and soil organic carbon (SOC) at the $CaCO_3$-bearing site and how this differed from the $CaCO_3$-free site. Text boxes representing geochemical variables are hollow, while text boxes representing changes in the SOC pools are filled. LFs, o-LF and HF refer to the light fractions (occluded and free-light fraction), occluded fractions specifically and heavy fractions, respectively. Arrows indicating interactions between geochemical variables are in full, while arrows indicating the impacts of geochemistry on SOC are dashed. Specific numbered arrows refer to the following mechanisms: **A)** Retention of available aluminium and its hydrolysis / buffering of soil pH. **B)** The dissolution of $CaCO_3$ releasing available calcium (Ca) and increasing pH. **C)** Accumulation of SOC by Ca, in turn, increases the exchange capacity of the soil and retains more exchangeable Ca. **D)** Ca inhibits the crystallisation of natural ferrihydrite, which, if past its point of zero charge, can adsorb and protect Ca. **E)** SOC inhibits the crystallisation of ferrihydrite, stabilising more SOC. **F)** Well crystalline Fe forms preferentially stabilise microbially-recycled SOC with higher stable carbon isotope compositions ($\delta^{13}C$ values). **G)** Ca flocculates dissolved organic carbon with lower $\delta^{13}C$ values. **H)** Poorly crystalline Fe forms may have stabilised occluded SOC. **I)** Ca increases the occlusion of SOC through flocculation. **J)** An increased SOC content increases biotic aggregate formation. **K)** Increased mineral coating decreases the SOC content of the LFs. **L)** Mineral coatings stabilises SOC. **M)** Near-neutral environments increases the efficiency of decomposition. **N)** More available Al decreases the efficiency of decomposition.

6.2 - The cascading influence of $CaCO_3$ on SOC

Soil organic carbon was strongly affected by an increase in Ca availability, driven by the presence of $CaCO_3$ at our Nant Valley sites.

Soil organic carbon content and $\delta^{13}C$ values were different at the otherwise similar sites with or without $CaCO_3$ at the Nant Valley alpage. Ca^{2+}, released during the dissolution of $CaCO_3$ (Eq. 6.2), can stabilise SOC through multiple mechanisms (Chapter 3). We tried to distinguish the potential role of Ca in SOC accumulation at the sites by isolating operationally-defined SOC pools related to different stabilisation mechanisms (free, occluded and mineral-associated SOC; Chapter 5). In this section (6.2) we will discuss the environmental processes that could have led to the differences between these pools and the potential role of Ca in these observations. The following synthesis will be ordered by decreasing mass of SOC to focus on the relatively more-important SOC stabilisation mechanisms first, which will also be covered in more detail.

The principal ways in which SOC differed between our sites were:

i) **Accumulation of mineral-associated SOC** - there was almost twice as much mineral-associated SOC at the $CaCO_3$-bearing site.
ii) **Differences in the quality of mineral-associated SOC** - $\delta^{13}C$ values of the mineral-associated SOC were typically lower at the $CaCO_3$-bearing profiles.
iii) **Accumulation of occluded SOC** - there was more occluded material at the $CaCO_3$-bearing site, particularly in the o-LF_{200}.
iv) **SOC contents of the LFs differed** - The SOC contents of the LFs were lower at the $CaCO_3$-free site.
v) **Differences in the quality of SOC within the LFs** - SOC in the LFs was more oxidatively transformed at the $CaCO_3$-bearing site, particularly in the occluded fractions.

6.2.1 - The accumulation of mineral-associated SOC

Our findings suggested that a higher Ca availability promoted the accumulation of mineral-associated SOC. Potential mechanisms underlying this accumulation are explored below.

6.2.1.1 - Conventional outer sphere polyvalent cation bridging

The outer sphere polyvalent cation bridging of SOC to mineral surfaces by Ca_{Exch} likely explains a proportion of the higher mass of mineral-associated SOC at the $CaCO_3$-bearing site (Fig. 6.1 C). However, the persistence of SOC in association with minerals (HF) at the $CaCO_3$-bearing site, in-spite of an increased abundance of Na^+ during DF, would seem to rule this out as the predominant mechanism. Exchange-like outer sphere interactions are weaker than inner sphere interactions (Sposito, 2016), meaning that they occur rapidly in soils according to the affinity of given cations for exchange sites,

their valence, hydrated ionic radius, and concentration (Essington, 2015). Monovalent Na^+ has less of an affinity for exchange sites on our HF than polyvalent Ca^{2+} (Sokoloff, 1938), due in part to its smaller valence and large hydrated radius (Kiriukhin and Collins, 2002). Yet, during DF, the concentration of Na^+ outweighed that of Ca^{2+} by several orders of magnitude. Consequently, if the bonds linking Ca^{2+} with SOC in the HF were purely outer sphere, Ca^{2+} would have likely exchanged with Na^+ during DF. This would have disrupted these bonds, causing SOC to be redistributed into the LFs, while reducing the mass of mineral-associated SOC.

Contrarily, we saw that the mass of SOC in the HF remained high and consistent at both sites, most closely representing the bulk SOC values. Thus, the interactions that bound SOC to the HF at the $CaCO_3$-bearing site seem to have been resistant to exchange-like reactions with Na^+. There are three potential hypotheses that could explain the persistence of mineral-associated SOC in the $CaCO_3$-bearing HF during DF:

i.i) The inner sphere complexation of SOC by Ca.

i.ii) The zonal structuring of OMA and protection of Ca_{Exch} / SOC from exchange-like reactions at the organo-mineral interface.

i.iii) Fe-Ca-ternary complexation of SOC.

6.2.1.2 - Inner sphere

Surface chemistry of inner sphere complexes

Metal cations can be adsorbed onto soil solid phases such as mineral surfaces or SOC functional groups through either the simple accumulation of an ion swarm around a negatively charged surface, outer sphere or direct inner sphere complexation (Sposito, 1981; Sposito, 2016). The propensity for a specific cation to form an inner sphere complex with a ligand / mineral surface is largely governed by local pH, ionic ratio of cation to ligand, ionic potential of the cation, Lewis nature of both the cation and surface, amongst other factors (Essington, 2015; Rahnemaie et al., 2006; Sposito, 2016). During inner sphere interactions the cation acts as a Lewis acid and the ligand a Lewis base. The availability of these ligands thus increases during deprotonation, which coincides with a soil pH range that is consistent with an increased Ca content. Inner sphere (covalent) complexes are more resistant than outer sphere complexes and thus, would be resistant to pure exchange-like (outer sphere) reactions (Rahnemaie et al., 2006; Sutton et al., 2005). Yet, there is still no evidence that Ca^{2+} could form inner sphere complexes with organic ligands or mineral surfaces in environmental samples and we still do not fully understand the thermodynamics of these processes.

Existence of inner sphere complexes

In Chapter 3, we hypothesised that, contrary to popular belief in soil sciences, SOC may be stabilised by inner-sphere complexes with Ca^{2+} (Fig. 6.1 C). This hypothesis was supported by chemical modelling studies (Bogatko et al., 2013; Iskrenova-Tchoukova et al., 2010), which indicated that Ca can, and predominantly does, form inner sphere complexes with certain functional groups of DOC (Kalinichev and Kirkpatrick, 2007; Sutton et al., 2005). We unsuccessfully attempted to extract this pool in Chapter 4, which was prevented by the simultaneous extraction of reactive $CaCO_3$ pools. However, the persistence of mineral-associated SOC during DF at the $CaCO_3$-bearing site (Chapter 5) may be evidence of the inner sphere complexation of SOC in these fractions. SOC complexed through inner sphere interactions with Ca would be more resistant to exchange-like reactions with Na^+ during DF. However, these forms of OMA have still not yet been identified in environmental samples. Comprehensive spectroscopic techniques are now needed to confirm the presence or absence, and nature of inner sphere bonds between SOC and Ca in a natural environment (discussed further in the opening perspectives section).

6.2.1.3 - Zonal structuring of OMA

A hypothesis to explain the retention of mineral-associated SOC at the $CaCO_3$-bearing site during DF, could be that outer sphere, exchange-like reactions between Ca_{Exch} and SOC were protected by the zonal structuring of OMA. Following the conceptual model presented by Kleber et al. (2007; Fig. 1.6), Ca^{2+} can contribute to the adsorption of SOC in either the direct contact or the kinetic zone of the organo-mineral interface. Speculatively, the flocculation of Ca^{2+} could, in theory, also increase the sorption of DOC / SOC by bridging another layer, an organo-cation layer, between the contact layer and the hydrophobic zone. In the hydrophobic zone, SOC is hypothesised to arrange into a micellar-like structure, with a hydrophobic interior and hydrophilic exterior (Kleber et al., 2007). If an outer sphere complexation of SOC by Ca was to occur within this conceptual zone of hydrophobic interactions, it could be, in theory, protected from exchange-like reactions with Na^+ by the micellar-like structure of OMA. This zonal structuring of OMA could then, in theory, be protecting outer sphere bonds between SOC and Ca^{2+} from exchange-like reactions during DF. However, this remains highly speculative and further experimentation with more advanced surface characterisation techniques and sorption experiments is still required to investigate how Ca_{Exch} influences the structure of OMA.

6.2.1.4 - Ca-Fe interactions

A co-stabilisation identified in experimental settings

This thesis may have provided weak supporting evidence for a potential co-stabilisation of SOC by Fe and Ca. Yet, before exploring these potential interactions in an environmental setting, it is first necessary to discuss two pivotal studies (Sowers et al., 2018a; Sowers et al., 2018b), which demonstrated that Ca / Fe could co-stabilise SOC in an experimental setting. In their first study (Fig. 6.2), Sowers et al.

(2018b) demonstrated that their experimental control (synthetic ferrihydrite) adsorbed less negatively charged DOC as pH levels increased towards its point of zero charge (PZC; pH 7-9; Schwertmann and Fechter, 1982). At lower pH, Ca addition increased DOC adsorption slightly relative to the control, but at higher pH, as the adsorption of the ferrihydrite decreased, Ca addition maintained high levels of DOC adsorption. Sowers et al. (2018b) hypothesised that at lower pH, the increased sorption during Ca addition was probably caused by Ca flocculating additional DOC onto the exterior of existing OMA (similar, conceptually, to the hypothesised organo-cation layer, discussed above). However, at a higher pH, as the surface charge of synthetic ferrihydrite decreased, Ca^{2+} bridged DOC onto the negatively charged ferrihydrite, co-stabilising it. In a later study, Sowers et al. (2018a) used STXM C-NEXAFS to elucidate that this accumulation was likely due to the formation of Fe-Ca-C ternary complexes. In theory, these experimental interactions would also be resistant to exchange-like reactions with Na^{+} and could thus explain a proportion of the SOC accumulated in OMA at the $CaCO_3$-bearing site. Yet, could these interactions exist in a natural environment like the $CaCO_3$-bearing site, and if so, how would they interact? We'll now explore this topic further in the following sections.

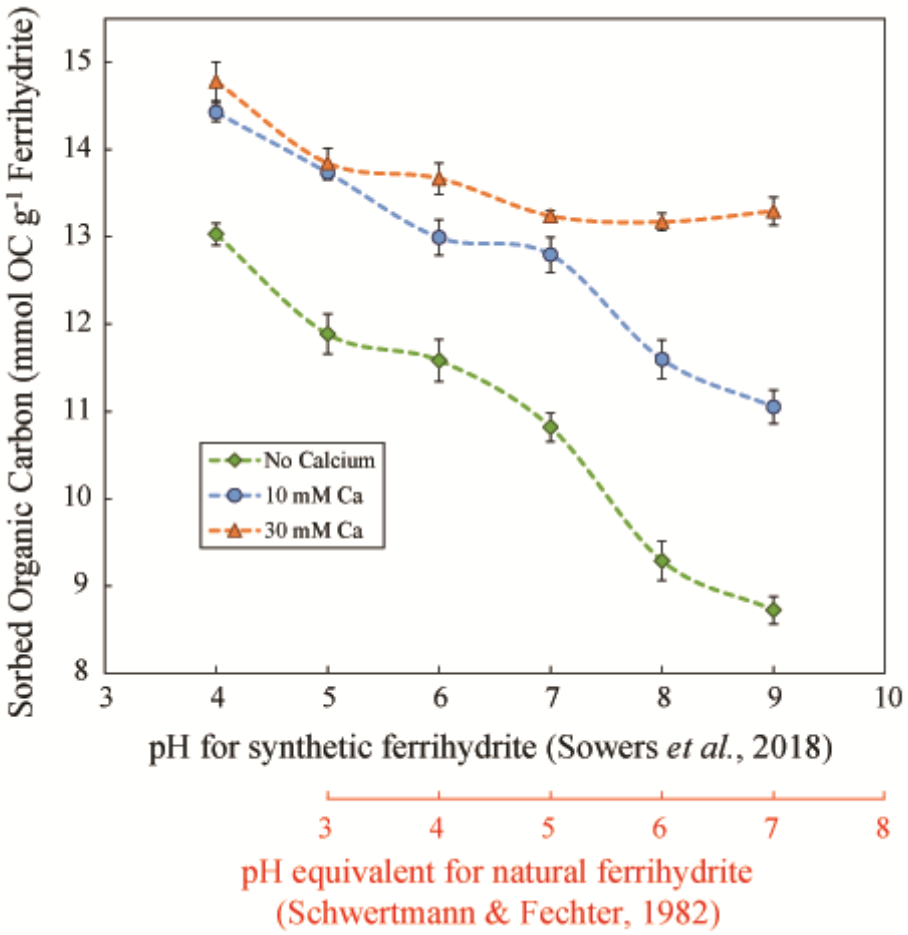

Fig. 6.2. The effect of calcium (Ca) addition (10 mM Ca or 30 mM Ca) on the adsorption of dissolved organic carbon by ferrihydrite over a pH range of 4 – 9 modified from Sowers et al. (2018b) published in Geochemical Transactions©. An initial dissolved organic carbon to iron ratio of 4.7 was used for all samples and experiments were performed in triplicate. The data points represent the mean of the triplicates, but it is not clear whether the error bars represent the standard deviation or standard error of these measurements. Below this we have plotted, in orange, a potential shift in the pH of these experiments caused by differences in the point of zero charge (PZC) of synthetic and natural ferrihydrite. The PZC of natural ferrihydrite (5.5-7) is lower than that of synthetic ferrihydrite (7-9; Schwertmann and Fechter, 1982) and we would thus expect the relationship witnessed with Ca to occur in natural soils at a lower pH.

The positive feedback Ca-Fe

In a natural soil environment, the potential interactions between Ca, Fe and SOC are likely to be far more complicated (Chapter 4). Firstly, due to the presence of impurities, the PZC of natural ferrihydrite (pH 5.5–7) is lower than that of synthetic ferrihydrite (pH 7-9; Schwertmann and Fechter, 1982) used in Sowers et al. (2018b). This means that a lower pH (pH >5.5) is required to change the surface charge of any natural ferrihydrite towards a negative charge (Fig. 6.2), at which point, it would interact more

strongly with positively charged Ca_{Exch}. The crystallisation of well crystalline Fe oxides from ferrihydrite could then be inhibited by this interaction with Ca_{Exch} (Fig. 6.1 D; Thompson et al., 2011). Both pH and Ca_{Exch} were increased by $CaCO_3$ dissolution at the $CaCO_3$-bearing site (Fig. 6.1 B; Eq. 6.2), which could therefore create a positive feedback between Ca_{Exch} sorption by Fe forms and the inhibition of their crystallisation. This interaction would create an intimate association between Ca and Fe that is driven by pH and likely explains the higher Fe_o/Fe_d ratios at the $CaCO_3$-bearing site (Chapter 4).

The effect of a Ca/Fe interaction on mineral-associated SOC

The potential positive feedback between the inhibition of Fe form crystallisation and the adsorption of Ca over a specific pH range may also have positively influenced the accumulation of SOC in OMA. It is highly probable that the more poorly crystalline Fe forms played some role in the accumulation of the higher mass of mineral-associated SOC at the $CaCO_3$-bearing site (Kramer and Chadwick, 2018). Like with Ca_{Exch}, the adsorption of organic colloids by poorly crystalline Fe forms is also known to inhibit their crystallisation (Fig. 6.1 E; Kleber and Jahn, 2007). However, while the higher pH at this site would have reduced the surface charge of poorly crystalline Fe forms and their adsorption of negatively charged SOC (Schwertmann and Fechter, 1982), Ca_{Exch} could have contributed to this accumulation by acting as a bridge between negatively charged surfaces (Sowers et al., 2018b). This would ensure that poorly crystalline Fe forms continue to stabilise negatively charged SOC through their co-association with Ca, even after the PZC of natural ferrihydrite has passed (Fig. 6.2; Sowers et al., 2018a; Sowers et al., 2018b). There was no correlation between SOC content and the free Fe (Fe_o) to Ca (Ca_{Exch}) ratio, but this metric may not act as an appropriate metric for these interactions. We can thus hypothesise that, Ca_{Exch} and poorly crystalline Fe forms may have been co-stabilising SOC on the HF at the $CaCO_3$-bearings site due to its higher pH. Speculatively, this form of stabilisation could also be partially protecting Ca_{Exch} from exchange-like reactions (Chan et al., 1979), explaining the persistence of these interactions during DF with Na^+.

Shifting pH - The transition between mechanisms

Interestingly, as the pH changed between profiles at the $CaCO_3$-bearing site, this relationship between Fe and Ca may have been destabilised, and instead shifted towards a competitive relationship. Profile B3 differed in characteristics from the other $CaCO_3$-bearing profiles (B1 & B2), and seemed to represent a transition between the two sites. Of the $CaCO_3$-bearing profiles, profile B3 was the furthest away from the adjacent cliffs and seemed to be the least impacted by the alluvio-colluvial inputs of limestone. Relative to B1 and B2, B3 had a slightly lower amount of $CaCO_3$, a lower pH, higher Fe_o/Fe_d ratios, and lower Ca_{Exch} content that were non-linear with SOC / depth (Fig. 4.14). As all profiles at the $CaCO_3$-bearing site had similar texture and SOC content, we hypothesised that this deviation in the Ca_{Exch} profile was likely caused by the occupation of exchange sites by poorly crystalline Fe forms (Chapter 4). This

suggests that, as the pH level dropped, there was direct competition between Fe and Ca for functional groups of SOC, which negatively impacted the retention of Ca_{Exch}. We can hypothesise that the lower pH at B3 increased the surface charge of poorly crystalline Fe forms, subsequently decreasing their interaction with Ca_{Exch} and increasing their role in the sorption of SOC, occupying exchange sites. Interestingly, differences in the quality of mineral-associated SOC at the two sites may have further hinted at their individual roles in OMA.

6.2.2 - Differences in the quality of mineral-associated SOC

Calcium-rich soils similar to the Nant Valley have been previously shown to contain an abundance of SOC with a fresh signal (Matteodo et al., 2018); but contrary to our hypothesis, this was related to a difference in the quality of mineral-associated SOC between our sites rather than occluded material (Chapter 5). Mineral-associated SOC typically had lower $\delta^{13}C$ values at the $CaCO_3$-bearing site (particularly at B1 & B2). These differences could have arisen from two specific mechanisms:

ii.i) Stronger stabilisation - Firstly, mineral-associated SOC could have been better protected at the $CaCO_3$-bearing site and thus, less oxidatively transformed because of its mineral-association.

ii.ii) Preferential stabilisation - Secondly, SOC could have been preferentially stabilised through the different forms of mineral association at our Nant Valley sites, thereby leading to the differences in quality of mineral-associated SOC.

While these differences could be explained by a higher degree of stabilisation at the $CaCO_3$-bearing site (Hypothesis ii.i above), within the literature, sorption mechanisms mediated by Ca are commonly hypothesised to provide a weaker degree of stabilisation relative to those mediated by Fe or Al forms (von Lützow et al., 2006; Wiesmeier et al., 2019). If mineral-associated SOC was more stable at the $CaCO_3$-bearing site, we would expect this site to always have lower HF $\delta^{13}C$ values than the $CaCO_3$-free site. Yet, at our sites, Profile B3 had $\delta^{13}C$ values that were more similar to the $CaCO_3$-free site. This transitional site thus questions this hypothesis (ii.i) and instead hints that the differences in the quality of mineral-associated SOC at our sites may be linked to the effects of a preferential stabilisation (hypothesis ii.ii).

SOC of varying quality may have been preferentially stabilised by the different, dominate forms of mineral-association at the two sites.

Within the literature, Fe oxides are thought to preferentially stabilise of microbial matter with higher $\delta^{13}C$ values (Fig. 6.1 F; Spielvogel et al., 2008), while Ca_{Exch} could be responsible for preferentially stabilising DOC with lower $\delta^{13}C$ values (Fig. 6.1 G; Minick et al., 2017). Our data, at the $CaCO_3$-bearing site, could support these hypotheses as poorly crystalline Fe forms seemed to be more dominant at B3

(Fig. 4.14 A), while Ca_{Exch} appeared more dominant in B1 and B2 (Fig. 4.14 C; Chapter 4). This, in turn, corresponded with changes in the HF $\delta^{13}C$ values at our $CaCO_3$-bearing site (Fig. 5.8; Chapter 5), which were more similar to the $CaCO_3$-free site at B3, but were lower at both B1 and B2. Thus, the HF $\delta^{13}C$ values may have identified a shift in the preferential stabilisation of mineral-associated SOC, caused by the dominance of different geochemical actors at our profiles (Fe oxides / Ca); but, to confirm this hypothesis, further investigation of the preferential stabilisation of SOC by different geochemical actors over a range of soil pH conditions is still needed.

6.2.3 - The accumulation of occluded SOC

There was more occluded SOC at the $CaCO_3$-bearing site and this is likely linked to the increased availability of Ca and SOC.

As hypothesised in Chapters 3, 4, and 5, there was more occluded SOC at the $CaCO_3$-bearing site. The role of $CaCO_3$ cementation, during evaporative processes (not discounting a potential role of biominerals; Bindschedler et al., 2016; Dincher et al., 2019; Zamanian et al., 2016), in the stabilisation of aggregates and accumulation of occluded SOC was likely inhibited by the humid conditions at the $CaCO_3$-bearing site. Likewise, while poorly crystalline Fe forms are thought to influence the occlusion of SOC (Fig. 6.1 H; Duiker et al., 2003), their variable charge and the increased pH at B1 and B2 would have probably diminished their direct role in the stabilisation of aggregates. Instead, it was likely the abiotic influence of the flocculation of soil separates by Ca_{Exch} (Fig. 6.1 I; Melvin et al., 2013; Muneer and Oades, 1989a; Muneer and Oades, 1989b; Muneer and Oades, 1989c; Paradelo et al., 2016) and the biotic influence of an increased SOC content (Fig. 6.1 J; Chenu, 1989; Chenu and Cosentino, 2011; Chenu and Plante, 2006; Costa et al., 2018), which augmented aggregation and increased occluded SOC mass at the $CaCO_3$-bearing site. Interestingly, Ca could also play a role in the promotion of biologically-formed aggregates at the $CaCO_3$-bearing site as it forms a key component linking EPS (personal discussion with Dr. Marco Keiluweit, 2018) and flocculating root mucilages into adhesive matrices that can cement aggregates (Czarnes et al., 2000; de Kerchove and Elimelech, 2007). Thus, we can hypothesise that there are probably several mechanisms through which an increased Ca availability directly impacted aggregate formation / stabilisation at the $CaCO_3$-bearing site, and subsequently, the accumulation of occluded SOC.

6.2.4 - Differences in SOC content of LFs

Soil organic carbon contents of the LFs were lower at the $CaCO_3$-free site and this is likely linked to an increased mineral coating on these fractions.

The SOC contents of the LFs were approximately 10 % higher (Fig. 5.4) at the $CaCO_3$-bearing site. This was most likely caused by a dilution effect on the SOC contents of the LFs by an increase in mineral coating (potentially mineral clay particles or well crystalline Fe oxides) at the $CaCO_3$-free site (Fig. 6.1

K). The quantification of the surficial chemistry (Fe, Al, Si) by the XPS did not seem to support this hypothesis, but it also failed to identify the larger differences that should exist between the LFs and HF. Furthermore, inspection of the fractions with optical microscopy during pre-testing did seem to weakly support this hypothesis (Appendix Fig. 8.17). Thus, it seems probable that the diluted SOC contents at the LFs were caused by increased mineral coating.

6.2.5 - Differences in the quality of SOC within the LFs

There were differences in the quality of SOC in the LFs and this was likely linked to a stabilisation by the aforementioned mineral coating and differences in geochemical environment between the sites.

Both $\delta^{13}C$ values and XPS measurements suggested that the LFs were less oxidatively transformed at the $CaCO_3$-free site, which could have been caused by two different mechanisms. Firstly, the above-hypothesised mineral coating (Al, Fe oxide and clay particles) on the LFs could inhibit their oxidative transformation through physical separation and sorption mechanisms (Fig. 6.1 L; Gu et al., 1994; Kaiser and Guggenberger, 2003). Secondly, the different geochemical conditions present at the two sites could have been promoting or inhibiting their respective microorganism communities. Near-neutral conditions like those at the $CaCO_3$-bearing site supposedly present near-optimum conditions for bacterial transformation of SOC (Fig. 6.1 M; Zelles et al., 1987); while, in contrast, Al^{3+} and H^+, which were more abundant at the $CaCO_3$-free site, are largely thought to stress bacterial communities (Jones et al., 2019; Scheel et al., 2008; Tate and Theng, 1980; Tonneijck et al., 2010). The toxic effects of Al^{3+} have long been hypothesised to stabilise SOC (Tate and Theng, 1980), although evidence for this can be contradictory (Marschner and Kalbitz, 2003). Thus, we can speculatively hypothesise that the increased abundance of available Al^{3+} at the $CaCO_3$-free site, relative to the $CaCO_3$-bearing site, may have inhibited the oxidation of easily accessible SOC (LFs; Fig. 6.1 N).

6.2.5.1 – Differences in microbial community and carbon use efficiency

Geochemistry may have also affected the composition of the microorganism communities, present at our sites. It is reasonably well established that an increasing pH is linked to a decreases in the fungal to bacterial ratio of soils at the global-scale (Bahram et al., 2018; Blagodatskaya and Anderson, 1999; Rousk et al., 2010; Rousk et al., 2009). As the differences in geochemistry at our sites differentiated their soil pH (Eq. 6.1 & 6.2), we can also assume that this may have affected the composition of the microbial communities at our sites. This could mean that there was a decreased fungal to bacterial ratio at our $CaCO_3$-bearing site.

Microorganism communities utilise SOC differently and as such, have different carbon use efficiencies. Carbon use efficiency is defined as the proportion of C assimilated by a microorganism that is used for growth and biomass (Bradford and Crowther, 2013). Although still in its infancy, early work is demonstrating that there is an exponential negative relationship between the fungal to bacterial ratio and

carbon use efficiency (Soares and Rousk, 2019). This implies that CUE is higher in bacterial-dominated soils, leading to an increased production of microbial metabolites, which can then be incorporated into the SOC pool. While there is not yet enough evidence of this relationship, an increase in pH could potentially be linked to an increase in carbon use efficiency, with shifting microbial community (Bahram et al., 2018; Rousk et al., 2010; Rousk et al., 2009; Soares and Rousk, 2019). Thus, the increased pH driven by the presence of $CaCO_3$ at the $CaCO_3$-bearing site, may be linked to a shift in microbial community, their carbon use efficiency, an increase in SOC content and a differential effect on the LFs at our sites. However, this is all based upon several assumptions and future investigation if there is a shift in microbial community between the sites and whether this change may have affected their carbon use efficiency and the LFs or SOC accumulation at our sites.

6.2.5.2 - Occlusion specific - differing levels of protection within different aggregates

Occluded SOC was more oxidised at the $CaCO_3$-bearing site, which was potentially evidence of increased biological aggregate formation

While the f-LF and occluded fractions had a similar ratio of aliphatic / aromatic to oxidised C moieties and $\delta^{13}C$ values at the $CaCO_3$-bearing site, the occluded SOC at the $CaCO_3$-free site was less oxidised than the f-LF. During biological aggregate formation SOC is decomposed prior to being occluded within its EPS bound aggregate (Fig. 6.1 J; Chenu and Cosentino, 2011). Thus, supporting the idea that biological aggregate formation was more abundant at the $CaCO_3$-bearing site, explaining a proportion of the larger occluded SOC pool at the $CaCO_3$-bearing site.

6.3 - Applications

6.3.1 - pH - the master variable and a linking theme?

This thesis supports the idea that pH should be incorporated into SOC models to parsimoniously improve their estimations of SOC content, by accounting for the geochemical controls on SOC persistence and accumulation.

There has been a recent revolution in our understanding of SOC, its decomposition (Lehmann and Kleber, 2015) and stabilisation within a soil profile (Schmidt et al., 2011). Unfortunately, conventional SOC models have still not fully incorporated this paradigm shift. SOC models have typically used climate (temperature / moisture) or clay content as the dominant variables for determining SOC content at the continental- to global scale (Coleman and Jenkinson, 1996; Parton, 1996). Climate has clear effects on SOC at the global scale (Davidson and Janssens, 2006; Schipper et al., 2014) and a finer texture (clay / fine silt content) does have well-established links to SOC stabilisation (Hosking, 1932); however, these are not the sole controls on SOC and this approach amounts to a rough generalisation at best.

It is clearly unjust to compare the alpage scale of the Nant Valley dataset to the results achieved by global SOC estimation methods, because results are scale dependent in soil science (Yudina and Kuzyakov, 2019). Yet, the $CaCO_3$-free site had a similar climate and a slightly higher clay content to the $CaCO_3$-bearing site. Consequently, SOC models based on clay and climate would estimate that the $CaCO_3$-free site had a slightly higher SOC content. However, SOC was actually twice as high at the $CaCO_3$-bearing site where the clay content was slightly smaller. This finding has recently been supported by Solly et al. (in review) who evaluated the variables that best predicted SOC content in a set of 1000 Swiss forest sites, demonstrating that clay content only predicted 7 % of the overall signal in their dataset. These findings further highlight the unreliability of estimations of SOC content made with models that use clay content as the sole variable.

Rasmussen et al. (2018) recently called for a movement "beyond clay", to find a new set of variables that more accurately predict SOM content. Rasmussen et al. (2018) analysis of 5,500 soil profiles suggested that Ca_{Exch} worked as an efficient predictor of SOM content in arid environments, while Al hydroxides and moisture content worked better in humid environments. This is once again, tracks with our understanding of Ca / Al chemistry on a global scale due to the leachable nature of Ca and the soluble nature of its main reservoir $CaCO_3$ (Likens et al., 1998). In a more humid environment, SOC should, in theory, be largely driven by Al / Fe hydroxides or a high water content (Histosols), as we can assume that with time, the presence of Ca_{Exch} would be reduced as it is leached from the system (unless restocked by Ca-rich parent material; Chapter 4). Thus, in their study, Rasmussen et al. (2018) seemed to have effectively identified a global transition from Ca-to-Al dominated biogeochemistry with climate, and their respective roles in SOC accumulation.

In Chapter 3 (Fig. 3.2), we hypothesised that pH could be used as a parsimonious variable (cheap and efficient) to incorporate this shift in geochemical controls on SOC cycling, into estimations of SOC content at the global scale. Unlike CEC, which correlates with the content of organic C in a soil because SOM is a predominate source of exchange sites, pH can act as a relatively independent measure of the shifting geochemical controls on SOC stabilisation (Rasmussen et al., 2018; Slessarev et al., 2016; Solly et al., in review). Unlike climate, which separates humid (largely buffered by available Al^{3+}; Eq. 6.1) from arid (largely buffered by $CaCO_3$; Eq. 6.2) environments (Slessarev et al., 2016), pH would also identify the presence of $CaCO_3$ in humid and temperate soils, like the $CaCO_3$-bearing site at the Nant Valley (and their potentially high SOC contents). In a case of apparent "multiple-independent" suggestion, both ourselves and Rasmussen et al. (2018) independently hypothesised this in the same edition of Biogeochemistry©. We have included an adapted version of their conceptual model below (Fig. 6.3), showing the shifting geochemical controls on SOC accumulation with pH. However, has this suggestion been supported by the empirical data gathered in Chapter 4 and 5?

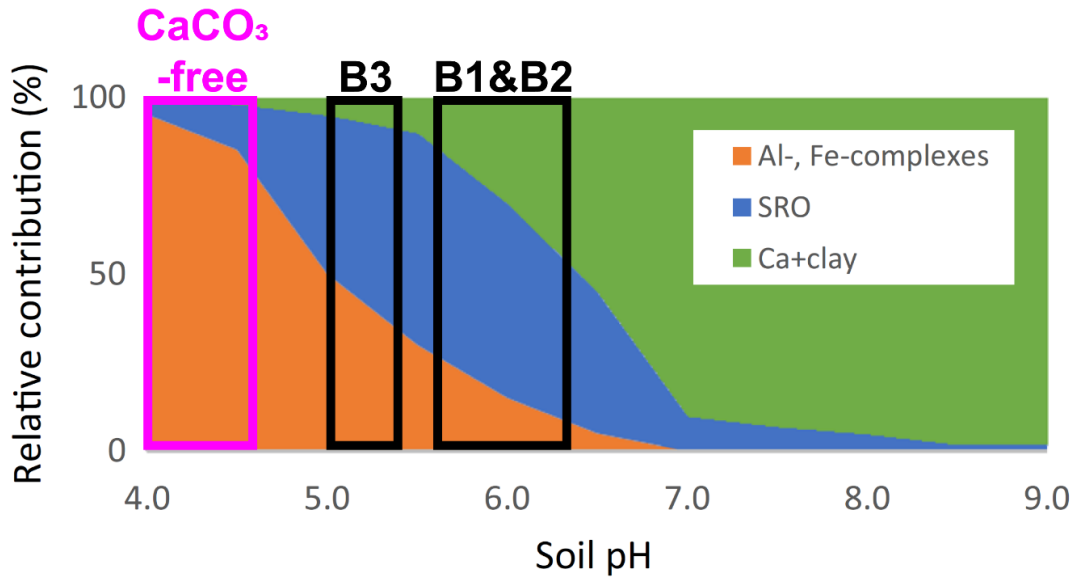

Fig. 6.3. A conceptual model of how horizon-level soil pH identifies a shift in the relative importance of different geochemical controls on soil organic carbon stabilisation. Image adapted from Rasmussen et al. (2018), published in Biogeochemistry©. Atop of their conceptual diagram we have highlighted the soil pH level of our samples with three boxes, grouped by the $CaCO_3$-free, B3, and the B1 / B2 profiles. It is worth noting that profile B3 did have one sample with a high pH (B3.7 = 6.5), which contained a distinct increase in calcium carbonate equivalent material and has not been included within its range.

As can be seen in Figure 6.3, the Nant Valley profiles plotted slightly lower than where we would expect them to, regarding the dominance of specific SOC stabilisation mechanisms at the Nant Valley. Yet, we measured our soil pH in 0.1 M $CaCl_2$, known to reduce soil pH by about 1.0 unit relative to soil pH in H_2O (Sumner, 1994), thereby explaining this shift. We found that the $CaCO_3$-free site had a relatively higher dominance of available Al forms and a Fe_o/Fe_d ratio of approximately 0.5, indicating a near-split between well crystalline and poorly crystalline Fe forms. Shifting to B3, we saw that poorly crystalline Fe seemed to dominate with its pH that was intermediate relative to the other profiles; while, Ca_{Exch} (and its potential co-stabilisation with Fe) seemed more dominant in both profile B1 & B2, which both had a higher pH. Thus, if the pH of the Nant Valley samples are shifted slightly higher (equivalent to that extracted by H_2O), the conceptual diagram of Rasmussen et al. (2018) seems to accurately predict observations from our dataset regarding the relative contribution of geochemical controls to SOC accumulation and cycling.

In Fig. 6.4 we have replotted Fig. 3.2, accounting for the results from this thesis and recent findings presented in the literature (Rasmussen et al., 2018; Sowers et al., 2018a; Sowers et al., 2018b). In this updated version we have split the role of well crystalline Fe oxides from that of poorly crystalline Fe oxides. We have also included the potential stabilisation of SOC by a Fe-Ca ternary complexation system. The environments in which this system could exist is once again predicted by pH, dictating at what point the surface charge of poorly crystalline Fe oxides begins to shift towards a negative charge

and can thus interact with Ca^{2+} (Schwertmann and Fechter, 1982; Sowers et al., 2018b). Overall, soil pH may help us parsimoniously reduce the uncertainties in traditional SOC models (Fig. 6.4), accounting for geochemical / climatic anomalies like the Nant Valley, and the shifting geochemical controls on SOC accumulation.

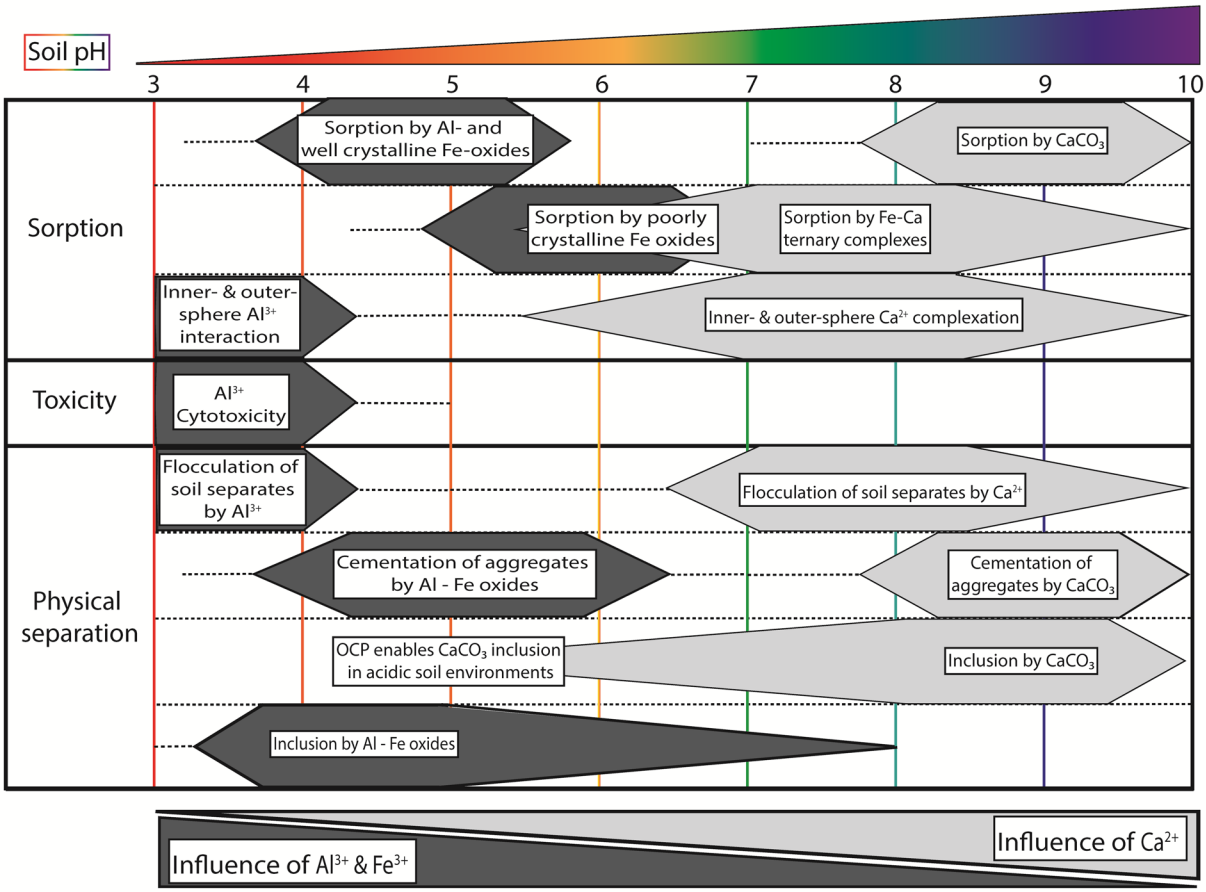

Fig. 6.4. An updated version of Fig. 3.2 detailing a shifting role of polyvalent cations in the stabilisation of soil organic carbon with increasing pH. Thresholds are based on values available in the literature and it is expected that adjustments will occur as more results become available. The sorption of Fe-Ca ternary complexes becomes more dominant as pH increases, which coincides with a decrease in the surface charge of poorly crystalline Fe forms. The text box of the sorption by poorly crystalline Fe forms, has been moved to the left to demonstrate the start of the Fe-Ca-ternary complex system.

6.3.2 - Is Ca-mediated occlusion really not important?

The small mass of SOC in our occluded pool suggests that future investigation into humid Ca-rich environments should instead focus predominantly on the importance of OMA mediated by Ca.

There has been much recent debate on the importance of aggregates and occlusion for the stabilisation and accumulation of SOC at different spatial scales. This debate has largely focused on whether or not, occlusion needs to be accounted for in models that estimate SOC content at a global scale (Kravchenko

et al., 2019; Wang et al., 2019; Yudina and Kuzyakov, 2019). An extrapolation of our results to this argument is impossible because of our study design (Chapter 4) and our operationally-defined occluded pool (Chapter 5; Kaiser and Berhe, 2014). Yet, to synthesise the discussion above, what insights about occlusion can be gained from our observations in Chapter 4 and 5?

In Chapter 5, we hypothesised that occlusion would play a relatively more important role in stabilising SOC at the $CaCO_3$-bearing sites, which in turn, would influence bulk SOC (Matteodo et al., 2018). There was more occluded material at the $CaCO_3$-bearing site, but contradicting our hypothesis, this occluded SOC was also more oxidatively transformed and played a minimal role in bulk SOC accumulation. This implies that Ca-mediated occlusion may not be as important to the accumulation of SOC in Ca-rich environment as first expected, contradicting our current understanding.

Yet, was material still occluded within our HF at the $CaCO_3$-bearing site? To prevent the potential redistribution of material between our fractions in Chapter 5, we did not sonicate above 590 J mL^{-1} (Kaiser and Berhe, 2014; Schmidt et al., 1999). SOC could still have been stabilised by both Ca-mediated occlusion and sorption within strong, nanoaggregates in the HF of the $CaCO_3$-bearing site. However, if these nanoaggregates were, as theorised, flocculated by outer sphere interactions with Ca (Ca-mediated occlusion), they should have been disrupted during the DF with SPT. Furthermore, at this smaller scale, where the conceptual separation of these mechanisms becomes near impossible (Sollins et al., 1996), an accumulation of SOC due to occlusion mediated by Ca would have been less apparent (Fig. 1.7). While we cannot rule out the possibility of Ca-mediated occlusion within strong nanoaggregates, this stabilisation was probably of less importance to the increased SOC content of the mineral-associated fraction than Ca-mediated OMA.

Contrasting this result, several key studies have repeatedly highlighted the importance of occlusion mediated by $CaCO_3$ to SOC in environments with a low aridity index (Blanco-Moure et al., 2012a; Blanco-Moure et al., 2012b; Fernández-Ugalde et al., 2014; Fernández-Ugalde et al., 2011; Virto et al., 2013). $CaCO_3$ has even been demonstrated to disrupt aggregate hierarchy and completely dominate the occlusion of SOC in certain semi-arid environments (Fernández-Ugalde et al., 2014). The high aridity index at the Nant Valley could potentially explain this disparity between our results. Humid conditions could have reduced the importance of the occluded pool at the $CaCO_3$-bearing site, by preventing the cementation of aggregates by $CaCO_3$. It seems that future studies on Ca-mediated accumulation of SOC in similar humid and temperate soil environments should instead focus on the mechanisms that increase the mineral-associated SOC content of Ca-rich soils.

6.3.3 - $CaCO_3$ and SOC management practices in agro-systems

This thesis supports the idea that liming could be a useful tool to help us achieve the targets set out by the 4 Per Mille Initiative, but this hypothesis still requires further investigation in different environments.

Could the findings discussed within this thesis be applied in the context of the 4 Per Mille Initiative? Lime ($CaCO_3$) has been applied agriculturally (liming) for millennia to help prevent soil acidification, which the Romans apparently quantified by taste (Barber, 1984). Furthermore, as shown in this thesis, applying $CaCO_3$ to agricultural soils could also positively influence SOC accumulation, potentially contributing to the direct (sorption / occlusion) and indirect (release of Ca^{2+} / pH changes / increased NPP / Fe form crystallinity) sequestration of SOC (Muneer and Oades, 1989a; Muneer and Oades, 1989b; Muneer and Oades, 1989c). As mentioned previously in Chapter 3, $CaCO_3$ application in agricultural soils has been reported to have mixed effects on SOC (Paradelo et al., 2015), with some authors reporting positive (Auler et al., 2019; Egan et al., 2018a; Muneer and Oades, 1989a; Muneer and Oades, 1989b), non-existent (Paradelo et al., 2016), or even negative effects (Chan and Heenan, 1999) of liming on SOC stocks. One major reason for this inconsistency could be the differences in initial parent material and soil type.

As supported by evidence presented in this thesis, flushing a biogeochemical reactor like a soil with $CaCO_3$ (during liming) could completely change its biogeochemistry and potentially alter its pedogenic trajectory. Soils will react differently to a significant anthropogenic input of $CaCO_3$, based upon their initial pedogenic conditions, particularly in regards to parent material and initial pH conditions. Whereas a $CaCO_3$-bearing or neutral environment may show little to no significant change upon $CaCO_3$-addition (Paradelo et al., 2016; Paradelo et al., 2015), an acidic deforested soil may exhibit more dramatic shifts in biogeochemistry (Carmeis Filho et al., 2017). Potential changes to an acidic system could include an increase in soil pH, Ca_{Exch} (Eq. 6.2), a shift in microorganism community (Rousk et al., 2010; Rousk et al., 2009), and a move away from Al / Fe dominated SOC stabilisation mechanisms (Adams et al., 2000; Chan and Heenan, 1999; Slessarev et al., 2016). Yet, this shift in system has rarely been investigated in detail, probably because it is contrary to the standard model of pedogenesis (Chadwick and Chorover, 2001), driven by the weathering of soils as a function of time (loss of soluble minerals prior to more insoluble minerals). Further investigation is still needed to evaluate the potential of liming to increase SOC accumulation in agro-soil systems under differing initial pedogenic / geochemical conditions. These investigations would also have to calculate the proportion of CO_2 given off during the dissolution of the applied lime (Eq. 6.2; Biasi et al., 2008), and compare this against the C sequestered through an accumulation of SOC. However, this thesis supports the idea that $CaCO_3$ application may help increase SOC contents of degraded agricultural soils (Minasny et al., 2017).

- Chapter 7: General conclusions & opening perspectives -

7.1 - Conclusions

The following synthesis will be structured by the principal research questions of the thesis, listed by their respective chapter number.

3. Can Ca mediate a stabilisation of SOC?

Calcium can mediate a stabilisation of SOC, increasing its resilience against oxidative transformation by microorganisms through several mechanisms. Evidence for this stabilisation dates back to Sokoloff (1938), but has been largely ignored since the works of Oades (1988). Investigations have only recently started to re-focus on these processes (Martí-Roura et al., 2019; Minick et al., 2017; Rasmussen et al., 2018; Solly et al., in review; Sowers et al., 2018b) and have highlighted a potential role of Ca in the stabilisation of SOC. Ca can mediate a stabilisation of SOC by facilitating or bridging organo-mineral, organo-cation, or organo-organic associations or by flocculating primary soil separates, which positively influences aggregation, subsequently occluding SOC. Ca seems to facilitate organo-mineral associations through the outer or inner sphere bridging complexation of SOC and through its interactions with Fe. It is possible that Ca plays an important role in the zonal structure of the organo-mineral interface; but further investigation with, more advanced, spectroscopic techniques is still required to investigate these OMA.

4. What is the influence of small quantities of $CaCO_3$ on the pedogenesis and biogeochemistry of soils that have developed under similar soil forming conditions, in a humid and temperate environment (Nant Valley, Switzerland)?

The presence of $CaCO_3$ created a state of pedogenic inertia at the Nant Valley that bifurcated the pedogenic trajectory and biogeochemistry of the studied soils. The dissolution of $CaCO_3$ caused a shift in the pedogenic trajectory of soils that had developed under otherwise similar soil forming conditions, away from Eutric Cambisols towards Cambic Phaeozems. $CaCO_3$ also had a cascading effect on the biogeochemistry of the $CaCO_3$-bearing site. The dissolution of $CaCO_3$ directly increased pH and Ca, which subsequently inhibited the crystallisation of Fe oxides and increased SOC contents at the $CaCO_3$-bearing site. This study thus supports the idea that liming could be used to help increase the SOC content of degraded agricultural soils, in line with the 4 Per Mille Initiative, but this still requires further investigation in different soil types.

5. How does SOC differ at the sites with or without $CaCO_3$ at the Nant Valley?

Soil organic carbon content and $\delta^{13}C$ values were significantly different between the Nant Valley sites with a natural variation in Ca. Bulk SOC was approximately twice as high at the $CaCO_3$-bearing site and had lower $\delta^{13}C$ values. As hypothesised, there was also more occluded SOC at the $CaCO_3$-bearing site; but contrary to our hypothesis, this seemed to provide little protection to the LFs, which were more

oxidatively transformed at the $CaCO_3$-bearing site. The LFs were likely stabilised at the $CaCO_3$-free site by mineral coating present on these fractions, which diluted their SOC content slightly. Ultimately both the free-light and occluded pool were of little overall significance to bulk SOC accumulation at either site due to their low mass of SOC.

It was instead, mineral-associated SOC that was of particular interest because of its larger mass of SOC. The Ca-rich soils ($CaCO_3$-bearing) contained twice as much C in organo-mineral association, relative to the soils with less Ca ($CaCO_3$-free site). The $CaCO_3$-free site displayed a typical increase in $\delta^{13}C$ values from the LFs to the HF, normally associated with a preferential stabilisation of microbially transformed SOC in the HF by Fe oxides. Yet, the HF at the $CaCO_3$-bearing site had $\delta^{13}C$ values that were more similar to the LFs. This likely arises from two complementary mechanisms. Firstly, SOC in the LFs is more efficiently oxidised in the near neutral environment of the $CaCO_3$-bearing site, so that it has $\delta^{13}C$ values that are more similar to the mineral-associated fraction. Secondly, Ca is likely flocculating and stabilising DOC with lower $\delta^{13}C$ values in the $CaCO_3$-bearing profiles, increasing the mass of mineral-associated SOC and causing the similarities between its qualities and that of the LFs.

6. Does Ca mediate an accumulation of SOC at the Nant Valley?

Our results strongly suggest a causal link between increased Ca availability and SOC accumulation. This suggests that Ca does play a role in the stabilisation of SOC at the Nant Valley. Ca seems to have played an important role in increasing the mass of occluded SOC, through its flocculation of soil separates and its positive effects on aggregation. More importantly, Ca seemed to increase the quantity of relatively fresh SOC within the OMA fractions at the $CaCO_3$-bearing site, which ultimately drove the differences in bulk SOC between our sites. This OMA was also resistant to an increased presence of Na^+ during DF, hinting that this accumulation was not predominantly driven by forms of outer sphere interaction, commonly assumed to be the main form of Ca bond in soil science. Yet, the role of Ca in accumulation of mineral-associated SOC was difficult to isolate from the effects of poorly crystalline Fe forms at the Nant Valley sites, which, like Ca, were also affected by the presence / absence of $CaCO_3$.

It seems that both Ca and poorly crystalline Fe forms acted to accumulate SOC in the OMA fractions of the $CaCO_3$-bearing site. This relationship seemed to differ with pH, which could be driving changes in the surface charge of poorly crystalline Fe forms. We can thus speculate that Ca and Fe may have been co-stabilising SOC at our profiles with a higher pH (B1 and B2), relative to B3, where poorly crystalline Fe forms seemed to be more dominant. This shift was detected by pH, which should be incorporated into SOC models to help parsimoniously improve their predictive power for geochemical-climatic anomalies, like the Nant Valley. Future investigation should now focus on further deciphering organo-mineral associations in similar Ca-rich environments with the methods outlined in the following section.

- Thank you for taking the time to read this thesis -

7.2 - Opening perspectives - the way forward

The following section will cover potential lines for the future investigation of Ca-SOC interactions. It will be structured by decreasing analytical scale, focusing first on potential study locations and geochemical settings, before discussing potential analytical approaches for the evaluation of OMA mediated by Ca.

7.2.1 - Future locations for the investigation of Ca

7.2.1.1 - The natural effects of $CaCO_3$ in humid environments - Slessarev et al. (2016)

As mentioned above in the discussion, the effects of $CaCO_3$ in humid environments have largely been overlooked. Fortunately, the study of Slessarev et al. (2016) highlighted potential locations for further evaluating the effects of $CaCO_3$ on humid environments. Their study identified locations with anomalously high pH, in spite of a high aridity index. These locations notably included: central and northern Europe, China, the Pacific Rim, and north-eastern North America. Future studies should seek to investigate these environments and the impact that $CaCO_3$ has on SOC in these regions.

7.2.1.2 - Liming - New Zealand and OCP systems

Further investigation into the effects of liming on different soil types could identify the potential of this process for increasing SOC sequestration of agro-ecosystems, in line with the 4 Per Mille Initiative. New Zealand could provide a great location to investigate the effects of liming due to its acidic pedogenic conditions (Podzols) and historic use of liming or soil flipping to increase agricultural production (Moir and Moot, 2014; Schiedung et al., 2019).

Another interesting location to further investigate the impact of $CaCO_3$-addition on SOC accumulation and stabilisation mechanisms would be adjacent to an active oxalate-carbonate pathway (OCP; Rowley et al., 2017). The OCP is a C sequestration pathway that results in the alkalinisation of the soil environment adjacent to a calcium oxalate (CaC_2O_4)-producing plant species, due to the oxidation of CaC_2O_4 by oxalotrophic microorganisms (Cailleau et al., 2011; Cailleau et al., 2014; Verrecchia et al., 2006). This oxidation eventually leads to the precipitation of $CaCO_3$ in the soil adjacent to the CaC_2O_4-producing plant species, sequestering atmospheric CO_2 and acting as a "natural liming" system. This natural liming should fundamentally alter SOC cycling adjacent to CaC_2O_4 producing trees over a period of time, shifting from Al- to Ca-dominated SOC stabilisation mechanisms with time in a threshold response. Future investigations could investigate this shift, coupled with agroforestry, to assess whether this natural liming positively affects SOC, as well as the sequestration of C as $CaCO_3$.

7.2.1.3 - A natural Ca-to-Al shift along a sequence in Hawaii

Hawaii provides another excellent opportunity to study the evolution from Ca- to Al-dominated stabilisation mechanisms. Hawaii presents a well-studied soil chronosequence created through the volcanism on the main island (Chadwick et al., 2003; Chorover et al., 2004; Mikutta et al., 2009). Ca

has been progressively leached from the soils of Hawaii, meaning that older soils have less Ca compared to the younger soils in the sequence (Mikutta et al., 2009). Significant studies have already investigated OMA in the Hawaiian soils (Chadwick et al., 2003; Chorover et al., 2004; Mikutta et al., 2009) providing ample evidence to build upon. Thus, Hawaii could provide a perfect location to further study the evolution of soils from Ca- to Al-dominated SOC stabilisation mechanisms with leaching.

7.2.2 - Experimental advances – probing Ca interactions

7.2.2.1 – Exploring the physical and chemical configuration of intact samples

Soil micromorphology is a powerful technique for the optical investigation of intact soils. It helps to give visual confirmation of the physical arrangement of a soil and can thus, provide invaluable evidence supporting chemical observations (Stoops, 2010; Verrecchia & Trumbino, in press). In soil micromorphology, a user can investigate intact soil samples with an optical microscope, after they have been cross-sectioned. This technique could be combined with a Wavelength-Dispersive Spectroscopy Electron Probe Microanalyser (thereafter electron microprobe) to chemically map the geochemical distributions of elements along the cross-sections, highlighting the chemical arrangement of different elements at the sites and their potential co-association. This could be used to quantify if Ca is spatially co-associated with Fe in physically in-tact samples.

7.2.2.2 – Exploring associations between elements and SOC with specific $\delta^{13}C$ values

To go one-step beyond this, we could also attempt to spatially quantify the co-association of Ca or Fe with C of specific $\delta^{13}C$ values in the HF to evaluate at a micro scale the preferential co-association of these elements. We would first have to chemically map the HF from the Nant Valley sites with the electron microprobe. Once mapped with the electron microprobe, we could pass the same samples on the secondary ionising mass spectrometer (SIMS; CAMECA IMS 1280HR; available at UNIL) to isotopically map $\delta^{13}C$ values on the same samples. This way we would be able to quantify the preferential association of Ca or Fe with each other or SOC with specific $\delta^{13}C$ values. While the co-association has been identified in experimental situations (Sowers et al., 2018a), this would provide valuable evidence of this system in natural samples. Yet, finding the right standards and ensuring that the samples were polished-flat correctly to reduce analytical bias caused by variations in surface topography, would be extremely challenging.

7.2.2.3 – Tracing the different stabilisation mechanisms.

NanoSIMS has been adopted widely within soil science for the investigation of organo-mineral associations (Mueller et al., 2013), particularly in relation to clay particles or Fe oxides (Heister et al., 2012; Rennert et al., 2014). These experiments typically involve incubating the clay and silt-sized fraction with isotopically labelled organic matter (^{13}C / ^{15}N) over a short-time period to observe how this freshly added material bonds to different minerals through sorption or occlusion (Mueller et al., 2012;

Vogel et al., 2014). This approach has demonstrated that SOC typically bonds to reactive mineral surfaces in surface areas such as pores, etches, or joins between two reactive mineral-bodies.

However, very few investigations have utilised NanoSIMS to investigate Ca-related processes in soils. A recent study used ^{44}Ca-labelled wollastonite ($^{44}Ca^{29}SiO_3$) to investigate the mobility of Ca during bimineralic reaction-rim growth in a CaO-MgO-SiO_2 system (Joachim et al., 2019). However, to our knowledge, no studies have yet used ^{44}Ca to directly investigate the mechanisms of SOC stabilisation and organo-mineral associations with a NanoSIMS. Samples and DF from the Nant Valley sites could be combined with various isotopic tracers and then measured with the NanoSIMS after a short-term incubation (Mueller et al., 2012; Vogel et al., 2014) The NanoSIMS would enable us to observe directly the spatial configuration of organo-mineral assemblages and tracers. Samples could be dosed with $^{44}CaCO_3$ or $^{44}CaCl_2$, tracing and mapping the reprecipitation and occlusion of $^{44}CaCO_3$ or the sorption of ^{44}Ca / ^{13}C / ^{15}N with a NanoSIMS. Samples with and without Ca could also be dosed with ^{13}C-enriched DOC, observing how DOC is stabilised differently in organo-mineral assemblages.

7.2.2.3 – Investigating the chemical structure of Ca-mediated organo-mineral association

One major weakness of this thesis is the lack of detailed spectroscopic work to explore our hypotheses, beyond the XPS data, the results of which were reasonably limited. The Ca-XPS did identify a Ca bond in the $CaCO_3$-bearing fractions, that was not present in the $CaCO_3$-free samples, but identification of the nature of this peak was prevented due to the limited chemical shift in the detailed Ca_{2p} region. There has been very little work that has used advanced Ca spectroscopy to evaluate different environmental samples, including hydroxyapatite samples (Eanes et al., 1981), analysis of Ca-acetate complexes in aqueous solutions (Muñoz Noval et al., 2018), or for the analysis of several inorganic and molecular calcium complexes (Martin-Diaconescu et al., 2015). The main work related to soils was completed by Sowers et al. (2018a), who used STXM C-NEXAFS to probe Fe-Ca-C ternary complexes in an experimental setting. Yet, overall OMA mediated by Ca have rarely been investigated with advanced spectroscopic techniques. Further investigation could use Ca / C (XAFS) or STXM C-NEXAFS to answer a whole range of important questions regarding these associations in different soils.

- This page is intentionally left blank -

- Chapter 8: Appendices -

Appendices list

The appendices of this thesis are ordered as follows:

8.1 - Supplementary Figures and Tables from the research chapters that were not included in the text.

8.2 - Maps.

8.3 - Soil profile data from the field.

8.4 - Full methods.

- 8.4.1 Preparation of soil
- 8.4.2 Lab analyses
- 8.4.3 Statistical methods

8.5 - Print copy of published papers.

- 8.5.1 Chapter 3: Rowley et al., 2018. Calcium-mediated stabilisation of soil organic carbon. *Biogeochemistry.* 137, 27-49.
- 8.5.2 Chapter 4: Rowley et al., 2020. A cascading influence of calcium carbonate on the biogeochemistry and pedogenic trajectories of subalpine soils, Switzerland. *Geoderma.* In press.
- 8.5.3 Matteodo et al., 2018. Decoupling of topsoil and subsoil controls on organic matter dynamics in the Swiss Alps. *Geoderma.* 330, 41-51.
- 8.5.4 Rowley et al., 2017. Moving carbon between spheres, the potential oxalate-carbonate pathway of *Brosimum alicastrum* Sw.; Moraceae. *Plant and soil.* 412, 465-479.

8.1 - Appendix (supplementary) Figures and Tables

This section will present any figures or tables in the supplementary information of the papers that hasn't been presented in the main thesis.

8.1.1 - Chapter 4

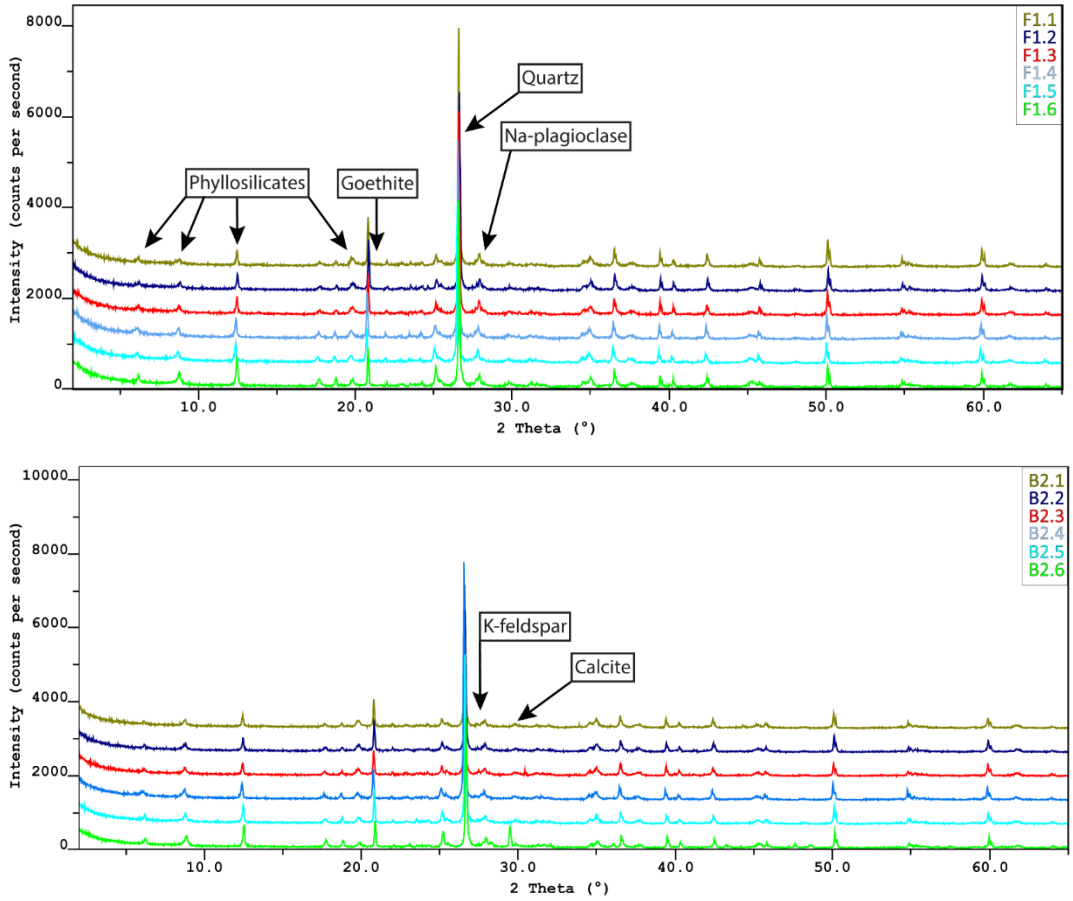

Appendix Fig. 8.1. Powder X-ray diffraction spectra for profiles F1 and B2. The main primary peaks are labelled.

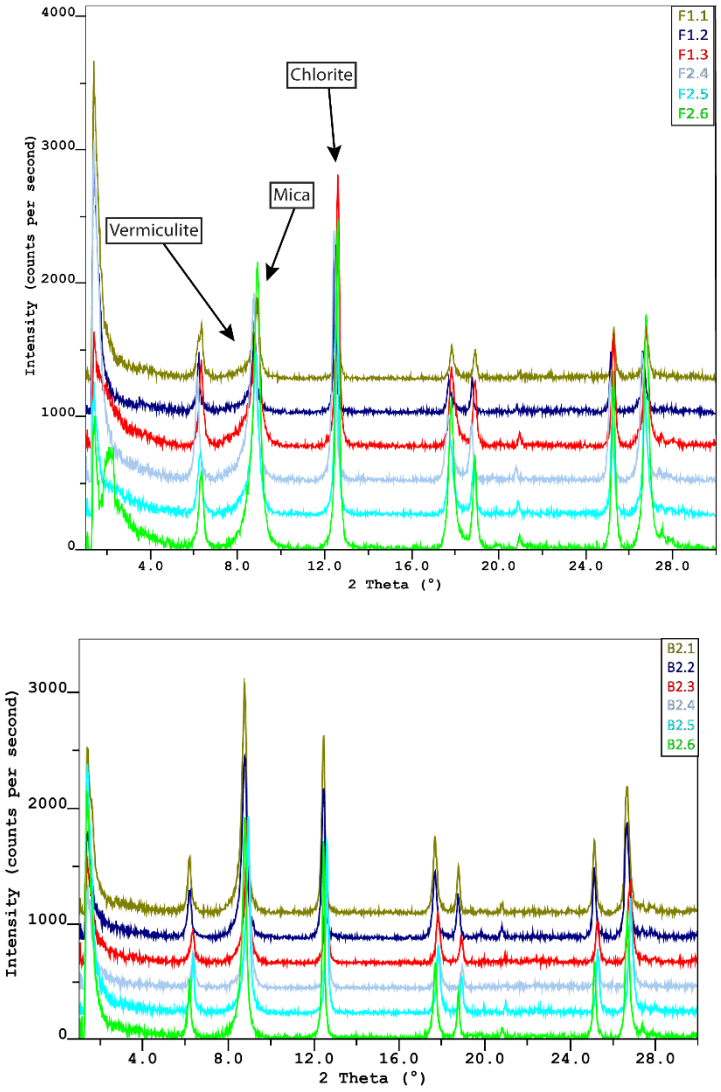

Appendix Fig. 8.2. X-ray diffraction spectra of oriented slides (< 2 µm) for profiles F1 and B2. The main primary peaks are labelled.

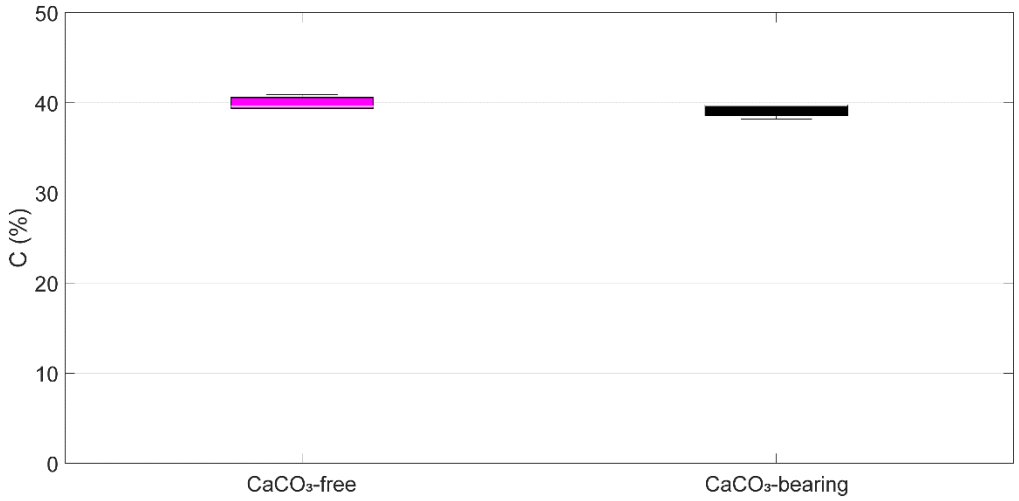

Appendix Fig. 8.3. Organic carbon contents for randomly sampled aboveground vegetation from the $CaCO_3$-free and $CaCO_3$-bearing sites.

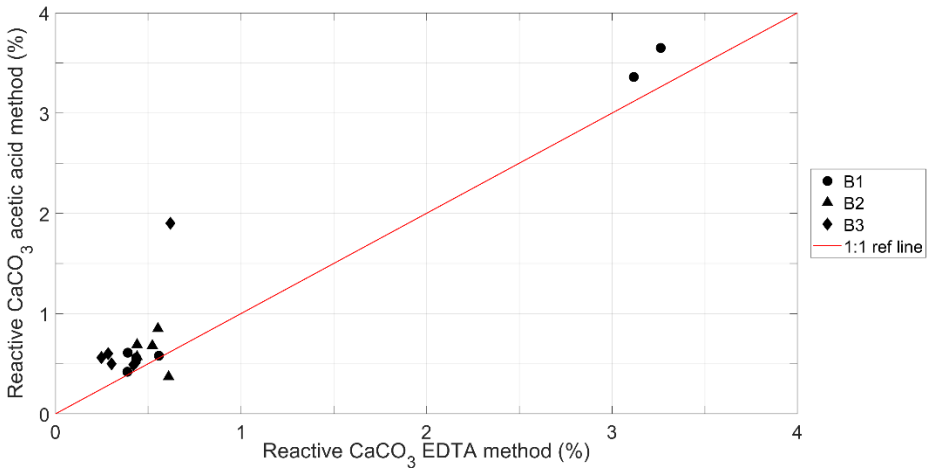

Appendix Fig. 8.4. Reactive carbonate quantified by the 0.4 M acetic acid (Loeppert et al. 1984) and 0.05 M disodium EDTA (Glover, 1961) methods at the $CaCO_3$-bearing (B1, B2, B3) profiles. For the EDTA method, extracted Ca was corrected for Ca_{Exch} content (0.0166 M cobalt hexamine) and expressed as equivalent $CaCO_3$. Estimates from the EDTA method tended to be slightly smaller than those from the acetic acid method. This may be due to incomplete displacement of the exchangeable pool by the 0.05 M disodium EDTA or the extraction of small amounts of reactive $CaCO_3$ by the cobalt hexamine.

Appendix Table 8.1. Total elemental compositions for the $CaCO_3$-free and $CaCO_3$-bearing profiles. Compositions were obtained by X-ray fluorescence and were corrected for loss on ignition during the fusion process.

Sample	Al g kg^{-1}	Ca g kg^{-1}	Cr g kg^{-1}	Fe g kg^{-1}	K g kg^{-1}	Mg g kg^{-1}	Mn g kg^{-1}	Na g kg^{-1}	Ni g kg^{-1}	P g kg^{-1}	Si g kg^{-1}	Ti g kg^{-1}
F1.1	88.8	3.0	0.2	49.7	22.6	12.1	0.7	7.3	0.1	1.8	320.3	5.3
F1.2	91.4	2.4	0.2	50.8	23.2	12.4	0.8	7.6	0.1	1.6	317.5	5.3
F1.3	91.3	2.3	0.2	51.2	23.4	12.7	0.9	7.8	0.1	1.5	316.7	5.2
F1.4	93.6	2.1	0.2	51.5	25.0	13.2	0.9	7.9	0.1	1.4	312.7	5.3
F1.5	97.4	1.9	0.2	52.5	26.5	13.8	0.9	7.9	0.1	1.2	307.8	5.5
F1.6	101.4	1.6	0.2	53.6	28.5	15.0	0.9	8.1	0.1	0.8	301.8	5.5
F2.1	87.1	2.2	0.1	49.3	21.2	11.6	0.7	7.6	0.1	1.8	323.1	5.0
F2.2	87.5	1.4	0.1	49.8	21.6	12.3	0.8	7.9	0.1	1.4	322.8	4.8
F2.3	87.6	1.3	0.1	50.0	22.2	12.5	0.9	8.0	0.1	1.4	322.5	4.8
F2.4	88.2	1.3	0.1	49.6	22.6	12.6	0.9	7.8	0.1	1.3	321.3	4.9
F2.5	90.2	1.2	0.2	50.2	23.5	13.2	0.9	8.0	0.1	1.2	318.8	4.8
F2.6	88.8	1.1	0.1	48.8	24.1	13.5	1.0	8.1	0.1	1.0	320.4	4.7
F3.1	88.4	3.4	0.1	49.1	22.7	12.0	0.9	7.6	0.1	2.3	320.4	5.1
F3.2	88.0	2.0	0.1	49.9	22.4	12.1	0.9	7.7	0.1	1.7	321.4	5.0
F3.3	87.0	1.6	0.1	49.8	22.2	12.2	0.9	7.9	0.1	1.5	321.9	4.9
F3.4	88.3	1.4	0.1	49.7	22.8	12.4	0.9	8.2	0.1	1.4	320.5	4.9
F3.5	90.0	1.4	0.1	49.9	23.3	12.4	0.9	7.8	0.1	1.3	319.6	5.0
F3.6	89.0	1.9	0.1	49.8	23.4	12.7	0.8	8.0	0.1	1.3	320.0	4.8
B1.1	91.0	28.7	0.2	52.4	26.6	15.3	0.7	6.1	0.1	2.9	293.2	5.6
B1.2	90.1	31.4	0.2	52.1	26.1	15.0	0.8	6.1	0.1	2.9	294.3	5.5
B1.3	91.8	12.7	0.2	52.9	27.4	15.1	1.0	6.1	0.1	3.3	299.9	5.5
B1.4	91.8	10.5	0.1	53.2	27.1	14.9	1.2	6.2	0.1	3.3	304.0	5.5
B1.5	90.1	9.3	0.1	52.9	26.6	14.7	1.1	6.1	0.1	3.3	306.8	5.3
B1.6	91.4	7.3	0.1	53.3	27.1	15.0	0.9	6.0	0.1	2.4	306.0	5.3
B2.1	93.6	13.9	0.2	50.7	27.3	15.0	0.8	6.5	0.1	5.4	296.9	5.6
B2.2	91.8	13.2	0.2	53.0	27.0	14.7	1.1	6.4	0.1	6.2	297.4	5.5
B2.3	91.0	11.9	0.2	52.4	26.7	14.5	1.2	6.5	0.1	6.4	300.0	5.5
B2.4	89.8	11.2	0.2	52.0	26.3	14.4	1.2	6.5	0.1	6.8	301.6	5.4
B2.5	90.8	10.5	0.2	51.1	25.8	14.7	1.0	6.7	0.1	6.8	303.8	5.5
B2.6	87.2	47.1	0.2	47.1	25.6	15.1	0.7	6.5	0.1	5.1	287.4	5.1
B3.1	93.0	9.7	0.2	47.8	27.9	14.6	0.8	6.5	0.1	5.8	303.4	5.5
B3.2	91.8	8.6	0.2	53.6	27.3	14.6	1.6	6.5	0.1	6.3	300.2	5.4
B3.3	91.8	8.6	0.2	53.4	27.1	14.6	1.6	6.5	0.1	6.5	299.8	5.4
B3.4	92.7	8.9	0.2	51.5	27.0	14.8	1.5	6.7	0.1	6.3	301.9	5.4
B3.5	94.5	8.1	0.2	52.0	27.6	15.2	1.3	6.7	0.1	5.4	301.0	5.5
B3.6	96.1	7.7	0.2	52.9	28.3	15.7	1.2	6.8	0.1	4.3	298.4	5.6
B3.7	94.7	13.0	0.2	53.3	27.8	15.7	0.9	6.7	0.1	3.0	299.3	5.4

Appendix Table 8.2. Mineralogy and texture of $CaCO_3$-free and $CaCO_3$-bearing profiles. Silicates and oxides were quantified on X-ray diffraction spectra, while total and reactive calcium carbonate equivalent (CCE) were quantified chemically (see Methods section). Samples for which the X-ray diffraction spectrum contained a clear calcite peak are marked in the total CCE column with an *.

Samples	Phyllo-silicates	Quartz	K-Feldspar	Na-Plagioc-lase	Goethi-te	Un-ident.	CCE-Total	CCE-React.	% React. $CaCO_3$	Clay < 2 µm	Silt 2-50 µm	Sand 50-2000 µm
	%	%	%	%	%	%	%	%	%	%	%	%
F1.1	42.8	44.4	0.0	5.5	1.5	5.9	0.0	0.0	0	18.4	67.9	13.7
F1.2	42.9	41.5	1.7	5.6	0.0	8.4	0.0	0.0	0	18.9	68.5	12.7
F1.3	41.3	38.3	1.5	6.5	1.5	10.9	0.0	0.0	0	18.6	68.2	13.2
F1.4	41.3	38.3	2.0	5.5	1.3	11.6	0.0	0.0	0	18.1	68.7	13.1
F1.5	41.5	36.5	3.4	6.5	0.0	12.1	0.0	0.0	0	17.7	69.1	13.2
F1.6	43.9	38.3	1.7	6.0	0.0	10.1	0.0	0.0	0	14.0	65.4	20.6
F2.1	45.7	41.8	1.7	4.9	0.0	5.8	0.0	0.0	0	18.4	64.1	17.5
F2.2	41.5	41.4	1.8	7.9	1.7	5.8	0.0	0.0	0	18.3	65.7	16.0
F2.3	45.1	43.6	1.8	5.8	1.6	2.1	0.0	0.0	0	18.1	65.7	16.2
F2.4	41.5	41.7	1.2	6.0	0.0	9.7	0.0	0.0	0	19.2	69.8	11.1
F2.5	42.6	41.0	1.2	4.8	0.0	10.4	0.0	0.0	0	17.4	68.4	14.2
F2.6	40.6	39.7	1.3	6.7	0.0	11.8	0.0	0.0	0	14.4	62.8	22.8
F3.1	40.8	42.5	0.0	7.2	0.0	9.5	0.0	0.0	0	21.1	68.6	10.3
F3.2	40.9	43.6	1.3	4.8	0.0	9.5	0.0	0.0	0	18.8	67.8	13.5
F3.3	40.8	44.4	1.5	7.3	1.2	4.8	0.0	0.0	0	17.7	67.4	15.0
F3.4	42.9	43.1	1.5	6.2	1.6	4.8	0.0	0.0	0	17.3	67.1	15.6
F3.5	42.8	38.9	1.7	6.2	0.0	10.5	0.0	0.0	0	17.8	68.7	13.6
F3.6	41.6	40.7	1.3	6.7	0.0	9.8	0.0	0.0	0	16.1	66.9	17.0
B1.1	42.9	39.8	2.1	4.1	0.0	7.3	3.8*	3.7	97	15.3	73.9	10.8
B1.2	45.3	36.7	2.0	4.2	0.0	5.8	4.2*	3.4	79	16.1	74.9	9.0
B1.3	47.0	38.2	2.0	3.8	0.0	9.0	1.1	0.6	54	16.5	73.9	9.7
B1.4	42.7	39.3	2.1	5.6	1.6	8.8	1.0	0.6	60	16.0	73.6	10.4
B1.5	43.2	43.1	2.0	3.6	0.0	8.1	0.8	0.6	67	15.2	73.1	11.7
B1.6	41.7	43.0	2.5	4.7	0.0	7.4	0.8*	0.4	53	15.3	72.9	11.9
B2.1	48.0	33.7	2.1	4.2	1.6	10.5	1.0	0.6	59	17.5	72.9	9.6
B2.2	47.5	33.6	2.3	4.5	1.7	9.9	1.0*	0.9	85	16.4	73.2	10.4
B2.3	45.7	34.7	3.7	3.9	1.9	10.1	1.0	0.7	69	15.4	73.8	10.8
B2.4	37.6	50.4	1.6	4.1	0.0	6.3	1.0	0.7	72	14.9	73.6	11.5
B2.5	40.0	41.0	2.0	4.3	1.3	10.9	0.9*	0.4	41	14.2	75.6	10.2
B2.6	35.8	36.6	2.3	6.1	0.0	9.7	6.2*	3.9	62	13.3	74.7	12.0
B3.1	53.6	31.9	2.5	8.5	0.0	3.6	0.7	0.6	82	15.8	74.1	10.1
B3.2	43.6	41.7	2.5	4.4	0.0	7.9	0.6	0.5	82	14.9	73.2	12.0
B3.3	51.2	35.5	2.3	4.3	0.0	6.8	0.6	0.5	86	14.5	74.4	11.2
B3.4	49.4	37.7	1.9	5.9	0.0	5.2	0.6	0.5	83	14.9	74.0	11.1
B3.5	47.6	36.9	1.9	4.8	0.0	8.9	0.6*	0.5	88	14.7	75.9	9.5
B3.6	47.0	37.6	1.8	4.4	0.0	8.6	0.6*	0.6	97	15.0	75.6	9.4
B3.7	41.7	37.6	2.0	5.3	1.7	10.2	1.9*	1.9	98	14.9	76.4	8.7

Un-ident.: Unidentified signal
Total and React. CCE: Total and reactive calcium carbonate equivalent material.
% React. $CaCO_3$: the percent of reactive CCE in the total CCE

Appendix Table 8.3. Relevant soil-surface carbon dioxide (CO_2) efflux data from Grand et al. (2016). For each site, the first column represents soil respiration rates; the second column represents estimated heterotrophic respiration, taken as 40% of clipped soil-surface CO_2 efflux (Hanson et al., 2000); the third column represents estimated heterotrophic respiration expressed per unit of soil organic carbon.

	$CaCO_3$-free			**$CaCO_3$-bearing**		
Month 2016	**Soil Respiration**	**Estimated heterotrophic respiration**	**Respiration / unit SOC**	**Soil Respiration**	**Estimated heterotrophic respiration**	**Respiration / unit SOC**
	µmol / m² / s	**µmol / m² / s**	**µmol / m² / s / SOC**	**µmol / m² / s**	**µmol / m² / s**	**µmol / m² / s / SOC**
July	8.3	3.3	1.3	6.1	2.4	0.5
Aug.	8.8	3.5	1.4	11.9	4.8	0.9
Sept.	5.6	2.2	0.9	8.9	3.6	0.7
Oct.	2.9	1.2	0.5	5.2	2.1	0.4

8.1.2 - Chapter 5

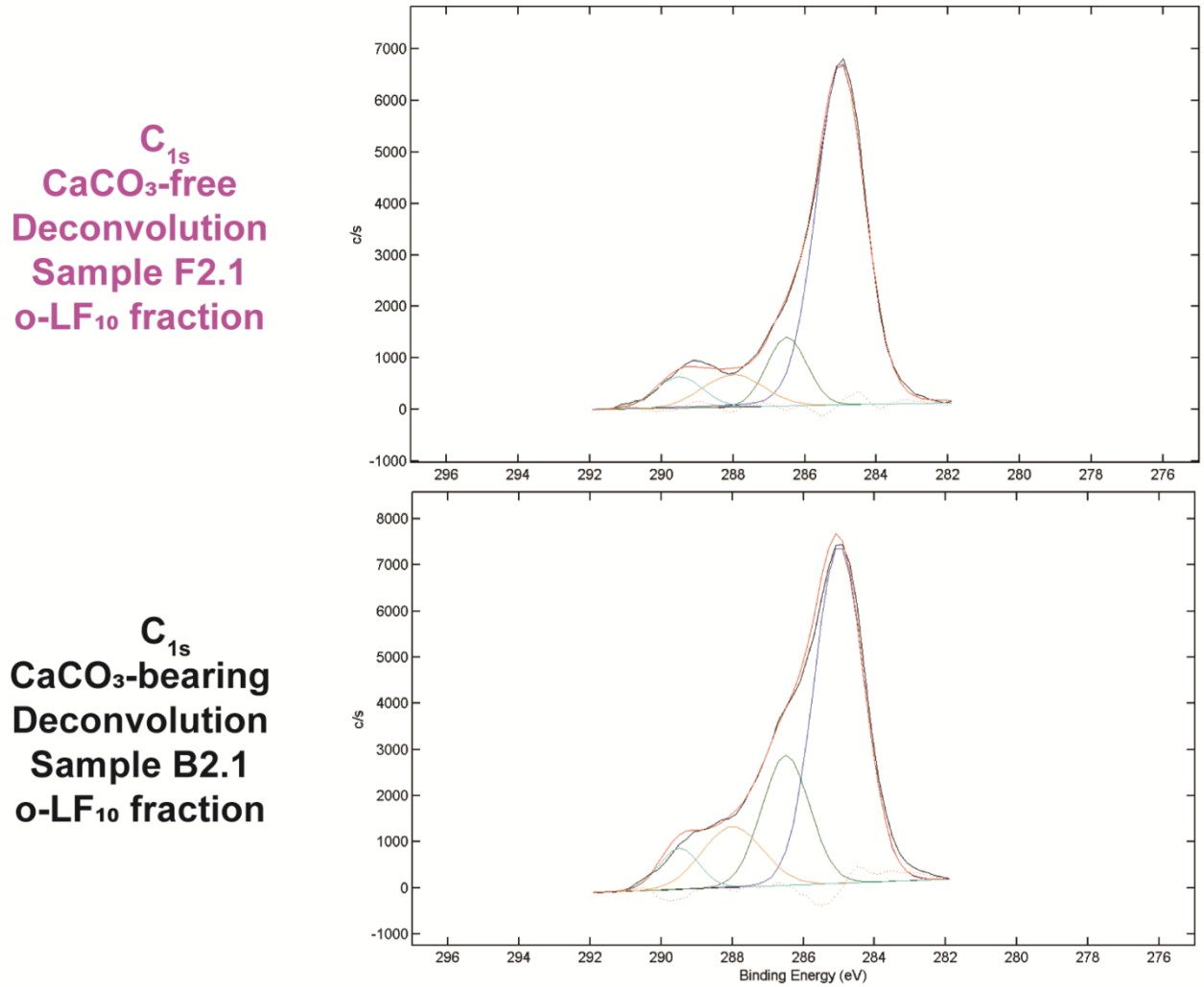

Appendix Fig. 8.5. Example of the deconvolution of the X-ray photoelectron spectroscopy attained carbon 1s orbital peak into four different sub peaks peaks, representing (from left-to-right): carboxylate (289.5 eV), carbonyl (288 eV), alcoholic / phenolic (286.5 eV), aromatic / aliphatic (285 eV) moieties. The two spectra have been centered at 285 eV.

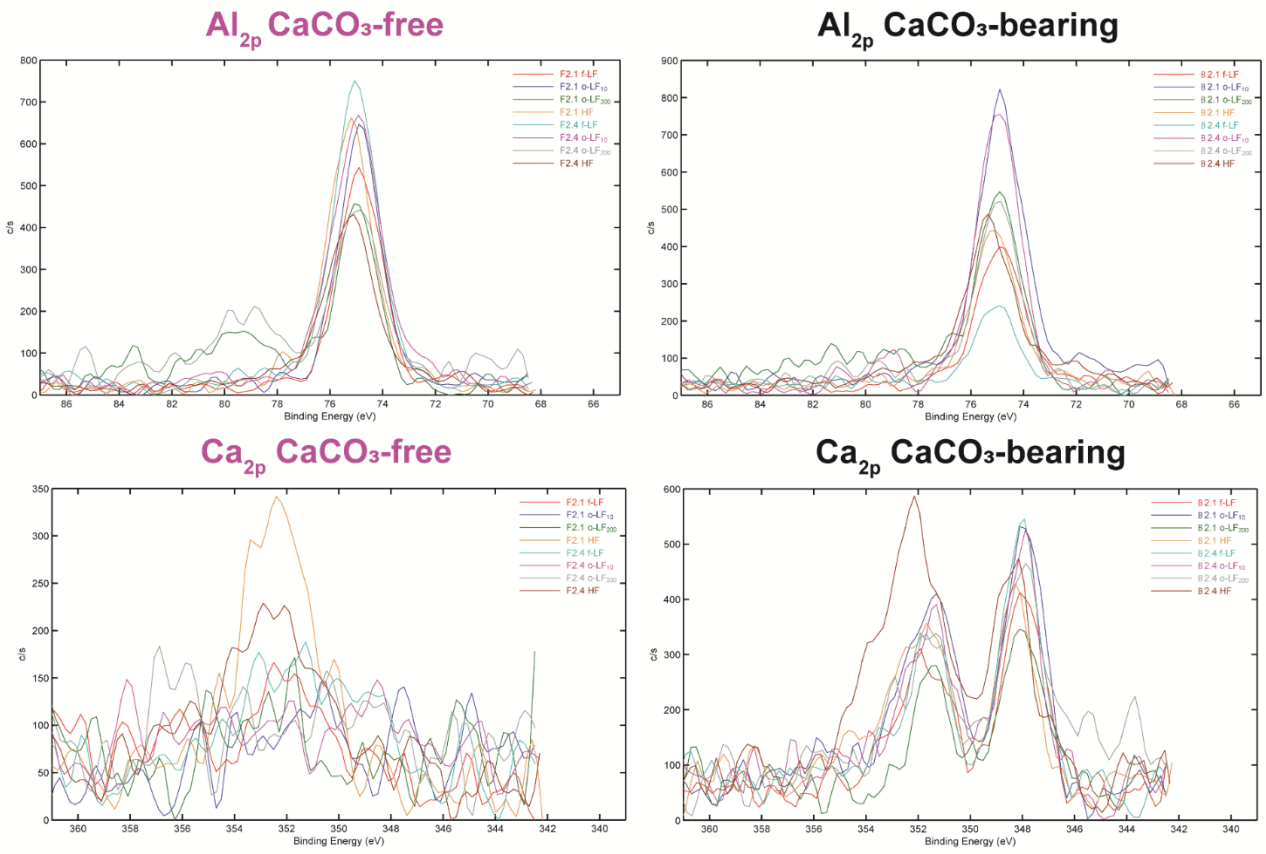

Appendix Fig. 8.6. Detailed X-ray photoelectron spectroscopy (XPS) in the electron binding energy range of photoelectrons ejected from the aluminium 2p and calcium 2p orbitals. Spectra include all of the density fractions from the $CaCO_3$-bearing (B2.1 and B2.4) and $CaCO_3$-free (F2.1 and F2.4) sample subset. The $Ca_{2F3/2}$ peak is difficult to distinguish due to the lack of a chemical shift in the Ca_{2p} region, lack of pre-existing XPS data on Ca-C interactions and location of the peak. The $Ca_{2F3/2}$ peak could be attributed to $CaCl_2$ or CaO type bonds (not $CaCO_3$ as it had been removed with a HCl fuimgation).

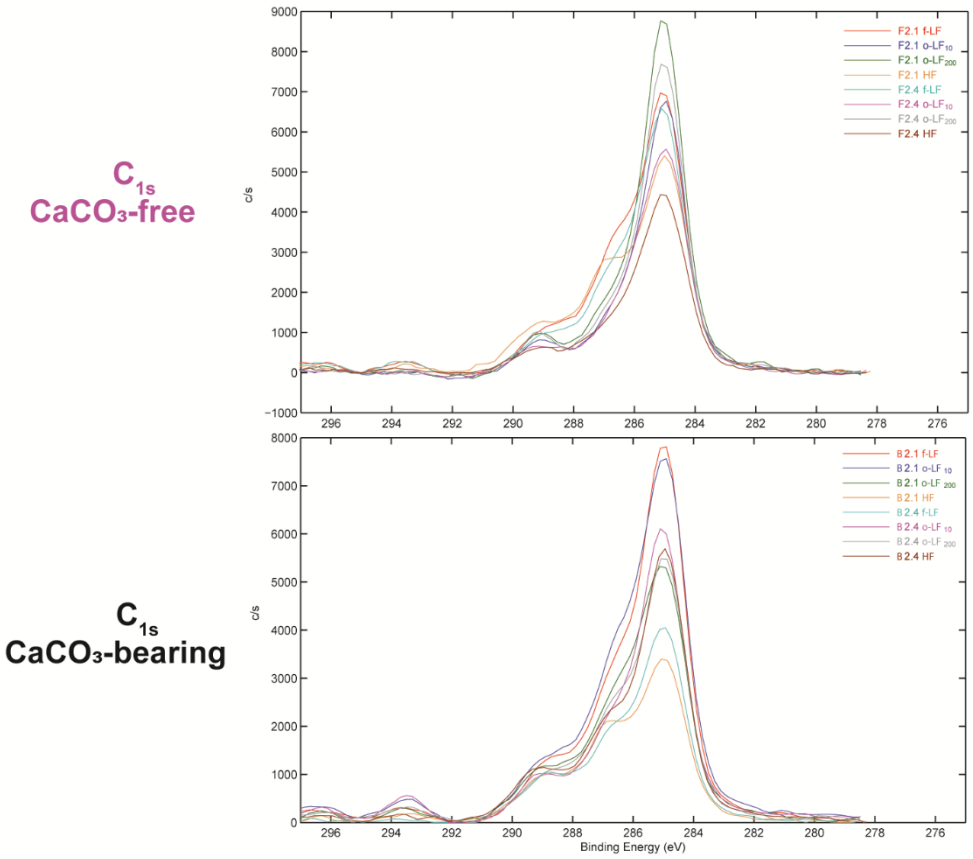

Appendix Fig. 8.7. Detailed X-ray photoelectron spectroscopy (XPS) in the electron binding energy range of photoelectrons ejected from the carbon 1s orbital. Spectra include all of the density fractions from the $CaCO_3$-bearing (B2.1 and B2.4) and $CaCO_3$-free (F2.1 and F2.4) sample subset.

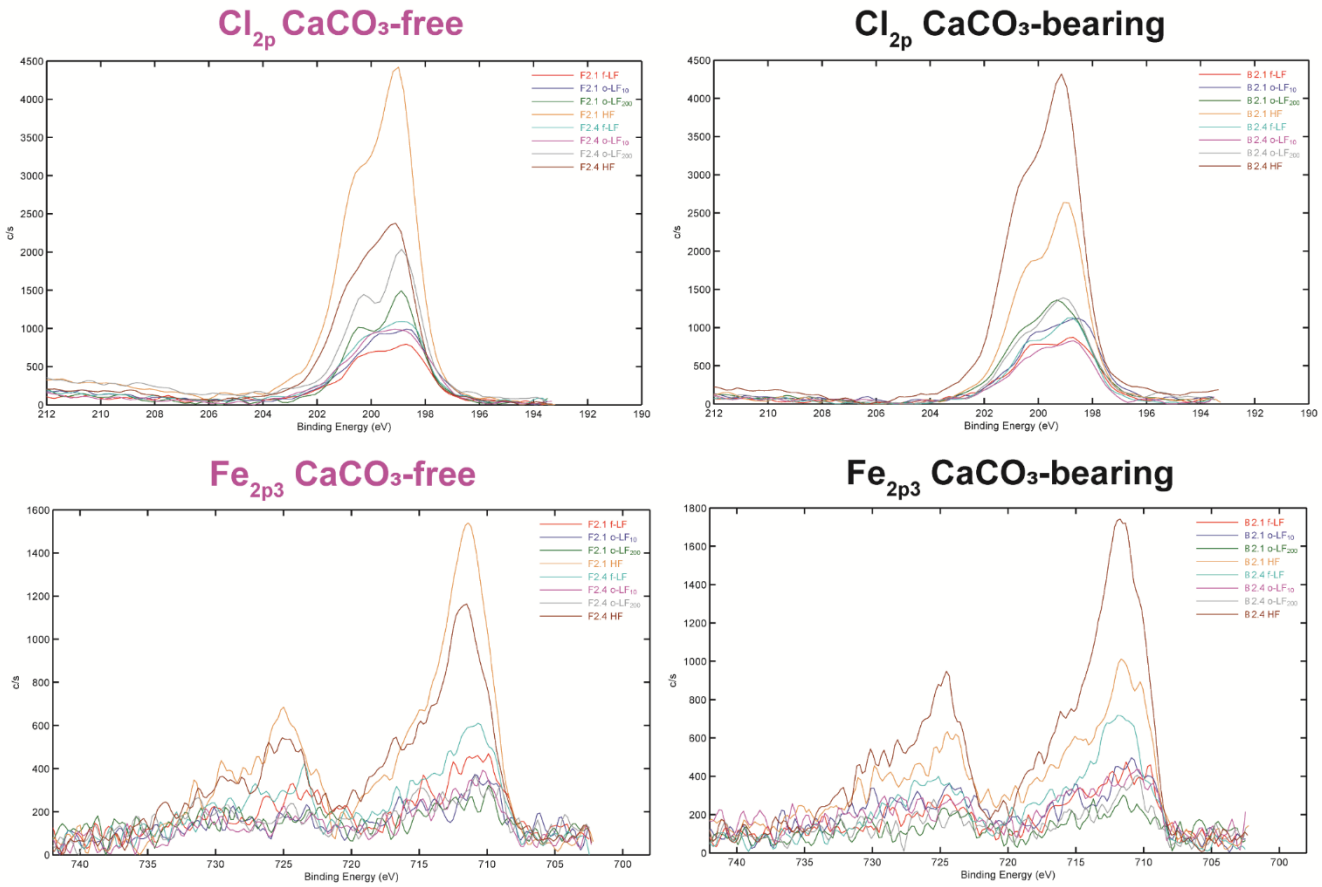

Appendix Fig. 8.8. Detailed X-ray photoelectron spectroscopy (XPS) in the electron binding energy range of photoelectrons ejected from the chlorine 2p and iron 2p3 orbitals. Spectra include all of the density fractions from the $CaCO_3$-bearing (B2.1 and B2.4) and $CaCO_3$-free (F2.1 and F2.4) sample subset.

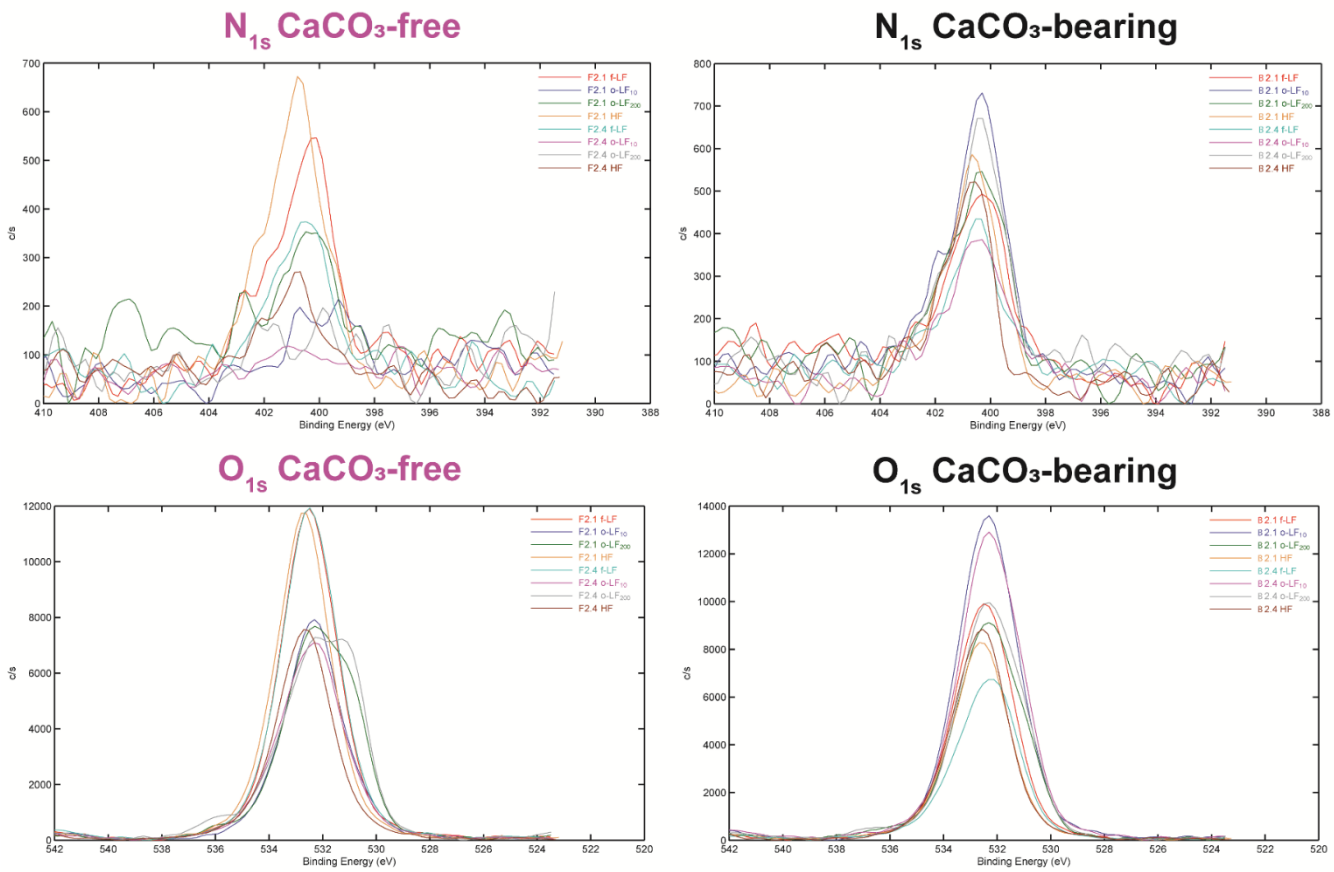

Appendix Fig. 8.9. Detailed X-ray photoelectron spectroscopy (XPS) in the electron binding energy range of photoelectrons ejected from the nitrogen 1s (N_{1s}) and oxygen 1s orbitals. Spectra include all of the density fractions from the $CaCO_3$-bearing (B2.1 and B2.4) and $CaCO_3$-free (F2.1 and F2.4) sample subset. There is a slight shift towards more protonated N_{1s} forms at the $CaCO_3$-free site, which has a more acidic pH (Jones and Singh, 2014).

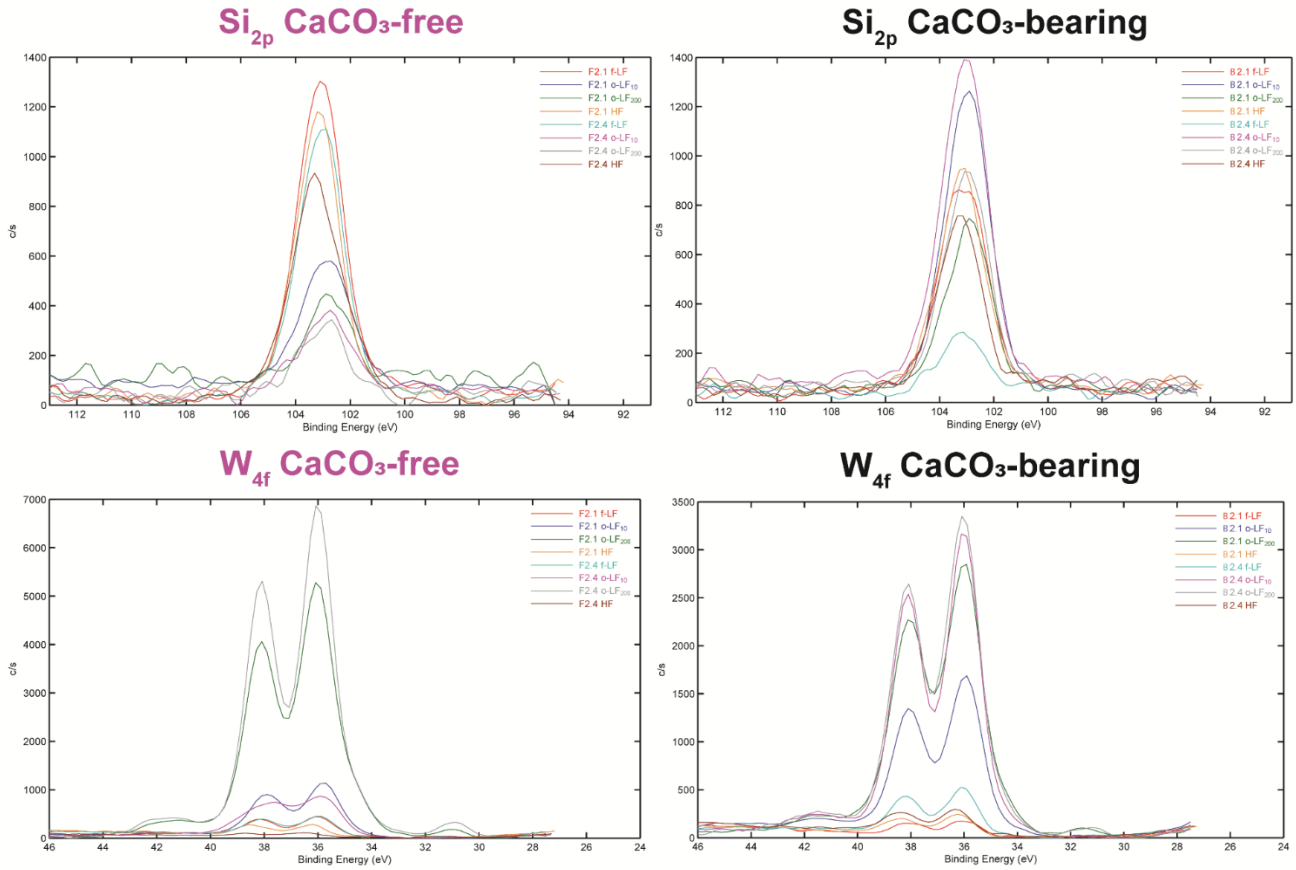

Appendix Fig. 8.10. Detailed X-ray photoelectron spectroscopy (XPS) in the electron binding energy range of photoelectrons ejected from the silicon 2p and tungsten 4f (W_{4f}) orbitals. Spectra include all of the density fractions from the $CaCO_3$-bearing (B2.1 and B2.4) and $CaCO_3$-free (F2.1 and F2.4) sample subset. Significant precipitation of calcium metatungstate would shift the W_{4f} from 35.5-36 eV towards 35 eV (Moulder and Chastain, 1992).

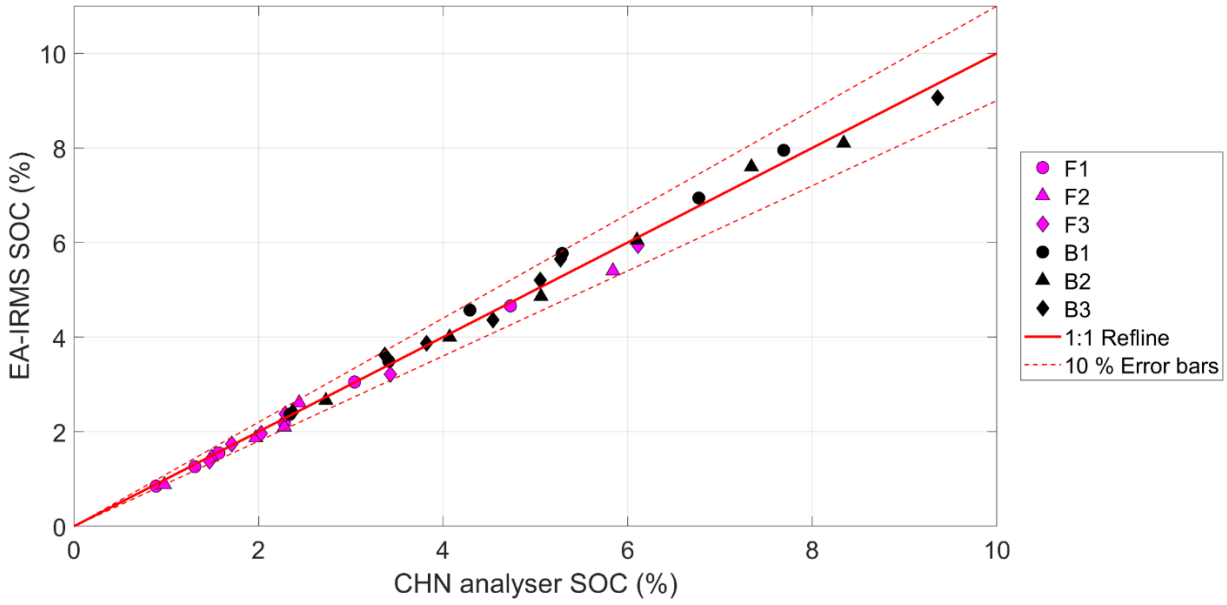

Appendix Fig. 8.11. Comparison of previous elemental analyser (CHN analyser) measurements of bulk soil (Chapter 4) at the $CaCO_3$-free (F1, F2, F3) and $CaCO_3$-bearing (B1, B2, B3) profiles with the elemental analyser isotope-ratio mass spectrometer (EA-IRMS) bulk soil data (Chapter 5). A 10 % uncertainty interval has been plotted in dashed red line, on either side of a 1:1 reference line in bold red, to represent the 5 % error margin in both machines.

Appendix Table 8.4. Mass of recovered material in different density fractions of the $CaCO_3$-free (F1, F2, F3) and $CaCO_3$-bearing (B1, B2, B3) profiles. There was insufficient material recovered in the F1.6 o-LF_{10} fraction for analysis. All figures are mean values of triplicates. Samples from the $CaCO_3$-bearing profiles with the highest calcium carbonate equivalent content are marked with an *.

	Bulk SOC				Mean fraction recoveries					Mean SOC content				Mean mass of SOC			
Sample	SOC content	Bulk Density	Sample SOC stock	Profile SOC Stock	f-LF	o-LF_{10}	o-LF_{200}	HF	Total recovery	f-LF	o-LF_{10}	o-LF_{200}	HF	f-LF	o-LF_{10}	o-LF_{200}	HF
	%	g cm^{-3}	kg C m^{-2}	kg C m^{-2}	mg	mg	mg	mg	%	%	%	%	%	mg C	mg C	mg C	mg C
F1.1	4.66	0.93	21.2		64.1	8.4	23.2	6712	99.1	22.2	16.9	16.3	4.4	14.2	1.4	3.7	296.9
F1.2	3.05	0.93	12.7		12.7	4.6	13.9	6823	99.5	18.3	17.6	15.3	2.8	2.3	0.7	2.1	193.3
F1.3	2.18	0.97	10.0	F1	8.6	5.0	11.9	6883	99.8	18.1	16.8	13.9	2.1	1.5	0.6	0.8	141.8
F1.4	1.55	0.97	13.5	12.8	5.8	1.4	9.3	6882	99.5	16.1	17.3	8.2	1.5	0.9	0.2	0.8	106.1
F1.5	1.26	1.07	11.5		4.8	1.3	4.3	6911	99.8	15.4	9.1	11.6	1.2	0.7	0.1	0.4	85.3
F1.6	0.85	1.07	11.5		4.3	0.1	0.4	6876	98.9	8.1		14.7	0.9	0.3		0.1	61.3
F2.1	5.36	0.93	23.7		80.0	16.6	25.2	6713	99.9	21.0	12.5	13.3	5.0	16.6	1.5	3.2	333.9
F2.2	2.55	0.93	11.3		10.7	10.1	13.4	6879	100.3	17.7	11.2	13.2	2.5	1.9	1.0	1.7	170.0
F2.3	2.08	0.97	9.6	F2	8.0	2.6	17.3	6894	100.4	15.7	14.6	9.8	1.8	1.3	0.4	1.5	125.3
F2.4	1.88	0.97	8.2	11.4	7.2	5.4	12.4	6904	100.3	17.9	11.9	11.6	1.8	1.3	0.6	1.4	122.2
F2.5	1.47	1.07	5.9		5.8	3.0	10.6	6913	100.2	16.3	11.5	10.4	1.6	1.0	0.3	0.8	110.9
F2.6	0.90	1.07	11.1		3.5	2.4	7.4	6910	99.7	15.4	7.4	8.6	0.9	0.5	0.2	0.4	64.3
F3.1	5.92	0.93	27.0		97.7	19.3	43.9	6608	99.2	23.0	16.5	18.2	5.6	22.4	3.1	7.9	371.4
F3.2	3.19	0.93	13.4		14.5	10.3	14.3	6817	99.7	23.0	6.1	14.2	3.0	3.4	0.7	2.1	203.0
F3.3	2.38	0.97	10.7	F3	6.9	12.7	16.2	6876	100.2	20.2	8.3	11.6	2.2	1.4	1.0	1.9	148.6
F3.4	1.97	0.97	7.6	11.7	5.4	5.0	7.4	6884	100.0	20.6	8.7	12.5	1.8	1.1	0.4	0.8	126.6
F3.5	1.76	1.07	7.0		5.7	5.8	7.0	6893	99.9	20.7	10.3	8.8	1.7	1.2	0.5	0.6	119.7
F3.6	1.37	1.07	8.1		7.4	0.7	6.9	6910	100.0	20.1	20.3	9.6	1.4	1.5	0.1	0.7	94.0
B1.1*	8.01	0.87	34.9		84.5	55.8	162.5	6469	99.1	26.5	14.1	23.9	6.3	22.4	7.9	37.9	407.0
B1.2*	7.08	0.87	30.2		61.8	48.4	136.9	6538	99.4	24.7	17.3	25.3	5.7	15.1	8.1	34.3	374.6
B1.3	5.81	0.93	24.3	**B1**	20.7	22.3	65.1	6667	99.0	24.1	12.0	22.4	5.1	5.0	2.7	13.4	342.4
B1.4	4.56	0.93	19.1	**24.2**	16.5	24.2	83.5	6748	100.2	25.5	13.8	20.9	4.0	4.2	3.2	17.3	268.7
B1.5	3.47	0.97	14.3		11.2	15.7	53.9	6814	100.2	27.1	13.7	16.0	3.2	3.0	2.2	8.6	218.9
B1.6	2.32	0.97	23.6		6.4	14.2	23.4	6871	100.3	21.6	9.3	15.2	2.1	1.4	1.4	3.3	146.9
B2.1	8.14	0.87	35.4		35.5	37.5	152.6	6493	99.0	28.5	21.5	21.6	7.3	10.1	7.8	32.4	475.3
B2.2	7.63	0.87	33.2		34.3	32.1	147.5	6565	99.9	30.0	20.5	21.8	6.8	10.3	6.3	31.9	446.1
B2.3	6.07	0.93	27.7	**B2**	31.1	33.1	86.1	6607	99.3	26.6	19.0	23.9	5.4	8.3	6.1	19.6	354.1
B2.4	4.83	0.93	21.9	**25.2**	32.3	21.4	83.7	6665	99.6	27.2	23.6	22.4	4.3	8.8	4.7	16.5	288.7
B2.5	3.96	0.97	18.7		31.6	22.5	39.1	6712	99.4	29.1	25.4	24.7	3.5	9.2	5.5	8.7	237.5
B2.6*	2.68	0.97	21.5		21.9	14.7	36.9	6697	98.2	27.0	25.6	19.4	2.5	5.9	3.7	7.0	165.7
B3.1	9.06	0.87	39.4		73.3	40.5	155.8	6474	99.2	26.5	21.4	23.0	8.3	19.3	8.2	35.8	537.5
B3.2	5.65	0.87	23.4		26.7	22.7	62.7	6661	98.9	30.2	20.0	21.9	5.1	8.1	4.4	12.3	336.5
B3.3	5.20	0.93	23.4		27.7	24.5	64.2	6670	99.0	31.2	19.8	23.2	4.7	8.7	4.6	15.0	312.0
B3.4	4.36	0.93	20.1	**B3**	21.0	19.9	54.7	6704	99.1	26.8	22.3	22.4	4.2	5.6	4.4	12.0	282.7
B3.5	3.87	0.97	17.8	**19.1**	15.3	16.5	46.7	6750	99.2	30.2	17.2	20.3	3.7	4.6	2.8	9.1	247.1
B3.6	3.62	0.97	17.2		14.1	15.3	40.5	6767	99.2	23.0	19.7	19.4	3.3	3.3	3.0	7.9	221.4
B3.7*	2.42	0.97	14.8		15.5	13.5	26.8	6757	98.3	27.6	20.5	19.2	2.3	4.3	2.8	3.8	154.8

f-LF: Free-light fraction
o-LF_{10}: occluded soil organic carbon pool separated after a sonication of 10 J mL^{-1}
o-LF_{200}: occluded soil organic carbon pool separated after a sonication of 200 J mL^{-1}
HF: Heavy fraction

Appendix Table 8.5. Stable carbon isotope compositons of the different density fractions of the $CaCO_3$-free (F1, F2, F3) and $CaCO_3$-bearing (B1, B2, B3) profiles. There was insufficient material recovered in the F1.6 o-LF_{10} fraction for analysis. All figures are mean values of triplicates.

Sample	Mean $\delta^{13}C$ values				Reconst. $\delta^{13}C$ values	Bulk $\delta^{13}C$ values
	f-LF	o-LF_{10}	o-LF_{200}	HF		
	‰	‰	‰	‰	‰	‰
F1.1	-27.2	-27.8	-27.0	-25.9	-26.0	-26.4
F1.2	-27.4	-27.2	-26.8	-25.8	-25.8	-25.8
F1.3	-28.1	-27.8	-27.4	-25.8	-25.9	-25.6
F1.4	-27.4	-26.7	-27.6	-25.7	-25.7	-25.3
F1.5	-28.0	-27.8	-28.1	-25.5	-25.6	-25.0
F1.6	-28.5		-18.7	-25.3	-25.4	-24.7
F2.1	-27.7	-27.7	-27.4	-25.7	-25.8	-26.3
F2.2	-27.7	-28.3	-27.5	-25.8	-25.8	-26.3
F2.3	-27.7	-27.8	-28.2	-25.8	-25.8	-25.6
F2.4	-27.0	-28.5	-28.1	-25.8	-25.8	-25.3
F2.5	-27.2	-28.7	-28.1	-25.7	-25.8	-25.1
F2.6	-27.2	-18.8	-29.1	-25.6	-25.6	-25.0
F3.1	-27.2	-27.7	-26.7	-25.8	-25.9	-26.6
F3.2	-26.8	-28.1	-26.9	-25.7	-25.7	-25.7
F3.3	-26.8	-28.8	-27.2	-25.8	-25.8	-25.5
F3.4	-26.4	-27.7	-27.4	-25.6	-25.6	-25.3
F3.5	-26.2	-27.8	-27.6	-25.5	-25.5	-24.9
F3.6	-25.2	-27.3	-27.9	-25.5	-25.5	-24.8
B1.1	-27.2	-27.4	-26.6	-26.5	-26.6	-27.4
B1.2	-27.0	-27.2	-26.4	-26.4	-26.4	-26.9
B1.3	-26.8	-27.1	-26.1	-26.2	-26.2	-26.4
B1.4	-26.3	-27.0	-25.9	-26.0	-26.0	-26.2
B1.5	-25.7	-27.0	-26.0	-25.9	-25.9	-25.6
B1.6	-26.2	-27.4	-26.5	-25.6	-25.6	-25.1
B2.1	-26.6	-26.7	-26.1	-26.1	-26.2	-26.9
B2.2	-25.7	-26.5	-26.0	-26.0	-26.0	-26.7
B2.3	-25.7	-26.1	-25.7	-26.0	-26.0	-26.3
B2.4	-25.2	-25.8	-25.3	-26.0	-25.9	-26.0
B2.5	-25.0	-25.6	-25.3	-26.0	-26.0	-25.8
B2.6	-25.0	-25.5	-25.5	-26.1	-26.0	-25.7
B3.1	-27.5	-26.7	-26.1	-25.9	-26.0	-26.8
B3.2	-25.9	-26.1	-25.7	-25.9	-25.9	-26.1
B3.3	-24.8	-26.0	-25.5	-25.7	-25.7	-26.0
B3.4	-25.4	-26.0	-25.3	-25.9	-25.8	-25.7
B3.5	-24.7	-26.2	-25.5	-25.6	-25.6	-25.6
B3.6	-25.9	-25.6	-25.0	-25.3	-25.3	-25.3
B3.7	-25.9	-25.8	-25.0	-25.3	-25.3	-25.1

f-LF: Free-light fraction
o-LF_{10}: occluded soil organic carbon pool separated after a sonication of 10 J mL^{-1}
o-LF_{200}: occluded soil organic carbon pool separated after a sonication of 200 J mL^{-1}
HF: Heavy fraction
Total recovery: sum of fraction masses, expressed as % of soil mass prior to fractionation.
Reconst. $\delta^{13}C$ values: average of fractions $\delta^{13}C$ values weighted according to the proportion of organic C in each fraction.
Bulk $\delta^{13}C$ values: actual $\delta^{13}C$ measurements performed on the unfractionated samples.

Appendix Table 8.6. Surficial (< 10 nm) chemical composition of the density fractions as measured qualitatively by X-ray photoelectron spectroscopy (XPS). Four samples were analysed, two from the $CaCO_3$-free (F2.1, F2.4) and two from the $CaCO_3$-bearing (B2.1, B2.4) site. The number and letter following the elemental symbols represent the orbital targeted by the XPS, from which a photoelectron was ejected.

Sample	Fraction	C_{1s} %	O_{1s} %	C:O ratio	N_{1s} %	Al_{2p} %	Ca_{2p} %	Cl_{2p} %	Fe_{2p3} %	K_{2p} %	Mg_{2s} %	Na_{1s} %	P_{2p} %	Si_{2p} %	Ti_{2p} %	W_{4f} %
F2.1	f-LF	51.2	35.6	1.4	0.6	3.1	0.0	2.2	0.0	0.0	0.0	0.7	0.4	6.2	0.0	0.0
	o-LF_{10}	54.6	31.6	1.7	3.7	4.3	0.1	2.4	0.0	0.0	0.0	0.3	0.0	2.3	0.1	0.6
	o-LF_{200}	56.8	32.2	1.8	1.4	2.6	0.0	2.8	0.1	0.0	0.0	0.3	0.1	0.0	0.0	3.7
	HF	45.6	34.5	1.3	2.6	2.2	0.4	8.7	1.8	0.0	0.0	0.2	0.6	3.3	0.2	0.0
F2.4	f-LF	49.3	36.7	1.3	0.7	3.8	0.1	2.4	0.8	0.0	0.0	0.4	0.2	5.3	0.3	0.1
	o-LF_{10}	51.9	33.9	1.5	0.9	6.1	0.5	4.3	0.4	0.0	0.0	0.0	0.0	1.5	0.1	0.5
	o-LF_{200}	50.9	33.6	1.5	1.7	3.8	0.3	3.2	0.2	0.0	0.0	0.1	0.0	0.9	0.4	4.9
	HF	49.3	33.3	1.5	0.0	2.8	0.4	7.5	0.6	0.0	0.0	0.8	0.0	5.2	0.2	0.0
B2.1	f-LF	55.8	33.0	1.7	3.0	1.5	0.3	1.5	0.0	0.0	0.0	0.2	0.0	4.7	0.0	0.0
	o-LF_{10}	48.8	38.9	1.3	1.1	2.2	0.3	2.7	0.9	0.0	0.0	0.0	0.1	4.1	0.4	0.6
	o-LF_{200}	48.2	34.6	1.4	2.7	4.9	1.0	3.6	0.0	0.0	0.0	0.1	0.0	2.5	0.5	1.9
	HF	45.8	34.1	1.3	1.7	3.0	0.5	7.2	0.9	0.0	0.0	1.5	1.0	4.2	0.3	0.0
B2.4	f-LF	51.9	37.5	1.4	0.6	2.3	0.5	3.8	1.1	0.0	0.0	0.0	1.1	0.8	0.2	0.2
	o-LF_{10}	43.7	40.2	1.1	0.0	4.3	0.5	1.6	0.4	0.0	0.0	1.8	1.1	4.9	0.0	1.5
	o-LF_{200}	48.6	36.8	1.3	2.8	2.5	0.6	2.6	0.0	0.0	0.0	1.3	0.0	2.2	0.3	2.2
	HF	51.9	30.0	1.7	0.0	2.8	0.7	9.5	1.5	0.0	0.0	0.2	0.4	2.6	0.2	0.0

8.2 - Maps

8.2.1 - Topographic map

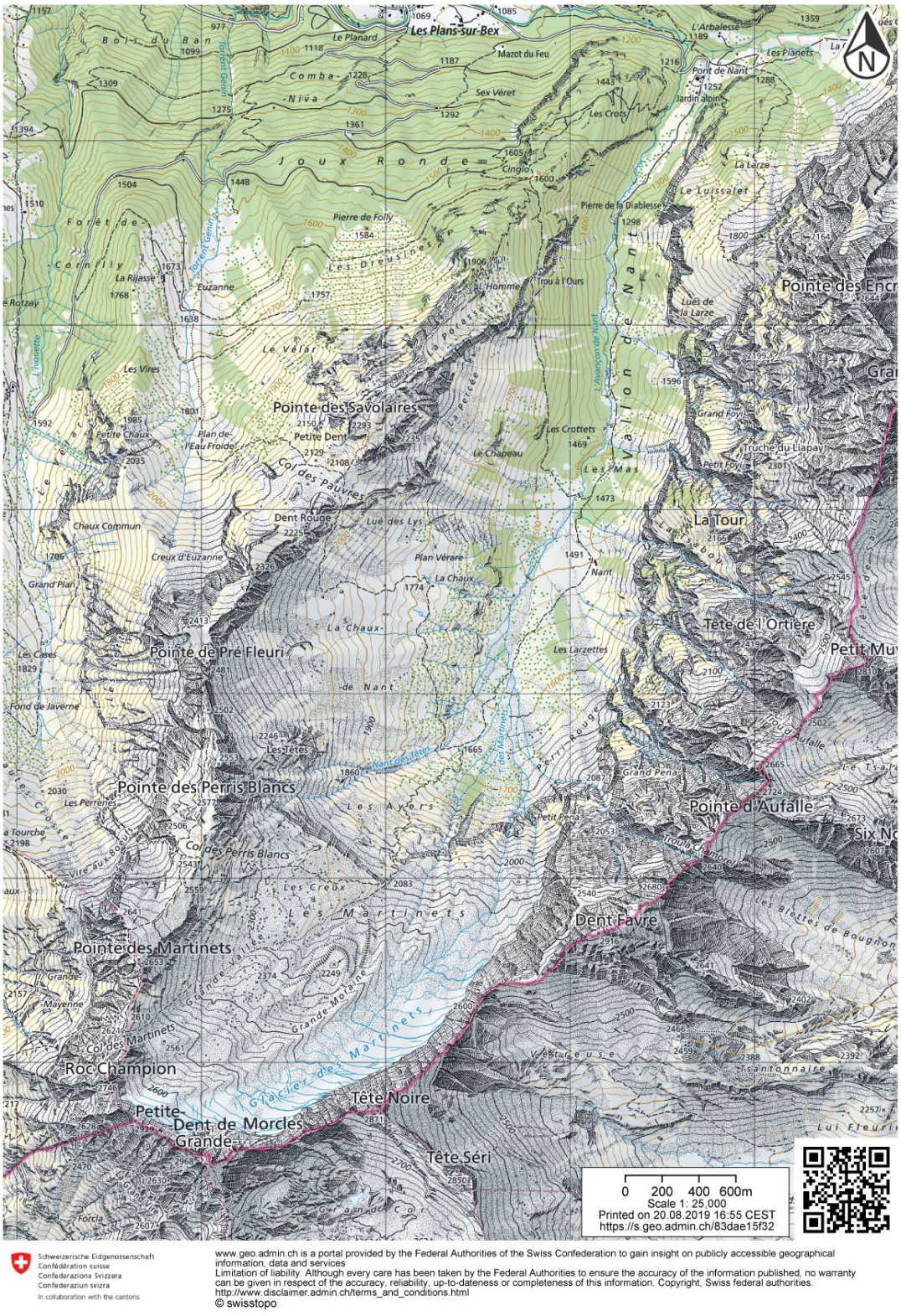

Appendix Fig. 8.12. Topographic map of the Nant Valley (SwissTopo, 2019). The line in pink separates the canton of Vaud (west) from Valais (east), Switzerland.

8.2.2 - Geological map

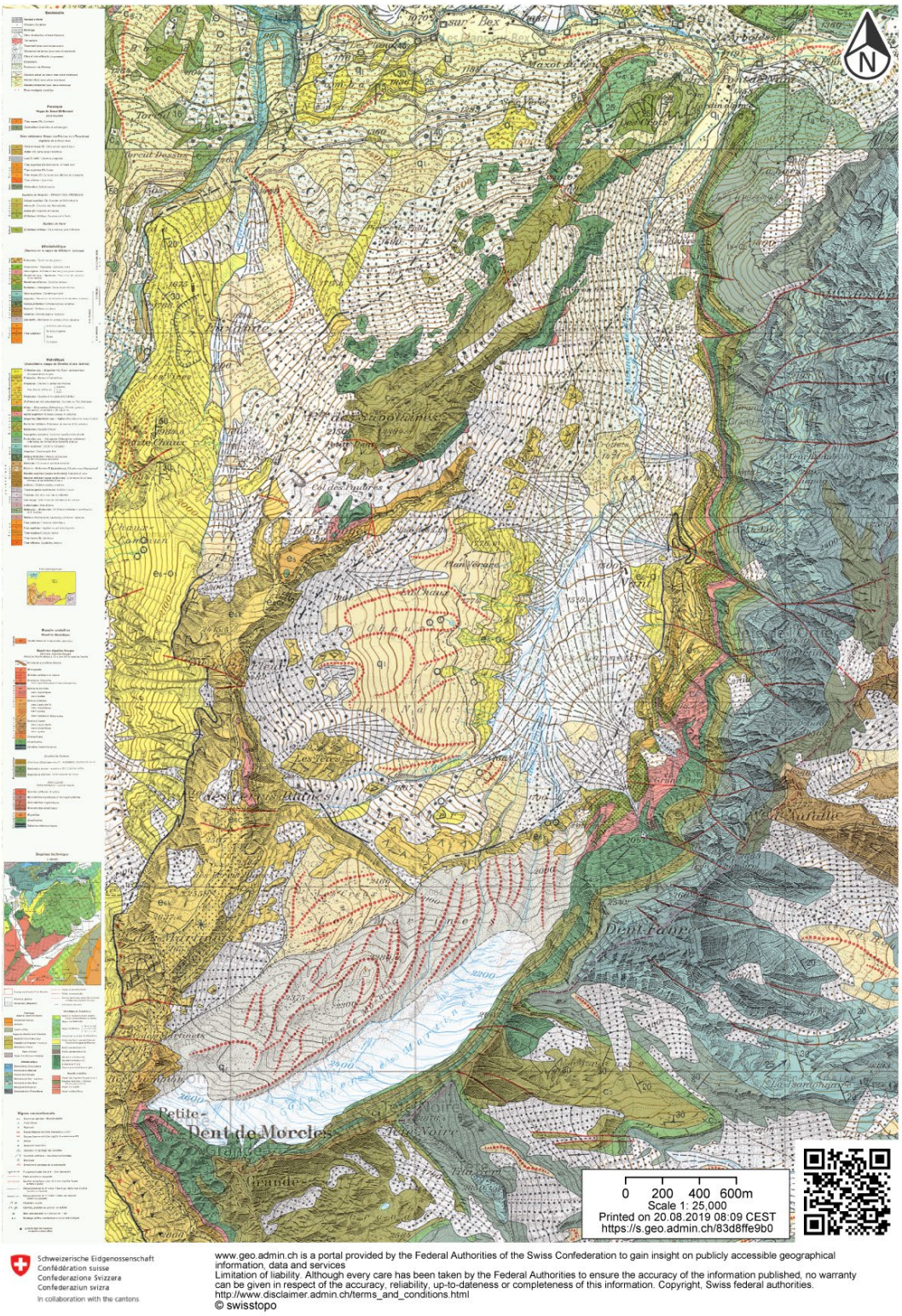

Appendix Fig. 8.13. Geological map of the Nant Valley (SwissTopo, 2019).

8.2.3 - Surficial formations map

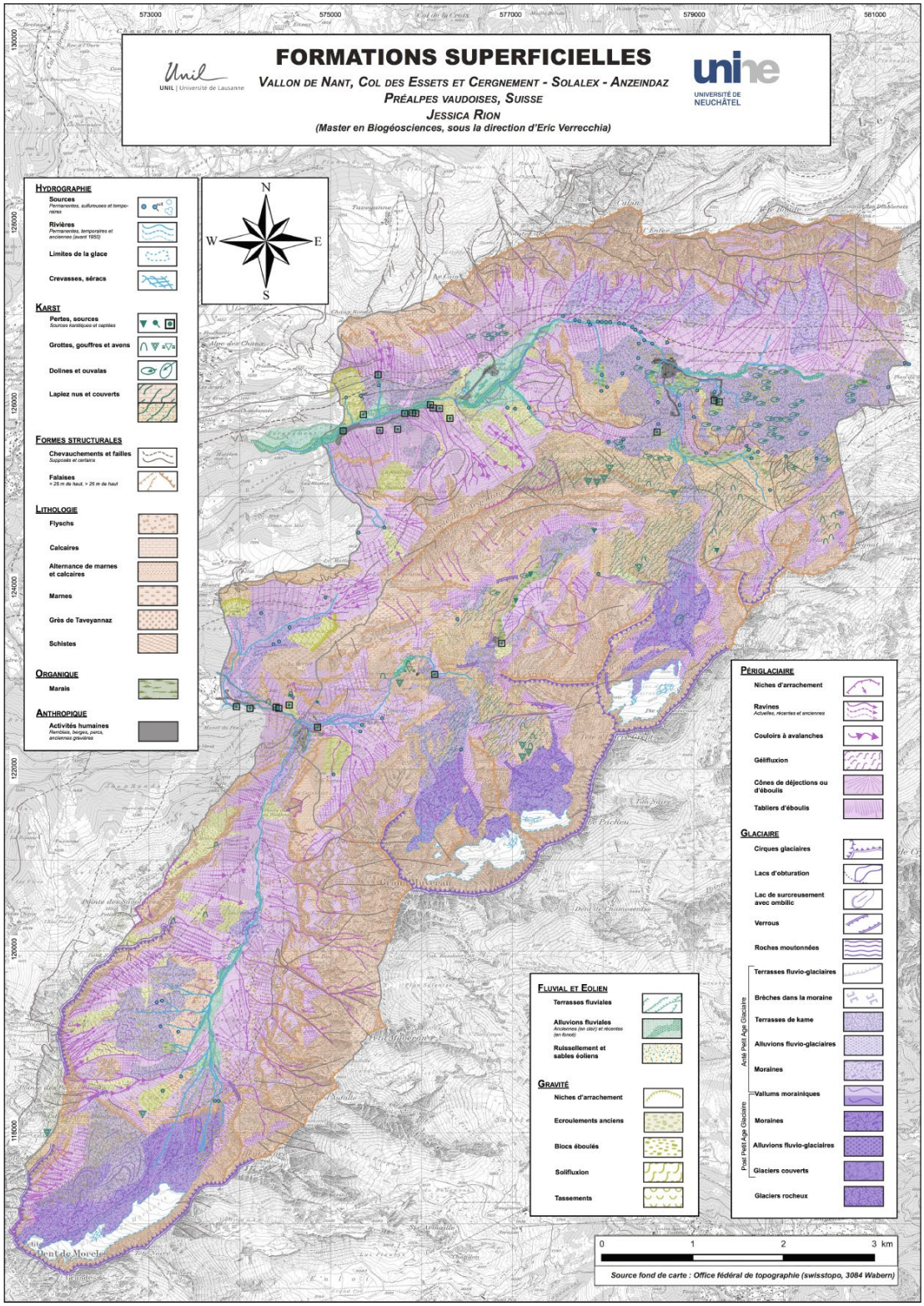

Appendix Fig. 8.14. Surficial formations map of the Nant Valley taken from Rion (2016). Legend in French, please ask for a translation if required.

8.2.4 - Vegetation map

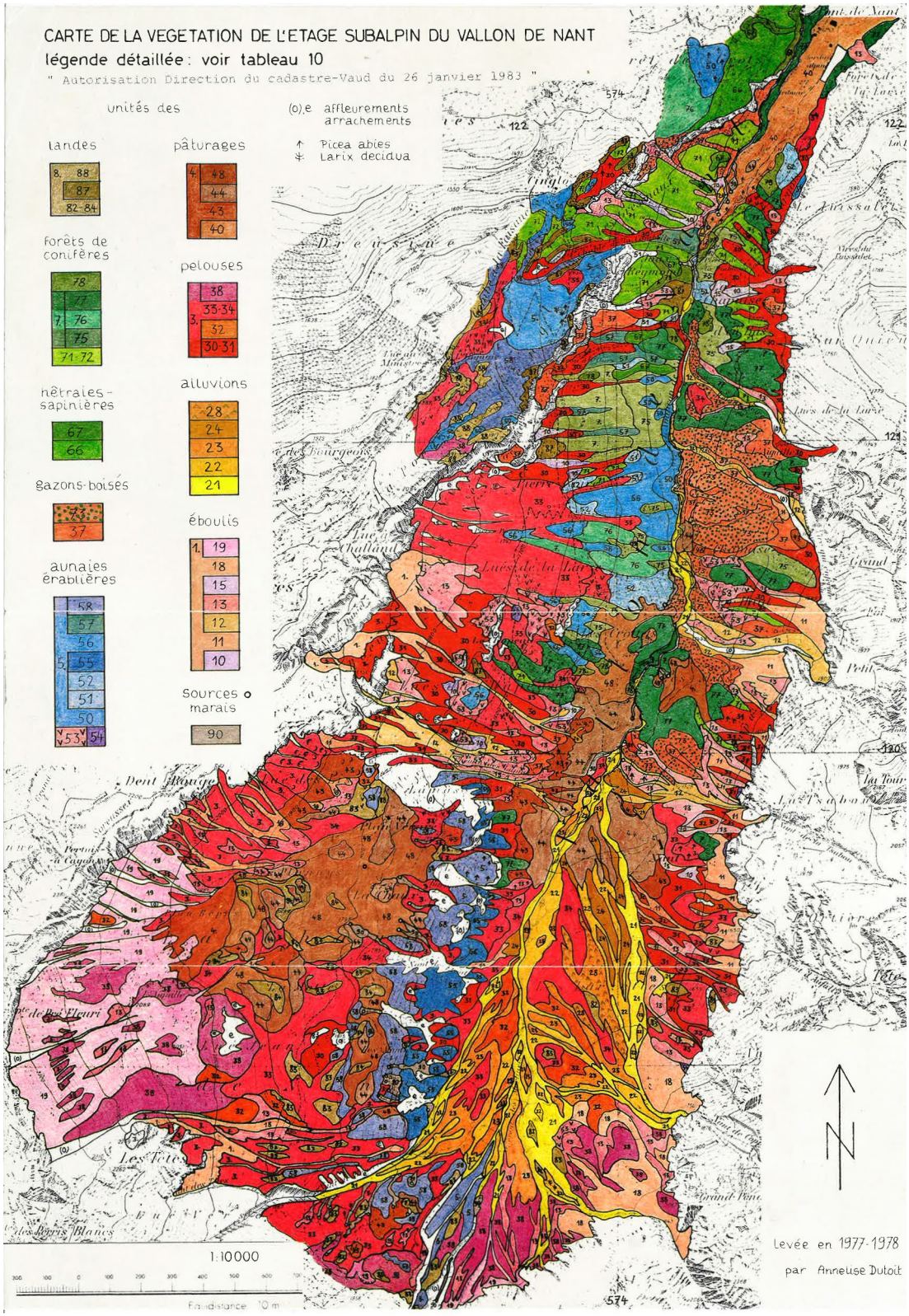

Appendix Fig. 8.15. Vegetation map of the Nant Valley taken from Dutoit (1983). The legend is in French on the following page. The sites are located upon the same vegetation structure, alpine grasslands (44; polygono-trisetion).

8.2.4.1 – Legend vegetation map

Appendix table 8.7. Index for the vegetation map in French (please ask for a translation if required), taken from Dutoit (1983).

10. INDEX DES UNITES CARTOGRAPHIQUES

N° VN	UNITES CARTOGRAPHIQUES	SYNTAXONOMIE UNITES SUPERIEURES	ASSOCIATIONS	TA-BLEAU	RELE-VES	PARA-GRAPHE
10	grt à Dryopteris robertiana et Rumex scutatus typique	Petasition paradoxi Zollitsch 66	Moehringio-Gymnocarpietum Jenny-Lips 30 em. Lippert 66	1 a	14-19	3.2
11	grt à Petasites paradoxus et Leontodon hyoseroides	Petasition paradoxi Zollitsch 66	Petasitetum paradoxi Beger 22	1 a	6-9	3.1.2
12	grt à Valeriana montana et Epilobium fleischeri	Petasition paradoxi Zollitsch 66	Petasitetum paradoxi Beger 22 epilobietosum Jenny-Lips 30	1 a	10-13	3.1.3
13	grt à Calamagrostis varia et Valeriana montana	(Petasition) - (Caricion ferrugineae)	stade pionnier du Laserpitio-Calamagrostietum (Kuhn 37, Moor 57) Th. Müller 61	1 a	22-29	3.3
15	grt à Dryopteris robertiana et Rumex scutatus, var. à Acer pseudoplatanus	Petasition paradoxi Zollitsch 66	Moehringio-Gymnocarpietum Jenny-Lips 30 em. Lippert 66 var. à Acer pseudoplatanus	1 a	20-21	3.2.2
18	grt à Adenostyles glabra et Thlaspi rotundifolium	Petasition paradoxi Zollitsch 66	grt original, aff. avec Petasitetum paradoxi Beger 22, Thlaspietum rotundifolii Br.-Bl. 26	1 a	1-5	3.1.1
19	grt à Thlaspi rotundifolium et Poa minor	Thlaspion rotundifolii Br.-Bl. 26	Thlaspietum rotundifolii Br.-Bl. 26 pro parte, var. à Doronicum grandiflorum	-	-	3.1.1
21	grt à Epilobium fleischeri et Hieracium staticifolium, ssgrt à Linaria alpina	Epilobion fleischeri G. Br.-Bl. 31	Epilobietum fleischeri Lüdi 21	2 a	1-10	4.2.1
22	grt à Epilobium fleischeri et Hieracium staticifolium, ssgrt à Tortella tortuosa	Epilobion fleischeri G. Br.-Bl. 31	Epilobietum fleischeri Lüdi 21	2 a	11-25	4.2.2
23	grt à Carex sempervirens et Dryas octopetala	Seslerion Br.-Bl. 26 contact Epilobion	(Seslerio-Caricetum sempervirentis Br.-Bl. 26 ericetosum)	2 a	26-30	4.3
24	(Poa alpina et Petasites paradoxus)	---	---	-	-	photo 6
28	grt à Larix decidua et Vaccinium myrtillus	Seslerion Br.-Bl. 26, contact Vaccinio-Piceetalia Br.-Bl. 39	---	2 a	31-33	4.3.2
30	grt à Carex ferruginea et Laserpitium latifolium	Caricion ferrugineae Br.-Bl. 31	Caricetum ferrugineae Lüdi 21 calamagrostietosum Oberd. 50 emend. 78	3 a	10-19	5.2.1
31	grt intermédiaire à Carex ferruginea et Petasites paradoxus	Caricion ferrugineae Br.-Bl. 31	---	3 a	21	5.2.2
32	grt à Carex sempervirens et Oxytropis jacquini	Seslerion coeruleae Br.-Bl. 26	Seslerio-Caricetum sempervirentis Br.-Bl. 26	3 a	1-9	5.1
33	grt à Carex ferruginea et Campanula rhomboidalis	Caricion ferrugineae Br.-Bl. 31	Caricetum ferrugineae Lüdi 21 norm.	3 a	20-32	5.2.2
34	grt intermédiaire à Carex ferruginea et Plantago lanceolata	Caricion ferrugineae Br.-Bl. 31	Caricetum ferrugineae Lüdi 21 (trifolietosum Oberd. 50 emend. 78)	3 a	24-27	5.2.2
37	Gazons-boisés; gazon rocailleux à recrû forestier	Seslerietalia variae Br.-Bl. 26	---	3 b	1-7	5.3.3 5.3.5
38	grt à Carex ferruginea et Festuca violacea	Caricion ferrugineae Br.-Bl 31	---	-	-	5.2.3
40	grt à Cynosurus cristatus et Leontodon autumnalis	Cynosurion Tx. 47	Festuco-Cynosuretum Tx. 42 (Crepido-Cynosuretum (Marschall 62, Knapp 62) Dietl 72)	4	2-5 (6)	6.2
43	grt à Phleum alpinum et Geranium silvaticum	Polygono-Trisetion Br.-Bl. 47, (Caricion ferrugineae Br.-Bl. 31)	---	4	10-11	6.3.2
44	grt à Phleum alpinum et Carum carvi	Polygono-Trisetion Br.-Bl. 47, (aff. Poion alpinae Oberd. 50)	(Phleo-Trisetetum (Br.-Bl. 48) Dietl 73)	4	7-9	6.3.1
48	grt à Nardus stricta et Hieracium auricula	Nardion Br.-Bl. 26	(Nardetum alpigenum Br.-Bl. 49)	4	1	6.1
50	Mégaphorbiée à Cicerbita alpina	Adenostylion alliariae Br.-Bl. 25	Cicerbito-Adenostyletum alliariae Br.-Bl. 50	5 a	21	7.6
51	Erablière à Agropyron caninum	Fraxino-Fagetea Moor 78 Lunario-Acerion Moor 75	Sorbo-Aceretum Moor 52	5 a	1-7	7.4.2

52	Erablière à Salix grandifolia	Lunario-Acerion Moor 75	(aff. Ulmo-Aceretum Issl. 27 Salicetum grandifoliae Br.-Bl. 50)	5 a	22-23	7.5.3
53	Fourré à Salix grandifolia	---	---	-	-	7.8.1
54	Reposoir et Mégaphorbiée au pied des parois	Arction Tx. 37 et Aegopodion podagrariae Tx. 75	Chenopodietum boni-henrici (Tx. 31) Th. Müll. ap. Oberd. 70 (grt à Chaerophyllum aureum et Myrrhis odorata Rich. 77)	-	-	7.8.2
55	Aunaie à Erable	Lunario-Acerion Moor 75 Adenostylion Br.-Bl. 25	rencontre Ulmo-Aceretum Issl. 27 et Alnetum viridis Br.-Bl. 18	5 b	11-18	7.7.3
56	Erablière à Laburnum alpinum	Lunario-Acerion Moor 75 (Adenostylion Br.-Bl. 25)	Ulmo-Aceretum Issl. 27 (stades ± évolués)	5 a	16-20	7.5.2
57	érablières à épicéas	Lunario-Acerion Moor 75	contact "avec futaies"	5 a	8-15	7.4.3
58	grt à Alnus viridis et Adenostyles alliariae; Aunaie Verte	Adenostylion Br.-Bl. 25	Alnetum viridis Br.-Bl. 18	5 b	1-10	7.7.2
66	Hêtraie-Sapinière à Festuca altissima	Abieti-Fagion Moor 78	Abieti-Fagetum Bartsch 40 festucetosum Kuoch 54	6	1-4	8.2.1
67	Hêtraie-Sapinière à Festuca altissima var. à Myrtille	Abieti-Fagion Moor 78	(Adenostylo glabrae-Fagetum Moor 70 luzuletosum Moor 70)	6	5-13	8.2.2
71	Forêt à Calamagrostis varia et Sesleria coerulea, Forêt à Graminées var. à Dryopteris robertiana	Vaccinio- Piceetalia Br.-Bl.39 Fraxino-Fagetea Moor 78 Seslerietalia Br.-Bl. 26 Thlaspietalia Br.-Bl. 26	---	7 b	1-8	8.4.1
72	Forêt à Calamagrostis varia et Sesleria coerulea, Forêt à Graminées var. à Chaerophyllum villarsii	Vaccinio-Piceetalia Br.-Bl. 39 Fraxino-Fagetea Moor 78 Seslerietalia Br.-Bl. 26 Thlaspietalia Br.-Bl. 26	---	7 b	9-13	8.4.2
73	Gazons-boisés; grt boisé aux clairières de gazon	Seslerietalia Br.-Bl. 26 Vaccino-Piceetalia Br.-Bl.39	---	3 b	8-13	5.3.4 5.3.5
75	Pessière à Fougères, var. à Cicerbita alpina	Vaccinio-Piceetea Br.-Bl. 39 Fraxino-Fagetea Moor 78 Betulo-Adenostyletea Br.-Bl.48	---	7 a	17-19	8.3.2 7.6
76	Sapinière à Erable	Fraxino-Fagetea Moor 78	vicariant altitudinal de l'Aceri-Fagetum Bartsch 40	6	14-20	8.2.3
77	Pessière à Fougères	Vaccinio-Piceetea Br.-Bl.39 Fraxino-Fagetea Moor 78 Piceo-Abietion prov.Ellenb. & Klötz. 72	(Dryopterido-Abietetum Ellenb. & Klötz. 72)	7 a	6-23	8.3.2
78	Pessière à Lonicera coerulea (Pessière sur blocs)	Vaccinio-Piceion Br.-Bl. 38	Asplenio-Piceetum (Aubert & Luquet 30) Moor 54	7 a	1-5	8.3.1
82	Lande fragmentaire des alluvions	Rhododendro-Vaccinion Br.-Bl. 26 Seslerietalia Br.-Bl. 26 (Seslerion Br.-Bl.26)	---	-	-	4.3.2 9.3
83	Pelouses à Rhododendron	Rhododendro-Vaccinion Br-Bl.26 Seslerietalia Br.-Bl. 26 (Caricion ferruginae Br.-Bl.31)	---	-	-	9.3
84	Pâturage à Rhododendron	Rhododendro-Vaccinion Br-Bl.26 (Poion alpinae Oberd. 50 & Nardion Br.-Bl. 26)	---	-	-	9.3
87	Lande à Rhododendron ferrugineux et à Mélèze (Lande subalpine)	Rhododendro-Vaccinion Br-Bl.26	Salici grandifoliae-Rhododendretum ferruginei Rich. 77	8	1-6	9.2.1
88	Lande à Empetrum hermaphroditum et Loiseleuria procumbens (Lande alpine)	Rhododendro-Vaccinion Br.-Bl. 26	aff. Vaccinio-Empetretum Br.-Bl. 26 et Arctostaphylo-Loiseleurietum. Oberd. 50	8	7-10	9.2.2
90	grt à Philonotis calcarea et Cratoneuron commutatum	Cratoneuro-Philonotidetalia Geissl. 76	Cratoneuro-Philonotidetum calcareae Geissl. 76	9	1-6	10.1
	grt à Carex davalliana et Carex flava	Tofieldietalia Prsg apud Oberd. 49	Caricetum davallianae W. Koch 28	9	7-10	10.2

8.3 - Profile Descriptions

8.3.1 - Key

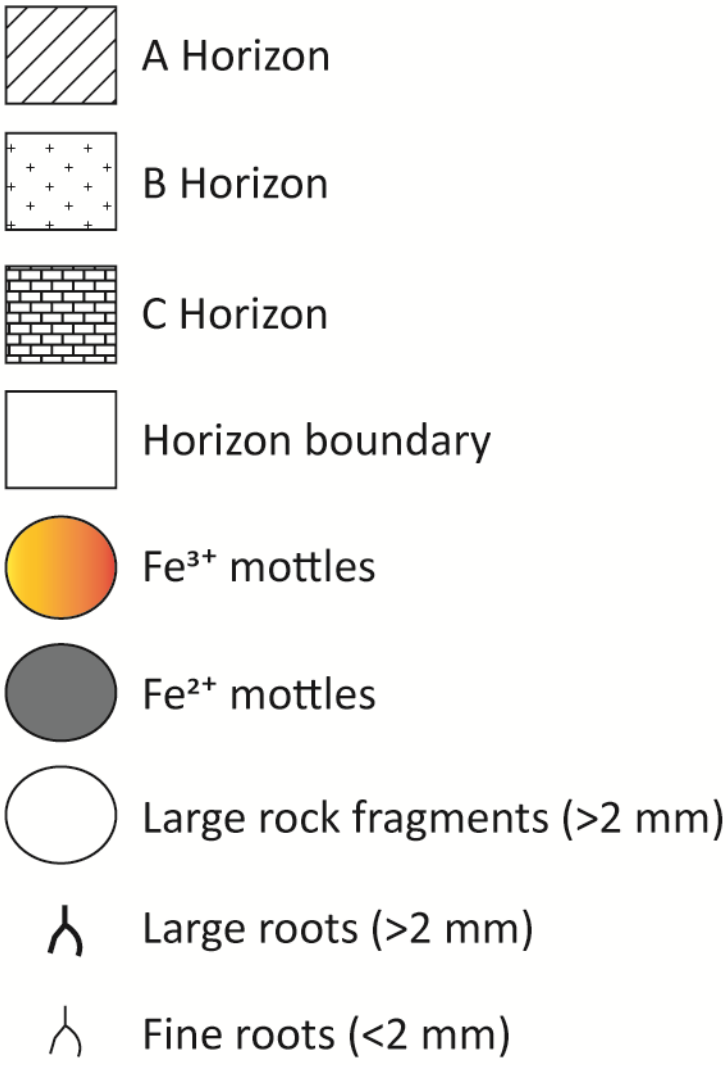

8.3.2 - Profile F1

WRB classification: Hypereutric Leptic Cambisols (Humic, Siltic) Drainage: Good

GPS location (Decimal degrees): N: 046.23130 E: 007.10038 Slope: 9° Aspect: E

Parent lithology : shist mixed colluvial-alluvial deposits eroded from the Morcles Nappe.

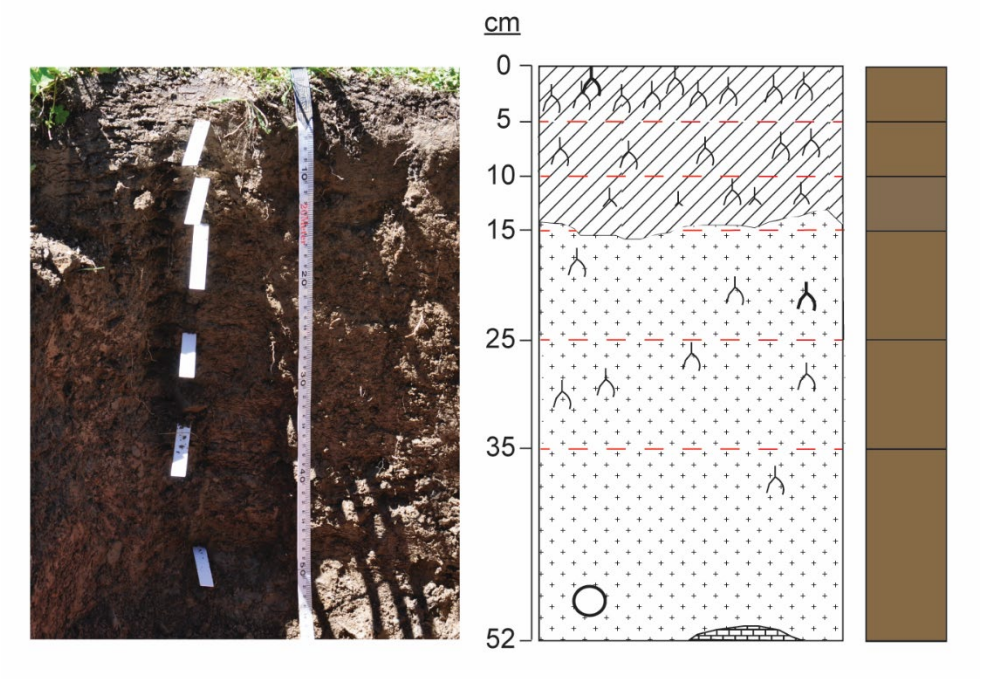

Depth (cm)	Horizon	Characteristics
0-5	Ah	Structure: Granular; Texture: Silty loam; Munsell: 10 yr 4 / 3; Roots: 50 %; Large rock fragments: 2 % Mottles: 30 % Effervescence: 0 / 4.
5-10	A1	Structure: Granular; Texture: Silty loam; Munsell: 10 yr 4 / 3; Roots: 30 %; Large rock fragments: 10 % Mottles: 15 % Effervescence: 0 / 4.
10-15	A2	Structure: Granular; Texture: Silty loam; Munsell: 10 yr 3 / 3; Roots: 20 %; Large rock fragments: 5 % Mottles: 2 % Effervescence: 0 / 4.
15-25	B1	Structure: Sub-angular / granular; Texture: Silty loam; Munsell: 10 yr 4 / 3; Roots: 5 %; Large rock fragments: 10 % Mottles: 0 % Effervescence: 0 / 4.
25-35	B2	Structure: Sub-angular; Texture: Silty loam; Munsell: 10 yr 4 / 3; Roots: 3 %; Large rock fragments: 15 % Mottles: 0 % Effervescence: 0 / 4.
35-52	B3	Structure: Sub-angular; Texture: Silty loam; Munsell: 10 yr 4 / 3; Roots: 0 %; Large rock fragments: 25 % Mottles: 0 % Effervescence: 0 / 4.

8.3.3 - Profile F2

WRB classification: Orthoeutric Leptic Cambisols (Humic, Siltic) Drainage: Good

GPS location (Decimal degrees): N: 046.23096 E: 007.10011 Slope: 11° Aspect: E

Parent lithology : shist mixed colluvial-alluvial deposits eroded from the Morcles Nappe.

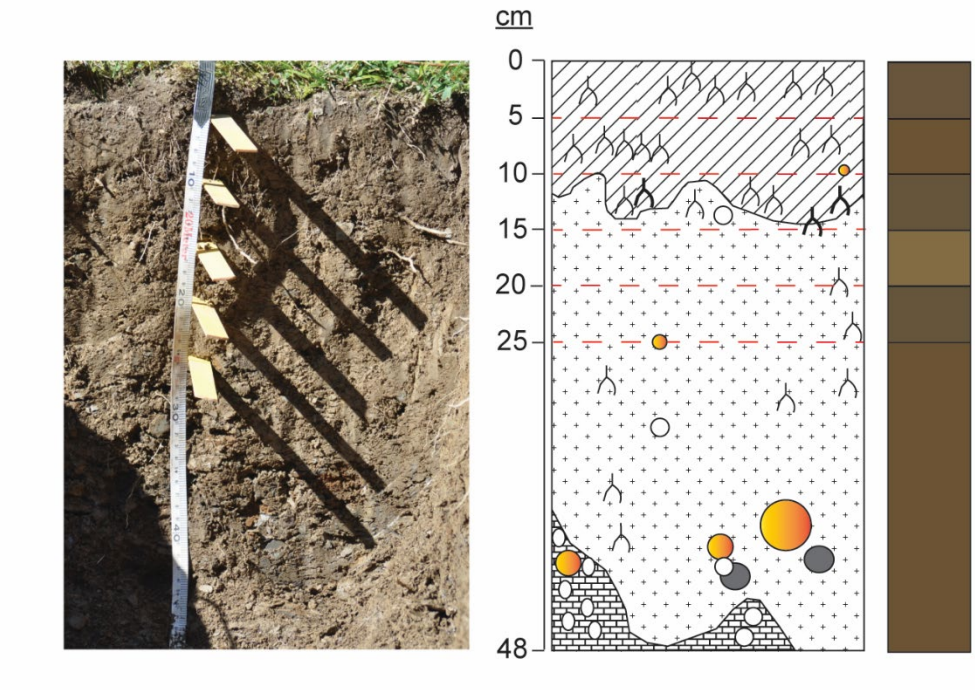

Depth (cm)	Horizon	Characteristics
0-5	Ah	Structure: Granular; Texture: Silty loam; Munsell: 10 yr 3 / 3; Roots: > 80 %; Large rock fragments: < 5 % Mottles: 30 % Effervescence: 0 / 4.
5-10	A	Structure: Granular; Texture: Silty loam; Munsell: 10 yr 4 / 3; Roots: 50 %; Large rock fragments: 5 % Mottles: 0 % Effervescence: 0 / 4.
10-15	AB	Structure: Granular / sub-angular; Texture: Silty loam; Munsell: 2.5 y 3 / 3; Roots: 35 %; Large rock fragments: 5 % Mottles: 5 % Effervescence: 0 / 4.
15-20	B1	Structure: Granular / sub-angular; Texture: Silty loam; Munsell: 2.5 y 4 / 4; Roots: 18 %; Large rock fragments: 10 % Mottles: < 5 % Effervescence: 0 / 4.
20-25	B2	Structure: Sub-angular; Texture: Silty loam; Munsell: 2.5 y 3 / 3; Roots: 10 %; Large rock fragments: 25 % Mottles: 0 % Effervescence: 0 / 4.
25-48	BC	Structure: Sub-angular; Texture: Silty loam; Munsell: 10 yr 4 / 3; Roots: 5 %; Large rock fragments: 35 % Mottles: 10 % Effervescence: 0 / 4.

8.3.4 - Profile F3

WRB classification: Orthoeutric Leptic Cambisols (Humic, Siltic) Drainage: Good

GPS location (Decimal degrees): N: 046.23094 E: 007.10026 Slope: 8° Aspect: EEN

Parent lithology : shist mixed colluvial-alluvial deposits eroded from the Morcles Nappe.

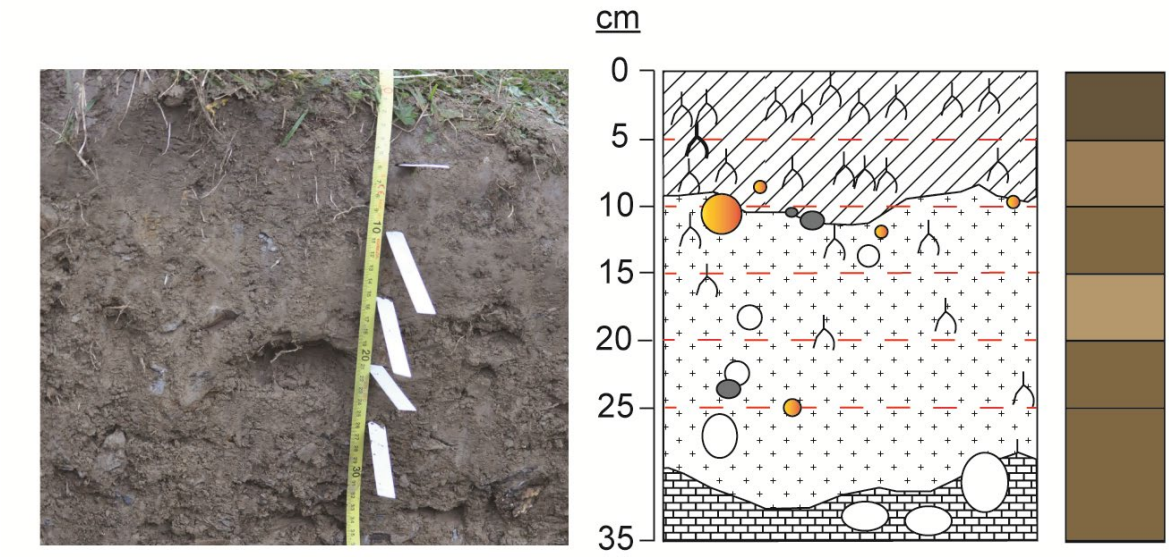

Depth (cm)	Horizon	Characteristics
0-5	Ah	Structure: Granular; Texture: Silty loam; Munsell: 2.5 y 3 / 3; Roots: 50 %; Large rock fragments: 2 % Mottles: 60 % Effervescence: 0 / 4.
5-10	A	Structure: Granular / sub-angular; Texture: Silty loam; Munsell: 2.5 y 5 / 4; Roots: 35 %; Large rock fragments: 10 % Mottles: 20 % Effervescence: 0 / 4.
10-15	B1	Structure: Granular / sub-angular; Texture: Silty loam; Munsell: 2.5 y 4 / 4; Roots: 20 %; Large rock fragments: 8 % Mottles: 5 % Effervescence: 0 / 4.
15-20	B2	Structure: Granular / sub-angular; Texture: Silty loam; Munsell: 2.5 y 4 / 6; Roots: 15 %; Large rock fragments: 20 % Mottles: < 5 % Effervescence: 0 / 4.
20-25	B3	Structure: Sub-angular; Texture: Silty loam; Munsell: 2.5 y 4 / 4; Roots: 2 %; Large rock fragments: 25 % Mottles: 2 % Effervescence: 0 / 4.
25-35	BC	Structure: Sub-angular; Texture: Silty loam; Munsell: 2.5 y 4 / 4; Roots: 1 %; Large rock fragments: 45 % Mottles: 2 % Effervescence: 0 / 4.

8.3.5 - Profile B1

WRB classification: Cambic Leptic Phaeozem (Siltic) Drainage: Good

GPS location (Decimal degrees): N: 046.22895 E: 007.10263 Slope: 6° Aspect: W

Parent lithology : carbonate-rich mixed colluvial-alluvial deposits eroded from the Morcles Nappe.

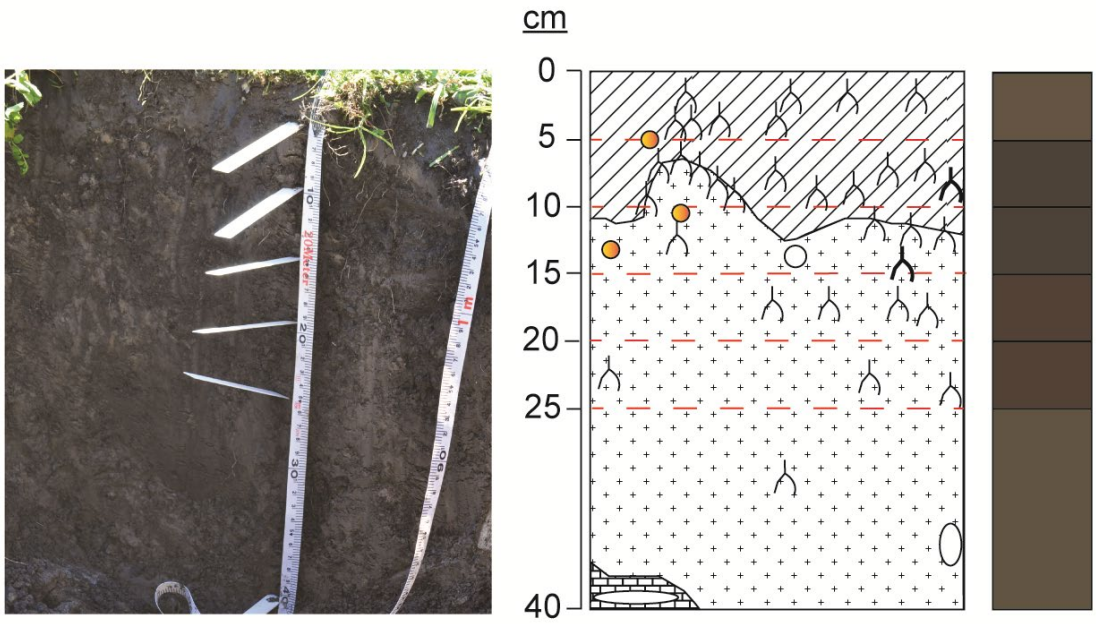

Depth (cm)	Horizon	Characteristics
0-5	Ah1	Structure: Granular; Texture: Silty loam; Munsell: 2.5 y 3 / 2; Roots: 70 %; Large rock fragments: 0 % Mottles: 10 % Effervescence: 3 / 4.
5-10	Ah2	Structure: Granular; Texture: Silty loam; Munsell: 2.5 y 2 / 1; Roots: 38 %; Large rock fragments: 2 % Mottles: 10 % Effervescence: 3 / 4.
10-15	ABh	Structure: Granular; Texture: Silty loam; Munsell: 5 y 1 / 2; Roots: 20 %; Large rock fragments: 10 % Mottles: 0 % Effervescence: 0 / 4.
15-20	Bh	Structure: Sub-angular; Texture: Silty loam; Munsell: 5 y 2 / 2; Roots: 5 %; Large rock fragments: 10 % Mottles: 0 % Effervescence: 1 / 4.
20-25	B1	Structure: Sub-angular; Texture: Silty loam; Munsell: 5 y 2 / 2; Roots: 5 %; Large rock fragments: 15 % Mottles: 0 % Effervescence: 1 / 4.
25-35	B2	Structure: Sub-angular; Texture: Silty loam; Munsell: 5 y 2 / 3; Roots: 1 %; Large rock fragments: 30 % Mottles: 0 % Effervescence: 2 / 4.

8.3.6 - Profile B2

WRB classification: Cambic Leptic Phaeozem (Siltic) Drainage: Good

GPS location (Decimal degrees): N: 046.22883 E: 007.10262 Slope: 7° Aspect: W

Parent lithology : carbonate-rich mixed colluvial-alluvial deposits eroded from the Morcles Nappe.

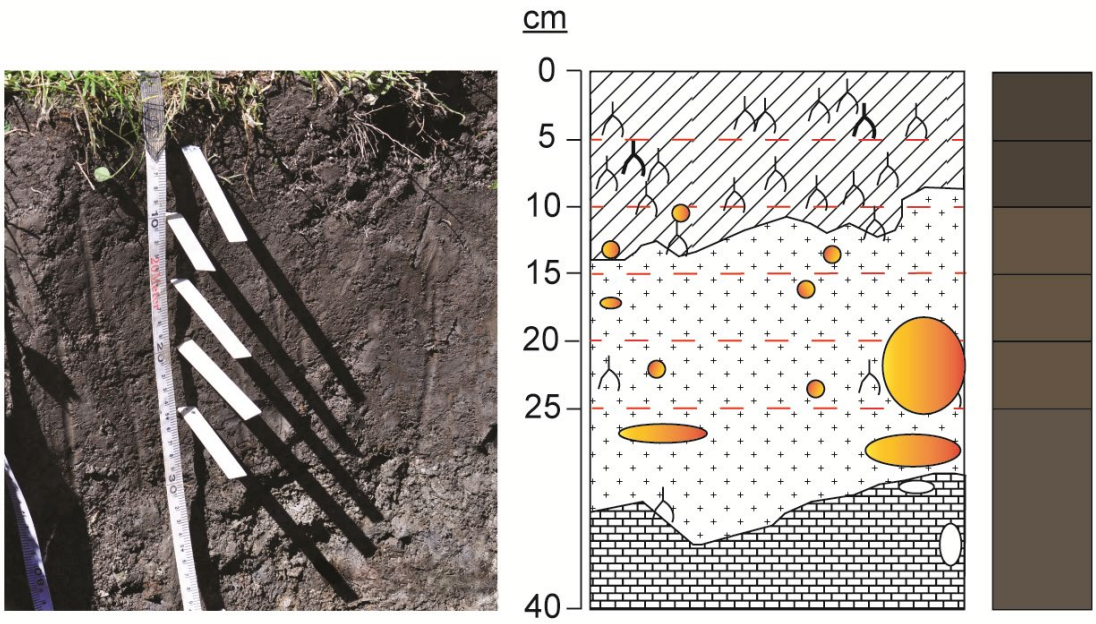

Depth (cm)	Horizon	Characteristics
0-5	Ah1	Structure: Granular; Texture: Silty loam; Munsell: 5 y 2 / 1; Roots: 35 %; Large rock fragments: 0 % Mottles: 5 % Effervescence: 0 / 4.
5-10	Ah2	Structure: Granular; Texture: Silty loam; Munsell: 5 y 2 / 1; Roots: 25 %; Large rock fragments: 0 % Mottles: 5 % Effervescence: 0 / 4.
10-15	ABh	Structure: Granular; Texture: Silty loam; Munsell: 2.5 y 3 / 2; Roots: 10 %; Large rock fragments: 2 % Mottles: 18 % Effervescence: 0 / 4.
15-20	Bh1	Structure: Granular / sub-angular; Texture: Silty loam; Munsell: 2.5 y 3 / 2; Roots: 10 %; Large rock fragments: 3 % Mottles: 10 % Effervescence: 1 / 4.
20-25	Bh2	Structure: Granular / sub-angular; Texture: Silty loam; Munsell: 2.5 y 3 / 2; Roots: 5 %; Large rock fragments: 3 % Mottles: 10 % Effervescence: 1 / 4.
25-40	BC	Structure: Sub-angular; Texture: Silty loam; Munsell: 2.5 y 3 / 1; Roots: 0 %; Large rock fragments: 40 % Mottles: 15 % Effervescence: 3 / 4.

8.3.7 - Profile B3

WRB classification: Cambic Leptic Phaeozem (Siltic) Drainage: Good

GPS location (Decimal degrees): N: 046.22886 E: 007.10240 Slope: 10° Aspect: NW

Parent lithology : carbonate-rich mixed colluvial-alluvial deposits eroded from the Morcles Nappe.

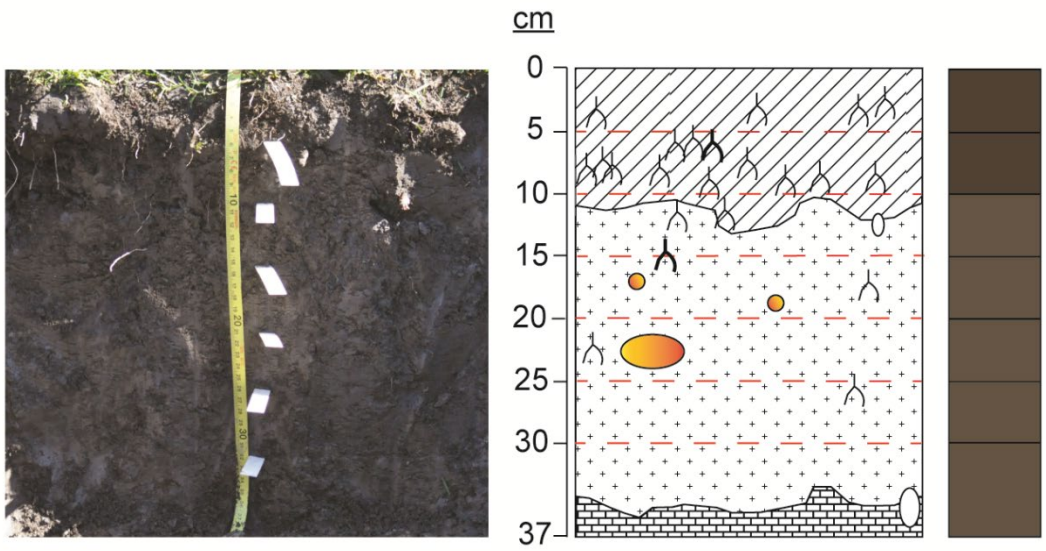

Depth (cm)	Horizon	Characteristics
0-5	Ah1	Structure: Granular; Texture: Silty loam; Munsell: 10 yr 2 / 2; Roots: 60 %; Large rock fragments: 0 % Mottles: 5 % Effervescence: 0 / 4.
5-10	Ah2	Structure: Granular / sub angular; Texture: Silty loam; Munsell: 10 yr 2 / 2; Roots: 20 %; Large rock fragments: 5 % Mottles: 15 % Effervescence: 1 / 4.
10-15	ABh	Structure: Granular / sub-angular; Texture: Silty loam; Munsell: 10 yr 3 / 2; Roots: 10 %; Large rock fragments: 3 % Mottles: 15 % Effervescence: 0 / 4.
15-20	Bh	Structure: Granular / sub-angular; Texture: Silty loam; Munsell: 10 yr 3 / 2; Roots: 5 %; Large rock fragments: 1 % Mottles: 15 % Effervescence: 0 / 4.
20-25	B1	Structure: Sub-angular; Texture: Silty loam; Munsell: 10 yr 3 / 2; Roots: 1 %; Large rock fragments: 5 % Mottles: 1 % Effervescence: 0 / 4.
25-30	B2	Structure: Angular; Texture: Silty loam; Munsell: 10 yr 3 / 2; Roots: 0 %; Large rock fragments: 2 % Mottles: 0 % Effervescence: 1 / 4.
30-37	BC	Structure: Angular; Texture: Silty loam; Munsell: 2.5 y 3 / 2; Roots: 0 %; Large rock fragments: 10 % Mottles: 0 % Effervescence: 2 / 4.

8.4 - Methods

8.4.1 - Preparation of soil samples

8.4.1.1 - Field moist soil

Several analyses required field moist soil (soil pH, oxalate and dithionite extraction). Field moist soil was carefully selected, ensuring coarse fragments or coarse organic matter (> 2 mm) were not included in these specific analyses.

8.4.1.2 - Air-dried (< 2 mm fraction)

Soils were air-dried and sieved to 2 mm as is the custom within soil sciences (van Reeuwijk, 2002).

1. Soils were dried at room temperature for over 1 month in Stephanie's office (the unofficial soil drying room).
2. Dried soil from each sample site was placed into a 2 mm sieve with a lid and base-pan.
3. Samples were shaken and left to repose for a moment.
4. All material that had not passed the sieve was then crushed in a pestle and mortar.
5. The material was then repassed through the sieves, repeating Steps 2 – 3, approximately six to ten times.
6. Most analysis was completed on this air-dried fraction.
7. All equipment was washed with ethanol and carefully dabbed dry with paper towel and compressed air.
8. Henceforth this < 2 mm fraction will be labelled air-dried soil.

8.4.1.3 - Ground soil (< 20 µm)

Ground soil was needed for several forms of analysis. A homogenous and representative sub-sample of air-dried soil was taken from each sample and ground to a fine powder for further analysis.

1. 25 g of air-dried soil was loaded into an agate crucible.
2. This soil was then crushed for 3 mins in a Siebtechnik Schibenschwingmuhle-TS vibrating disc-mill.
3. Samples were then loaded into glass receptacles and all equipment was washed with distilled water and dried with compressed air and gently with paper towel.

8.4.1.4 - Density fractionation

Individual SOC pools were fractioned by density (SPT; Sometu-Europe) and sequential sonication, into free-light (f-LF), 2 occluded-light fractions separated at 10 J mL^{-1} and 200 J mL^{-1} sonication energies (o-LF_{10}, o-LF_{200} respectively), and a heavy fraction (HF; Golchin et al., 1994; Poeplau et al., 2018; Viret and Grand, 2019).

f-LF

1. 7 g of air-dried soil from each sample was added to a 50 mL labelled falcon tube.
2. 35 mL of SPT (1.6 g cm^{-3}) was added to the sample with a graduated cylinder.
3. The tube was then gently inverted until all material was suspended.
4. Samples were then placed and balanced within a swing-bucket centrifuge.
5. Tubes were left to rest for 30 mins to ensure the fractionation of various particles with differing densities.
6. Samples were then centrifuged at 1080 g for 30 mins.
7. The f-LF (floating material on the SPT) was then decanted into an acid washed vacuum filtration unit with 0.45 μm nitrocellulose paper.
8. Tubes were twisted during inversion to ensure that all material adhering to the side of the tube was decanted into the filtration unit.
9. Any remaining f-LF material was then carefully scraped from the sides of the tubes using an acid washed plastic spatula so as not to scrape the tubes' sides.
10. The scraping spatula was rinsed thoroughly with deionised water between washes.
11. Once the f-LF from all samples were in the vacuum filtration units, a vacuum pump was switched on, filtering the SPT from the f-LF.
12. This SPT was then recombined with the remaining sample still in the falcon tube.
13. The f-LF was then re-suspended with 50 mL of deionised water and left to rest for a least 10 mins.
14. The f-LF was then thoroughly rinsed and filtered, washing the side of the funnel and material three times with deionised water in a squeezy bottle. Between each rinse, the f-LF sat thoroughly submerged in deionised water to ensure it was rinsed properly.
15. The f-LF was then washed off the filter paper and into an aluminium drying boat with deionised water, being careful to not overfill the boat or damage the paper, while ensuring no material remains on the filter o-ring.
16. All material was already rinsed on the filter paper during the three complete rinses, but this was triple checked before passing the funnels for acid washing.
17. The f-LF was then dried in an oven at 65°C, until the remaining deionised water in all the aluminium boats had been removed. Samples were then left for another 12 h to dry thoroughly.

$O\text{-}LF_{10}$ & $o\text{-}LF_{200}$

1. After removing the f-LF, the remaining sample were re-suspended in the SPT by shaking them carefully.
2. Tubes were then sonicated using a pre-calibrated sonicator (see the calibration section below for more details for more details) at 10 J mL^{-1} (25 s). The sonicator was used at a maximum of 20 % amplitude to reduce the movement of material up the sonicator node.

3. During sonication, samples were kept in an ice slurry to efficiently dissipate any heat transfer from the sonication node.
4. Occluded material that had travelled up the sonicator node was washed back into the sample tube with 1 mL of fresh 1.6 g cm^{-3} SPT using an autopipette.
5. The sonicator node was washed with deionised water between samples, waiting until it dripped dry, before gently dabbing the node dry with tissue paper. Prior to sonicating another sample, the node was checked to ensure that no paper was stuck to it.
6. Samples were then re-centrifuged at 1080 g for 30 mins
7. The suspended o-LF_{10} was then fractionated, filtered, rinsed and oven dried in the same manner as the f-LF.
8. SPT was recombined with the o-LF_{200} and pellets were re-suspended with a quick blast upside down on a vortex agitator.
9. The remaining sample was then sonicated at 190 J mL^{-1} (8m16s for 36 mL), totalling 200 J mL^{-1} sonication.
10. Material was washed off the sonicator node again. The sonicator node was washed three times with deionised water between uses, to prevent any potential SPT precipitation on the node.
11. Tubes were reposed, balanced within the centrifuge and rested for 30 mins.
12. Tubes were then centrifuged at 1830g for 30 mins.
13. The o-LF_{200} floating material was then fractionated from the HF in the same manner as the f-LF and o-LF_{10}.
14. The SPT was then filtered from the o-LF_{200} and removed for recycling later (see the section below on SPT recycling for more details).
15. Samples were then rinsed and oven dried.

HF

1. An acid washed glass bead (1 mm diameter) and 40 mL of deionised water were added to the remaining HF pellet. The glass bead broke up dense aggregates that developed during the rinsing process, particularly in the $CaCO_3$-bearing site (Appendix Fig. 8.16). This in turn caused large recoveries because of the retention of SPT in the HF.
2. This mixture was then agitated with a vortex until the pellet was broken up.

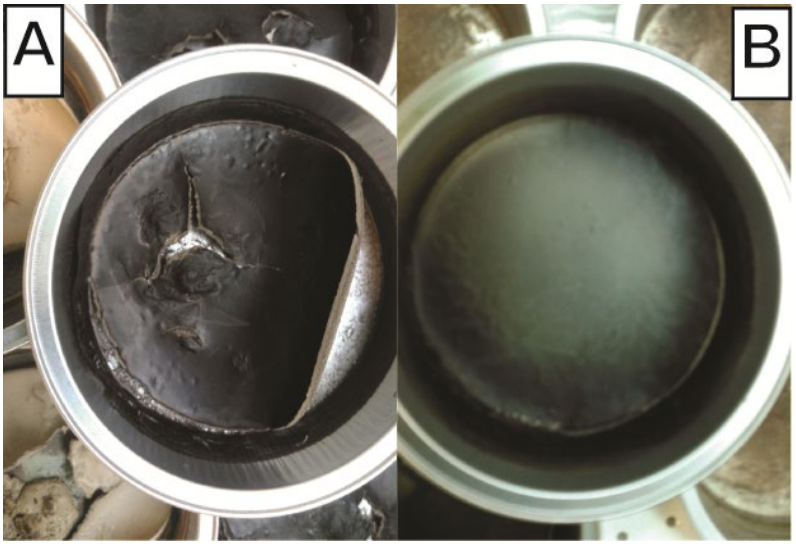

Appendix Fig. 8.16. Density fractionation pre-testing revealed a glass bead was necessary to ensure that the heavy fraction (HF) were thoroughly rinsed. **A)** This sample was not agitated with a glass bead (1 mm) and could not be rinsed properly. The HF aggregated and created a ball that still contained sodium polytungstate (SPT). B) This sample was agitated with a glass bead during the rinsing process and the HF was rinsed homogeneously, removing all SPT.

3. Samples were then placed on a rotary shaker and agitated at 200 rpm for 10 mins.
4. Samples were then centrifuged at 7,500 g for 30 mins. The supernatant was removed gently, pouring it against the direction of the cake so as not to dislodge loose material at the rim of the tube.
5. The supernatant was not completely removed if the cake became un-stabilised, as it was of the utmost importance not to preferentially lose fine material. The rinse water was poured into a large beaker to check for loses of material during the rinsing process. If there were significant loses we started the process again.
6. A second aliquot of deionised water (40 mL) was added to the sample and the process restarted.
7. This process was repeated a total of five times to completely remove the SPT (< 50 µS).
8. On the 4th rinse, 1mL of 2 M NaCl was added to the 40 mL of deionised water (50 mM NaCl) to prevent destabilisation of the cake on the 4th and 5th rinses.
9. Once rinsed five times, the tube was vortexed with a little deionised water.
10. The remaining HF slurry was then rinsed into an aluminium boat.
11. The glass ball was removed straight away with tweezers rinsing any material back into the boat.
12. After ensuring that all the HF material was transferred into the boat, the tube was disposed of and the HF was oven dried.

Material recovery

1. Once oven dried, material in the aluminium weigh boats was left to cool within a desiccator.
2. Material was then scraped off the boats at a constant pressure using a plastic spatula so as not to damage the boat. Pre-testing demonstrated that the metal spatula was more efficient, but also attacked the aluminium boats, as was confirmed using optical microscopy (Appendix Fig. 8.17 A & B). The material was scraped onto a pre-weighed weighing paper and weighed. All scraping was carried out atop a white plastic tray to prevent any loss of material.

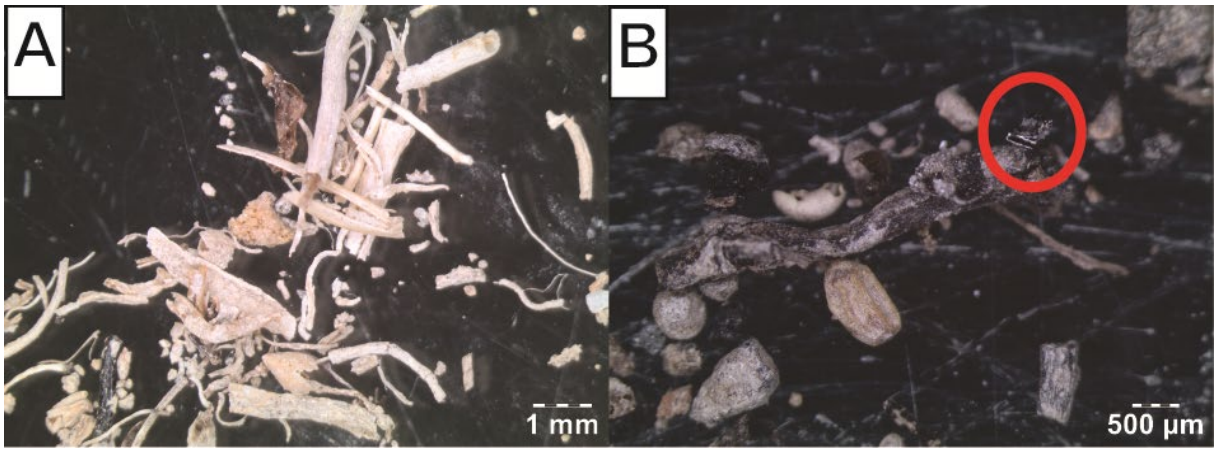

Appendix Fig. 8.17. Micrographs of the free-light fraction from the: **A)** $CaCO_3$-free site, **B)** $CaCO_3$-bearing site. This inspection revealed that the metal spatula was too aggressive to recover material for the fractions, as it grated the aluminium boats (grated material circled in red), which contained the fractions after drying. It also revealed that the $CaCO_3$-free site seemed to have more mineral coating.

3. Once all the material was removed from the boat, fractions were then moved into a pestle and mortar, and crushed to a fine and homogeneous particle size.
4. To remove SIC from the LFs, all LFs were moved into a pre-weighed glass vials and fumigated, like in Chapter 4 (see the fumigation section in 8.4.2.6 below).
5. A representative subsample of each HF was moved to an acid washed glass desiccator vial for fumigation, as in Chapter 4 (see the fumigation section in 8.4.2.6 below).
6. Total recovery for all samples ranged between 98.2–100.4 %. There was no material recovered in the F1.6 o-LF_{10}.

8.4.1.5 - Preparations for DF

Grading SPT to a specific density

1. To ensure SPT was at 1.6 g cm^{-3}, SPT was slowly added to a deionised water solution, heated in a beaker on a hotplate at 80 °C (or warm to touch) with an acid washed stirring magnet.

2. Due to the potential precipitation of Ca-metatungstate, SPT was always kept in plastic containers between the evaporation steps on the hotplate in glass.
3. Once cool the density of SPT solutions was confirmed using a floating densimeter in the 1.5-2 g cm^{-3} range.

Recycling SPT

Due to the expensive nature of heavy density solutions SPT was recycled several times before disposal according to Six et al. (1999). A recycling column was used (the construction of which is explored in the next section).

1. The SPT was first filtered through 2.5 µm filter papers
2. The SPT was first then added to a glass beaker and heated on a hotplate at 80 °C (or until warm to touch) with a stirring magnet.
3. 15 mL L^{-1} H_2O_2 (35%) was then added to the warm contaminated SPT solution to oxidise any organic material that passed the filter.
4. After 24 H, the SPT was removed from the heating plate and stored in a plastic container.
5. The SPT was then left to rest for 7 – 10 days with the lid left slightly open, to degas excess H_2O_2
6. 2 L of deionised water was then passed through the recycling column (Appendix Fig. 8.18; see below for details on its construction), prior to passing the SPT through.

Appendix Fig. 8.18. Sodium polytungstate rinsing column.

7. The SPT was then passed through the recycling column, passing 2.5 µm filters at the top and bottom.
8. Each litre that passed the unit was marked on tape at the base of the stand. Filters on the top and bottom of the column were also changed every day.
9. After passing all the H_2O_2 oxidised / evaporated SPT through the column, 200 – 400 mL of deionised water was passed through the columns twice, to ensure that any remaining SPT was rinsed from the columns. This rinse liquid was then combined with the SPT to be evaporated.
10. The rinse water was then evaporated from the SPT on a heating plate with a stirring magnet.
11. 15 mL L^{-1} ethanol was added to the evaporating solution to digest any excess H_2O_2.
12. The recycled SPT was then evaporated to the desired density, checking density on the hot plate. Hotplate temperatures were reduced markedly if the SPT was left overnight to prevent potential "evaporation" accidents.
13. **The temperature of the SPT should only be warm to touch.**
14. After the solution had cooled to room temperature in a plastic container, it was brought to the desired density by adding deionised water.

Changing columns

1. Dispose of the activated charcoal and filter papers.
2. Store the cationic (Na^+) exchange resin for regeneration.
3. Clean and acid wash everything (3 M HCl).
4. Set up the column as follows (Appendix Fig. 8.18):
    a. Cut two circular 6 µm filters for each column and place at the bottom of the columns.
    b. Next place into the column:
        i. 5 cm of glass wool column (*laine de verre*)
        ii. 10 cm of cationic exchange resin (Dowex® Marathon™ C Na^+-form, strongly acidic, 20-50 mesh)
        iii. 5 cm of glass wool column (*laine de verre*)
        iv. 7 cm activated charcoal
        v. Then another 3cm of glass wool column (*laine de verre*)
    c. Make sure any liquid that goes in and out of the columns is filtered on 2.5 µm filters at the top and at the bottom

Regenerating the cationic exchange resin

1. Put the resin in a 2 M NaCl solution for 1 h while mixing slowly.
2. Remove the solution
3. Repeat steps a further 2 times
4. Rinse the resin three times with deionised water

8.4.2 - Lab analyses

8.4.2.1 - Soil pH

Soil pH was measured potentiometrically using a glass-body combination electrode (Thermo Scientific Orion ROSS probe) on field moist samples in 0.1 M $CaCl_2$ solution (1:2 ratio).

1. 10 g of field moist soil was combined with 20 mL of 0.1 M $CaCl_2$ in 50 mL centrifuge tubes.
2. Suspensions were then agitated with a pipette tip.
3. Suspensions were left to equilibrate for 10 mins from the start time and were then stirred a second time.
4. Suspensions were then left to settle for another 20 mins.
5. The pH of suspensions was then measured using the electrode, rinsing the electrode between samples using distilled water.

8.4.2.2 - Texture - Particle size distributions

Texture was determined using laser diffraction (Pansu and Gautheyrou, 2006). The Beckman Coulter LS13320 Particle Sizing Analyser was run using the default optical model (Fraunhofer.rf780d) in auto-

dilution mode. Measurements were taken when an obscuration of 12 % was obtained. Pre-treatment of samples prior to measurement included:

1. 1 g of air-dried soil from each sample was placed in a 50 mL centrifuge tube.
2. Samples were not de-carbonated in an attempt to preserve any $CaCO_3$ (< 2 mm), which were present at the $CaCO_3$-bearing site.
3. Soil organic matter was digested with increasing concentrations of H_2O_2 (10-35 %). Oxidation of the organic matter was completed slowly as the reaction can quickly escalate, causing samples to spill over, and then the extraction must be restarted.
    a. pH was kept around neutrality throughout the destruction of organic matter with NaOH to prevent destruction of mineral components due to the acidification associated with the destruction of organic matter.
        i. pH was checked with indicator paper and corrected around neutrality at each step after step c.
    b. 2 mL of distilled water was first added to the samples.
    c. 2 mL of 10 % H_2O_2 was added to the samples, before agitating them.
    d. After agitation, the lids were left on the samples, but unscrewed to allow for the release of gases.
    e. Tubes were then left for 12 h under the fume hood.
    f. After this, the tubes were heated at 45°C in an oven.
    g. 2 h later, 1 mL of 35 % H_2O_2 was added to the samples.
    h. Samples were then left to repose for another 12 h.
    i. Samples were then put back into the oven for 12 h.
    j. Every 8 to 16 h 2 – 4 mL of 35 % H_2O_2 was added to the samples, agitating them and then replacing them in the oven, until all organic matter had been oxidised and there was no further evidence of reaction upon H_2O_2 addition. This took approximately 1.5 weeks.
    k. Samples were then left with their lids off in the oven and evaporated down to < 10 mL.
4. Samples were then chemically dispersed with 1 mL of 40 g L^{-1} sodium hexametaphosphate, shaking them on a rotary table at 100 rpm.
5. Samples were then washed into 15 mL tubes designed for the auto-sampler of the Beckman Coulter LS13320 Particle Sizing Analyser.

8.4.2.3 - XRF

The total elemental compositions of samples were determined using X-ray fluorescence (XRF; PANalytical PW2400 WDXRF spectrometer). Samples were prepared for analysis using a lithium tetraborate ($Li_2B_4O_7$) fusion.

1. 3 g of crushed sample was weighed into a clean pre-weighed crucible.
2. Samples were then heated for 3 h at 1050°C in a Solo 111-13/10/30 Furnace.
3. The samples were then left to cool at room temperature.
4. The loss of combustibles was then calculated for correction of elemental compositions later.
5. Samples were then homogenised using a pestle and mortar.
6. 1.2 g of each homogenised sample was then combined with 6 g of $Li_2B_4O_7$ and crushed in a pestle and mortar for 3 mins.
7. Samples were then loaded into a platinum crucible and fused twice in a PANalytical Perl X3 Fuser at 1250 °C.
8. The fuser then loaded the fused samples into a platinum plate, where they cooled.
9. Glass samples are then removed from their platinum holder and stored in plastic containers, until they are measured with the XRF.

8.4.2.4 - XRD

Bulk

Bulk mineralogy (Appendix Fig. 8.1) was determined on ground samples prepared according to Adatte et al. (1996) using X-ray diffraction (XRD; Thermo ARL X'TRA Powder Diffractometer).

1. Approximately 800 mg of ground sample was pressed (20 bars) in a powder holder covered with blotting paper.
2. Pressed samples were then analysed using Cu Kα radiation at 45 kV / 40 mA with a 13 s counting time per 0.02° for 2 θ in the 1-65° range.
3. Samples were rotated at a range of 1° min^{-1} with an acquisition step size of 0.03 – 0.05° 2 θ using a 0 / 0 type goniometer with a 250 mm radius.
4. A spectral counter (THERMO ARL water cooled silicon detector) was used to eliminate Cu Kβ and Fe parasitic emissions.

Clay

Samples from a randomly selected profile at each site were also prepared for clay mineralogical analysis (Appendix Fig. 8.2) according to Adatte et al. (1996).

1. Samples from profiles F1 and B2 were mixed with deionised water.
2. Samples were agitated and combined with 10 % HCl to remove carbonate.
3. Insoluble residues were washed by centrifugation until neutral pH was acquired.
4. Different size fractions (< 2 µm and < 16 µm) were separated by sedimentation according to Stokes' law.
5. Selected fractions were then pipetted onto glass plates and air-dried.
6. Resulting oriented slides were analysed by XRD before and after ethylene glycol solvation.

8.4.2.5 - Extractions

Extractions of varying strength were used on the soil samples to evaluate different elements within our soils (described below). Analysis of the various extractions was completed using an ICP-OES in a 2 % HNO_3 matrix. All samples were run with process blanks and 20 % random blind measurements to ensure quantification of replicability and analytical error. The machine was run with analytical blanks and standards throughout its runs. A internal Sc standard was also used to check for machine drift and correct measurements. All extractions were completed using acid washed (3M HCl) equipment.

Selective dissolution of Al and Fe forms

X-ray diffraction works well on repeating crystalline structures, but struggles on poorly crystalline reactive minerals. These reactive minerals, such as Al and Fe oxides can be semi-quantified using selective dissolution techniques (Parfitt and Childs, 1988b). Selective dissolution techniques extract minerals based on their resistance to dissolution by an array of chemical reagents and can be combined to withdraw an approximation of the specific reactive mineral phase contents (Eusterhues et al., 2003). Two dissolution techniques were combined to analyse reactive Al and Fe phases at the Nant Valley; ammonium oxalate acid buffer (McKeague and Day, 1966) and citrate-bicarbonate-dithionite (Mehra and Jackson, 1958) extractions. Both extracts were completed on field moist samples as Al and Fe oxides are known to be affected by drying (Schwertmann, 1964).

Ammonium oxalate acid buffer extraction

Oxalate extracts Al and Fe (Al_o and Fe_o) associated with organic complexes and short range order mineral phases. The Al_o and Fe_o were extracted using an ammonium oxalate acid buffer (pH 3), created by combining 0.2 M ammonium oxalate ($[NH_4]_2C_2O_4.H_2O$; 4 / 7 parts) with 0.2 M oxalic acid ($H_2C_2O_4.2H_2O$; 3 / 7 parts).

1. 1 g of moist soil sample was combined with 100 mL of ammonium oxalate acid buffer solution in 250 mL polypropylene centrifuge tubes.
2. The tubes will then be concealed from light using aluminium foil and shaken at 250 rpm for 4 h.
3. The samples were reposed for 1 h.
4. Extracts will then be centrifuged at 7,500 g for 30 mins.
5. Extracts were then vacuum filtrated (0.45 μm) and diluted (x 100) for analysis on the ICP-OES.

Dithionite extraction

Dithonite is a strong and versatile reducing agent (Williamson, 1989) and can be used to extract Al and Fe from crystalline or non-crystalline species, secondary oxyhydroxides, and organic complexes (Dahlgren, 1994). The dithionite reaction needs to be buffered between pH 7 – 8 (Mehra and Jackson, 1958) to efficiently extract Al and Fe (Al_d and Fe_d). This is achieved with a sodium-citrate-bicarbonate

buffer. The buffer is created by combining 0.3 M trisodium citrate dihydrate ($Na_3C_6H_5O_7 . 2H_2O$; 8 / 9 parts) with 1 M sodium bicarbonate ($NaHCO_3$).

1. 1 g of field moist soil from each sample was added to 100 mL of the sodium-citrate-bicarbonate buffer, and heated in a water bath (Memmert WNE 29) at 75-80 °C.
    a. The water level must not be too high as it causes the tubes to fall over, but must be high enough to ensure that the samples stay at the correct temperature.
2. Once brought up to temperature, 1 g of dithionite ($Na_2S_2O_4$) was added to the solution using a calibrated measuring spoon and stirred for 10 mins intermittently with a pipette tip.
3. A second 1 g portion was then added to the samples, before stirring them for a further 10 mins discontinuously.
4. Once the mineral soils greyed completely (30 mins), the solutions were removed from the water bath and reposed / chilled at room temperature for 1 h.
5. Samples were then centrifuged at 7,500 g.
6. Samples were vacuum filtrating (0.45 µm).
7. Filtered samples were then diluted (x 100) with 2 % HNO_3 for ICP-OES analysis.

Ca extractions

Cobalt hexamine extract (0.0166 M)

Cobalt hexamine (cohex) extract was selected as the main exchangeable extract after pre-testing revealed that it was least aggressive against $CaCO_3$ in soil samples from the Nant Valley with mixed $CaCO_3$ contents (Appendix Fig. 8.19). The cohex extraction was adapted from Aran et al. (2008). The cobalt hexamine extraction works via compulsive exchange as cobalt has a strong affinity for exchange sites. The compulsive exchange method of calculating CEC (difference in cobalt concentration between the blank and samples) was not used as a CEC measure, due to its erratic behaviour and lack of reproducibility during pre-testing. Therefore the sum of exchangeable cations was used instead, not including H^+.

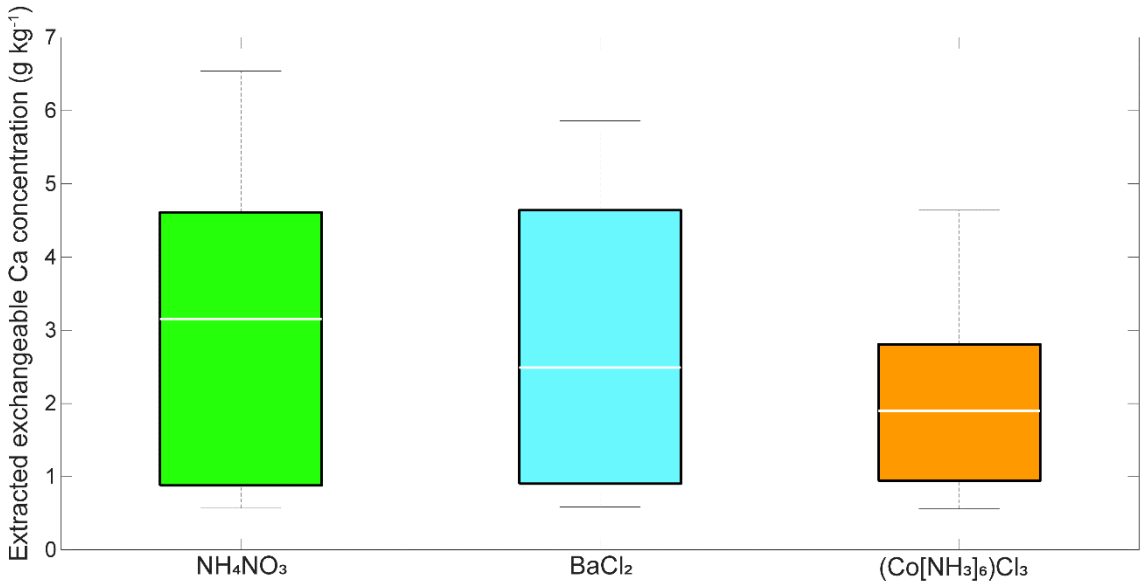

Appendix Fig. 8.19. A comparison of different exchangeable extracts on soils of mixed calcium carbonate contents from the Nant Valley.

1. 2 g of air-dried soil was combined with 40 mL of 0.0166 M cohex.
2. Samples were shaken at 120 rpm for 1 h on a rotary shaker.
3. Samples were then vacuum filtered using 0.45 µm nitrocellulose filter papers.
4. Filtered samples were diluted (x 25) and acidified with 2 % HNO_3.
5. Acidified extracts were then measured using the ICP-OES.

Water extractable extract

Water extractable elements were extracted with a method adapted from Tirmizi et al. (2006). Extraction time was kept as small as possible to prevent the dissolution of reactive $CaCO_3$ by deionised water, which acidifies upon exposure to CO_2^{Atm} and its absorption (H_2CO_3).

1. 5 g of air-dried soil (< 2 mm) was combined with 20 mL of deionised water ($_{dd}H_2O$).
2. Samples were then shaken for 30 mins at 250 rpm on a rotary shaker.
3. Samples were then left to repose for 30 mins.
4. Extracts were centrifuged at 1080 g for 15 mins.
5. Extracts were then filtered using 8 µm filter papers.
6. Filtered extracts were acidified and diluted with 2 % HNO_3.
7. Diluted extracts were then measured on the ICP-OES.

KCl extract (2 M)

An exchangeable cation extraction method adapted from Keeney and Nelson (1982). This extract is also used for the extraction of available nitrogen.

1. 5 g of air-dried soil ws combined with 25 mL of 2 M KCl.

2. Samples were then shaken for 30 mins at 180 rpm on a rotary shaker.
3. Extracts were then vacuum filtered through 0.45 µm nitrocellulose filters.
4. Samples were diluted (x 50) and acidified with 2 % HNO_3.
5. Diluted extracts were then measured using an ICP-OES.

Na_2EDTA extract (0.05 M)

A Na_2EDTA extraction was used in an attempt to extract a more resistant exchangeable pool (Lo and Yang, 1999), but was also aggressive against reactive $CaCO_3$ (Glover, 1961).

1. 2 g of air-dried soil was combined with 40 mL of 0.05 M Na_2EDTA.
2. Samples were then shaken for 2 h at 250 rpm on a rotary shaker.
3. Extracts were then vacuum filtered through 0.45 µm nitrocellulose filters.
4. Samples were diluted (x 50) and acidified with 2 % HNO_3.
5. Diluted extracts were then measured using an ICP-OES.

$CuCl_2$ extract (0.5 M)

A $CuCl_2$ extraction was also used to extract a more resistant exchangeable pool (Barra et al., 2001; Juo and Kamprath, 1979), but it was also aggressive against reactive $CaCO_3$. While this method worked on a limited number of samples, giving reproducible data, it also coated the ICP-OES torch in Cu. This Cu was removed in an acid bath with a low-level sonication, but we would recommend further dilution, prior to analysis, if you are to use this method.

1. 2 g of air-dried soil was combined with 20 mL of 0.5 M $CuCl_2$.
2. Samples were then shaken for 2 h at 250 rpm on a rotary shaker.
3. Extracts were centrifuged at 1080 g for 30 mins.
4. Extracts were then vacuum filtered through 0.45 µm nitrocellulose filters.
5. Samples were diluted (x 50) and acidified with 2 % HNO_3.
6. Diluted extracts were then measured using an ICP-OES.
7. Remember that $CuCl_2$ is toxic and must be disposed of with due care.

NH_4NO_3 extract (1 M)

As can be seen in Appendix Fig. 8.19 the NH_4NO_3 extract was not retained as it was aggressive towards reactive $CaCO_3$ during method, development but for clarity it's explained below. The method was adapted from Bélanger et al. (2008).

1. A sub-sample of soils with mixed carbonate contents were selected.
2. 8 g of air-dried soil from these soils was combined with 40 mL of 1 M NH_4Cl.
3. Samples were then shaken for 1 h at 200 rpm on a rotary shaker.
4. Extracts were then vacuum filtered through 0.45 µm nitrocellulose filters.
5. Samples were diluted (x 50) and acidified with 2 % HNO_3.

6. Diluted extracts were then measured using an ICP-OES.

$BaCl_2$ extract (0.1 M)

As with the NH_4NO_3 the $BaCl_2$ extract was not retained as it was relatively more aggressive towards reactive $CaCO_3$ during method development (Appendix Fig. 8.19), but for clarity it's explained below. The method was adapted from Gillman and Sumpter (1986).

1. A sub-sample of soils with mixed carbonate contents were selected.
2. 2.5 g of air-dried soil from these soils was combined with 25 mL of 0.1 M $BaCl_2$.
3. Samples were then shaken for 1 h at 250 rpm on a rotary shaker.
4. Extracts were then vacuum filtered through 0.45 µm nitrocellulose filters.
5. Samples were diluted (x 50) and acidified with 2 % HNO_3.
6. Diluted extracts were then measured using an ICP-OES.

8.4.2.6 - Soil organic carbon and total nitrogen analysis / fumigation

Bulk organic C and total nitrogen contents were quantified on AGB and ground soil samples by dry combustion in Chapter 4 and 5 (Thermoscientific Flash 2000 CHN Elemental Analysers and Carlo Erba 1108, respectively).

Fumigation

Prior to analysis SIC needed to be removed from ground samples to prevent over-estimation of the SOC content in the $CaCO_3$-bearing site (and potential $\delta^{13}C$ value bias from $CaCO_3$ later in Chapter 5). Removal of SIC is normally achieved with repeated rinsing with HCl and H_2O, however, this also removes acid and water soluble SOC and is both time and labour intensive. We used a 12 M HCl fumigation process (Harris et al., 2001; Ramnarine et al., 2011) instead as it can achieve SIC removal quicker and without the loss of soluble SOC. Samples typically lose weight upon fumigation when SIC is removed. Samples gained weight during the fumigation process, due most likely to the formation of a green rust, which could be seen on the samples.

1. 510 mg of ground sample was oven dried at 65 °C for 24 h.
2. Samples were removed from the oven and left to dry in a desiccator.
3. Samples were then re-weighed after cooling.
4. Samples were remoistened carefully with 150 µL of deionised water ($_{dd}H_2O$).
5. Samples were then fumigated in a desiccator with 100 mL of 10.8 M HCl for 24 h.
6. Samples were then removed from the desiccator and left to evaporate for 72 h (so as to not corrode the drying oven).
7. Samples were then re-dried at 65 °C for 24 h and re-weighed to calculate the weight gain during the fumigation process.

8. A correction factor similar to the humidity residual correction was then used to correct SOC contents of analysed samples.
9. Approximately 10-15 mg of fumigated samples were then weighed into tin boats using a microbalance and pyrolysed using a Thermoscientific Flash 2000 CHN Elemental Analyser.
10. Samples were measured in duplicate to check the replicability of our measurements and standards were pyrolysed throughout the analysis to check for machine drift.

$\delta^{13}C$ values

The content of C and stable C isotope composition of both bulk samples, triplicates of density fractions, AGB and BGB were quantified using a Carlo Erba 1108 elemental analyser connected to a Thermo Fisher Delta V isotope ratio mass spectrometer (EA-IRMS). The EA-IRMS was operated in continuous He flow mode via a split interface (Conflo II). Combustion occurred in an O_2 atmosphere at 1020°C. Standards and blind replicates where measured throughout the run. The stable C isotope composition is reported as $\delta^{13}C$ value in ‰ relative to known standards (Eq. 5.2). All analysis was run with a minimum of 10 % blind replicates, unless run in triplicate (density fractions).

8.4.2.7 - X-ray photoelectron spectroscopy

All the fractions of a surface and subsoil sample from the same randomly-selected profile at each site were measured (all fractions from samples B2.1, B2.4, F2.1, F2.4) using a PHI VersaProbe II scanning XPS microprobe (Physical Instruments AG, Germany). X-ray photoelectron spectroscopy (XPS) measurements were made at the Surface Characterization Laboratory, Ecole Polytechnique Federale de Lausanne. Fractions were analysed with a monochromatic Al Kα X-ray source (1486.6 eV) of 45.7 W power and a beam size of 200 µm. The spherical capacitor was set at 45° take-off angle respective to the surface of samples. Samples were scanned twice, once coarsely (region scans), with a pass energy of 187.85 eV, yielding the principle elements of interest. The samples were than scanned in more detail (survey scans) using a pass energy of 46.95 eV. Exposure time was < 30 mins to prevent X-ray induced alteration of the density fractions and subsequent false structural C assignments (Dengis et al., 1995). Vacuum inside the main chamber was in low 10 torr during measurements (-7 Pa). Sample charging during analysis caused peak shifts of < 3 eV, which were corrected based on the maximum principal C_{1s} sub peak, centering at 285 eV (Mikutta et al., 2009).

8.4.3 - Statistical methods

As the statistical methods have been thoroughly explored in previous parts of this thesis, this specific section will present some of the code used in SAS for the linear mixed models, principal component and factor analysis. Code for specific graphics will not be presented in this section, but can be requested by email.

8.4.3.1 - Linear mixed models

Analysis of bulk soil measurements in Chapter 4

```
PROC MIXED data = DCP method = reml plots=residualpanel (conditional) boxplot;
class RPL DG DGPL Pronew ;
model SM = RPL|DGPL /ddfm=satterth htype=1,3 residual;
repeated DGPL / type=ar(1) subject=Pronew group=RPL*DG;
lsmeans RPL DGPL RPL|DGPL;
RUN;

PROC MIXED data = DCP method = reml plots=residualpanel (conditional) boxplot;
class RPL DG DGPL Pronew ;
model SM = RPL|DGPL /ddfm=satterth htype=1,3 residual;
repeated DGPL / type=ar(1) subject=Pronew group=RPL*DG;
lsmeans RPL DGPL RPL|DGPL;
RUN;
```

Analysis of triplicates in Chapter 5

```
'For triplicates data';

PROC MIXED data = C13DF method = reml plots=residualpanel (conditional) boxplot;
class RandomProfile Fraction LForHF Site Depth Profile Sample ;
model _13C = Site|Depth|Fraction /ddfm=satterth htype=1,3 residual;
random Depth/ type=AR(1) subject=Profile group=Site;
repeated Fraction/type=vc subject=sample*RandomProfile group=LForHF;
lsmeans Depth Fraction Site|Fraction;
RUN;
'LForHF tests';

PROC MIXED data = C13DF method = reml plots=residualpanel (conditional) boxplot;
class RandomProfile Fraction LForHF Site Depth Profile Sample ;
model SOC = Site|LForHF /ddfm=satterth htype=1,3 residual;
random Depth/ type=AR(1) subject=Profile group=Site;
repeated Fraction/type=vc subject=sample*RandomProfile group=LForHF;
lsmeans Site|LForHF;
RUN;
```

8.4.3.2 – Principal component and factor analysis

Principal component analysis

```
PROC PRINCOMP data=PCA out=PCAPCA
        plots(ncomp=3)=pattern(vector circles=0.25 0.5 0.75 1.0);
        ID SamN;
        var Clay FineSilt Coarsesilt Finesand Sand   CaCO3React      CaCO3Total       Phyllosilicates
        Quartz   Feldspar Plagioclase        Goethite AlXRF   CaXRF  FeXRF   MgXRF SiXRF CaSat AlSat;
RUN;
```

Factor analysis

```
PROC FACTOR data=PCA out=DCPvari method=principal nfactor=5 rotate=quartimax
cov
        plots(vector nplot=3)= loadings(circles=0.25 0.5 0.75 1.0) scree;
        var Clay FineSilt Coarsesilt Finesand Sand   CaCO3React      CaCO3Total Phyllosilicates
        Quartz   Feldspar Plagioclase Goethite AlXRF         CaXRF FeXRF MgXRF    SiXRF CaSat AlSat;
RUN;
```

8.6 - Full Papers

8.6.1 - Chapter 3 - Ca-mediated stabilisation of SOC

- This page is intentionally left blank -

Biogeochemistry (2018) 137:27–49
https://doi.org/10.1007/s10533-017-0410-1

SYNTHESIS AND EMERGING IDEAS

Calcium-mediated stabilisation of soil organic carbon

Mike C. Rowley · Stéphanie Grand · Éric P. Verrecchia

Received: 7 August 2017 / Accepted: 10 December 2017 / Published online: 19 December 2017

Abstract Soils play an essential role in the global cycling of carbon and understanding the stabilisation mechanisms behind the preservation of soil organic carbon (SOC) pools is of globally recognised significance. Until recently, research into SOC stabilisation has predominantly focused on acidic soil environments and the interactions between SOC and aluminium (Al) or iron (Fe). The interactions between SOC and calcium (Ca) have typically received less attention, with fewer studies conducted in alkaline soils. Although it has widely been established that exchangeable Ca (Ca_{Exch}) positively correlates with SOC concentration and its resistance to oxidation, the exact mechanisms behind this relationship remain largely unidentified. This synthesis paper critically assesses available evidence on the potential role of Ca in the stabilisation of SOC and identifies research topics that warrant further investigation. Contrary to the common view of the chemistry of base cations in soils, chemical modelling indicates that Ca^{2+} can readily exchange its hydration shell and create inner sphere complexes with organic functional groups. This review therefore argues that both inner- and outer-sphere bridging by Ca^{2+} can play an active role in the stabilisation of SOC. Calcium carbonate ($CaCO_3$) can influence occluded SOC stability through its role in the stabilisation of aggregates; however, it could also play an unaccounted role in the direct sorption and inclusion of SOC. Finally, this review highlights the importance of pH as a potential predictor of SOC stabilisation mechanisms mediated by Al- or Fe- to Ca, and their respective effects on SOC dynamics.

Keywords Calcium · Soil organic carbon stabilisation · Sorption · Occlusion · Polyvalent cation bridging · Organo-mineral interactions

Responsible Editor: Marc G. Kramer.

Mike C. Rowley and Stéphanie Grand contributed equally to this work.

M. C. Rowley (✉) · S. Grand · É. P. Verrecchia
Institut des Dynamiques de la Surface Terrestre (IDYST), Faculté des Géosciences et de l'Environnement (FGSE), Université de Lausanne, Bât. Géopolis, Lausanne 1015, Switzerland
e-mail: mike.rowley@unil.ch

Introduction

Soil organic carbon stabilisation

Soils are the largest actively cycling terrestrial C reservoir and play an essential role in the global cycling of C. Improving our understanding of this C reservoir and modelling its dynamics are fundamental to predicting its sensitivity to future change (Brovkin and Goll 2015). However, current models suffer from

large uncertainties caused by the complexities of SOC and its physicochemical interactions with the soil matrix (Friedlingstein et al. 2006). Models require further mechanistic research on the variables that drive SOC dynamics to improve their accuracy (Campbell and Paustian 2015). Therefore, understanding the mechanisms behind the accumulation and persistence of SOC is of globally recognised importance.

Soil organic C stabilisation broadly refers to mechanisms believed to impede the decomposition of organic matter, promoting its accumulation and persistence in soils. Conversely, decomposition refers to the progressive oxidative transformation of organic inputs, during which a fraction of the organic matter is volatilised as carbon dioxide, while residues become increasingly laden with functional groups, such as carboxyl, phenol, or hydroxyl groups (Guggenberger and Zech 1993; Oste et al. 2002; Peinemann et al. 2005). Sollins et al. (1996) originally proposed three theoretical mechanisms that confer stability to SOC: (i) an inherent recalcitrance or thermodynamic stability of soil organic matter (SOM) and its subsequent selective preservation by decomposers, (ii) the physical occlusion of SOC from decomposers, and (iii) sorption of SOC to inorganic soil components resulting in organo-mineral or organo-cation complexes.

It was previously thought that the primary mechanism behind the persistence of SOC was the selective preservation of thermodynamically stable or recalcitrant substrates by decomposers (Aber et al. 1990; Sollins et al. 1996), causing their accrual within the soil matrix. However, as hypothesised by Oades (1988), there is little evidence for the preservation of complex cell-wall materials like lignin and suberin in stable SOC pools (Gleixner et al. 1999, 2002; Rumpel and Kögel-Knabner 2011; Schmidt et al. 2011). Contrarily, recent evidence suggests that selective preservation is only relevant at the beginning of the SOC decomposition continuum (Dignac et al. 2005; Gleixner et al. 1999, 2002; Lehmann and Kleber 2015; Schmidt et al. 2011) or within organic horizons (Lemma et al. 2007; Preston et al. 2009). The stabilisation and maintenance of SOC in mineral soil horizons, over medium- to long-time periods, is now predominantly thought to be driven by specific ecosystem properties rather than the inherent recalcitrance of SOC (Schmidt et al. 2011).

The established paradigm: ecosystem properties limiting SOC decomposition

Important ecosystem properties that contribute to SOC stabilisation include:

(i) the physical separation of substrates from decomposers over plurimetric to micrometric scales;
(ii) interactions between SOC and cations or minerals;
(iii) the occurrence of temperature or moisture conditions that are incompatible with enzymatic reactions;
(iv) toxicity effects of metal ions like Al^{3+}.

The first and second processes are the most widespread as they occur, theoretically at least, in all soils. The state of knowledge on these processes is briefly synthesised below.

Physical separation

Soil organic carbon (SOC) can be stabilised by its physical separation from decomposers, their enzymes, and the necessary components of aerobic decomposition, such as oxygen or moisture. This physical constrainment can occur over large spatial scales in biologically limiting environments, like those present in Histosols or Cryosols, where waterlogged or frozen conditions severely limit the oxidative degradation of organic substrates (Dörfer et al. 2013), but can also occur at smaller spatial scales. Mechanisms for small scale physical separation include hydrophobic interactions arranging substrates into a micellar structure (Chassin 1979), SOC inclusion within a mineral or cogenetic mineral assemblage (Bindschedler et al. 2016), SOC intercalation within phyllosilicates (Theng et al. 1986), and occlusion of SOC within pedogenic aggregates (Adu and Oades 1978). Thus, the physical constrainment of aerobic decomposition can occur over plurimetric to micrometric scales and stabilises SOC in nearly all soil environments.

Formation of soil aggregates is the most widespread microscale process that leads to the physical separation of SOC, typically labelled as occluded SOC. The relation between aggregation and the stability or accumulation of SOC has been repeatedly demonstrated (Denef et al. 2004; Moni et al. 2010; Monreal

et al. 1997; Plante et al. 2002; Skjemstad et al. 1993; Virto et al. 2008, 2010). Formation of aggregates has conventionally been thought to involve the electrostatic flocculation of soil separates into stable domains 2–20 μm in size (Ghezzehei 2011), which are then bound by organic or inorganic cementing agents (Jastrow 1996; Six et al. 2004). Much emphasis has been placed on biological mechanisms that can control aggregation, such as the physical meshing of soil particles by roots and fungi or the excretion of extracellular polysaccharides/polymeric substances by microorganisms and roots (Balesdent et al. 2000; Chenu and Cosentino 2011; Six et al. 2002, 2004). In the theory of biological-controlled aggregate formation (Chenu 1989; Oades and Waters 1991; Oades 1993; Tisdall 1996), fresh SOC acts as an aggregate formation nucleus, stimulating localised activity of microorganism communities. These microorganisms excrete extracellular polysaccharide/polymeric substances that adhere to soil particles, which binds them together, creating a shell around the decomposing SOC nucleus and eventually occluding the SOC residue within (Chenu and Cosentino 2011). When driven by biology, soil structure is typically arranged into a spatial hierarchy, with distinct physical classes of aggregates that are often classified as macroaggregates (> 250 μm) or microaggregates (< 250 μm; Asano and Wagai 2014; Elliott 1986; Oades 1984; Six et al. 2000, 2004; Tisdall 1996; Tisdall and Oades 1982). These aggregate classes have different properties (size, structural stability, porosity, hydrophilicity), which confer different stabilities to the SOC occluded within (Chenu and Cosentino 2011; Dexter 1988; Kleber et al. 2007; Sutton et al. 2005; von Lützow et al. 2006; Zheng et al. 2016). It is largely accepted that in this hierarchy, microaggregates are formed within macroaggregates, which then break apart because of their weaker binding agents and larger planes of weakness, distributing microaggregates into the soil matrix (Oades 1984; Six et al. 2004; Tisdall 1996). These microaggregates are typically considered more stable because of their stronger binding agents and reduced macroporosity, increasing the stability of SOC occluded within (Denef et al. 2004; Tisdall and Oades 1982). Yet despite the recent emphasis on biological controls on soil aggregation, it should be noted that soil aggregation, its hierarchy, and the occlusion of SOC is also influenced by inorganic components of the soil matrix.

Abiotic agents, such as the composition of the mineral soil matrix, can indeed play a dominant role in aggregate formation and stability and therefore, influence occluded SOC. Polyvalent cations are known to increase aggregation in soils by flocculating negatively charged soil separates (Bronick and Lal 2005; Érika et al. 2016; Grant et al. 1992). Inorganic components can also increase the stability of aggregates through cementation, with examples including poorly crystalline minerals (Rasmussen et al. 2005), well crystallised Fe oxides (Oades and Waters 1991; Zhao et al. 2017), or carbonates (Falsone et al. 2010; Fernández-Ugalde et al. 2011, 2014; Virto et al. 2011). Inorganic components have been documented to reinforce both macroaggregates (Fernández-Ugalde et al. 2011; Virto et al. 2013) and microaggregates (Falsone et al. 2010). Some authors have pointed out that when predominantly controlled by inorganic agents, like Fe oxides in Ferralsols (Oxisols; Oades and Waters 1991), soil structure may not display the hierarchical organisation commonly associated with biology. However, when compared to biotic processes, inorganic controls on SOC occlusion have received relatively little attention recently.

Sorption

SOC can also be stabilised through sorptive interactions. These interactions include adsorption to minerals, like phyllosilicate clays, Al-, Fe-, Mn-oxides, poorly crystalline minerals, or polyvalent cations forming bridges to mineral or other organic soil constituents. A positive relationship between the resistance of SOC to chemical oxidation and the presence of specific reactive mineral species was first described by Hosking (1932). Since then, the presence of reactive minerals or metals has been repeatedly shown to correlate with increased SOC stocks (Baldock and Skjemstad 2000; Grand and Lavkulich 2011; Sokoloff 1938; Torn et al. 1997) and the resistance of SOC to microbial degradation in incubation experiments (Minick et al. 2017; Rasmussen et al. 2006; Whittinghill and Hobbie 2012). Soil organic C complexed by minerals generally exhibits older ^{14}C-derived ages than other SOC pools (Kleber et al. 2011; Rasmussen et al. 2005; Schrumpf et al. 2013; Spielvogel et al. 2008; Trumbore 1993); thus adsorption plays a clear role in the stabilisation of SOC over long time periods. However, there is still some level of

confusion within the field regarding the chemistry involved. Therefore, the main bonding mechanisms between organic and inorganic soil components are discussed briefly below.

Bonding mechanisms

There is a range of bonding mechanisms that can link organic molecules to minerals or metal cations (Table 1). The prevalence of each bonding mechanism will vary with soil texture, mineralogy, and concentration of cations. SOC can be stabilised through either inner- or outer-sphere interactions with minerals or metal cations (Sposito 2008; Sutton et al. 2005). Inner sphere complexes occur when a substance can closely approach a mineral's surface or metal ion, usually resulting in direct chemisorption; see Eq. 1 for an example. In outer sphere interactions, water molecules prevent the direct approach or sorption of a substance to a mineral's surface or metal ion; instead, the charges are countered through a diffuse charged zone (Oldham 2008). In soil, inner- and outer-sphere interactions act in combination to stabilise SOC over medium- to long-time periods, so that it becomes difficult, if not impossible, to ascribe SOC stabilisation in a given horizon to specific modes of interaction. However, a basic understanding of the fundamental chemical mechanisms at play is useful to inform our interpretation of operationally-defined SOC pools (see section below on sorption processes involving Ca).

$$\| - \mathrm{M} - \mathrm{OH} + \mathrm{HO} - \mathrm{R} \rightarrow \| - \mathrm{M} - \mathrm{O} - \mathrm{R} + \mathrm{H_2O}. \quad (1)$$

Equation 1: Ligand exchange between a mineral (M) and a hydroxyl functional group on an organic substrate (R) that results in the direct and strong adsorption of SOC. Equation adapted from Huang and Schnitzer (1986).

Stabilisation by sorption

SOC can be stabilised by organo-cation or organo-mineral interactions through several mechanisms. The primary SOC stabilisation mechanism of adsorption consists of the removal of SOC from solution and transfer to a solid phase. This transfer increases the stability of SOC by reducing the chance of diffusive encounter with degrading enzymes. It can occur whenever organic compounds become adsorbed to mineral surfaces (Kaiser and Guggenberger 2000; Kalbitz et al. 2005), but also when the concentration of cations becomes sufficient for soluble organic polymers to flocculate and precipitate (Baldock and Skjemstad 2000). Much of the research on flocculation thresholds has focused on acid soils dominated by Al chemistry (Boudot 1992; Matus et al. 2006; Rasmussen et al. 2006). In these soils, it has been shown that extensive flocculation and precipitation can be expected at a C:Al ratio in the order of 10–30 or lower (Jansen et al. 2003; Scheel et al. 2007; Skjemstad et al. 1992). The flocculation of dissolved organics by other cations in natural soils has not been as extensively studied.

Beyond the effect of sorption on the partition of SOC between the liquid and solid phase, substrates can also be stabilised by other mechanisms, such as the toxicity effects of certain metals, the inactivation of enzymes during sorption, or steric hindrance. It has been proposed that environmental cytotoxicity could result in the stabilisation of organics complexed by some metals such as Al (Tate and Theng 1980). Al^{3+} is toxic and is thought to limit decomposer activity in acidic soil environments (Tonneijck et al. 2010), although evidence for this can be contradictory (Marschner and Kalbitz 2003). The extra-cellular enzymes responsible for much of SOM decomposition can also be rendered inactive by adsorption onto mineral surfaces, due to structural modifications in their conformation at the adsorption interface (Quiquampoix and Burns 2007). Steric hindrance is a general mechanism involving the lack-of-fit between a substrate and a catalyst (an enzyme) caused by changes in tertiary structure, which is a common consequence of sorptive interactions in soil (Quiquampoix and Burns 2007; Zimmerman and Ahn 2010). Therefore, the spatial arrangement of adsorbed elements along the molecular interface plays an important role in the stabilisation of SOC during adsorption.

Although it was previously proposed that adsorption occurred uniformly over mineral surfaces, resulting in a monolayer coverage (Keil et al. 1994), this has now been challenged by empirical evidence suggesting that organic loading instead occurs in distinct reactive 'hotspots' (Hedges and Keil 1995; Kaiser and Guggenberger 2003; Vogel et al. 2014). Vogel et al. (2014) recently utilised scanning electron microscopy

Table 1 Mechanisms of interaction between soil organic carbon substrates and minerals or metal ions

Mechanism	Nature	Type of interaction	Description
Ligand exchange (Mikutta et al. 2014) Ligand exchange is the formation of new coordination complexes with metals	Covalent to ionic bond	Inner sphere	Strong bonding to a metal via the direct substitution of one outgoing ligand (for instance, a hydroxyl group) by an incoming one (for instance, an organic molecule with a hydroxyl, phenol, or carboxyl functional group)—see Eq. 1. There is no change in oxidation state at the metal centre and charge is conserved during the reaction
Chelation (Ahmed and Holmström 2014) Chelation is the formation of polydentate coordination complexes with metals. Compared to monodentate complexes, they have a greater stability	Covalent to ionic bond	Inner sphere	A special case of ligand exchange, where the incoming ligand (usually an organic molecule) is polydentate and thus able to replace two or more of the simple outgoing ligands bound to the central metal.
Cation bridging (Iskrenova-Tchoukova et al. 2010) Cation bridging allows for the interaction of two negatively charged surfaces such as a phyllosilicate and an organic anion	Direct cation bridging Mostly ionic bond	Inner sphere	A bond formed when the hydration shell of a polyvalent cation is displaced. The organic anion becomes directly coordinated to the cation, as in ligand exchange
	Exchangeable (water) bridging Van der Waals forces (see below)	Outer sphere	Here water is not displaced and the cation interacts with the organic anion essentially through hydrogen bonding (see below). Both polyvalent and monovalent cations can participate in this type of interaction. It has sometimes been labelled 'water bridging', although this term remains ambiguous, as it has also been used to describe ligand exchange reactions. The term 'exchangeable bridging', which has been coined to describe the cation exchange phenomenon, may be more descriptive
Hydrophobic interactions (Spaccini et al. 2002) These occur whenever non-polar substances exist in a polar solvent, such as water	Entropy-driven structure	Outer sphere	Aggregation of non-polar substances caused by the repulsion of hydrophobic molecule by water. Hydrophobic interactions also take place during the clustering of amphiphillic molecules into bilayers and micelles (hydrophilic exterior protecting a hydrophobic core)
Other 'weak' interactions (van der Waals) (Israelachvili 2011) While weak, these forces are additive meaning that in complex substrates such as those commonly found in SOC, many van der Waals interactions can combine to create apparent strong sorption	Dipole–dipole force	Outer sphere	The electrostatic attraction between molecules with permanent polarity, arising from differences in the electronegativity of their atomic constituents
	Hydrogen bonding	Outer sphere	Hydrogen bonding refers to a specific type of dipole–dipole interaction, which occurs when a hydrogen atom bonded to a strongly electronegative atom (typically F, O, or N) interacts with another electronegative atom. These interactions are stronger than ordinary dipole–dipole forces
	London dispersion (induced dipole) force	Outer sphere	Temporary and weak attractive force arising from the unequal movement of electrons within a molecule, turning it momentarily into a dipole. Unlike dipole–dipole interactions, the London dispersion force does not arise from a difference in the electronegativity of component atoms, but merely the correlated movements of electrons in interacting molecules

The references point to one recent example of study in soil science

and NanoSIMS to observe the direct adsorption of isotopically labelled SOM on a clay fraction during incubation. The authors found that SOM was preferentially associated with rough areas of nano-mineral clusters, including micropores, etch pits, and cracks. However, the preservation of organic C at these stabilisation 'hotspots' is difficult to ascribe to a single mechanism. As hypothesised by Kögel-Knabner et al. (2008), adsorption of SOC within these rough areas provides a twofold stabilisation of SOC, where the accessibility of the substrate to decomposers is reduced and the substrate is concomitantly stabilised by the aforementioned mechanisms of sorption. Therefore, at the molecular-scale, it seems that stabilisation by both physical separation and adsorption simultaneously co-occur (Fig. 1) and become indistinguishable (Chenu and Plante 2006; Kögel-Knabner et al. 2008; Vogel et al. 2014), thus questioning the conceptual segregation of the mechanisms enumerated by Sollins et al. (1996).

Ca-mediated SOC stabilisation

Ca–SOC interactions

Research into SOC stabilisation has typically focused on acidic soil environments and the effects of Al^{3+} or Fe^{3+} or their poorly crystalline forms on SOC (Grünewald et al. 2006; Kögel-Knabner et al. 2008). Basic soil environments, and potential interactions between the Ca and C cycles have received comparatively less attention (Grünewald et al. 2006). Yet, Ca is the most abundant alkaline earth metal in the Earth's crust, making up 2.94% of the upper continental crust (Wedepohl 1995). Furthermore, calcareous or Ca-rich

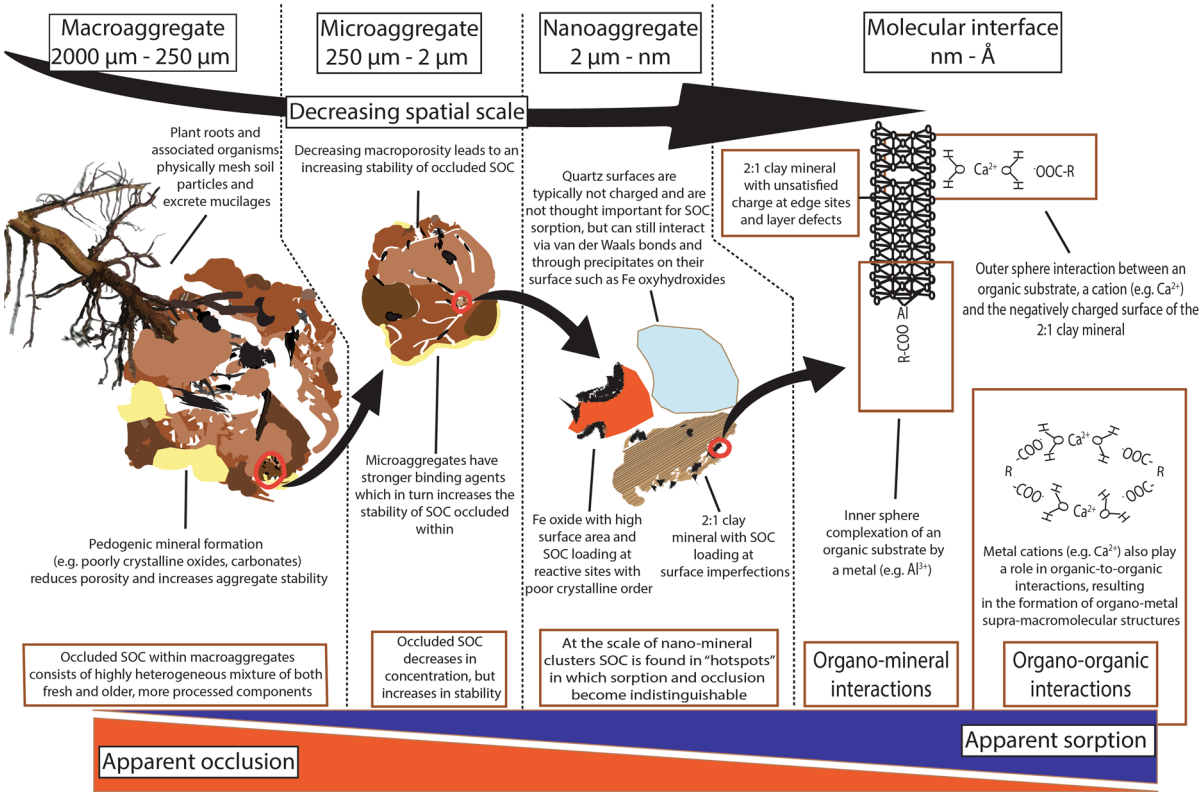

Fig. 1 Occlusion and sorption co-stabilise soil organic carbon at all spatial scales, but this co-occurrence becomes more apparent at the nano-scale where they become operationally indistinguishable

soils cover more than 30% of the Earth's surface (Bertrand et al. 2007; Chen and Barak 1982) and basic soils account for at least 12% of the world's soil resources (Grünewald et al. 2006). Ca^{2+} within a soil matrix typically originates from the weathering of lithosphere or surficial formations (Dijkstra et al. 2003; Likens et al. 1998), decomposition of Ca^{2+}-rich organic materials (Ranjbar and Jalali 2012), the lateral movement of Ca^{2+}-rich water (Clarholm and Skyllberg 2013), atmospheric dust deposition (Dijkstra et al. 2003; Pulido-Villena et al. 2006) or anthropogenic inputs. Ca^{2+} is weathered with relative ease from both primary and secondary minerals (Likens et al. 1998) and has therefore typically been thought to persist or accumulate chiefly in semi-arid to arid environments. However, Ca-rich environments also exist within temperate regions on soils developed from calcareous parent material, out-of-equilibrium with climate (Slessarev et al. 2016). High Ca concentrations are also commonly found in the topsoil of acid soils derived from crystalline lithologies due to biological cycling (Cailleau et al. 2004; Federer and Hornbeck 1985; Grand & Lavkulich 2013; Likens et al. 1998; Ross et al. 1991). Therefore, Ca^{2+} is an environmentally ubiquitous cation that could potentially play an unaccounted role in the stabilisation of SOC.

The first investigation into the interactions between Ca and SOC was published almost 80 years ago by Sokoloff (1938), who provided experimental evidence that organic matter solubility decreased upon addition of Ca when compared to Na addition. Since then, research in Ca-rich field environments has highlighted a positive correlation between exchangeable Ca^{2+} (Ca_{Exch}) and SOC concentration (see Fig. 2; Bertrand et al. 2007; Bruckert et al. 1986; Clough and Skjemstad 2000; Duchaufour 1982; Gaiffe et al. 1984; Oades 1988; Paul et al. 2003; Shang and Tiessen 2003). As an example, Yang et al. (2016) recently established that alpine grassland soils in the Neotropics contained nearly double the concentration of SOC (405.3 ± 41.7 t ha^{-1}) when developed on Ca-rich, calcareous lithology than their acidic counterparts (226.0 ± 5.6 t ha^{-1}). Similarly, O'Brien et al. (2015) and Li et al. (2017) demonstrated that Ca_{Exch} was the strongest explanatory variable for SOC concentration of grasslands. However, identification of the exact mechanisms responsible for this widespread correlation remain elusive.

A simple case of co-occurrence?

The positive correlation between Ca_{Exch} and SOC could be explained by their simple co-occurrence, as an increase in SOC concentration generally increases the cation exchange capacity (CEC) of a soil (Yuan et al. 1967). Calcium is a plant macronutrient and there is evidence that Ca also has a localised positive effect on net primary productivity (NPP) and SOM inputs through above-ground and below-ground biomass (Briedis et al. 2012b; Carmeis Filho et al. 2017; Paradelo et al. 2015). This localised effect on NPP has been shown to positively influence the accumulation of SOC in limed Ferralsols (Oxisols; Briedis et al.

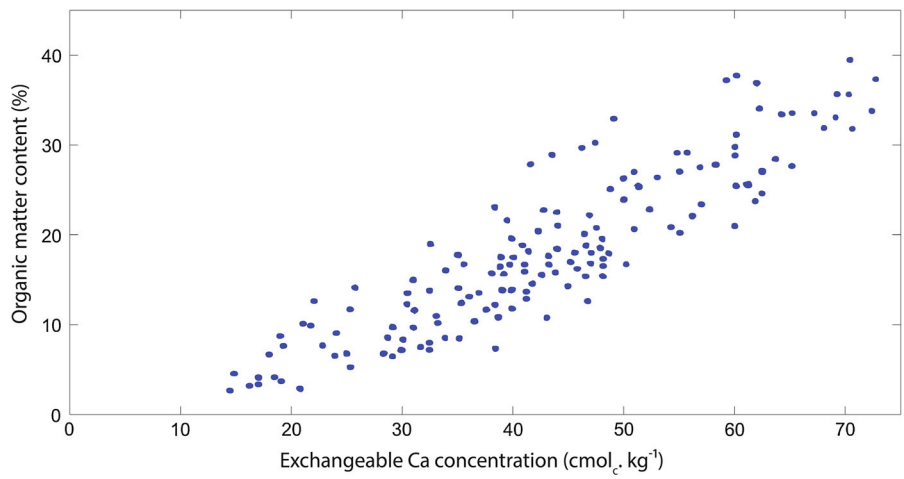

Fig. 2 Positive relationship between exchangeable calcium (centimoles of charge per kg) and soil organic carbon concentration (%) in the Jura Mountain range, adapted from Gaiffe and Schmitt (1980)

2012b; Carmeis Filho et al. 2017) and could explain a portion of the differences in SOC concentration observed between acidic and calcareous soils. However, these explanations fail to account for the decrease in respiration rate (per unit C) associated with Ca prevalence and observed in multiple field studies (Groffman et al. 2006; Hobbie et al. 2002) or incubation experiments (Minick et al. 2017; Whittinghill and Hobbie 2012). These results are at first glance counter-intuitive since the addition of Ca^{2+} to an edaphic ecosystem is also linked to a change in decomposer communities composition from fungi- to bacterial dominance (Blagodatskaya and Anderson 1999; Rousk et al. 2009, 2010) and an improvement in conditions for bacterial decomposition (Illmer and Schinner 1991; Ivarson 1977; Zelles et al. 1987), at least partially due to the buffering of soil pH to circumneutral levels (Narendrula-Kotha and Nkongolo 2017). It would thus be expected that the rate of enzymatic decomposition of SOC would increase when Ca^{2+} saturates the exchange complex (Andersson et al. 1999; Chan and Heenan 1999; Thirukkumaran and Morrison 1996). This could be the case in the organic (litter) layer (Minick et al. 2017), but is generally not observed in the mineral soil. Contrary to hypotheses formulated in both studies, Hobbie et al. (2002) and Groffman et al. (2006) found that microbial respiration was actually lower in Ca-rich environments, even though physicochemical conditions for microbial activity were improved. Furthermore, lab experiments have shown that Ca_{Exch} concentration is correlated with a reduction in SOC leaching losses (Minick et al. 2017), photo-oxidation (7%; Clough and Skjemstad 2000) and respiration as CO_2 during incubation (Minick et al. 2017; Whittinghill and Hobbie 2012). Therefore, Ca_{Exch} seems to be linked to a reduction in the propensity of C substrates for decomposition that is not solely linked to its effects on NPP or microbial ecology.

Consequently, this review will investigate the potential mechanisms behind the stabilisation and accumulation of SOC mediated by Ca and its mineral forms, namely their influence on:

(i) aggregation and the occlusion of SOC;
(ii) inclusion of SOC within pedogenic- or biogenic-$CaCO_3$;
(iii) organo-mineral and organo-cation interactions.

Mechanisms for Ca-mediated SOC stabilisation

Occlusion: Ca and aggregation

The Ca ion and aggregates

It is widely accepted that Ca^{2+} has a significant positive effect on aggregation and soil structural stability and therefore, indirectly influences the accumulation and occlusion of SOC. Early authors demonstrated an influence of Ca^{2+} on soil aggregation (Martin et al. 1955; Peterson 1947). This dependence was further investigated by Gaiffe et al. (1984) who demonstrated that the removal of Ca_{Exch} and its replacement by K_{Exch} led to a disruption of aggregates. As theorised by Edwards and Bremner (1967), one of the main mechanisms thought to be behind this stabilisation is the flocculation of negatively charged separates by outer sphere interactions involving Ca^{2+}, which is explored further in the following section on sorption processes. This process operates in the bulk soil and it has also been hypothesised that Ca^{2+} could play a role in flocculating particles in the gut of certain earthworm species, leading to the formation of 'Ca humates' (Satchell 1967). This was supported by the results of Shipitalo and Protz (1989) who utilised micromorphology and chemical pre-treatments to infer that Ca probably played a role in flocculating particles within earthworm casts of certain species, stabilising the microaggregates within them. Another mechanism for the stabilisation of aggregates in Ca-rich environments involves the formation of complexes between Ca and high-molecular weight organic compounds such as root mucilages or microbial polysaccharides/polymeric substances. It has been shown that these substances readily complex Ca^{2+} and create gel-like structures that bind aggregates (Czarnes et al. 2000; de Kerchove and Elimelech 2007; Erktan et al. 2017; Gessa and Deiana 1992). In particular, galacturonic acids, a common root mucilage, display a high affinity towards Ca, which links polymer chains to form an adhesive matrix (de Kerchove and Elimelech 2007). Czarnes et al. (2000) also showed that these polygalacturonic acid gels increase the hydrophobicity of aggregates, thereby increasing their stability during wetting and drying cycles. Further investigation is needed to analyse the

role that adhesive Ca-mucilage matrices play in aggregate stabilisation and the occlusion of SOC.

The effects of carbonate on aggregates

Interactions between Ca-bearing secondary minerals and soil structure have been extensively covered in the literature because of the use of liming ($CaCO_3$ addition) in agriculture. There have been many experiments that have documented the positive effects of the addition of calcite/aragonite ($CaCO_3$) or gypsum ($CaSO_4.2H_2O$) on the structure of non-calcareous soils (Armstrong and Tanton 1992; Baldock et al. 1994; Briedis et al. 2012a; Grant et al. 1992; Grünewald et al. 2006; Inagaki et al. 2017; Kaiser et al. 2014; Melvin et al. 2013; Muneer and Oades 1989a; Paradelo et al. 2016). Some authors have also assessed the effects of $CaCO_3$ removal from calcareous soils on aggregate stability, finding that the treatment reduced soil structural stability and increased porosity (Falsone et al. 2010; Muneer and Oades 1989c; Toutain 1974; Virto et al. 2011). Furthermore and reminiscent of the work of Oades and Waters (1991) on Fe oxides in Ferralsols (Oxisols), Fernández-Ugalde et al. (2011) demonstrated that the hierarchical model of aggregation was partially disrupted by carbonate. In the semi-arid Mediterranean soils of their study, the authors showed that the abundance of $CaCO_3$ controlled macroaggregate turnover and increased their stability, to the extent that the usual disruption of macroaggregates, leading to the release of constituent microaggregates, was prevented (Fernández-Ugalde et al. 2011; Oades 1984).

There are several mechanisms by which $CaCO_3$ could positively affect aggregate stability and the occlusion of SOC. $CaCO_3$ is easily weathered and acts as an abundant source of Ca^{2+}, thus encouraging the flocculation of soil separates and aggregation through the mechanisms listed above (Baldock and Skjemstad 2000; Clough and Skjemstad 2000; Wuddivira and Camps-Roach 2007). Carbonate ions are also capable of reprecipitation with Ca^{2+} under the right environmental conditions, forming secondary $CaCO_3$ crystals (from micrite to sparite) that cement aggregates (Fernández-Ugalde et al. 2011, 2014; Shang and Tiessen 2003; Virto et al. 2013). This mechanism was analysed in detail by Falsone et al. (2010), who utilised N_2 adsorption and Hg porosimetry to demonstrate that this formation of secondary $CaCO_3$ crystals decreased aggregate porosity in the 2–50 nm range and thus, decreased the accessibility of intra-microaggregate SOC to decomposers. Certain earthworm species have also been shown to cement particles that pass through their gut with a mixture of poorly crystalline biogenic carbonates (calcite, vaterite, aragonite) excreted from their calciferous glands (Brinza et al. 2014; Edwards and Bohlen 1995). The cementing effect of carbonates on aggregates is well-documented in arid soils in which large concentrations of pedogenic carbonates are found (Fernández-Ugalde et al. 2011, 2014; Virto et al. 2013). However, it may also play a role in humid or sub-humid environments where carbonate-rich parent materials are continually getting dissolved and locally reprecipitated, but this still needs to be investigated further.

Although it is widely accepted that the occurrence of $CaCO_3$ positively affects soil structure and offers favourable conditions for the stabilisation of SOC by occlusion, its actual consequence on occluded SOC stocks is less clear. In a recent review, Paradelo et al. (2015) concluded that while $CaCO_3$ addition had a clear positive effect on soil structure, its effect on occluded SOC stocks was uncertain. Positive (Egan et al. 2018; Muneer and Oades 1989a, b), non-existent (Paradelo et al. 2016) or negative effects (Chan and Heenan 1999) of $CaCO_3$-amendment on occluded SOC have indeed been reported. In some instances, it may be difficult to disentangle the integrative effects of agricultural management from the simple effects of $CaCO_3$ additions. In natural, unamended soils, Fernández-Ugalde et al. (2014) showed that carbonates had a positive effect on occluded SOC stocks. This finding needs to be replicated in a range of natural soils, as differences in initial conditions (e.g. texture, mineralogy, organic inputs and their distribution) could reasonably result in different outcomes.

Inclusion

Inclusion is defined as the envelopment of SOC within a mineral or cogenetic mineral assemblage that leads to its physical protection (Babel 1975). Stabilisation of SOC by inclusion works through a similar mechanism to intercalation or occlusion, by physically separating a substrate from decomposers. SOC may be trapped within any form of pedogenic carbonates, but its inclusion may not be quantitatively important when

carbonate formation chiefly occurs through abiotic processes. Diaz et al. (2016) recently dated small concentrations of SOC (0.1–0.5%) included within pedogenic carbonate nodules in Cameroon with C^{14} measurement, recording ages ranging between 8000 and 13,000 years. This highlights the potential of this mechanism to stabilise SOC over long time periods, but probably only in small concentrations.

Calcium carbonate is one of the most abundant biominerals on Earth and can be synthesised by a wide range of terrestrial organisms (Skinner and Jahren 2007). Biomineralisation of $CaCO_3$ can either be induced within cells, mediated by biological activity that stimulates physicochemical precipitation, or initiated by the presence of an existing biological matrix that initiates crystal nucleation and growth in the extracellular environment (Bindschedler et al. 2016). During each of these forms of biomineralisation, SOC can become included and encapsulated within the crystal structure (Verrecchia et al. 1995). A few specific examples of biogenic carbonate forms include calcified root cells, fungal filaments and rhizoliths (calcified roots; e.g. Becze-Deàk et al. 1997; Jaillard et al. 1991; Monger et al. 1991), calcified earthworm biospheriods (Barta 2011), and the mineralisation of bacterial or fungal organic templates (Bindschedler et al. 2014; Cailleau et al. 2009). Another mechanism for the inclusion of SOC could be biomineralisation pathways such as the oxalate-carbonate pathway (Verrecchia 1990). The oxalate-carbonate pathway involves biomineralisation of $CaCO_3$ during the bacterial catabolism of calcium oxalate-rich SOC produced by plants or fungi. It thus intimately links SOC to the nucleation site of $CaCO_3$ biomineralisation and could allow its inclusion within the crystal matrix in both acidic (Cailleau et al. 2004, 2005; Verrecchia et al. 2006) and calcareous soils (Rowley et al. 2016). However, there has been very little direct quantification of the concentrations or ^{14}C ages of SOC included within biogenic carbonate forms, which could potentially contain much higher SOC concentrations than abiotically-formed pedogenic carbonates. Therefore, further investigation is now needed to quantify the inclusion of SOC within biogenic carbonate and its role in SOC dynamics.

Sorption: Ca, minerals and organics

Organo-mineral interactions with calcite

Lithogenic and pedogenic $CaCO_3$ could also play a key role in the stabilisation of SOC via adsorption. Most of the research into direct organo-calcite interactions has focused on the interactions between DOC and calcite in sorption experiments. Earlier work by Suess (1970) and Carter (1978) showed that DOC could be directly adsorbed onto $CaCO_3$, while Suzuki (2002) more recently showed that $CaCO_3$ was an effective adsorbant of DOC from black tea solutions, possibly due to its high point of zero charge (9.5; Grünewald et al. 2006). Thomas et al. (1993b) more specifically studied the affinity of different synthetic carbonates for common organic functional groups and demonstrated that calcite, dolomite, and magnesite all sorbed a wide range of organic compounds, which included carboxylic acids, alcohols, sulphates, sulfonates, amines, amino acids and carboxylated polymers. Interestingly, interaction with DOC has been shown to modify carbonate precipitation equilibria, by inhibiting either further crystal precipitation (Inskeep and Bloom 1986; Reddy et al. 1990; Reynolds 1978) or the dissolution of sorbent minerals (Thomas et al. 1993a). Jin and Zimmerman (2010) established that $CaCO_3$ obtained from aquifers preferentially adsorbed dissolved organic matter with a high molecular weight, which the authors attributed to a form of outer sphere interaction. It has been theorised that the kinetics of DOC adsorption by carbonates may be biphasic, occurring through an initial rapid phase of outer sphere interactions, which is then followed by a slower phase of inner sphere and hydrophobic interactions that in turn protect the carbonate surface from dissolution (Jin and Zimmerman 2010; Lee et al. 2005; Thomas et al. 1993b). While these DOC adsorption experiments have provided interesting insight into potential $CaCO_3$–SOC interactions, there has been relatively little direct research on the adsorption of SOC by different forms of calcite/aragonite in soils. Measurements of soil carbonate content commonly differentiate between a reactive and a total pool (Pansu and Gautheyrou 2006), but there is little evidence for the role of these operationally-defined pools in adsorption of SOC. Further research should focus on the effects of the supposedly reactive, poorly

crystalline or amorphous $CaCO_3$ pool on the adsorption of SOC in natural environments.

Outer sphere processes

Irrespective of their carbonate content, many soils have significant concentrations of free Ca^{2+} which may also contribute to the stabilisation of SOC. The widely observed correlation between Ca_{Exch} and SOC has led to the implicit assumption that Ca^{2+} predominantly affects SOC through weak outer sphere interactions (von Lützow et al. 2006), such as those contributing to the retention of exchangeable cations (Table 1). This form of cation bridging by Ca^{2+} has been highlighted as an important component of SOC stabilisation by many authors and is well-documented (Clough and Skjemstad 2000; Edwards and Bremner 1967; Oades 1988). As illustrated in the lyotropic series, cations' outer sphere (exchangeable) behaviour is related to the size of their hydration shell and valence. This is confirmed by chemical modelling, which indicates that exchangeable bridges by Ca^{2+} typically have a larger residence time than those of monovalent cations, like Na^{+}, because the charge-to-hydration radius ratio of Na^{+} prevents it from efficiently countering the repulsion between negatively-charged surfaces (Iskrenova-Tchoukova et al. 2010; Sutton et al. 2005). Thus, Ca^{2+} is a fundamental flocculating agent of natural systems because of its ability to form efficient outer sphere bridge units.

However, it is interesting to note that Al^{3+} and H^{+} rate higher than Ca^{2+} on the lyotropic series and should thus cause similar or higher levels of apparent flocculation in soils in which they are abundant, such as most acid soils. Yet, it is widely observed that colloidal mobility is enhanced in acidic environments where Al^{3+} and H^{+} dominate and there is little or no Ca^{2+} present, such as those associated with the formation of Luvisols (Lavkulich and Arocena 2011). It is also worth considering that the innate reversibility of outer sphere interactions should mean that exchangeable Ca bridges would not be inherently persistent in natural soils. These considerations lead us to explore the possibility that interactions between Ca and SOC are not solely attributable to outer sphere (exchangeable) processes and that, despite its correlative association with SOC, Ca_{Exch} may not be solely responsible for the bulk of SOC stabilisation in Ca-rich soils.

Inner sphere processes

It is generally observed that each cation has a different range of interactions in soils. For instance, trivalent Fe is seldom found in large amounts as a free ion in soil, as it very readily hydrolyses to form insoluble precipitates under most environmentally-relevant conditions. Al^{3+} also hydrolyses into insoluble hydroxides at slightly acidic to basic pH, while in acidic soils, it is found to participate both in outer sphere, cation exchange and inner sphere, ligand exchange reactions. Ca^{2+} is thought to retain its hydration shell and behave strictly like an exchangeable cation, as are other 'base' cations such as Mg^{2+}, K^{+} and Na^{+} (Essington 2004). However in soil science, the fundamental controls on the propensity of each cation to form inner sphere complexes with SOM are not as well understood as the affinity of cations for non-specific exchange sites.

One of the reasons for this is that there are many factors that can influence inner sphere complexation of SOM by ions in the soil matrix, including characteristics of cations (ionic potential, electronegativity, polarisability of their electron cloud, hydrated radii, propensity to retain their hydration shell), of ligands (amount and type of organic functional groups) and of the environment (pH, ionic strength, solution composition, metal-to-ligand ratio, pressure and temperature conditions; Essington 2004). Cations can be broadly split into three classes (Class A, B, and intermediate/C) based upon the polarisability of their electron cloud, which in turn, indicates how likely they are to form inner sphere complexes with specific ligands (Ahrland et al. 1958; Pearson 1963; Schwarzenbach 1961). Class A cations are weakly polarisable and tend to form complexes with O-containing ligands, such as carboxylate functional groups through ionic bonding. On the other hand, Class B cations have a labile electron cloud and tend to form complexes with N- or S-bearing ligands through more covalent bonding (Langmuir 1997; Sposito 2008). Al^{3+} and the base cations, including Ca^{2+}, are considered group A cations, indicating that they may theoretically form inner sphere complexes with widely-occurring O-bearing ligands such as carboxylate groups (Sposito 2008). However, each cation's actual behaviour in soil cannot be predicted from one or a couple of first-principles only, as it results from the interaction of several factors. For instance, Na is not generally seen to engage in inner sphere complexation in soils, while

K only does so in the interlayer of specific phyllosilicates. Advanced chemical modelling can offer insight into these issues.

Authors have modelled the interactions between dissolved organic C (DOC) and Ca^{2+} in an attempt to investigate their molecular-scale interactions (Aristilde and Sposito 2008; Benedetti et al. 1995). These models suggest that Ca^{2+} can bind to SOC through both inner sphere and outer sphere processes (Bogatko et al. 2013; Iskrenova-Tchoukova et al. 2010; Kalinichev and Kirkpatrick 2007; Sutton et al. 2005). Sutton et al. (2005) modelled the complexation of deprotonated carboxyl groups by Ca^{2+} and found that their interactions were predominantly inner sphere (75%). The model of Kalinichev and Kirkpatrick (2007) also confirmed that Ca^{2+} could form direct cation bridges with carboxylate and to a lesser extent, phenolic and other –OH functional groups, unlike Mg^{2+}, whose hydration water is more tightly held (Dontsova and Norton 2002; Kalinichev and Kirkpatrick 2007; Tipping 2005). Chemical modelling thus indicates that Ca^{2+} can interact with SOC through inner- and outer-sphere processes, thereby potentially increasing SOC stability against decomposition or leaching (Minick et al. 2017).

Building empirical evidence for Ca–SOC interactions

While models predict that Ca^{2+} can form both inner- and outer-sphere bridges with SOC, empirical evidence of these associations in natural environments remains scarce. Density fractionation, which separates free, occluded and mineral-associated SOC (Golchin et al. 1994) has the potential to offer insight. When performed sequentially (Sollins et al. 2009), density fractionation can separate SOC fractions associated with different minerals; furthermore, because the method uses extremely concentrated salt solutions (usually Na polytungstate), outer sphere associations are not expected to survive the treatment, meaning that only strong (inner sphere) association with minerals are considered. Wen et al. (2017) recently showed that there was more SOC associated with calcite-rich than with dolomite-rich heavy fractions, possibly corroborating modelling predictions of stronger SOC association with Ca than Mg (Kalinichev and Kirkpatrick 2007). The occluded fraction was however not separated from the mineral-associated fraction, so that the results remain somewhat equivocal. Further density fractionation studies analysing the relative role of occlusion and sorption for SOC accumulation in Ca-rich soils would undoubtedly prove informative. Density fractionation is however a costly and time-consuming technique (Poeplau et al. In review) and may be difficult to use in calcareous soils, since polytungstate left in contact with free Ca for extended periods can precipitate as insoluble Ca-metatungstate. Methods applicable to the bulk soil would constitute useful complements to fractionation approaches.

Selective extractions on bulk soil have typically been used to analyse the effects of cation pools on SOC stocks. As indicated in Fig. 2, the operationally defined Ca_{Exch} pool, extracted by salt solutions, represents a reactive and abundant pool of Ca^{2+} that is regularly correlated with SOC concentration (Bruckert et al. 1986; Gaiffe and Schmitt 1980; Li et al. 2017; O'Brien et al. 2015), thus highlighting its potential as an indicator variable for the measurement of Ca^{2+} interacting with SOC. However, by definition, Ca_{Exch} only represents Ca^{2+} engaged in outer sphere interactions. The selective chemical extraction of the inner sphere Ca pool, corresponding to pyrophosphate extractions for Al and Fe in acidic soil environments (Bascomb 1968; Parfitt and Childs 1988; Rasmussen et al. 2006), is challenging due to the insolubility of most chelating agents once complexed by Ca (e.g., Ca-pyrophosphate or Ca-oxalate). In a recent study, van der Heijden et al. (2017) isolated a "non-crystalline pool of Ca" in acidic, base-poor soils, which may have included a significant contribution of Ca complexed by SOM, but the extract (dilute oxalic + nitric acid) was not specific to organic complexes. Extraction with other chelating agents that remain soluble in their Ca form (e.g. ethylenediaminetetraacetic acid, EDTA; Bélanger et al. 2008) or with salts of strong cation complexants (e.g. copper chloride; Barra et al. 2001; Juo and Kamprath 1979) may be informative; however, these extractants could also attack the mineral $CaCO_3$ pool, making their use difficult in calcareous soils.

Alternatively, X-ray absorption spectroscopy (XAS) could eventually be used to investigate the coordination environment of Ca^{2+}–SOC complexes under different environmental conditions. As an example, Martin-Diaconescu et al. (2015) have recently successfully probed the coordination environment of synthetic Ca complexes. While powerful, these direct spectroscopic techniques require the use

of synchrotron light source and can only be applied to small amounts of samples with limited compositional complexity. We are still lacking a method that allows for the routine assessment of inner sphere Ca–SOM complexes and their relative importance in different soils, which constitutes a significant research gap given the potential for inner sphere interactions to stabilise SOM with increased efficiency (Mikutta et al. 2007), and perhaps through ecosystem disturbance events (Basile-Doelsch et al. 2009; Grand and Lavkulich 2012).

Implications for conceptual models of SOC cycling

Despite the growing body of evidence supporting a major role for specific soil minerals and cations in SOC stabilisation (Doetterl et al. 2015), soil mineralogy and geochemistry are largely absent from leading models of SOC cycling. The following section will discuss a few processes that have the potential to improve representations of SOC stabilisation, with particular emphasis on Ca-rich soils.

Digressing from the expected profile-scale depth distributions

In addition to their influence on the total amount of SOC retained in soil, polyvalent cations are suspected to influence its vertical distribution in soil profiles. Current pedometric approaches to mapping soil C acknowledge the importance of accounting for soil type when estimating the vertical distribution of SOC (Kempen et al. 2011; Wiese et al. 2016). Polyvalent cations can indeed cause departures from the generally assumed exponential decline of SOC concentration with depth (Hilinski 2001). A classical example involves Podzols characterised by the effective translocation of Al–SOC complexes to deep soil horizons (Ferro-Vázquez et al. 2014; Grand and Lavkulich 2011). Contrastingly, Calcisols have an accumulation of Ca-saturated SOC in surface horizons (Yang et al. 2016). This accumulation of Ca-saturated SOC is likely caused by the complexation, flocculation, and precipitation of organic acids and clays in the presence of Ca, precluding their translocation to subsoil horizons. Two of the most common low molecular weight organic acids (oxalic and citric acids) in soil notably form sparingly soluble salts in the presence of Ca (calcium oxalate $K_{sp} \approx 10^{-8.5}$; Certini et al. 2000), preventing their translocation, whereas their Al and Fe counterparts are highly soluble (Gadd 1999). The fundamental differences in how polyvalent cations modulate SOC inputs, stability and depth distributions highlight the critical importance of accounting for geochemical factors when modelling SOC dynamics.

Preferential sorption

Integrating a geochemical dimension into conceptual models of SOM dynamics is also important because the formation of organo-mineral complexes appears to be a preferential process, with selectivity exhibited by both the organic and mineral component (Spielvogel et al. 2008). Very little is actually known about the preferential nature of organo-mineral interactions in soils. To date, there is some evidence within the literature that specific organic compounds such as N-rich microbial metabolites, microbial cell-wall fragments, and possibly pyrogenic C may be selectively sorbed by soil minerals (Brodowski et al. 2007; Jin and Zimmerman 2010; Miltner et al. 2012; Scheel et al. 2008; Schurig et al. 2013; Spielvogel et al. 2008). Furthermore, it has been suggested that some reactive mineral surfaces, such as those of Al and Fe phases, may be disproportionally involved in the sorption of specific classes of organics, such as proteins, lignin, and phenolic compounds (Heckman et al. 2013; Kögel-Knabner et al. 2008; Xiao et al. 2015). However, there have been very few studies looking at the potential preferential sorption of organic compounds in Ca-rich edaphic environments.

If molecular scale stabilisation of SOC by Ca^{2+} predominantly occurs through inner- or outer-sphere cation bridging, then it should preferentially target functional groups such as carboxyls and phenols. Römkens and Dolfing (1998) and Kaiser (1998) accordingly demonstrated that Ca^{2+} preferentially flocculated and precipitated high molecular weight DOC compounds, which contained higher proportions of carboxylic and phenolic functional groups. There is also evidence for the preferential adsorption of negatively charged products of lignin degradation (syringyl units; Grünewald et al. 2006) and DOC (Jin and Zimmerman 2010; Jin et al. 2014) by calcite. The implications of this hypothesis for our understanding of SOC dynamics could be profound. It could

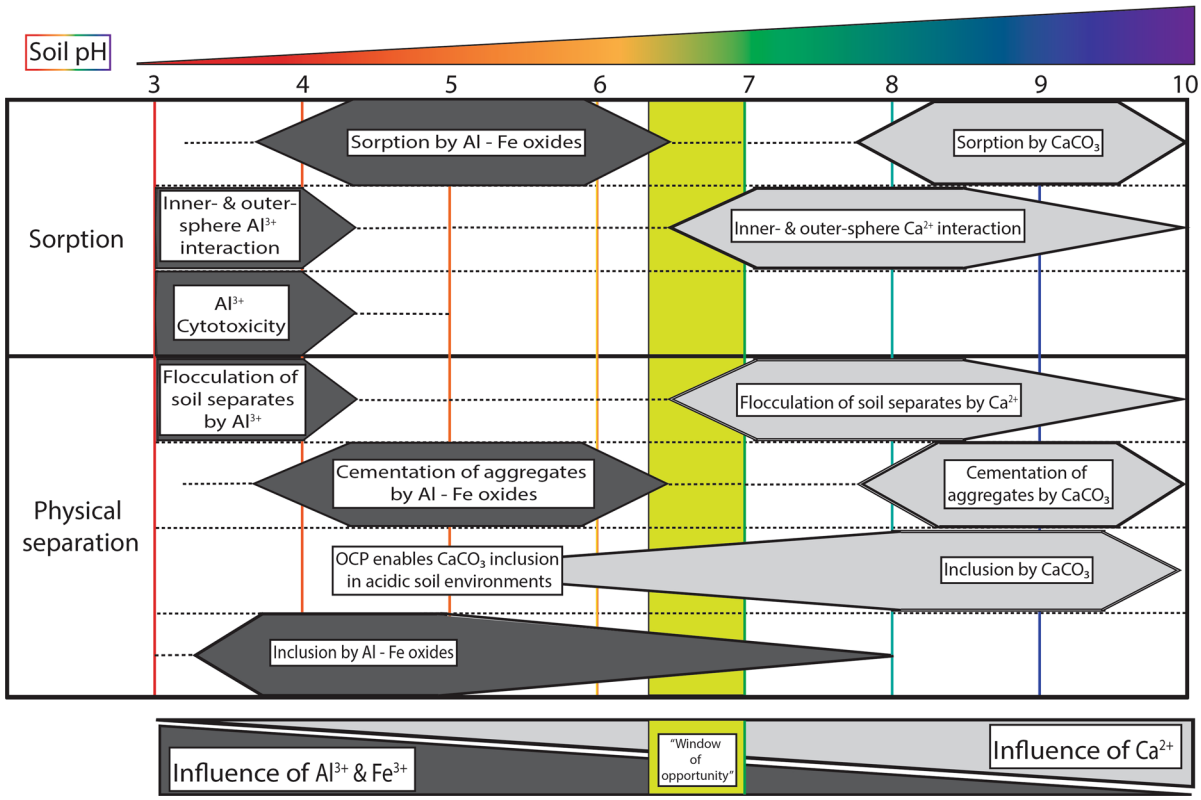

Fig. 3 The shifting role of polyvalent cations in the stabilisation of SOC with increasing pH. A 'window of opportunity' for microbial decomposition is highlighted in green according to the proposition of (Clarholm and Skyllberg 2013). Thresholds are based on values available in the literature and it is expected that adjustments will occur as more results become available. Al–Fe oxides refer to true oxides as well as oxyhydroxides and their poorly crystalline forms. *OCP* oxalate-carbonate pathway

potentially provide a mechanism to bridge the two competing hypotheses of SOC persistence, i.e. biochemical recalcitrance *vs.* mineral association, since organic compounds with different compositions could have different probabilities for sorptive preservation. This perspective is highly relevant to SOC modelling. As an example, the CENTURY model assumes universal preservation of lignin in stable SOC pools (Parton 1996; Parton et al. 2015), which has been questioned by experimental evidence (Gleixner et al. 1999, 2002). Accruing evidence on selective sorption of specific compounds to minerals or cations, including lignin derivatives, could speak in favour of considering SOC biochemical composition as a predictor of residence time, but the parametrisation would have to be adjusted for different geochemical environments.

Conversely, Minick et al. (2017) demonstrated that high additions of Ca at the Hubbard Brook experimental forest specifically reduced the mineralisation of ^{13}C-depleted SOC, which should represent a relatively fresh pool, little affected by oxidative transformation (Rumpel and Kögel-Knabner 2011), thus contradicting the hypothesis that Ca^{2+} preferentially stabilises oxidised SOC. Yet stabilisation of ^{13}C-depleted SOC could simply imply that occlusion was the predominant mechanism of SOC stabilisation at the Hubbard Brook forest. SOC occlusion could limit the mineralisation of ^{13}C-depleted sources because aggregates occlude a heterogeneous mixture of both ^{13}C-enriched, decomposed and relatively fresh, ^{13}C-depleted particulate-organic matter (Poeplau et al. In review). However, this still requires further evidence. Future investigation should specifically focus on the relative importance of occlusion and adsorption for SOC stabilisation, as influenced by the geochemical environment (dominant free cation) and the composition of organic components (esp. prevalence of functional groups).

pH: the master variable for SOC stabilisation mechanisms?

As pH shifts from acidic to basic conditions, so does the importance of SOC stabilisation by different polyvalent cations and their mineral forms, moving from Al^{3+} or Fe^{3+} to Ca^{2+}, respectively (Tipping 2005). The prevalence of each cation is indeed largely linked to soil pH due to the buffering capacity of primary and secondary minerals, notably calcite and Al oxides (Oste et al. 2002; Slessarev et al. 2016). As each cation is associated with different SOC stabilisation mechanisms (Fig. 3), this shift in pH could arguably be used to predict the concentration and types of SOC being stabilised in each environment. Therefore, we propose the following conceptual model: in acidic environments, complexation of organic ligands by free Al^{3+} and Fe^{3+} as well as their mineral forms (Kalbitz and Kaiser 2008; Scheel et al. 2008) and the cementation of aggregates by Fe oxides (Oades and Waters 1991; Zhao et al. 2017) are likely to control SOC stabilisation. There could also be a localised effect of Ca in the topsoil of these acidic environments caused by biological cycling and resulting accumulation of Ca (Clarholm and Skyllberg 2013). As soil pH increases above 6, Ca^{2+} becomes more prevalent and consequently, there should be increased evidence of SOC stabilisation by inner- and outer-sphere Ca^{2+} bridging or Ca-mediated aggregation (Kayler et al. 2011). As soil pH increases further to pH > 8.3, excess Ca^{2+} will begin to precipitate as $CaCO_3$, reducing the stabilisation by free Ca^{2+} at the expense of $CaCO_3$-mediated mechanisms (Lindsay 1979). When soil pH starts to increase beyond pH 9.5, soils will become increasingly sodic and dominated by Na^+, which tends to disperse soil separates, reducing occlusion (Wong et al. 2010) and sorption of SOC (Iskrenova-Tchoukova et al. 2010; Sutton et al. 2005), and consequently weaken SOC stabilisation.

As indicated by Fig. 3, stabilisation of SOC by polyvalent cations is expected to be weakest at near-neutral levels of pH, which also coincides with optimum conditions for bacterial mineralisation (Groffman et al. 2006; Illmer and Schinner 1991; Ivarson 1977; Whittinghill and Hobbie 2012; Zelles et al. 1987). This was suggested previously by Clarholm and Skyllberg (2013) as a "window of opportunity" (highlighted in green; Fig. 3) for C mineralisation. Taking this reasoning a step further, we hypothesize that low and high pH environments will afford different capacities for SOC stabilisation. Given the documented efficiency of sorption by Al and Fe forms and of aggregation by Ca, we postulate that adsorption by Al–Fe oxides generally dominates SOC stabilisation at low pH, stabilising SOC for long time periods; but as the pH increases beyond the "window of opportunity", it could be expected that the dominant stabilisation mechanism would be occlusion within aggregates, potentially involving larger amounts of SOC but for shorter durations. However, due to the relatively limited body of work on Ca-mediated SOC stabilisation mechanisms, these hypotheses currently remain speculative; the dominant SOC stabilisation mechanisms associated with each cation, the amount of SOC they can affect and the relative strength of the conferred protection still require confirmation. Nonetheless, pH has the potential to act as a fundamental indicator of the mechanisms controlling SOC stabilisation. Therefore, this review suggests that SOC models should consider incorporating pH as a master variable to represent the effects of different stabilisation mechanisms by polyvalent cations and their mineral forms on the accumulation and persistence of SOC.

Conclusions

Although an addition of Ca^{2+} generally improves microbial conditions for decomposition by increasing pH and reducing stress from H^+, it can counter-intuitively reduce respiration rates through the stabilisation of SOC. The main mechanisms behind Ca-mediated SOC stabilisation are likely linked to the ability of Ca^{2+} to bridge negatively charged surfaces. Chemical modelling indicates that Ca^{2+} can bridge SOC and minerals through both inner- and outer-sphere interactions, but this still requires empirical confirmation. When scaled up, Ca bridging also positively affects soil structure; yet surprisingly little is known about the implication for the amount and stability of occluded SOC. The relative prevalence of occlusion and adsorption for SOC stabilisation in Ca-influenced soils needs to be determined, as it could have important consequences for the stabilisation of SOC in terms of its maximum amount, mean residence time but also composition. Indeed, there is some evidence that adsorption could preferentially involve

some classes of organic compounds whereas occlusion may be relatively indiscriminate, at least at the macroscopic level. Soil pH could also play a fundamental role in predicting the occurrence of these stabilisation mechanisms and should be considered for inclusion in current SOC models. In order to better represent interactions between the C and Ca cycle in conceptual and numerical models of SOC cycling, we suggest that further mechanistic investigation should focus on the quantification of the relative prevalence and strength of each stabilisation mechanism and their variation across pH thresholds.

Acknowledgements A special acknowledgement must be paid to Dr. Michèle Gaiffe for allowing us to modify her previous diagram and include it in the paper. Thanks also to Dr. Pascal Vittoz, Dr. David Sebag, Prof. Jasquelin Peña, Magali Matteodo, Dr. Nathalie Diaz, Finaritra Randevoson, and Fabienne Dietrich for enjoyable and profitable conversations regarding the manuscript. Special thanks to the Canton de Vaud and IDYST for financially supporting this work and the "*Conseil de coordination scientifique du Vallon de Nant*" for research permissions.

References

Aber JD, Melillo JM, McClaugherty CA (1990) Predicting long-term patterns of mass loss, nitrogen dynamics, and soil organic matter formation from initial fine litter chemistry in temperate forest ecosystems. Can J Bot 68(10):2201–2208

Adu JK, Oades JM (1978) Physical factors influencing decomposition of organic materials in soil aggregates. Soil Biol Biochem 10(2):109–115

Ahmed E, Holmström SJM (2014) Siderophores in environmental research: roles and applications. Microb Biotechnol 7(3):196–208

Ahrland S, Chatt J, Davies NR (1958) The relative affinities of ligand atoms for acceptor molecules and ions. Q Rev 12(3):265–276

Andersson S, Nilsson I, Valeur I (1999) Influence of dolomitic lime on DOC and DON leaching in a forest soil. Biogeochemistry 47(3):295–315

Aristilde L, Sposito G (2008) Molecular modeling of metal complexation by a fluoroquinolone antibiotic. Environ Toxicol Chem 27(11):2304–2310

Armstrong ASB, Tanton TW (1992) Gypsum applications to aggregated saline—sodic clay topsoils. J Soil Sci 43(2):249–260

Asano M, Wagai R (2014) Evidence of aggregate hierarchy at micro- to submicron scales in an allophanic Andisol. Geoderma 216:62–74

Babel U (1975) Micromorphology of soil organic matter. In: Gieseking JE (ed) Soil components: organic components, vol 1. Springer, Berlin, pp 369–473

Baldock JA, Skjemstad JO (2000) Role of the soil matrix and minerals in protecting natural organic materials against biological attack. Org Geochem 31(7–8):697–710

Baldock J, Aoyama M, Oades J, Grant C (1994) Structural amelioration of a South Australian red-brown earth using calcium and organic amendments. Soil Res 32(3):571–594

Balesdent J, Chenu C, Balabane M (2000) Relationship of soil organic matter dynamics to physical protection and tillage. Soil Tillage Res 53(3–4):215–230

Barra CM, Curtius AJ, de Campos RC, Perez DV (2001) Evaluation of four aluminum extraction methods using selected Brazilian soils. Commun Soil Sci Plant Anal 32(11–12):1969–1980

Barta G (2011) Secondary carbonates in loess-paleosoil sequences: a general review. Central Eur J Geosci 3(2):129–146

Bascomb CL (1968) Distribution of pyrophosphate extractable iron and organic carbon in soils of various groups. J Soil Sci 19(2):251–268

Basile-Doelsch I, Brun T, Borschneck D, Masion A, Marol C, Balesdent J (2009) Effect of landuse on organic matter stabilized in organomineral complexes: a study combining density fractionation, mineralogy and δ13C. Geoderma 151(3):77–86

Becze-Deàk J, Langohr R, Verrecchia EP (1997) Small scale secondary $CaCO_3$ accumulations in selected sections of the European loess belt. Morphological forms and potential for paleoenvironmental reconstruction. Geoderma 76(3):221–252

Bélanger N, Paré D, Hendershot WH (2008) Chapter 27—determining nutrient availability in forest soils. In: Carter MR, Gregorich EG (eds) Soil sampling and methods of analysis. Canadian Society of Soil Science, Pinawa, p 1224

Benedetti MF, Milne CJ, Kinniburgh DG, Van Riemsdijk WH, Koopal LK (1995) Metal ion binding to humic substances: application of the non-ideal competitive adsorption model. Environ Sci Technol 29(2):446–457

Bertrand I, Delfosse O, Mary B (2007) Carbon and nitrogen mineralization in acidic, limed and calcareous agricultural soils: apparent and actual effects. Soil Biol Biochem 39(1):276–288

Bindschedler S, Cailleau G, Braissant O, Milliere L, Job D, Verrecchia EP (2014) Unravelling the enigmatic origin of calcitic nanofibres in soils and caves: purely physicochemical or biogenic processes? Biogeosciences 11(10):2809–2825

Bindschedler S, Cailleau G, Verrecchia E (2016) Role of fungi in the biomineralization of calcite. Minerals 6(2):41

Blagodatskaya EV, Anderson T-H (1999) Adaptive responses of soil microbial communities under experimental acid stress in controlled laboratory studies. Appl Soil Ecol 11(2–3):207–216

Bogatko S, Cauët E, Bylaska E, Schenter G, Fulton J, Weare J (2013) The aqueous Ca^{2+} system, in comparison with

Zn^{2+}, Fe^{3+}, and Al^{3+}: an ab initio molecular dynamics study. Chem Eur J 19(9):3047–3060

Boudot J-P (1992) Relative efficiency of complexed aluminum noncrystalline Al hydroxide, allophane and imogolite in retarding the biodegradation of citric acid. Geoderma 52(1):29–39

Briedis C, de Moraes Sá JC, Caires EF, de Fátima Navarro J, Inagaki TM, Boer A, de Oliveira Ferreira A, Neto CQ, Canalli LB, Bürkner dos Santos J (2012a) Changes in organic matter pools and increases in carbon sequestration in response to surface liming in an oxisol under long-term no-till. Soil Sci Soc Am J 76(1):151–160

Briedis C, Sá JCdM, Caires EF, Navarro JdF, Inagaki TM, Boer A, Neto CQ, Ferreira AdO, Canalli LB, Santos JBd (2012b) Soil organic matter pools and carbon-protection mechanisms in aggregate classes influenced by surface liming in a no-till system. Geoderma 170:80–88

Brinza L, Schofield PF, Hodson ME, Weller S, Ignatyev K, Geraki K, Quinn PD, Mosselmans JFW (2014) Combining μXANES and μXRD mapping to analyse the heterogeneity in calcium carbonate granules excreted by the earthworm *Lumbricus terrestris*. J Synchrotron Radiat 21(Pt 1):235–241

Brodowski S, Amelung W, Haumaier L, Zech W (2007) Black carbon contribution to stable humus in German arable soils. Geoderma 139(1–2):220–228

Bronick CJ, Lal R (2005) Soil structure and management: a review. Geoderma 124(1–2):3–22

Brovkin V, Goll D (2015) Land unlikely to become large carbon source. Nat Geosci 8(12):893

Bruckert S, Gaiffe M, Duquet B, Tavant Y, Tavant H (1986) Rôle du flux de calcium sur la stabilisation de la matière organique des sols. Ann Sci Univ France Comté Besançon 4(6):25–29

Cailleau G, Braissant O, Verrecchia EP (2004) Biomineralization in plants as a long-term carbon sink. Naturwissenschaften 91(4):191–194

Cailleau G, Braissant O, Dupraz C, Aragno M, Verrecchia EP (2005) Biologically induced accumulations of $CaCO_3$ in orthox soils of Biga, Ivory Coast. Catena 59(1):1–17

Cailleau G, Verrecchia EP, Braissant O, Emmanuel L (2009) The biogenic origin of needle fibre calcite. Sedimentology 56(6):1858–1875

Campbell EE, Paustian K (2015) Current developments in soil organic matter modeling and the expansion of model applications: a review. Environ Res Lett 10(12):123004

Carmeis Filho ACA, Penn CJ, Crusciol CAC, Calonego JC (2017) Lime and phosphogypsum impacts on soil organic matter pools in a tropical oxisol under long-term no-till conditions. Agric Ecosyst Environ 241:11–23

Carter P (1978) Adsorption of amino acid-containing organic matter by calcite and quartz. Geochim Cosmochim Acta 42(8):1239–1242

Certini G, Corti G, Ugolini FC (2000) Vertical trends of oxalate concentration in two soils under Abies alba from Tuscany (Italy). J Plant Nutr Soil Sci 163(2):173–177

Chan KY, Heenan DP (1999) Lime-induced loss of soil organic carbon and effect on aggregate stability. Soil Sci Soc Am J 63(6):1841–1844

Chassin P (1979) Determination of the angle of contact of humic acids diols solutions—consequences on the mechanisms of aggregate destruction. Ann Agron 30(6):481–491

Chen Y, Barak P (1982) Iron nutrition of plants in calcareous soils. In: Brady NC (ed) Advances in agronomy. Academic Press, Waltham, pp 217–240

Chenu C (1989) Influence of a fungal polysaccharide, scleroglucan, on clay microstructures. Soil Biol Biochem 21(2):299–305

Chenu C, Cosentino D (2011) Microbial regulation of soil structural dynamics. In: Ritz K, Young IM (eds) The architecture and biology of soils: life in inner space. CABI, Cambridge, pp 37–70

Chenu C, Plante AF (2006) Clay-sized organo-mineral complexes in a cultivation chronosequence: revisiting the concept of the 'primary organo-mineral complex'. Eur J Soil Sci 57(4):596–607

Clarholm M, Skyllberg U (2013) Translocation of metals by trees and fungi regulates pH, soil organic matter turnover and nitrogen availability in acidic forest soils. Soil Biol Biochem 63:142–153

Clough A, Skjemstad JO (2000) Physical and chemical protection of soil organic carbon in three agricultural soils with different contents of calcium carbonate. Aust J Soil Res 38(5):1005–1016

Czarnes S, Hallett PD, Bengough AG, Young IM (2000) Root- and microbial-derived mucilages affect soil structure and water transport. Eur J Soil Sci 51(3):435–443

de Kerchove AJ, Elimelech M (2007) Formation of polysaccharide gel layers in the presence of Ca^{2+} and K^{+} ions: measurements and mechanisms. Biomacromol 8(1):113–121

Denef K, Six J, Merckx R, Paustian K (2004) Carbon sequestration in microaggregates of no-tillage soils with different clay mineralogy. Soil Sci Soc Am J 68(6):1935–1944

Dexter AR (1988) Advances in characterization of soil structure. Soil and Tillage Research 11(3):199–238

Diaz N, Dietrich F, King GE, Valla PG, Sebag D, Herman F, Verrecchia EP (2016) A 20-ka reconstruction of a Sahelo-Sudanian paleoenvironment using multi-method dating on pedogenic carbonate. In: EGU general assembly conference abstracts, vol 18, p 4243

Dignac MF, Bahri H, Rumpel C, Rasse DP, Bardoux G, Balesdent J, Girardin C, Chenu C, Mariotti A (2005) Carbon-13 natural abundance as a tool to study the dynamics of lignin monomers in soil: an appraisal at the Closeaux experimental field (France). Geoderma 128(1–2):3–17

Dijkstra FA, Van Breemen N, Jongmans AG, Davies GR, Likens GE (2003) Calcium weathering in forested soils and the effect of different tree species. Biogeochemistry 62(3):253–275

Doetterl S, Stevens A, Six J, Merckx R, Van Oost K, Casanova Pinto M, Casanova-Katny A, Munoz C, Boudin M, Zagal Venegas E, Boeckx P (2015) Soil carbon storage controlled by interactions between geochemistry and climate. Nature Geosci 8(10):780–783

Dontsova KM, Norton LD (2002) Clay dispersion, infiltration, and erosion as influenced by exchangeable Ca and Mg. Soil Sci 167(3):184–193

Dörfer C, Kühn P, Baumann F, He J-S, Scholten T (2013) Soil organic carbon pools and stocks in permafrost-affected soils on the Tibetan Plateau. PLoS ONE 8(2):e57024

Duchaufour R (1982) Pedology: pedogenesis and classification. Springer, Dordrecht

Edwards CA, Bohlen PJ (1995) Biology and ecology of earthworms. Springer, Dordrecht

Edwards AP, Bremner JM (1967) Microaggregates in soil. J Soil Sci 18(1):64

Egan G, Crawley MJ, Fornara DA (2018) Effects of long-term grassland management on the carbon and nitrogen pools of different soil aggregate fractions. Sci Total Environ 613–614(Suppl C):810–819

Elliott ET (1986) Aggregate structure and carbon, nitrogen, and phosphorus in native and cultivated soils. Soil Sci Soc Am J 50(3):627–633

Érika AdS, Geraldo CdO, Carla EC, José MdL, Laura BBdM, Pedro ANB (2016) Stability of soil aggregates in Latosols and Cambisols via standard method and sonification. Afr J Agric Res 11(39):3894–3903

Erktan A, Balmot J, Merino-Martín L, Monnier Y, Pailler F, Coq S, Abiven S, Stokes A, Le Bissonnais Y (2017) Immediate and long-term effect of tannins on the stabilization of soil aggregates. Soil Biol Biochem 105:197–205

Essington ME (2004) Soil and water chemistry. An intergrative approach. CRC Press, Boca Raton

Falsone G, Catoni M, Bonifacio E (2010) Effects of calcite on the soil porous structure: natural and experimental conditions. Agrochimica 54(1):1–12

Federer CA, Hornbeck JW (1985) The buffer capacity of forest soils in new England. Water Air Soil Pollut 26(2):163–173

Fernández-Ugalde O, Virto I, Barré P, Gartzia-Bengoetxea N, Enrique A, Imaz MJ, Bescansa P (2011) Effect of carbonates on the hierarchical model of aggregation in calcareous semi-arid Mediterranean soils. Geoderma 164(3–4):203–214

Fernández-Ugalde O, Virto I, Barré P, Apesteguía M, Enrique A, Imaz MJ, Bescansa P (2014) Mechanisms of macroaggregate stabilisation by carbonates: implications for organic matter protection in semi-arid calcareous soils. Soil Res 52(2):180–192

Ferro-Vázquez C, Nóvoa-Muñoz JC, Costa-Casais M, Klaminder J, Martínez-Cortizas A (2014) Metal and organic matter immobilization in temperate Podzols: a high resolution study. Geoderma 217–218:225–234

Friedlingstein P, Cox P, Betts R, Bopp L, Von Bloh W, Brovkin V, Cadule P, Doney S, Eby M, Fung I, Bala G, John J, Jones C, Joos F, Kato T, Kawamiya M, Knorr W, Lindsay K, Matthews HD, Raddatz T, Rayner P, Reick C, Roeckner E, Schnitzler KG, Schnur R, Strassmann K, Weaver AJ, Yoshikawa C, Zeng N (2006) Climate-carbon cycle feedback analysis: results from the (CMIP)-M-4 model intercomparison. J Clim 19(14):3337–3353

Gadd GM (1999) Fungal production of citric and oxalic acid: importance in metal speciation, physiology and biogeochemical processes. In: Poole RK (ed) Advances in microbial physiology. Academic Press, New York, pp 47–92

Gaiffe M, Schmitt A (1980) Sols et végétation à l'étage montagnard dans les forêts du Jura Central. Science du sol: Bulletin l'Association Francaise pour l'Étude du sol 4:265–296

Gaiffe M, Duquet B, Tavant H, Tavant Y, Bruckert S (1984) Biological stability and physical stability of a clay-humus complex placed under different conditions of calcium or potassium saturation. Plant Soil 77(2–3):271–284

Gessa C, Deiana S (1992) Ca-polygalacturonate as a model for a soil-root interface: II. Fibrillar structure and comparison with natural root mucilage. Plant Soil 140(1):1–13

Ghezzehei TA (2011) Soil structure. In: Huang PA, Li Y, Sumner ME (eds) Handbook of soil sciences. CRC Press, Boca Raton, pp 1–18

Gleixner G, Bol R, Balesdent J (1999) Molecular insight into soil carbon turnover. Rapid Commun Mass Spectrom 13(13):1278–1283

Gleixner G, Poirier N, Bol R, Balesdent J (2002) Molecular dynamics of organic matter in a cultivated soil. Org Geochem 33(3):357–366

Golchin A, Oades JM, Skjemstad JO, Clarke P (1994) Study of free and occluded particulate organic-matter in soils by solid-state C-13 CP/MAS NMR-spectroscopy and scanning electron microscopy. Aust J Soil Res 32(2):285–309

Grand S, Lavkulich LM (2011) Depth distribution and predictors of soil organic carbon in Podzols of a forested watershed in southwestern Canada. Soil Sci 176(4):164–174

Grand S, Lavkulich LM (2012) Effects of forest harvest on soil carbon and related variables in Canadian spodosols. Soil Sci Soc Am J 76(5):1816–1827

Grand S, Lavkulich LM (2013) Potential influence of poorly crystalline minerals on soil chemistry in Podzols of southwestern Canada. Eur J Soil Sci 64(5):651–660

Grant CD, Dexter AR, Oades JM (1992) Residual effects of additions of calcium compounds on soil structure and strength. Soil Tillage Res 22(3):283–297

Groffman PM, Fisk MC, Driscoll CT, Likens GE, Fahey TJ, Eagar C, Pardo LH (2006) Calcium additions and microbial nitrogen cycle processes in a Northern Hardwood Forest. Ecosystems 9(8):1289–1305

Grünewald G, Kaiser K, Jahn R, Guggenberger G (2006) Organic matter stabilization in young calcareous soils as revealed by density fractionation and analysis of lignin-derived constituents. Org Geochem 37(11):1573–1589

Guggenberger G, Zech W (1993) Dissolved organic carbon control in acid forest soils of the Fichtelgebirge (Germany) as revealed by distribution patterns and structural composition analyses. Geoderma 59(1):109–129

Heckman K, Grandy AS, Gao X, Keiluweit M, Wickings K, Carpenter K, Chorover J, Rasmussen C (2013) Sorptive fractionation of organic matter and formation of organo-hydroxy-aluminum complexes during litter biodegradation in the presence of gibbsite. Geochim Cosmochim Acta 121:667–683

Hedges JI, Keil RG (1995) Sedimentary organic-matter preservation—an assessment and speculative synthesis. Mar Chem 49(2–3):81–115

Hilinski T (2001) Implementation of exponential depth distribution of organic carbon in the CENTURY model. Colorado State University, Department of Soil and Crop Science, Fort Collins

Hobbie SE, Miley TA, Weiss MS (2002) Carbon and nitrogen cycling in soils from acidic and nonacidic tundra with

different glacial histories in Northern Alaska. Ecosystems 5(8):0761–0774
Hosking JS (1932) The influence of hydrogen-ion concentration on the decomposition of soil organic matter by hydrogen peroxide. J Agric Sci 22:92–100
Huang PM, Schnitzer M (1986) Interactions of soil minerals with natural organics and microbes. The Soil Science Society of America, Madison
Illmer P, Schinner F (1991) Effects of lime and nutrient salts on the microbiological activities of forest soils. Biol Fertil Soils 11(4):261–266
Inagaki TM, de Moraes Sá JC, Caires EF, Gonçalves DRP (2017) Why does carbon increase in highly weathered soil under no-till upon lime and gypsum use? Sci Total Environ 599–600:523–532
Inskeep WP, Bloom PR (1986) Kinetics of calcite precipitation in the presence of water-soluble organic ligands1. Soil Sci Soc Am J 50(5):1167–1172
Iskrenova-Tchoukova E, Kalinichev AG, Kirkpatrick RJ (2010) Metal cation complexation with natural organic matter in aqueous solutions: molecular dynamics simulations and potentials of mean force. Langmuir 26(20):15909–15919
Israelachvili JN (2011) 6—Van der Waals forces. Intermolecular and Surface Forces, 3rd edn. Academic Press, San Diego, pp 107–132
Ivarson KC (1977) Changes in decompostion rate, microbial population and carbohydrate content of an acid peat bog after liming and reclamation. Can J Soil Sci 57(2):129–137
Jaillard B, Guyon A, Maurin AF (1991) Structure and composition of calcified roots, and their identification in calcareous soils. Geoderma 50(3):197–210
Jansen B, Nierop KGJ, Verstraten JM (2003) Mobility of Fe(II), Fe(III) and Al in acidic forest soils mediated by dissolved organic matter: influence of solution pH and metal/organic carbon ratios. Geoderma 113(3):323–340
Jastrow JD (1996) Soil aggregate formation and the accrual of particulate and mineral-associated organic matter. Soil Biol Biochem 28(4–5):665–676
Jin J, Zimmerman AR (2010) Abiotic interactions of natural dissolved organic matter and carbonate aquifer rock. Appl Geochem 25(3):472–484
Jin J, Zimmerman AR, Moore PJ, Martin JB (2014) Organic and inorganic carbon dynamics in a karst aquifer: Santa Fe River Sink-Rise system, north Florida, USA. J Geophys Res Biogeosci 119(3):340–357
Juo ASR, Kamprath EJ (1979) Copper chloride as an extractant for estimating the potentially reactive aluminum pool in acid soils1. Soil Sci Soc Am J 43(1):35–38
Kaiser K (1998) Fractionation of dissolved organic matter affected by polyvalent metal cations. Org Geochem 28(12):849–854
Kaiser K, Guggenberger G (2000) The role of DOM sorption to mineral surfaces in the preservation of organic matter in soils. Org Geochem 31(7–8):711–725
Kaiser K, Guggenberger G (2003) Mineral surfaces and soil organic matter. Eur J Soil Sci 54(2):219–236
Kaiser M, Ghezzehei TA, Kleber M, Myrold DD, Berhe AA (2014) Influence of calcium carbonate and charcoal applications on organic matter storage in silt-sized aggregates formed during a microcosm experiment. Soil Sci Soc Am J 78(5):1624–1631
Kalbitz K, Kaiser K (2008) Contribution of dissolved organic matter to carbon storage in forest mineral soils. J Plant Nutr Soil Sci 171(1):52–60
Kalbitz K, Schwesig D, Rethemeyer J, Matzner E (2005) Stabilization of dissolved organic matter by sorption to the mineral soil. Soil Biol Biochem 37(7):1319–1331
Kalinichev AG, Kirkpatrick RJ (2007) Molecular dynamics simulation of cationic complexation with natural organic matter. Eur J Soil Sci 58(4):909–917
Kayler ZE, Kaiser M, Gessler A, Ellerbrock RH, Sommer M (2011) Application of delta C-13 and delta N-15 isotopic signatures of organic matter fractions sequentially separated from adjacent arable and forest soils to identify carbon stabilization mechanisms. Biogeosciences 8(10):2895–2906
Keil RG, Tsamakis E, Fuh CB, Giddings JC, Hedges JI (1994) Mineralogical and textural controls on the organic composition of coastal marine-sediments—hydrodynamic separation using splitt-fractionation. Geochim Cosmochim Acta 58(2):879–893
Kempen B, Brus DJ, Stoorvogel JJ (2011) Three-dimensional mapping of soil organic matter content using soil type-specific depth functions. Geoderma 162(1–2):107–123
Kleber M, Sollins P, Sutton R (2007) A conceptual model of organo-mineral interactions in soils: self-assembly of organic molecular fragments into zonal structures on mineral surfaces. Biogeochemistry 85(1):9–24
Kleber M, Nico PS, Plante A, Filley T, Kramer M, Swanston C, Sollins P (2011) Old and stable soil organic matter is not necessarily chemically recalcitrant: implications for modeling concepts and temperature sensitivity. Glob Change Biol 17(2):1097–1107
Kögel-Knabner I, Guggenberger G, Kleber M, Kandeler E, Kalbitz K, Scheu S, Eusterhues K, Leinweber P (2008) Organo-mineral associations in temperate soils: integrating biology, mineralogy, and organic matter chemistry. J Plant Nutr Soil 171(1):61–82
Langmuir D (1997) Aqueous environmental geochemistry. Prentice Hall, Upper Saddle River
Lavkulich LM, Arocena JM (2011) Luvisolic soils of Canada: genesis, distribution, and classification. Can J Soil Sci 91(5):781–806
Lee YJ, Elzinga EJ, Reeder RJ (2005) Cu(II) adsorption at the calcite–water interface in the presence of natural organic matter: kinetic studies and molecular-scale characterization. Geochim Cosmochim Acta 69(1):49–61
Lehmann J, Kleber M (2015) The contentious nature of soil organic matter. Nature 528(7580):60–68
Lemma B, Nilsson I, Kleja DB, Olsson M, Knicker H (2007) Decomposition and substrate quality of leaf litters and fine roots from three exotic plantations and a native forest in the southwestern highlands of Ethiopia. Soil Biol Biochem 39(9):2317–2328
Li D, Wen L, Yang L, Luo P, Xiao K, Chen H, Zhang W, He X, Chen H, Wang K (2017) Dynamics of soil organic carbon and nitrogen following agricultural abandonment in a karst region. J Geophys Res Biogeosci 122:230–242
Likens GE, Driscoll CT, Buso DC, Siccama TG, Johnson CE, Lovett GM, Fahey TJ, Reiners WA, Ryan DF, Martin CW, Bailey SW (1998) The biogeochemistry of calcium at Hubbard Brook. Biogeochemistry 41(2):89–173

Lindsay W (1979) Chemical equilibria in soils. Wiley, New York

Marschner B, Kalbitz K (2003) Controls of bioavailability and biodegradability of dissolved organic matter in soils. Geoderma 113(3–4):211–235

Martin JP, Martin WP, Page JB, Raney WA, de Ment JD (1955) Soil aggregation. In: Norman AG (ed) Advances in agronomy. Academic Press, Waltham, pp 1–37

Martin-Diaconescu V, Gennari M, Gerey B, Tsui E, Kanady J, Tran R, Pécaut J, Maganas D, Krewald V, Gouré E, Duboc C, Yano J, Agapie T, Collomb M-N, DeBeer S (2015) Ca K-edge XAS as a probe of calcium centers in complex systems. Inorg Chem 54(4):1283–1292

Matus F, Amigo X, Kristiansen SM (2006) Aluminium stabilization controls organic carbon levels in Chilean volcanic soils. Geoderma 132(1):158–168

Melvin AM, Lichstein JW, Goodale CL (2013) Forest liming increases forest floor carbon and nitrogen stocks in a mixed hardwood forest. Ecol Appl 23(8):1962–1975

Mikutta R, Mikutta C, Kalbitz K, Scheel T, Kaiser K, Jahn R (2007) Biodegradation of forest floor organic matter bound to minerals via different binding mechanisms. Geochim Cosmochim Acta 71(10):2569–2590

Mikutta R, Lorenz D, Guggenberger G, Haumaier L, Freund A (2014) Properties and reactivity of Fe-organic matter associations formed by coprecipitation versus adsorption: clues from arsenate batch adsorption. Geochim Cosmochim Acta 144:258–276

Miltner A, Bombach P, Schmidt-Brucken B, Kastner M (2012) SOM genesis: microbial biomass as a significant source. Biogeochemistry 111(1–3):41–55

Minick KJ, Fisk MC, Groffman PM (2017) Soil Ca alters processes contributing to C and N retention in the Oa/A horizon of a northern hardwood forest. Biogeochemistry 132:343–357

Monger HC, Daugherty LA, Lindemann WC, Liddell CM (1991) Microbial precipitation of pedogenic calcite. Geology 19(10):997–1000

Moni C, Rumpel C, Virto I, Chabbi A, Chenu C (2010) Relative importance of sorption versus aggregation for organic matter storage in subsoil horizons of two contrasting soils. Eur J Soil Sci 61(6):958–969

Monreal CM, Schulten HR, Kodama H (1997) Age, turnover and molecular diversity of soil organic matter in aggregates of a Gleysol. Can J Soil Sci 77(3):379–388

Muneer M, Oades JM (1989a) The role of Ca-organic interactions in soil aggregate stability.1. Laboratory studies with glucose-C-14, $CaCO_3$ and $CaSO_4.2H_2O$. Aust J Soil Res 27(2):389–399

Muneer M, Oades JM (1989b) The role of Ca-organic interactions in soil aggregate stability.2. Field studies with C-14-labelled straw, $CaCO_3$ and $CaSO_4.2H_2O$. Aust J Soil Res 27(2):401–409

Muneer M, Oades JM (1989c) The role of Ca-organic interactions in soil aggregate stability. 3. Mechanisms and models. Aust J Soil Res 27(2):411–423

Narendrula-Kotha R, Nkongolo KK (2017) Microbial response to soil liming of damaged ecosystems revealed by pyrosequencing and phospholipid fatty acid analyses. PLoS ONE 12(1):e0168497

Oades JM (1984) Soil organic matter and structural stability: mechanisms and implications for management. Plant Soil 76(1/3):319–337

Oades JM (1988) The retention of organic matter in soils. Biogeochemistry 5(1):35–70

Oades JM (1993) The role of biology in the formation, stabilization and degradation of soil structure. Geoderma 56(1):377–400

Oades J, Waters A (1991) Aggregate hierarchy in soils. Soil Res 29(6):815–828

O'Brien SL, Jastrow JD, Grimley DA, Gonzalez-Meler MA (2015) Edaphic controls on soil organic carbon stocks in restored grasslands. Geoderma 251–252:117–123

Oldham KB (2008) A Gouy–Chapman–Stern model of the double layer at a (metal)/(ionic liquid) interface. J Electroanal Chem 613(2):131–138

Oste LA, Temminghoff EJM, Riemsdijk WHV (2002) Solid-solution partitioning of organic matter in soils as influenced by an increase in pH or Ca concentration. Environ Sci Technol 36(2):208–214

Pansu M, Gautheyrou J (2006) Handbook of soil analysis: mineralogical, organic and inorganic methods. Springer, Berlin

Paradelo R, Virto I, Chenu C (2015) Net effect of liming on soil organic carbon stocks: a review. Agric Ecosyst Environ 202:98–107

Paradelo R, van Oort F, Barre P, Billiou D, Chenu C (2016) Soil organic matter stabilization at the pluri-decadal scale: insight from bare fallow soils with contrasting physico-chemical properties and macrostructures. Geoderma 275:48–54

Parfitt RL, Childs CW (1988) Estimation of forms of Fe and Al—a review, and analysis of contasting soils by dissolution and mossbauer methods. Aust J Soil Res 26(1):121–144

Parton WJ (1996) The CENTURY model. In: Powlson DS, Smith P, Smith JU (eds) Evaluation of soil organic matter models: using existing long-term datasets. Springer, Berlin, pp 283–291

Parton WJ, Del Grosso SJ, Plante AF, Adair EC, Lutz SM (2015) Modeling the dynamics of soil organic matter and nutrient cycling. In: Paul EA (ed) Soil microbiology, ecology and biochemistry, 4th edn. Academic Press, Boston, pp 505–537

Paul EA, Morris SJ, Six J, Paustian K, Gregorich EG (2003) Interpretation of soil carbon and nitrogen dynamics in agricultural and afforested soils. Soil Sci Soc Am J 67(5):1620–1628

Pearson RG (1963) Hard and soft acids and bases. J Am Chem Soc 85(22):3533–3539

Peinemann N, Guggenberger G, Zech W (2005) Soil organic matter and its lignin component in surface horizons of salt-affected soils of the Argentinian Pampa. Catena 60(2):113–128

Peterson JB (1947) Calcium linkage, a mechanism in soil granulation. Soil Sci Soc Am J 12:29–34

Plante AF, Feng Y, McGill WB (2002) A modeling approach to quantifying soil macroaggregate dynamics. Can J Soil Sci 82(2):181–190

Preston CM, Nault JR, Trofymow JA (2009) Chemical changes during 6 years of decomposition of 11 litters in some canadian forest sites. Part 2. 13C abundance, solid-state

13C NMR spectroscopy and the meaning of "lignin". Ecosystems 12(7):1078–1102
Pulido-Villena E, Reche I, Morales-Baquero R (2006) Significance of atmospheric inputs of calcium over the southwestern Mediterranean region: high mountain lakes as tools for detection. Glob Biogeochem Cycles 20(2):1–8
Quiquampoix H, Burns RG (2007) Interactions between proteins and soil mineral surfaces: environmental and health consequences. Elements 3(6):401–406
Ranjbar F, Jalali M (2012) Calcium, magnesium, sodium, and potassium release during decomposition of some organic residues. Commun Soil Sci Plant Anal 43(4):645–659
Rasmussen C, Torn MS, Southard RJ (2005) Mineral assemblage and aggregates control carbon dynamics in a California conifer forest. Soil Sci Soc Am J 69(6):1711–1721
Rasmussen C, Southard RJ, Horwath WR (2006) Mineral control of organic carbon mineralization in a range of temperate conifer forest soils. Glob Change Biol 12(5):834–847
Reddy KJ, Lindsay WL, Workman SM, Drever JI (1990) Measurement of calcite ion activity products in soils. Soil Sci Soc Am J 54(1):67–71
Reynolds RC (1978) Polyphenol inhibition of calcite precipitation in Lake Powell 1. Limnol Oceanogr 23(4):585–597
Römkens PFAM, Dolfing J (1998) Effect of Ca on the solubility and molecular size distribution of DOC and Cu binding in soil solution samples. Environ Sci Technol 32(3):363–369
Ross DS, Bartlett RJ, Magdoff FR (1991) Exchangeable cations and the pH-independent distribution of cation exchange capacities in Spodosols of a forested watershed. In: Wright RJ, Baligar VC, Murrmann RP (eds) Proceedings of the second international symposium on plant-soil interactions at low pH, 24–29 June 1990, Beckley, WV. Springer, Dordrecht, pp 81–92
Rousk J, Brookes PC, Baath E (2009) Contrasting soil pH effects on fungal and bacterial growth suggest functional redundancy in carbon mineralization. Appl Environ Microbiol 75(6):1589–1596
Rousk J, Baath E, Brookes PC, Lauber CL, Lozupone C, Caporaso JG, Knight R, Fierer N (2010) Soil bacterial and fungal communities across a pH gradient in an arable soil. Int Soc Microb Ecol J 4(10):1340–1351
Rowley MC, Estrada-Medina H, Tzec-Gamboa M, Rozin A, Cailleau G, Verrecchia EP, Green I (2016) Moving carbon between spheres, the potential oxalate-carbonate pathway of Brosimum alicastrum Sw Moraceae. Plant Soil 412:465–479
Rumpel C, Kögel-Knabner I (2011) Deep soil organic matter-a key but poorly understood component of terrestrial C cycle. Plant Soil 338(1–2):143–158
Satchell JE (1967) Lumbricidae. In: Burgess A, Raw F (eds) Soil biology. Academic Press, London, pp 259–322
Scheel T, Dörfler C, Kalbitz K (2007) Precipitation of dissolved organic matter by aluminum stabilizes carbon in acidic forest soils. Soil Sci Soc Am J 71(1):64–74
Scheel T, Jansen B, Van Wijk AJ, Verstraten JM, Kalbitz K (2008) Stabilization of dissolved organic matter by aluminium: a toxic effect or stabilization through precipitation? Eur J Soil Sci 59(6):1122–1132
Schmidt MWI, Torn MS, Abiven S, Dittmar T, Guggenberger G, Janssens IA, Kleber M, Kögel-Knabner I, Lehmann J, Manning DAC, Nannipieri P, Rasse DP, Weiner S, Trumbore SE (2011) Persistence of soil organic matter as an ecosystem property. Nature 478(7367):49–56
Schrumpf M, Kaiser K, Guggenberger G, Persson T, Kögel-Knabner I, Schulze ED (2013) Storage and stability of organic carbon in soils as related to depth, occlusion within aggregates, and attachment to minerals. Biogeosciences 10(3):1675–1691
Schurig C, Smittenberg RH, Berger J, Kraft F, Woche SK, Goebel MO, Heipieper HJ, Miltner A, Kaestner M (2013) Microbial cell-envelope fragments and the formation of soil organic matter: a case study from a glacier forefield. Biogeochemistry 113(1–3):595–612
Schwarzenbach G (1961) The general, selective, and specific formation of complexes by metallic cations. Adv Inorg Chem Radiochem 3:257–285
Shang C, Tiessen H (2003) Soil organic C sequestration and stabilization in karstic soils of Yucatan. Biogeochemistry 62(2):177–196
Shipitalo MJ, Protz R (1989) Chemistry and micromorphology of aggregation in earthworm casts. Geoderma 45(3):357–374
Six J, Paustian K, Elliott ET, Combrink C (2000) Soil structure and organic matter I. Distribution of aggregate-size classes and aggregate-associated carbon. Soil Sci Soc Am J 64(2):681–689
Six J, Conant RT, Paul EA, Paustian K (2002) Stabilization mechanisms of soil organic matter: implications for C-saturation of soils. Plant Soil 241(2):155–176
Six J, Bossuyt H, Degryze S, Denef K (2004) A history of research on the link between (micro)aggregates, soil biota, and soil organic matter dynamics. Soil Tillage Res 79(1):7–31
Skinner HCW, Jahren AH (2007) 8.04—biomineralization A2—Holland, Heinrich D. In: Turekian KK (ed) Treatise on geochemistry. Pergamon, Oxford, pp 1–69
Skjemstad JO, Fitzpatrick RW, Zarcinas BA, Thompson CH (1992) Genesis of Podzols on coastal dunes in southern Queensland. 2. Geochemistry and forms of elements as deduced from various soil extraction procedures. Aust J Soil Res 30(5):615–644
Skjemstad JO, Janik LJ, Head MJ, McClure SG (1993) High energy ultraviolet photo-oxidation: a novel technique for studying physically protected organic matter in clay- and silt-sized aggregates. J Soil Sci 44(3):485–499
Slessarev EW, Lin Y, Bingham NL, Johnson JE, Dai Y, Schimel JP, Chadwick OA (2016) Water balance creates a threshold in soil pH at the global scale. Nature 540(7634):567–569
Sokoloff VP (1938) Effect of neutral salts of sodium and calcium on carbon and nitrogen of soils. J Agric Res 57:0201–0216
Sollins P, Homann P, Caldwell BA (1996) Stabilization and destabilization of soil organic matter: mechanisms and controls. Geoderma 74(1–2):65–105
Sollins P, Kramer MG, Swanston C, Lajtha K, Filley T, Aufdenkampe AK, Wagai R, Bowden RD (2009) Sequential density fractionation across soils of contrasting mineralogy: evidence for both microbial- and mineral-controlled soil organic matter stabilization. Biogeochemistry 96(1–3):209–231
Spaccini R, Piccolo A, Conte P, Haberhauer G, Gerzabek MH (2002) Increased soil organic carbon sequestration through

hydrophobic protection by humic substances. Soil Biol Biochem 34(12):1839–1851
Spielvogel S, Prietzel J, Kögel-Knabner I (2008) Soil organic matter stabilization in acidic forest soils is preferential and soil type-specific. Eur J Soil Sci 59(4):674–692
Sposito G (2008) The chemistry of soils. Oxford University Press, Oxford
Suess E (1970) Interaction of organic compounds with calcium carbonate—I. Association phenomena and geochemical implications. Geochim Cosmochim Acta 34(2):157–168
Sutton R, Sposito G, Diallo MS, Schulten H-R (2005) Molecular simulation of a model of dissolved organic matter. Environ Toxicol Chem 24(8):1902–1911
Suzuki S (2002) Black tea adsorption on calcium carbonate: a new application to chalk powder for brown powder materials. Colloids Surf A 202(1):81–91
Tate KR, Theng BKG (1980) Organic matter and its interactions with inorganic soil constiuents. In: Theng BKG (ed) Soils with variable charge. Soil Bureau, Lower Hutt, pp 225–249
Theng BKG, Churchman GJ, Newman RH (1986) The occurrence of interlayer clay-organic complexes in two New Zealand soils. Soil Sci 142(5):262–266
Thirukkumaran CM, Morrison IK (1996) Impact of simulated acid rain on microbial respiration, biomass, and metabolic quotient in a mature sugar maple (Acersaccharum) forest floor. Can J For Res 26(8):1446–1453
Thomas MM, Clouse JA, Longo JM (1993a) Adsorption of organic compounds on carbonate minerals. 3. Influence on dissolution rates. Chem Geol 109(1–4):227–237
Thomas MM, Clouse JA, Longo JM (1993b) Adsorption of organic compounds on carbonate minerals: 1. Model compounds and their influence on mineral wettability. Chem Geol 109(1–4):201–213
Tipping E (2005) Modelling Al competition for heavy metal binding by dissolved organic matter in soil and surface waters of acid and neutral pH. Geoderma 127(3–4):293–304
Tisdall JM (1996) Formation of soil aggregates and accumulation of soil organic matter. In: Carter MRS, Stewart BA (eds) Structure and organic matter storage in agricultural soils. CRC Press, Boca Raton, pp 57–86
Tisdall JM, Oades JM (1982) Organic-matter and water-stable aggregates in soils. J Soil Sci 33(2):141–163
Tonneijck FH, Jansen B, Nierop KGJ, Verstraten JM, Sevink J, De Lange L (2010) Towards understanding of carbon stocks and stabilization in volcanic ash soils in natural Andean ecosystems of northern Ecuador. Eur J Soil Sci 61(3):392–405
Torn MS, Trumbore SE, Chadwick OA, Vitousek PM, Hendricks DM (1997) Mineral control of soil organic carbon storage and turnover. Nature 389(6647):170–173
Toutain F (1974) Etude écologique de l'humidificaton dans les hetraies acidiphiles. In. Université de Nancy, Nancy
Trumbore SE (1993) Comparison of carbon dynamics in tropical and temperate soils using radiocarbon measurements. Glob Biogeochem Cycles 7(2):275–290
van der Heijden G, Legout A, Mareschal L, Ranger J, Dambrine E (2017) Filling the gap in Ca input-output budgets in base-poor forest ecosystems: the contribution of non-crystalline phases evidenced by stable isotopic dilution. Geochim Cosmochim Acta 209:135–148
Verrecchia EP (1990) Litho-diagenetic implications of the calcium oxalate-carbonate biogeochemical cycle in semiarid Calcretes, Nazareth, Israel. Geomicrobiol J 8(2):87–99
Verrecchia EP, Freytet P, Verrecchia KE, Dumont J-L (1995) Spherulites in calcrete laminar crusts; biogenic $CaCO_3$ precipitation as a major contributor to crust formation. J Sediment Res 65(4a):690
Verrecchia EP, Braissant O, Cailleau G (2006) The oxalate–carbonate pathway in soil carbon storage: the role of fungi and oxalotrophic bacteria. Cambridge University Press, Cambridge
Virto I, Barre P, Chenu C (2008) Microaggregation and organic matter storage at the silt-size scale. Geoderma 146(1–2):326–335
Virto I, Moni C, Swanston C, Chenu C (2010) Turnover of intra- and extra-aggregate organic matter at the silt-size scale. Geoderma 156(1–2):1–10
Virto I, Gartzia-Bengoetxea N, Fernandez-Ugalde O (2011) Role of organic matter and carbonates in soil aggregation estimated using laser diffractometry. Pedosphere 21(5): 566–572
Virto I, Barré P, Enrique A, Poch RM, Fernández-Ugalde O, Imaz MJ, Bescansa P (2013) Micromorphological analysis on the influence of the soil mineral composition on short-term aggregation in semi-arid Mediterranean soils. Span J Soil Sci 3(2):116–129
Vogel C, Mueller CW, Hoeschen C, Buegger F, Heister K, Schulz S, Schloter M, Kögel-Knabner I (2014) Submicron structures provide preferential spots for carbon and nitrogen sequestration in soils. Nat Commun 5(2947):1–7
von Lützow M, Kögel-Knabner I, Ekschmitt K, Matzner E, Guggenberger G, Marschner B, Flessa H (2006) Stabilization of organic matter in temperate soils: mechanisms and their relevance under different soil conditions - a review. Eur J Soil Sci 57(4):426–445
Wedepohl HK (1995) The composition of the continental crust. Geochim Cosmochim Acta 59(7):1217–1232
Wen L, Li D, Chen H, Wang K (2017) Dynamics of soil organic carbon in density fractions during post-agricultural succession over two lithology types, southwest China. J Environ Manag 201:199–206
Whittinghill KA, Hobbie SE (2012) Effects of pH and calcium on soil organic matter dynamics in Alaskan tundra. Biogeochemistry 111(1–3):569–581
Wiese L, Ros I, Rozanov A, Boshoff A, de Clercq W, Seifert T (2016) An approach to soil carbon accounting and mapping using vertical distribution functions for known soil types. Geoderma 263:264–273
Wong VNL, Greene RSB, Dalal RC, Murphy BW (2010) Soil carbon dynamics in saline and sodic soils: a review. Soil Use Manag 26(1):2–11
Wuddivira MN, Camps-Roach G (2007) Effects of organic matter and calcium on soil structural stability. Eur J Soil Sci 58(3):722–727
Xiao J, Wen Y, Li H, Hao J, Shen Q, Ran W, Mei X, He X, Yu G (2015) In situ visualisation and characterisation of the capacity of highly reactive minerals to preserve soil organic matter (SOM) in colloids at submicron scale. Chemosphere 138:225–232
Poeplau C, Don A, Six J, Kaiser M, Benbi D, Chenu C, Cotrufo FM, Derrien D, Gioacchini P, Grand S, Gregorich E,

Griepentrog M, Gunina A, Haddix M, Kuzyakov Y, Kühnel A, Macdonald LM, Soong J, Trigalet S, Vermeire M-L, Rovira P, van Wesemaell B, Wiesmeier M, Yeasmin S, Yevdokimov I, Nieder R (in review) Isolating soil organic carbon fractions with varying turnover rates – A comprehensive comparison of fractionation methods

Yang S, Cammeraat E, Jansen B, Cerli C, Kalbitz K (2016) Organic carbon stabilization of soils formed on acidic and calcareous bedrocks in Neotropical alpine grassland, Peru. EGU General Assembly 2016, held 17-22 April, 2016 in Vienna, Austria

Yuan TL, Gammon N, Leighty RG (1967) Relative contribution of organic and clay fractions to cation-exchange capacity of sandy soils from several soil groups. Soil Sci 104(2):123–128

Zelles L, Scheunert I, Kreutzer K (1987) Bioactivity in limed soil of a spruce forest. Biol Fertil Soils 3(4):211–216

Zhao J, Chen S, Hu R, Li Y (2017) Aggregate stability and size distribution of red soils under different land uses integrally regulated by soil organic matter, and iron and aluminum oxides. Soil Tillage Res 167:73–79

Zheng W, Morris EK, Lehmann A, Rillig MC (2016) Interplay of soil water repellency, soil aggregation and organic carbon. A meta-analysis. Geoderma 283:39–47

Zimmerman AR, Ahn M-Y (2010) Organo-mineral–enzyme interaction and soil enzyme activity. In: Shukla G, Varma A (eds) Soil enzymology. Soil biology, vol 22. Springer, Berlin, pp 271–292

- This page is intentionally left blank -

8.6.2 - Chapter 4 – $CaCO_3$ trajectories biogeochemistry

- This page is intentionally left blank -

Geoderma 361 (2020) 114065

Contents lists available at ScienceDirect

Geoderma

journal homepage: www.elsevier.com/locate/geoderma

A cascading influence of calcium carbonate on the biogeochemistry and pedogenic trajectories of subalpine soils, Switzerland

Mike C. Rowley[a,*], Stephanie Grand[a], Thierry Adatte[b], Eric P. Verrecchia[a]

[a] IDYST – Institute of Earth Surface Dynamics, Faculty of Geosciences and Environment, Université de Lausanne, Switzerland
[b] ISTE – Institute of Earth Sciences, Faculty of Geosciences and Environment, Université de Lausanne, Switzerland

ARTICLE INFO

Handling Editor: David Laird

Keywords:
Pedogenic inertia
Pedogenic thresholds
Soil inorganic carbon
Soil organic carbon
Pedogenic oxides

ABSTRACT

Soil research in temperate to cool and humid regions has typically focused on acidic soils; there has been relatively little investigation of the effects of calcium carbonate ($CaCO_3$) on unamended soil properties or function in these environments. The object of this study was to characterise the effects of small amounts of $CaCO_3$ on pedogenic trajectories and soil biogeochemistry in a humid subalpine valley of Switzerland. To isolate the influence of $CaCO_3$, six profiles were selected that had developed under almost identical conditions for soil formation, *i.e.* climate, topography, vegetation structure, time since deglaciation, silicate mineralogy and texture. The main difference between the profiles was that three contained a small quantity of $CaCO_3$ (< 6.2%; thereafter, '$CaCO_3$-bearing') while the remaining three contained no detectable $CaCO_3$ (thereafter, '$CaCO_3$-free'). The presence of $CaCO_3$ was associated with cascading changes in soil biogeochemistry. These changes included higher pH, an order of magnitude higher extractable Ca and twice as much soil organic carbon (SOC). $CaCO_3$-bearing profiles also displayed a higher proportion of poorly crystalline Fe forms. The higher pH at the $CaCO_3$-bearing site was attributable to the weak buffering provided by $CaCO_3$ dissolution, which in turn maintained the relatively higher extractable Ca. Exchangeable Ca (Ca_{Exch}) and other reactive Ca forms could help stabilise SOC, contributing to its accumulation through processes such as flocculation and subsequent occlusion within aggregates and/or sorption to mineral surfaces. The increased SOC, Ca_{Exch} and pH at the $CaCO_3$-bearing site could in turn be inhibiting the crystallisation of disordered Fe forms, but further research is required to confirm this effect and isolate the exact mechanisms. Overall, this study shows that the presence of small amounts of $CaCO_3$ in humid environments has a far-reaching influence on soil biogeochemistry and further supports the idea that indicators of Ca prevalence have the potential to improve regional SOC estimates.

1. Introduction

Calcium carbonate ($CaCO_3$) accounts for an important fraction of C present in soils, linking the long-term geological C cycle with the faster biogeochemical cycling of soil organic carbon (SOC; Gao et al., 2017; Hasinger et al., 2015; Sanderman, 2012; Zamanian et al., 2016). Globally, the presence of $CaCO_3$ in soils is inversely correlated to effective precipitation because of its susceptibility to chemical weathering (Arkley, 1963; Jenny, 1941; Slessarev et al., 2016). However, there remains clear outliers in this global correlation, as $CaCO_3$-bearing soils can be found in humid environments and are typically related to lithological $CaCO_3$ reservoirs that are yet to be exhausted by leaching (Slessarev et al., 2016). Furthermore, while the precipitation of $CaCO_3$ by physicochemical processes is not typically favoured in humid or acidic environments (Barta et al., 2018; Cerling, 1984), it can still occur through the direct and indirect results of biological processes (Bindschedler et al., 2016; Cailleau et al., 2005; Hasinger et al., 2015). Thus, $CaCO_3$ in soils can persist in a state of disequilibrium with climate, when driven by reserves of calcareous parent material or biological processes.

The aforementioned disequilibrium is an example of pedogenic inertia, defined as the persistence of certain soil conditions or processes in spite of the presence of extrinsic pedogenic factors that favour their discontinuation (Bryan and Teakle, 1949). The extrinsic pedogenic factors refer to four of the five conventional factors of pedogenesis (parent material, biota, topography and climate; Jenny, 1941), excluding time which acts as a vector (Muhs, 1984). In the previously used example, the state of pedogenic inertia exists because an intrinsic pedogenic factor, the continued and slow dissolution of $CaCO_3$, prevents the expression of an acidic soil favoured since deglaciation by the

* Corresponding author at: Bureau 4633, Bâtiment Geopolis, UNIL Quartier Mouline, Lausanne 1015, Switzerland.
E-mail address: mike.rowley@unil.ch (M.C. Rowley).

https://doi.org/10.1016/j.geoderma.2019.114065
Received 21 August 2019; Received in revised form 29 October 2019; Accepted 30 October 2019
Available online 03 December 2019

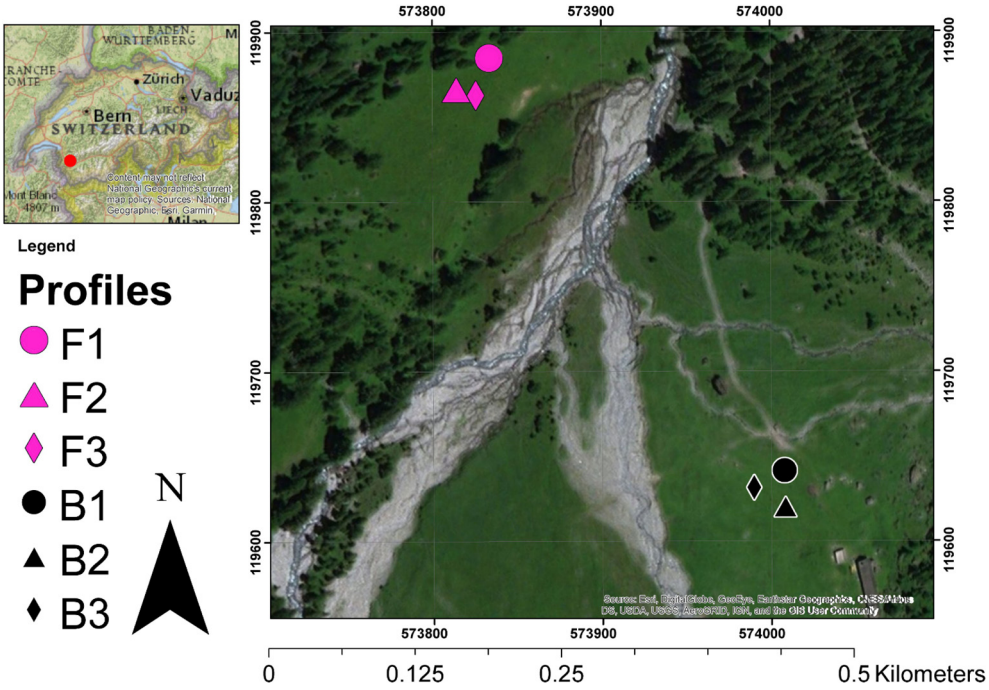

Fig. 1. Profile locations in the Nant valley, Vaud Alps, Switzerland. Coordinates are in CH1903 LV03 (ESRI, 2019). Profiles labelled with an F (F1, F2, F3) are at the $CaCO_3$-free site and profiles labelled with a B (B1, B2, B3) are at the $CaCO_3$-bearing site.

extrinsic factor of climate (Chadwick and Chorover, 2001). In turn, this inertia can diverge the trajectory of pedogenesis, as evidenced by the wide array of soils that develop on parent material containing varied $CaCO_3$ content in humid or mountainous environments (Kowalska et al., 2019). Unless there is a change in extrinsic factors, pedogenic inertia is by nature a transient condition that will eventually cease in a threshold response. Pedogenic thresholds are defined as limits in intrinsic pedogenic factors or soil properties, that once breached, cause rapid and irreversible transformations in pedogenesis and biogeochemistry (Chadwick and Chorover, 2001; Muhs, 1984). In the case of $CaCO_3$, a threshold may occur when its concentration becomes too low to provide pH buffering to the soil system, triggering changes in soil biogeochemistry.

The presence of $CaCO_3$ plays a commanding role in governing soil biogeochemistry. The primary mechanism for this is the buffering of soil pH caused by the consumption of H^+ during acid hydrolysis of $CaCO_3$ (Bache, 1984; Zamanian et al., 2016). pH is known as a master variable in soil ecosystems and impacts many biological and chemical processes, such as the composition of microbial communities (Bahram et al., 2018; Rousk et al., 2010), mineral weathering rates (Chadwick and Chorover, 2001), redox chemistry (Bartlett and James, 1993) and the speciation and lability of many elements (Sposito, 2016). The dissolution of $CaCO_3$ also provides a continued supply of Ca^{2+}, which has long been thought to promote the accumulation of SOC in $CaCO_3$-bearing soils through occlusion (Grant et al., 1992; Muneer and Oades, 1989) and sorption processes (Edwards and Bremner, 1967; Kalinichev and Kirkpatrick, 2007; see review in Rowley et al., 2018). Recent evidence has highlighted a potential stabilisation of SOC by Fe-Ca-ternary complexation (Sowers et al., 2018a,b), which could be more prevalent in $CaCO_3$-bearing soils than acidic profiles with limited exchangeable Ca (Ca_{Exch}). However, further research is still needed to evidence links between Ca, SOC, and reactive forms of Fe in different soil environments. In particular, the effects of small amounts of $CaCO_3$, commonly found in cool humid edaphic environments, on soil biogeochemistry still require further investigation.

Therefore, the objective of this paper is to quantify the impact of small amounts of $CaCO_3$ on the pedogenesis and biogeochemistry of soils in a humid environment (Nant Valley, Vaud Alps, Switzerland). To isolate the effects of $CaCO_3$ on pedogenesis at the Nant Valley, six soil profiles were selected that had developed under near-identical conditions for soil formation (Jenny, 1941) or extrinsic pedogenic factors (Chadwick and Chorover, 2001; Muhs, 1984), except that three profiles contained a small quantity of $CaCO_3$ ($< 6.2\%$ $CaCO_3$) while the other three were devoid of carbonates. Our hypothesis was that the presence or absence of $CaCO_3$ would trigger a threshold response, resulting in large divergences in pedogenesis and soil biogeochemistry, particularly regarding the accumulation of SOC.

2. Materials and methods

2.1. Site description and sampling

This study was completed in the Nant Valley (573′000, 119′000 CH1903 LV03), a partially glaciated watershed in the Vaud Alps, Switzerland. The valley is orientated north-south and situated on the Morcles Nappe, a near-recumbent anticline consisting of Jurassic and Cretaceous shallow-water limestones intercalated with marl and shale deposits (Austin et al., 2008). Sampling took place in a pastoral area of the valley floor (*ca.* 1500 m elevation above sea level), which is lightly-grazed by heifers during summer months. This area receives approximately 1800 mm yr^{-1} precipitation, has a mean annual temperature of 6 °C (Vittoz and Gmür, 2008) and is typically covered in snow from December to April.

Two sampling sites were selected that represented a range of $CaCO_3$ contents, while having developed under near-identical soil forming conditions. Potential variations in the $CaCO_3$ content were identified in the field using an auger, 10% v/v HCl and a field pH meter (Hellige pH Indicator). Retained sites were located on subalpine prairies and thus had the same vegetation structure, which had previously been characterised in detail (Grand et al., 2016; Vittoz and Gmür, 2008). Soils at each site developed in mixed alluvial, morainic and colluvial materials issued from the Morcles Nappe (Grand et al., 2016; Perret and Martin, 2014), deposited around the time of the retreat of the Martinets Glacier (*ca.* 15 Ka; Seguinot et al., 2018). Sites all had a minimal slope, the

same altitude, similar climate due to their proximity to each other (*ca.* 400 m apart) and equivalent irradiance.

Three profiles were dug at each sampling site in July–August 2016 (Fig. 1). Profiles were classified as Eutric Cambisols (siltic) with no HCl effervescence on the northwest bank and Cambic Phaeozems (siltic) that effervesced on the southeast bank of the Nant River (IUSS Working Group WRB, 2015). For brevity, the Eutric Cambisols will henceforth be labelled as $CaCO_3$-free (profiles F1, F2, F3, in fuchsia) and the Cambic Phaeozems will be labelled as $CaCO_3$-bearing (profiles B1, B2, B3, in black). Profiles were sampled at 6–7 depth intervals (Table 1) to a maximum depth of 50 cm, sampling the deepest layers first to prevent intra-profile contamination. Samples were labelled from 1 to 6 / 7 with increasing depth (*e.g.*, F1.1-to-F1.6) and then transported to the University of Lausanne in sealed bags. Aboveground biomass (AGB) was also randomly sampled from the sites to quantify potential differences in vegetative inputs at the sites.

2.2. Laboratory analyses

Samples were air-dried and sieved to 2 mm. All analyses were completed on this fine earth fraction unless stated otherwise and results were corrected for residual humidity (van Reeuwijk, 2002). Sub-samples were ground to a fine powder (*ca.* 20 μm) for 3 min in an agate crucible with a vibrating-disc mill (Siebtechnik Schibenschwingmuhle-TS). AGB samples were oven-dried (40 °C), ground by hand and homogenised for further analysis. Quality control procedures included the analysis of an internal standard when appropriate, as well as the inclusion of blanks and quality checks. A minimum of 10% blind replicates were included in all analyses. All plastic and glassware were acid washed (3 M HCl) to remove trace contamination.

2.2.1. pH and texture

Soil pH was measured potentiometrically using a glass-body combination electrode (Thermo Scientific Orion ROSS Probe) on field moist samples in a 0.1 M $CaCl_2$ solution (1:2 soil:solution mass ratio). Texture was determined using laser diffraction (0.01–2000 μm; Pansu and Gautheyrou, 2006). Pre-treatment included digestion of soil organic matter with increasing concentrations of H_2O_2 (10–35%). During the procedure, pH was kept around neutrality with NaOH to prevent destruction of mineral components due to acidification. Samples were then shaken with sodium hexametaphosphate for 16 h to chemically disperse particles prior to measurement with a Beckman Coulter LS13320 Particle Sizing Analyser. The analyser pump speed was set at 80% (*ca.* 9500 mL min^{-1}) and samples were weakly sonicated in both the auto-sampler and analyser (4/8 setting; *ca.* 2 J mL^{-1}) prior to measurement. The analyser was run using the default optical model (Fraunhofer.rf780d) in auto-dilution mode. Measurements were taken when an obscuration of 12% was attained.

2.2.2. Elemental analysis

The total elemental composition was quantified on ground samples using X-ray fluorescence (XRF; PANalytical PW2400 WDXRF Spectrometer) following lithium tetraborate fusion (PANalytical Perl X3 Fuser). Results were corrected for loss-on-ignition at 1050 °C (Solo 111–13/10/30). Organic C and total nitrogen were quantified on AGB and soil ground samples by dry combustion (Carlo Erba 1108 and Thermo Scientific Flash 2000 CHN Elemental Analysers). Soil samples were fumigated for 24 h with 12 M HCl in order to remove inorganic C prior to CHN elemental analysis (Harris et al., 2001; Ramnarine et al., 2011). Samples were weighed to the nearest milligram before and after fumigation to correct for mass changes. All samples gained mass due to the formation of small quantities of chloride green rust, likely formed from the reaction of Fe oxides with Cl^- (Ramnarine et al., 2011).

2.2.3. Mineralogy

Bulk mineralogy was determined on ground samples prepared according to Adatte et al. (1996) using X-ray diffraction (XRD; Thermo ARL X'TRA Powder Diffractometer). Approximately 800 mg of ground sample was pressed (20 bars) in a powder holder covered with blotting paper. Pressed samples were then analysed using Cu Kα radiation at 45 kV / 40 mA with a 13 s counting time per 0.02° for 2 θ in the 1-65° range. Samples were rotated at a range of 1° min^{-1} with an acquisition step size of 0.03 – 0.05° 2 θ using a θ / θ type goniometer with a 250 mm radius. A spectral counter (Thermo ARL Water-cooled Silicon Detector) was used to eliminate Cu Kβ and Fe parasitic emissions. The bulk mineralogy of samples was then quantified using external standards (Adatte et al., 1996).

Samples from a randomly selected profile at each site were also prepared for clay mineralogical analysis according to Adatte et al. (1996). Briefly, samples from profiles F1 and B2 were mixed with deionised water, agitated, and combined with 10% HCl to remove carbonates. Insoluble residues were washed by centrifugation until neutral pH was acquired. Different size fractions (< 2 μm and < 16 μm) were separated by sedimentation according to Stokes' law. Selected fractions were then pipetted onto glass plates and air-dried. Resulting oriented slides were analysed by XRD before and after ethylene glycol solvation (heating to 450 °C).

Total carbonate content expressed as $CaCO_3$ equivalent material (CCE) was determined using a weak acid dissolution followed by measurement of the pH of the extractant (Loeppert et al., 1984). The method was selected for its reproducibility in quantifying low amounts of $CaCO_3$, for which the XRD detection limit is around 1% (Loeppert and Suarez, 1996). The method was also adapted to measure reactive carbonates, by measuring extracts shortly after the addition of the weak acid. Briefly, 2 g of soils were placed in 50 mL centrifuge tubes and shaken on a rotary shaker (250 rpm) with 25 mL 0.4 M acetic acid. Holes approximately 1 mm in diameter were made in the lids to allow for degassing during the reaction. The pH of standards (reagent grade $CaCO_3$) and samples solutions was measured (Thermo-Fisher Scientific Orion Star A111 Probe) at 1 h (reactive carbonates) and 16 h (total carbonate) after the addition of acetic acid. Quality control was assured by running blind, analytical and spiked replicates (Loeppert and Suarez, 1996).

2.2.4. Extractable cations

Fe and Al present in pedogenic oxides were extracted using a citrate-bicarbonate dithionite solution (Fe_d or Al_d; Mehra and Jackson, 1958), while poorly crystalline and monomeric Fe and Al forms were extracted with an oxalate solution (Fe_o or Al_o; McKeague and Day, 1966). The ratio of oxalate-to-dithionite extractable Fe (Fe_o/Fe_d) was used as a measure of the crystallinity of Fe oxides (Skjemstad et al., 1992). One surficial sample (B3.1) contained more Fe_o than Fe_d (*ca.* 20%; Table 1). The citrate-bicarbonate dithionite extraction is typically less selective and extracts more Fe than the oxalate extraction (Dahlgren, 1994), but it can be less efficient at extracting chelated Fe (Rennert, 2019), potentially explaining the Fe_o/Fe_d ratio > 1.

Exchangeable cations were extracted from field moist samples using a 0.0166 M cobalt hexamine (Cohex; $[Co(NH_3)_6]Cl_3$) extraction (Aran et al., 2008). Pre-testing demonstrated that this extraction was the least aggressive towards carbonates (data not shown). Cation exchange capacity (CEC_{SUM}) was calculated as the sum of extracted exchangeable cations ($cmol_c$ kg^{-1}), excluding H^+. Ca was also quantified in several other soil extracts including, in order of expected increasing extraction strength: deionised water (1:4 ratio; Tirmizi et al., 2006), 2 M KCl (1:5 ratio; Keeney and Nelson, 1982), 0.05 M disodium EDTA (1:20 ratio; Lo and Yang, 1999) and 0.5 M $CuCl_2$ extraction (1:10 ratio; Barra et al., 2001). All extracts were vacuum-filtered (0.45 μm) and diluted with 2% HNO_3 prior to analysis on an ICP-OES (Perkin Elmer Optima 8300 Inductively Coupled Plasma–optical Emission Spectrometer).

2.3. Statistical analyses of soil variables

The effects of $CaCO_3$ on soil variables were investigated using linear mixed models in SAS 9.4™. The estimation method was set to restricted (residual) maximum likelihood. Conditional residuals were plotted against predicted values to evaluate deviations from homoscedasticity and goodness of fit. Residuals were also checked for normality with QQ-plots (Galecki and Burzykowski, 2015). The significance of fixed effects was evaluated using type III F-tests. The denominators' degrees of freedom were computed using the Satterthwaite adjustment (Satterthwaite, 1946). For significant fixed effects, comparison of means was carried out using t-tests without multiple inference adjustment (Webster, 2007). The alpha level of significance was set at $\alpha = 0.05$ for all tests. All reported means are conditional least-square means ± the standard error of the mean (SEM). Means for profiles are the unweighted average of sampling intervals.

Models included site ($CaCO_3$-bearing or free), depth classes and their interaction as fixed effects. Observations were blocked by profile and a different variance was computed for each site since observations from the $CaCO_3$-bearing site typically had a higher dispersion than those from the $CaCO_3$-free site. For extractable Fe, dispersion was also higher for surface samples and the variance was additionally allowed to vary with depth. To account for the autocorrelation of observations within profiles, depth was set as a repeated measure effect with a first-order autoregressive covariance structure. Choice of covariance structure was made based on the Bayesian Information Criteria.

A Pearson's correlation coefficient heat map was created to explore linear associations between variables using the Corrplot Package (Wei and Simko, 2017) in R (2019). Variables in the heat map were ordered hierarchically into two separate groups using the complete-linkage method (Sørensen, 1948). A principal component analysis (PCA) was conducted on the correlation matrix to synthesise relationships between variables. A factor analysis was completed on the first 5 principal components (accounting for > 82% of variance) using a quartimax orthogonal rotation (Neuhaus and Wrigley, 1954). The purpose of the quartimax rotation is to minimise the number of original variables associated with each factor to simplify interpretation. Observations were then plotted according to their factor 1 and 2 scores in Matlab®.

Finally, differences in the shape of the depth curve of SOC between the sites were explored by examining scatterplots of SOC versus depth. Linear regressions were fitted to the data for each site. A higher root mean square error (RMSE) was considered as an indication of lack-of-fit (departure from the linear trend). Residuals from the linear regression were also tested for normality using the Shapiro-Wilk test, with departures from normality used as another indicator of deviation from the linear trend.

3. Results

3.1. Soil texture, composition and silicate mineralogy

Soil texture was similar between the two sites (Fig. 2). All samples had a silty-loam texture and were comprised of six predominant textural populations (Suppl. Fig. 1). There was slightly less silt at the $CaCO_3$-free site than at the $CaCO_3$-bearing site (67.3 ± 0.7% versus 74.1 ± 0.4%), and consequently more sand- (15 ± 0.8% versus 10.6 ± 0.5%) and clay-sized particles (17.8 ± 0.3% versus 15.3 ± 0.3%). The surficial samples of F1 and F2 (F1.1, F2.1, F2.2 and F2.3) as well as one deep sample (F2.6) had a more pronounced peak in the fine sand population (Suppl. Fig. 1), which occurred at the expense of fine silt populations.

Major elemental compositions were mostly similar at both sites (Suppl. Table 1). Ti and other transition/post-transition metals were largely invariant. The main differences pertained to Ca, which was approximately an order of magnitude higher at the $CaCO_3$-bearing site (14.7 ± 3.3 g kg^{-1}) than at the $CaCO_3$-free site (1.9 ± 0.2 g kg^{-1}).

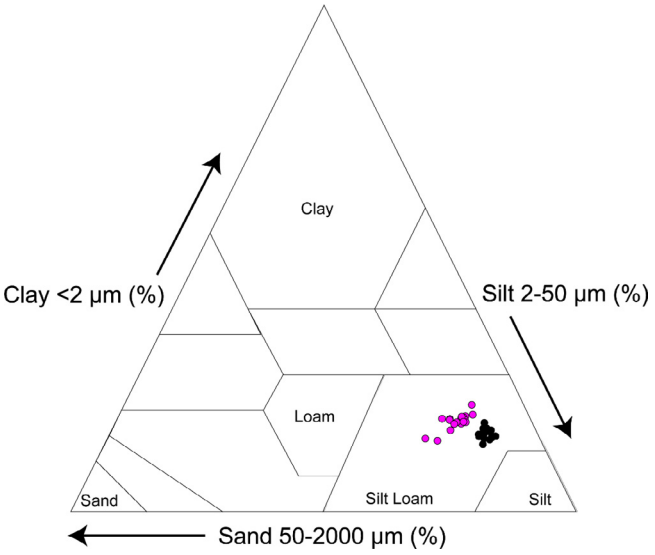

Fig. 2. Texture of samples from the $CaCO_3$-free (fuchsia dots) and $CaCO_3$-bearing (black dots) profiles.

There was a corresponding decrease in Si at the $CaCO_3$-bearing site (299.8 ± 1.5 g kg^{-1}), relative to the $CaCO_3$-free site (318.3 ± 3.4 g kg^{-1}). There were also small differences in the amounts of other elements including Mg and P, which were slightly higher at the $CaCO_3$-bearing site (14.9 ± 0.1 g kg^{-1} Mg; 4.9 ± 0.8 g kg^{-1} P) than at the $CaCO_3$-free site (12.7 ± 0.3 g kg^{-1} Mg; 1.4 ± 0.1 g kg^{-1} P). K was also marginally higher at the $CaCO_3$-bearing site (26.9 ± 0.3 g kg^{-1} versus 23.4 ± 0.9 g kg^{-1}), while Na was slightly higher at the $CaCO_3$-free site (7.8 ± 0.0 g kg^{-1} versus 6.4 ± 0.1 g kg^{-1}). Overall, the main difference in major elements composition between the sites consisted of an increase in Ca at the expense of Si in the $CaCO_3$-bearing profiles.

Silicate mineralogy was also similar between the $CaCO_3$-bearing and $CaCO_3$-free sites (Suppl. Table 2). Both sites had a bulk mineralogy that was predominated by quartz (38–41%) and phyllosilicates (42–44%), with small amounts of Na-plagioclase (5%), K-feldspar (2%) and goethite (1%), while 8% of the diffraction signal remained unquantified. Average Na-plagioclase content was slightly higher at the $CaCO_3$-free site (6.1 ± 0.2%) relative to the $CaCO_3$-bearing (4.8 ± 0.3%), while average content of K-feldspar was marginally higher at the $CaCO_3$-bearing site (2.2 ± 0.1%) relative to the $CaCO_3$-free site (1.5 ± 0.2%). The phyllosilicate mineralogy was also remarkably similar between the two sites and consistent throughout the analysed profiles. The phyllosilicate population in both the randomly selected profiles (F1 and B2) was predominantly formed of chlorite and mica, with a small quantity of illite-vermiculite mixed layer minerals.

3.2. Soil pH, $CaCO_3$ and Ca forms

Soil pH was higher at the $CaCO_3$-bearing site (range = 5–6.5) than the $CaCO_3$-free (range = 4–4.6). pH also increased significantly with depth at both sites (Table 1). The amount of $CaCO_3$ equivalent material (CCE) was below detectable limits in profiles from the $CaCO_3$-free site. Profiles from the $CaCO_3$-bearing site typically contained about 0.5% reactive CCE and 0.8% total CCE (Fig. 3), except for four samples, also identified by XRD, which contained several percent of $CaCO_3$. These four samples consisted of two surficial samples (B1.1, B1.2) and two of the deepest samples (B2.6, B3.7). The overall proportion of reactive carbonates, operationally-defined as having reacted with 0.4 M acetic acid in under 1 h, was high (74.4 ± 3.7% average; Suppl. Table 2).

As with total Ca, extractable Ca was approximately an order of magnitude higher at the $CaCO_3$-bearing than at the $CaCO_3$-free site

Table 1
Selected properties of the study profiles at the Nant valley. Profiles F1, F2 and F3 are Eutric Cambisols ($CaCO_3$-free) and profiles B1, B2 and B3 are Cambic Phaeozems ($CaCO_3$-bearing).

Sample name	Depth intervals (cm)	Genetic Horizons	pH	Al_{Exch} cmol.$_c$ kg^{-1}	Ca_{Exch} cmol.$_c$ kg^{-1}	CEC_{sum} cmol.$_c$ kg^{-1}	Ca_{Exch} saturation %	Al_{Exch} saturation %	TON %	SOC %	C:N ratio	Al_o g kg^{-1}	Fe_o g kg^{-1}	Al_d g kg^{-1}	Fe_d g kg^{-1}	Fe_o/Fe_d ratio
F1.1	0–5	Ah	4.1	0.4	6.2	7.3	84.9	5.7	0.6	4.7	8.0	2.6	13.2	3.2	24.0	0.6
F1.2	5–10	A1	4.3	0.3	4.5	5.3	84.9	6.4	0.4	3.0	7.5	2.8	12.5	3.3	23.0	0.5
F1.3	10–15	A2	4.3	0.2	4.1	4.7	87.0	5.2	0.3	2.3	7.3	3.1	11.8	3.3	22.3	0.5
F1.4	15–25	B1	4.5	0.2	3.8	4.6	82.8	5.1	0.2	1.6	6.8	2.6	12.1	3.8	24.6	0.5
F1.5	25–35	B2	4.5	0.2	4.1	4.6	89.1	4.5	0.2	1.3	6.1	2.9	11.2	3.9	25.4	0.4
F1.6	35–52	B3	4.6	0.1	4.3	4.6	93.3	1.5	0.2	0.9	5.3	2.5	9.1	3.0	22.8	0.4
F2.1	0–5	Ah	4.0	1.3	4.4	6.1	72.6	20.6	0.7	5.8	8.6	2.9	11.1	3.7	23.7	0.5
F2.2	5–10	A	4.2	1.5	1.6	3.2	48.4	45.7	0.3	2.4	7.7	3.1	11.5	3.6	22.1	0.5
F2.3	10–15	AB	4.2	1.4	1.5	3.0	50.0	44.5	0.3	2.3	7.5	2.8	10.6	3.9	23.1	0.5
F2.4	15–20	B1	4.3	1.0	1.7	2.8	61.1	36.7	0.3	2.0	7.3	2.9	10.8	3.7	21.8	0.5
F2.5	20–25	B2	4.4	0.9	1.6	2.6	62.9	34.5	0.2	1.5	6.7	2.8	9.9	3.9	23.3	0.4
F2.6	25–40	BC	4.4	0.8	1.6	2.5	63.5	33.1	0.2	1.0	5.6	2.1	7.4	3.0	19.7	0.4
F3.1	0–5	Ah	4.3	0.5	7.6	9.0	84.1	5.7	0.7	6.1	8.5	2.8	12.2	3.3	21.7	0.6
F3.2	5–10	A	4.4	0.9	3.2	4.5	71.2	19.8	0.4	3.4	7.8	3.0	11.6	3.6	21.8	0.5
F3.3	10–15	B1	4.5	0.9	2.6	3.8	66.9	23.5	0.3	2.3	7.4	2.7	9.9	3.6	21.5	0.5
F3.4	15–20	B2	4.4	1.1	1.7	3.0	56.4	34.8	0.3	2.0	7.3	3.0	10.6	4.3	24.6	0.4
F3.5	20–25	B3	4.5	1.1	1.9	3.2	58.1	33.8	0.2	1.7	7.4	3.2	10.5	4.1	22.9	0.5
F3.6	25–40	BC	4.5	1.1	1.7	3.1	54.3	35.9	0.2	1.5	7.5	3.2	10.1	3.8	20.5	0.5
B1.1	0–5	Ah1	6.3	0	23.2	23.7	97.6	0.0	0.8	7.7	9.2	0.9	13.1	0.9	24.7	0.5
B1.2	5–10	Ah2	6.4	0	23.0	23.4	98.4	0.0	0.8	6.8	8.9	1.0	14.0	1.0	25.4	0.6
B1.3	10–15	ABh	6.3	0	20.3	20.6	98.5	0.0	0.6	5.3	8.7	1.2	15.3	1.0	24.5	0.6
B1.4	15–20	Bh	6.4	0	16.9	17.2	98.4	0.0	0.5	4.3	8.5	1.4	17.9	1.2	26.8	0.7
B1.5	20–25	B1	6.4	0	15.2	15.5	98.3	0.0	0.4	3.4	8.3	1.2	15.3	1.2	26.3	0.6
B1.6	25–40	B2	6.3	0	11.8	12.0	98.2	0.0	0.3	2.3	7.8	1.3	13.8	1.4	29.9	0.5
B2.1	0–5	Ah1	5.7	0	23.5	23.8	98.7	0.0	0.9	8.3	9.2	1.6	17.6	1.3	20.2	0.9
B2.2	5–10	Ah2	5.7	0	18.4	18.6	98.8	0.0	0.8	7.3	9.3	1.6	20.8	1.5	25.1	0.8
B2.3	10–15	ABh	5.8	0	18.8	19.1	98.9	0.0	0.7	6.1	9.2	1.7	21.5	1.5	26.0	0.8
B2.4	15–20	Bh1	5.8	0	16.9	17.3	97.6	0.0	0.5	5.1	9.4	1.7	22.4	1.5	25.3	0.9
B2.5	20–25	Bh2	5.9	0	14.6	14.7	98.9	0.0	0.4	4.1	9.5	1.6	20.9	1.6	30.1	0.7
B2.6	25–40	BC	6.5	0	12.8	13.1	98.0	0.0	0.3	2.7	9.0	0.9	15.5	1.0	22.1	0.7
B3.1	0–5	Ah1	5.0	0	13.5	14.5	93.0	0.0	1.1	9.4	8.8	2.0	21.4	1.7	17.4	1.2
B3.2	5–10	Ah2	5.3	0	11.3	12.0	94.4	0.0	0.6	5.3	8.9	2.0	20.8	1.8	25.6	0.8
B3.3	10–15	ABh	5.1	0	12.3	12.9	95.3	0.0	0.5	5.1	9.4	1.9	21.1	1.8	26.3	0.8
B3.4	15–20	Bh	5.2	0	13.4	14.4	93.2	0.0	0.5	4.5	9.4	1.9	26.7	1.6	27.5	1.0
B3.5	20–25	B1	5.3	0	12.5	12.9	97.0	0.0	0.4	3.8	8.8	1.6	17.9	1.6	26.6	0.7
B3.6	25–30	B2	5.2	0	12.1	12.5	96.8	0.0	0.4	3.4	9.0	1.3	14.2	1.5	26.7	0.5
B3.7	30–37	BC	6.4	0	12.0	12.3	97.7	0.0	0.3	2.4	8.6	0.9	12.1	1.2	25.4	0.5

Genetic horizons; characterised according to FAO (2006).
Ca_{Exch}, Al_{Exch}: exchangeable Ca and Al.
CEC_{sum}: cation exchange capacity calculated as the sum of exchangeable cations, not including H^+.
TON, SOC and C:N ratio: total nitrogen, soil organic carbon and the ratio of the two
Fe_o, Al_o: oxalate-extractable Fe and Al.
Fe_d, Al_d: dithionite-extractable Fe and Al.

(Fig. 4). CEC_{SUM} was also higher at the $CaCO_3$-bearing (16.6 ± 1.9 cmol$_c$ kg^{-1}) than at the $CaCO_3$-free site (4.3 ± 0.6 cmol$_c$ kg^{-1}). This difference reflected the higher Ca_{Exch} content (Suppl. Fig. 2) at the $CaCO_3$-bearing site (16.1 ± 2.1 cmol$_c$ kg^{-1}) relative to the $CaCO_3$-free site (3.2 ± 0.8 cmol$_c$ kg^{-1}), as Ca was the predominant exchangeable cation at both sites. The Ca saturation of the exchange complex was high at both sites, but was greatest and had a smaller range at the $CaCO_3$-bearing site (93–99%) than at the $CaCO_3$-free site (48–93%). This difference was reflected in corresponding increases in Al saturation, as exchangeable Al (Al_{Exch}) was consistently detected at the $CaCO_3$-free site only.

Extraction efficiency of Ca increased in the order of H_2O < KCl ≈ Cohex < EDTA < $CuCl_2$. 2 M KCl extracted similar amounts of Ca as 0.0166 M Cohex at both sites, indicating that these two extracts effectively targeted the classical, exchangeable pool. The EDTA and $CuCl_2$ also extracted the exchangeable Ca pool at the $CaCO_3$-free site (Fig. 4), but extracted more Ca at the $CaCO_3$-bearing site, particularly in the samples with higher $CaCO_3$ contents.

3.3. Multivariate exploration of texture and mineralogy

Correlation analysis (Fig. 5) showed that there was a strong positive correlation between $CaCO_3$ and total Ca. There was also a strong positive correlation between CEC_{SUM} and Ca_{Exch}. On the other hand, there was a strong anti-correlation between Ca_{Exch}/Ca saturation and Al_{Exch}/Al saturation. Strong anti-correlations were also detected between fine silt and fine sand/clay contents, reflecting the fact that soil texture was dominated by silt populations, which exerted a 'dilution' effect (Bern, 2009) on other size classes (simplex behaviour). Total Mg and total Ca were also significantly anti-correlated with changes in total Si, which dominated major element composition, highlighting another 'dilution' effect.

A PCA (Suppl. Fig. 3A) followed by a factor analysis (Suppl. Fig. 3B) demonstrated that sites were clearly split along multivariate factor 1 (Suppl. Fig. 3C). This factor represented the abundance of Ca (as shown by the correlation with total Ca, $CaCO_3$ and Ca_{Sat}) and the anti-correlation between total Ca / Mg and total Si / quartz. The second factor

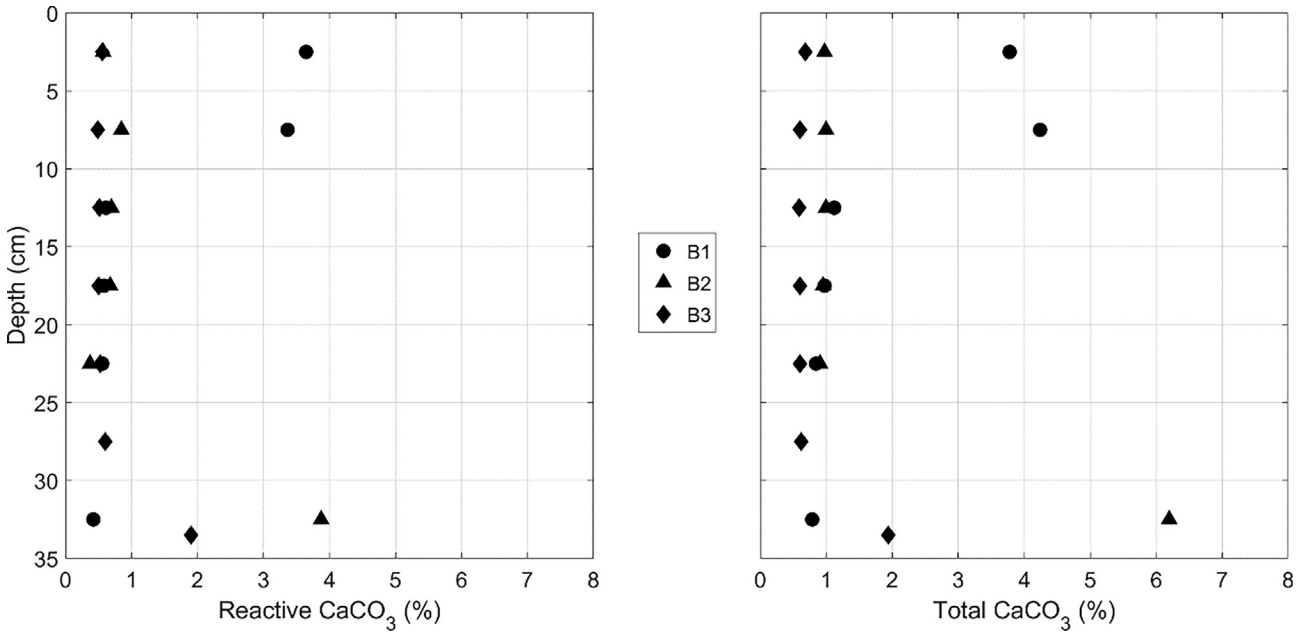

Fig. 3. Reactive and total contents of calcium carbonate equivalent for $CaCO_3$-bearing profiles (B1, B2, B3). Calcium carbonate equivalent contents were below the limits of detection at the $CaCO_3$-free site.

was a proxy for texture. There was no difference between sites along this factor, except for the fact that observations from the $CaCO_3$-free site showed a higher dispersion (had both lower and higher scores than observations from the $CaCO_3$-bearing site). Thus, overall differences in texture and silicate mineralogy were relatively small, but there were clear differences related to the presence or absence of $CaCO_3$, which differentiated the sites (Suppl. Fig. 3C).

3.4. Organic matter and free Al and Fe

Al_o was lower at the $CaCO_3$-bearing site (1.5 ± 0.2 g kg^{-1}) than at the $CaCO_3$-free (2.8 ± 0.2 g kg^{-1}), and did not vary with depth. Al_o displayed a strong negative correlation with pH (Fig. 6; R^2 = 0.88). Al_d was generally equal to Al_o at the $CaCO_3$-bearing site, suggesting that dithionite and oxalate quantitatively extracted the same Al pool. Al_d was however higher than Al_o at the $CaCO_3$-free site, suggesting that some Al substitution (Al incorporation into the crystalline lattice of Fe oxides dissolved by the dithionite treatment) had taken place.

Extractable Fe was an order of magnitude higher than extractable Al at both sites. There was an effect of depth on the amount of Fe_o, which became larger mid-profile (15–20 cm). There was also a significant influence of depth on the proportion of oxalate-to-dithionite extractable Fe, which typically decreased with depth, except for samples at 15–20 cm (Fig. 7). Both dithionite and oxalate extractable Fe were higher at the $CaCO_3$-bearing site (Fe_d = 25.3 ± 0.3 g kg^{-1}; Fe_o = 18.2 ± 1.6 g kg^{-1}) than at the $CaCO_3$-free (Fe_d = 22.7 ± 0.4 g kg^{-1}; Fe_o = 10.9 ± 0.5 g kg^{-1}). The proportion of oxalate-to-dithionite extractable Fe was also higher at the $CaCO_3$-bearing site (0.73 ± 0.06) than the $CaCO_3$-free (0.48 ± 0.01). Thus, extractable Fe was more abundant and predominantly found in poorly crystalline or monomeric forms at the $CaCO_3$-bearing site.

Organic carbon contents of AGB were similar between the sites (Suppl. Fig. 4). AGB estimates, reported in Blattner, were 281 g m^{-2} at the $CaCO_3$-bearing sites and 350 g m^{-2} at the $CaCO_3$-free site. We thus calculated that above-ground C amounted to 110 g C m^{-2} at the $CaCO_3$-bearing site and 140 g C m^{-2} at the $CaCO_3$-free site.

In contrast, SOC was approximately twice as high at the $CaCO_3$-bearing site (5.2 ± 0.2%) compared to the $CaCO_3$-free soils (2.5 ± 0.1%), decreasing systematically with depth at both sites (Fig. 8). SOC decreased with depth more linearly at the $CaCO_3$-bearing site (RMSE of linear relationship = 3.36) than at the $CaCO_3$-free (RMSE = 6.76; Suppl. Fig. 5A:C). The distribution of residuals from the linear relationship between SOC and depth at the $CaCO_3$-bearing site were normally distributed (p = 0.69), while the residuals at the $CaCO_3$-free site were not (p = 0.02). Total nitrogen followed an almost identical pattern and was thus higher at the $CaCO_3$-bearing site

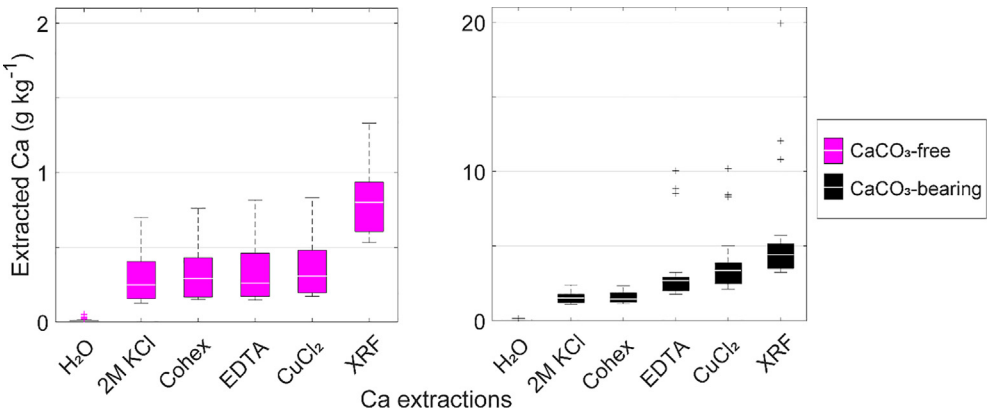

Fig. 4. Calcium content of $CaCO_3$-free and $CaCO_3$-bearing profiles. From left to right are deionised water, 2 M potassium chloride, 0.0166 M cobalt hexamine (Cohex), 0.05 M disodium EDTA and 0.5 M copper chloride extracts measured on an inductively coupled plasma optical emission spectrometer and total contents measured with X-ray fluorescence (XRF). Y scales differ by an order of magnitude. Bottom and top edges of the boxes in the box plot represent the 25th and 75th percentiles, the middle bars represent the median. Whiskers represent the range of most extreme data points not considered as outliers, while '+' represent outliers defined as values outside of the ± 2.7 standard deviation range.

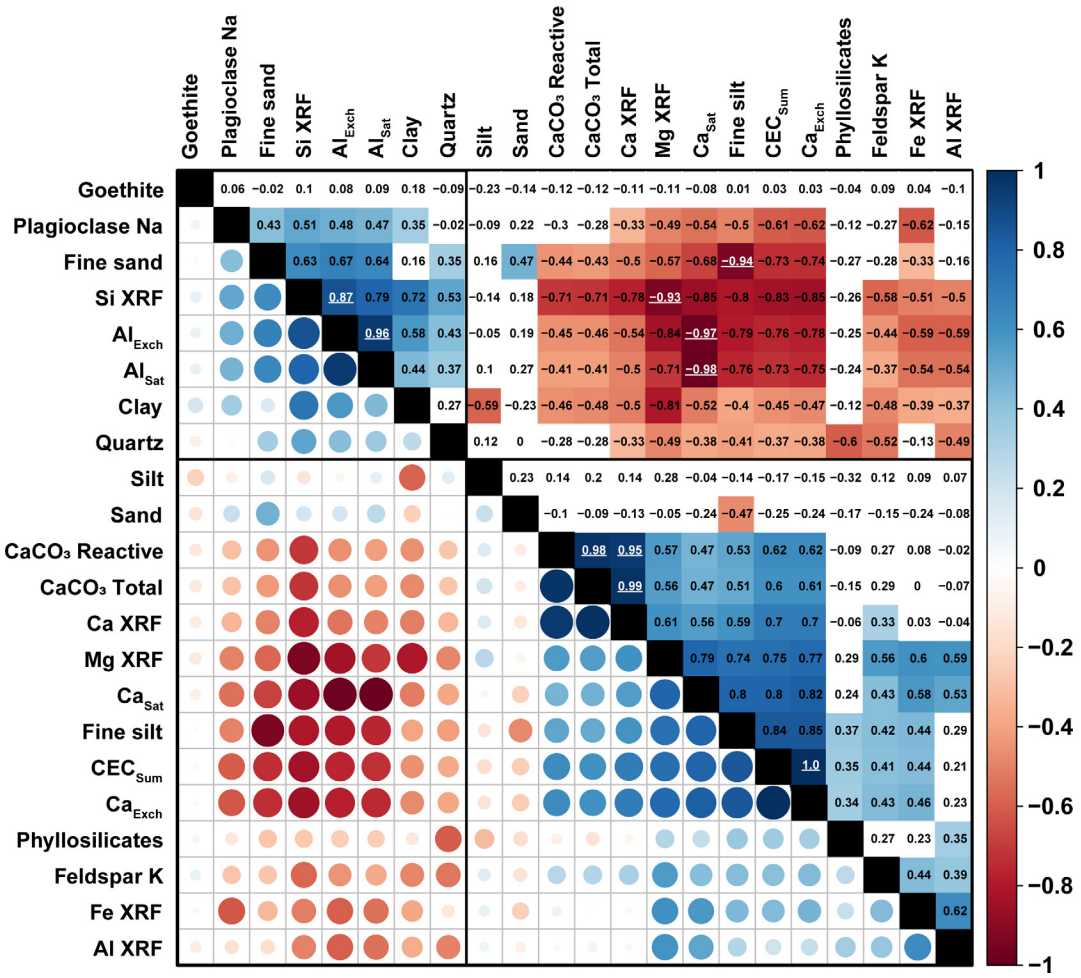

Fig. 5. Pearson's correlation coefficient matrix divided into two parts. The lower-left part represents the value of positive (blue) and negative (red) correlation coefficients as variations in circle size. The upper-right part displays the actual Pearson's correlation coefficients. Boxes in the upper-right part are only coloured in if the relationship is significant ($\alpha = 0.05$). Strong correlation coefficients are highlighted in white and underlined ($r \geq 0.85$). The different variables are hierarchically clustered using the complete-linkage method into two separate groups, highlighted with black rectangles in bold. (For interpretation of the references to colour in this figure legend, the reader is referred to the web version of this article.)

(0.6 ± 0.0%) than at the $CaCO_3$-free (0.3 ± 0.0%). Total N also decreased systematically with depth. The C:N ratio was low at both sites (Suppl. Fig. 6). It was slightly higher at the $CaCO_3$-bearing site (8.9 ± 0.3) than at the $CaCO_3$-free site (7.2 ± 0.3), but the differences were very small.

4. Discussion

In this study, we aimed to determine the influence of small amounts of $CaCO_3$ on pedogenesis and biogeochemistry. We used a naturally occurring gradient in $CaCO_3$ content affecting otherwise highly similar

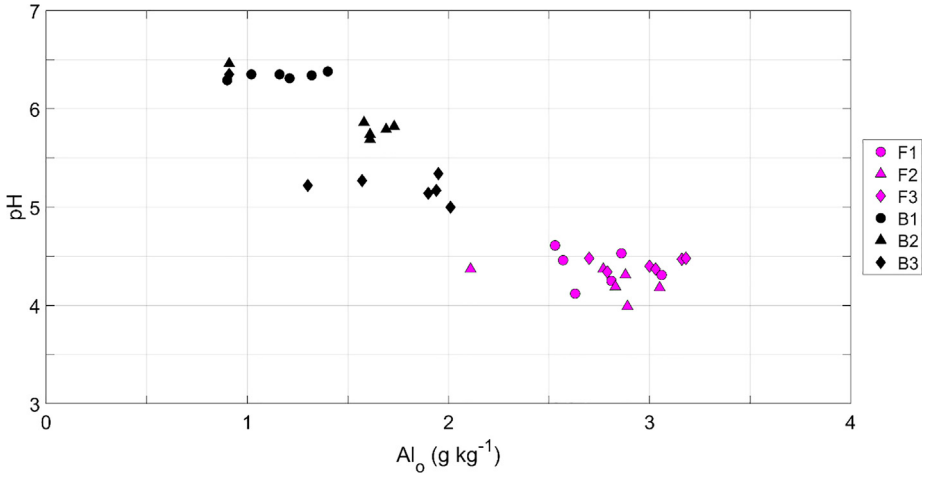

Fig. 6. Negative relationship between soil pH and oxalate extractable aluminium (Al_o) for $CaCO_3$-free (F1, F2, F3) and $CaCO_3$-bearing profiles (B1, B2, B3).

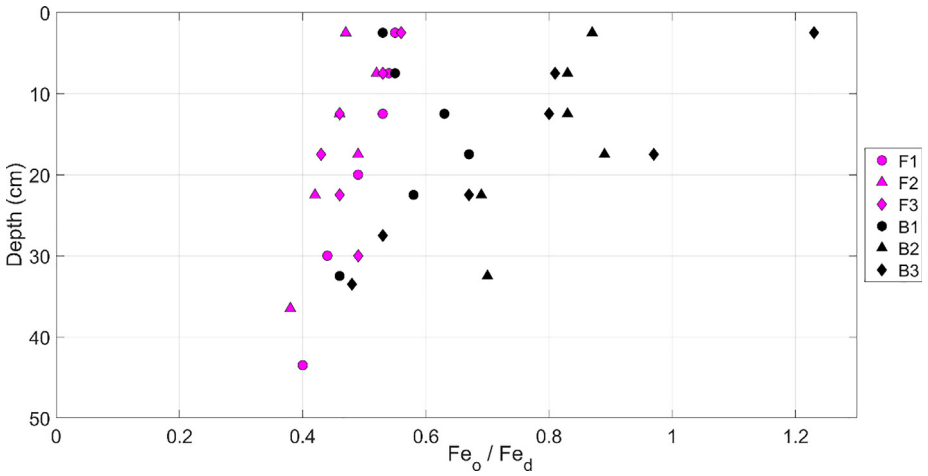

Fig. 7. Ratio between oxalate (Fe_o) and dithionite (Fe_d) extractable Fe contents for $CaCO_3$-free (F1, F2, F3) and $CaCO_3$-bearing (B1, B2, B3) profiles.

soils. With the constraints of finding near-identical soil forming conditions, we retained only 6 profiles, which were all located in close proximity (< 500 m). With such a low sample size, two things must be kept in mind:

(1) The generalisation of findings to other soils is not supported by this experimental layout (but remains possible if a detailed mechanistic understanding is attained).
(2) Only large effects could be statistically detected.

It was of prime importance that the soils be similar except for the presence/absence of $CaCO_3$, in order to isolate the role of $CaCO_3$ from other pedogenic variables. Homogeneity of parent material was of particular importance and is discussed further below.

4.1. Parent material

Textural analysis confirmed field observations that the parent material was homogeneous, with all samples plotting within the silt loam class. Both sites had 6 predominant textural populations, the modes of which are commonly encountered in previously glaciated landscapes (Boulton, 1978). The total composition of major elements were also similar between the sites. There was however a clear increase in Ca at the $CaCO_3$-bearing sites due to the presence of $CaCO_3$. This increase in Ca also caused a proportional decrease in Si (silicates) due to a 'dilution' effect. The slightly higher Mg content at the $CaCO_3$-bearing site could be due to partial substitution of Mg for Ca in calcite (0.3% in measured coarse fragments) or the presence of poorly crystalline dolomite and accessory ferromagnesian minerals. P was also slightly elevated at the $CaCO_3$-bearing site, which could be a reflection of its lower mobility in Ca-bearing geochemical environments (von Wandruszka, 2006). K was marginally higher at the $CaCO_3$-bearing site and Na was higher at the $CaCO_3$-free site, which corresponded to small differences in K-feldspar and Na-plagioclase abundances, respectively. Relatively immobile elements such as Ti and other transition / post-transition metals showed near-uniform distribution between samples from different profiles, collected at different depths, pointing to a common source for parent materials. Neoformation of pedogenic clay was incipient at both sites, with only small quantities of an illite-vermiculite mixed-layer mineral detected (Egli et al., 2003; Zollinger et al., 2013). Most of the phyllosilicates originated from the physical disintegration of shale components of the Morcles Nappe.

While the siliceous component of the parent material at the two sites was near-homogeneous, there was a natural variation in $CaCO_3$ present at the alpage. This was likely due to the variability in $CaCO_3$ content of surficial deposits issued from the Morcles Nappe. The Grand Muveran cliffs protruding on the southeast side of the study area contain calcareous material, while the slopes of La Chaux on the northwest side essentially consist of shales. Thus, during the partial alluvio-colluvial reworking of the moraine and slope deposits that occurred following deglaciation, some carbonates were added to the $CaCO_3$-bearing site while little to no carbonates were added to the $CaCO_3$-free site.

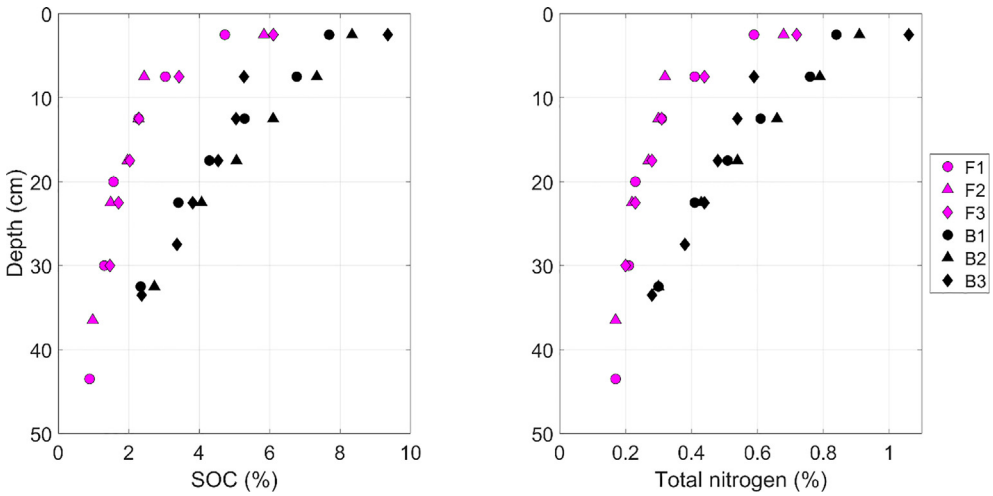

Fig. 8. Soil organic carbon (SOC) and total nitrogen contents for $CaCO_3$-free (F1, F2, F3) and $CaCO_3$-bearing (B1, B2, B3) profiles.

$CaCO_3$ was identified as being predominantly reactive at the Nant Valley (Fig. 3) by the adapted Loeppert et al. (1984) method. This method is not typically used for the measurement of reactive carbonates, but its results were in reasonable agreement with the EDTA extraction (Suppl. Fig. 7), which has been used previously for the estimation of reactive carbonates (Glover, 1961). Thus, $CaCO_3$ was most likely predominantly reactive at the $CaCO_3$-bearing site, increasing the likelihood that it would play an active role in soil biogeochemistry.

Another difference between the sites was that free Fe forms were significantly less crystalline at the $CaCO_3$-bearing profiles, relative to the $CaCO_3$-free profiles. The sorption of organic colloids (Filimonova et al., 2016; Kleber and Jahn, 2007) and cations such as Ca_{Exch} (Thompson et al., 2011), which were more abundant at the $CaCO_3$-bearing site, could have inhibited the formation of well-crystallised Fe forms. The increased pH at this site may have also indirectly influenced the crystallinity of Fe forms via its influence on their variable surface charge and their interaction with Ca_{Exch} (Schwertmann and Fechter, 1982), but this would still require further investigation. While the presence of $CaCO_3$ seemed to favour the prevalence of disordered Fe forms, the Fe_o/Fe_d ratio did not vary systematically with SOC, Ca_{Exch} or pH making it hazardous to attribute the differences in crystallinity to a single factor. It seems more likely that a mixture of indirect influences of $CaCO_3$ were involved in explaining the decreased crystallinity of Fe forms at the $CaCO_3$-bearing site.

4.2. Accumulation of SOC

Soil organic carbon was approximately twice as high at the $CaCO_3$-bearing site compared to the $CaCO_3$-free site. A potential explanation for this accumulation could involve the higher primary productivity of grasses at the $CaCO_3$-bearing site. Yet, AGB was slightly higher at the $CaCO_3$-free site relative to the $CaCO_3$-bearing site. Increased root turnover or exudation at the $CaCO_3$-bearing site could explain part of the differences in SOC, but this effect should be relatively small due to the similarities between vegetation structure at the sites (Vittoz and Gmür, 2008). Instead, it was probably the difference in the efficiency of SOC stabilisation that drove the relative accumulation of SOC observed at the $CaCO_3$-bearing site.

In a previous study, Grand et al. (2016) demonstrated that soil respiration was higher at the $CaCO_3$-bearing site than the $CaCO_3$-free site for 3 out of 4 of the measured months (July–Oct.); yet estimated heterotrophic respiration (Hanson et al., 2000) was actually lower throughout the entire measurement period, when expressed per unit SOC (Suppl. Table 3). This suggests that SOC at the $CaCO_3$-bearing site has a certain biogeochemical stability, which may be contributing towards its accumulation (Whittinghill and Hobbie, 2012). Due to similarities between the sites, this stability cannot be explained by differences in texture or clay mineralogy. Potential geochemical controls that could influence the accumulation of SOC at the Nant Valley include the prevalence of reactive Ca and Fe forms, which are discussed further below.

4.2.1. Reactive Ca forms

We found a weak positive correlation between Ca_{Exch} and SOC at our sites (Suppl. Fig. 8C), which was particularly evident in the $CaCO_3$-bearing profiles with higher pH and Ca_{Exch}. CEC_{sum} was also higher at the $CaCO_3$-bearing sites (Suppl. Fig. 8D); this was partly attributable to the higher SOC content acting as loci for cation exchange, as clay mineralogy and texture were homogeneous at the sites. Thus, the commonly observed correlation between SOC and Ca_{Exch} could partially be explained by the increase in cation exchange sites provided by SOC (Briedis et al., 2012). However, there is evidence that Ca can also influence SOC dynamics (Groffman et al., 2006; Hobbie et al., 2002; Martí-Roura et al., 2019; Minick et al., 2017; Whittinghill and Hobbie, 2012) through several mechanisms (see Rowley et al., 2018 for more details). In our study, the two-fold increase in SOC at the $CaCO_3$-bearing site supports the hypothesis that reactive Ca is causally linked to the accumulation and stabilisation of SOC. Future investigation should focus on the mechanisms by which Ca influences SOC dynamics.

4.2.2. Analysing Ca forms

Exchangeable Ca may not be the only reactive Ca pool that influences SOC. It has been hypothesised that Ca could also stabilise SOC through inner sphere complexes (Rowley et al., 2018). This is supported by chemical modelling (Iskrenova-Tchoukova et al., 2010; Kalinichev and Kirkpatrick, 2007; Sutton et al., 2005), but as of yet, there is no direct evidence of this in soils. We attempted to extract this tightly bound, 'chelated Ca' pool using selective extractions, as has been done with the selective dissolution of free Fe and Al. Our more aggressive extracts, EDTA and $CuCl_2$, yielded the same quantity of Ca as the exchangeable cations extracts (KCl/Cohex) at the $CaCO_3$-free site, but more Ca than the exchangeable cations extracts at the $CaCO_3$-bearing site. This was particularly apparent in samples with higher amounts of $CaCO_3$ and it thus seems as though both EDTA and $CuCl_2$ were aggressive towards reactive $CaCO_3$, but failed to target Ca pools other than the exchangeable pool at $CaCO_3$-free sites. Thus, the existence in soils of a tightly-bound Ca pool which is distinct from reactive $CaCO_3$, and its selective extraction, remains an open question.

4.2.3. Fe forms

It is widely established that poorly crystalline Fe forms can stabilise SOC (Kögel-Knabner et al., 2008; von Lützow et al., 2006). In our study, SOC displayed a weak positive correlation with Fe_o, which was particularly evident in the profiles with the highest amounts of extractable Fe (Suppl. Fig. 8B). The same trend was observed for the degree of crystallinity of Fe oxides (Fe_o/Fe_d; Suppl. Fig. 8A), as the amount of crystalline oxides was comparatively similar between profiles and it was mainly the amount of Fe_o that changed. The $CaCO_3$-bearing profiles displayed an increase in Fe_o/Fe_d ratio mid-profile (15–20 cm; Fig. 7), potentially due to the mobility of poorly crystalline Fe species during brief suboxic events linked to snowmelt. It is possible that this pattern had some influence over the more linear SOC decline with depth at these sites (Suppl. Fig. 5A:C). Overall, our results support a positive relation between SOC accumulation and the amount of poorly crystalline Fe.

4.2.4. Ca and Fe interactions

It is interesting to note that our data hint at some kind of interaction or competition between Ca and Fe forms (Suppl. Fig. 8A:D). Profiles B1 and B2 showed no association between SOC and Fe_o but were instead characterised by a strong correlation between SOC and Ca_{Exch}. On the contrary, in profile B3, where pH and $CaCO_3$ were slightly lower than in the other $CaCO_3$-bearing profiles, SOC was significantly related to Fe_o and much less so to Ca_{Exch}. Speculatively, we propose that some organic functional groups may interact either with exchangeable cations or with reactive oxides depending on the prevailing biogeochemical conditions (pH and the prevalence of free elements), which may lead to a change in the relative importance of SOC stabilisation mechanisms (Rasmussen et al., 2018; Rowley et al., 2018).

Furthermore, a synergistic stabilisation of dissolved organic C by poorly crystalline Fe and Ca_{Exch}, involving the formation of Fe-Ca-organic C ternary complexes, has recently been described (Sowers et al., 2018a,b). Hypothetically, this could also have exerted a positive feedback on the stabilisation of SOC at the $CaCO_3$-bearing sites (Fig. 9), as disordered Fe forms that are favoured by the higher SOC, Ca_{Exch} and pH would in turn further contribute to an accumulation of SOC, rendered particularly effective by the presence of significant amounts of extractable Ca. This potential relationship between Ca and Fe and its impacts on SOC stabilisation and accumulation should now be investigated further in Ca-rich soils.

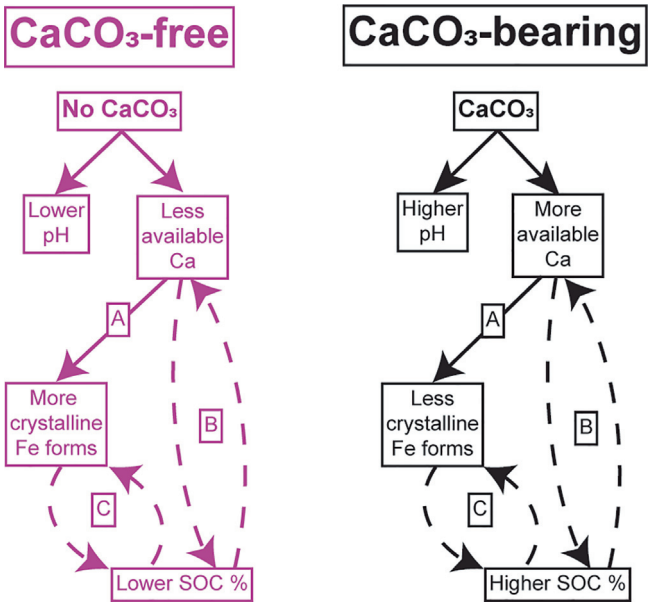

Fig. 9. A conceptual diagram of differences in biogeochemistry at the $CaCO_3$-free and $CaCO_3$-bearing sites, attributable to the cascading influence of $CaCO_3$. Direct interactions between geochemical variables are signified by straight arrows, while potential positive/negative feedback systems are signified by curved dashed arrows. The lettered interactions refer to: A) Ca-Fe interactions, where sorption of Ca by Fe oxides can prevent their further crystallisation (Thompson et al., 2011); B) Soil organic carbon (SOC)-Ca feedback loop, where SOC can be directly stabilised by Ca (Rowley et al., 2018), while SOC also provides exchange sites for the continued retention of available Ca forms; C) Fe-SOC feedback loop, where poorly crystalline Fe forms retain and stabilise SOC, while SOC can also inhibit the crystallisation of Fe forms (Kleber and Jahn, 2007).

4.3. Implications for modelling efforts

There is growing evidence that geochemical indicators are important parameters for modelling the persistence of SOC (Rasmussen et al., 2018; Vaughan et al., 2019). Indeed, models that infer SOC dynamics from clay content and climate would be unable to represent the difference in SOC content attributed here to the presence or absence of $CaCO_3$. Rasmussen et al. (2018) recently questioned the use of clay and climate as sole variables for modelling SOC and our results are in close agreement with their broader analysis of 5500 soil profiles. Models based on climate and clay content may be particularly inappropriate in situations where soil geochemistry is in disequilibrium with climate (occurrence of pedogenic inertia) and/or variations in types and crystallinity of Fe phases exist. Furthermore, modelling the depth distribution of SOC using an exponential decay function would have also misrepresented the different SOC-depth trends present at the sites, further underestimating SOC stocks at the $CaCO_3$-bearing site. These errors could however be reduced by accounting for differences in soil geochemistry and their subsequent effects on the accumulation of SOC and its depth distribution.

4.4. Synthesis – cascading biogeochemistry and the shift in geochemical controls on SOC stabilisation with pH

The divergence in biogeochemistry at the Nant Valley sites is caused by a state of pedogenic inertia, driven by the cascading influence of $CaCO_3$ dissolution (Fig. 9). The $CaCO_3$-bearing site exists in a state of disequilibrium with climate as the pedogenic threshold of $CaCO_3$ removal has not yet been breached. This threshold is unlikely to be breached in the near-future, due the presence of the adjacent calcareous cliffs and their alluvio-colluvial inputs, so that the site will likely continue to retain its Mollic nature, high pH, and base saturation (Phaeozem).

Upon weathering, reactive $CaCO_3$ buffered pH levels (Likens et al., 1998), releasing Ca_{Exch} into the soil solution. This Ca_{Exch} can stabilise SOC (Oades, 1988; Rowley et al., 2018), which likely contributed to its accumulation in the $CaCO_3$-bearing profiles (x2). The presence of $CaCO_3$ also seemed to indirectly participate in the stabilisation of poorly crystalline Fe forms, which in turn, may have exerted a positive feedback on the retention of SOC, possibly involving ternary Fe-Ca-SOC complexes (Sowers et al., 2018a,b).

In contrast, the $CaCO_3$-free profiles had a lower pH. These acidic conditions in turn seemed to favour the prevalence of more crystalline Fe oxides such as goethite and higher amounts of reactive Al forms such as Al_{Exch} and Al_o (Adams et al., 2000). This confirms the long-held notion that decreasing soil pH identifies a shift along a weathering sequence from Ca-to-Al dominated biogeochemistry (Adams et al., 2000; Slessarev et al., 2016). In turn, this shift can be linked to different SOC stabilisation mechanisms (Rasmussen et al., 2018; Rowley et al., 2018), which could be used to help model the persistence of SOC. Thus, this study further supports the notion that soil pH could be used as an efficient and parsimonious variable for improving regional models of pedogenesis, biogeochemical functioning, and even SOC stabilisation (Clarholm and Skyllberg, 2013; Rowley et al., 2018). Future studies should investigate the potential of soil pH as a widely available indicator to account for the effects of geochemistry on SOC and improving the accuracy of regional SOC estimates.

Declaration of Competing Interest

The authors declare that they have no known competing financial interests or personal relationships that could have appeared to influence the work reported in this paper.

Acknowledgements

The authors would like to acknowledge Prof. Jasquelin Pena for the discussion that led to this paper. Thanks to Dr. Pascal Vittoz for many profitable discussions regarding the vegetation at the Nant Valley and *P. dactylifera*. Thanks to Dr. Magali Matteodo, Maïté Buttet and Mélanie Delasoie for help with the sampling campaigns. Thanks to Dr. Jorge Spangenberg, Céline Blattner, Mélanie Delasoie and Franziska Fischer for help with measurements. Special thanks to the Canton de Vaud and IDYST for financially supporting this work and the "*Conseil de Coordination Scientifique du Vallon de Nant, Université de Lausanne*" for research permissions.

Appendix A. Supplementary data

Supplementary data to this article can be found online at https://doi.org/10.1016/j.geoderma.2019.114065.

References

Adams, M.L., Hawke, D.J., Nilsson, N.H.S., Powell, K.J., 2000. The relationship between soil solution pH and Al3+ concentrations in a range of South Island (New Zealand) soils. Soil Res. 38 (1), 141–154.
Adatte, T., Stinnesbeck, W., Keller, G., 1996. Lithostratigraphic and mineralogic correlations of near K/T boundary clastic sediments in northeastern Mexico: implications for origin and nature of deposition. Geol. Soc. Am. Spec. Papers 307.
Aran, D., Maul, A., Masfaraud, J.-F., 2008. A spectrophotometric measurement of soil cation exchange capacity based on cobaltihexamine chloride absorbance. C.R. Geosci. 340 (12), 865–871.
Arkley, R.J., 1963. Calculation of carbonate and water movement in soil from climatic data. Soil Sci. 96 (4), 239–248.
Austin, N., Evans, B., Herwegh, M., Ebert, A., 2008. Strain localization in the Morcles nappe (Helvetic Alps, Switzerland). Swiss J. Geosci. 101 (2), 341–360.
Bache, B.W., 1984. The role of calcium in buffering soils. Plant, Cell Environ. 7 (6), 391–395.
Bahram, M., Hildebrand, F., Forslund, S.K., Anderson, J.L., Soudzilovskaia, N.A.,

Bodegom, P.M., Bengtsson-Palme, J., Anslan, S., Coelho, L.P., Harend, H., Huerta-Cepas, J., Medema, M.H., Maltz, M.R., Mundra, S., Olsson, P.A., Pent, M., Põlme, S., Sunagawa, S., Ryberg, M., Tedersoo, L., Bork, P., 2018. Structure and function of the global topsoil microbiome. Nature 560 (7717), 233–237.
Barra, C.M., Curtius, A.J., de Campos, R.C., Perez, D.V., 2001. Evaluation of four aluminum extraction methods using selected Brazilian soils. Commun. Soil Sci. Plant Anal. 32 (11–12), 1969–1980.
Barta, G., Bradák, B., Novothny, Á., Markó, A., Szeberényi, J., Kiss, K., Kovács, J., 2018. The influence of paleogeomorphology on the stable isotope signals of paleosols. Geoderma 330, 221–231.
Bartlett, R.J., James, B.R., 1993. Redox chemistry of soils. Adv. Agron. 50 (50), 151–208.
Bern, C.R., 2009. Soil chemistry in lithologically diverse datasets: the quartz dilution effect. Appl. Geochem. 24 (8), 1429–1437.
Bindschedler, S., Cailleau, G., Verrecchia, E., 2016. Role of fungi in the biomineralization of calcite. Minerals 6 (2), 41.
Boulton, G.S., 1978. Boulder shapes and grain-size distributions of debris as indicators of transport paths through a glacier and till genesis. Sedimentology 25 (6), 773–799.
Briedis, C., de Moraes Sá, J.C., Caires, E.F., de Fátima Navarro, J., Inagaki, T.M., Boer, A., de Oliveira Ferreira, A., Neto, C.Q., Canalli, L.B., Bürkner dos Santos, J., 2012. Changes in organic matter pools and increases in carbon sequestration in response to surface liming in an Oxisol under long-term no-till. Soil Sci. Soc. Am. J. 76 (1), 151–160.
Bryan, W.H., Teakle, L.J.H., 1949. Pedogenic inertia: a concept in soil science. Nature 164, 969.
Cailleau, G., Braissant, O., Dupraz, C., Aragno, M., Verrecchia, E.P., 2005. Biologically induced accumulations of CaCO3 in orthox soils of Biga, Ivory Coast. Catena 59 (1), 1–17.
Cerling, T.E., 1984. The stable isotopic composition of modern soil carbonate and its relationship to climate. Earth Planet. Sci. Lett. 71 (2), 229–240.
Chadwick, O.A., Chorover, J., 2001. The chemistry of pedogenic thresholds. Geoderma 100 (3–4), 321–353.
Clarholm, M., Skyllberg, U., 2013. Translocation of metals by trees and fungi regulates pH, soil organic matter turnover and nitrogen availability in acidic forest soils. Soil Biol. Biochem. 63, 142–153.
Dahlgren, R.A., 1994. Quantification of allophane and imogolite. In: J.E. Amonette, Y.L. W. (Eds.), Quantitative methods in soil mineralogy. Soil Science Society of America, Madison, WI, pp. 430–451.
Edwards, A.P., Bremner, J.M., 1967. Microaggregates in soil. J. Soil Sci. 18 (1), 64.
Egli, M., Mirabella, A., Fitze, P., 2003. Formation rates of smectites derived from two Holocene chronosequences in the Swiss Alps. Geoderma 117 (1), 81–98.
ESRI, 2019. World Imagery and national geographic base maps. ESRI, pp. World imagery "Sources: Esri, DigitalGlobe, GeoEye, i-cubed, USDA FSA, USGS, AEX, Getmapping, Aerogrid, IGN, IGP, swisstopo, and the GIS User Community" / National geographic "Sources: National Geographic, Esri, DeLorme, HERE, UNEP-WCMC, USGS, NASA, ESA, METI, NRCAN, GEBCO, NOAA, iPC".
FAO, 2006. Guidelines for soil description. FAO - Food and Agriculture Organization of the United Nations, Rome.
Filimonova, S., Kaufhold, S., Wagner, F.E., Häusler, W., Kögel-Knabner, I., 2016. The role of allophane nano-structure and Fe oxide speciation for hosting soil organic matter in an allophanic Andosol. Geochimica et Cosmochimica Acta 180, 284-302.
Galecki, A., Burzykowski, T., 2015. Linear mixed-effects models using R: A step-by-step approach. Springer New York, New York.
Gao, Y., Tian, J., Pang, Y., Liu, J., 2017. Soil inorganic carbon sequestration following afforestation is probably induced by pedogenic carbonate formation in Northwest China. Front. Plant Sci. 8 (1282).
Glover, E.D., 1961. Method of solution of calcareous materials using the complexing agent, EDTA. J. Sedimentary Res. 31 (4), 622–626.
Grand, S., Rubin, A., Verrecchia, E.P., Vittoz, P., 2016. Variation in soil respiration across soil and vegetation types in an alpine valley. PLoS ONE 11 (9), e0163968.
Grant, C.D., Dexter, A.R., Oades, J.M., 1992. Residual effects of additions of calcium compounds on soil structure and strength. Soil Tillage Res. 22 (3), 283–297.
Groffman, P.M., Fisk, M.C., Driscoll, C.T., Likens, G.E., Fahey, T.J., Eagar, C., Pardo, L.H., 2006. Calcium additions and microbial nitrogen cycle processes in a Northern Hardwood Forest. Ecosystems 9 (8), 1289–1305.
Hanson, P.J., Edwards, N.T., Garten, C.T., Andrews, J.A., 2000. Separating root and soil microbial contributions to soil respiration: A review of methods and observations. Biogeochemistry 48 (1), 115–146.
Harris, D., Horwath, W.R., van Kessel, C., 2001. Acid fumigation of soils to remove carbonates prior to total organic carbon or carbon-13 isotopic analysis. Soil Sci. Soc. Am. J. 65 (6), 1853–1856.
Hasinger, O., Spangenberg, J.E., Millière, L., Bindschedler, S., Cailleau, G., Verrecchia, E.P., 2015. Carbon dioxide in scree slope deposits: A pathway from atmosphere to pedogenic carbonate. Geoderma 247–248, 129–139.
Hobbie, S.E., Miley, T.A., Weiss, M.S., 2002. Carbon and nitrogen cycling in soils from acidic and nonacidic tundra with different glacial histories in Northern Alaska. Ecosystems 5 (8), 0761–0774.
Iskrenova-Tchoukova, E., Kalinichev, A.G., Kirkpatrick, R.J., 2010. Metal cation complexation with natural organic matter in aqueous solutions: molecular dynamics simulations and potentials of mean force. Langmuir 26 (20), 15909–15919.
IUSS Working Group WRB, 2015. World reference base for soil resources 2014, update 2015. No 106. FAO, Rome.
Jenny, H., 1941. Factors of soil formation: a system of quantitative pedology. McGraw-Hill, University of Michigan.
Kalinichev, A.G., Kirkpatrick, R.J., 2007. Molecular dynamics simulation of cationic complexation with natural organic matter. Eur. J. Soil Sci. 58 (4), 909–917.
Keeney, D.R., Nelson, D.W., 1982. Nitrogen in organic forms. In: A.L.e.a. Page (Ed.), Methods of soil analysis. American Society of Agronomy, Madison, WI.
Kleber, M., Jahn, R., 2007. Andosols and soils with andic properties in the German soil taxonomy. J. Plant Nutr. Soil Sci. 170 (3), 317–328.
Kögel-Knabner, I., Guggenberger, G., Kleber, M., Kandeler, E., Kalbitz, K., Scheu, S., Eusterhues, K., Leinweber, P., 2008. Organo-mineral associations in temperate soils: Integrating biology, mineralogy, and organic matter chemistry. J. Plant Nutr. Soil Sci.-Zeitschrift Fur Pflanzenernahrung Und Bodenkunde 171 (1), 61–82.
Kowalska, J.B., Zaleski, T., Józefowska, A., Mazurek, R., 2019. Soil formation on calcium carbonate-rich parent material in the outer Carpathian Mountains – a case study. Catena 174, 436–451.
Likens, G.E., Driscoll, C.T., Buso, D.C., Siccama, T.G., Johnson, C.E., Lovett, G.M., Fahey, T.J., Reiners, W.A., Ryan, D.F., Martin, C.W., Bailey, S.W., 1998. The biogeochemistry of calcium at Hubbard Brook. Biogeochemistry 41 (2), 89–173.
Lo, I.M.C., Yang, X.Y., 1999. EDTA extraction of heavy metals from different soil fractions and synthetic soils. Water Air Soil Pollut. 109 (1), 219–236.
Loeppert, R.H., Hallmark, C.T., Koshy, M.M., 1984. Routine procedure for rapid determination of soil carbonates. Soil Sci. Soc. Am. J. 48 (5), 1030–1033.
Loeppert, R.H., Suarez, D.L., 1996. Carbonate and gypsum. In: D.L. Sparks, A.L. Page, P.A. Helmke, R.H. Loeppert (Eds.), Methods of soil analysis part 3—chemical methods. SSSA Book Series. Soil Science Society of America, American Society of Agronomy, Madison, WI.
Martí-Roura, M., Hagedorn, F., Rovira, P., Romanyà, J., 2019. Effect of land use and carbonates on organic matter stabilization and microbial communities in Mediterranean soils. Geoderma 351, 103–115.
McKeague, J.A., Day, D.H., 1966. Dithionite- and oxalate-extractable Fe and Al as aids in differentiating various classes of soils. Can. J. Soil Sci. 46 (1), 13.
Mehra, O.P., Jackson, M.L., 1958. Iron oxide removal from soils and clays by a dithionite-citrate system buffered with sodium bicarbonate. Clays Clay Miner. 7 (1), 317–327.
Minick, K.J., Fisk, M.C., Groffman, P.M., 2017. Soil Ca alters processes contributing to C and N retention in the Oa/A horizon of a northern hardwood forest. Biogeochemistry 1–15.
Muhs, D.R., 1984. Intrinsic thresholds in soil systems. Phys. Geogr. 5 (2), 99–110.
Muneer, M., Oades, J.M., 1989. The role of Ca-organic interactions in soil aggregate stability.3. Mechanisms and models. Aust. J. Soil Res. 27 (2), 411–423.
Neuhaus, J.O., Wrigley, C., 1954. The quartimax rotation. Br. J. Statistical Psychol. 7 (2), 81–91.
Oades, J.M., 1988. The retention of organic matter in soils. Biogeochemistry 5 (1), 35–70.
Pansu, M., Gautheyrou, J., 2006. Handbook of Soil Analysis: Mineralogical, Organic and Inorganic Methods. Springer, Berlin; New York.
Perret, A., Martin, S., 2014. Carte Géomorphologique Du Vallon De Nant & Étude De La Marge Proglaciaire Du Glacier Des Martinets. Bulletin Annuel De La Murithienne 132, 69–82.
R, 2019. R: A language and environment for statistical computing. In: R.C. Team (Ed.). R Foundation for Statistical Computing, Vienna, Austria.
Ramnarine, R., Voroney, R.P., Wagner-Riddle, C., Dunfield, K.E., 2011. Carbonate removal by acid fumigation for measuring the δ13C of soil organic carbon. Can. J. Soil Sci. 91 (2), 247–250.
Rasmussen, C., Heckman, K., Wieder, W.R., Keiluweit, M., Lawrence, C.R., Berhe, A.A., Blankinship, J.C., Crow, S.E., Druhan, J.L., Hicks Pries, C.E., Marin-Spiotta, E., Plante, A.F., Schädel, C., Schimel, J.P., Sierra, C.A., Thompson, A., Wagai, R., 2018. Beyond clay: towards an improved set of variables for predicting soil organic matter content. Biogeochemistry 137 (3), 297–306.
Rennert, T., 2019. Wet-chemical extractions to characterise pedogenic Al and Fe species – a critical review. Soil Res. 57 (1), 1–16.
Rousk, J., Baath, E., Brookes, P.C., Lauber, C.L., Lozupone, C., Caporaso, J.G., Knight, R., Fierer, N., 2010. Soil bacterial and fungal communities across a pH gradient in an arable soil. Int. Soc. Microbial Ecol. J. 4 (10), 1340–1351.
Rowley, M.C., Grand, S., Verrecchia, É.P., 2018. Calcium-mediated stabilisation of soil organic carbon. Biogeochemistry 137 (1), 27–49.
Sanderman, J., 2012. Can management induced changes in the carbonate system drive soil carbon sequestration? A review with particular focus on Australia. Agric. Ecosyst. Environ. 155, 70–77.
Satterthwaite, F.E., 1946. An approximate distribution of estimates of variance components. Biometrics Bull. 2 (6), 110–114.
Schwertmann, U., Fechter, H., 1982. The point of zero charge of natural and synthetic ferrihydrites and its relation to adsorbed silicate. Clay Miner. 17 (4), 471–476.
Seguinot, J., Jouvet, G., Huss, M., Funk, M., Ivy-Ochs, S., Preusser, F., 2018. Modelling last glacial cycle ice dynamics in the Alps. Cryosphere Discuss. 2018, 1–30.
Skjemstad, J., Fitzpatrick, R., Zarcinas, B., Thompson, C., 1992. Genesis of podzols on coastal dunes in southern Queensland. II. Geochemistry and forms of elements as deduced from various soil extraction procedures. J. Soil Res. 30 (5), 615–644.
Slessarev, E.W., Lin, Y., Bingham, N.L., Johnson, J.E., Dai, Y., Schimel, J.P., Chadwick, O.A., 2016. Water balance creates a threshold in soil pH at the global scale. Nature 540 (7634), 567–569.
Sørensen, T.J., 1948. A method of establishing groups of equal amplitude in plant sociology based on similarity of species content and its application to analyses of the vegetation on Danish commons. I kommission hos E. Munksgaard, København.
Sowers, T., Adhikari, D., Wang, J., Yang, Y., Sparks, D.L., 2018a. Spatial associations and chemical composition of organic carbon sequestered in Fe, Ca, and organic carbon ternary systems. Environ. Sci. Technol.
Sowers, T.D., Stuckey, J.W., Sparks, D.L., 2018b. The synergistic effect of calcium on organic carbon sequestration to ferrihydrite. Geochem. Trans. 19, 4.
Sposito, G., 2016. The Chemistry of Soils. 3rd ed. Oxford University Press, Oxford.
Sutton, R., Sposito, G., Diallo, M.S., Schulten, H.-R., 2005. Molecular simulation of a model of dissolved organic matter. Environ. Toxicol. Chem. 24 (8), 1902–1911.
Thompson, A., Rancourt, D.G., Chadwick, O.A., Chorover, J., 2011. Iron solid-phase

differentiation along a redox gradient in basaltic soils. Geochim. Cosmochim. Acta 75 (1), 119–133.
Tirmizi, S.A., Wattoo, F.H., Wattoo, M.H.S., Khokhar, N.M., Iqbal, J., 2006. Analytical investigation of soil inorganic elements in cotton cultivated areas of Vehari - Pakistan. J. Chem. Soc. Pak. 27 (6), 606–610.
van Reeuwijk, L.P., 2002. Procedures for soil analysis. 6th ed. FOA - Food and Agriculture Organization of United Nations: International Soil Reference and information Center (ISRIC), Wageningen, The Netherlands.
Vaughan, E., Matos, M., Ríos, S., Santiago, C., Marín-Spiotta, E., 2019. Clay and climate are poor predictors of regional-scale soil carbon storage in the US Caribbean. Geoderma 354, 113841.
Vittoz, P., Gmür, P., 2008. Introduction aux Journées de la biodiversité dans le Vallon de Nant. In: A.-C.P. Clot, D. Cherix, F. Dessimox, J.-L. Gattolliat, P. Gmür, P. Vittoz, M. Vust (Eds.), Biodiversité du Vallon de Nant Premières Journées de la biodiversité en Suisse romande (5 et 6 juillet, 2008) Mémoire Vol 23. Société vaudoise des Sciences naturelles, Vaud, Switzerland.
von Lützow, M., Kögel-Knabner, I., Ekschmitt, K., Matzner, E., Guggenberger, G., Marschner, B., Flessa, H., 2006. Stabilization of organic matter in temperate soils: mechanisms and their relevance under different soil conditions - a review. Eur. J. Soil Sci. 57 (4), 426–445.
von Wandruszka, R., 2006. Phosphorus retention in calcareous soils and the effect of organic matter on its mobility. Geochem. Trans. 7 (1), 6.
Webster, R., 2007. Analysis of variance, inference, multiple comparisons and sampling effects in soil research. Eur. J. Soil Sci. 58 (1), 74–82.
Wei, T., Simko, V., 2017. R package “corrplot”: Visualization of a Correlation Matrix.
Whittinghill, K.A., Hobbie, S.E., 2012. Effects of pH and calcium on soil organic matter dynamics in Alaskan tundra. Biogeochemistry 111 (1–3), 569–581.
Zamanian, K., Pustovoytov, K., Kuzyakov, Y., 2016. Pedogenic carbonates: forms and formation processes. Earth Sci. Rev. 157, 1–17.
Zollinger, B., Alewell, C., Kneisel, C., Meusburger, K., Gaertner, H., Brandova, D., Ivy-Ochs, S., Schmidt, M.W.I., Egli, M., 2013. Effect of permafrost on the formation of soil organic carbon pools and their physical-chemical properties in the Eastern Swiss Alps. Catena 110, 70–85.

8.6.3 - Matteodo et al., 2018

- This page is intentionally left blank -

Geoderma 330 (2018) 41–51

Contents lists available at ScienceDirect

Geoderma

journal homepage: www.elsevier.com/locate/geoderma

Decoupling of topsoil and subsoil controls on organic matter dynamics in the Swiss Alps

Magalì Matteodo[a], Stephanie Grand[a,*,1], David Sebag[a,b,1], Mike C. Rowley[a], Pascal Vittoz[a], Eric P. Verrecchia[a]

[a] Institute of Earth Surface Dynamics (IDYST), Faculty of Geosciences and Environment (FGSE), University of Lausanne, 1015 Lausanne, Switzerland
[b] Normandie University, UNIROUEN, UNICAEN, CNRS, M2C, 76000 Rouen, France

ARTICLE INFO

Handling Editor: A.B. McBratney

Keywords:
Alpine environment
Organic matter stabilisation
Ecosystem properties
Litter decomposition
Rock-Eval pyrolysis
Thermal stability

ABSTRACT

Our understanding of mechanisms governing soil organic matter (OM) stability is evolving. It is gradually becoming accepted that soil OM stability is not primarily regulated by the molecular structure of plant inputs, but instead by the biotic and abiotic properties of the edaphic environment. Moreover, several experimental studies conducted in artificial systems have suggested that mechanisms regulating OM stability may differ with depth in the soil profile. Up to now however, there is very limited field-scale evidence regarding the hierarchy of controls on soil OM dynamics and their changes with soil depth.

In this study, we take advantage of the high heterogeneity of ecological conditions occurring in the alpine belt to identify the major determinants of OM dynamics and how their significance varies with depth in the soil profile. Aboveground litter, mineral topsoil, and subsoil samples originating from 46 soil profiles spanning a wide range of soil and vegetation types were analysed. We used Rock-Eval pyrolysis, a technique that investigates the thermal stability of OM, as an indicator of OM dynamics.

Our results show a clear divergence in predictors of OM thermal stability in the litter, topsoil, and subsoil layers. The composition of OM correlated with its thermal stability in the litter layer but not in mineral soil horizons, where the supply rate of fresh organic material and the physical and chemical characteristics of the pedogenic environment appeared important instead. This study offers direct confirmation that soil OM dynamics are influenced by different ecosystem properties in each soil layer. This has important implications for our understanding of carbon cycling in soils under a changing climate.

1. Introduction

Soil organic matter (OM) provides essential ecosystem services as it contributes to soil fertility, water quality and retention, biodiversity, resistance to soil erosion, and could play a fundamental role in the mitigation of climate change (Adhikari and Hartemink, 2016). Therefore, it is necessary to understand the mechanisms governing its stability, namely its preservation from mineralisation (Plante et al., 2011; Sollins et al., 1996; von Lützow et al., 2006) in order to maintain soil OM stocks and their associated functions. It was previously widely held that mineralisation rates of soil OM reflected the kinetics of enzymatic reactions and were consequently largely dependent on the intrinsic molecular composition of plant litter entering the soil system (Davidson and Janssens, 2006). This concept has been formalised under the term "selective degradation" (Sollins et al., 1996), and assumed that soil microorganisms preferentially decomposed the inherently labile components of OM, causing the accrual of recalcitrant components (Aber et al., 1990; Melillo et al., 1982). Recent studies have however questioned the idea that organic molecules could be inherently "stable" or "recalcitrant" (Lehmann and Kleber, 2015; Marschner et al., 2008) by showing that potentially persistent organic molecules, such as lignin, could be mineralised relatively quickly in soils (Gleixner et al., 1999, 2002; Heim and Schmidt, 2007). Contrarily, supposedly labile compounds, such as polysaccharides and proteins, can persist in soil for several decades, centuries or even millennia before being mineralised (Derrien et al., 2006; Gleixner et al., 1999, 2002). These long residence times can be in large part attributed to protection or stabilisation by soil minerals (Gleixner et al., 2002; Spielvogel et al., 2008). These recent findings have led to the proposal of a new paradigm, conceptualised by Schmidt et al. (2011). It suggests that selective degradation only plays an essential role in the initial stages of litter decomposition on the soil surface, while its importance becomes marginal when organic material

* Corresponding author.
E-mail address: stephanie.grand@unil.ch (S. Grand).
[1] Shared authorship: Stephanie Grand and David Sebag contributed equally to the work.

https://doi.org/10.1016/j.geoderma.2018.05.011
Received 27 November 2017; Received in revised form 7 May 2018; Accepted 9 May 2018
Available online 30 May 2018

is incorporated into the mineral soil. In the mineral soil, OM decomposition rates would instead mainly be driven by its spatial accessibility to microorganisms, their enzymes and the necessary compounds of decomposition (mainly oxygen and moisture), and by the type and number of interactions established with mineral surfaces (Lehmann and Kleber, 2015; Schimel and Schaeffer, 2012; Sollins et al., 1996; von Lützow et al., 2006). OM stability in the mineral soil would thus be mainly governed by ecosystem properties such as climate, soil texture, mineralogy and geochemistry (see synthesis by Schmidt et al., 2011 and references therein).

Even though considerably high proportions (between 30 and 63%) of carbon (C) are stored in the subsoil, between 30 and 100 cm deep (Batjes, 1996), most of the studies on soil OM stabilisation mechanisms have focused on the topsoil (Rumpel and Kögel-Knabner, 2011). This may have resulted in a significant bias in our understanding of drivers of OM stability. Indeed, manipulative laboratory experiments suggest that factors controlling C dynamics in topsoil and subsoil may be substantially different. Fierer et al. (2003) and Salomé et al. (2010) incubated topsoil and subsoil material and found that water potential and supply of fresh organic material were important for surface horizons, while nutrient input, temperature, and the physical accessibility of organic substrates appeared as the main regulatory mechanisms of C mineralisation in the subsurface soil layers. Whether this divergence of controls on soil OM stability is operative under field conditions remains however difficult to evaluate.

Indeed, there is no universally recognised mean to assess soil OM stability. Many different fractionation techniques have been devised based on physical, chemical, or biological properties of OM (see Kögel-Knabner et al., 2008 for a review). Physical and chemical fractionation techniques separate soil OM into operationally-defined pools whose relevance to field-scale OM dynamics remains difficult to assess (Diochon et al., 2016). Investigations that consider the bulk sample without pre-treatment may allow for a more integrative assessment of OM stability. In this respect, biological mineralisation during long-term incubation experiments is generally favoured (Plante et al., 2011), but the inherent soil disturbance and the long durations of incubation required to be fully informative (up to several decades) represent an impediment. Thermal decomposition techniques offer a promising alternative to study soil OM stability. Results from thermal decomposition studies are consistent with those of incubation experiments (Plante et al., 2011) and some physical fractionation schemes (Gregorich et al., 2015; Saenger et al., 2015). The pertinence of thermal techniques is based on the assumption, validated by Plante et al. (2011), that the thermal stability of OM is related to its chemical properties or biological stability, as the activation energy required for thermal bond cleavage correlates to the chemical energy required for enzymatic cleavage (Kögel-Knabner et al., 2008). Schiedung et al. (2017) recently showed that thermal oxidation between 200 and 400 °C was a poor predictor of old (17 years or older) versus recent vegetation inputs. Pyrolysis techniques appear better suited to assess biological stability, as persistent OM tends to disintegrate at higher temperatures than labile OM (Barré et al., 2016). The Rock-Eval pyrolysis technique is now widely employed for routine analysis of OM in soil samples (see Sebag et al., 2016 for a review). This method quantifies total organic and inorganic C contents of a sample (either soil or litter) and provides a wide range of parameters that can be used to evaluate OM composition and its thermal stability. When compared to other methods used to quantify pools of recent or labile C (as assessed using ^{14}C dating, incubation and physical fractionation), Rock-Eval analysis performed most effectively (Soucémarianadin et al., 2018a; Vinduskova et al., 2015).

In this study, the thermal stability of OM, taken as an indicator of OM dynamics, was measured using Rock-Eval pyrolysis in litter (Oi horizon), topsoil mineral (A horizons), and subsoil mineral layers (including E, B, and C horizons) of 46 subalpine-alpine soil profiles. These soil profiles spanned eight types of vegetation communities and a wide range of soil pH and moisture conditions. The specific aims of this research were (1) to identify the major predictors of OM thermal stability and (2) to assess how their relative importance varied with soil depth. We hypothesised that there would be a clear shift in determinants of OM thermal stability between soil layers, with the influence of plant inputs being restricted to organic layers while the properties of the mineral phase would become prominent at depth.

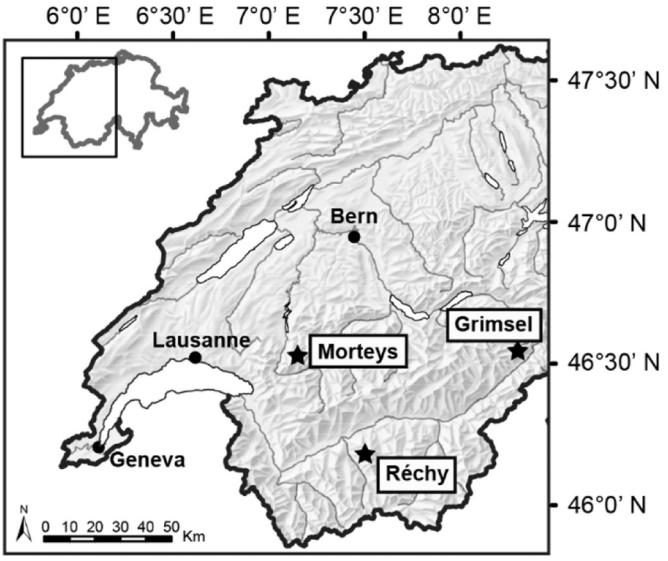

Fig. 1. Location of the three study sites (represented by a star) in Switzerland.

2. Methods

2.1. Sampling design

The 46 soil profiles were selected across three sites of northern and western central Alps in Switzerland (Fig. 1) differing in terms of lithology (Table 1). The Morteys site is underlain by compact limestone and calcareous surficial deposits, while the soil parent materials of the Grimsel site are mainly granite, gneiss, and granodiorite (Oberhänsli et al., 1988). The Réchy area is underlain by a variety of bedrock types including gneiss, mica schist, quartzite, calcschist, marble, and "cornieule" (a dolomite-gypsum greywacke). The three study sites were

Table 1
Characteristics of the study sites: coordinates, mean annual temperatures (MAT), mean annual precipitations (MAP), elevation ranges (with median between brackets), vegetation belt, vegetation types present, lithology, and number of soil profiles excavated at each study site. MAT and MAP are extrapolated according to Zimmermann and Kienast (1999) with a 25 m grid cell size.

	Morteys	Grimsel	Réchy
Latitude	46°32′N	46°32′N	46°10′N
Longitude	7°09′E	8°16′E	7°30′E
MAT [°C]	2.1	−0.44	−0.53
MAP [mm]	1650	2071	1480
Elevation [m]	1698–2232 (1884)	2310–2650 (2329)	2430–2697 (2573)
Vegetation belt	Upper subalpine	Lower alpine	Lower alpine
Vegetation types	Calcareous grasslands, subalpine pastures, calcareous snowbeds	Siliceous subalpine and alpine grasslands, typical snowbeds	Siliceous alpine grasslands, typical and wet snowbeds, windy ridges
Lithology	Limestone	Granite, gneiss, granodiorite	Gneiss, micaschists, quartzite, calcshists, marble, dolomite
No. of soil profiles	18	11	17

covered with glaciers during the last Pleistocene glaciation (Würm). The onset of the melting of the Rhône glacier in Switzerland is dated circa 21,000 years before present and continued to the oldest Dryas, around 16,000 years before present (Ivy-Ochs et al., 2004). This must be considered as the maximum soil age at our study sites. A variety of morphodynamic processes triggered the removal, transport, and accumulation of material during the Quaternary, leading to a complex mosaic of sediments of different ages (Baruck et al., 2016; Theurillat et al., 1998). Therefore, surficial deposits such as scree slope, moraine, and loess deposits are frequently found as soil parent materials. The climatic conditions differ slightly between the three study sites consistently with their biogeographic region and elevational belt. Due to its internal position in the Alps, the climate of the Réchy area tends towards drier continental conditions, while Morteys and Grimsel have a slightly more humid and oceanic climate (Table 1). All soil profiles are located above the present treeline. However, because of extensive grazing and deforestation in the Middle Age, the present treeline elevation is lower than it would be if driven purely by climatic influences (Favilli et al., 2010). We can estimate that the Morteys study site is located around the potential treeline (upper subalpine and lower alpine belt) and the Grimsel and Réchy sites slightly above it (lower alpine and alpine belt; Table 1).

Vascular plant species were exhaustively inventoried around each soil profile. Then, for simplification and standardisation purposes, the plant inventories with similar species composition and estimated cover were grouped by cluster analysis and, based on its dominant species, each group was associated to a specific plant community of the Swiss vegetation classification system (Delarze et al., 2015). This procedure identified a total of eight types of plant communities growing on the 46 soil profiles: (i) calcareous grasslands, (ii) subalpine pastures, (iii) windy ridges, (iv) calcareous snowbeds, (v) siliceous subalpine grasslands, (vi) siliceous alpine grasslands, (vii) typical (siliceous) snowbeds and (viii) wet snowbeds. Each vegetation type mirrors the ecological conditions where plants grow (Suppl. Table 1) and can therefore be considered as an “eco-unit” (Saenger et al., 2013). Vegetation in most plots was extensively grazed by cow, goat, or sheep for 2–4 months in summer, with the strongest grazing impact expected in subalpine pastures.

2.2. Soil description and analyses

Soil description was performed following the guidelines provided by the Food and Agriculture Organization of the United Nations (FAO, 2006). Depth, colour (according to the Munsell soil colour chart), relative abundance of calcium carbonate (established by 10% HCl test), structure, percentage of skeleton (rock fragments > 2 mm) and abundance of fine roots (< 2 mm in diameter) in each soil horizon were estimated in the field. Organic (Oi, Oe and Oa), mineral topsoil (A), and mineral subsoil horizons (E, B, and C) have been initially named according to Baize and Girard (2009) and then converted to the international FAO nomenclature (FAO, 2006). Classification of soils followed IUSS Working Group (2015) and that of humus forms followed Jabiol et al. (2013).

Samples were collected in a total of 231 horizons, including the organic horizons. Sampling occurred in early summer, within the three months following snow melt, irrespective of the vegetation type. Samples were dried at 45 °C. Mineral soil samples were then sieved at 2 mm (fine earth fraction) and a part of the sieved sample was crushed to powder in an agate mortar. The organic samples were ground to 0.12 mm mesh size with a pulveriser (14 Fritsch Tracomme AG). pH was measured in water (pH_{H2O}) with a lab pH meter (Metrohm SA) fitted with a double-junction combined glass electrode. The measurement was conducted in a suspension of fine earth in deionized water (1:2.5 soil water ratio) after 2 h of agitation. The texture of the fine earth fraction was assessed by laser diffraction. Prior to particle size analysis, calcium carbonate was removed by reaction with 10% HCl which was subsequently rinsed off until a pH > 6 was reached. The OM was then removed with 10–35% hydrogen peroxide (H_2O_2). During and after the OM digestion, excess acidity was neutralised with sodium hydroxide (NaOH) 0.1–0.5 M. Finally, soil mineral particles suspended in dilute Na-hexametaphosphate (40 g/L) were analysed in the diffractometer (Malvern™ Mastersizer 2000). Organic carbon and total nitrogen were measured on the dried crushed samples with a CHNS Elemental analyser (EA1108-Carlo Erba Instrument). Calcium carbonate was removed prior to analysis by addition of 10% HCl and subsequent rinsing. The C/N ratio was calculated for each organic and topsoil mineral layer. Unfortunately, N concentration in subsoil horizons was below the reliable quantification limit precluding the interpretation of C/N ratios there.

The total organic carbon (TOC) concentration and the OM properties of the 231 samples were obtained by thermal analysis performed with a Rock-Eval 6 Pyrolyser (Vinci Technologies). Twenty samples had TOC concentrations that were too low for reliable analysis (TOC < 0.2%) and/or abnormal pyrolysis curves (no smooth pyrograms in the S2, S3 or S4 regions indicative of measurement failure) and were deleted from the dataset; therefore 211 samples were retained for the analyses. Between 40 and 70 mg of dried crushed sample were pyrolysed in an inert N_2 atmosphere with increasing temperatures from 200 up to 650 °C with a heating rate of 25 °C/min. The residual sample was then oxidised under oxygenated atmosphere starting at a temperature of 400 increasing until 850 °C with the same heating rate.

The two phases of thermal decomposition released hydrocarbon compounds (HC), CO_2, and CO which were detected continuously. The sum of these C fractions (excluding the CO_2 released above 400 °C during N_2-pyrolysis and above 650 °C during oxidation, which corresponds to the mineral C) represents the TOC concentration (Lafargue et al., 1998). The TOC concentration correlated very well with the organic C concentration measured by elemental analysis ($r^2 = 0.98$, Suppl. Fig. 1). All element concentrations were calculated on an oven-dried soil basis. The hygroscopic moisture correction factor was determined by oven-drying dried crushed samples at 55 °C during 30 h for organic layers and 105 °C during 24 h for the other layers. The amount of HC released relative to TOC is called the Hydrogen Index (HI) and is considered proportional to the atomic H:C ratio in the sample. Similarly, the amount of CO_2 and CO released relative to TOC is called the Oxygen Index (OI) and it is considered proportional to the atomic O:C ratio. The HI and OI are regarded as proxies of the organic matter stoichiometry or composition (Carrie et al., 2012).

The amount of HC released during pyrolysis between 200 and 650 °C forms a bell curve called the S2 pyrogram. The shape of this pyrogram is sample-specific and is indicative of the thermal stability of organic molecules in the sample. The area under the S2 pyrogram was subdivided into four sections (A1, A2, A3 and A4) using temperature cut-offs frequently used in the literature (Sebag et al., 2016): 200–340 °C for A1, 340–400 °C for A2, 400–460 °C for A3 and 460–650 °C for A4. Thermally labile organic molecules release high quantities of HC during the early stage of the pyrolysis process (i.e. large A1 and A2 areas), while thermally stable organic molecules crack later (i.e. large A3 and A4 areas). On this basis, the thermal stability of each sample was represented by two indices previously proposed by Sebag et al. (2016): the R-Index representing thermally refractory OM [$R = (A3 + A4) / (A1 + A2 + A3 + A4)$], and the I-Index representing thermally labile OM [$I = \log_{10}(A1 + A2) / (A3)$]. These two indices are negatively correlated and only the R-Index was retained as an indicator of OM thermal stability in the present study (Suppl. Fig. 2).

The R-Index was preferred over other Rock-Eval parameters such as the OI, the HI, or temperatures at which 50% of C was evolved during the pyrolysis or oxidation phase (T50_HC_PYR or T50_CO2_OX, respectively), for the following reasons: (1) the OI and HI are more directly interpretable as indicators of OM stoichiometry than its stability; (2) T50_CO2_OX has been shown to correlate poorly with other measures of OM stability (Soucémarianadin et al., 2018a,b); and (3)

Table 2
Eighteen investigated potential drivers of OM thermal stability grouped under thematic categories. The scale (ordinal drivers), units (continuous ones), range, indications on whether they were included in the linear mixed models (LMM) specific to each soil horizon and their relative importance calculated with the IT-AIC analysis are given. Some drivers were excluded from the models to avoid collinearities or because they were not relevant in the soil horizon considered.

Category	Potential drivers of OM thermal stability	Remarks	Scale or unit	Range (median)	Relative importance in litter horizons	Relative importance in mineral topsoil	Relative importance in mineral subsoil
Site conditions	Mean summer temperature	Monthly average temperature for the period 1961–1990	°C	4.8–10.0 (6.6)	< 0.01	0.08	0.01
	Mean annual moisture Index	Precipitation - potential evapotranspiration (period 1961–1990)	mm	7147–15,108 (8658)	0.01	0.04	0.01
	North-South gradient	Equals to 0 - cosinus [radian (Aspect)]	–	From −1 (North) to 1 (South) (−0.03)	Collinear with solar radiation and Vegetation PC2 scores	< 0.03	< 0.01
	Mean summer solar radiation	Global potential shortwave radiation	KJ/day	17,080–28,902 (27030)	Collinear with North-South gradient and Vegetation PC2 scores	0.04	< 0.01
Vegetation type	Vegetation PC1 scores	Proportion of acidophilic species	Scores on the PC1 axis of a PCA based on species composition	From −0.3 to 0.2 (0.05)	< 0.01	Collinear with pH	0.49
	Vegetation PC2 scores	Proportion of hygrophilic species	Scores on the PC2 axis of a PCA based on species composition	From −0.2 to 0.2 (−0.01)	0.7	0.06	0.02
Soil properties	pH	For the litter layers, is the value of the first A horizon in the corresponding soil	–	3–7.9 (5.4)	Collinear with Vegetation PC1 scores	0.04	< 0.01
	Presence of carbonates	For the litter layers, it corresponds to the presence of carbonates within the soil profile	0 (absence), 1 (presence)	–	0.03	0.04	0.02
	Clay	Mineral particles < 0.002 mm diameter	% of fine earth fraction	1.1–48.5 (4.3)	Not relevant	Collinear with Sand	Collinear with Sand
	Silt	Mineral particles 0.002–0.063 mm diameter	% of fine earth fraction	31.7–87.1 (57.7)	Not relevant	0.06	0.47
	Sand	Mineral particles 0.063–2 mm diameter	% of fine earth fraction	3.2–65.4 (22.9)	Not relevant	0.04	0.51
Humus form properties	Humus Index	Modified from Ponge et al. (2002)	2 (Mesomull & Euanmoor), 3 (Oligomull), 4 (Dysmull), 5 (Hemimoder & Amphi), 7 (Dysmoder), 8 (Hemimor & Humimor)	2–8 (4)	0.02	0.03	< 0.01
	Waterlogged conditions	Presence of Anmoor humus forms (Jabiol et al., 2013)	0 (absence), 1 (presence)	–	0.02	0.05	0.01
	Rhizic humus form	Presence of > 25% of dead or living roots in the total volume of the O and A horizons combined (Jabiol et al., 2013)	0 (absence), 1 (presence)	–	Not relevant	< 0.03	0.01
OM properties	TOC	Total organic carbon concentration	% of fine earth fraction	0.45–59 (6.2)	< 0.01	1	< 0.01
	Hydrogen Index (HI)	Amount of hydrocarbons (HC) released relative to TOC	mg HC/g TOC	44.9–524.5 (267.3)	0.36	0.03	0.32
	Oxygen Index (OI)	Amount of CO and CO2 released relative to TOC	mg CO + CO2/g TOC	107.8–464.6 (216.2)	< 0.01	0.04	0.03
	C/N	Total carbon/total nitrogen	–	7.3–70.2 (14.7)	0.72	0.09	Not determined

T50_HC_PYR is by definition very close to and highly correlated with the R-Index, making its use redundant. Finally, Sebag et al. (2016) has shown that the R-Index is an appropriate proxy for OM dynamics during the decomposition process.

2.3. Potential drivers of OM thermal stability

A total of eighteen quantitative variables in five categories (site conditions, vegetation type, soil properties, humus forms and OM composition) were chosen for their potential impact on OM stability (Table 2). The mean air temperature in summer (June to September included), the average summer solar radiation and the mean annual moisture index (precipitation-evapotranspiration) were extrapolated for each soil location from the Swiss meteorological stations (www.meteoswiss.ch) according to Zimmermann and Kienast (1999). The aspect was measured in the field with a compass and then converted to a "North-South (NS) gradient" by the formula:

$$NS_{gradient} = 0 - \cos[radian(Aspect)].$$

The vegetation type was taken into account by performing a principle component analysis (PCA) based on the species composition and cover (after Hellinger transformation; see Legendre and Gallagher, 2001) recorded at each study point. Scores on the first two axes (Suppl. Fig. 3) were retained for subsequent analyses. The two resulting variables were respectively called Vegetation PC1 scores and Vegetation PC2 scores. To facilitate interpretation of these principal components, Landolt ecological indicator values (Landolt et al., 2010) expressing plant-specific requirements for soil pH (R) and moisture (F) were associated to each plant species of the dataset. A global indicator values for each plant inventory was calculated with the species cover as a weight. Finally, the Pearson correlation coefficient between the mean indicator values and the PC1 and PC2 scores of each plant inventory were calculated. Landolt's R value, corresponding to an increasing preference for alkaline soils, correlated strongly and negatively with Vegetation PC1 scores (Pearson's $r = -0.88$, 95% confidence interval = $-0.93 < r < -0.80$). Landolt's F value, corresponding to increasing requirement for soil moisture, was positively correlated with Vegetation PC2 scores ($r = 0.54$, $-0.30 < r < -0.72$). Vegetation PC1 scores were thus mainly related to the proportion of acidophilic species, and separated plant communities typically associated with calcareous versus siliceous substrates. Instead, Vegetation PC2 scores reflected in part the contribution of hygrophilic species and distinguished grasslands from snowbeds.

Soil properties included pH_{H2O}, clay (< 2 µm), silt (2–63 µm) and sand (63–2000 µm) percentages and the occurrence of carbonate (presence/absence of 10% HCl reaction). The humus form, i.e. the sequence of organic and underlying topsoil mineral horizons, was selected to represent the integrated effects of plant and decomposer communities. In this study, the humus form was represented by the Humus Index (modified after Ponge et al., 2002) spanning from 2 (MULL) to 8 (MOR). The presence of waterlogged and rhizic conditions (binary variables) was assigned, respectively, to the histic Anmoor humus forms (Jabiol et al., 2013) and to humus forms having > 25% of dead or living roots in the total volume (Jabiol et al., 2013). The OM properties consisted in the TOC concentration and three indices of OM composition: the HI and OI from Rock-Eval pyrolysis and the C/N ratio.

Finally, we also investigated the relation between class variables and OM thermal stability. Class variables included the lithological origin of soil's parent material, pedogenic environments and horizon type. Soil's parental lithology was assigned using our field observations as well as existing geological and geomorphological maps (www.swisstopo.admin.ch). We assigned three categories of parental lithologies: (1) a "calcareous" category referring to limestones, calcareous sandstones, marbles, and surficial deposits (screes and moraines) derived almost exclusively from these materials; (2) a "mixed" category containing surficial deposits of mixed origin (sedimentary, metamorphic, and igneous components); and (3) a "Si-rich" category containing granite, gneiss, quartzite, and surficial deposits derived almost exclusively from these materials. Pedogenic environments and horizon types were assigned on the basis of field description and results of soil lab analyses. We recognised four main types of pedogenic environments based on the degree of soil development and organic matter mobility. First, weakly differentiated solums (Cambisols, Leptosols, Regosols, Gleysols, Stagnosols) were set apart from podzolic solums with strong horizon differentiation. Secondly, within weakly-differentiated solums, we set apart circumneutral (subsoil pH > 6) from acid (subsoil pH < 5.6) profiles, hypothesising a difference in organic matter dynamics due to charge, dispersion and opportunity for mineral-association (Rowley et al., 2018). Likewise, we set apart Humic Podzols characterized by a strong accumulation of organic compounds to the subsoil, from Ferric Podzols where subsoil accumulation is dominated by Fe and Al compounds. We grouped horizon types following the same guiding principles into four general classes. The "podzolic" class included podzolic E, humic B (Bh), ferric B (Bs) and podzolic C horizons. The "weakly differentiated" class included Bsi (siliceous, low Ca saturation), Bci (absence of Ca-carbonate but high Ca saturation), Bca (presence of calcium carbonate) and C horizons. The next class was associated with soils with expressed redoximorphic features and included Bg (stagnic conditions) and Br (strong reducing conditions) horizons. The last class referred to buried A horizons (FAO, 2006).

2.4. Statistical analysis

The litter (Oi horizon), topsoil mineral (A horizon) and subsoil mineral layers (E, B and C horizons) were considered separately in the statistical analyses. The Oe and Oa horizons were excluded because of their low occurrence in the data set (respectively 6 and 4% of the samples). An information theoretic framework based on the Aikaike's information criterion (IT-AIC, Burnham and Anderson, 2002) was employed in order to find the dominant factors influencing OM thermal stability in each layer. Contrary to the traditional null hypothesis testing (Anderson et al., 2000), the IT-AIC approach fundamentally explores range of alternative fits (a "model set") potentially associated to a certain phenomenon and highlights the strongest associations worthy of further investigations (Symonds and Moussall, 2011). In the present study, a set of linear mixed-effects models (LMM) was built with the R-Index as dependent variable and the potential drivers of Table 2 as independent variables, standardised to a mean of 0 and a standard deviation of 0.5 according to Gelman (2008). The study sites and mean horizon depth were set as random effects in order to discount their potential influence on OM thermal stability. The independent variables (predictors) to be included in the models were scrutinised in order to avoid problematic collinearities. For each layer, groups of variables having a Spearman's rank correlation coefficient higher than 0.7 were identified, and the strongest predictor was retained. We also checked that the choice of the alternative variable did not affect ranking of the other predictors. The model set was composed of every possible combination of the variables, including an intercept-only model. According to Harrell (2001), the number of predictor variables simultaneously considered in each model should not exceed 1/10 of the sample size to avoid over-parameterisation. As the sample size of the litter layers was 33, the maximal number of predictors simultaneously considered in each model was set to 3. The same maximum number of predictors was used for mineral topsoil and subsoil horizons, although the number of samples was higher (77 and 69, respectively), to ensure that each analysis operated under similar constraints. The models composing the set were then compared and ranked by their AIC_C (modified version of AIC recommended for small sample sizes; $AICc = AIC + (2k^2 + 2k) / (n - k - 1)$, with n = sample size and k = number of estimated parameters). The approximation power of each model was expressed as the difference (ΔAIC_C) between the AIC_C of the best model (the lowest AIC_C value) and the AIC_C value for each of the other models. The ΔAIC_C was

then used to calculate the Aikaike weight (w_i) representing, for a given model, the probability to be the best approximating model within the model set. In this study, a "top model set" was created by subsetting the models that had a cumulative Aikaike weight of ≤ 0.95. Then, within the top model set, the relative importance of each variable was calculated by summing the Aikaike weights of the model(s) containing that variable. The factors having the strongest effect on the response variable were those with the highest summed Aikaike weights, i.e. having a relative importance tending towards 1 (Burnham and Anderson, 2002).

The relationship between the response variable (R-Index) and the factors having the highest relative importance was measured by the Pearson correlation coefficient and its 95% confidence intervals. The lower the confidence interval width, the higher the probability of the Pearson correlation coefficient to correctly reflect population correlation.

Finally, the role of class variables (soil parent material, pedogenic process, horizon type) on OM thermal stability, which could not be evaluated through the IT-AIC analysis, was investigated using a one-way analysis of variance (ANOVA). Diagnostics for assumptions of normality, homoscedasticity, and goodness-of-fit were performed on residual plots. For significant effects, pairwise *t*-tests without adjustment for multiple inferences (Webster, 2007) were performed to identify significant differences between R-Index means. The alpha level for significance was set to $\alpha = 0.05$ for all tests.

3. Results

3.1. Thermal stability of the OM increases with depth in the soil profile

The R-Index, i.e. the proportion of refractory compounds in the pyrolysed OM, increased with depth in the soil profile, from litter to topsoil and subsoil mineral layers. In contrast, the I-index, a proxy for preservation thermally labile, decreased with depth (Suppl. Fig. 2). This progressive increase in OM thermal stability with depth was observed in each of the eight vegetation types.

3.2. Factors influencing OM thermal stability in the litter layer

According to the IT-AIC analysis, OM thermal stability in the litter layer was mainly related to the OM stoichiometry (C/N ratio and Hydrogen Index, HI) and the proportion of hygrophilic species (Vegetation PC2 scores; Fig. 2). The R-Index correlated negatively with the C/N ratio ($r = -0.72$, $-0.85 < r < -0.50$) and positively with Vegetation PC2 scores ($r = 0.79$, $0.61 < r < 0.89$). The Hydrogen Index (HI), representing the proportion of hydrogen (H) relative to C atoms in OM, ranked as the third most important factor and was negatively related to the R-Index ($r = -0.65$, $-0.81 < r < -0.39$; Suppl. Fig. 4). The litter from snowbeds showed the lowest C/N ratios and HI values but the highest OM thermal stability.

3.3. Factors influencing OM thermal stability in the mineral topsoil

In the topsoil (A horizons), the thermal stability of the OM was predominantly related to its concentration (Fig. 3). The correlation between the R-Index and total organic C (TOC) concentration was negative and relatively weak ($r = -0.53$, $-0.67 < r < -0.34$). When the topsoil was OM-rich (TOC > 15%), the OM thermal stability was comparatively low. In some cases, these OM-rich A horizons were water-saturated for more than six months per year and displayed a hydromorphic humus type (classified as Anmoor; Jabiol et al., 2013). In others cases, the OM-rich A horizons had a large proportion of roots, and finally some of them presented a certain amount of fragmented litter homogeneously mixed with the fine earth fraction, likely resulting from bioturbation.

It should be noted that 28 of the 46 soil profiles presented several A horizons. In these cases, the OM of the most surficial A horizon systematically had a lower thermal stability than the underlying one (Suppl. Fig. 5), indicating increasing proportions of thermally stable OM with depth. To further investigate the hierarchy of predictors of OM thermal stability, we repeated the analysis with depth included as a fixed effect rather than a random one. This allowed us to compare the effectiveness of explanatory variables compared to that of depth. The main predictor of OM thermal stability remained the TOC concentration and was very closely followed by depth (Suppl. Fig. 6). This means that the predictive power of TOC concentration is of the same order as that of depth. The correlation between TOC concentration and depth was relatively weak ($r = -0.48$).

3.4. Factors influencing OM thermal stability in the mineral subsoil

The OM thermal stability in the subsoil was negatively related to the sand content and positively to the proportion of acidophilic species

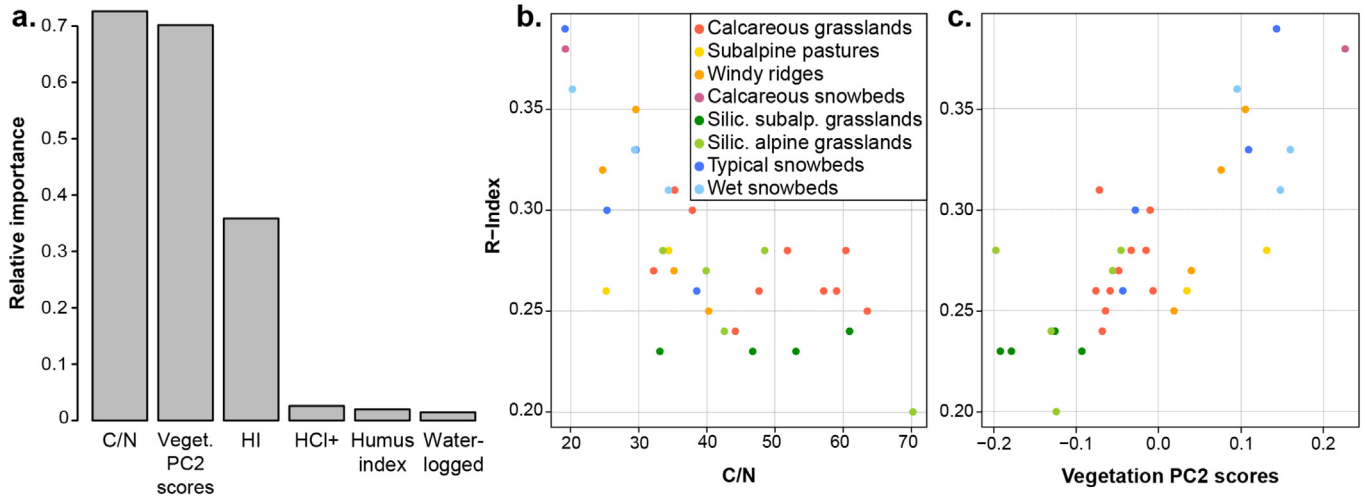

Fig. 2. Predictors of OM thermal stability in the litter layer. (a) The six main explanatory variables influencing the R-Index in the litter layers, ranked according to their relative importance. "Veget. PC2 scores": scores on the 2nd axis of a principle component analysis based on vegetation composition and cover, corresponding to a gradient of increasing contribution of hygrophilic species; "HI": Hydrogen Index; "HCl+": visible effervescence upon strong acid addition due to the presence of carbonate in the soil; (b and c) R-Index values plotted against the two most important predictors, C/N and Vegetation PC2 scores. Colours represent the eight plant communities. "Silic.": siliceous. "subalp.": subalpine.

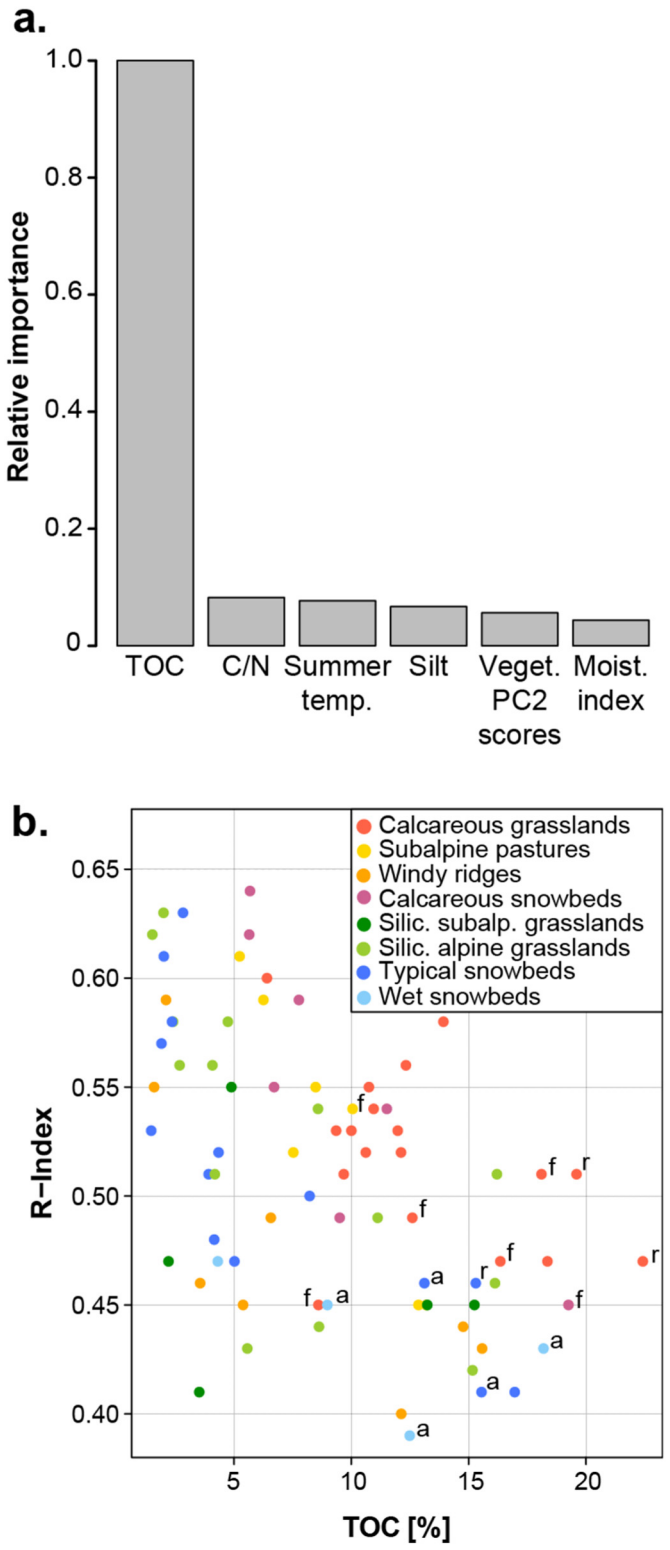

Fig. 3. Predictors of OM thermal stability in the mineral topsoil. (a) The six main explanatory variables influencing the R-Index in the topsoil, ranked by their relative importance. "TOC": total organic C concentration; "Summer temp.": mean summer temperature; "Silt": % of mineral particles having a diameter between 0.002 and 0.063 mm; "Moist. Index": mean annual moisture index (precipitation – potential evapotranspiration) (b) R-Index values plotted against the organic C concentration (TOC %). Colours represent the eight plant communities, while letters represent peculiarities of the A horizon. "a": hydromorphic A (Anmoor in Jabiol et al., 2013); "r": rhizic humus form, presence of > 25% of dead and living roots in the total volume of O and A horizons combined (Jabiol et al., 2013); "f": fragmented litter homogeneously mixed with fine earth fraction.

(Vegetation PC1 scores; Fig. 4b and c). The correlation remained weak in both cases ($r = -0.33$, $-0.52 < r < -0.10$ and $r = 0.25$, $0.01 < r < 0.46$, respectively). Silt and HI ranked respectively as third and fourth most important predictors (Suppl. Fig. 7). For comparison, the predictive power of these factors greatly exceeded that of horizon depth when included as a fixed effect (Suppl. Fig. 8). The correlation between the R-Index and texture variables (sand and silt proportion) was mainly driven by three eluvial (E) horizons, which were particularly sandy. If these three samples were removed from the analysis, the importance of texture was reduced and Vegetation PC1 scores became the most important predictor, followed by sand and silt proportions (not shown).

This study took place in the alpine environment, with little human activity, and as such the respective vegetation type reflected each site's ecological conditions (Vonlanthen et al., 2006; Grand et al., 2016). Vegetation PC1 scores represented a gradient of plant community preference for alkaline soils (Landolt et al., 2010) and could thus be considered as a proxy for soil geochemistry, as determined by the nature of the geological substrate and pedogenic environment. The nature of the geological substrate indeed explained 74% of the variance in Vegetation PC1, while the pedogenic environment explained 62% of the variance in Vegetation PC1 (Suppl. Fig. 9). This interpretation is confirmed by the correlation between Vegetation PC1 and soil pH (Suppl. Fig. 10).

Soil geochemistry was best represented by class variables that were not suited to the IT-AIC analysis. We therefore conducted a separate analysis of variance to test the effect of geological and soil classes on the R-Index of subsoil horizons (Suppl. Fig. 11). Geological classes explained 19% of the variance in the R-Index, with samples associated with Si-rich lithologies having a significantly higher R-Index than samples associated with calcareous or mixed lithologies. Soil classes explained 26% of the variance in the R-Index, with ferric podzols having a significantly higher R-Index than other soils.

Moreover, thermal stability of subsoil layers varied according to the type of horizon considered (Fig. 4d) and the pattern was not reducible to horizon depth, as could be observed in the topsoil (Suppl. Fig. 5). E horizons showed the lowest R-Index values, reaching the same range of thermal stability displayed by A horizons (Fig. 3), while buried A horizons (IIA; corresponding to fossil soils) showed among the highest R-Index values. B and C horizons showed intermediate values. Significant differences could be noted according to the different pedogenic processes at work: in podzolic profiles, OM thermal stability increased dramatically from eluvial (E) to illuvial horizons and was highest in horizons dominated by the accumulation of sesquioxides (E ~ Bh < Bs ~ podzolic C). In weakly developed soils, OM thermal stability increased slightly from carbonate-rich to siliceous horizons (Bca < Bsi). In redoximorphic horizons, OM thermal stability was generally variable and within range of other acid B and C horizons. Overall, the horizon type and associated pedogenic process had detectable effects on the OM thermal stability of the mineral subsoil layers.

4. Discussion

Due to its complex topography, geology, and geomorphology, the Alpine environment generates steep natural gradients of vegetation, soil moisture, texture, and geochemistry over very short spatial scales. This natural variability was used to explore controls on OM thermal stability. Study sites displayed a small climatic gradient (restricted region in the Alps and limited elevation range). Accordingly, climate-related variables (mean summer temperature, moisture index, and solar irradiance) were not found to be important predictors of OM thermal stability in the data set, likely due to the comparatively small range of variation in these factors. Furthermore, anthropogenic impact on these soils were not believed to have exerted a paramount influence since study sites have never been ploughed, but have been used for extensive pasture, largely replacing natural grazing by deer, gams or ibex.

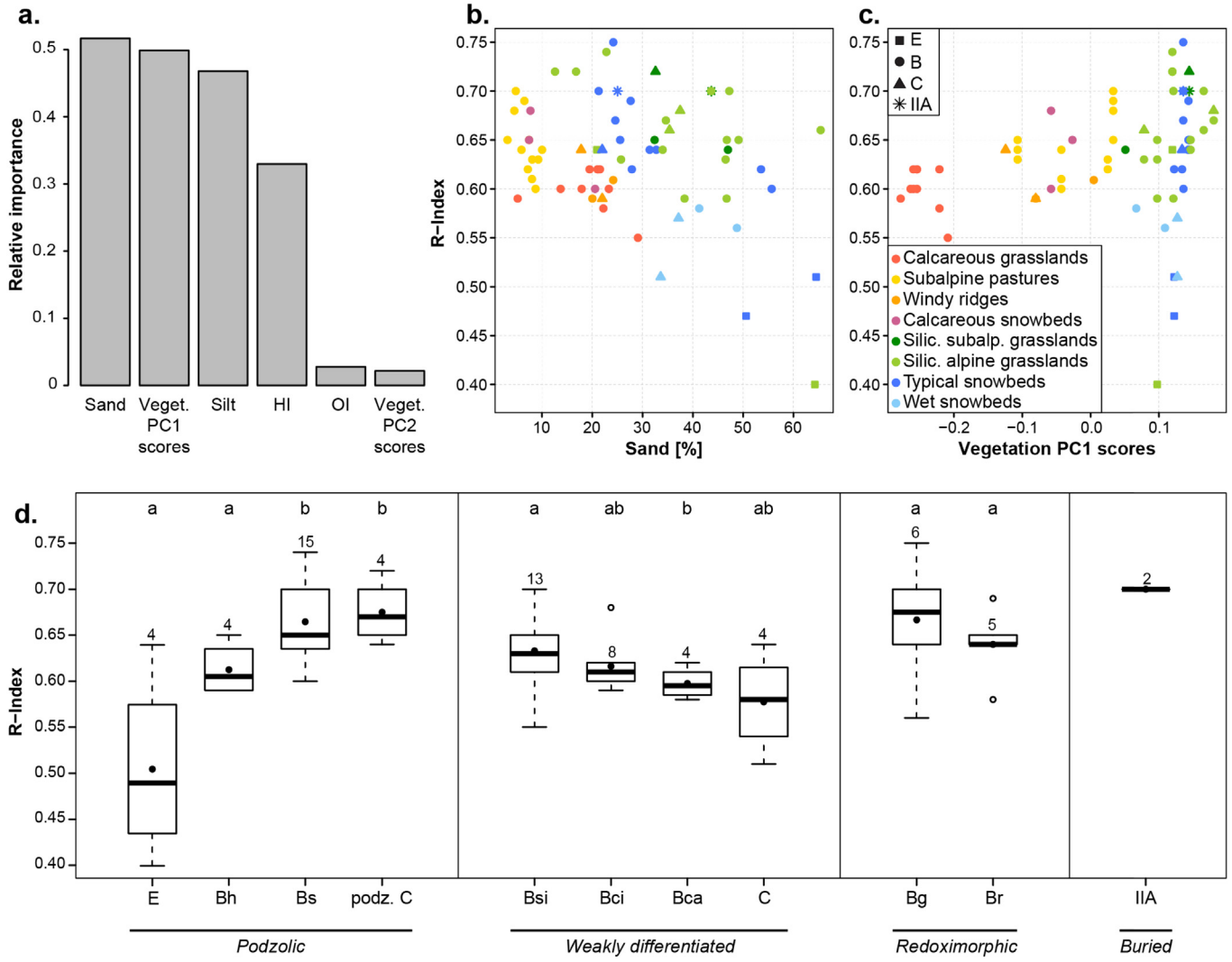

Fig. 4. Predictors of OM thermal stability in the subsoil. (a) The six main explanatory variables influencing the R-Index in the subsoil, ranked by their relative importance. "Veget. PC1 scores": scores on the 1st axis of a principle component analysis based on vegetation composition and cover, corresponding to a shift from calcophilic to acidophilic species. (b and c) R-Index values plotted against the two most important variables, Sand and Vegetation PC1 scores. Colours represent the eight plant communities and symbols represent the horizon categories. (d) Boxplots of R-Index by mineral horizon types. The first four horizon types represent the podzolic soil sequence, including "E" (eluvial horizon); "Bh" (illuvial accumulation of organic matter); "Bs" (illuvial accumulation of sesquioxides); "podzolic C" (C horizon underlying a podzolic profile). The next four horizon types are found in weakly-developed solums, such as Cambisols, Leptosols, and Regosols, and include: "Bsi" (siliceous, low Ca saturation); "Bci" (absence of Ca-carbonate but high Ca saturation); "Bca" (presence of Ca carbonate); "C" (subsoil horizon weakly affected by pedogenic processes). The next two horizon types are found in soils with expressed redoximorphic features and include "Bg" (stagnic conditions) and "Br" (strong reducing conditions) horizons. The last class "IIA" refers to buried A horizons (FAO, 2006). Black dots represent the mean values, the black line is the median, and boxes are limited by 1st and 3rd quartiles. Numbers of observations are indicated above boxplots. Letters above boxplots indicate significant differences (p-value < 0.05) calculated by pairwise *t*-tests conducted within broad classes of horizon types.

We used the Rock-Eval R-Index, which gives a snapshot of the proportion of thermally refractory compounds found within the OM, as a proxy for organic matter dynamics, broadly understood as processes leading to changes in OM properties. The use of Rock-Eval pyrolysis allowed us to evaluate OM properties similarly across all soil layers without applying any pre-treatment, and thus eliminated the risk of creating experimental artefacts. As expected from results of other studies employing Rock-Eval analysis (Sebag et al., 2016 and references therein), we found that the contribution from thermally stable OM progressively increased with depth in the soil profile (Suppl. Fig. 1). This is in accordance with the generally accepted idea that in the absence of perturbations, soil OM stability and residence time tend to increase with depth (van der Voort et al., 2016). However, the R-Index of subsoil horizons retained significant variability (Fig. 4d). Moreover, differences in subsoil horizons could not be predicted from differences observed in the litter layer or even the A horizon (Suppl. Fig. 12). As an example, wet snowbeds had relatively high R-Index values in the litter layer, but showed the lowest values in mineral horizons; siliceous subalpine grasslands had among the lowest R-Index values in the litter and topsoil horizons, but they showed the highest values in the subsoil (Suppl. Fig. 13). This indicated that soil OM dynamics, as represented by changes in OM thermal properties, followed diverging trajectories with depth in different edaphic environments. In the next sections, we will explore the factors correlated with OM thermal stability in each major soil layer (litter, topsoil, and subsoil) and their significance.

In the litter layer, the thermal stability of OM varied according to its stoichiometry (C/N and Hydrogen Index – HI) and to the plant community producing it (Vegetation PC2 scores). Differences in the C/N and HI in the litter layer may arise both from the initial biochemical OM composition and from the litter mineralisation degree. Variations in C/N ratios were driven by differences in N rather than organic C concentration (Suppl. Fig. 14). Plants with efficient N uptake mediated by

mycorrhizal fungi or N-fixing capacity may produce N-enriched litter. These characteristics are present in some vascular plant and moss species of snowbeds (Woolgrove and Woodin, 1996; Mullen et al., 1998), which showed the lowest C/N ratio and highest R-Index values (Suppl. Figs. 13 & 14). The process might be further enhanced by N accumulation in the snowpack, acting as a scavenger of air pollution (Knutson et al., 1976). On the other hand, N accumulation (Aber and Melillo, 1982; Manzoni et al., 2008) and OM dehydrogenisation (Barré et al., 2016; Sebag et al., 2016) typically occur during decomposition. Low C/N and HI values may be used as an indicator of the mineralisation degree (Grand and Lavkulich, 2012). The inverse relation between the litter thermal stability and the C/N and HI values may reflect the fact that a more thermally recalcitrant OM is produced as decomposition proceeds. In this study, litter was collected in summer and thus essentially consisted in material that had senesced nearly a year ago (during the previous fall). The concomitant increase in thermal stability and the proportion of hygrophilic species could also indicate that longer periods of snow cover favour decomposition (Baptist et al., 2010; Hobbie and Chapin, 1996) and selectively preserve thermally resistant components (Sebag et al., 2016). Overall, the increase in the R-Index, concomitant with the increase in N and decrease in H content, corroborates the common observation that OM properties in the litter layer simply reflect the quality of plant inputs and the extent of decomposition.

In the A horizons, the main predictor of OM thermal stability, among the 18 factors under study, was the concentration of soil C (Fig. 3), which is in turn related to the balance between mechanisms governing the fresh OM inputs and those controlling its mineralisation or deep translocation. The predictive power of organic C concentration on OM thermal stability was surprisingly large, matching that of depth (Suppl. Fig. 6). The main split seemed to occur at an organic C concentration of about 15%. Below this threshold, the R-Index of OM was highly variable while above this threshold, the R-Index was consistently low (Fig. 3). Many of the organic C rich samples had unusually large amounts of roots or visible litter fragments (indicative of active bioturbation delivering plant material to the mineral soil). Other displayed traces of hydromorphy. Our sample set, restricted to a semi-natural environment, thus contained a significant proportion of samples with a high concentration of fresh OM displaying a thermally labile signature. In the same way, Sebag et al. (2006) observed lower R-indices in soil layers under dense plant cover (large inputs) when compared to sparse vegetation (low inputs).

These findings indicate that the thermal signature of OM in the A horizon was related to physical processes of OM delivery into the mineral soil. The thermally labile signature of the OM-rich samples could be due to several processes. Roots or litter-rich samples probably record a kinetic phenomenon in which the thermal signature of the OM is constantly 'refreshed' by abundant new inputs. A decline in enzymatic efficiency at high substrate availability might play a role (Schimel and Weintraub, 2003). For hydromorphic samples, it is well-known that oxygen limitation can initiate a transition towards alternative respiratory pathways that are less energy efficient, and thus a reduction in decomposition (Schlesinger and Bernhardt, 2013). Furthermore, at high organic loadings, the potential for OM stabilisation by interactions with mineral surfaces decreases (Six et al., 2002). Organic-rich samples are thus likely dominated by light particulate OM fractions, which generally represents a thermally labile OM pool (Saenger et al., 2015; Soucémarianadin et al., 2018a). Overall, our results indicate that thermal stability of topsoil OM is controlled by pedogenic processes rather than OM composition or stoichiometry.

In subsoil mineral layers, OM thermal stability was mainly related to texture and Vegetation PC1. However, the predictive power of these factors was modest, indicating that a major part of OM thermal stability in the subsoil remained unexplained by the present dataset. Vegetation PC1 represented a gradient of calcophilic to acidophilic species and could thus be interpreted as a proxy for soil geochemistry (Suppl. Figs. 9 & 10). Recognising the indirectness in inferring soil geochemistry from plant communities, we performed an additional analysis of variance which confirmed that geological and pedogenic classes had a strong explanatory power on R-Index variations in the subsoil (Suppl. Fig. 11). Variance explained by geology (19%) and soil (26%) classes were actually larger than that explained by Vegetation PC1 (6%). This result concurs with a recent study of instantaneous OM mineralisation rates (represented by soil-surface efflux, also known as soil respiration) in mountain soils, which found that 17% of the variation in whole-soil respiration could be explained by soil classes (Grand et al., 2016). Soucémarianadin et al. (2018b) suggested that soil class could constitute an integrated parameter capturing important differences in OM turnover; yet, pedogenic parameters are conspicuously absent from most models of soil OM cycling. Interestingly, we found that texture (% sand, silt, or clay) was only slightly related to the R-Index of OM in subsoil layers once special pedogenic dynamics were accounted for, such as that associated with the E horizons of podzols. This finding is consistent with the results of a recent large meta-analysis (Rasmussen et al., 2018) which showed that chemical and mineralogical parameters far exceeded the predictive power of clay on soil OM stabilisation.

Moreover, significant differences in OM thermal stability were observed between subsoil horizon types (Fig. 4d), which could not be simply explained by an increase in the R-Index with depth. We instead hypothesise that various stabilisation mechanisms, associated to specific pedogenic processes, could be responsible for the observed variations. According to von Lützow et al. (2008), stabilisation mechanisms are indeed horizon-specific in Podzols. The potential for organo-mineral interactions is thought to be low in eluvial horizons, where long-chain alkyl structures could accumulate (Rumpel et al., 2004), perhaps as a result of hydrophobic separation from decomposers. Complexation of organics with monomeric Al and Fe has been proposed as the main stabilisation mechanism in Bh horizons while Bs and podzolic C horizons typically contain highly oxidised OM stabilised by organo-mineral interactions, such as ligand-exchange (Rumpel et al., 2004; von Lützow et al., 2008). Interestingly, OM thermal stability in Podzol mineral layers measured in this study increased in the order E ~ Bh < Bs layers (Fig. 4d). In accordance with the conceptual model outlined by Rumpel et al. (2004), a possible interpretation is that E horizons contained mostly C and H-rich, thermally unstable moieties (Suppl. Fig. 15), while Bh and Bs horizon were enriched in partially dehydrogenated, thermally stable molecules. Moreover, our results might suggest that OM interaction with metals, believed to dominate in Bh horizons, have a weaker effect on OM properties than interactions with poorly crystalline oxides and aluminosilicates, expected in Bs horizons.

A potential stabilisation mediated by Ca was less apparent in our dataset (Fig. 4d), but OM present in Ca-rich horizons (Bca) was more thermally labile, and thus perhaps less processed, than the OM present in Ca-poor horizons (Bsi). This may indicate that aggregation and protection of some thermally labile OM by occlusion within aggregates were more pronounced in Ca-rich horizons (Rowley et al., 2018). Moreover, plant roots were visibly more abundant in the calcareous subsoils than in their siliceous counterparts, and their turnover could partly explain the large concentration of labile OM in Ca-rich B horizons. Redoximorphic processes (Bg and Br horizons) were not associated with a specific OM thermal signature, perhaps due to the typically seasonal nature of waterlogging in alpine soils. Overall, our result supports a dominant role of the geochemical properties of the mineral matrix on OM dynamics in the subsoil. Further investigation is needed to establish whether the thermal resistance measured by Rock-Eval pyrolysis is indeed reflective of the type of organo-mineral association involved.

As previously proposed by Salomé et al. (2010), this study confirmed a substantial decoupling between organic, topsoil, and subsoil mineral horizons in terms of factors influencing OM dynamics, as represented by its thermal stability. This study was consistent with the repeated findings of litter bag experiments (e.g. Preston et al., 2009)

showing that the intrinsic properties of OM (litter source) and its selective degradation play a role at the beginning of the OM decomposition continuum (Lehmann and Kleber, 2015), in the litter layer, before any pervasive opportunity for interaction with the mineral matrix. Contrarily, in the topsoil and subsoil mineral layers, our data showed that OM dynamics were influenced by the pedogenic environment, rather than being an intrinsic property driven by its initial composition. In these layers, the vegetation type played an indirect role on soil OM thermal stability by determining the rate of plant inputs entering the soil system and its vertical distribution along the soil profile (Jobbagy and Jackson, 2000), rather than by determining its quality. As observed in many studies (Kögel-Knabner et al., 2008; Rumpel et al., 2002), soil OM dynamics in subsoil horizons seemed to be driven by the types and intensity of organo-mineral interactions and physical protection from decomposers. Consistently with our initial hypothesis, our study thus evidenced a clear shift in determinants of OM dynamics between soil horizons, with the influence of the litter source and OM stoichiometry seeming preeminent in organic layers and properties of the mineral phase rising to the forefront in the subsoil.

It should be noted that the 18 factors explored in this study were not exhaustive. In particular, we expect that measures of the molecular composition of plant materials and composition of the decomposer community could yield important further insights into OM dynamics in the litter layer. In the mineral soil, we used proxies for soil mineralogy and geochemistry (lithological origin of soil's parent material, pedogenesis, presence of acidophilic/calcophilic species). We expect that detailed measures of mineralogical and geochemical parameters (e.g., specific surface area, clay mineralogy, oxide content and crystallinity, carbonate content and crystallinity, base saturation, etc.) would provide more details on processes governing OM dynamics in the mineral soil. Furthermore, our study was restricted to semi-natural grasslands of the alpine and subalpine belts. This area is characterized by uncultivated, young soils with relatively small amounts of secondary minerals. Other studies in areas with diverse land uses and more pedogenetically advanced profiles are needed to extend these results beyond mountain regions.

It is generally thought that global warming will increase soil organic C mineralisation (Leifeld et al., 2009; Schimel, 1995). The present study suggests that the effects of climate change will not be reducible to changes in OM mineralisation rates as a result of the temperature-dependency of enzymatic degradation (Q10-effects); indeed, pure Q10-effects are likely to be of minor importance when compared to broader ecosystem consequences. Our study suggests that shifts in plant communities and in pedogenic trajectories could result in drastically altered OM dynamics. This constitutes a critical research gap which undermines our capacity to predict the future of OM storage in soils.

5. Conclusions

Building upon the theoretical framework of Schmidt et al. (2011), this study investigated ecosystem-scale controls on soil OM dynamics in a wide range of soils co-occurring in a restricted geographical area of the Swiss Alps. We used OM thermal stability as a proxy for OM dynamics, broadly understood as processes leading to patterns of OM distribution and properties. The study of the whole soil profile allowed to show a radical shift in the nature of predictors of OM dynamics between soil layers. In the litter layer, the OM thermal stability was related to its composition (a product of the initial composition of plant inputs and probably more importantly, their degree of microbial processing), suggesting a dominant biological and biochemical control. In the topsoil, OM thermal stability was mainly related to the OM content, which represented the balance between factors influencing inputs (litter in-mixing, fine root density) and outputs (waterlogging). In the subsoil, geochemical and pedogenetic parameters rose to the forefront as predictors of OM thermal stability. These results suggest that soil horizons act as interacting yet distinct functional units in terms of OM dynamics and are likely to respond differently to external forcing. Therefore, next-generation conceptual or numerical models of soil OM cycling would be greatly improved by the implementation of depth-resolved schemes. Moreover, multi-disciplinary approaches, as the present one, may prove to be particularly relevant for the understanding and the prediction of soil OM fate under fast climate change.

Contribution statement

M.M. and P.V. designed the sampling strategy, performed vegetation records and soil descriptions in the field. M.M. analysed soil samples. M.M., S.G., and D.S. analysed data. P.V. and E.P.V. supervised the work. E.P.V. funded the work and contributed to design the sampling strategy. All co-authors contributed to the writing and the interpretation of data.

Acknowledgments

We thank Marie-José Petétot for her help in plant inventories and soil descriptions of the Morteys site, and analysis of the relative soil samples. We thank also Loïc Liberati, Swanee Messerli, Jessica Rion, Aurélie Rubin, Ayumi Koishi, Yohan Ancey and Jérémy Tritz for their help in the field, pH measurements and sample preparations. Dr. Thierry Adatte (ISTE, University of Lausanne) performed Rock-Eval and CHNS analyses. We are very grateful to Aline Buri for her suggestions on statistical analyses. The “Fondation Herbette” kindly supported Dr. David Sebag during his stays at the University of Lausanne.

Appendix A. Supplementary data

Supplementary data to this article can be found online at https://doi.org/10.1016/j.geoderma.2018.05.011.

References

Aber, J.D., Melillo, J.M., 1982. Nitrogen immobilization in decaying hardwood leaf litter as a function of initial nitrogen and lignin content. Can. J. Bot. 60, 2263–2269.
Aber, J.D., Melillo, J.M., Mcclaugherty, C.A., 1990. Predicting long-term patterns of mass-loss, nitrogen dynamics, and soil organic-matter formation from initial fine litter chemistry in temperate forest ecosystems. Can. J. Bot. 68, 2201–2208.
Adhikari, K., Hartemink, A.E., 2016. Linking soils to ecosystem services - a global review. Geoderma 262, 101–111.
Anderson, D.R., Burnham, K.P., Thompson, W.L., 2000;al.,. Null hypothesis testing: problems, prevalence, and an alternative. J. Wildl. Manag. 64, 912–923.
Baize, D., Girard, M.-C., 2009. Référentiel pédologique. Association française pour l'étude du sol (AFES), Versailles Cedex.
Baptist, F., Yoccoz, N.G., Choler, P., 2010. Direct and indirect control by snow cover over decomposition in alpine tundra along a snowmelt gradient. Plant Soil 328, 397–410.
Barré, P., Plante, A.F., Cécillon, L., Lutfalla, S., Baudin, F., Bernard, S., et al., 2016. The energetic and chemical signatures of persistent soil organic matter. Biogeochemistry 130, 1–12.
Baruck, J., Nestroy, O., Sartori, G., Baize, D., Traidl, R., Vrščaj, B., et al., 2016. Soil classification and mapping in the Alps: the current state and future challenges. Geoderma 264, 312–331.
Batjes, N.H., 1996. Total carbon and nitrogen in the soils of the world. Eur. J. Soil Sci. 47, 151–163.
Burnham, K.P., Anderson, D.R., 2002. Model selection and multimodel inference. In: A Practical Information-Theoretic Approach, 2nd ed. Springer, New York.
Carrie, J., Sanei, H., Stern, G., 2012. Standardisation of Rock-Eval pyrolysis for the analysis of recent sediments and soils. Org. Geochem. 46, 38–53.
Davidson, E.A., Janssens, I.A., 2006. Temperature sensitivity of soil carbon decomposition and feedbacks to climate change. Nature 440, 165–173.
Delarze, R., Gonseth, Y., Eggenberg, S., Vust, M., 2015. Guide des milieux naturels de Suisse, 3rd ed. Rossolis, Bussigny.
Derrien, D., Marol, C., Balabane, M., Balesdent, J., 2006. The turnover of carbohydrate carbon in a cultivated soil estimated by C-13 natural abundances. Eur. J. Soil Sci. 57, 547–557.
Diochon, A., Gillespie, A.W., Ellert, B.H., Janzen, H.H., Gregorich, E.G., 2016. Recovery and dynamics of decomposing plant residue in soil: an evaluation and three fractionation methods. Eur. J. Soil Sci. 67, 196–205.
FAO, 2006. Guidelines for soil description, 4th ed. Food and Agriculture Organization of the United Nations (FAO), Rome, Italy.
Favilli, F., Cherubini, P., Collenberg, M., Egli, M., Sartori, G., Schoch, W., Haeberli, W., 2010. Charcoal fragments of Alpine soils as an indicator of landscape evolution during the Holocene in Val di Sole (Trentino, Italy). The Holocene 20, 67–79.

Fierer, N., Allen, A.S., Schimel, J.P., Holden, P.A., 2003. Controls on microbial CO_2 production: a comparison of surface and subsurface soil horizons. Glob. Chang. Biol. 9, 1322–1332.
Gelman, A., 2008. Scaling regression inputs by dividing by two standard deviations. Stat. Med. 27, 2865–2873.
Gleixner, G., Bol, R., Balesdent, J., 1999. Molecular insight into soil carbon turnover. Rapid Commun. Mass Spectrom. 13, 1278–1283.
Gleixner, G., Poirier, N., Bol, R., Balesdent, J., 2002. Molecular dynamics of organic matter in a cultivated soil. Org. Geochem. 33, 357–366.
Grand, S., Lavkulich, L.M., 2012. Effect of forest harvest on soil carbon and related variables in Canadian Spodosols. Soil Sci. Soc. Am. J. 76, 1816–1827.
Grand, S., Rubin, A., Verrecchia, E.P., Vittoz, P., 2016. Variation in soil respiration across soil and vegetation types in an Alpine valley. PLoS One 11, e0163968.
Gregorich, E.G., Gillespie, A.W., Beare, M.H., Curtin, D., Sanei, H., Yanni, S.F., 2015. Evaluating biodegradability of soil organic matter by its thermal stability and chemical composition. Soil Biol. Biochem. 91, 182–191.
Harrell, F.E., 2001. Regression Modeling Strategies: With Applications to Linear Models, Logistic Regression, and Survival Analysis. Springer, New York.
Heim, A., Schmidt, M.W.I., 2007. Lignin turnover in arable soil and grassland analysed with two different labelling approaches. Eur. J. Soil Sci. 58, 599–608.
Hobbie, S.E., Chapin, F.S., 1996. Winter regulation of tundra litter carbon and nitrogen dynamics. Biogeochemistry 35, 327–338.
IUSS Working Group, 2015. World reference base for soil resources 2014, update 2015. International soil classification system for naming soils and creating legends for soil maps. In: World Soil Resources Reports No. 106. FAO, Rome.
Ivy-Ochs, S., Schafer, J., Kubik, P.W., Synal, H.A., Schluchter, C., 2004. Timing of deglaciation on the northern Alpine foreland (Switzerland). Eclogae Geol. Helv. 97, 47–55.
Jabiol, B., Zanella, A., Ponge, J.-F., Sartori, G., Englisch, M., Delft, B., et al., 2013. A proposal for including humus forms in the World Reference Base for Soil Resources (WRB-FAO). Geoderma 192, 286–294.
Jobbagy, E.G., Jackson, R.B., 2000. The vertical distribution of soil organic carbon and its relation to climate and vegetation. Ecol. Appl. 10, 423–436.
Knutson, E.O., Sood, S.K., Stockham, J.D., 1976. Aerosol collection by snow and ice crystals. Atmos. Environ. 10, 395–402.
Kögel-Knabner, I., Guggenberger, G., Kleber, M., Kandeler, E., Kalbitz, K., Scheu, S., et al., 2008. Organo-mineral associations in temperate soils: integrating biology, mineralogy, and organic matter chemistry. J. Plant Nutr. Soil Sci. 171, 61–82.
Lafargue, E., Marquis, F., Pillot, D., 1998. Rock-Eval 6 applications in hydrocarbon exploration, production, and soil contamination studies. Rev. Inst. Fr. Pétrol. 53, 421–437.
Landolt, E., Bäumler, B., Erhardt, A., Hegg, O., Klötzli, F.A., Lämmler, W., et al., 2010. Flora Indicativa. Ecological Indicator Values and Biological Attributes of the Flora of Switzerland and the Alps. Haupt, Bern, Switzerland.
Legendre, P., Gallagher, E.D., 2001. Ecologically meaningful transformations for ordination of species data. Oecologia 129, 271–280.
Lehmann, J., Kleber, M., 2015. The contentious nature of soil organic matter. Nature 528, 60–68.
Leifeld, J., Zimmermann, M., Fuhrer, J., Conen, F., 2009. Storage and turnover of carbon in grassland soils along an elevation gradient in the Swiss Alps. Glob. Chang. Biol. 15, 668–679.
Manzoni, S., Jackson, R.B., Trofymow, J.A., Porporato, A., 2008. The global stoichiometry of litter nitrogen mineralization. Science 321, 684–686.
Marschner, B., Brodowski, S., Dreves, A., Gleixner, G., Gude, A., Grootes, P.M., et al., 2008. How relevant is recalcitrance for the stabilization of organic matter in soils? J. Plant Nutr. Soil Sci. 171, 91–110.
Melillo, J.M., Aber, J.D., Muratore, J.F., 1982. Nitrogen and lignin control of hardwood leaf litter decomposition dynamics. Ecology 63, 621–626.
Mullen, R.B., Schmidt, S.K., Jaeger, C.H., 1998. Nitrogen uptake during snowmelt by the snow buttercup, *Ranunculus adoneus*. Arct. Alp. Res. 30, 121–125.
Oberhänsli, R., Schenker, F., Mercolli, I., 1988. Indications of Variscan nappe tectonics in the Aar Massif. Schweiz. Mineral. Petrogr. Mitt. 68, 509–520.
Plante, A.F., Fernandez, J.M., Haddix, M.L., Steinweg, J.M., Conant, R.T., 2011. Biological, chemical and thermal indices of soil organic matter stability in four grassland soils. Soil Biol. Biochem. 43, 1051–1058.
Ponge, J.F., Chevalier, R., Loussot, P., 2002. Humus index: an integrated tool for the assessment of forest floor and topsoil properties. Soil Sci. Soc. Am. J. 66, 1996–2001.
Preston, C.M., Nault, J.R., Trofymow, J.A., Smyth, C., Grp, C.W., 2009. Chemical changes during 6 years of decomposition of 11 litters in some Canadian forest sites. Part 1. Elemental composition, tannins, phenolics, and proximate fractions. Ecosystems 12, 1053–1077.
Rasmussen, C., Heckman, K., Wieder, W.R., Keiluweit, M., Lawrence, C.R., Behre, A.A., et al., 2018. Beyond clay: towards an improved set of variables for predicting soil organic matter content. Biogeochemistry 137, 297–306.
Rowley, M., Grand, S., Verrecchia, E., 2018. Calcium-mediated stabilisation of soil organic carbon. Biogeochemistry 137, 27–49.
Rumpel, C., Kögel-Knabner, I., 2011. Deep soil organic matter-a key but poorly understood component of terrestrial C cycle. Plant Soil 338, 143–158.
Rumpel, C., Kögel-Knabner, I., Bruhn, F., 2002. Vertical distribution, age, and chemical composition of organic, carbon in two forest soils of different pedogenesis. Org. Geochem. 33, 1131–1142.
Rumpel, C., Eusterhues, K., Kögel-Knabner, I., 2004. Location and chemical composition of stabilized organic carbon in topsoil and subsoil horizons of two acid forest soils. Soil Biol. Biochem. 36, 177–190.
Saenger, A., Cecillon, L., Sebag, D., Brun, J.J., 2013. Soil organic carbon quantity, chemistry and thermal stability in a mountainous landscape: a Rock-Eval pyrolysis survey. Org. Geochem. 54, 101–114.
Saenger, A., Cecillon, L., Poulenard, J., Bureau, F., De Danieli, S., Gonzalez, J.M., Brun, J.J., 2015. Surveying the carbon pools of mountain soils: a comparison of physical fractionation and Rock-Eval pyrolysis. Geoderma 241, 279–288.
Salomé, C., Nunan, N., Pouteau, V., Lerch, T.Z., Chenu, C., 2010. Carbon dynamics in topsoil and in subsoil may be controlled by different regulatory mechanisms. Glob. Chang. Biol. 16, 416–426.
Schiedung, M., Don, A., Wordell-Dietrich, P., Alcántara, V., Kuner, P., Guggenberger, G., 2017. Thermal oxidation does not fractionate soil organic carbon with differing biological stabilities. J. Plant Nutr. Soil Sci. 180, 18–26.
Schimel, D.S., 1995. Terrestrial ecosystems and the carbon-cycle. Glob. Chang. Biol. 1, 77–91.
Schimel, J.P., Schaeffer, S.M., 2012. Microbial control over carbon cycling in soil. Front. Microbiol. http://dx.doi.org/10.3389/fmicb.2012.00348.
Schimel, J.P., Weintraub, M.N., 2003. The implications of exoenzyme activity on microbial carbon and nitrogen limitation in soil: a theoretical model. Soil Biol. Biochem. 35, 549–563.
Schlesinger, W.H., Bernhardt, E.S., 2013. Biogeochemistry: An Analysis of Global Change, 3rd ed. Elsevier/Academic Press.
Schmidt, M.W.I., Torn, M.S., Abiven, S., Dittmar, T., Guggenberger, G., Janssens, I.A., et al., 2011. Persistence of soil organic matter as an ecosystem property. Nature 478, 49–56.
Sebag, D., Disnar, J.R., Guillet, B., Di Giovanni, C., Verrecchia, E.P., Durand, A., 2006. Monitoring organic matter dynamics in soil profiles by 'Rock-Eval pyrolysis': bulk characterization and quantification of degradation. Eur. J. Soil Sci. 57, 344–355.
Sebag, D., Verrecchia, E.P., Cécillon, L., Adatte, T., Albrecht, R., Aubert, M., et al., 2016. Dynamics of soil organic matter based on new Rock-Eval indices. Geoderma 284, 185–203.
Six, J., Conant, R.T., Paul, E.A., Paustian, K., 2002. Stabilization mechanisms of soil organic matter: implications for C-saturation of soils. Plant Soil 241, 155–176.
Sollins, P., Homann, P., Caldwell, B.A., 1996. Stabilization and destabilization of soil organic matter: mechanisms and controls. Geoderma 74, 65–105.
Soucémarianadin, L., Cécillon, L., Chenu, C., Baudin, F., Nicolas, M., Girardin, C., Barré, P., 2018a. Is Rock-Eval 6 thermal analysis a good indicator of soil organic carbon lability? A method-comparison study in forest soils. Soil Biol. Biochem. 117, 108–116.
Soucémarianadin, L.N., Cécillon, L., Guenet, B., Chenu, C., Baudin, F., Nicolas, M., et al., 2018b. Environmental factors controlling soil organic carbon stability in French forest soils. Plant Soil. http://dx.doi.org/10.1007/s11104-018-3613-x.
Spielvogel, S., Prietzel, J., Kögel-Knabner, I., 2008. Soil organic matter stabilization in acidic forest soils is preferential and soil type-specific. Eur. J. Soil Sci. 59, 674–692.
Symonds, M.R.E., Moussall, I.A., 2011. A brief guide to model selection, multimodel inference and model averaging in behavioural ecology using Akaike's information criterion. Behav. Ecol. Sociobiol. 65, 13–21.
Theurillat, J.P., Felber, F., Geissler, P., Gobat, J.-M., Fierz, M., Fischlin, A., et al., 1998. Sensitivity of plant and soil ecosystems of the Alps to climate change. In: Cebon, P., Davies, H.C., Imboden, D., Jaeger, C.C. (Eds.), Views From the Alps. MIT Press, Massachusetts, pp. 225–308.
van der Voort, T.S., Hagedorn, F., McIntyre, C., Zell, C., Walthert, L., Schleppi, P., et al., 2016. Variability in C-14 contents of soil organic matter at the plot and regional scale across climatic and geologic gradients. Biogeosciences 13, 3427–3439.
Vinduskova, O., Sebag, D., Cailleau, G., Brus, J., Frouz, J., 2015. Methodological comparison for quantitative analysis of fossil and recently derived carbon in mine soils with high content of aliphatic kerogen. Org. Geochem. 89-90, 14–22.
von Lützow, M., Kögel-Knabner, I., Ekschmitt, K., Matzner, E., Guggenberger, G., Marschner, B., Flessa, H., 2006. Stabilization of organic matter in temperate soils: mechanisms and their relevance under different soil conditions - a review. Eur. J. Soil Sci. 57, 426–445.
von Lützow, M., Kögel-Knabner, I., Ludwig, B., Matzner, E., Flessa, H., Ekschmitt, K., et al., 2008. Stabilization mechanisms of organic matter in four temperate soils: development and application of a conceptual model. J. Plant Nutr. Soil Sci. 171, 111–124.
Vonlanthen, C.M., Bühler, A., Veit, H., Kammer, P.M., Eugster, W., 2006. Alpine plant communities: a statistical assessment of their relation to microclimatological, pedological, geomorphological, and other factors. Phys. Geogr. 27, 137–154.
Webster, R., 2007. Analysis of variance, inference, multiple comparisons and sampling effects in soil research. Eur. J. Soil Sci. 58, 74–82.
Woolgrove, C.E., Woodin, S.J., 1996. Ecophysiology of a snow-bed bryophyte *Kiaeria starkei* during snowmelt and uptake of nitrate from meltwater. Can. J. Bot. 74, 1095–1103.
Zimmermann, N.E., Kienast, F., 1999. Predictive mapping of alpine grasslands in Switzerland: species versus community approach. J. Veg. Sci. 10, 469–482.

- This page is intentionally left blank -

8.6.4 - Rowley et al., 2017

- This page is intentionally left blank -

Plant Soil (2017) 412:465–479
DOI 10.1007/s11104-016-3135-3

REGULAR ARTICLE

Moving carbon between spheres, the potential oxalate-carbonate pathway of *Brosimum alicastrum* Sw.; Moraceae

Mike C. Rowley · Héctor Estrada-Medina · Magnolia Tzec-Gamboa · Aviram Rozin · Guillaume Cailleau · Eric P. Verrecchia · Iain Green

Received: 31 August 2016 / Accepted: 26 October 2016 / Published online: 16 December 2016

Abstract
Aims The Oxalate-Carbonate Pathway (OCP) is a biogeochemical process that transfers atmospheric CO_2 into the geologic reservoir as $CaCO_3$; however, until now all investigations on this process have focused on species with limited food benefits. This study evaluates a potential OCP associated with *Brosimum alicastrum*, a Neotropical species with agroforestry potential (*ca.* 70–200 kg-nuts yr^{-1}), in the calcareous soils of Haiti and Mexico.
Methods / results Enzymatic analysis demonstrated significant concentrations of calcium oxalate (5.97 % D.W.) were associated with *B. alicastrum* tissue in all sample sites. The presence of oxalotrophism was also confirmed with microbiological analyses in both countries. High concentrations of total calcium (>7 g kg^{-1}) and lithogenic carbonate obscured the localised alkalinisation and identification of secondary carbonate associated with the OCP at most sample sites, except Ma Rouge, Haiti. Soils adjacent to subjects in Ma Rouge demonstrated an increase in pH (0.63) and $CaCO_3$ concentration (5.9 %) that, when coupled with root-like secondary carbonate deposits in Mexico, implies that the OCP does also occur in calcareous soils.
Conclusions Therefore this study confirms that the OCP also occurs in calcareous soils, adjacent to *B. alicastrum*, and could play a fundamental and un-accounted role in the global calcium-carbon coupled cycle.

Keywords Oxalate-Carbonate Pathway (OCP) · *Brosimum alicastrum* · Calcium oxalate · Carbon-calcium cycle · Oxalotrophic bacteria

Responsible Editor: Hans Lambers.

Study locations Merida, Yucatán Peninsula, Mexico: Oxtapacab (20.77111°N / 89.50417 °W), San Jose Tzal (20.824167 °N / 89.66111 °W), Tzucacab (20.07083 °N / 89.05055 °W) and Haiti: Anse-à-Pitres (18.04306 °N / 71.75833 °W), Anse-Rouge (19.63333 °N / 73.05000 °W).

Highlights
1) Calcium oxalate identified in all analysed *Brosimum alicastrum*.
2) CaOx crystals probably help its younger form augment incident UV-radiation in light-limited environments.
3) Ma Rouge, a Haitian sampling site, demonstrated signs of early onset oxalotrophy.
4) Root-like secondary carbonate deposits were discovered in Mexico.
5) Evidence suggests that *Brosimum alicastrum* is oxalogenic and that oxalogenesis can occur in calcareous environments.

This research's sampling was funded by Bournemouth University, Biomimicry Europa, and Sadhana Forest.

Electronic supplementary material The online version of this article (doi:10.1007/s11104-016-3135-3) contains supplementary material, which is available to authorized users.

M. C. Rowley · G. Cailleau · E. P. Verrecchia
Université de Lausanne, Faculté des Géosciences et de l'Environnement (GSE), Institut des Dynamiques de la Surface Terrestre (IDYST), Lausanne, Switzerland

Introduction

Soils play a major role in the cycling of carbon (C) and understanding the processes that regulate C migration

from one reservoir to the next is of globally recognised significance. The Oxalate-Carbonate Pathway (OCP; Fig. 1) is a biogeochemical cycle that results in the transfer of atmospheric carbon dioxide (CO_2^{Atm}) into the geologic C reservoir within soils, as calcium carbonate ($CaCO_3$). The process probably plays an important role in the regulation of CO_2^{Atm} within the global C cycle (Cailleau et al. 2005; Cailleau et al. 2014) when the source of calcium (Ca) is provided by silicate rocks. OCP has several key components, involving; calcium oxalate (CaOx; $CaC_2O_4 \bullet n\ H_2O$) producing plants, fungi, phytophagous invertebrates, and oxalotrophic bacteria (Cailleau et al. 2004, 2011; Cailleau et al. 2014; Garvie 2006). The first stage commences when CO_2^{Atm} is fixed by RuBisCo during photosynthesis, forming biomass and oxalic acid ($H_2C_2O_4$; Fig 2). Oxalic acid can then be converted into insoluble CaOx crystals ($K_{sp} \approx 10^{-8.5}$; Certini et al. 2000; Monje and Baran 2002; Palak et al. 2012) by plants within specialised cells called crystal idioblasts (Faheed et al. 2013; Franceschi and Nakata 2005; Nakata 2002, 2003). These CaOx crystals are subsequently released during herbivory and decomposition, creating a CaOx pool adjacent to the producing species, in its rhizosphere (Cailleau et al. 2011; Jayasuriya 1955), stomachs of endopedonic species (Bassalik 1913), or within phytoabrasions (Cailleau et al. 2004; Verrecchia et al. 2006). Consequently, this pool of CaOx can then be catabolised by bacteria, labelled oxalotrophic through either the common glycolate- (Bravo et al. 2013; Chandra and Shethna 1977; Tamer and Aragno 1980) or less common serine-pathway (Sahin 2003), precipitating C as $CaCO_3$ and creating a distinct local alkalinisation of acidic soils (Cromack et al. 1977; Fig. 3). Therefore, an active OCP has the ability to biominerally transfer CO_2^{Atm} within the geologic reserve.

Although there have been numerous studies on the OCP, analysis has typically focused on tree species in

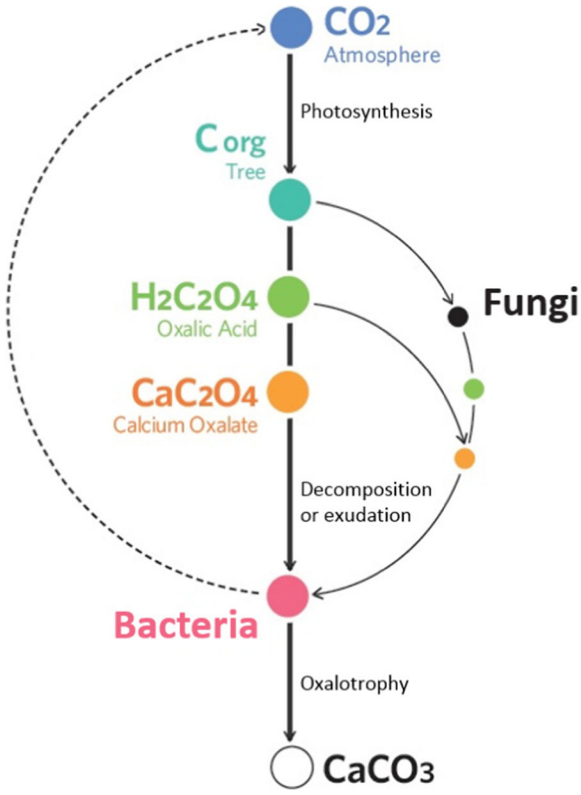

Fig. 1 A simplified model of the Oxalate-Carbonate Pathway (OCP), a process that transfers carbon dioxide from atmosphere to secondary calcium carbonate. As described by Cailleau et al. (2014), the process commences when a calcium oxalate producing species (Tree) organically sequesters carbon during photosynthesis (Corg), converting it into oxalic acid and then calcium oxalate. Once released from organic material during decomposition or as exudes, calcium oxalate is subsequently catabolised by oxalotrophic bacteria (Bact.), converting one mol as carbonate and releasing another as respired carbon dioxide. Fungi also assist in the process by either breaking down oxalic rich matter and depositing calcium oxalate for catabolism by bacteria, or by fungal oxalotrophy

$$\mathbf{1.)\ C_6H_{12}O_6 + O_2 \Longrightarrow 2C_3H_4O_3 + 2\ H_2O}$$

$$\mathbf{2.)\ 2C_3H_4O_3 + 2\ CO_2 \Longrightarrow 2\ C_4H_4O_5}$$

$$\mathbf{3.)\ 2\ C_4H_4O_5 + 2\ H_2O \Longrightarrow 2\ H_2C_2O_4 + 2\ H_4C_2O_2}$$

$$\mathbf{4.)\ 2\ Ca^{2+} + 2\ H_2C_2O_4 + O_2 \Longrightarrow 2\ CaC_2O_4.H_2O}$$

Fig. 2 Oxalic acid production and subsequent precipitation of calcium oxalate from glucose. 1.) Glucose is first oxidated to form pyruvate. 2.) Then pyruvate is carboxylated to produce oxaloacetate. 3.) The subsequent hydrolysis of oxaloacetate forms oxalate and acetate. 4.) Where Ca^{2+} can then react with oxalic acid to form calcium oxalate as either mono- or di-hydrate crystals (Verrecchia 1990; Verrecchia et al. 2006)

H. Estrada-Medina · M. Tzec-Gamboa
Universidad Autónoma de Yucatán, Campus de Ciencias Biológicas y Agropecuarias, Mérida, Mexico

A. Rozin
Sadhana Forest, Auroville, Tamil Nadu, India

M. C. Rowley (✉) · I. Green
Bournemouth University, Faculty of Science and Technology, Poole, UK
e-mail: mike.rowley@unil.ch

$$1000CaC_2O_4 \,.\, n\,H_2O + 372\,O_2 + 32\,NH_4^+ \Rightarrow 32\,C_4H_8O_2N^+_{Biomass} + 936\,CaCO_3 + 64\,Ca(OH_2)_{aq} \cdots + (1000.(n-2) + 1872)\,H_2O + 936\,CO_2$$

Fig. 3 Oxalotrophic catabolism of calcium oxalate by bacteria (in Verrecchia et al. 2006, from Harder et al. 1974)

acidic soil environments. At current, investigations have confirmed 24 species are associated with active OCPs (Braissant et al. 2002; Cailleau et al. 2004; Cailleau et al. 2014; Ferro 2012; Garvie 2003, 2006; Monje and Baran 2002), typically utilising the emblematic localised alkalinisation of acidic soils as a geochemical proxy for oxalogenesis. The most heavily investigated OCP is associated with *Milicia excelsa Welw.* (Moraceae) in ferralitic soils of Africa (Aragno et al. 2010; Braissant et al. 2004; Braissant et al. 2002; Cailleau et al. 2005; Cailleau et al. 2004; Martin et al. 2012). For which, Cailleau et al. (2011) demonstrated a potential sequestration of *ca.* 1 t C as $CaCO_3$ throughout a model individual's lifetime. Later work identified a further two species within the Moraceae family (Cailleau et al. 2014), associated with an OCP, while earlier work has demonstrated CaOx production in several other species within the family (Wu and Kuo Huang 1997), including the food-producing genus *Brosimum* (Scholz et al. 2007). However, most studies on the OCP have focused on species without agroforestry potential and there has currently been no investigations into a potential OCP associated with the Moraceae genus *Brosimum.*

Brosimum alicastrum Swartz, Moraceae *(B. alicastrum)* is a large Neotropical, ever-green, canopy-emergent tree species utilised in Central America for agroforestry purposes and conservation marketing operations. It is common throughout the dry and wet semi-evergreen forests of the Caribbean, Central America, and Northern-South America (Ortiz et al. 1995; Yates and Ramirez-Sosa 2004). The species has a height range of around 20–40 m, increasing with precipitation, and a common Diameter at Breast Height (DBH) of 1–1.5 m, increasing North–south (Peters 1983, 1989). It is a species shown to be drought resistant (Brewer et al. 2003; Querejeta et al. 2006), growing well in Leptosols of different biomes, while producing nutritious nuts (Peters and Pardo-tejeda 1982). These natural products can be processed to form a range of foods, medicines and excellent fodder for almost all large gregarious mammals, (Gillespie et al. 2004; Ricogray et al. 1991). The species starts seed production after reaching sexual maturity (i.e. 5–7-yr) and, thereafter, an individual can produce around 70–200 kg-seeds yr^{-1} (±30 kg) throughout its 150–200-yr life cycle (Gillespie et al. 2004; Ortiz et al. 1995; Peters 1983, 1989). Furthermore, recent work by Woda and Martinez (2013) has shown that *B. alicastrum*'s seeds have an established, economic harvest return of US $ 650 ha yr^{-1} in Honduras, almost doubling that of maize (US $ 326 ha yr^{-1}); thus, highlighting the potential of *B. alicastrum* as an effective agroforestry crop.

If *B. alicastrum* was found to be in association with an active OCP, it would represent an ideal agroforestry crop with biomineral C fixation capabilities. However, currently the OCP has only been identified in acidic soils, free from inherited carbonate (Cailleau et al. 2014), unlike the predominate habitat of *B. alicastrum* (Peters and Pardo-tejeda 1982). The presence of carbonate in calcareous soils increases the complexity of identifying an OCP (Cailleau et al. 2014), but shouldn't prevent its identification through the analysis of the process' constituents and geochemical proxies. Therefore, the aim of this work is to ascertain if *B. alicastrum* is associated with an active oxalate-carbonate pathway in the calcareous soils of Haiti and Mexico, via the following questions:

1) Does *B. alicastrum* produce CaOx, and if so, is there geochemical evidence of an active OCP adjacent to the species in calcareous soils?
2) Are there oxalotrophic bacterial communities in calcareous soils adjacent to subject *B. alicastrum* in both Haiti and Mexico?
3) What is the C fixation potential of a model *B. alicastrum* agroforestry system in calcareous soils?

Materials & methods

Site settings

Calcareous sample sites were selected with notable environmental and biogeographical similarities in Anse-à-

Pitres (A, B - Banane, C - Bony, D – Ma Rouge) and Anse Rouge (E), Haiti and, the Yucatán Peninsula (F - Tzucacab, G - Oxtapacab, H – San Jose Tzal), Mexico (Fig. 4). The Yucatán sites sit atop a partially emergent carbonate platform of low-lying, Tertiary limestone karst and were typically characterised as either Calcic or Calcaric Leptosols or Cambisols in Oxtapacab and San Joze Tazal, or Luvisols in Tzucacab (Ramos 1975; Shang and Tiessen 2003; WRB 2015) that receive an annual rainfall of approximately 1,100 mm yr^{-1} (Giddings and Soto 2003). Mexico provided mature trees in contrast with Haiti, where only recent plantations were available for sampling. Anse-à-Pitres and Anse Rouge also sit atop Tertiary limestone karst, with thin eroded soils that were predominately classified as Calcaric or Calcic Cambisols, although several sites in Ma Rouge presented a non-calcareous nature (just below classification of Calcaric ≤2 % $CaCO_3$; WRB 2015). Accurate climatic data on the two regions is sparse, but both regions are subject to an annual hurricane season of fluctuating strength (Whigham and Lynch 1998; Whigham et al. 2003), which just preceded sampling for this investigation (2013).

Sampling

A sample of 50 subject *B. alicastrum* of varying size and maturity were selected from both study countries (20 Mexican, 30 Haitian) using stratified-random techniques. Two samples were taken from each subject, an experimental sample from adjacent to the subject and a control sample, exogenous of the subject's zone of lateral edaphic influence (3.5–25 m depending on subject height). To analyse the bulk differences between adjacent and control sites, all soil profiles were taken to their shallow bedrock (10–40 cm) and bulked.

Samples of *B. alicastrum* tissue were taken from each subject for biogeochemical analyses. 3 Foliar and 3 branch samples were taken from the lowest branches of each subject, mid-branch, ensuring uniformity

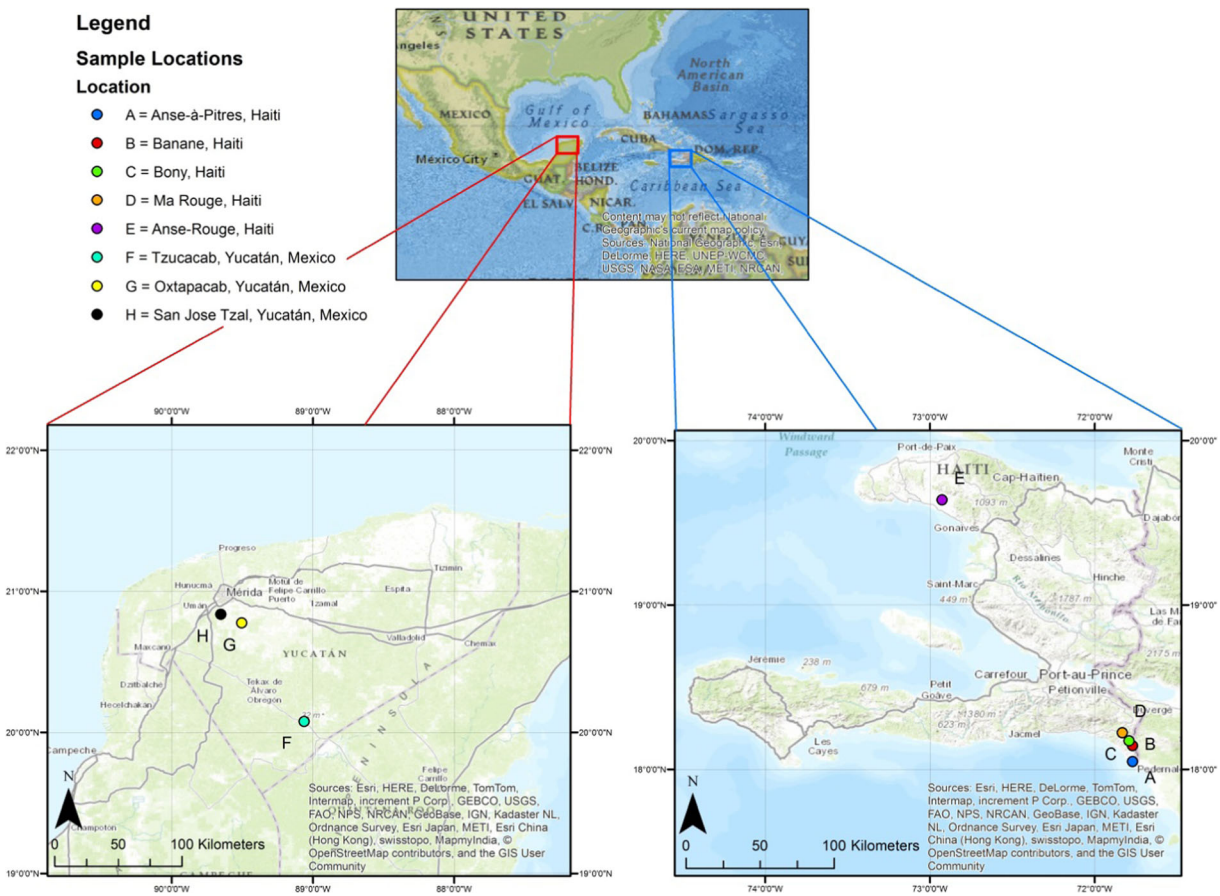

Fig. 4 Sample sites in Haiti and Mexico (Esri 2014)

amongst samples in both countries. Root and bark samples were only taken from Mexican subjects to restrict the damage to the younger trees in Haiti. Subject locations were recorded using GPS systems (Opteka GPS & Garmin GPS 76) and measurements of DBH, soil sample depth, and height, were obtained using 30 m tape and, where necessary, in conjunction with a clinometer (Sokkia No. 8047).

Sample preparation

All soil and plant samples, except those for bacterial analyses, were air-dried in the field to prevent decomposition and decay, and then transported to Bournemouth for laboratory analyses via courier. Bournemouth samples were autoclaved (Astell Swiftlock Securetouch +; 121 °C for 30 mins) on arrival as part of the plant health licence (Food, Environment and Rural Affairs) for importing foreign soils and plant material into the UK. Soil samples were then sieved to fine earth fraction (<2 mm) for chemical analysis, while plant samples were homogenised using a rotor mill and stainless steel-bore mill kit (Retsch MM200). Field-moist samples from each study site, except Anse Rouge, were sent urgently to a laboratory in the Yucatan for bacterial analysis and stored at 4 °C prior to examination. Live samples from Haiti were delayed in Mexican customs for a month, but were also held at 4 °C.

Calcium oxalate analysis

Microscopy

The presence of CaOx in *B. alicastrum* tissue was first identified using optical and Scanning Electron Microscopy (SEM). Samples were prepared for optical microscopy using techniques adapted from Ilarslan et al. (2001). Various tissues from both countries were submerged in Carnoy Fluid (3:1 ethyl alcohol: acetic acid) and left in Petri dishes for 24 h, then re-submerged in ethyl alcohol for 1.5 h. Samples were then coated in 2.5 % sodium hypochlorite and rested for 4 h before mounting with glycerine-gelatine. Slides were observed with an Olympus BX51 compound microscope, using both dark and light field microscopy, and images were captured with an Olympus DP70 Digital Microscope Camera (Olympus Inc.).

SEM and Energy Dispersive X-ray Spectroscopic (SEM/EDS) techniques adapted from Garvie (2003) were used to image and detect the composition of observed crystals. Homogenised plant tissue was applied to alloy stubs using adhesive stickers and AuPd sputter coated (B-7341 Agar Auto Sputter Coater) for 40–60 s. Samples were subsequently analysed in high vacuum using a Jeol JSM-6010 Plus/LV SEM, with an INCA X-sight 8129 EDS system (ETAS Inc.), and InTouchScreen software. All EDS readings represent a percentage of the analysed substance's atomic weight and were recorded in K-band. Furthermore, surficial measurements are considered semi-quantitative as these measurements are applied to 3-dimensional objects.

Enzymatic oxalate analysis

Calcium oxalate concentrations of each *B. alicastrum* sample were quantified using a commercial Enzymatic Oxalate Kit (EOK; Trinity Biotech Plc; Cailleau et al. 2014; Certini et al. 2000). The EOK functions through the oxidation of oxalate by the enzyme (oxalate oxidase) into CO_2 and hydrogen peroxide, which is subsequently oxidized by peroxidase, 3-methyl-2-benzthiazlinone hydrazine (MBTH) and 3-dimethylamino benzoic acid (DMAB) into an indamine dye with a maximum absorbance of 590 nm. Sub-samples of 0.1 g were taken from each plant tissue sample and placed into 30 mL tubes, combined with 5 mL 1 M hydrochloric acid (HCl) extractant and shaken for 16 h at 150 revs min^{-1} (Bibby Stuart Orbital Shaker SO1). The extractants were then centrifuged at 3,000 revs min^{-1} for 5 mins (Heraeus Instruments Megafuge 1.0) and 1 mL supernatant transferred into new 30 mL tubes. This was subsequently combined with 4 mL Ultra-Pure H_2O (Millipore™; 18.2 mΩ at 25 °C) and 0.4 mL 2 M sodium hydroxide (NaOH) for pH correction (pH 5–7) and, thereafter, the manufacturer's instructions were followed. Absorbance was then measured at 590 nm using a Carey 50 UV/vis spectrophotometer (Varian Inc.) after 20 min had elapsed to allow full colour development. Certain soil samples were also measured with the same techniques, adjusting the extraction procedure for the lower concentrations of oxalate. The kits reported the oxalate concentration in mg kg^{-1} which was then adjusted by multiplying the concentrations by the difference in M.W. (1.66) between whewellite (CaOx monohydrate; $CaC_2O_4.H_2O$ M.W.: 142.112 g M^{-1}) and oxalate ($C_2O_4^{-2}$ M.W.: 88.019 g M^{-1}) to give CaOx monohydrate concentrations of each sample.

Total carbon analysis

Total C was ascertained using dry combustion techniques adapted from Wright and Bailey (2001), analysing the tissue of randomly selected *B. alicastrum* subjects from each sampling location. Briefly, triplicates of 1–2 mg of homogenised sample were placed into a tin capsule (Barry and Pinkard 2013; Schutz et al. 2009) and combusted at 1,600 °C in a thermal elemental analyser (Thermo Finnegan FlashEA 1112), standardising peak integration by combusting 2.5-Bis (5–tert-butyl-benzoxazol-2-yl) thiophene (BBOT).

Analysis of edaphic variables associated with the OCP

Loss on ignition

Organic matter content (% OM) of each soil sample was calculated through loss on ignition (Cailleau et al. 2014). 1 g of oven dried (105 °C; Memmert UN 55) soil was furnaced (Carbolite model OAF 11 / 1) at 450 °C for 12 h and the percentage mass loss on ignition calculated.

Soil pH

pH_{H2O} was measured using techniques adapted from Cailleau et al. (2005). 4 g of soil was combined with 10 mL of distilled water ($_d$ H_2O), reposed for 16 h and measured in triplicate with a pH meter (Hach H135 Mini-lab Pro).

ICP-OES

The elemental composition of all soil samples was ascertained using a Vista-Pro CCD Simultaneous Inductively Coupled Plasma-Optical Emission Spectrometer (ICP-OES; Varian inc.) and different extraction methods. Exchangeable concentrations (Ca^{exch} and P^{exch}) were extracted using 1 M ammonium nitrate (NH_4NO_3) extraction technique adapted from MAFF (1986). 0.5 g of soil was combined with 10 mL 1 M NH_4NO_3 in 30 mL polypropylene tubes and shaken for 33 min at 250 revs min^{-1}, the reposed solution was then filtered (Whatman No. 42) and analysed on the ICP-OES. Total concentrations (Ca^{Tot}) were extracted using nitric acid (HNO_3) digestion in a microwave (Anton Parr Multiwave 3000). 0.1 g of soil from each sample was digested with 6 mL 70 % HNO_3 (Fisher Scientific Primar Plus Trace Metal grade) at 200 °C / 20 Bar (800 W), for 30 mins. The microwaved solutions were then filtered (No. 42) and diluted (50 mL) with Ultra-pure H_2O. Quality Control was ensured through the analysis of process blanks and CRM samples (NWRI/INRE TH-2; extraction efficiency $Ca = 100.00$ %, $RSD = 3.98$; $P = 87.18$ %, $RSD = 5.59$).

Soil carbonate

Calcium carbonate concentration was evaluated with a back titration (Cailleau et al. 2014). Briefly, 1 g of soil was combined with 0.25 M Sulphuric acid (H_2SO_4) and then back-titrated with 0.5 M NaOH until a pH 7 was attained. It was not possible to confirm pure presence of $CaCO_3$ using XRD and although a potential error induced by the presence of magnesium carbonate ($MaCO_3$) is small enough to preclude (Cailleau et al. 2005), $CaCO_3$ concentrations are reported as (Ca_{1-x}, Mg_x) CO_3 % D.W..

Identification of oxalotrophy

Oxalotrophic bacterial analysis was completed on each study site, except Anse Rouge, utilising techniques adapted from Braissant et al. (2004). For each study site, 2 g of field moist sample was placed into a 50 mL centrifuge tube and vortexed for 1 min with 20 mL of 1 % sodium hexametaphosphate ($[NaPO_3]_6$), before reposing for a further 20 mins at room temperature. Serial dilutions (10^{-2} a 10^{-4}) were made with 0.9 % sodium chloride (NaCl) solution and then propagated on petri dishes with two layers of media (Aragno and Schlegel 1992). The first layer was a Schegel medium (7 g L^{-1}), while the second layer consisted of Schegel medium with 4 g L^{-1} CaOx monohydrate ($CaC_2O_4.H_2O$), diluted to 10^{-2} or 10^{-4}. Dishes were then incubated at 30 °C for 10–15 days and counted for colonies, every 72 h after the 3rd day of incubation.

Inverse modelling of a potential OCP

The quantity of CO_2^{Atm} captured during OCP bio-induced $CaCO_3$ precipitation associated with an ideal oxalotrophic system was evaluated through the inverse modelling of observed variables and previous literature values (Benjamin et al. 2001; Cairns et al. 1997; Cairns

et al. 2003; Gill and Jackson 2000; Peters 1989), using inverse modelling equations given in the Supplementary information. The model estimates a potential maximum biomineral $CaCO_3$ precipitation and organic C sequestration associated with a *B. alicastrum* OCP by inverse modelling the biochemical characteristics ascertained with the aforementioned methods.

Statistical analysis

Statistical analysis was utilised to evaluate the potential oxalogenesis of *B. alicastrum*. All data was tested for homoscedasticity (Levene's test, $p > 0.05$) and then analysed with partial correlation. Two-way ANOVAs or independent t-tests were applied using IBM SPSS Statistics Version 21, testing the differences between adjacent and control samples, in both countries.

Results

Calcium oxalate analysis

Microscopy

Optical microscopy revealed crystal deposits throughout *B. alicastrum* OM. Prismatic crystals were typically associated with the vascular structure of OM, while druse crystal deposits were associated with the lamina of *B. alicastrum* foliar tissue, from both Haiti and Mexico (Fig. 5). Crystals were present in all forms of sampled *B. alicastrum* tissue (leaf, branch, bark, and root), even in the youngest measured subjects (<0.5 yrs), while in-situ SEM/EDS analyses detected Ca, C, and oxygen in the crystals. Their composition and crystallographic habiti (Verrecchia et al. 1993) confirmed their CaOx monohydrate nature (Fig. 5).

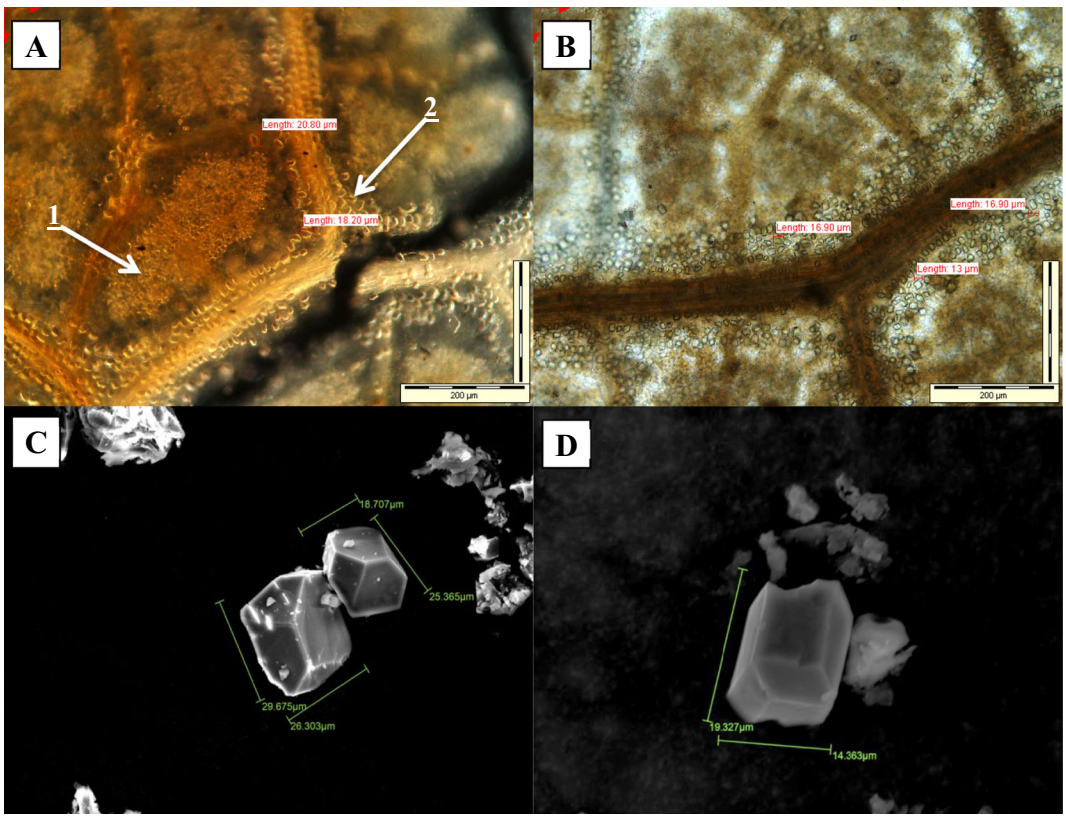

Fig. 5 Calcium oxalate crystals observed and imaged in *Brosimum alicastrum* tissue using optical and scanning electron microscopy. **a** Druse / sand CaOx crystals (1) associated with the lamina, and prismatic CaOx crystals (2) associated with the vascular system of foliar tissue from a Haitian subject. **b** Prismatic and druse CaOx crystals in foliar tissue from a Mexican subject. **c** Prismatic CaOx crystal isolated from the rhytidome of a Mexican subject. **d** Prismatic CaOx crystal isolated from a Mexican subject's root tissue all of which are prismatic habiti common in whewellite

Enzymatic oxalate analysis

Enzymatic oxalate kit analyses quantified the presence of CaOx monohydrate in *B. alicastrum* tissue (Fig. 6). Highest concentrations of CaOx were discovered in Haitian leaf matter, while concentrations decreased with age, between the younger Haitian (mean = 97.26 g kg^{-1}) and mature Mexican subjects (mean = 42.66 g kg^{-1}, $t_{[19]} = 4.385$, $p = 0.001$). High mean concentrations of CaOx were also found in *B. alicastrum* bark (72.79 g kg^{-1}) and root (57.86 g kg^{-1}) material from Mexico, with the lowest concentrations found in branch material of both countries (mean = 38.30 g kg^{-1}). CaOx production did not correlate with Ca^{Exch} ($r^2 = 0.208$, $n = 50$) or P^{Exch} ($r^2 = 0.004$, $n = 50$).

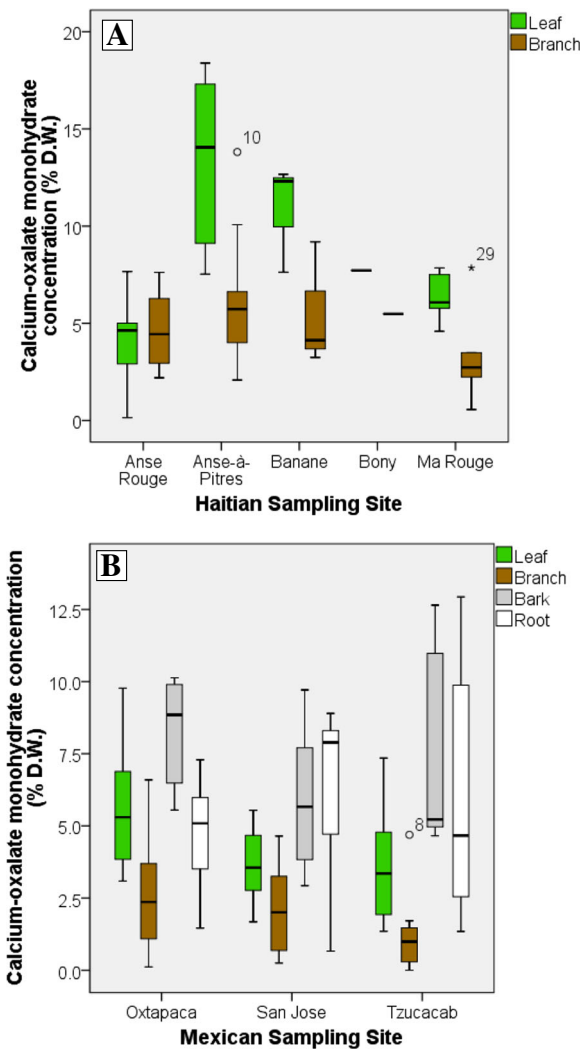

Fig. 6 Box plot graphs displaying oxalate concentrations (% D.W.) of subject Brosimum alicastrum leaf and branch tissue at Haitian sampling sites (**a**), and leaf, bark, root and branch tissue at Mexican sampling sites (**b**)

Analysis of edaphic variables associated with the OCP

The effect of *B. alicastrum* on emblematic edaphic variables associated with the OCP was tested using two-way ANOVAs. The presence of *B. alicastrum* had a negligible effect on all edaphic variables related to the OCP, at all sites combined ($[Ca_{1-x}, Mg_x] CO_3$ $F_{[1,3]} = 0.545$, $p = 0.462$, Ca^{Tot} $F_{[1,\ 3]} = 0.189$, $p = 0.665$ & pH $F_{[1,\ 3]} = 0.07$, $p = 0.787$), except Ma Rouge, Haiti. Ma Rouge displayed the lowest background concentrations of Ca^{Tot} (mean = 6.74 g kg^{-1}) and, although the subjects at Ma Rouge were very young (0.5–2 yrs), the adjacent samples demonstrated clear germinal indications of oxalotrophy (Table 1), namely: (i) a distinct localised alkalinisation, (ii) an increase in concentrations of Ca^{Tot}, (iii; Ca_{1-x}, Mg_x) CO_3 concentration (Fig. 7; Cailleau et al. 2014), and (iv) P^{Exch}, which is unrelated to the OCP, but can be an indicator of CaOx production and release, which subsequently liberates inorganic-bound P (Cannon et al. 1995). There was also an increase in Ca^{Exch} (mean increase 2.73 g kg^{-1}) in the adjacent Ma Rouge sites, but not others ($F_{[1,\ 3]} = 0.002$, $p = 0.962$), indicative of localised Ca cycling by the trees (Jobbágy and Jackson 2001).

Oxalotrophic microbial analysis

Oxalotrophy was detected in cultures from all sampling locations, in both Haiti and Mexico. All samples, except one experimental sample and four control Haitian samples, tested positive for oxalotroph colonies. Haitian study sites displayed a lower frequency of positive colonies than Mexican sites which could be due to the delay in customs; thus, making a direct comparison between the two impossible.

Sampling observations

Multiple mechanisms for the release of *B. alicastrum* produced CaOx were identified in association with subjects in both countries, for instance: phytophagous invertebrate predation (termite) and mycological decomposition (Fig. 8). Secondary carbonate deposits, confirmed through effervescence with 2 M HCl, were found in association with the largest subjects in Mexico. These carbonate deposits were typically concentric, located mid-soil profile, in-between the root network of the subjects, and were

Table 1 Independent samples t-tests comparing the means of edaphic variables related to the oxalate-carbonate pathway, in the adjacent and control profiles at the Ma Rouge sampling site

Variable	Adjacent		Control		t	P	Eta^2
	Mean	SD	Mean	SD			
pH	7.94	0.24	7.31	0.17	5.38	0.00	0.74
Ca^{Tot} (g kg^{-1})	42.79	31.00	6.74	1.91	2.84	0.04	0.45
(Ca_{1-x}, Mg_x) CO_3 (% D.W.)	11.05	4.60	5.15	4.46	2.26	0.48	0.34
P^{Exch} x 10^{-3} (g kg^{-1})	8.09	3.37	1.63	1.40	4.34	0.00	0.65

different in colour, texture and friability from the lithogenic carbonate, crumbling easily upon extraction (Fig. 8).

Carbon capture potential

The calculated values given in Tables 2 and 3 represent an ideal model of oxalotrophy, CaOx production, organic C sequestration, and also decomposition. Whereby, all CaOx and C captured by *B. alicastrum* as either organic C sequestration or $CaCO_3$ precipitation, is stored within the associated C reserve. CaOx concentrations (% D.W.) are calculated from the CaOx concentrations ascertained with the enzymatic oxalate analysis multiplied by the molecular weight of CaOx monohydrate (whewellite; $CaC_2O_4.H_2O$ M.W.: 142.112 g M^{-1}), the most abundant form of CaOx in plants (Aragno et al. 2010).

Discussion

Calcium oxalate and *B. alicastrum*

The present study has demonstrated that CaOx is ubiquitous throughout all forms of analysed *B. alicastrum* tissues, and that production commences at a young age for the species (<0.5 yrs). CaOx concentrations in subject tissue regularly exceeded 5 % D.W. (Libert and Franceschi 1987) and the mean oxalate concentration for all sampled tissues in both Haiti and Mexico was 5.97 % D.W. (59.71 g kg^{-1}, $n = 140$). Furthermore, inverse modelling of the species' biochemical analysis revealed that *B. alicastrum* deposits significant quantities of CaOx into its surrounding edaphic ecosystem on an averaged, annual basis throughout its lifetime. The quantities of oxalate within its tissue are proportionally

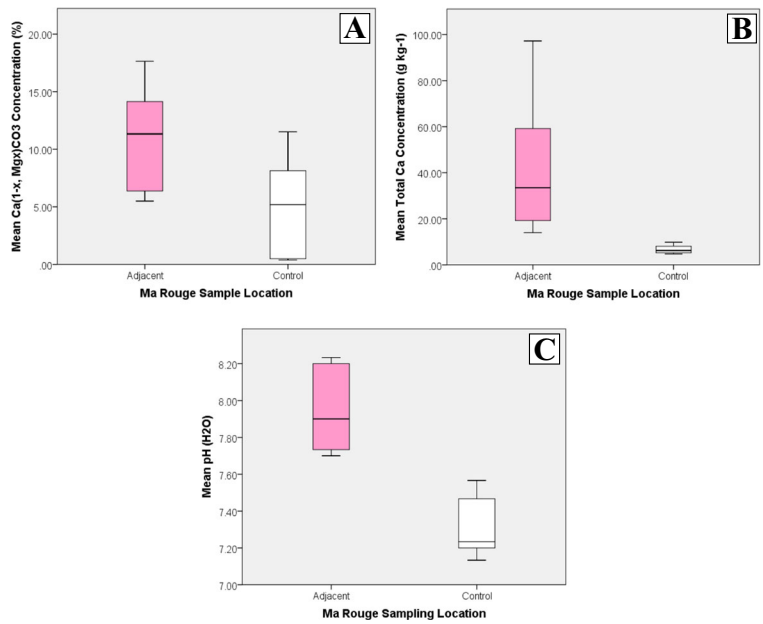

Fig. 7 Box plot graphs displaying soil variables associated with the OCP from adjacent and control (3.5 m distance) samples at Ma Rouge Haiti, which displayed the lowest background concentrations of total Ca, in the following order: (**a**) soil pH values, (**b**) total calcium concentration and (**c**) calcium carbonate concentration, the purity of which was not ascertained

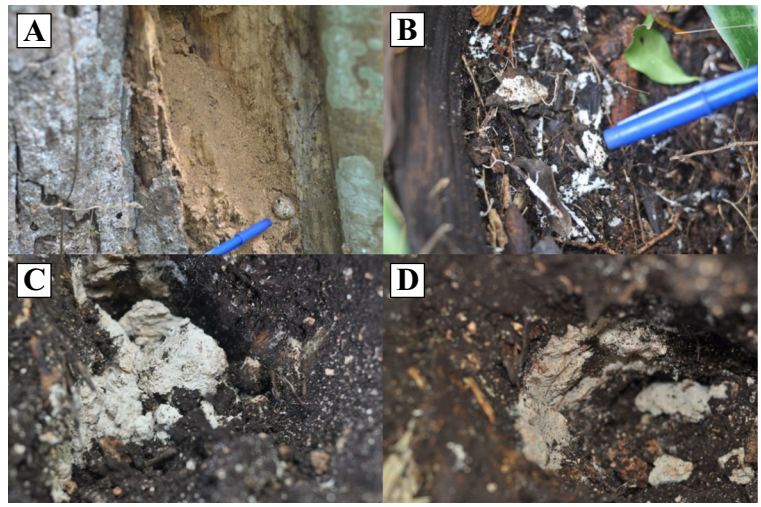

Fig. 8 Photographic observations from sampling. **a** Evidence of phytophagous invertebrate predation. **b** Mycological degradation of CaOx rich tissue in the rhizosphere adjacent to a Mexican subject. **c** Idiosyncratic carbonate mineral deposit, concentric and root-like in structure, located within the root network of a Mexican subject. **d** Concentric carbonate-rich mineral deposit at 1 m distance from a Mexican subject

magnified by the species large biomass; thus, creating a potent source of potential OCP C storage if planted in an acidic soil environment free from a lithogenic carbonate source.

The primary phyto-function of CaOx production in *B. alicastrum* remains unclear. Contrary to previous studies, this investigation found no significant relationship between *B. alicastrum*'s CaOx production and Ca^{Exch} (Austenfeld and Leder 1978; Rasmussen and Smith 1961; Volk et al. 2002) or P^{Exch} (Cannon et al. 1995; Knight et al. 1992) concentrations in most sites, providing weak evidence that CaOx production is utilised for the phyto-regulation of Ca^{Exch} or release of P^{Exch} from inorganic-pools. Equally, the use of *B. alicastrum* tissue for fodder and the non-raphide morphology or size of crystals (Sakai et al. 1984; Salinas et al. 2001) indicate that the species does not use CaOx production as an herbivory deterrent. However, the concentrated production of druse crystals in the lamina of *B. alicastrum* foliar tissue could distribute UV light to chloroplasts, increasing incident UV absorbency in understory environments, as originally hypothesised by Franceschi (2001) and later demonstrated experimentally by Kuo-Huang et al. (2007) in *Peperomia glabella*. This hypothesis explains the observed decrease in subject foliar CaOx concentration with age, while also explaining *B. alicastrum's* high survival rates under dense canopy (>80 %; Laborde and Corrales-Ferrayola 2012). Therefore, a role for *B. alicastrum* CaOx druse crystal production in the maximisation of incident UV light is hypothesised.

Table 2 Mean calcium oxalate and carbon contents of *B. alicastrum* tissue from both countries used in the inverse modelling of the carbon capture ability of an ideal individual or hectare population

Tissue type	Mean calcium oxalate content (% D.W.)	Mean total carbon (% D.W.)
Leaf	7.54	35.68
Branch	3.91	41.63
Bark	7.28	45.70
Root	5.79	41.34
Mean tissue	5.97	39.98

During this investigation, the root network of *B. alicastrum* was of particular interest. *B. alicsatrum* has a root network that is mainly concentrated in the upper soil and bedrock layers (Querejeta et al. 2006). The EOK analyses indicated that *B. alicastrum* root tissue contains a significant concentration of CaOx, which, when coupled with the Cairns et al. (1997) root / shoot ratio (0.26) and Gill and Jackson (2000) root turnover rate (0.1 yr^{-1}), predict that *B. alicastrum* deposits significant quantities of CaOx directly into its rhizosphere through the continuous decomposition and regeneration of root OM. Furthermore, investigations have demonstrated that *B. alicastrum* roots have strong associations with mycorrhizal fungi (Allen et al. 2003; Allen et al. 2005) that, Bravo et al. (2013) demonstrated act as highways for the dispersal of oxalotrophic bacteria to oxalate, creating an ideal mutualistic habitat for oxalotrophy.

Table 3 Estimates for the carbon capture ability of an ideal *B. alicastrum* individual and hectare plantation of 400 individuals

Predictions	Total calcium oxalate output (kg)	Potential biomineral precipitation of captured CO_2^{ATM} as $CaCO_3$ (kg)	Potential organic carbon sequestration of CO_2^{Atm} as biomass (kg)	Potential total CO_2 capture (kg)	Annual CO_2 capture (kg yr^{-1} MLE^{-1})
Individual	1590	479	39,633	40,112	267
1 ha plantation (400 individuals)	636,000	191,600	15,853,200	16,048,800	106,800

OCP and carbonate soils

All the constituents of an active OCP in ferralitic soils have now been identified by this investigation in calcareous ecosystems adjacent to *B. alicastrum* in both Haiti and Mexico. These constituents include: an oxalate producing species (*B. alicastrum*), phytophagous invertebrate predation and mycological decomposition of CaOx rich tissue, significant oxalotrophic bacterial communities, and secondary $CaCO_3$. Furthermore a calcareous sample site in Haiti, Ma Rouge, has demonstrated clear, emblematic, early indications of oxalotrophy adjacent to subjects (Table 2) even though the subjects are still very young (0.5–2 yrs). This was contrary to our hypothesis that the trees would be too young to have affected their local edaphic ecosystem; but, at the time of sampling, the Ma Rouge trees had already grown to 1.4–1.8 m in height and were producing significant quantities of CaOx, which was also detectable in the soils adjacent to them (5–25 g kg^{-1}). As demonstrated by Bravo et al. (2011), this soil CaOx pool can be catabolised quickly upon entry into the edaphic ecosystem when in the presence of oxalotrophs. Which, when coupled with positive identification of oxalotrophy in soils found adjacent to *B. alicastrum* in Ma Rouge, strongly suggests that, like suggested by Verrecchia et al. (1993), an OCP can occur in calcareous environments and secondary carbonate deposits found in association with the root networks in Mexico are generated through an active OCP.

Although there was evidence of oxalotrophy in Ma Rouge, typical edaphic variables associated with the OCP were suppressed in most sites. This could be because of the higher concentrations of Ca (Ca^{Exch} & Ca^{Tot}) masking the typical indicators of an OCP. Ma Rouge displayed the lowest concentrations of Ca (Ca^{Exch} & Ca^{Tot}) or $CaCO_3$ (2 sites below the calcaric threshold) of any site samples. The site was also the only site to present evidence of Ca^{Exch} cycling by the plants (Jobbágy and Jackson 2001). However, the passive cycling of Ca could not explain the observed increase in $CaCO_3$ content of adjacent samples. On the contrary, there was a larger increase in adjacent concentrations of Ca^{Tot}, relative to Ca^{Exch}, which, as a plant nutrient would be actively cycled by plants. This increase is most likely linked to the $CaCO_3$ increase adjacent to the species, as will be the localised alkalinisation. A significant saturation of exchange complex by Ca (>4.47 g kg^{-1}) of a deprotonated alkaline soil would typically suppress the localised alkalinisation associated with an OCP in ferralitic environments; but, the observed increase in $CaCO_3$ would further increase pH as seen in Ma Rouge. Although the presence of lithogenic $CaCO_3$ makes it difficult to discern secondary $CaCO_3$ deposits and thereby, identify an active OCP (Cailleau et al. 2014), the root-like position, colour, shape, texture and friability of secondary $CaCO_3$ deposits in Mexico were all suggestive of an OCP associated with *B. alicastrum*. Therefore, Ca and C cycling of the OCP in calcareous environments needs to be studied in more detail to identify alternate indicators of the process in alkaline soils.

In calcareous environments, plants under stress from high Ca^{Exch} concentrations, typically increase CaOx production as a Ca detoxification mechanism (Austenfeld and Leder 1978; Molano-Flores 2001; Rasmussen and Smith 1961; Volk et al. 2002; Webb 1999). This increased production of CaOx would theoretically lead to a larger pool available for oxalotrophy relative to a ferralitic environment, subsequently increasing the C cycling of the process. However, an identifiable C sequestration of a calcareous OCP must be ruled out because CO_2 is concomitantly released into the soil matrix when Ca^{2+} is liberated during the

$$2H^+ + CaCO_3 \Leftrightarrow Ca^{2+} + CO_2 + H_2O$$

Fig. 9 The acidic dissolution of limestone frees Ca in the soil solution for the OCP, but also degases carbon dioxide. This supposes the presence of strong acids. However, for the details of the general balance of the OCP involving calcium carbonate, calcium oxalate, and CO_2, please see Verrecchia et al. (2006)

dissolution of $CaCO_3$ in calcareous environments (Fig. 9). This means that a calcareous OCP system cannot truly be considered a C sink, but instead a C capturer, as the allochthonous, non-carbonate origin of the Ca^{2+} precipitated as $CaCO_3$ cannot be confirmed in this complex system. Instead, this work has confirmed that *B. alicastrum* is an oxalogenic species which is known to have significant agroforestry potential (Woda and Martinez 2013) and if planted in a location free from lithogenic $CaCO_3$, would act as an efficient agroforestry and C capture tool.

Conclusion

Calcium oxalate production takes place throughout *B. alicastrum* tissue and the compound likely plays an important role in the species' adolescent form, maximising photosynthesis, through the augmentation of incident UV radiation in the lamina, in light-limited environments. This research has also identified oxalotrophic bacterial communities in soils from Haiti and Mexico, providing further evidence for previous suggestions that oxalotrophism is globally diverse. Furthermore, this study has provided experimental evidence for the hypothesis of Verrecchia et al. (1993) that, the OCP can occur in calcareous environments. Thus, when planted in soils free from lithogenic carbonate, *B. alicastrum* would represent a valuable C sequestration and agroforestry crop which would have the ability to biomineralally sequester C via an active OCP, while providing food for Neotropical communities in countries such as Haiti, Mexico or Belize. Further investigation is now required to:

1. Analyse *B. alicastrum* in acidic soil environments,
2. Assess the isotopic signatures of discovered carbonate deposits,
3. Assess the origin of Ca sources in calcareous OCP systems,
4. Identify more oxalogenic species with significant agroforestry potential, to facilitate integration of this biogeochemical C management solution into current agroforestry systems.

Acknowledgments The authors would like to acknowledge and thank the entire Sadhana Forest organisation, not only for their financial contribution, but also their continued council, volunteering and friendly support throughout this research. We would like to thank Dr. David Sebag for his excellent internal review and improvements to our draft manuscript. The authors would also like to acknowledge Chris R., Bournemouth University, and Daniel Rodary of Biomimicry Europa for financial contributions towards the research. Thanks furthermore to Oscar Alvárez Rivera, Beatriz Aguilar Silveira, : Pete Armstrong for his much appreciated graphical support, FERA - license number: 111808/198476/3, Artik 29 & Hebert, Erika Vohman of the The Maya Nut Institute, Adolfo of Colatinco, Paola Barbuto, Lydia Maschin, Carlyle Collins, Erica, Chris & Heather.

References

Allen EB, Allen ME, Egerton-Warburton L, Corkidi L, Gomez-Pompa A (2003) Impacts of early- and late-seral mycorrhizae during restoration in seasonal tropical forest, Mexico. Ecol Appl 13:1701–1717. doi:10.1890/02-5309

Allen MF, Allen EB, Gomez-Pompa A (2005) Effects of mycorrhizae and nontarget organisms on restoration of a seasonal tropical forest in Quintana Roo, Mexico: Factors limiting tree establishment. Restor Ecol 13:325–333. doi:10.1111/j.1526-100X.2005.00041.x

Aragno M, Schlegel HG (1992) The mesophilic hydrogen-oxidizing (Knallgas) bacteria. In: Balows A, Trüper HG, Dworkin M, Harder W, Schleifer H (eds) The prokaryotes, 2nd edn. Springer, Berlin

Aragno A, Verrecchia EP, Job D, Cailleau G, Braissant O, Khammar N, Ferro K, Mota M, Guggiari M, Martin G (2010) Calcium carbonate biomineralization in ferralitic, tropical soils through the oxalate-carbonate pathway. BGS Bull 30:127–130

Austenfeld F-A, Leder U (1978) Über den Oxalathaushalt von Salicornia europaea L. unter dem Einfluß variierter Erdalkalisalz-Gaben. Zeitschr für Pflanzenphysiol 88:403–412. doi:10.1016/S0044-328X(78)80256-6

Barry KM, Pinkard EA (2013) Growth and photosynthetic responses following defoliation and bud removal in eucalypts.

For Ecol Manage 293:9–16. doi:10.1016/j.foreco.2012.12.012

Bassalik K (1913) Ueber die Verarbeitung der Oxalsäure durch Bacillus extorquens. Jahrbüch für Wissenschaft Botan 53: 255–302

Benjamin TJ, Montañez PI, Jaménez JJM, Gillespie AR (2001) Carbon, water and nutrient flux in Maya homegardens in the Yucatán peninsula of México. Agroforest Syst 53:103–111. doi:10.1023/a:1013312217471

Braissant O, Verrecchia EP, Aragno M (2002) Is the contribution of bacteria to terrestrial carbon budget greatly underestimated? Naturwissenschaften 89:366–370. doi:10.1007/s00114-002-0340-0

Braissant O, Cailleau G, Aragno M, Verrecchia EP (2004) Biologically induced mineralization in the tree Milicia excelsa (Moraceae): its causes and consequences to the environment. Geobiology 2:59–66. doi:10.1111/j.1472-4677.2004.00019.x

Bravo D, Braissant O, Solokhina A, Clerc M, Daniels AU, Verrecchia E, Junier P (2011) Use of an isothermal microcalorimetry assay to characterize microbial oxalotrophic activity. Fems Microbiol Ecol 78:266–274. doi:10.1111/j.1574-6941.2011.01158.x

Bravo D, Cailleau G, Bindschedler S, Simon A, Job D, Verrecchia E, Junier P (2013) Isolation of oxalotrophic bacteria able to disperse on fungal mycelium. Fems Microbiol Lett 348:157–166. doi:10.1111/1574-6968.12287

Brewer SW, Rejmanek M, Webb MAH, Fine PVA (2003) Relationships of phytogeography and diversity of tropical tree species with limestone topography in southern Belize. J Biogeogr 30:1669–1688. doi:10.1046/j.1365-2699.2003.00971.x

Cailleau G, Braissant O, Verrecchia EP (2004) Biomineralization in plants as a long-term carbon sink. Naturwissenschaften 91: 191–194. doi:10.1007/s00114-004-0512-1

Cailleau G, Braissant O, Dupraz C, Aragno M, Verrecchia EP (2005) Biologically induced accumulations of CaCO3 in orthox soils of Biga, Ivory Coast. Catena 59:1–17. doi:10.1016/j.catena.2004.06.002

Cailleau G, Braissant O, Verrecchia EP (2011) Turning sunlight into stone: the oxalate-carbonate pathway in a tropical tree ecosystem. Biogeosciences 8:1755–1767. doi:10.5194/bg-8-1755-2011

Cailleau G, Mota M, Bindschedler S, Junier P, Verrecchia EP (2014) Detection of active oxalate–carbonate pathway ecosystems in the Amazon Basin: global implications of a natural potential C sink. Catena 116:132–141. doi:10.1016/j.catena.2013.12.017

Cairns MA, Brown S, Helmer EH, Baumgardner GA (1997) Root biomass allocation in the world's upland forests. Oecologia 111:1–11. doi:10.1007/s004420050201

Cairns MA, Olmsted I, Granados J, Argaez J (2003) Composition and aboveground tree biomass of a dry semi-evergreen forest on Mexico's Yucatan Peninsula. For Ecol Manage 186:125–132. doi:10.1016/s0378-1127(03)00229-9

Cannon JP, Allen EB, Allen MF, Dudley LM, Jurinak JJ (1995) The effects of oxalates produced by salsola-tragus on the phosphorus-nutrition of stipa-pulchra. Oecologia 102:265–272. doi:10.1007/bf00329792

Certini G, Corti G, Ugolini FC (2000) Vertical trends of oxalate concentration in two soils under Abies alba from Tuscany (Italy). J Plant Nutr Soil Sci 163:173–177. doi:10.1002/(sici)1522-2624(200004)163:2<173::aid-jpln173>3.0.co;2-h

Chandra TS, Shethna YI (1977) Oxalate, formate, formamide, and methanol metabolism in Thiobacillus novellus. J Bacteriol 131:389–398

Cromack K, Sollins P, Todd RL, Fogel R, Todd AW, Fender WM, Crossley ME, Crossley DA (1977) The role of oxalic acid and bicarbonate in calcium cycling by fungi and bacteria: some possible implications for soil animals. Ecol Bull 25: 246–252. http://www.jstor.org/stable/20112586

Esri (2014) Basemap, sources: National Geographic, Esri, DeLorme, HERE, UNEP-WCMC, USGS, NASA, ESA< METI, NRCRAn, GEBCO, NOAA, iPC

Faheed F, Mazen A, Abd Elmohsen S (2013) Physiological and ultrastructural studies on calcium oxalate crystal formation in some plants. Turk J Botan 37:139–152. doi:10.3906/bot-1112-19

Ferro KI (2012) The impact of oxalogenic plants on soil carbon dynamics - formation of a millennium storage as calcium carbonate. Université de Neuchâtel, Neuchâtel

Franceschi V (2001) Calcium oxalate in plants. Trends Plant Sci 6: 331. doi:10.1016/S1360-1385(01)02014-3

Franceschi VR, Nakata PA (2005) Calcium oxalate in plants: formation and function. Annu Rev Plant Biol 56:41–71. doi:10.1146/annurev.arplant.56.032604.144106

Garvie LAJ (2003) Decay-induced biomineralization of the saguaro cactus (Carnegiea gigantea). Am Mineral 88: 1879–1888

Garvie LAJ (2006) Decay of cacti and carbon cycling. Naturwissenschaften 93:114–118. doi:10.1007/s00114-005-0069-7

Giddings L, Soto M (2003) Rhythms of precipitation in the Yucatán Peninsula. In: Gomez-Pompa A, Allen MF, Fedick SL, Jiménez-Osornio JJ (eds) The lowland maya area: three millennia at the human-wildland influence. Food Products Press, Oxford

Gill RA, Jackson RB (2000) Global patterns of root turnover for terrestrial ecosystems. New Phytol 147:13–31. doi:10.1046/j.1469-8137.2000.00681.x

Gillespie AR, Bocanegra-Ferguson DM, Jimenez-Osornio JJ (2004) The propagation of Ramon (Brosimum alicastrum Sw.; Moraceae) in Mayan homegardens of the Yucatan peninsula of Mexico. New Forest 27:25–38. doi:10.1023/a:1025081224852

Harder W, Wiersma M, Groen L (1974) Transport of substrates and energetics of growth of Pseudomonas oxalaticus during growth on formate or oxalate in continous culture. J Gen Microbiol 81:R2–R3

Ilarslan H, Palmer RG, Horner HT (2001) Calcium oxalate crystals in developing seeds of soybean. Ann Bot 88:243–257. doi:10.1006/anbo.2001.1453

Jayasuriya GCN (1955) The isolation and characterisitics of an oxalate-decomposing organism. J Gen Microbiol 12:419–428

Jobbágy EG, Jackson RB (2001) The distribution of soil nutrients with depth: global patterns and the imprint of plants. Biogeochem 53:51–77. doi:10.1023/a:1010760720215

Knight WG, Dudley LM, Jurinak JJ (1992) Oxalate effects on solution phosphorus in a calcareous soil. Arid Soil Res Rehab 6:11–20

Kuo-Huang LL, Maurice SBK, Franceschi VR (2007) Correlations between calcium oxalate crystals and photosynthetic activities in palisade cells of shade-adapted Peperomia glabella. Botan Stud 48:155–164

Laborde J, Corrales-Ferrayola I (2012) Direct seeding of Brosimum alicastrum Sw. (Moraceae) and Enterolobium cyclocarpum (Jacq.) Griseb. (Mimosaceae) in different habitats in the dry tropics of central Veracruz. Acta Botanica Mexican 100:107–134

Libert B, Franceschi VR (1987) Oxalate in crop plants. J Agric Food Chem 35:926–938. doi:10.1021/jf00078a019

MAFF (1986) The analysis of agricultural materials: a manual of the analytical methods used by the agricultural development and advisory service, 2nd ed. Her Majesty's Stationery Office, London

Martin G, Guggiari M, Bravo D, Zopfi J, Cailleau G, Aragno M, Job D, Verrecchia E, Junier P (2012) Fungi, bacteria and soil pH: the oxalate-carbonate pathway as a model for metabolic interaction. Environ Microbiol 14:2960–2970. doi:10.1111/j.1462-2920.2012.02862.x

Molano-Flores B (2001) Herbivory and calcium concentrations affect calcium oxalate crystal formation in leaves of Sida (Malvaceae). Ann Bot 88:387–391. doi:10.1006/anbo.2001.1492

Monje PV, Baran EJ (2002) Characterization of calcium oxalates generated as biominerals in cacti. Plant Physiol 128:707–713. doi:10.1104/pp.010630

Nakata PA (2002) Calcium oxalate crystal morphology. Trends Plant Sci 7:324–324. doi:10.1016/s1360-1385(02)02285-9

Nakata PA (2003) Advances in our understanding of calcium oxalate crystal formation and function in plants. Plant Sci 164:901–909. doi:10.1016/s0168-9452(03)00120-1

Ortiz M, Azanón Y, Melgar M, Elias L (1995) The corn tree (Brosimum alicastrum): a food for the tropics. In: Simopoulos AP (ed) Plants in human nutrition, world review of nutrition and diabetics. Kargel Publishers, Basel

Palak VR, Harisha CR, Prakapati PK (2012) Importance of calcium oxalate crystals in panchavalkala. Int J Pharmacog Phytochem Res 4:112–116

Peters CM (1983) Observations on Maya subsistence and the ecology of a tropical tree. Amer Antiq 48:610–615. doi:10.2307/280569

Peters CM (1989) Reproduction, growth and the population dynamics of *Brosimum alicastrum* Sw. in a moist tropical forest of Central Veracruz, Mexico.

Peters CM, Pardo-tejeda E (1982) Brosimum-alicastrum (Moraceae) - uses and potential in Mexico. Econom Botan 36:166–175. doi:10.1007/bf02858712

Querejeta JI, Estrada-Medina H, Allen MF, Jimenez-Osornio JJ, Ruenes R (2006) Utilization of bedrock water by Brosimum alicastrum trees growing on shallow soil atop limestone in a dry tropical climate. Plant and Soil 287:187–197. doi:10.1007/s11104-006-9065-8

Ramos EL (1975) Geological summary of the Yucatan Peninsula. In: Nairn AEM, Stehli FG (eds) The Gulf of Mexico and the Caribbean. Springer US, Boston

Rasmussen G, Smith PF (1961) Effects of calcium, potassium, and magnesium on oxalic, malic, and citric acid content of Valencia orange leaf tissue. Plant Physiol 36:99-. doi:10.1104/pp.36.1.99

Rico-gray V, Chemas A, Mandujano S (1991) Uses of tropical deciduous forest species by the Yucatecan Maya. Agroforest Syst 14:149–161. doi:10.1007/bf00045730

Sahin N (2003) Oxalotrophic bacteria. Res Microbiol 154:399–407. doi:10.1016/s0923-2508(03)00112-8

Sakai WS, Shiroma SS, Nagao MA (1984) A study of raphide microstructure in relation to irritation. Scan Electron Microscop II(Pt 2):979–986

Salinas ML, Ogura T, Soffchi L (2001) Irritant contact dermatitis caused by needle-like calcium oxalate crystals, raphides in Agave tequilana among workers in tequila distilleries and agave plantations. Contact Dermatitis 44:94–96. doi:10.1034/j.1600-0536.2001.440208.x

Scholz G, Liebner F, Koch G, Bues C-T, Guenther B, Baeucker E (2007) Chemical, anatomical and technological properties of Snakewood Brosimum guianense (Aubl.) Huber. Wood Sci Technol 41:673–686. doi:10.1007/s00226-007-0149-2

Schutz AEN, Bond WJ, Cramer MD (2009) Juggling carbon: allocation patterns of a dominant tree in a fire-prone savanna. Oecologia 160:235. doi:10.1007/s00442-009-1293-1

Shang C, Tiessen H (2003) Soil organic C sequestration and stabilization in karstic soils of Yucatan. Biogeochem 62:177–196. doi:10.1023/a:1021123728639

Tamer AÜ, Aragno M (1980) Isolement, characterisation et essai d'identifcation de bactéries capables d'utiliser l'oxalate comme seule source de carbone et d'énergie. Bull Soc Neuchâtel Sci Nature 103:91–104

Verrecchia EP (1990) Litho-diagenetic implications of the calcium oxalate-carbonate biogeochemical cycle in semiarid Calcretes, Nazareth, Israel. Geomicrobiol J 8:87–99. doi:10.1080/01490459009377882

Verrecchia EP, Dumont J-L, Verrecchia KE (1993) Role of calcium oxalate biomineralization by fungi in the formation of calcretes; a case study from Nazareth, Israel. J Sediment Res 63:1000–1006. doi:10.1306/d4267c6c-2b26-11d7-8648000102c1865d

Verrecchia EP, Braissant O, Cailleau G (2006) The oxalate–carbonate pathway in soil carbon storage: the role of fungi and oxalotrophic bacteria. Cambridge University Press

Volk GM, Lynch-Holm VJ, Kostman TA, Goss LJ, Franceschi VR (2002) The role of druse and raphide calcium oxalate crystals in tissue calcium regulation in Pistia stratiotes leaves. Plant Biol 4:34–45. doi:10.1055/s-2002-20434

Webb MA (1999) Cell-mediated crystallization of calcium oxalate in plants. Plant Cell 11:751–761

Whigham DF, Lynch JF (1998) Responses of plants and birds to hurricane disturbances in a dry tropical forest of Quintana Roo, Mexico. In: Dallmeier F, Comiskey JA (eds) Forest biodiversity in North, Central and South America, and the Caribbean. The Parthenon Publishing Group, Paris

Whigham DF, Olmsted I, Cabrera Cano E, Curtis AB (2003) Impacts of hurricanes on the forests of Quintana Roo, Yucatán Peninsula, Mexico. In: Gomez-Pompa A, Allen MF, Fedick SL, Jiménez-Osornio JJ (eds) The lowland

Maya area: three millennia at the human-wildland influence. Food Products Press, Oxford

Woda C, Martinez M (2013) Nueces de Masica (*Brosimum alicastrum*) como alimento humano – el potencial de producción de un bosque tropical húmedo en Honduras. Sistema de Investigación Nacional Forestal, Áreas Protegidas y Vida Silvestre – SINFOR El VIII Congresso Forestal Centroamericano, San Pedro Sula, Honduras

WRB W-IWG (2015) World reference base for soil resources 2014, update 2015. In: WS Resources (ed) No 106. FAO, Rome

Wright AF, Bailey JS (2001) Organic carbon, total carbon, and total nitrogen determinations in soils of variable calcium carbonate contents using a Leco CN-2000 dry combustion analyzer. Commun Soil Sci Plant Anal 32:3243–3258. doi:10.1081/css-120001118

Wu CC, Kuo Huang LL (1997) Calcium crystals in the leaves of some species of Moraceae. Botan Bull Acad Sin 38:97–104

Yates S, Ramirez-Sosa CR (2004) Ethnobotanical knowledge of Brosimum alicastrum (Moraceae) among urban and rural El Salvadorian adolescents. Econom Botan 58:72–77. doi:10.1663/0013-0001(2004)058[0072:ekobam]2.0.co;2

- This page is intentionally left blank -

References

Aber, J.D., Melillo, J.M., McClaugherty, C.A., 1990. Predicting long-term patterns of mass loss, nitrogen dynamics, and soil organic matter formation from initial fine litter chemistry in temperate forest ecosystems. Canadian Journal of Botany 68(10), 2201-2208.

Abou Neel, E.A., Aljabo, A., Strange, A., Ibrahim, S., Coathup, M., Young, A.M., Bozec, L., Mudera, V., 2016. Demineralization-remineralization dynamics in teeth and bone. Int J Nanomedicine 11, 4743-4763.

Accoe, F., Boeckx, P., Cleemput, O.V., Hofman, G., 2003. Relationship between soil organic C degradability and the evolution of the δ13C signature in profiles under permanent grassland. Rapid Communications in Mass Spectrometry 17(23), 2591-2596.

Accoe, F., Boeckx, P., Cleemput, O.V., Hofman, G., Zhang, Y., Li, R.h., Guanxiong, C., 2002. Evolution of the δ13C signature related to total carbon contents and carbon decomposition rate constants in a soil profile under grassland. Rapid Communications in Mass Spectrometry 16(23), 2184-2189.

Adams, M.L., Hawke, D.J., Nilsson, N.H.S., Powell, K.J., 2000. The relationship between soil solution pH and Al3+ concentrations in a range of South Island (New Zealand) soils. Soil Research 38(1), 141-154.

Adatte, T., Stinnesbeck, W., Keller, G., 1996. Lithostratigraphic and mineralogic correlations of near K/T boundary clastic sediments in northeastern Mexico: Implications for origin and nature of deposition. Geological Society of America Special Papers 307.

Adhikari, D., Sowers, T., Stuckey, J.W., Wang, X., Sparks, D.L., Yang, Y., 2019. Formation and redox reactivity of ferrihydrite-organic carbon-calcium co-precipitates. Geochimica et Cosmochimica Acta 244, 86-98.

Adu, J.K., Oades, J.M., 1978. Physical factors influencing decomposition of organic materials in soil aggregates. Soil Biology and Biochemistry 10(2), 109-115.

Ahmed, E., Holmström, S.J.M., 2014. Siderophores in environmental research: roles and applications. Microbial Biotechnology 7(3), 196-208.

Ahrens, D.C., Samson, P.J.-. 2010. Extreme weather and climate. Brooks Cole, Belmont USA.

Ahrland, S., Chatt, J., Davies, N.R., 1958. The relative affinities of ligand atoms for acceptor molecules and ions. Quarterly Reviews, Chemical Society 12(3), 265-276.

Andersson, S., Nilsson, I., Valeur, I., 1999. Influence of dolomitic lime on DOC and DON leaching in a forest soil. Biogeochemistry 47(3), 295-315.

Aran, D., Maul, A., Masfaraud, J.-F., 2008. A spectrophotometric measurement of soil cation exchange capacity based on cobaltihexamine chloride absorbance. Comptes Rendus Geoscience 340(12), 865-871.

Archer, M.D., Barber, J. (Eds.), 2004. Molecular to global photosynthesis. Series on Photoconversion of Solar Energy, Volume 2. Imperial College Press, 788 pp.

Aristilde, L., Sposito, G., 2008. Molecular modeling of metal complexation by a fluoroquinolone antibiotic. Environmental Toxicology and Chemistry 27(11), 2304-2310.

Arkley, R.J., 1963. Calculation of carbonate and water movement in soil from climatic data. Soil Science 96(4), 239-248.

Armstrong, A.S.B., Tanton, T.W., 1992. Gypsum applications to aggregated saline—sodic clay topsoils. Journal of Soil Science 43(2), 249-260.

Asano, M., Wagai, R., 2014. Evidence of aggregate hierarchy at micro- to submicron scales in an allophanic Andisol. Geoderma 216, 62-74.

Auler, A.C., Caires, E.F., Pires, L.F., Galetto, S.L., Romaniw, J., Charnobay, A.C., 2019. Lime effects in a no-tillage system on Inceptisols in Southern Brazil. Geoderma Regional 16, e00206.

Austin, N., Evans, B., Herwegh, M., Ebert, A., 2008. Strain localization in the Morcles nappe (Helvetic Alps, Switzerland). Swiss Journal of Geosciences 101(2), 341-360.

Babel, U., 1975. Micromorphology of soil organic matter. In: J.E. Gieseking (Ed.), Soil Components: Vol. 1: Organic Components. Springer Berlin Heidelberg, Berlin, Heidelberg, pp. 369-473.

Bache, B.W., 1984. The role of calcium in buffering soils. Plant, Cell & Environment 7(6), 391-395.

Bahram, M., Hildebrand, F., Forslund, S.K., Anderson, J.L., Soudzilovskaia, N.A., Bodegom, P.M., Bengtsson-Palme, J., Anslan, S., Coelho, L.P., Harend, H., Huerta-Cepas, J., Medema, M.H., Maltz, M.R., Mundra, S., Olsson, P.A., Pent, M., Põlme, S., Sunagawa, S., Ryberg, M., Tedersoo, L., Bork, P., 2018. Structure and function of the global topsoil microbiome. Nature 560(7717), 233-237.

Baldock, J., Aoyama, M., Oades, J., Grant, C., 1994. Structural amelioration of a South Australian red-brown earth using calcium and organic amendments. Soil Research 32(3), 571-594.

Baldock, J.A., Skjemstad, J.O., 2000. Role of the soil matrix and minerals in protecting natural organic materials against biological attack. Organic Geochemistry 31(7–8), 697-710.

Balesdent, J., Chenu, C., Balabane, M., 2000. Relationship of soil organic matter dynamics to physical protection and tillage. Soil & Tillage Research 53(3-4), 215-230.

Balesdent, J., Mariotti, A., 1996. Mass spectrometry of soils. Mass Spectrometry of Soils, edited by: Boutton, TW and Yamasaki, SI, Marcel Dekker, New York.

Barber, S.A., 1984. Liming materials and practices. In: F. Adams (Ed.), Soil acidity and liming. Agronomy Monograph. American Society of Agronomy, Crop Science Society of America, Soil Science Society of America, Madison, WI, pp. 171-209.

Barra, C.M., Curtius, A.J., de Campos, R.C., Perez, D.V., 2001. Evaluation of four aluminum extraction methods using selected Brazilian soils. Communications in Soil Science and Plant Analysis 32(11-12), 1969-1980.

Barta, G., 2011. Secondary carbonates in loess-paleosoil sequences: a general review. Central European Journal of Geosciences 3(2), 129-146.

Barta, G., Bradák, B., Novothny, Á., Markó, A., Szeberényi, J., Kiss, K., Kovács, J., 2018. The influence of paleogeomorphology on the stable isotope signals of paleosols. Geoderma 330, 221-231.

Bartlett, R.J., James, B.R., 1993. Redox chemistry of soils. Advances in Agronomy, Vol 50 50, 151-208.

Bascomb, C.L., 1968. Distribution of pyrophosphate extractable iron and organic carbon in soils of various groups. Journal of Soil Science 19(2), 251-268.

Bashkin, V.N., 2002. Interactions of biogeochemical cycles. In: V.N. Bashkin (Ed.), Modern Biogeochemistry. Springer Netherlands, Dordrecht, pp. 199-237.

Basile-Doelsch, I., Brun, T., Borschneck, D., Masion, A., Marol, C., Balesdent, J., 2009. Effect of landuse on organic matter stabilized in organomineral complexes: A study combining density fractionation, mineralogy and δ13C. Geoderma 151(3), 77-86.

Batjes, N.H., 1996. Total carbon and nitrogen in the soils of the world. European Journal of Soil Science 47(2), 151-163.

Becze-Deàk, J., Langohr, R., Verrecchia, E.P., 1997. Small scale secondary CaCO3 accumulations in selected sections of the European loess belt. Morphological forms and potential for paleoenvironmental reconstruction. Geoderma 76(3), 221-252.

Bélanger, N., Paré, D., Hendershot, W.H., 2008. Chapter 27 - Determining nutrient availability in forest soils. In: M.R. Carter, E.G. Gregorich (Eds.), Soil sampling and methods of analysis. Canadian Society of Soil Science ; CRC Press, Pinawa, Manitoba, Boca Raton, FL, pp. 1224.

Benedetti, M.F., Milne, C.J., Kinniburgh, D.G., Van Riemsdijk, W.H., Koopal, L.K., 1995. Metal ion binding to humic substances: application of the non-ideal competitive adsorption model. Environmental Science & Technology 29(2), 446-457.

Benson, A., Calvin, M., 1950. The path of carbon in photosynthesis: VII. Respiration and photosynthesis. Journal of Experimental Botany, 63-68.

Bern, C.R., 2009. Soil chemistry in lithologically diverse datasets: The quartz dilution effect. Applied Geochemistry 24(8), 1429-1437.

Bertrand, I., Delfosse, O., Mary, B., 2007. Carbon and nitrogen mineralization in acidic, limed and calcareous agricultural soils: Apparent and actual effects. Soil Biology and Biochemistry 39(1), 276-288.

Biasi, C., Lind, S.E., Pekkarinen, N.M., Huttunen, J.T., Shurpali, N.J., Hyvönen, N.P., Repo, M.E., Martikainen, P.J., 2008. Direct experimental evidence for the contribution of lime to CO2 release from managed peat soil. Soil Biology and Biochemistry 40(10), 2660-2669.

Bindschedler, S., Cailleau, G., Braissant, O., Milliere, L., Job, D., Verrecchia, E.P., 2014. Unravelling the enigmatic origin of calcitic nanofibres in soils and caves: purely physicochemical or biogenic processes? Biogeosciences 11(10), 2809-2825.

Bindschedler, S., Cailleau, G., Verrecchia, E., 2016. Role of fungi in the biomineralization of calcite. Minerals 6(2), 41.

Blagodatskaya, E.V., Anderson, T.-H., 1999. Adaptive responses of soil microbial communities under experimental acid stress in controlled laboratory studies. Applied Soil Ecology 11(2–3), 207-216.

Blanco-Moure, N., Angurel, L.A., Moret-Fernández, D., López, M.V., 2012a. Tensile strength and organic carbon of soil aggregates under long-term no tillage in semiarid Aragon (NE Spain). Geoderma 189–190, 423-430.

Blanco-Moure, N., Moret-Fernández, D., López, M.V., 2012b. Dynamics of aggregate destabilization by water in soils under long-term conservation tillage in semiarid Spain. Catena 99, 34-41.

Blattner, C., 2017. L'influence des facteurs environnementaux sur la respiration des sols au Vallon de Nant (VD), Université de Lausanne / Université de Geneve, Lausanne.

Bogatko, S., Cauët, E., Bylaska, E., Schenter, G., Fulton, J., Weare, J., 2013. The aqueous Ca2+ system, in comparison with Zn2+, Fe3 +, and Al3 +: An Ab Initio molecular dynamics study. Chemistry – A European Journal 19(9), 3047-3060.

Bond-Lamberty, B., Bailey, V.L., Chen, M., Gough, C.M., Vargas, R., 2018. Globally rising soil heterotrophic respiration over recent decades. Nature 560(7716), 80-83.

Boström, B., Comstedt, D., Ekblad, A., 2007. Isotope fractionation and 13C enrichment in soil profiles during the decomposition of soil organic matter. Oecologia 153(1), 89-98.

Boudot, J.-P., 1992. Relative efficiency of complexed aluminum noncrystalline Al hydroxide, allophane and imogolite in retarding the biodegradation of citric acid. Geoderma 52(1), 29-39.

Boulton, G.S., 1978. Boulder shapes and grain-size distributions of debris as indicators of transport paths through a glacier and till genesis. Sedimentology 25(6), 773-799.

Bradford, M., Crowther, T., 2013. Carbon use efficiency and storage in terrestrial ecosystems. The New phytologist 199, 7-9.

Braghiere, R.K., Quaife, T., Black, E., He, L., Chen, J.M., 2019. Underestimation of Global Photosynthesis in Earth System Models Due to Representation of Vegetation Structure. Global Biogeochemical Cycles n/a(n/a).

Bravo, D., Cailleau, G., Bindschedler, S., Simon, A., Job, D., Verrecchia, E., Junier, P., 2013. Isolation of oxalotrophic bacteria able to disperse on fungal mycelium. Fems Microbiology Letters 348(2), 157-166.

Briedis, C., de Moraes Sá, J.C., Caires, E.F., de Fátima Navarro, J., Inagaki, T.M., Boer, A., de Oliveira Ferreira, A., Neto, C.Q., Canalli, L.B., Bürkner dos Santos, J., 2012a. Changes in organic matter pools and increases in carbon sequestration in response to surface liming in an Oxisol under long-term no-till. Soil Science Society of America Journal 76(1), 151-160.

Briedis, C., Sá, J.C.d.M., Caires, E.F., Navarro, J.d.F., Inagaki, T.M., Boer, A., Neto, C.Q., Ferreira, A.d.O., Canalli, L.B., Santos, J.B.d., 2012b. Soil organic matter pools and carbon-protection mechanisms in aggregate classes influenced by surface liming in a no-till system. Geoderma 170, 80-88.

Brinza, L., Schofield, P.F., Hodson, M.E., Weller, S., Ignatyev, K., Geraki, K., Quinn, P.D., Mosselmans, J.F.W., 2014. Combining μXANES and μXRD mapping to analyse the heterogeneity in calcium carbonate granules excreted by the earthworm Lumbricus terrestris. Journal of Synchrotron Radiation 21(Pt 1), 235-241.

Brodowski, S., Amelung, W., Haumaier, L., Zech, W., 2007. Black carbon contribution to stable humus in German arable soils. Geoderma 139(1), 220-228.

Bronick, C.J., Lal, R., 2005. Soil structure and management: a review. Geoderma 124(1–2), 3-22.

Bruckert, S., Gaiffe, M., Duquet, B., Tavant, Y., Tavant, H., 1986. Rôle du flux de calcium sur la stabilisation de la matière organique des sols. Ann. Sci. Univ. France-Comté, Besançon 4(6), 25-29.

Bryan, W.H., Teakle, L.J.H., 1949. Pedogenic inertia : a concept in soil science. Nature 164, 969.

Burgin, A.J., Yang, W.H., Hamilton, S.K., Silver, W.L., 2011. Beyond carbon and nitrogen: how the microbial energy economy couples elemental cycles in diverse ecosystems. Frontiers in Ecology and the Environment 9(1), 44-52.

Burns, R.G., 2010. How do microbial extracellular enzymes locate and degrade natural and synthetic polymers in soil. In: J. Xu, P.M. Huang (Eds.), Molecular environmental soil science at the interfaces in the Earth's critical zone. Springer Berlin Heidelberg, Berlin, Heidelberg, pp. 294-297.

Cailleau, G., Braissant, O., Dupraz, C., Aragno, M., Verrecchia, E.P., 2005. Biologically induced accumulations of CaCO3 in orthox soils of Biga, Ivory Coast. Catena 59(1), 1-17.

Cailleau, G., Braissant, O., Verrecchia, E.P., 2004. Biomineralization in plants as a long-term carbon sink. Naturwissenschaften 91(4), 191-194.

Cailleau, G., Braissant, O., Verrecchia, E.P., 2011. Turning sunlight into stone: the oxalate-carbonate pathway in a tropical tree ecosystem. Biogeosciences 8(7), 1755-1767.

Cailleau, G., Mota, M., Bindschedler, S., Junier, P., Verrecchia, E.P., 2014. Detection of active oxalate–carbonate pathway ecosystems in the Amazon Basin: Global implications of a natural potential C sink. Catena 116, 132-141.

Cailleau, G., Verrecchia, E.P., Braissant, O., Emmanuel, L., 2009. The biogenic origin of needle fibre calcite. Sedimentology 56(6), 1858-1875.

Carbone, M.S., Still, C.J., Ambrose, A.R., Dawson, T.E., Williams, A.P., Boot, C.M., Schaeffer, S.M., Schimel, J.P., 2011. Seasonal and episodic moisture controls on plant and microbial contributions to soil respiration. Oecologia 167(1), 265-278.

Carmeis Filho, A.C.A., Penn, C.J., Crusciol, C.A.C., Calonego, J.C., 2017. Lime and phosphogypsum impacts on soil organic matter pools in a tropical Oxisol under long-term no-till conditions. Agriculture, Ecosystems & Environment 241, 11-23.

Cerli, C., Celi, L., Kalbitz, K., Guggenberger, G., Kaiser, K., 2012. Separation of light and heavy organic matter fractions in soil - Testing for proper density cut-off and dispersion level. Geoderma 170, 403-416.

Cerling, T.E., 1984. The stable isotopic composition of modern soil carbonate and its relationship to climate. Earth and Planetary Science Letters 71(2), 229-240.

Cerri, C.C., Volkoff, B., Andreaux, F., 1991. Nature and behaviour of organic matter in soils under natural forest, and after deforestation, burning and cultivation, near Manaus. Forest Ecology and Management 38(3), 247-257.

Certini, G., Corti, G., Ugolini, F.C., 2000. Vertical trends of oxalate concentration in two soils under Abies alba from Tuscany (Italy). Journal of Plant Nutrition and Soil Science 163(2), 173-177.

Chadwick, O.A., Chorover, J., 2001. The chemistry of pedogenic thresholds. Geoderma 100(3–4), 321-353.

Chadwick, O.A., Gavenda, R.T., Kelly, E.F., Ziegler, K., Olson, C.G., Elliott, W.C., Hendricks, D.M., 2003. The impact of climate on the biogeochemical functioning of volcanic soils. Chemical Geology 202(3), 195-223.

Chan, K.Y., Davey, B.G., Geering, H.R., 1979. Adsorption of magnesium and calcium by a soil with variable charge. Soil Science Society of America Journal 43(2), 301-304.

Chan, K.Y., Heenan, D.P., 1999. Lime-induced loss of soil organic carbon and effect on aggregate stability. Soil Science Society of America Journal 63(6), 1841-1844.

Chassin, P., 1979. Determination of the angle of contact of humic acids diols solutions - consequences on the mechanisms of aggregate destruction. Ann Agron 30(6), 481-491.

Chen, Y., Barak, P., 1982. Iron nutrition of plants in calcareous soils. In: N.C. Brady (Ed.), Advances in Agronomy. Academic Press, pp. 217-240.

Chenu, C., 1989. Influence of a fungal polysaccharide, scleroglucan, on clay microstructures. Soil Biology and Biochemistry 21(2), 299-305.
Chenu, C., Cosentino, D., 2011. Microbial regulation of soil structural dynamics. In: K. Ritz, I.M. Young (Eds.), The architecture and biology of soils: life in inner space. CABI, pp. 37-70.
Chenu, C., Plante, A.F., 2006. Clay-sized organo-mineral complexes in a cultivation chronosequence: revisiting the concept of the 'primary organo-mineral complex'. European Journal of Soil Science 57(4), 596-607.
Chi, J., Zhang, W., Wang, L., Putnis, C.V., 2019. Direct observations of the occlusion of soil organic matter within calcite. Environmental Science & Technology.
Chorover, J., Amistadi, M.K., Chadwick, O.A., 2004. Surface charge evolution of mineral-organic complexes during pedogenesis in Hawaiian basalt. Geochimica Et Cosmochimica Acta 68(23), 4859-4876.
Ciais, P., Chris, S., Govindasamy, B., Bopp, L., Brovkin, V., Canadell, J., Chhabra, A., Defries, R., Galloway, J., Heimann, M., 2013. Carbon and other biogeochemical cycles. In: T.F. Stocker, D. Qin, G.-K. Plattner, M. Tignor, S.K. Allen, J. Boschung, A. Nauels, Y. Xia, V. Bex, P.M. Midgley (Eds.), Climate Change 2013: The Physical Science Basis. Contribution of Working Group I to the Fifth Assessment Report of the Intergovernmental Panel on Climate Change Cambridge University Press, Cambridge, UK and New York, USA, pp. 465-570.
Ciais, P., Tan, J., Wang, X., Roedenbeck, C., Chevallier, F., Piao, S.L., Moriarty, R., Broquet, G., Le Quéré, C., Canadell, J.G., Peng, S., Poulter, B., Liu, Z., Tans, P., 2019. Five decades of northern land carbon uptake revealed by the interhemispheric CO2 gradient. Nature 568(7751), 221-225.
Clarholm, M., Skyllberg, U., 2013. Translocation of metals by trees and fungi regulates pH, soil organic matter turnover and nitrogen availability in acidic forest soils. Soil Biology and Biochemistry 63, 142-153.
Clough, A., Skjemstad, J.O., 2000. Physical and chemical protection of soil organic carbon in three agricultural soils with different contents of calcium carbonate. Australian Journal of Soil Research 38(5), 1005-1016.
Coleman, K., Jenkinson, D.S., 1996. RothC-26.3 - A model for the turnover of carbon in soil. In: D.S. Powlson, P. Smith, J.U. Smith (Eds.), Evaluation of soil organic matter models. Springer Berlin Heidelberg, Berlin, Heidelberg, pp. 237-246.
Cook, J., Oreskes, N., Doran, P.T., Anderegg, W.R.L., Verheggen, B., Maibach, E.W., Carlton, J.S., Lewandowsky, S., Skuce, A.G., Green, S.A., Nuccitelli, D., Jacobs, P., Richardson, M., Winkler, B., Painting, R., Rice, K., 2016. Consensus on consensus: a synthesis of consensus estimates on human-caused global warming. Environmental Research Letters 11(4), 048002.
Coplen, T.B., 2011. Guidelines and recommended terms for expression of stable-isotope-ratio and gas-ratio measurement results. Rapid Communications in Mass Spectrometry 25(17), 2538-2560.
Costa, O.Y.A., Raaijmakers, J.M., Kuramae, E.E., 2018. Microbial extracellular polymeric substances: Ecological function and impact on soil aggregation. Front Microbiol 9, 1636-1636.
Czarnes, S., Hallett, P.D., Bengough, A.G., Young, I.M., 2000. Root- and microbial-derived mucilages affect soil structure and water transport. European Journal of Soil Science 51(3), 435-443.
Dahlgren, R.A., 1994. Quantification of allophane and imogolite. In: J.E. Amonette, Y.L. W. (Eds.), Quantitative methods in soil mineralogy. Soil Science Society of America, Madison, WI, pp. 430-451.
Davidson, E.A., Janssens, I.A., 2006. Temperature sensitivity of soil carbon decomposition and feedbacks to climate change. Nature 440(7081), 165-173.
de Kerchove, A.J., Elimelech, M., 2007. Formation of polysaccharide gel layers in the presence of Ca2+ and K+ ions: measurements and mechanisms. Biomacromolecules 8(1), 113-121.
Decad, G.M., Nikaido, H., 1976. Outer membrane of gram-negative bacteria. XII. Molecular-sieving function of cell wall. Journal of bacteriology 128(1), 325-336.
Delasoie, M., 2018. Distribution des compartiments de calcium dans des sols du Vallon de Nant (VD): bilans de calcium et relations avec la matière organique du sol, Universite de Lausanne, Lausanne.

Demarty, M., Morvan, C., Thellier, M., 1984. Calcium and the cell wall. Plant, Cell & Environment 7(6), 441-448.
Demri, B., Muster, D., 1995. XPS study of some calcium compounds. Journal of Materials Processing Technology 55(3), 311-314.
Denef, K., Six, J., Merckx, R., Paustian, K., 2004. Carbon sequestration in microaggregates of no-tillage soils with different clay mineralogy. Soil Science Society of America Journal 68(6), 1935-1944.
Dengis, P.B., Gerin, P.A., Rouxhet, P.G., 1995. X-ray photoelectron spectroscopy analysis of biosurfaces: examination of performances with yeast cells and related model compounds. Colloids and Surfaces B: Biointerfaces 4(4), 199-211.
Diaz, N., Dietrich, F., King, G.E., Valla, P.G., Sebag, D., Herman, F., Verrecchia, E.P., 2016. A 20-ka reconstruction of a Sahelo-Sudanian paleoenvironment using multi-method dating on pedogenic carbonate, EGU General Assembly Conference Abstracts, pp. 4243.
Dijkstra, F.A., Van Breemen, N., Jongmans, A.G., Davies, G.R., Likens, G.E., 2003. Calcium weathering in forested soils and the effect of different tree species. Biogeochemistry 62(3), 253-275.
Dincher, M., Calvaruso, C., Turpault, M.-P., 2019. Major element residence times in humus from a beech forest: The role of element forms and recycling. Soil Biology and Biochemistry, 107674.
Doetterl, S., Stevens, A., Six, J., Merckx, R., Van Oost, K., Casanova Pinto, M., Casanova-Katny, A., Munoz, C., Boudin, M., Zagal Venegas, E., Boeckx, P., 2015. Soil carbon storage controlled by interactions between geochemistry and climate. Nature Geosci 8(10), 780-783.
Dokuchaev, V.V., 1883. Russian chernozem:(Russkiĭ chernozem), 1. Russkaya kollektsiya, St Petersbourg.
Dontsova, K.M., Norton, L.D., 2002. Clay dispersion, infiltration, and erosion as influenced by exchangeable Ca and Mg. Soil Science 167(3), 184-193.
Duchaufour, R., 1982. Pedology: Pedogenesis and classification. Springer, Netherlands.
Duiker, S.W., Rhoton, F.E., Torrent, J., Smeck, N.E., Lal, R., 2003. Iron (hydr)oxide crystallinity effects on soil aggregation. Soil Science Society of America Journal 67(2), 606-611.
Dutoit, A., 1983. La végétation de l'étage subalpin du Vallon de Nant, Université de Lausanne, Lausanne, 131 + annexes pp.
Eanes, E.D., Powers, L., Costa, J.L., 1981. Extended X-ray absorption fine structure (EXAFS) studies on calcium in crystalline and amorphous solids of biological interest. Cell Calcium 2(3), 251-262.
EASAC, 2018. Negative emission technologies: what role in meeting Paris Agreement targets? Policy report., 35. European Academies Science Advisory Council.
Edwards, A.P., Bremner, J.M., 1967. Microaggregates in soil. Journal of Soil Science 18(1), 64.
Edwards, C.A., Bohlen, P.J., 1995. Biology and ecology of earthworms. 3 ed. Springer, Netherlands.
Egan, G., Crawley, M.J., Fornara, D.A., 2018a. Effects of long-term grassland management on the carbon and nitrogen pools of different soil aggregate fractions. Science of The Total Environment 613-614, 810-819.
Egan, G., Crawley, M.J., Fornara, D.A., 2018b. Effects of long-term grassland management on the carbon and nitrogen pools of different soil aggregate fractions. Science of The Total Environment 613-614(Supplement C), 810-819.
Egli, M., Mirabella, A., Fitze, P., 2003. Formation rates of smectites derived from two Holocene chronosequences in the Swiss Alps. Geoderma 117(1), 81-98.
Elliott, E.T., 1986. Aggregate structure and carbon, nitrogen, and phosphorus in native and cultivated soils. Soil Science Society of America Journal 50(3), 627-633.
Érika, A.d.S., Geraldo, C.d.O., Carla, E.C., José, M.d.L., Laura, B.B.d.M., Pedro, A.N.B., 2016. Stability of soil aggregates in Latosols and Cambisols via standard method and sonification. African Journal of Agricultural Research 11(39), 3894-3903.
Erktan, A., Balmot, J., Merino-Martín, L., Monnier, Y., Pailler, F., Coq, S., Abiven, S., Stokes, A., Le Bissonnais, Y., 2017. Immediate and long-term effect of tannins on the stabilization of soil aggregates. Soil Biology and Biochemistry 105, 197-205.
ESRI, 2019. World Imagery and national geographic base maps. ESRI, pp. World imagery "Sources: Esri, DigitalGlobe, GeoEye, i-cubed, USDA FSA, USGS, AEX, Getmapping, Aerogrid, IGN, IGP,

swisstopo, and the GIS User Community" / National geographic "Sources: National Geographic, Esri, DeLorme, HERE, UNEP-WCMC, USGS, NASA, ESA, METI, NRCAN, GEBCO, NOAA, iPC".
Essington, M.E., 2015. Soil and water chemistry. An intergrative approach. CRC Press, Boca Raton, Florida, USA.
Eusterhues, K., Rumpel, C., Kleber, M., Kögel-Knabner, I., 2003. Stabilisation of soil organic matter by interactions with minerals as revealed by mineral dissolution and oxidative degradation. Organic Geochemistry 34(12), 1591-1600.
Falsone, G., Catoni, M., Bonifacio, E., 2010. Effects of calcite on the soil porous structure: natural and experimental conditions. Agrochimica 54(1), 1-12.
Federer, C.A., Hornbeck, J.W., 1985. The buffer capacity of forest soils in new England. Water, Air, and Soil Pollution 26(2), 163-173.
Fernández-Ugalde, O., Virto, I., Barré, P., Apesteguía, M., Enrique, A., Imaz, M.J., Bescansa, P., 2014. Mechanisms of macroaggregate stabilisation by carbonates: implications for organic matter protection in semi-arid calcareous soils. Soil Research 52(2), 180-192.
Fernández-Ugalde, O., Virto, I., Barré, P., Gartzia-Bengoetxea, N., Enrique, A., Imaz, M.J., Bescansa, P., 2011. Effect of carbonates on the hierarchical model of aggregation in calcareous semi-arid Mediterranean soils. Geoderma 164(3–4), 203-214.
Ferro-Vázquez, C., Nóvoa-Muñoz, J.C., Costa-Casais, M., Klaminder, J., Martínez-Cortizas, A., 2014. Metal and organic matter immobilization in temperate podzols: A high resolution study. Geoderma 217–218(0), 225-234.
Filimonova, S., Kaufhold, S., Wagner, F.E., Häusler, W., Kögel-Knabner, I., 2016. The role of allophane nano-structure and Fe oxide speciation for hosting soil organic matter in an allophanic Andosol. Geochimica et Cosmochimica Acta 180, 284-302.
Foote, E., Silliman, B., Dan, J.D., Gray, A., Agassiz, L., Gibbs, W., 1856. On the heat in the Sun's rays. The American Journal of Science and Arts 22(31), 362.
Frederick, S.E., Gruber, P.J., Tolbert, N.E., 1973. The occurrence of glycolate dehydrogenase and glycolate oxidase in green plants: an evolutionary survey. Plant physiology 52(4), 318-323.
Gadd, G.M., 1999. Fungal production of citric and oxalic acid: importance in metal speciation, physiology and biogeochemical processes. In: R.K. Poole (Ed.), Advances in Microbial Physiology. Academic Press, pp. 47-92.
Gaiffe, M., Duquet, B., Tavant, H., Tavant, Y., Bruckert, S., 1984. Biological stability and physical stability of a clay-humus complex placed under different conditions of calcium or potassium saturation. Plant and Soil 77(2-3), 271-284.
Gaiffe, M., Schmitt, A., 1980. Sols et végétation à l'étage montagnard dans les forêts du Jura Central. Science du sol: Bulletin l'Association Francaise pour l'Étude du sol 4, 265-296.
Galecki, A., Burzykowski, T., 2015. Linear mixed-effects models using R: A step-by-step approach. Springer New York, New York.
Gao, Y., Tian, J., Pang, Y., Liu, J., 2017. Soil inorganic carbon sequestration following afforestation is probably induced by pedogenic carbonate formation in Northwest China. Frontiers in Plant Science 8(1282).
Garten, C.T., 2006. Relationships among forest soil C isotopic composition, partitioning, and turnover times. Canadian Journal of Forest Research 36(9), 2157-2167.
Garten, C.T., Cooper, L.W., Post, W.M., Hanson, P.J., 2000. Climate Controls on Forest Soil C Isotope Ratios in the Southern Appalachian Mountains. Ecology 81(4), 1108-1119.
Garten, C.T., Hanson, P.J., 2006. Measured forest soil C stocks and estimated turnover times along an elevation gradient. Geoderma 136(1), 342-352.
Garten, C.T., Hanson, P.J., Todd, D.E., Lu, B.B., Brice, D.J., 2007. Natural 15N- and 13C-Abundance as Indicators of Forest Nitrogen Status and Soil Carbon Dynamics. In: R. Michener, K. Lajtha (Eds.), Stable Isotopes in Ecology and Environmental Science. Blackwell Publishing LTd, Malden, pp. 61-82.
Gessa, C., Deiana, S., 1992. Ca-polygalacturonate as a model for a soil-root interface: II. Fibrillar structure and comparison with natural root mucilage. Plant and Soil 140(1), 1-13.

Ghezzehei, T.A., 2011. Soil structure. In: P.A. Huang, Y. Li, M.E. Sumner (Eds.), Handbook of soil sciences. Handbook of Soil Science. CRC Press, pp. 1-18.
Gigon, O., 2012. L'influence des formations superficielles sur la genèse des sols du Vallon de Nant (VD), Université de Lausanne / Université de Neuchâtel, Lausanne.
Gillman, G.P., Sumpter, E.A., 1986. Modification to the compulsive exchange method for measuring exchange characteristics of soils. Soil Research 24(1), 61-66.
Gleixner, G., Bol, R., Balesdent, J., 1999. Molecular insight into soil carbon turnover. Rapid Communications in Mass Spectrometry 13(13), 1278-1283.
Gleixner, G., Poirier, N., Bol, R., Balesdent, J., 2002. Molecular dynamics of organic matter in a cultivated soil. Organic Geochemistry 33(3), 357-366.
Glover, E.D., 1961. Method of solution of calcareous materials using the complexing agent, EDTA. Journal of Sedimentary Research 31(4), 622-626.
Gobat, J.M., Aragno, M., Matthey, W., 2004. The living soil. Fundamentals of Soil Science and Soil Biology. Science Publishers, Enfield (USA) / Plymouth (UK).
Golchin, A., Oades, J.M., Skjemstad, J.O., Clarke, P., 1994. Study of free and occluded particulate organic matter in soils by solid-state c-13 CP/MAS NMR-spectroscopy and scanning electron-microscopy. Australian Journal of Soil Research 32(2), 285-309.
Goudie, A., 1973. Duricrusts in Tropical and Subtropical Landscapes. Oxford, Clarendon Press: Oxford University Press.
Grand, S., Lavkulich, L.M., 2011. Depth distribution and predictors of soil organic carbon in Podzols of a forested watershed in southwestern Canada. Soil Sci 176(4), 164-174.
Grand, S., Lavkulich, L.M., 2012. Effects of forest harvest on soil carbon and related variables in canadian Spodosols. Soil Science Society of America Journal 76(5), 1816-1827.
Grand, S., Lavkulich, L.M., 2013. Potential influence of poorly crystalline minerals on soil chemistry in Podzols of southwestern Canada. European Journal of Soil Science 64(5), 651-660.
Grand, S., Rubin, A., Verrecchia, E.P., Vittoz, P., 2016. Variation in soil respiration across soil and vegetation types in an alpine valley. PLOS ONE 11(9), e0163968.
Grant, C.D., Dexter, A.R., Oades, J.M., 1992. Residual effects of additions of calcium compounds on soil structure and strength. Soil and Tillage Research 22(3), 283-297.
Greczynski, G., Hultman, L., 2017. C 1s Peak of Adventitious Carbon Aligns to the Vacuum Level: Dire Consequences for Material's Bonding Assignment by Photoelectron Spectroscopy. Chemphyschem 18(12), 1507-1512.
Groffman, P.M., Fisk, M.C., Driscoll, C.T., Likens, G.E., Fahey, T.J., Eagar, C., Pardo, L.H., 2006. Calcium additions and microbial nitrogen cycle processes in a Northern Hardwood Forest. Ecosystems 9(8), 1289-1305.
Grosse, G., Harden, J., Turetsky, M., McGuire, A.D., Camill, P., Tarnocai, C., Frolking, S., Schuur, E.A.G., Jorgenson, T., Marchenko, S., Romanovsky, V., Wickland, K.P., French, N., Waldrop, M., Bourgeau-Chavez, L., Striegl, R.G., 2011. Vulnerability of high-latitude soil organic carbon in North America to disturbance. Journal of Geophysical Research: Biogeosciences 116(G4).
Grünewald, G., Kaiser, K., Jahn, R., Guggenberger, G., 2006. Organic matter stabilization in young calcareous soils as revealed by density fractionation and analysis of lignin-derived constituents. Organic Geochemistry 37(11), 1573-1589.
Gu, B.H., Schmitt, J., Chen, Z.H., Liang, L.Y., McCarthy, J.F., 1994. Adsorption and desorption of natural organic-matter on iron-oxide - mechanisms and models. Environmental Science & Technology 28(1), 38-46.
Hagedorn, F., Saurer, M., Blaser, P., 2004. A 13C tracer study to identify the origin of dissolved organic carbon in forested mineral soils. European Journal of Soil Science 55(1), 91-100.
Hanson, P.J., Edwards, N.T., Garten, C.T., Andrews, J.A., 2000. Separating root and soil microbial contributions to soil respiration: A review of methods and observations. Biogeochemistry 48(1), 115-146.

Harris, D., Horwath, W.R., van Kessel, C., 2001. Acid fumigation of soils to remove carbonates prior to total organic carbon or carbon-13 isotopic analysis. Soil Science Society of America Journal 65(6), 1853-1856.

Hasinger, O., Spangenberg, J.E., Millière, L., Bindschedler, S., Cailleau, G., Verrecchia, E.P., 2015. Carbon dioxide in scree slope deposits: A pathway from atmosphere to pedogenic carbonate. Geoderma 247–248, 129-139.

Heckman, K., Grandy, A.S., Gao, X., Keiluweit, M., Wickings, K., Carpenter, K., Chorover, J., Rasmussen, C., 2013. Sorptive fractionation of organic matter and formation of organo-hydroxy-aluminum complexes during litter biodegradation in the presence of gibbsite. Geochimica Et Cosmochimica Acta 121, 667-683.

Hedges, J.I., Keil, R.G., 1995. Sedimentary organic-matter preservation - an assessment and speculative synthesis. Marine Chemistry 49(2-3), 81-115.

Heinze, C., Meyer, S., Goris, N., Anderson, L., Steinfeldt, R., Chang, N., Le Quéré, C., Bakker, D.C.E., 2015. The ocean carbon sink – impacts, vulnerabilities and challenges. Earth Syst. Dynam. 6(1), 327-358.

Heister, K., Hoeschen, C., Pronk, G.J., Mueller, C.W., Koegel-Knabner, I., 2012. NanoSIMS as a tool for characterizing soil model compounds and organomineral associations in artificial soils. Journal of Soils and Sediments 12(1), 35-47.

Hilinski, T., 2001. Implementation of exponential depth distribution of organic carbon in the CENTURY model, Colorado State University, Department of Soil and Crop Science.

Hobbie, E.A., Macko, S.A., Shugart, H.H., 1999. Insights into nitrogen and carbon dynamics of ectomycorrhizal and saprotrophic fungi from isotopic evidence. Oecologia 118(3), 353-360.

Hobbie, S.E., Miley, T.A., Weiss, M.S., 2002. Carbon and nitrogen cycling in soils from acidic and nonacidic tundra with different glacial histories in Northern Alaska. Ecosystems 5(8), 0761-0774.

Hosking, J.S., 1932. The influence of hydrogen-ion concentration on the decomposition of soil organic matter by hydrogen peroxide. Journal of Agricultural Science 22, 92-100.

Huang, P.M., Schnitzer, M., 1986. Interactions of soil minerals with natural organics and microbes. SSSA special publication. The Soil Science Society of America, Madison, Wis., USA.

Illmer, P., Schinner, F., 1991. Effects of lime and nutrient salts on the microbiological activities of forest soils. Biology and Fertility of Soils 11(4), 261-266.

Inagaki, T.M., de Moraes Sá, J.C., Caires, E.F., Gonçalves, D.R.P., 2017. Why does carbon increase in highly weathered soil under no-till upon lime and gypsum use? Science of The Total Environment 599–600, 523-532.

Inskeep, W.P., Bloom, P.R., 1986. Kinetics of calcite precipitation in the presence of water-soluble organic ligands. Soil Science Society of America Journal 50(5), 1167-1172.

Iovieno, P., Bååth, E., 2008. Effect of drying and rewetting on bacterial growth rates in soil. FEMS Microbiology Ecology 65(3), 400-407.

IPCC, 2014. Climate change 2014: Impacts, adaptation, and vulnerability. Summaries, frequently asked questions, and cross-chapter boxes. A contribution of working group II to the fifth assessment report of the Intergovernmental Panel on Climate Change [Field, C.B., V.R. Barros, D.J. Dokken, K.J. Mach, M.D. Mastrandrea, T.E. Bilir, M. Chatterjee, K.L. Ebi, Y.O. Estrada, R.C. Genova, B. Girma, E.S. Kissel, A.N. Levy, S. MacCracken,P.R. Mastrandrea, and L.L. White (eds.)]. World Meteorological Organization, Geneva, Switzerland.

Iskrenova-Tchoukova, E., Kalinichev, A.G., Kirkpatrick, R.J., 2010. Metal cation complexation with natural organic matter in aqueous solutions: molecular dynamics simulations and potentials of mean force. Langmuir 26(20), 15909-15919.

Israelachvili, J.N., 2011. 6 - Van der Waals forces, Intermolecular and surface forces Academic Press, San Diego, pp. 107-132.

IUSS Working Group WRB, 2015. World reference base for soil resources 2014, update 2015. No 106. FAO, Rome.

Ivarson, K.C., 1977. Changes in decompostion rate, microbial population and carbohydrate content of an acid peat bog after liming and reclamation. Canadian Journal of Soil Science 57(2), 129-137.
Jaillard, B., Guyon, A., Maurin, A.F., 1991. Structure and composition of calcified roots, and their identification in calcareous soils. Geoderma 50(3), 197-210.
Jansen, B., Nierop, K.G.J., Verstraten, J.M., 2003. Mobility of Fe(II), Fe(III) and Al in acidic forest soils mediated by dissolved organic matter: influence of solution pH and metal/organic carbon ratios. Geoderma 113(3), 323-340.
Jastrow, J.D., 1996. Soil aggregate formation and the accrual of particulate and mineral-associated organic matter. Soil Biology and Biochemistry 28(4–5), 665-676.
Jenkinson, D., Adams, D., Wild, A., 1991. Model estimates of CO2 emissions from soil in response to global warming. Nature 351: 304-306. Nature 351, 304-306.
Jenny, H., 1941. Factors of soil formation: a system of quantitative pedology. McGraw-Hill, University of Michigan.
Jin, J., Zimmerman, A.R., 2010. Abiotic interactions of natural dissolved organic matter and carbonate aquifer rock. Applied Geochemistry 25(3), 472-484.
Jin, J., Zimmerman, A.R., Moore, P.J., Martin, J.B., 2014. Organic and inorganic carbon dynamics in a karst aquifer: Santa Fe River Sink-Rise system, north Florida, USA. Journal of Geophysical Research: Biogeosciences 119(3), 340-357.
Joachim, B., Heinrich, W., Hoschen, C., Abart, R., 2019. The effect of H2O fluid on relative component mobilities in a bimineralic reaction rim in the system CaO-MgO-SiO2. European Journal of Mineralogy 31(1), 61-72.
Jones, D.L., Cooledge, E.C., Hoyle, F.C., Griffiths, R.I., Murphy, D.V., 2019. pH and exchangeable aluminum are major regulators of microbial energy flow and carbon use efficiency in soil microbial communities. Soil Biology and Biochemistry, 107584.
Jones, E., Singh, B., 2014. Organo-mineral interactions in contrasting soils under natural vegetation. Frontiers in Environmental Science 2(2).
Juo, A.S.R., Kamprath, E.J., 1979. Copper chloride as an extractant for estimating the potentially reactive aluminum pool in acid soils. Soil Science Society of America Journal 43(1), 35-38.
Kaiser, K., 1998. Fractionation of dissolved organic matter affected by polyvalent metal cations. Organic Geochemistry 28(12), 849-854.
Kaiser, K., Eusterhues, K., Rumpel, C., Guggenberger, G., Kögel-Knabner, I., 2002. Stabilization of organic matter by soil minerals — investigations of density and particle-size fractions from two acid forest soils. Journal of Plant Nutrition and Soil Science 165(4), 451-459.
Kaiser, K., Guggenberger, G., 2003. Mineral surfaces and soil organic matter. European Journal of Soil Science 54(2), 219-236.
Kaiser, K., Guggenberger, G., Haumaier, L., Zech, W., 1997. Dissolved organic matter sorption on sub soils and minerals studied by 13C-NMR and DRIFT spectroscopy. European Journal of Soil Science 48(2), 301-310.
Kaiser, K., Guggenberger, G., Zech, W., 2001. Isotopic fractionation of dissolved organic carbon in shallow forest soils as affected by sorption. European Journal of Soil Science 52(4), 585-597.
Kaiser, M., Berhe, A.A., 2014. How does sonication affect the mineral and organic constituents of soil aggregates?-A review. Journal of Plant Nutrition and Soil Science 177(4), 479-495.
Kaiser, M., Berhe, A.A., Sommer, M., Kleber, M., 2012. Application of ultrasound to disperse soil aggregates of high mechanical stability. Journal of Plant Nutrition and Soil Science 175(4), 521-526.
Kaiser, M., Ghezzehei, T.A., Kleber, M., Myrold, D.D., Berhe, A.A., 2014. Influence of calcium carbonate and charcoal applications on organic matter storage in silt-sized aggregates formed during a microcosm experiment. Soil Science Society of America Journal 78(5), 1624-1631.
Kalbitz, K., Kaiser, K., 2008. Contribution of dissolved organic matter to carbon storage in forest mineral soils. Journal of Plant Nutrition and Soil Science-Zeitschrift Fur Pflanzenernahrung Und Bodenkunde 171(1), 52-60.

Kalinichev, A.G., Kirkpatrick, R.J., 2007. Molecular dynamics simulation of cationic complexation with natural organic matter. European Journal of Soil Science 58(4), 909-917.
Kandasamy, S., Bejugam, N., 2016. Perspectives on the Terrestrial Organic Matter Transport and Burial along the Land-Deep Sea Continuum: Caveats in Our Understanding of Biogeochemical Processes and Future Needs, 3.
Kayler, Z.E., Kaiser, M., Gessler, A., Ellerbrock, R.H., Sommer, M., 2011. Application of delta C-13 and delta N-15 isotopic signatures of organic matter fractions sequentially separated from adjacent arable and forest soils to identify carbon stabilization mechanisms. Biogeosciences 8(10), 2895-2906.
Keeney, D.R., Nelson, D.W., 1982. Nitrogen in organic forms. In: A.L.e.a. Page (Ed.), Methods of soil analysis. American Society of Agronomy, Madison, WI.
Kelleher, B.P., Simpson, A.J., 2006. Humic substances in soils: are they really chemically distinct? Environmental Science & Technology 40(15), 4605-4611.
Kempen, B., Brus, D.J., Stoorvogel, J.J., 2011. Three-dimensional mapping of soil organic matter content using soil type-specific depth functions. Geoderma 162(1-2), 107-123.
Kiriukhin, M.Y., Collins, K.D., 2002. Dynamic hydration numbers for biologically important ions. Biophysical Chemistry 99(2), 155-168.
Kleber, M., Jahn, R., 2007. Andosols and soils with andic properties in the German soil taxonomy. Journal of Plant Nutrition and Soil Science 170(3), 317-328.
Kleber, M., Lehmann, J., 2019. Humic substances extracted by alkali are invalid proxies for the dynamics and functions of organic matter in terrestrial and aquatic ecosystems. Journal of Environmental Quality 48(2), 207-216.
Kleber, M., Nico, P.S., Plante, A., Filley, T., Kramer, M., Swanston, C., Sollins, P., 2011. Old and stable soil organic matter is not necessarily chemically recalcitrant: implications for modeling concepts and temperature sensitivity. Global Change Biology 17(2), 1097-1107.
Kleber, M., Sollins, P., Sutton, R., 2007. A conceptual model of organo-mineral interactions in soils: self-assembly of organic molecular fragments into zonal structures on mineral surfaces. Biogeochemistry 85(1), 9-24.
Koerselman, W., Arthur, F.M.M., 1996. The vegetation N:P ratio: a new tool to detect the nature of nutrient limitation. Journal of Applied Ecology 33(6), 1441-1450.
Kögel-Knabner, I., Guggenberger, G., Kleber, M., Kandeler, E., Kalbitz, K., Scheu, S., Eusterhues, K., Leinweber, P., 2008. Organo-mineral associations in temperate soils: Integrating biology, mineralogy, and organic matter chemistry. Journal of Plant Nutrition and Soil Science-Zeitschrift Fur Pflanzenernahrung Und Bodenkunde 171(1), 61-82.
Konings, A.G., Bloom, A.A., Liu, J., Parazoo, N.C., Schimel, D.S., Bowman, K.W., 2019. Global satellite-driven estimates of heterotrophic respiration. Biogeosciences 16(11), 2269-2284.
Kowalska, J.B., Zaleski, T., Józefowska, A., Mazurek, R., 2019. Soil formation on calcium carbonate-rich parent material in the outer Carpathian Mountains – A case study. Catena 174, 436-451.
Kramer, M.G., Chadwick, O.A., 2018. Climate-driven thresholds in reactive mineral retention of soil carbon at the global scale. Nature Climate Change 8(12), 1104-1108.
Kravchenko, A., Otten, W., Garnier, P., Pot, V., Baveye, P.C., 2019. Soil aggregates as biogeochemical reactors: Not a way forward in the research on soil–atmosphere exchange of greenhouse gases. Global Change Biology 25(7), 2205-2208.
Krebs, H.A., Johnson, W.A., 1937. The role of citric acid in intermediate metabolism in animal tissues. Enzymologia 4, 148-156.
Kreyling, O., Kölbl, A., Spielvogel, S., Rennert, T., Kaiser, K., Kögel-Knabner, I., 2013. Density fractionation of organic matter in dolomite-derived soils. Journal of Plant Nutrition and Soil Science 176(4), 509-519.
Kuzyakov, Y., Friedel, J.K., Stahr, K., 2000. Review of mechanisms and quantification of priming effects. Soil Biology and Biochemistry 32(11–12), 1485-1498.

Laine, J., Silvola, J., Tolonen, K., Alm, J., Nykänen, H., Vasander, H., Tapani, S., Ilkka, S., Jukka, S., Martikainen, P.J., 1996. Effect of water-level drawdown on global climatic warming: Northern peatlands. Ambio 25(3), 179-184.

Lal, R., 2004. Soil carbon sequestration impacts on global climate change and food security. Science 304(5677), 1623.

Lal, R., 2009. Challenges and opportunities in soil organic matter research. European Journal of Soil Science 60(2), 158-169.

Langmuir, D., 1997. Aqueous environmental geochemistry. Prentice Hall, Upper Saddle River, N.J.

Lavkulich, L.M., Arocena, J.M., 2011. Luvisolic soils of Canada: Genesis, distribution, and classification. Canadian Journal of Soil Science 91(5), 781-806.

Lee, X., Wu, H.-J., Sigler, J., Oishi, C., Siccama, T., 2004. Rapid and transient response of soil respiration to rain. Global Change Biology 10(6), 1017-1026.

Lee, Y.J., Elzinga, E.J., Reeder, R.J., 2005. Cu(II) adsorption at the calcite–water interface in the presence of natural organic matter: Kinetic studies and molecular-scale characterization. Geochimica et Cosmochimica Acta 69(1), 49-61.

Lehmann, J., Kleber, M., 2015. The contentious nature of soil organic matter. Nature 528(7580), 60-68.

Li, D., Wen, L., Yang, L., Luo, P., Xiao, K., Chen, H., Zhang, W., He, X., Chen, H., Wang, K., 2017. Dynamics of soil organic carbon and nitrogen following agricultural abandonment in a karst region. Journal of Geophysical Research: Biogeosciences.

Likens, G.E., Driscoll, C.T., Buso, D.C., Siccama, T.G., Johnson, C.E., Lovett, G.M., Fahey, T.J., Reiners, W.A., Ryan, D.F., Martin, C.W., Bailey, S.W., 1998. The biogeochemistry of calcium at Hubbard Brook. Biogeochemistry 41(2), 89-173.

Lindsay, W., 1979. Chemical equilibria in soils, Chemical equilibria in soils. John Wiley Sons.

Lo, I.M.C., Yang, X.Y., 1999. EDTA extraction of heavy metals from different soil fractions and synthetic soils. Water, Air, and Soil Pollution 109(1), 219-236.

Loeppert, R.H., Hallmark, C.T., Koshy, M.M., 1984. Routine procedure for rapid determination of soil carbonates. Soil Science Society of America Journal 48(5), 1030-1033.

Loeppert, R.H., Suarez, D.L., 1996. Carbonate and gypsum. In: D.L. Sparks, A.L. Page, P.A. Helmke, R.H. Loeppert (Eds.), Methods of soil analysis part 3—chemical methods. SSSA Book Series. Soil Science Society of America, American Society of Agronomy, Madison, WI.

Löhnis, F., 1926. Nitrogen availability of green manures. Soil Science 22(4), 253-290.

Lovelock, J.E., 1989. Geophysiology, the science of Gaia. Reviews of Geophysics 27(2), 215-222.

Lüthi, D., Le Floch, M., Bereiter, B., Blunier, T., Barnola, J.-M., Siegenthaler, U., Raynaud, D., Jouzel, J., Fischer, H., Kawamura, K., Stocker, T.F., 2008. High-resolution carbon dioxide concentration record 650,000–800,000 years before present. Nature 453, 379.

Marschner, B., Kalbitz, K., 2003. Controls of bioavailability and biodegradability of dissolved organic matter in soils. Geoderma 113(3–4), 211-235.

Martí-Roura, M., Hagedorn, F., Rovira, P., Romanyà, J., 2019. Effect of land use and carbonates on organic matter stabilization and microbial communities in Mediterranean soils. Geoderma 351, 103-115.

Martin-Diaconescu, V., Gennari, M., Gerey, B., Tsui, E., Kanady, J., Tran, R., Pécaut, J., Maganas, D., Krewald, V., Gouré, E., Duboc, C., Yano, J., Agapie, T., Collomb, M.-N., DeBeer, S., 2015. Ca K-edge XAS as a probe of calcium centers in complex systems. Inorganic Chemistry 54(4), 1283-1292.

Martin, J.P., Martin, W.P., Page, J.B., Raney, W.A., de Ment, J.D., 1955. Soil aggregation. In: A.G. Norman (Ed.), Advances in agronomy. Academic Press, pp. 1-37.

Mason-Jones, K., Banfield, C.C., Dippold, M.A., 2019. Compound-specific 13C stable isotope probing confirms synthesis of polyhydroxybutyrate by soil bacteria. Rapid Communications in Mass Spectrometry 33(8), 795-802.

Matteodo, M., Grand, S., Sebag, D., Rowley, M.C., Vittoz, P., Verrecchia, E.P., 2018. Decoupling of topsoil and subsoil controls on organic matter dynamics in the Swiss Alps. Geoderma 330, 41-51.

Matus, F., Amigo, X., Kristiansen, S.M., 2006. Aluminium stabilization controls organic carbon levels in Chilean volcanic soils. Geoderma 132(1), 158-168.
Mayer, L.M., Xing, B., 2001. Organic matter–surface area relationships in acid soils. Soil Science Society of America Journal 65(1), 250-258.
McKeague, J.A., Day, D.H., 1966. Dithionite- and oxalate-extractable Fe and Al as aids in differentiating various classes of soils. Canadian Journal of Soil Science 46(1), 13-&.
Mehra, O.P., Jackson, M.L., 1958. Iron oxide removal from soils and clays by a dithionite-citrate system buffered with sodium bicarbonate. Clays and Clay Minerals 7(1), 317-327.
Melvin, A.M., Lichstein, J.W., Goodale, C.L., 2013. Forest liming increases forest floor carbon and nitrogen stocks in a mixed hardwood forest. Ecological Applications 23(8), 1962-1975.
Mikutta, R., Lorenz, D., Guggenberger, G., Haumaier, L., Freund, A., 2014. Properties and reactivity of Fe-organic matter associations formed by coprecipitation versus adsorption: Clues from arsenate batch adsorption. Geochimica et Cosmochimica Acta 144, 258-276.
Mikutta, R., Mikutta, C., Kalbitz, K., Scheel, T., Kaiser, K., Jahn, R., 2007. Biodegradation of forest floor organic matter bound to minerals via different binding mechanisms. Geochimica Et Cosmochimica Acta 71(10), 2569-2590.
Mikutta, R., Schaumann, G.E., Gildemeister, D., Bonneville, S., Kramer, M.G., Chorover, J., Chadwick, O.A., Guggenberger, G., 2009. Biogeochemistry of mineral–organic associations across a long-term mineralogical soil gradient (0.3–4100kyr), Hawaiian Islands. Geochimica et Cosmochimica Acta 73(7), 2034-2060.
Millière, L., Gussone, N., Moritz, T., Bindschedler, S., Verrecchia, E., 2019. Origin of strontium and calcium in pedogenic needle fibre calcite (NFC). Chemical Geology 524.
Miltner, A., Bombach, P., Schmidt-Brucken, B., Kastner, M., 2012. SOM genesis: microbial biomass as a significant source. Biogeochemistry 111(1-3), 41-55.
Minasny, B., Malone, B.P., McBratney, A.B., Angers, D.A., Arrouays, D., Chambers, A., Chaplot, V., Chen, Z.-S., Cheng, K., Das, B.S., Field, D.J., Gimona, A., Hedley, C.B., Hong, S.Y., Mandal, B., Marchant, B.P., Martin, M., McConkey, B.G., Mulder, V.L., O'Rourke, S., Richer-de-Forges, A.C., Odeh, I., Padarian, J., Paustian, K., Pan, G., Poggio, L., Savin, I., Stolbovoy, V., Stockmann, U., Sulaeman, Y., Tsui, C.-C., Vågen, T.-G., van Wesemael, B., Winowiecki, L., 2017. Soil carbon 4 per mille. Geoderma 292, 59-86.
Minick, K.J., Fisk, M.C., Groffman, P.M., 2017. Soil Ca alters processes contributing to C and N retention in the Oa/A horizon of a northern hardwood forest. Biogeochemistry, 1-15.
Moir, J.L., Moot, D.J., 2014. Medium-term soil pH and exchangeable aluminium response to liming at three high country locations. Proceedings of the New Zealand Grassland Association 76, 41-46.
Monger, H.C., Daugherty, L.A., Lindemann, W.C., Liddell, C.M., 1991. Microbial precipitation of pedogenic calcite. Geology 19(10), 997-1000.
Moni, C., Rumpel, C., Virto, I., Chabbi, A., Chenu, C., 2010. Relative importance of sorption versus aggregation for organic matter storage in subsoil horizons of two contrasting soils. European Journal of Soil Science 61(6), 958-969.
Monreal, C.M., Schulten, H.R., Kodama, H., 1997. Age, turnover and molecular diversity of soil organic matter in aggregates of a Gleysol. Canadian Journal of Soil Science 77(3), 379-388.
Moulder, J.F., Chastain, J., 1992. Handbook of X-ray photoelectron spectroscopy: A reference book of standard spectra for identification and interpretation of XPS data. Physical Electronics Division, Perkin-Elmer Corporation.
Mueller, C.W., Koelbl, A., Hoeschen, C., Hillion, F., Heister, K., Herrmann, A.M., Koegel-Knabner, I., 2012. Submicron scale imaging of soil organic matter dynamics using NanoSIMS - From single particles to intact aggregates. Organic Geochemistry 42(12), 1476-1488.
Mueller, C.W., Rethemeyer, J., Kao-Kniffin, J., Löppmann, S., Hinkel, K.M., G. Bockheim, J., 2015. Large amounts of labile organic carbon in permafrost soils of northern Alaska. Global Change Biology 21(7), 2804-2817.

Mueller, C.W., Weber, P.K., Kilburn, M.R., Hoeschen, C., Kleber, M., Pett-Ridge, J., 2013. Chapter one - Advances in the analysis of biogeochemical Interfaces: NanoSIMS to investigate soil microenvironments. In: D.L. Sparks (Ed.), Advances in Agronomy. Academic Press, pp. 1-46.

Muhs, D.R., 1984. Intrinsic thresholds in soil systems. Physical Geography 5(2), 99-110.

Muneer, M., Oades, J.M., 1989a. The role of Ca-organic interactions in soil aggregate stability .1. Laboratory studies with glucose-C-14, CaCO3 and CaSO4.2H2O. Australian Journal of Soil Research 27(2), 389-399.

Muneer, M., Oades, J.M., 1989b. The role of Ca-organic interactions in soil aggregate stability .2. Field studies with C-14-labelled straw, CaCO3 AND CaSO4.2H2O. Australian Journal of Soil Research 27(2), 401-409.

Muneer, M., Oades, J.M., 1989c. The role of Ca-organic interactions in soil aggregate stability .3. Mechanisms and models. Australian Journal of Soil Research 27(2), 411-423.

Muñoz Noval, Á., Nishio, D., Kuruma, T., Hayakawa, S., 2018. Coordination and structure of Ca(II)-acetate complexes in aqueous solution studied by a combination of Raman and XAFS spectroscopies. Journal of Molecular Structure 1161, 512-518.

Narendrula-Kotha, R., Nkongolo, K.K., 2017. Microbial response to soil liming of damaged ecosystems revealed by pyrosequencing and phospholipid fatty acid analyses. Plos One 12(1), e0168497.

Natelhoffer, K., Fry, B., 1988. Controls on natural nitrogen-15 and carbon-13 abundances in forest soil organic matter. Soil Science Society of America Journal 52(6), 1633-1640.

Neuhaus, J.O., Wrigley, C., 1954. The quartimax rotation. British Journal of Statistical Psychology 7(2), 81-91.

NOAA, N.O.A.A., 2019. Earth System Research Laboratory - Global Monitoring Division. Pieter Tans & Ralph Keeling, Scripps Institution of Oceanography.

O'Brien, S.L., Jastrow, J.D., Grimley, D.A., Gonzalez-Meler, M.A., 2015. Edaphic controls on soil organic carbon stocks in restored grasslands. Geoderma 251–252, 117-123.

Oades, J., Waters, A., 1991. Aggregate hierarchy in soils. Soil Research 29(6), 815-828.

Oades, J.M., 1984. Soil organic matter and structural stability: mechanisms and implications for management. Plant and Soil 76(1/3), 319-337.

Oades, J.M., 1988. The retention of organic matter in soils. Biogeochemistry 5(1), 35-70.

Oades, J.M., 1993. The role of biology in the formation, stabilization and degradation of soil structure. Geoderma 56(1), 377-400.

Oldham, K.B., 2008. A Gouy–Chapman–Stern model of the double layer at a (metal)/(ionic liquid) interface. Journal of Electroanalytical Chemistry 613(2), 131-138.

Orlov, D.S., 1995. Humic substances of soils and general theory of humification. A.A. Balkema, Rotterdam, Nethelands.

Oste, L.A., Temminghoff, E.J.M., Riemsdijk, W.H.V., 2002. Solid-solution partitioning of organic matter in soils as influenced by an increase in pH or Ca concentration. Environmental Science & Technology 36(2), 208-214.

Pansu, M., Gautheyrou, J., 2006. Handbook of soil analysis : mineralogical, organic and inorganic methods. Springer, Berlin ; New York.

Paradelo, R., van Oort, F., Barre, P., Billiou, D., Chenu, C., 2016. Soil organic matter stabilization at the pluri-decadal scale: Insight from bare fallow soils with contrasting physicochemical properties and macrostructures. Geoderma 275, 48-54.

Paradelo, R., Virto, I., Chenu, C., 2015. Net effect of liming on soil organic carbon stocks: A review. Agriculture, Ecosystems & Environment 202, 98-107.

Parfitt, R.L., Childs, C.W., 1988a. Estimation of forms of Fe and Al - a review, and analysis of contasting soils by dissolution and mossbauer methods. Australian Journal of Soil Research 26(1), 121-144.

Parfitt, R.L., Childs, C.W., 1988b. Estimation of forms of Fe and Al - A review, and analysis of contrasting soils by dissolution and mossbauer methods. Australian Journal of Soil Research 26(1), 121-144.

Parton, W.J., 1996. The CENTURY model. In: D.S. Powlson, P. Smith, J.U. Smith (Eds.), Evaluation of soil organic matter models: using existing long-term datasets. Springer Berlin Heidelberg, Berlin, Heidelberg, pp. 283-291.

Parton, W.J., Del Grosso, S.J., Plante, A.F., Adair, E.C., Lutz, S.M., 2015. Modeling the dynamics of soil organic matter and nutrient cycling. In: E.A. Paul (Ed.), Soil Microbiology, Ecology and Biochemistry (Fourth Edition). Academic Press, Boston, pp. 505-537.

Paul, E.A., Morris, S.J., Six, J., Paustian, K., Gregorich, E.G., 2003. Interpretation of soil carbon and nitrogen dynamics in agricultural and afforested soils. Soil Science Society of America Journal 67(5), 1620-1628.

Pearson, R.G., 1963. Hard and soft acids and bases. Journal of the American Chemical Society 85(22), 3533-3539.

Perret, A., Martin, S., 2014. Carte Géomorphologique Du Vallon De Nant & Étude De La Marge Proglaciaire Du Glacier Des Martinets. Bulletin Annuel De La Murithienne 132, 69-82.

Peterson, J.B., 1947. Calcium linkage, a mechanism in soil granulation. Soil Science Society of America Journal 12, 29-34.

Plante, A.F., Feng, Y., McGill, W.B., 2002. A modeling approach to quantifying soil macroaggregate dynamics. Canadian Journal of Soil Science 82(2), 181-190.

Poeplau, C., Don, A., Six, J., Kaiser, M., Benbi, D., Chenu, C., Cotrufo, M.F., Derrien, D., Gioacchini, P., Grand, S., Gregorich, E., Griepentrog, M., Gunina, A., Haddix, M., Kuzyakov, Y., Kühnel, A., Macdonald, L., Soong, J., Trigalet, S., Nieder, R., 2018. Isolating organic carbon fractions with varying turnover rates in temperate agricultural soils – A comprehensive method comparison, 125.

Pohl, M., Hoffmann, M., Hagemann, U., Giebels, M., Albiac Borraz, E., Sommer, M., Augustin, J., 2015. Dynamic C and N stocks – key factors controlling the C gas exchange of maize in heterogenous peatland. Biogeosciences 12(9), 2737-2752.

Powers, J.S., Schlesinger, W.H., 2002. Geographic and vertical patterns of stable carbon isotopes in tropical rain forest soils of Costa Rica. Geoderma 109(1), 141-160.

Prentice, I.C., Farquhar, G., Fasham, M., Goulden, M., Heimann, M., Jaramillo, V., Kheshgi, H., LeQuéré, C., Scholes, R., Wallace, D.W., 2001. The carbon cycle and atmospheric carbon dioxide. Cambridge University Press.

Preston, C.M., Nault, J.R., Trofymow, J.A., 2009. Chemical changes during 6 years of decomposition of 11 litters in some canadian forest sites. Part 2. 13C abundance, solid-state 13C NMR spectroscopy and the meaning of “lignin”. Ecosystems 12(7), 1078-1102.

Pulido-Villena, E., Reche, I., Morales-Baquero, R., 2006. Significance of atmospheric inputs of calcium over the southwestern Mediterranean region: High mountain lakes as tools for detection. Global Biogeochemical Cycles 20(2), 1-8.

Quiquampoix, H., Burns, R.G., 2007. Interactions between proteins and soil mineral surfaces: environmental and health consequences. Elements 3(6), 401-406.

R, 2019. R: A language and environment for statistical computing. In: R.C. Team (Ed.). R Foundation for Statistical Computing, Vienna, Austria.

Rahnemaie, R., Hiemstra, T., van Riemsdijk, W.H., 2006. Inner- and outer-sphere complexation of ions at the goethite–solution interface. Journal of Colloid and Interface Science 297(2), 379-388.

Ramnarine, R., Voroney, R.P., Wagner-Riddle, C., Dunfield, K.E., 2011. Carbonate removal by acid fumigation for measuring the δ13C of soil organic carbon. Canadian Journal of Soil Science 91(2), 247-250.

Ranjbar, F., Jalali, M., 2012. Calcium, magnesium, sodium, and potassium release during decomposition of some organic residues. Communications in Soil Science and Plant Analysis 43(4), 645-659.

Rasmussen, C., Heckman, K., Wieder, W.R., Keiluweit, M., Lawrence, C.R., Berhe, A.A., Blankinship, J.C., Crow, S.E., Druhan, J.L., Hicks Pries, C.E., Marin-Spiotta, E., Plante, A.F., Schädel, C., Schimel, J.P., Sierra, C.A., Thompson, A., Wagai, R., 2018. Beyond clay: towards an improved set of variables for predicting soil organic matter content. Biogeochemistry 137(3), 297-306.

Rasmussen, C., Southard, R.J., Horwath, W.R., 2006. Mineral control of organic carbon mineralization in a range of temperate conifer forest soils. Global Change Biology 12(5), 834-847.
Rasmussen, C., Torn, M.S., Southard, R.J., 2005. Mineral assemblage and aggregates control carbon dynamics in a California conifer forest. Soil Science Society of America Journal 69(6), 1711-1721.
Rayleigh, L., 1896. Theoretical considerations respecting the separation of gases by diffusion and similar processes. The London, Edinburgh, and Dublin Philosophical Magazine and Journal of Science 42(259), 493-498.
Reddy, K.J., Lindsay, W.L., Workman, S.M., Drever, J.I., 1990. Measurement of calcite ion activity products in soils. Soil Science Society of America Journal 54(1), 67-71.
Rennert, T., 2019. Wet-chemical extractions to characterise pedogenic Al and Fe species – a critical review. Soil Research 57(1), 1-16.
Rennert, T., Händel, M., Höschen, C., Lugmeier, J., Steffens, M., Totsche, K.U., 2014. A NanoSIMS study on the distribution of soil organic matter, iron and manganese in a nodule from a Stagnosol. European Journal of Soil Science 65(5), 684-692.
Reynolds, R.C., 1978. Polyphenol inhibition of calcite precipitation in Lake Powell 1. Limnology and Oceanography 23(4), 585-597.
Ries, J.B., Cohen, A.L., McCorkle, D.C., 2009. Marine calcifiers exhibit mixed responses to CO2-induced ocean acidification. Geology 37(12), 1131-1134.
Rion, J., 2016. Photodétection et cartographie des formations superficielles, Université de Lausanne, Lausanne.
Römkens, P.F.A.M., Dolfing, J., 1998. Effect of Ca on the solubility and molecular size distribution of DOC and Cu binding in soil solution samples. Environmental Science & Technology 32(3), 363-369.
Ross, D.S., Bartlett, R.J., Magdoff, F.R., 1991. Exchangeable cations and the pH-independent distribution of cation exchange capacities in Spodosols of a forested watershed. In: R.J. Wright, V.C. Baligar, R.P. Murrmann (Eds.), Plant-Soil Interactions at Low pH: Proceedings of the Second International Symposium on Plant-Soil Interactions at Low pH, 24–29 June 1990, Beckley West Virginia, USA. Springer Netherlands, Dordrecht, pp. 81-92.
Rousk, J., Baath, E., Brookes, P.C., Lauber, C.L., Lozupone, C., Caporaso, J.G., Knight, R., Fierer, N., 2010. Soil bacterial and fungal communities across a pH gradient in an arable soil. International Society for Microbial Ecology Journal 4(10), 1340-1351.
Rousk, J., Brookes, P.C., Baath, E., 2009. Contrasting soil pH effects on fungal and bacterial growth suggest functional redundancy in carbon mineralization. Applied and Environmental Microbiology 75(6), 1589-1596.
Rovira, P., Casals, P., Romanyà, J., Bottner, P., Coûteaux, M.-M., Ramon Vallejo, V., 1998. Recovery of fresh debris of different sizes in density fractions of two contrasting soils. European Journal of Soil Biology 34(1), 31-37.
Rowley, M.C., Estrada-Medina, H., Tzec-Gamboa, M., Rozin, A., Cailleau, G., Verrecchia, E.P., Green, I., 2017. Moving carbon between spheres, the potential oxalate-carbonate pathway of Brosimum alicastrum Sw.; Moraceae. Plant and Soil 412(1), 465-479.
Rowley, M.C., Grand, S., Verrecchia, É.P., 2018. Calcium-mediated stabilisation of soil organic carbon. Biogeochemistry 137(1), 27-49.
Rubin, A., 2013. Dynamiques temporelles et spatiales de la respiration des sols au Vallon de Nant (VD), Université de Lausanne / Université de Neuchâtel, Lausanne.
Rumpel, C., Kögel-Knabner, I., 2011. Deep soil organic matter-a key but poorly understood component of terrestrial C cycle. Plant and Soil 338(1-2), 143-158.
Sanderman, J., 2012. Can management induced changes in the carbonate system drive soil carbon sequestration? A review with particular focus on Australia. Agriculture, Ecosystems & Environment 155, 70-77.
Satchell, J.E., 1967. Lumbricidae. Soil biology, 259-322.

Satterthwaite, F.E., 1946. An approximate distribution of estimates of variance components. Biometrics Bulletin 2(6), 110-114.
Schaetzl, R.J., Thompson, M.L., 2015. Soil Genesis and Geomorphology. 2nd ed. Cambridge Univeristy Press, New York, U.S.A.
Scheel, T., Dörfler, C., Kalbitz, K., 2007. Precipitation of dissolved organic matter by aluminum stabilizes carbon in acidic forest soils. Soil Science Society of America Journal 71(1), 64-74.
Scheel, T., Jansen, B., Van Wijk, A.J., Verstraten, J.M., Kalbitz, K., 2008. Stabilization of dissolved organic matter by aluminium: a toxic effect or stabilization through precipitation? European Journal of Soil Science 59(6), 1122-1132.
Schiedung, M., Tregurtha, C.S., Beare, M.H., Thomas, S.M., Don, A., 2019. Deep soil flipping increases carbon stocks of New Zealand grasslands. Global Change Biology 25(7), 2296-2309.
Schipper, L.A., Hobbs, J.K., Rutledge, S., Arcus, V.L., 2014. Thermodynamic theory explains the temperature optima of soil microbial processes and high Q10 values at low temperatures. Global Change Biology 20(11), 3578-3586.
Schlesinger, W.H., 2003. Introduction to volume 8. In: H.D. Holland, K.K. Turekian (Eds.), Treatise on geochemistry. Pergamon, Oxford, pp. xv-xix.
Schlesinger, W.H., Andrews, J.A., 2000. Soil respiration and the global carbon cycle. Biogeochemistry 48(1), 7-20.
Schlesinger, W.H., Bernhardt, E.S., 2013. Biogeochemistry : an analysis of global change. 3rd ed. Elsevier Inc., Oxford, England.
Schmidt, M.W.I., Rumpel, C., Kögel-Knabner, I., 1999. Evaluation of an ultrasonic dispersion procedure to isolate primary organomineral complexes from soils. European Journal of Soil Science 50(1), 87-94.
Schmidt, M.W.I., Torn, M.S., Abiven, S., Dittmar, T., Guggenberger, G., Janssens, I.A., Kleber, M., Kögel-Knabner, I., Lehmann, J., Manning, D.A.C., Nannipieri, P., Rasse, D.P., Weiner, S., Trumbore, S.E., 2011. Persistence of soil organic matter as an ecosystem property. Nature 478(7367), 49-56.
Schrumpf, M., Kaiser, K., Guggenberger, G., Persson, T., Koegel-Knabner, I., Schulze, E.D., 2013. Storage and stability of organic carbon in soils as related to depth, occlusion within aggregates, and attachment to minerals. Biogeosciences 10(3), 1675-1691.
Schurig, C., Smittenberg, R.H., Berger, J., Kraft, F., Woche, S.K., Goebel, M.O., Heipieper, H.J., Miltner, A., Kaestner, M., 2013. Microbial cell-envelope fragments and the formation of soil organic matter: a case study from a glacier forefield. Biogeochemistry 113(1-3), 595-612.
Schwarzenbach, G., 1961. The general, selective, and specific formation of complexes by metallic cations. Advances in Inorganic Chemistry and Radiochemistry 3, 257-285.
Schwertmann, U., 1964. Differenzierung der Eisenoxide des Bodens durch Extraktion mit Ammoniumoxalat-Lösung. Zeitschrift für Pflanzenernährung, Düngung, Bodenkunde 105(3), 194-202.
Schwertmann, U., Fechter, H., 1982. The point of zero charge of natural and synthetic ferrihydrites and its relation to adsorbed silicate. Clay Minerals 17(4), 471-476.
Seguinot, J., Jouvet, G., Huss, M., Funk, M., Ivy-Ochs, S., Preusser, F., 2018. Modelling last glacial cycle ice dynamics in the Alps. The Cryosphere Discuss. 2018, 1-30.
Shang, C., Tiessen, H., 2003. Soil organic C sequestration and stabilization in karstic soils of Yucatan. Biogeochemistry 62(2), 177-196.
Shipitalo, M.J., Protz, R., 1989. Chemistry and micromorphology of aggregation in earthworm casts. Geoderma 45(3), 357-374.
Six, J., Bossuyt, H., Degryze, S., Denef, K., 2004. A history of research on the link between (micro)aggregates, soil biota, and soil organic matter dynamics. Soil & Tillage Research 79(1), 7-31.
Six, J., Conant, R.T., Paul, E.A., Paustian, K., 2002. Stabilization mechanisms of soil organic matter: Implications for C-saturation of soils. Plant and Soil 241(2), 155-176.

Six, J., Paustian, K., Elliott, E.T., Combrink, C., 2000. Soil structure and organic matter I. Distribution of aggregate-size classes and aggregate-associated carbon. Soil Science Society of America Journal 64(2), 681-689.

Six, J., Schultz, P.A., Jastrow, J.D., Merckx, R., 1999. Recycling of sodium polytungstate used in soil organic matter studies. Soil Biology & Biochemistry 31(8), 1193-1196.

Skinner, H.C.W., Jahren, A.H., 2007. 8.04 - Biomineralization A2 - Holland, Heinrich D. In: K.K. Turekian (Ed.), Treatise on Geochemistry. Pergamon, Oxford, pp. 1-69.

Skjemstad, J.O., Fitzpatrick, R.W., Zarcinas, B.A., Thompson, C.H., 1992. Genesis of podzols on coastal dunes in southern Queensland. 2. Geochemistry and forms of elements as deduced from various soil extraction procedures. Australian Journal of Soil Research 30(5), 615-644.

Skjemstad, J.O., Janik, L.J., Head, M.J., McClure, S.G., 1993. High energy ultraviolet photo-oxidation: a novel technique for studying physically protected organic matter in clay- and silt-sized aggregates. Journal of Soil Science 44(3), 485-499.

Slessarev, E.W., Lin, Y., Bingham, N.L., Johnson, J.E., Dai, Y., Schimel, J.P., Chadwick, O.A., 2016. Water balance creates a threshold in soil pH at the global scale. Nature 540(7634), 567-569.

Soares, M., Rousk, J., 2019. Microbial growth and carbon use efficiency in soil: Links to fungal-bacterial dominance, SOC-quality and stoichiometry. Soil Biology and Biochemistry 131, 195-205.

Sokoloff, V.P., 1938. Effect of neutral salts of sodium and calcium on carbon and nitrogen of soils. Journal of Agricultural Research 57, 0201-0216.

Sollins, P., Homann, P., Caldwell, B.A., 1996. Stabilization and destabilization of soil organic matter: Mechanisms and controls. Geoderma 74(1-2), 65-105.

Sollins, P., Kramer, M.G., Swanston, C., Lajtha, K., Filley, T., Aufdenkampe, A.K., Wagai, R., Bowden, R.D., 2009. Sequential density fractionation across soils of contrasting mineralogy: evidence for both microbial- and mineral-controlled soil organic matter stabilization. Biogeochemistry 96(1-3), 209-231.

Sollins, P., Swanston, C., Kleber, M., Filley, T., Kramer, M., Crow, S., Caldwell, B.A., Lajtha, K., Bowden, R., 2006. Organic C and N stabilization in a forest soil: Evidence from sequential density fractionation. Soil Biology and Biochemistry 38(11), 3313-3324.

Solly, E.F., Weber, V., Zimmermann, S., Walthert, L., Hagedorn, F., Schmidt, M.W.I., in review. Is the content and potential preservation of soil organic carbon reflected by cation exchange capacity? A case study in Swiss forest soils. Biogeosciences Discuss. 2019, 1-32.

Sørensen, T.J., 1948. A method of establishing groups of equal amplitude in plant sociology based on similarity of species content and its application to analyses of the vegetation on Danish commons. I kommission hos E. Munksgaard, København.

Sowers, T., Adhikari, D., Wang, J., Yang, Y., Sparks, D.L., 2018a. Spatial associations and chemical composition of organic carbon sequestered in Fe, Ca, and organic carbon ternary systems. Environmental Science & Technology.

Sowers, T.D., Stuckey, J.W., Sparks, D.L., 2018b. The synergistic effect of calcium on organic carbon sequestration to ferrihydrite. Geochemical Transactions 19, 4.

Spaccini, R., Piccolo, A., Conte, P., Haberhauer, G., Gerzabek, M.H., 2002. Increased soil organic carbon sequestration through hydrophobic protection by humic substances. Soil Biology and Biochemistry 34(12), 1839-1851.

Spielvogel, S., Prietzel, J., Kögel-Knabner, I., 2008. Soil organic matter stabilization in acidic forest soils is preferential and soil type-specific. European Journal of Soil Science 59(4), 674-692.

Sposito, G., 1981. The thermodynamics of soil solutions. Oxford University Press.

Sposito, G., 2016. The chemistry of soils. 3rd ed. Oxford University Press, Oxford.

Stevenson, F.J., 1994. Humus chemistry: genesis, composition, reactions. Journal of Chemical Education, 72. 2nd edition ed. American Chemical Society.

Stockmann, U., Padarian, J., McBratney, A., Minasny, B., de Brogniez, D., Montanarella, L., Hong, S.Y., Rawlins, B.G., Field, D.J., 2015. Global soil organic carbon assessment. Global Food Security 6, 9-16.

Stoops, G., 2010. Interpretation of Micromorphological Features of Soils and Regoliths. 2nd ed. Elsevier, Amsterdam.
Suess, E., 1970. Interaction of organic compounds with calcium carbonate—I. Association phenomena and geochemical implications. Geochimica et Cosmochimica Acta 34(2), 157-168.
Sumner, M.E., 1994. Measurement of soil pH: Problems and solutions. Communications in Soil Science and Plant Analysis 25(7-8), 859-879.
Sutton, R., Sposito, G., Diallo, M.S., Schulten, H.-R., 2005. Molecular simulation of a model of dissolved organic matter. Environmental Toxicology and Chemistry 24(8), 1902-1911.
Suzuki, S., 2002. Black tea adsorption on calcium carbonate: A new application to chalk powder for brown powder materials. Colloids and Surfaces A: Physicochemical and Engineering Aspects 202(1), 81-91.
SwissTopo, 2019. Swiss map resources, ETH Zurich, pp. © 2019 swisstopo (JD100042).
Tate, K.R., Theng, B.K.G., 1980. Organic matter and its interactions with inorganic soil constiuents. In: B.K.G. Theng (Ed.), Soils with variable charge. Soil Bureau, Lower Hutt, New Zealand, pp. 225-249.
Theng, B.K.G., Churchman, G.J., Newman, R.H., 1986. The occurrence of interlayer clay-organic complexes in two New Zealand soils. Soil Science 142(5), 262-266.
Thirukkumaran, C.M., Morrison, I.K., 1996. Impact of simulated acid rain on microbial respiration, biomass, and metabolic quotient in a mature sugar maple (Acersaccharum) forest floor. Canadian Journal of Forest Research 26(8), 1446-1453.
Thomas, G.W., Hargrove, W.L., 1984. The chemistry of soil acidity. Soil acidity and liming, e3-56.
Thomas, M.M., Clouse, J.A., Longo, J.M., 1993a. Adsorption of organic compounds on carbonate minerals. 3. Influence on dissolution rates. Chemical Geology 109(1), 227-237.
Thomas, M.M., Clouse, J.A., Longo, J.M., 1993b. Adsorption of organic compounds on carbonate minerals: 1. Model compounds and their influence on mineral wettability. Chemical Geology 109(1), 227-237.
Thompson, A., Rancourt, D.G., Chadwick, O.A., Chorover, J., 2011. Iron solid-phase differentiation along a redox gradient in basaltic soils. Geochimica et Cosmochimica Acta 75(1), 119-133.
Tipping, E., 2005. Modelling Al competition for heavy metal binding by dissolved organic matter in soil and surface waters of acid and neutral pH. Geoderma 127(3-4), 293-304.
Tirmizi, S.A., Wattoo, F.H., Wattoo, M.H.S., Khokhar, N.M., Iqbal, J., 2006. Analytical investigation of soil inorganic elements in cotton cultivated areas of Vehari - Pakistan. Journal of the Chemical Society of Pakistan 27(6), 606-610.
Tisdall, J.M., 1996. Formation of soil aggregates and accumulation of soil organic matter. In: M.R.S. Carter, B. A., (Ed.), Structure and organic matter storage in agricultural soils. CRC Press, Boca Raton, pp. 57-86.
Tisdall, J.M., Oades, J.M., 1982. Organic-matter and water-stable aggregates in soils. Journal of Soil Science 33(2), 141-163.
Tonneijck, F.H., Jansen, B., Nierop, K.G.J., Verstraten, J.M., Sevink, J., De Lange, L., 2010. Towards understanding of carbon stocks and stabilization in volcanic ash soils in natural Andean ecosystems of northern Ecuador. European Journal of Soil Science 61(3), 392-405.
Torn, M.S., Swanston, C.W., Castanha, C., Trumbore, S.E., 2009. Storage and turnover of organic matter in soil. In: N. Senesi, B. Xing, P.M. Huang (Eds.), Biophysico-chemical processes involving natural nonliving organic matter in environmental systems. John Wiley & Sons, Inc., New Jersey, U.S.A., pp. 183-218.
Torn, M.S., Trumbore, S.E., Chadwick, O.A., Vitousek, P.M., Hendricks, D.M., 1997. Mineral control of soil organic carbon storage and turnover. Nature 389(6647), 170-173.
Toutain, F., 1974. Etude écologique de l'humidificaton dans les hetraies acidiphiles, Université de Nancy., Nancy, France.
Trenberth, K.E., 2011. Changes in precipitation with climate change. Climate Research 47(1-2), 123-138.

Trumbore, S.E., 1993. Comparison of carbon dynamics in tropical and temperate soils using radiocarbon measurements. Global Biogeochemical Cycles 7(2), 275-290.
Trumbore, S.E., Davidson, E.A., Barbosa de Camargo, P., Nepstad, D.C., Martinelli, L.A., 1995. Belowground cycling of carbon in forests and pastures of eastern Amazonia. Global Biogeochemical Cycles 9(4), 515-528.
Tyndall, J., 1859. On the transmission of heat of different qualities through gases of different kinds. Proceedings of the Royal Institution 3, 155-158.
UN General Assembly, 2015. Transforming our world: the 2030 Agenda for Sustainable Development. In: T.g. assembly (Ed.). United Nations.
UNEP (Ed.), 1992. World atlas of desertification (United nations environment programme). Land Degradation & Development, 3. John Wiley & Sons, Ltd, London, 249-249 pp.
UNFCC, 2016. Report of the confrerence of the parties on its twenty-first session, held in Paris from 30 November to 13 December 2015, I/CP.21 Report No. 21. UNFCC United Nations Framework Convention on Climate Chaange.
van der Heijden, G., Legout, A., Mareschal, L., Ranger, J., Dambrine, E., 2017. Filling the gap in Ca input-output budgets in base-poor forest ecosystems: The contribution of non-crystalline phases evidenced by stable isotopic dilution. Geochimica et Cosmochimica Acta 209, 135-148.
van Reeuwijk, L.P., 2002. Procedures for soil analysis. 6th ed. FOA - Food and Agriculture Organization of United Nations: International Soil Reference and information Center (ISRIC), Wageningen, The Netherlands.
Vaughan, E., Matos, M., Ríos, S., Santiago, C., Marín-Spiotta, E., 2019. Clay and climate are poor predictors of regional-scale soil carbon storage in the US Caribbean. Geoderma 354, 113841.
Verrecchia, E.P., 1990. Litho-diagenetic implications of the calcium oxalate-carbonate biogeochemical cycle in semiarid Calcretes, Nazareth, Israel. Geomicrobiology Journal 8(2), 87-99.
Verrecchia, E.P., Braissant, O., Cailleau, G., 2006. The oxalate–carbonate pathway in soil carbon storage: the role of fungi and oxalotrophic bacteria. Fungi in Biogeochemical Cycles. Cambridge University Press.
Verrecchia, E.P., Freytet, P., Verrecchia, K.E., Dumont, J.-L., 1995. Spherulites in calcrete laminar crusts; biogenic CaCO ₃ precipitation as a major contributor to crust formation. Journal of Sedimentary Research 65(4a), 690.
Viret, F., Grand, S., 2019. Combined size and density fractionation of soils for investigations of organo-mineral interactions.
Virto, I., Barre, P., Chenu, C., 2008. Microaggregation and organic matter storage at the silt-size scale. Geoderma 146(1-2), 326-335.
Virto, I., Barré, P., Enrique, A., Poch, R.M., Fernández-Ugalde, O., Imaz, M.J., Bescansa, P., 2013. Micromorphological analysis on the influence of the soil mineral composition on short-term aggregation in semi-arid Mediterranean soils. Spanish Journal of Soil Science 3(2), 116-129.
Virto, I., Gartzia-Bengoetxea, N., Fernandez-Ugalde, O., 2011. Role of organic matter and carbonates in soil aggregation estimated using laser diffractometry. Pedosphere 21(5), 566-572.
Virto, I., Moni, C., Swanston, C., Chenu, C., 2010. Turnover of intra- and extra-aggregate organic matter at the silt-size scale. Geoderma 156(1–2), 1-10.
Vittoz, P., Gmür, P., 2008. Introduction aux Journées de la biodiversité dans le Vallon de Nant. In: A.-C.P. Clot, D. Cherix, F. Dessimox, J.-L. Gattolliat, P. Gmür, P. Vittoz, M. Vust (Eds.), Biodiversité du Vallon de Nant Premières Journées de la biodiversité en Suisse romande (5 et 6 juillet, 2008) Mémoire Vol 23. Société vaudoise des Sciences naturelles, Vaud, Switzerland.
Vogel, C., Mueller, C.W., Hoeschen, C., Buegger, F., Heister, K., Schulz, S., Schloter, M., Kögel-Knabner, I., 2014. Submicron structures provide preferential spots for carbon and nitrogen sequestration in soils. Nature Communications 5(2947), 1-7.
von Lützow, M., Kögel-Knabner, I., Ekschmitt, K., Matzner, E., Guggenberger, G., Marschner, B., Flessa, H., 2006. Stabilization of organic matter in temperate soils: mechanisms and their relevance under different soil conditions - a review. European Journal of Soil Science 57(4), 426-445.

von Wandruszka, R., 2006. Phosphorus retention in calcareous soils and the effect of organic matter on its mobility. Geochemical Transactions 7(1), 6.
W. Carter, P., 1978. Adsorption of amino acid-containing organic matter by calcite and quartz. Geochimica et Cosmochimica Acta 42(8), 1239-1242.
Wang, B., Brewer, P.E., Shugart, H.H., Lerdau, M.T., Allison, S.D., 2019. Soil aggregates as biogeochemical reactors and implications for soil–atmosphere exchange of greenhouse gases—A concept. Global Change Biology 25(2), 373-385.
Webster, R., 2007. Analysis of variance, inference, multiple comparisons and sampling effects in soil research. European Journal of Soil Science 58(1), 74-82.
Wedepohl, H.K., 1995. The composition of the continental crust. Geochimica et Cosmochimica Acta 59(7), 1217-1232.
Wei, T., Simko, V., 2017. R package "corrplot": Visualization of a Correlation Matrix.
Wen, L., Li, D., Chen, H., Wang, K., 2017. Dynamics of soil organic carbon in density fractions during post-agricultural succession over two lithology types, southwest China. Journal of Environmental Management 201, 199-206.
Whittinghill, K.A., Hobbie, S.E., 2012. Effects of pH and calcium on soil organic matter dynamics in Alaskan tundra. Biogeochemistry 111(1-3), 569-581.
Wiese, L., Ros, I., Rozanov, A., Boshoff, A., de Clercq, W., Seifert, T., 2016. An approach to soil carbon accounting and mapping using vertical distribution functions for known soil types. Geoderma 263, 264-273.
Wiesmeier, M., Spörlein, P., Geuß, U., Hangen, E., Haug, S., Reischl, A., Schilling, B., von Lützow, M., Kögel-Knabner, I., 2012. Soil organic carbon stocks in southeast Germany (Bavaria) as affected by land use, soil type and sampling depth. Global Change Biology 18(7), 2233-2245.
Wiesmeier, M., Urbanski, L., Hobley, E., Lang, B., von Lützow, M., Marin-Spiotta, E., van Wesemael, B., Rabot, E., Ließ, M., Garcia-Franco, N., Wollschläger, U., Vogel, H.-J., Kögel-Knabner, I., 2019. Soil organic carbon storage as a key function of soils - A review of drivers and indicators at various scales. Geoderma 333, 149-162.
Williamson, K.L., 1989. Reduction of indigo - sodium hydrosulfite as a reducing agent Journal of Chemical Education 66(4), 359-359.
Wong, V.N.L., Greene, R.S.B., Dalal, R.C., Murphy, B.W., 2010. Soil carbon dynamics in saline and sodic soils: a review. Soil Use and Management 26(1), 2-11.
Wuddivira, M.N., Camps-Roach, G., 2007. Effects of organic matter and calcium on soil structural stability. European Journal of Soil Science 58(3), 722-727.
Xiao, J., Wen, Y., Li, H., Hao, J., Shen, Q., Ran, W., Mei, X., He, X., Yu, G., 2015. In situ visualisation and characterisation of the capacity of highly reactive minerals to preserve soil organic matter (SOM) in colloids at submicron scale. Chemosphere 138, 225-232.
Yang, S., Cammeraat, E., Jansen, B., Cerli, C., Kalbitz, K., 2016. Organic carbon stabilization of soils formed on acidic and calcareous bedrocks in Neotropical alpine grassland, Peru. EGU General Assembly 2016, held 17-22 April, 2016 in Vienna Austria.
Yeasmin, S., Singh, B., Johnston, C.T., Sparks, D.L., 2017. Organic carbon characteristics in density fractions of soils with contrasting mineralogies. Geochimica et Cosmochimica Acta 218, 215-236.
Yuan, G., Soma, M., Seyama, H., Theng, B.K.G., Lavkulich, L.M., Takamatsu, T., 1998. Assessing the surface composition of soil particles from some Podzolic soils by X-ray photoelectron spectroscopy. Geoderma 86(3), 169-181.
Yuan, T.L., Gammon, N., Leighty, R.G., 1967. Relative contribution of organic and clay fractions to cation-exchange capacity of sandy soils from several soil groups. Soil Science 104(2), 123-128.
Yudina, A., Kuzyakov, Y., 2019. Saving the face of soil aggregates. Global Change Biology 0(ja).
Zamanian, K., Pustovoytov, K., Kuzyakov, Y., 2016. Pedogenic carbonates: forms and formation processes. Earth-Science Reviews 157, 1-17.
Zelles, L., Scheunert, I., Kreutzer, K., 1987. Bioactivity in limed soil of a spruce forest. Biology and Fertility of Soils 3(4), 211-216.

Zemek, J., Olejnik, K., Klapetek, P., 2008. Photoelectron spectroscopy from randomly corrugated surfaces. Surface Science 602(7), 1440-1446.

Zhao, J., Chen, S., Hu, R., Li, Y., 2017. Aggregate stability and size distribution of red soils under different land uses integrally regulated by soil organic matter, and iron and aluminum oxides. Soil and Tillage Research 167, 73-79.

Zhu, Z., Piao, S., Myneni, R.B., Huang, M., Zeng, Z., Canadell, J.G., Ciais, P., Sitch, S., Friedlingstein, P., Arneth, A., Cao, C., Cheng, L., Kato, E., Koven, C., Li, Y., Lian, X., Liu, Y., Liu, R., Mao, J., Pan, Y., Peng, S., Peñuelas, J., Poulter, B., Pugh, T.A.M., Stocker, B.D., Viovy, N., Wang, X., Wang, Y., Xiao, Z., Yang, H., Zaehle, S., Zeng, N., 2016. Greening of the Earth and its drivers. Nature Climate Change 6, 791.

Zimmerman, A.R., Ahn, M.-Y., 2010. Organo-mineral–enzyme interaction and soil enzyme activity. 22, 271-292.

Zollinger, B., Alewell, C., Kneisel, C., Meusburger, K., Gaertner, H., Brandova, D., Ivy-Ochs, S., Schmidt, M.W.I., Egli, M., 2013. Effect of permafrost on the formation of soil organic carbon pools and their physical-chemical properties in the Eastern Swiss Alps. Catena 110, 70-85.